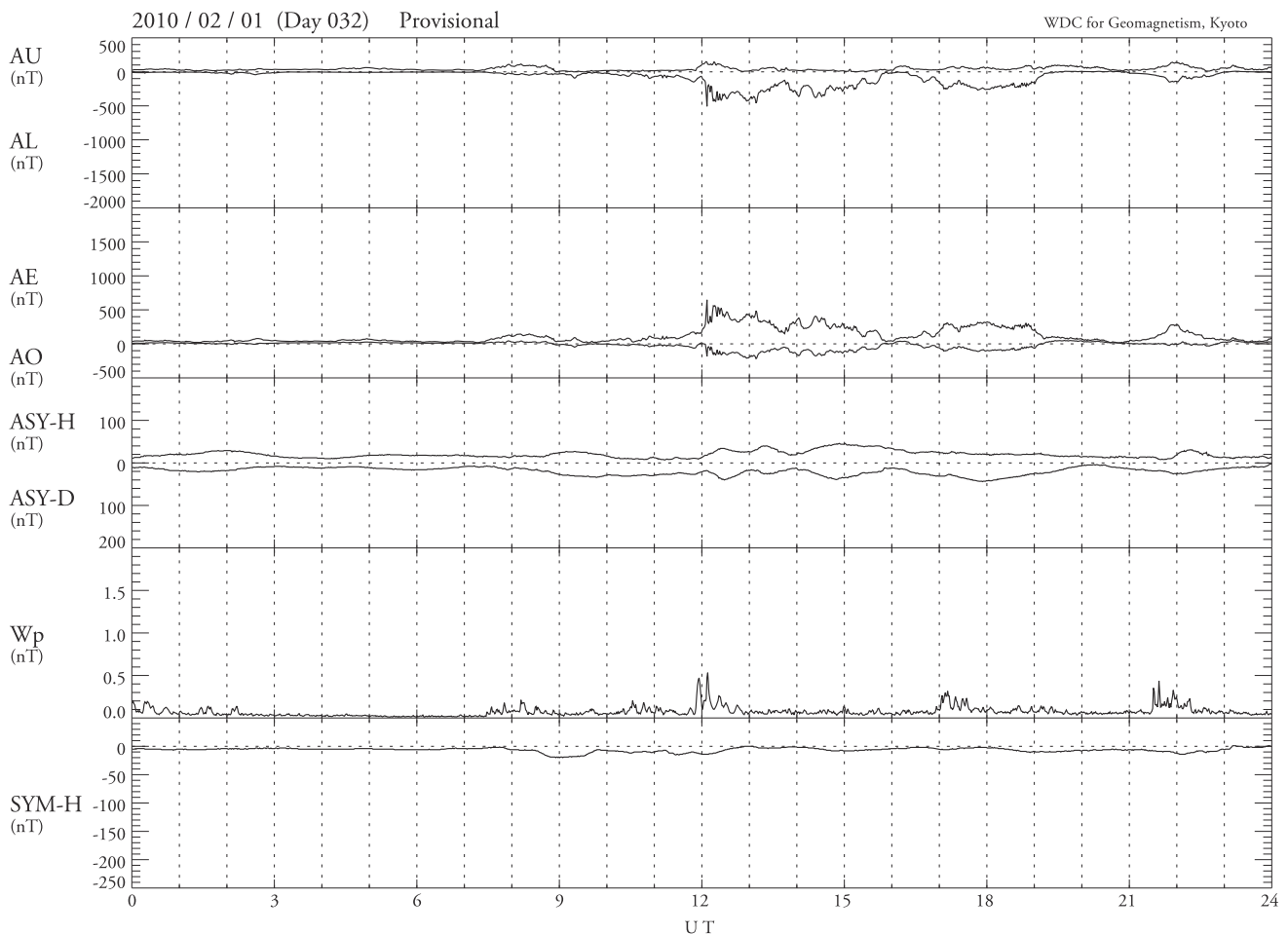


High-Time Resolution Geomagnetic Indices

AE, ASY, W_p , and SYM

No. 2 2010



March 2012

Data Analysis Center for Geomagnetism and Space Magnetism
Graduate School of Science, Kyoto University
Kyoto, Japan

High-Time Resolution Geomagnetic Indices

AE, ASY, W_p , and SYM

No. 2

2010

March 2012

Data Analysis Center for Geomagnetism and Space Magnetism
Graduate School of Science
Kyoto University

Preface

This data book displays geomagnetic indices in a stack for quick and easy search of substorm onset/geomagnetic storm. The geomagnetic indices include the AE (Auroral Electrojet) indices, the ASY (ASYmmetric disturbance) index, the Wp (Wave planetary) index, and the SYM (SYMmetric disturbance) index. All of them have a time resolution of 1 min. The AE and ASY indices are considered to reflect occurrence of high-latitude negative bays and mid-latitude positive bays, respectively, both of which appear at substorm onset. The Wp index, a newly proposed index, represents Pi2 wave power on the nightside at low-latitude, which is a good indicator of substorm onset. The SYM index expresses the symmetric disturbance field, which is essentially the same as Sugiura's hourly Dst index; thus geomagnetic storms can be found by its large negative values. Detailed information of these indices is given in later sections.

Substorm onset can be identified by enhancements of the AE/ASY/Wp indices (or decrease of the AL index). However, since the AE/ASY/Wp indices reflect different substorm signatures, it is natural that their behaviors or time scales of variations at substorm onset are different from each others. For instance, the AE and ASY indices continue to increase for a few tens of minutes to 1 hour after substorm onset and decay in the order of 1 hour, while the Wp index increases in a short time (~10 min) at substorm onset and returns to its initial values within a few tens of minutes. There is also the difference in sensitivity to substorm onset among these indices.

Please note that the plotted indices may contain artificial noises, though we tried to eliminate them as much as possible. Users are suggested to contact us for further information or digital data before presentation and publication.

M. Nosé, T. Iyemori, Y. Odagi, M. Takeda, H. Toh, Y. Koyama, and N. Takeuchi
Data Analysis Center for Geomagnetism and Space Magnetism
Graduate School of Science, Kyoto University
Bldg. #1, Oiwake-cho, Kitashirakawa, Sakyo-ku, Kyoto 606-8502, Japan
Tel: +81-75-753-3929
Fax: +81-75-722-7884
E-mail: nose@kugi.kyoto-u.ac.jp (M. Nosé)
iyemori@kugi.kyoto-u.ac.jp (T. Iyemori)
WWW: <http://wdc.kugi.kyoto-u.ac.jp>

Acknowledgments

The data used in this data book are kindly provided by the following institutes (in alphabetical order). Observatory abbreviation codes are shown in parentheses. We thank all of the staff in these institutes for making geomagnetic field data available.

- Arctic and Antarctic Research Institute (DIK, CCS, TIK, PBK)
- Department of Earth and Environmental Sciences, Ludwig Maximilians Universität (FUR)
- DTU Space, Technical University of Denmark (NAQ, TDC)
- Ecole et Observatoire des Sciences de la Terre (AMS)
- Geological Survey of Canada (YKC, FCC, SNK)
- Geological Survey of Sweden (ABK)
- Geoscience Australia (CNB, LRM)
- Hermanus Magnetic Observatory (HER)
- Indian Institute of Geomagnetism (ABG)
- Institute de Physique du Globe de Paris (CLF, PPT)
- Institute of the Ionosphere of Republic Kazakhstan (AAA)
- Kakioka Magnetic Observatory (MMB, KAK)
- Kandilli Observatory and Earthquake Research Institute, Boğazici University (IZN)
- Observatori de l'Ebre (OE), CSIC, Universitat Ramon Llull (EBR)
- University of Iceland (LRV)
- Urumqi Geomagnetic Observatory, Seismological Bureau of Xinjiang Uygur Autonomous Region (WMQ)
- U.S. Geological Survey (HON, BOU, FRD, SJD, TUC, BRW, CMO)

1. AE Indices

1.1. Introduction

The Auroral electrojet (AE) index was originally introduced by *Davis and Sugiura (1966)* as a measure of global electrojet activity in the auroral zone. After the initial development at the NASA/Goddard Space Flight Center, the calculation of the index was first performed at the Geophysical Institute of the University of Alaska, which published hourly values of the index for the years 1957-1964. The production of 2.5 min values was then made at the Goddard Space Flight Center for the period from September 1964 to June 1968. After these early publications, the index was regularly issued by the World Data Center A for Solar-Terrestrial Physics (WDC-A for STP) in Boulder, Colorado, which published 2.5 min values for the years 1966–1974 and 1.0 min values for 1975 and the first 4 months of 1976.

When it became difficult for the WDC-A for STP to continue producing the AE index, WDC-C2 (operated by the Data Analysis Center for Geomagnetism and Space Magnetism, Faculty of Science, Kyoto University) began to produce the AE index from the International Magnetospheric Study period (1978–1979) onwards. Since then, WDC-C2 for Geomagnetism (renamed WDC for Geomagnetism, Kyoto after 2000) has been publishing 1.0 min values of the AE index.

1.2. Method of derivation

The AE index is derived from geomagnetic variations in the horizontal component observed at selected 12 observatories along the auroral zone in the northern hemisphere. To normalize the data, a base value for each station is first calculated for each month by averaging all the data from the station on the five international quietest days. This base value is subtracted from each value of one-minute data obtained at the station during that month. Then among the data from all the stations at each given time (UT), the largest and smallest values are selected. The AU and AL indices are respectively defined by the largest and the smallest values so selected. The symbols, AU and AL, derive from the fact that these values form the upper and lower envelopes of the superposed plots of all the data from these stations as functions of UT. The difference, AU minus AL, defines the AE index, and the mean value of the AU and AL, i.e. $(AU+AL)/2$, defines the AO index. The term “AE indices” is usually used to represent these four indices (AU, AL, AE and AO). The AU and AL indices are intended to express the strongest current intensity of the eastward and westward auroral electrojets, respectively. The AE index represents the overall activity of the electrojets, and the AO index provides a measure of the equivalent zonal current.

A list of the AE stations is compiled in Table 1 and their locations are shown in Figure 1. It should be noted that some of the stations have closed and been replaced by new stations. Cape Wellen was closed in 1996 and was not replaced until the introduction of Pebek in April 2001. Great Whale River observatory was closed in July 1984 and followed by a new station at Poste-de-la-Baleine, in September 1984. Then Poste-de-la-Baleine was replaced by Sanikiluaq in November and December 2007.

Table 1. List of the 12 AE stations. Stations above (below) a double line are currently working stations (old stations).

Observatory	Abbrev.	Geographic		Geomagnetic		Notes
		Lat. (°)	Lon. (°)	Lat.(°)	Lon. (°)	
Abisko	ABK	68.36	18.82	66.06	114.66	
Dixon Island	DIK	73.55	80.57	64.04	162.53	
Cape Chelyuskin	CCS	77.72	104.28	67.48	177.82	
Tixie Bay	TIK	71.58	129.00	61.76	193.71	
Pebek	PBK	70.09	170.93	63.82	223.31	Open. in 2001/04
Barrow	BRW	71.30	203.25	69.57	246.18	
College	CMO	64.87	212.17	65.38	261.18	
Yellowknife	YKC	62.40	245.60	68.87	299.53	
Fort Churchill	FCC	58.80	265.90	67.98	328.36	
Sanikiluaq	SNK	56.5	280.8	66.6	349.7	Open. in 2007/12
Narssarsuaq	NAQ	61.20	314.16	69.96	37.95	
Leirvogur	LRV	64.18	338.30	69.32	71.04	
Cape Wellen	CWE	66.17	190.17	62.88	241.36	Clos. in 1996
Great Whale River	GWR	55.27	282.22	65.45	351.77	Clos. in 1984/07
Poste-de-la-Baleine	PBQ	55.27	282.22	65.45	351.77	Open. in 1984/09 Clos. in 2007/11

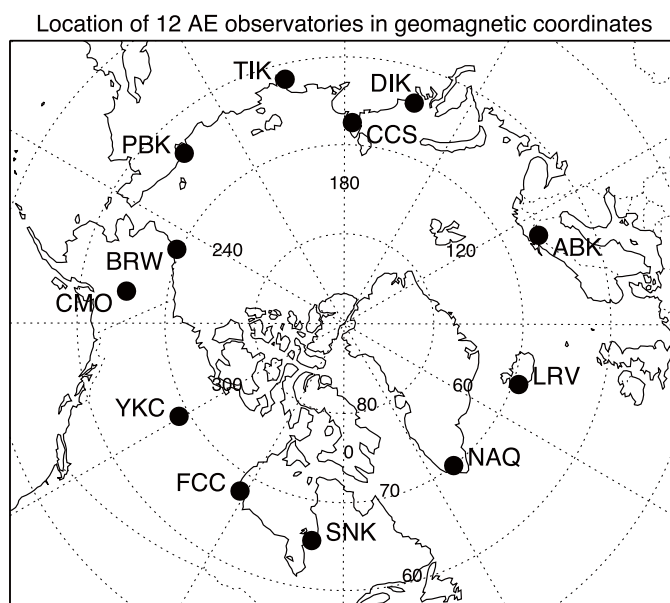


Figure 1. Location of the current AE observatories in geomagnetic coordinates. Latitude circles are drawn at 10° intervals and longitude are separated by 30° intervals.

2. SYM/ASY Indices

2.1. Introduction

To describe the geomagnetic disturbance fields in mid-latitudes with high-time (i.e., 1 minute) resolution, a longitudinally asymmetric (ASY) and a symmetric (SYM) disturbance index are introduced and derived for both H and D components, that is, for the components in the horizontal (dipole pole) direction H (SYM-H, ASY-H) and in the orthogonal (East-West) direction D (SYM-D, ASY-D). The symmetric disturbance field in H, SYM-H, is essentially the same as Sugiura's hourly Dst index (*Sugiura and Poros, 1971*), although we use 1 minute values from different sets of stations with a slightly different coordinate system. Similarly, the ASY-H asymmetric disturbance component in H is close to the asymmetric indices proposed by *Kawasaki and Akasofu (1971)*, *Crooker and Siscoe (1971)*, or *Clauer et al. (1983)*. ASY-D used in this data book was introduced and discussed by *Iyemori (1990, 1996)*. It has been shown that the variation of the asymmetric H component correlates well with the AE index (e.g. *Crooker, 1972; Clauer and McPherron, 1980*). The results of an examination of the correlation between the ASY-D and the AE indices or the IMF-Bz and a discussion of the meaning of these indices will be published in somewhere else. Although there exists rather a good correlation between both ASYs and the AE indices, it should be noted that there are some essential differences between them and we should be careful when we use the ASY indices as a monitor of disturbances in the polar region.

2.2. Method of derivation

Shown in Table 2 and Figure 2 are a list of geomagnetic observatories used here and their distribution in the geomagnetic dipole coordinate system, respectively. It should be noted that some of the stations used here (i.e., Urumqi, Fredericksburg, Boulder, Tucson, Memambetsu, Martin de Vivies and Chambon-la-Foret) are at higher latitudes than those used in the derivation of Sugiura's standard Dst index (i.e., Honolulu, Kakioka, Hermanus, and San Juan). Only six of the stations are used for the derivation of each month, some stations being replaced by others depending on the availability and the condition of the data of the month. The data are processed in units of one month. Therefore some gap in the magnitude is seen between successive months. The derivation procedure essentially consists of the following four steps.

(1) Subtraction of the geomagnetic main field and the Sq field to calculate the disturbance field component

The geomagnetic field consists of the main field, the solar quiet (Sq) daily variation, and the disturbance field. To get the disturbance field, the geomagnetic main field and the Sq field have to be subtracted. To calculate the base value including the Sq field, the data of international five quiet days are used. That is, the original data of the international 5-Q days of the month that include the Sq field as well as the geomagnetic main field are averaged every minute and fitted by B-spline functions. For some special cases where some of the 5-Q days are not suitable for the purpose because of missing data etc., another quiet day is selected from international 10 quiet days of the month. The fitted values are then subtracted from original data to get the disturbance component.

(2) Coordinate transformation to a dipole coordinate system

In a geomagnetic storm period, the ring current is the main source of the disturbance field in the H component observed at mid-latitudes. As the ring current flows in the magnetosphere at a distance of several R_E (radius of the Earth) and in the equatorial plane, its geomagnetic effect should be nearly parallel to the dipole axis. On the other hand, the H direction at each observatory is generally different from the dipole pole direction because of the non-dipole component or local geomagnetic anomalies. Therefore the ring current effect is mixed into the D component. To minimize the ring current effect in the D-component, the data are transformed to the dipole coordinate system at each station. The differences between the dipole pole position and local geomagnetic direction are shown in Table 1.

(3) Calculation of the longitudinally symmetric component, SYM-H and SYM-D

The longitudinally symmetric component is calculated by averaging the disturbance component at each minute for the 6 stations. For the H component, a latitudinal correction is made on the averaged value to get the value (SYM-H) which corresponds to Sugiura's equatorial Dst index, that is, it is divided by the 6-station average of $\cos \theta_m$, where θ_m is the dipole latitude of each station, though the stations used, the coordinate system and the method to subtract the base value with Sq current effect are different from his method of derivation. On the symmetric component of D (SYM-D), we make no latitudinal correction at all.

(4) Calculation of the asymmetric component, ASY-H and ASY-D

The asymmetric component at each station is obtained by subtracting the symmetric component from each disturbance field. For the H component, the symmetric part is subtracted after making a latitudinal correction assuming that the SYM-H represents the magnitude of the uniform field parallel to the dipole axis generated by the ring current. After subtracting the symmetric part, a latitudinal correction is made by multiplying the normalization coefficient for each station which is determined empirically as the standard deviations of the asymmetric variation for the 6 stations become equal. The ASY-H and the ASY-D indices are defined as the range between the maximum and minimum deviation at each moment for the H and the D component, respectively.

Table 2. List of the SYM/ASY stations.

Observatory	Abbrev.	Geographic		Geomagnetic		Apex	Rotation
		Lat. (°)	Lon. (°)	Lat.(°)	Lon. (°)		
San Juan	SJG	18.110	293.850	28.04	6.54	30.3	-8.9
Fredericksburg	FRD	38.200	282.630	48.14	353.93	50.3	0.4
Boulder	BOU	40.130	254.760	48.24	321.28	49.5	2.5
Tucson	TUC	32.170	249.270	39.73	316.74	40.3	2.7
Papeete	PPT	-17.567	210.426	-15.13	285.49	17.5	0.76
Honolulu	HON	21.320	202.000	21.71	270.27	22.8	0.5
Memambetsu	MMB	43.910	144.189	35.63	211.74	36.9	-16.1
Urumqi	WMQ	43.800	87.700	34.34	162.53	38.7	7.66
Alma Ata	AAA	43.250	76.920	34.50	153.04	38.3	11.0
Alibag	ABG	18.638	72.872	10.37	146.55	13.4	6.8
Martin de Vivies	AMS	-37.796	77.574	-46.22	144.93	49.2	-32.4
Hermanus	HER	-34.425	19.225	-34.08	84.63	42.7	-10.1
Chambon-la-Foret	CLF	48.025	2.261	49.75	85.80	44.2	13.6

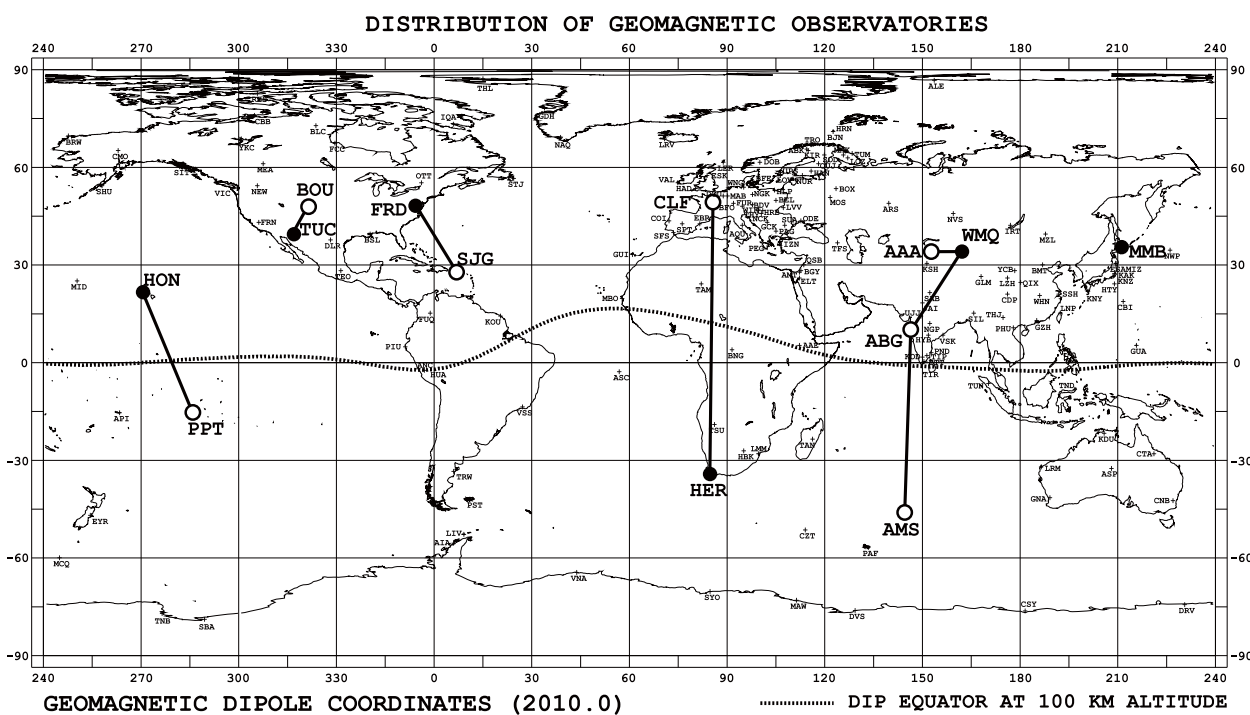


Figure 2. Location of the SYM/ASY observatories in geomagnetic coordinates. The observatories normally used are shown by the solid circles. The stations replaced in some special cases are shown by the open circles connected by solid lines.

3. Wp index

3.1. Introduction

Pi2 pulsations are defined as geomagnetic variations with periods of 40-150 seconds and irregular (damped) waveforms (*Jacobs et al.*, 1964). Previous studies reported that Pi2 pulsations can serve as a diagnostic indicator of substorm onset (*Saito et al.*, 1976a, b; *Sakurai and Saito*, 1976). They appear almost simultaneously with auroral breakups (e.g., *Gelpi et al.*, 1987), energetic particle injection in the inner magnetosphere (e.g., *Saka et al.*, 1996), and magnetic field dipolarization (e.g., *Yumoto et al.*, 1989). Since low-latitude Pi2 pulsations have dominant power near midnight, multiple ground stations distributing longitudinally are needed for their detection. Recently a large number of geomagnetic stations have started recording geomagnetic field variations with a time resolution of 1 min. This development facilitates the routine derivation of a new index measuring Pi2 power. In this data book, using data from the longitudinal network of 11 ground stations, we calculate a new substorm index, the “Wp index” (Wave and planetary).

3.2. Method of derivation

Figure 3 shows the locations of geomagnetic stations used to derive the Wp index. The coordinates of the stations are listed in Table 3. Since Canberra, Learmonth, and Tristan da Cunha are located in the southern hemisphere, their locations are plotted as geomagnetically conjugate points in Figure 3. The absolute values of geomagnetic latitude of these 11 stations range between 21° and 49°. The largest longitudinal separation between the stations is about 52° (between Urumqi and Iznik). Therefore the longitudinal network of these stations is dense enough that at least one station is always positioned on the nightside where low-latitude Pi2 pulsations can be clearly observed.

Using the 1-s data from the 11 stations, we calculate the Wp index as follows. A schematic figure of the calculation procedure is shown in Figure 4.

1. The magnetic field in the horizontal plane is converted into H_N - H_E coordinates, where the H_N and H_E components are parallel and perpendicular to the local magnetic field, respectively. The H_E component is positive eastward. The orientation of the local magnetic field (i.e., declination) at each station is calculated by using the IGRF-11 model. Table 3 lists the declination on 1 January 2005, which is applied in subsequent periods. In the calculation of the Wp index, only the H_N component is used (Figure 4a).

2. Wavelet analysis is applied to geomagnetic field data for a segment of 512 second length. The data segment is shifted forward by 60 seconds and the wavelet analysis is repeated (Figure 4b). The frequency bands of wavelet function with $j=4$ and 5 are 5.2-20.8 mHz and 10.4-41.7 mHz, respectively, which cover a frequency range of Pi2 pulsations (6.67-25.0 mHz). The wavelet coefficients of $j=4$ and 5 ($a_{4,k}$ and $a_{5,k}$) are computed so that their magnitude represents a maximum amplitude of the corresponding wavelet functions in nT.

3. Using the obtained wavelet coefficients, we calculate wavelet power with a time resolution of 1 min (Figure 4c). The wavelet power is defined as an average of wavelet coefficients of $j=4$ and 5 ($a_{4,k}$ and

$a_{5,k}$) in a given 1-minute bin. This process results in a time series of 1-minute wavelet power (i.e., 1440 data points/1 day) for each station, which is named the W_{ABB} index, where “W” stands for “Wave” and “ABB” is the 3-letter abbreviation code of the station.

4. The Wp index is derived from the W_{ABB} indices at 11 stations. Since Pi2 pulsations have dominant power on the nightside, we use only W_{ABB} from stations located at 1800-0400 MLT. The Wp index is simply defined as an average of W_{ABB} of the stations in this MLT range (Figure 4d).

Table 3. List of the 11 Wp stations.

Observatory	Abbrev.	Geographic		Geomagnetic		Declination. (°)
		Lat. (°)	Lon. (°)	Lat.(°)	Lon. (°)	
Tucson	TUC	32.17	249.27	39.88	316.11	10.4
Honolulu	HON	21.32	202.00	21.64	269.74	9.8
Canberra	CNB	-35.32	149.36	-42.71	226.94	12.4
Kakioka	KAK	36.23	140.19	27.37	208.75	-7.2
Learmonth	LRM	-22.22	114.10	-32.42	186.45	0.5
Urumqi	WMQ	43.80	87.70	34.11	162.21	2.8
Izник	IZN	40.50	29.73	37.74	109.58	4.7
Fürstentfeldbruck	FUR	48.17	11.28	48.38	94.61	2.0
Ebro	EBR	40.82	0.50	43.18	81.31	-0.7
Tristan da Cunha	TDC	-37.25	347.50	-31.55	53.42	-23.8
San Juan	SJG	18.11	293.85	28.31	6.08	-12.7

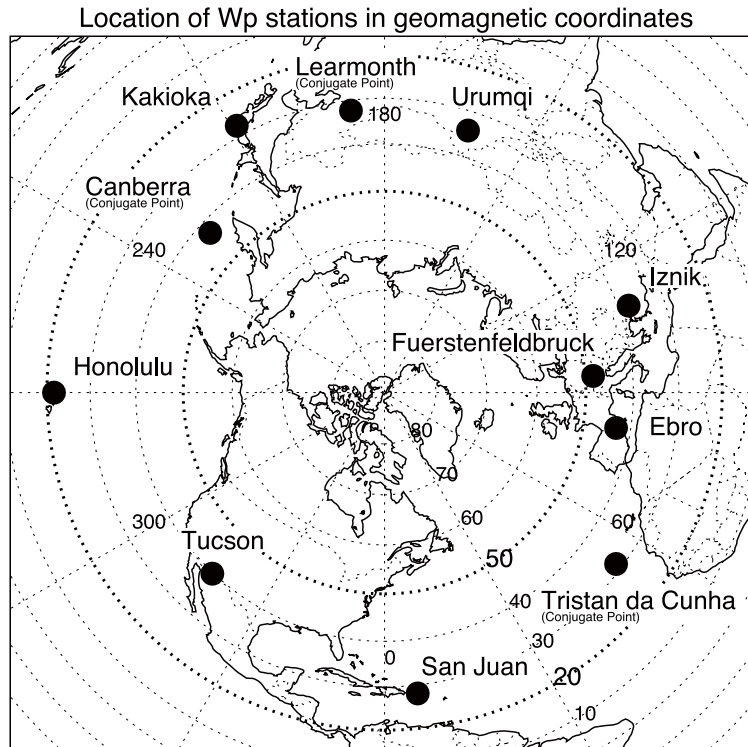


Figure 3. Location of geomagnetic stations in geomagnetic coordinates used to derive the Wp index. Dotted thick circles indicate geomagnetic latitudes of 20° and 50° .

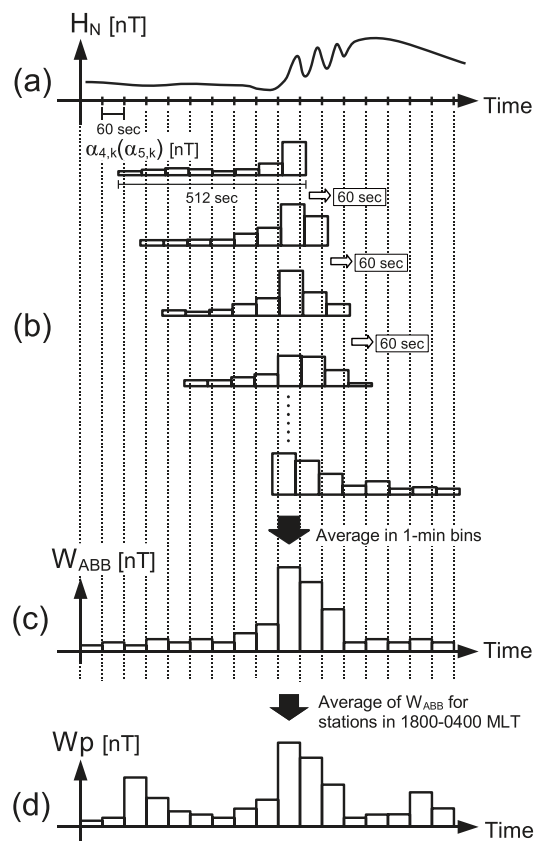
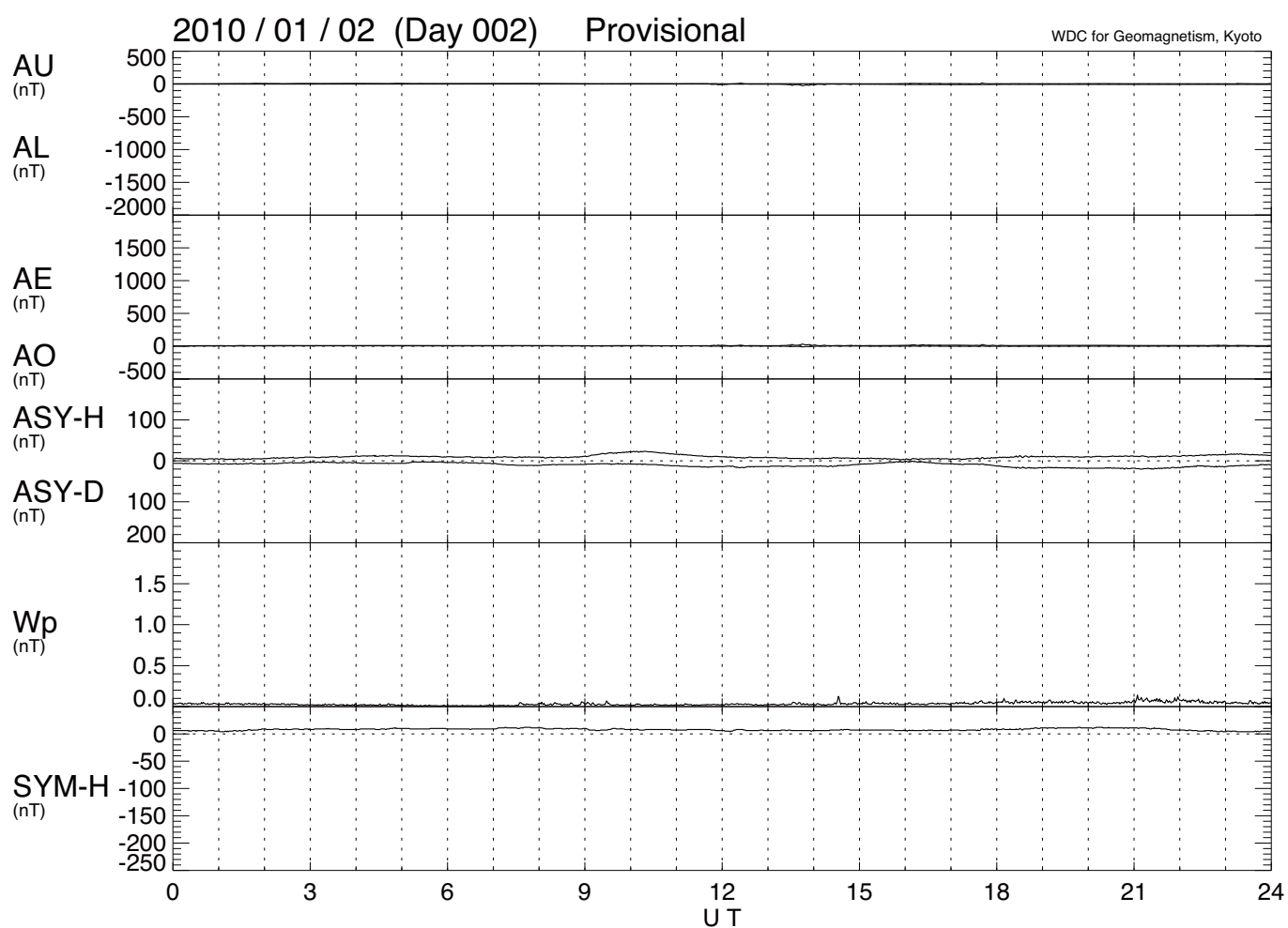
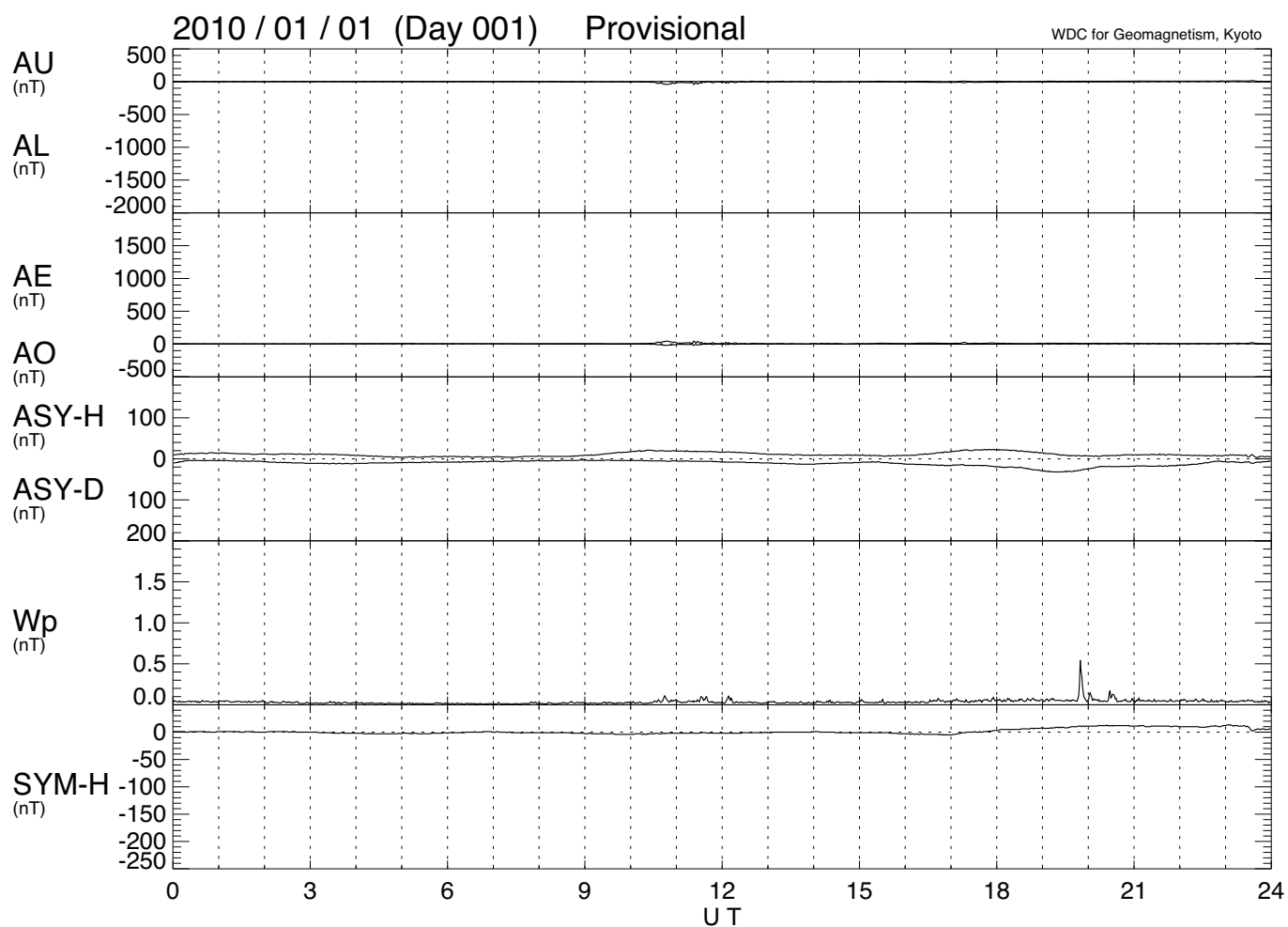
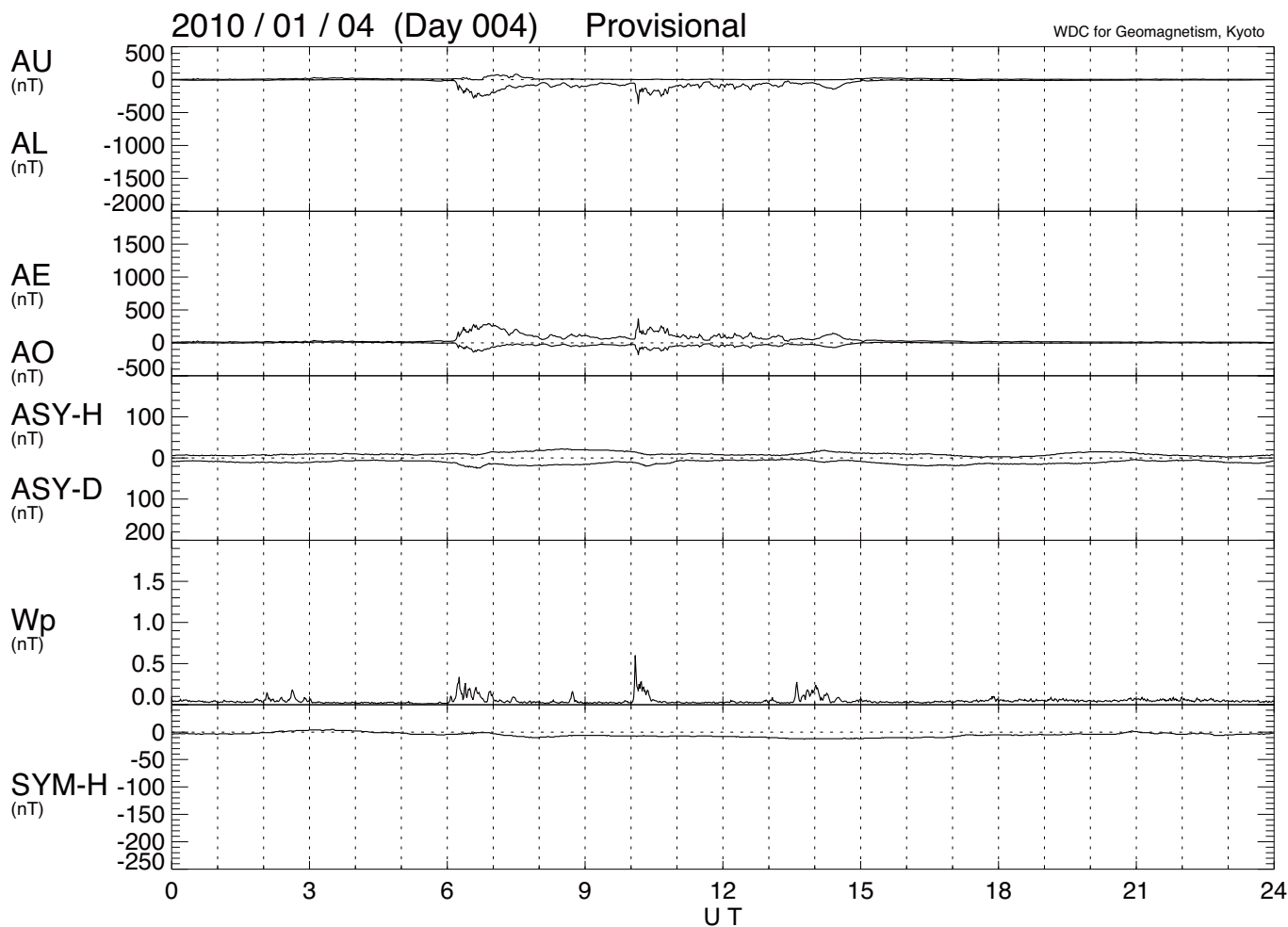
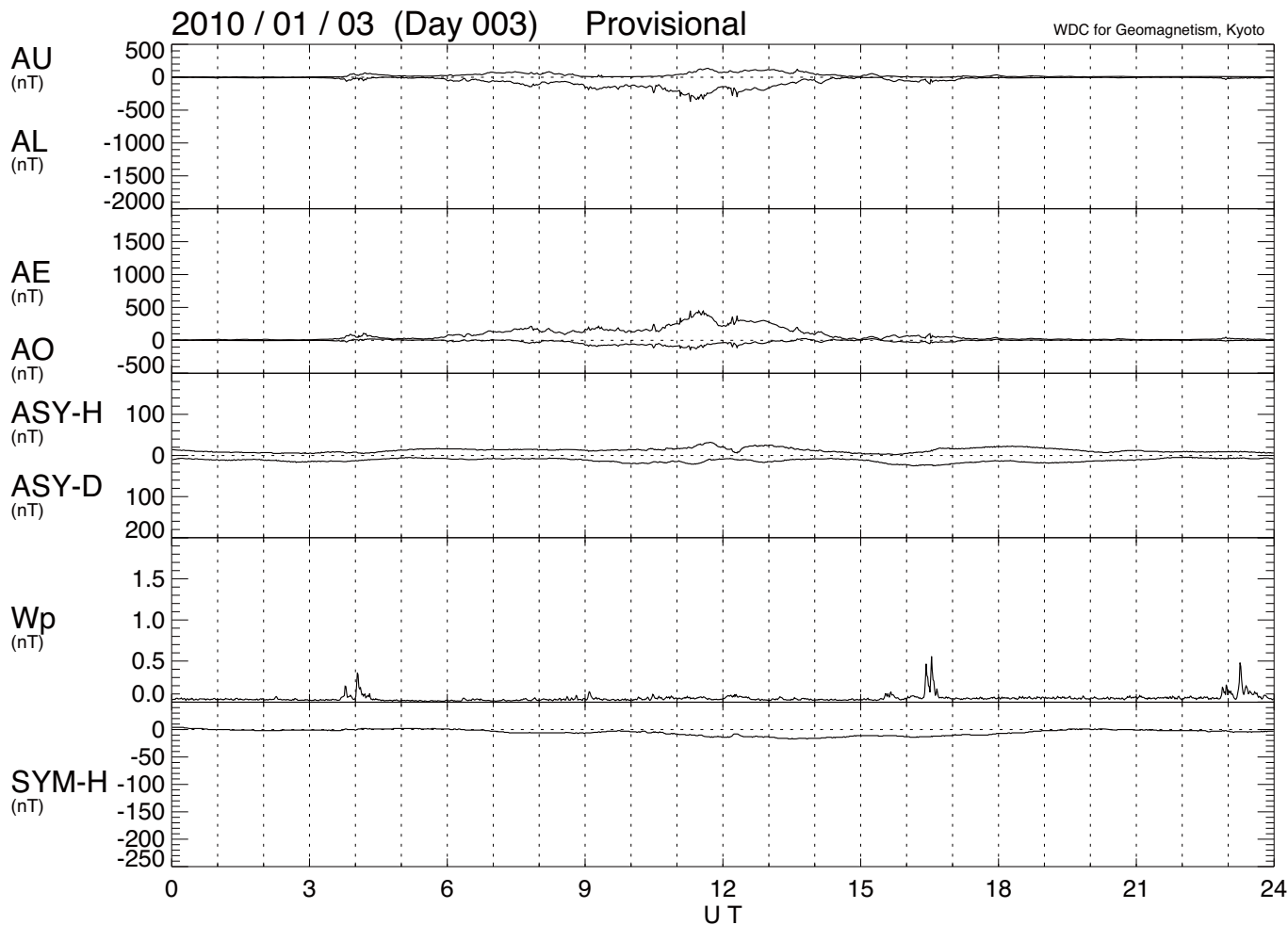


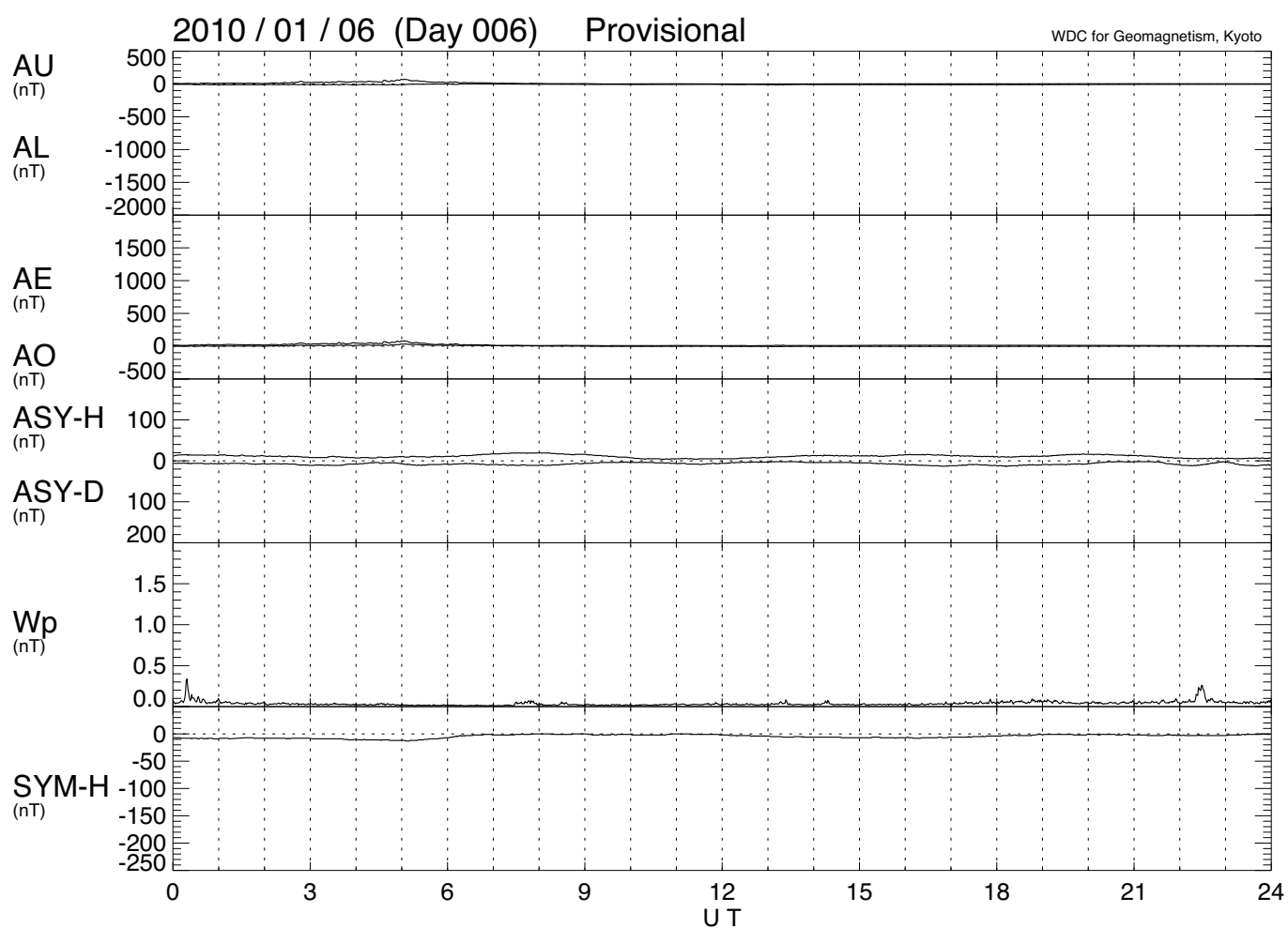
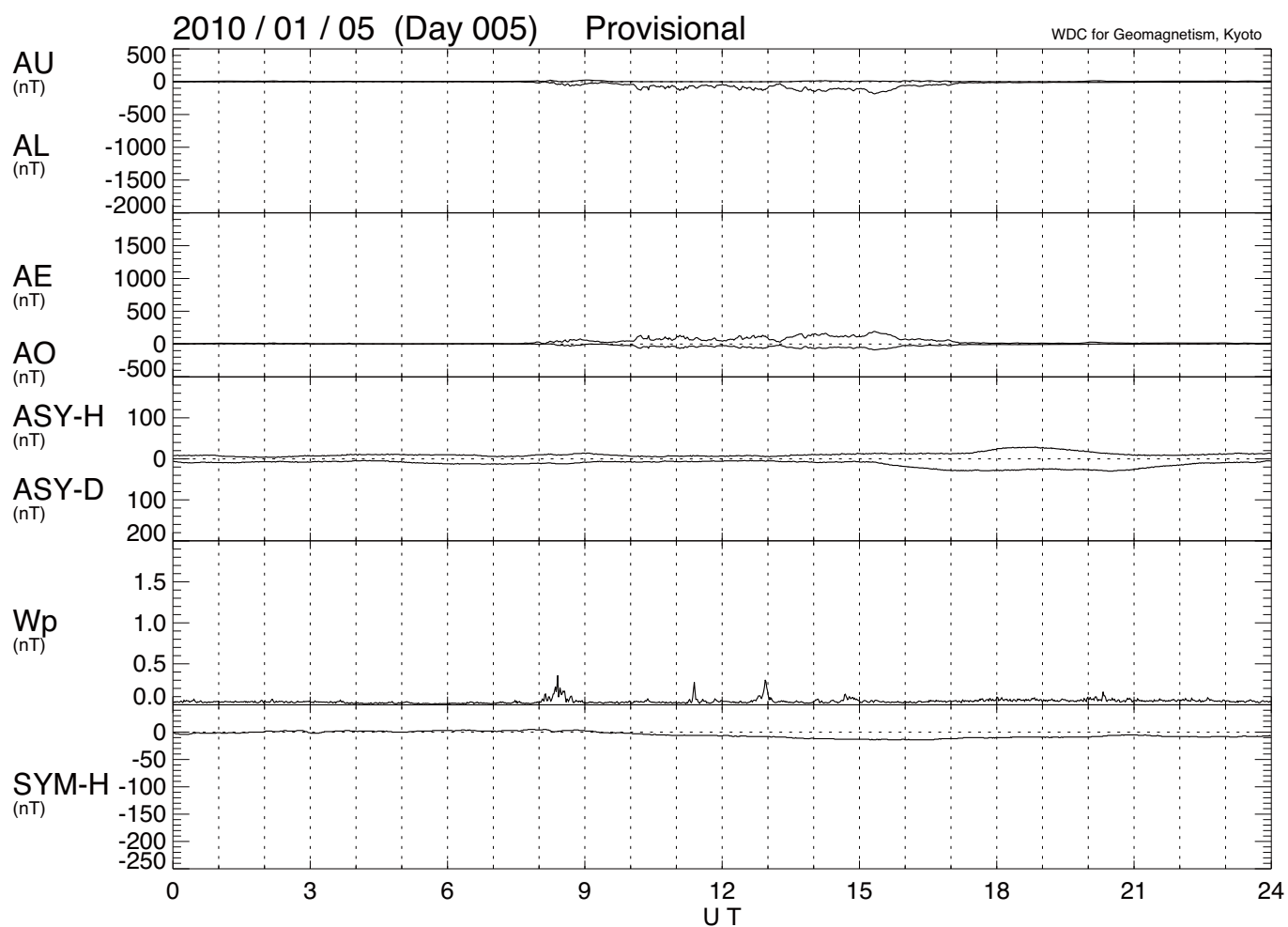
Figure 4. Schematic figure of calculation procedure of the Wp index.

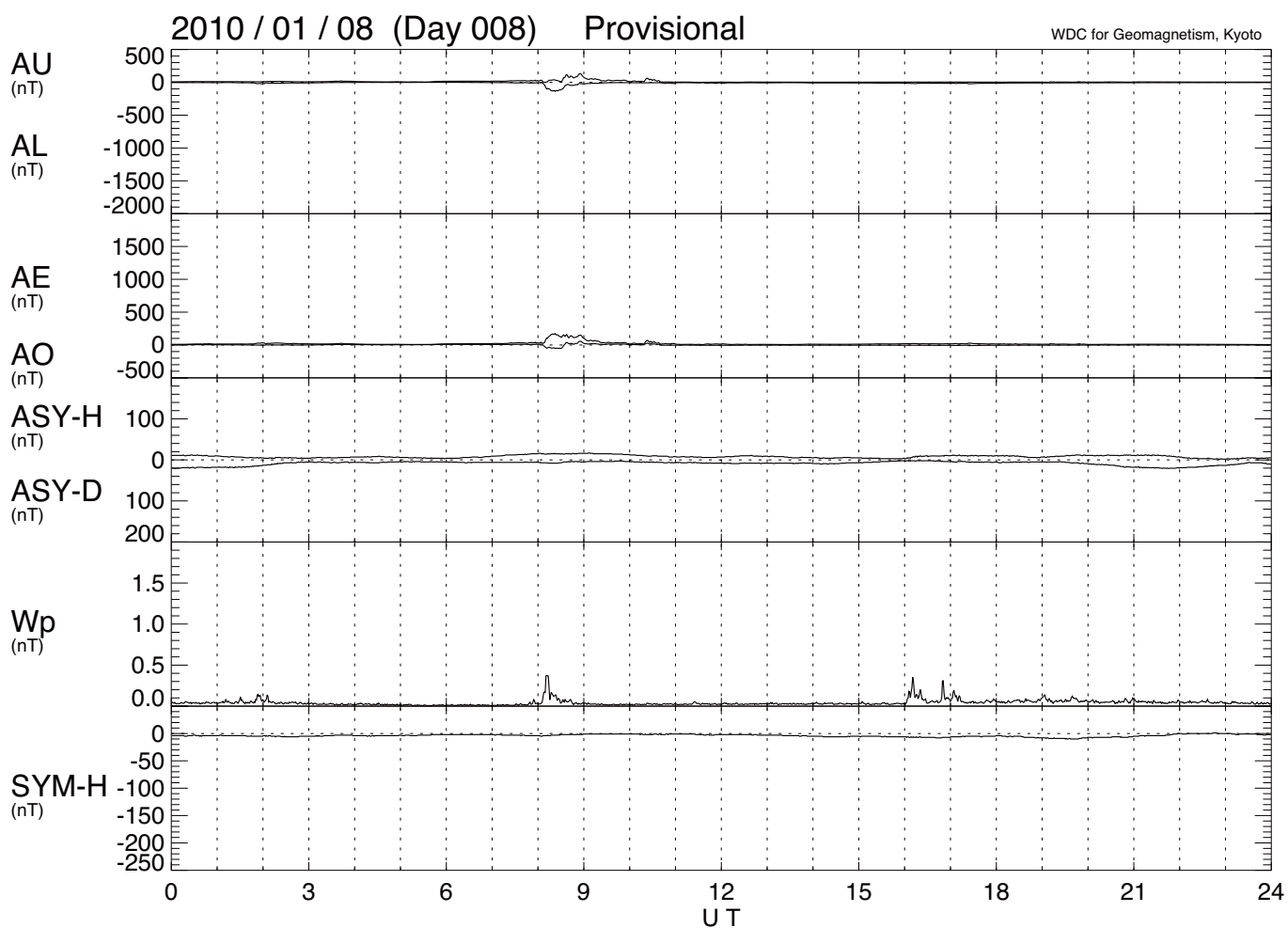
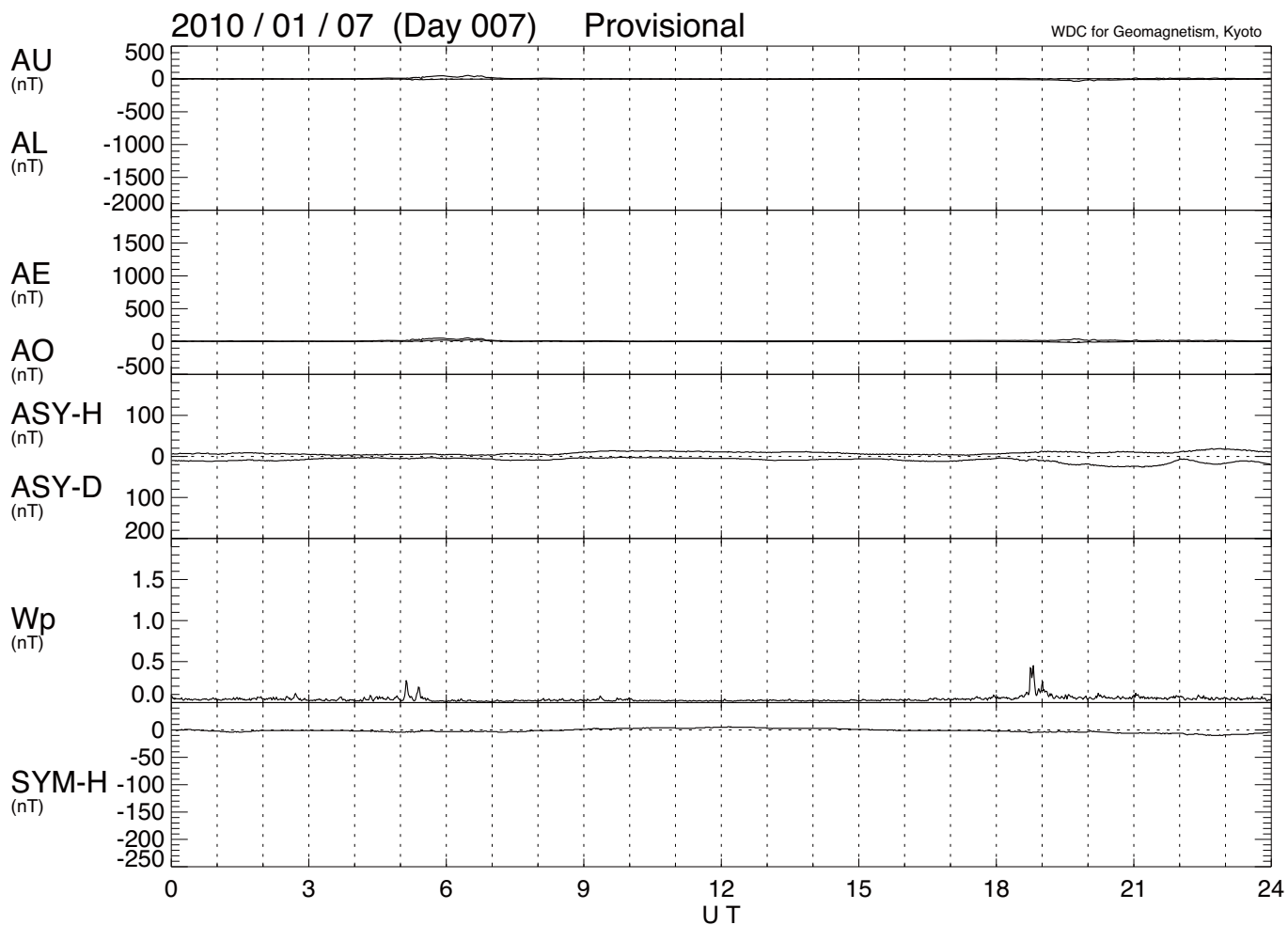
References

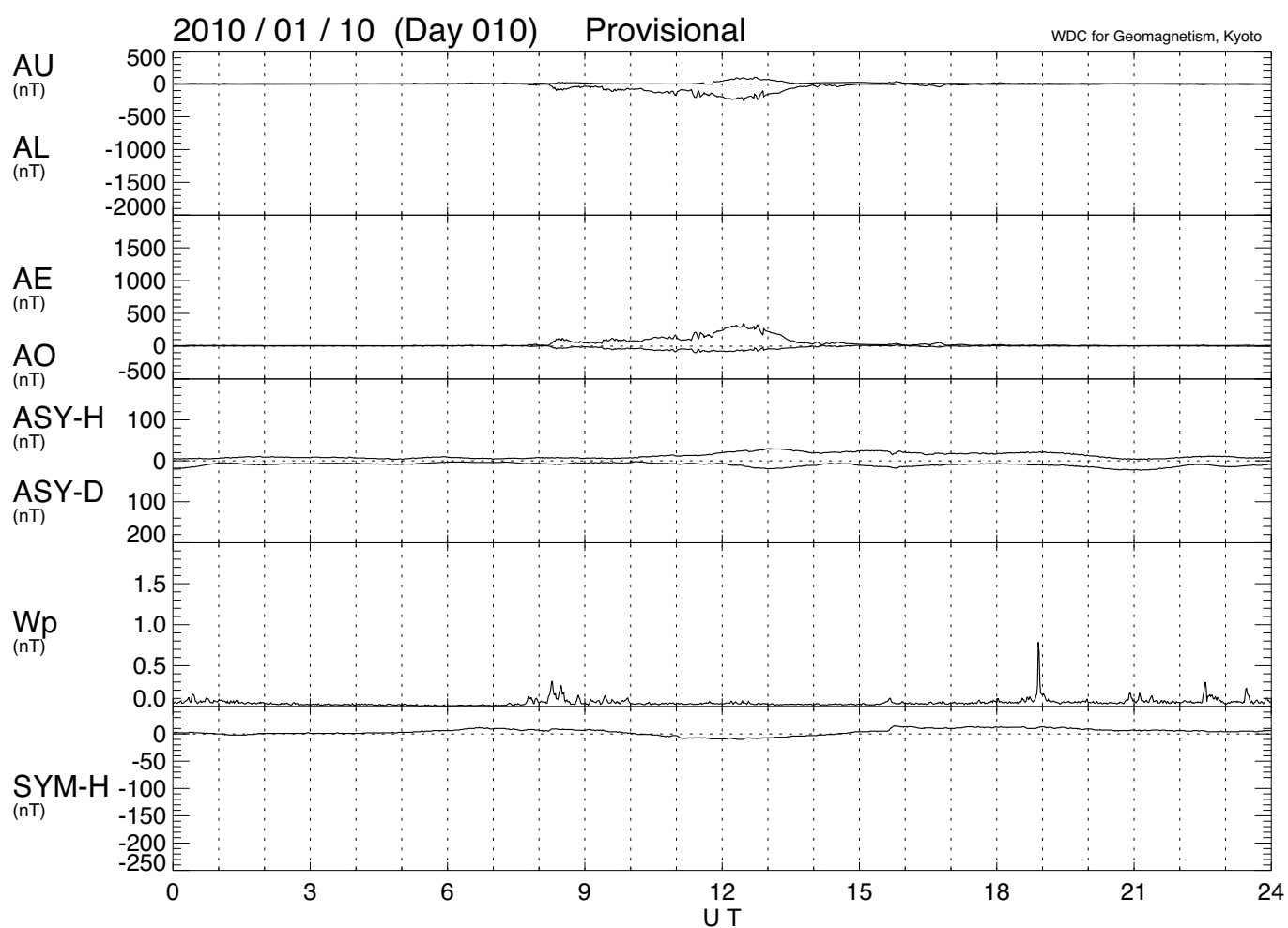
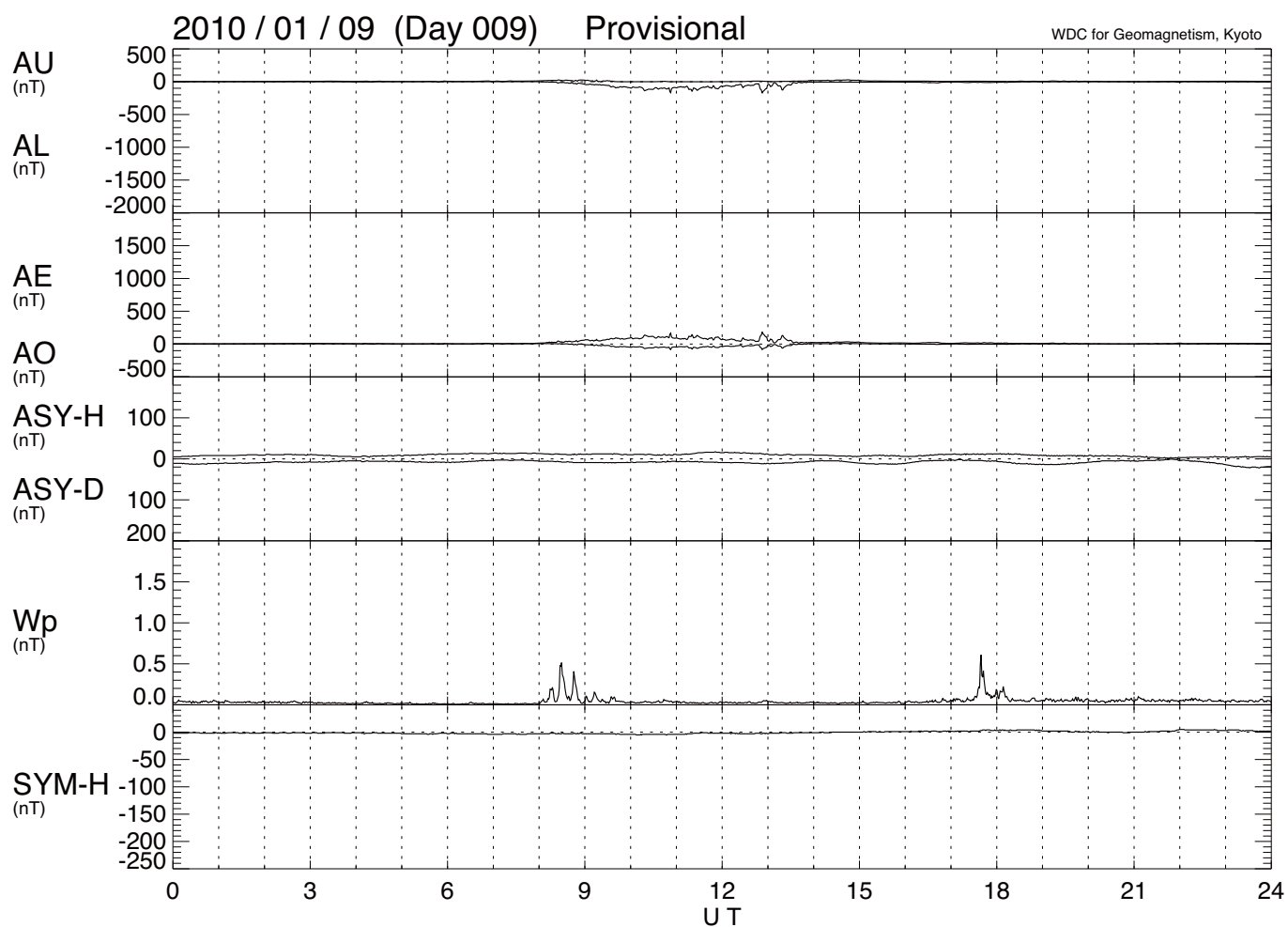
- Clauer, C. R. and R. L. McPherron, The relative importance of the interplanetary electric field and magnetospheric substorms on the partial ring current development, *J. Geophys. Res.*, *85*, 6747-6759, 1980.
- Clauer, C. R., R. L. McPherron, and C. Searls, Solar wind control of the low- latitude asymmetric magnetic disturbance field, *J. Geophys. Res.*, *88*, 2123-2130, 1983.
- Crooker, N. C. and G. L. Siscoe, A study of the geomagnetic disturbance field asymmetry, *Radio Sci.*, *6*, 495-501, 1971.
- Crooker, N. C., High-time resolution of the low-latitude asymmetric disturbance in the geomagnetic field, *J. Geophys. Res.*, *77*, 773-775, 1972.
- Davis, T. N., and M. Sugiura, Auroral electrojet activity index AE and its universal time variations, *J. Geophys. Res.*, *71*, 785-801, 1966.
- Gelpi, C., W. J. Hughes, and H. J. Singer, A comparison of magnetic signatures and DMSP auroral images at substorm onset - Three case studies, *J. Geophys. Res.*, *92*, 2447-2460, 1987.
- Iyemori, T., Storm-time magnetospheric currents inferred from mid-latitude geomagnetic field variations, *J. Geomag. Geoelectr.*, *42*, 1249-1265, 1990.
- Iyemori, T. and D. R. K. Rao, Decay of the Dst field of geomagnetic disturbance after substorm onset and its implication to storm-substorm relation, *Ann. Geophys.*, *14*, 608-618, 1996.
- Jacobs, J. A., Y. Kato, S. Matsushita, and V. A. Troitskaya, Classification of geomagnetic micropulsations, *J. Geophys. Res.*, *69*, 180-181, 1964.
- Kawasaki, K., and S.-I. Akasofu, Low-latitude DS component of geomagnetic storm field, *J. Geophys. Res.*, *76*, 2396-2405, 1971.
- Saito, T., K. Yumoto, and Y. Koyama, Magnetic pulsation Pi2 as a sensitive indicator of magnetospheric substorm, *Planet. Space Sci.*, *24*, 1025-1029, 1976a.
- Saito, T., T. Sakurai, and Y. Koyama, Mechanism of association between Pi2 pulsation and magnetospheric substorm, *J. Atmos. Sol. Terr. Phys.*, *38*, 1265-1277, 1976b.
- Saka, O., O. Watanabe, M. Shinohara, H. Tachihara, and D. N. Baker, A comparison of the occurrence of very-low-latitude Pi2 pulsations with magnetic-field and energetic-particle flux variations (30-300 keV) at geosynchronous altitudes, *J. Geomag. Geoelectr.*, *48*, 1431-1441, 1996.
- Sakurai, T., and T. Saito, Magnetic pulsations Pi2 and substorm onset, *Planet. Space Sci.*, *24*, 573-575, 1976.
- Sugiura, M., and D. J. Poros, Hourly values of equatorial Dst for years 1957 to 1970, *Rep. X-645-71-278*, Goddard Space Flight Center, Greenbelt, Maryland, 1971.
- Yumoto, K., T. Saito, K. Takahashi, F. W. Menk, B. J. Fraser, T. A. Potemra, and L. J. Zanetti, Some aspects of the relation between Pi1-2 magnetic pulsations observed at L=1.3-2.1 on the ground and substorm-associated magnetic field variations in the near earth magnetotail observed by AMPTE CCE, *J. Geophys. Res.*, *94*, 3611-3618, 1989.

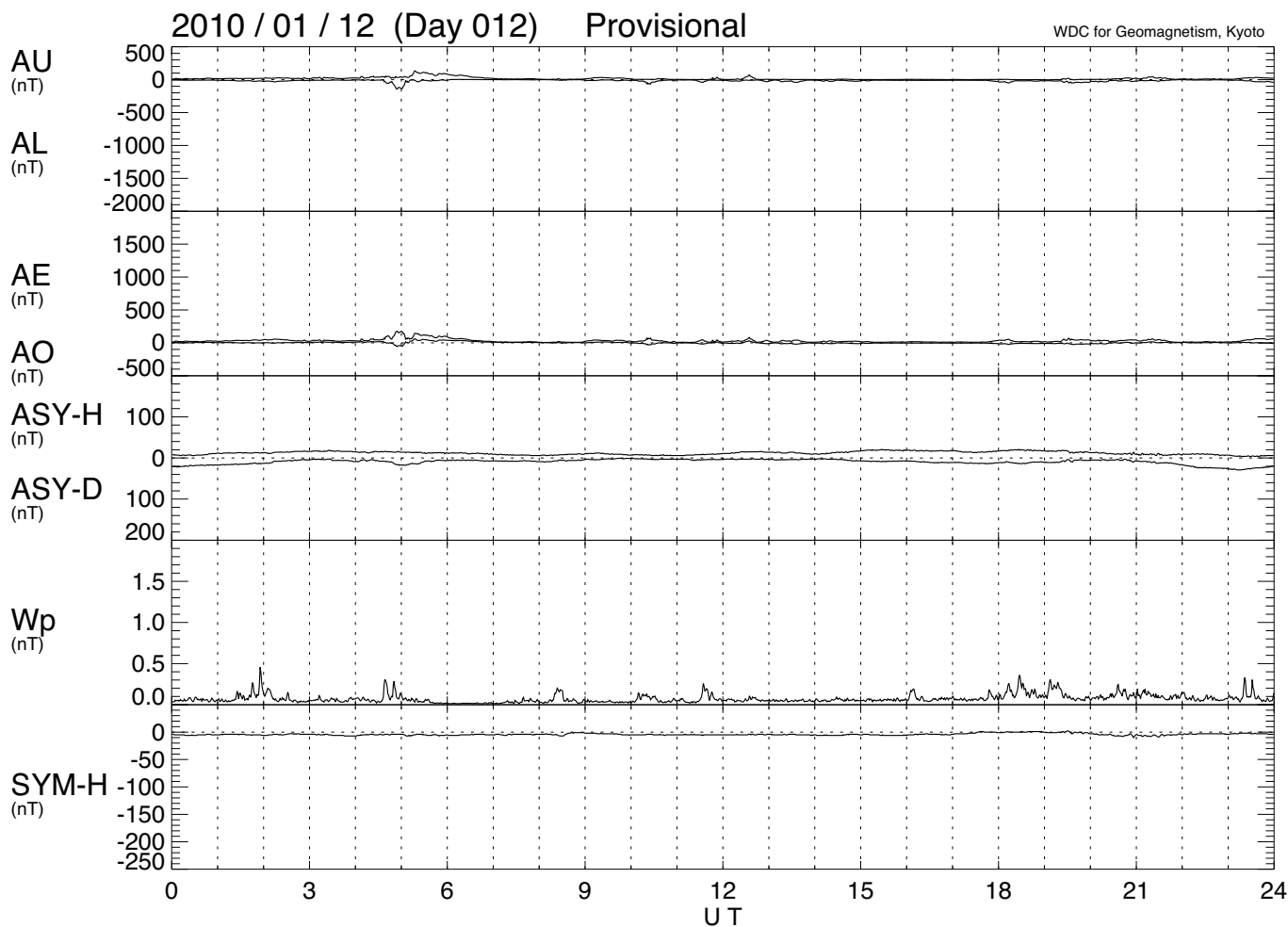
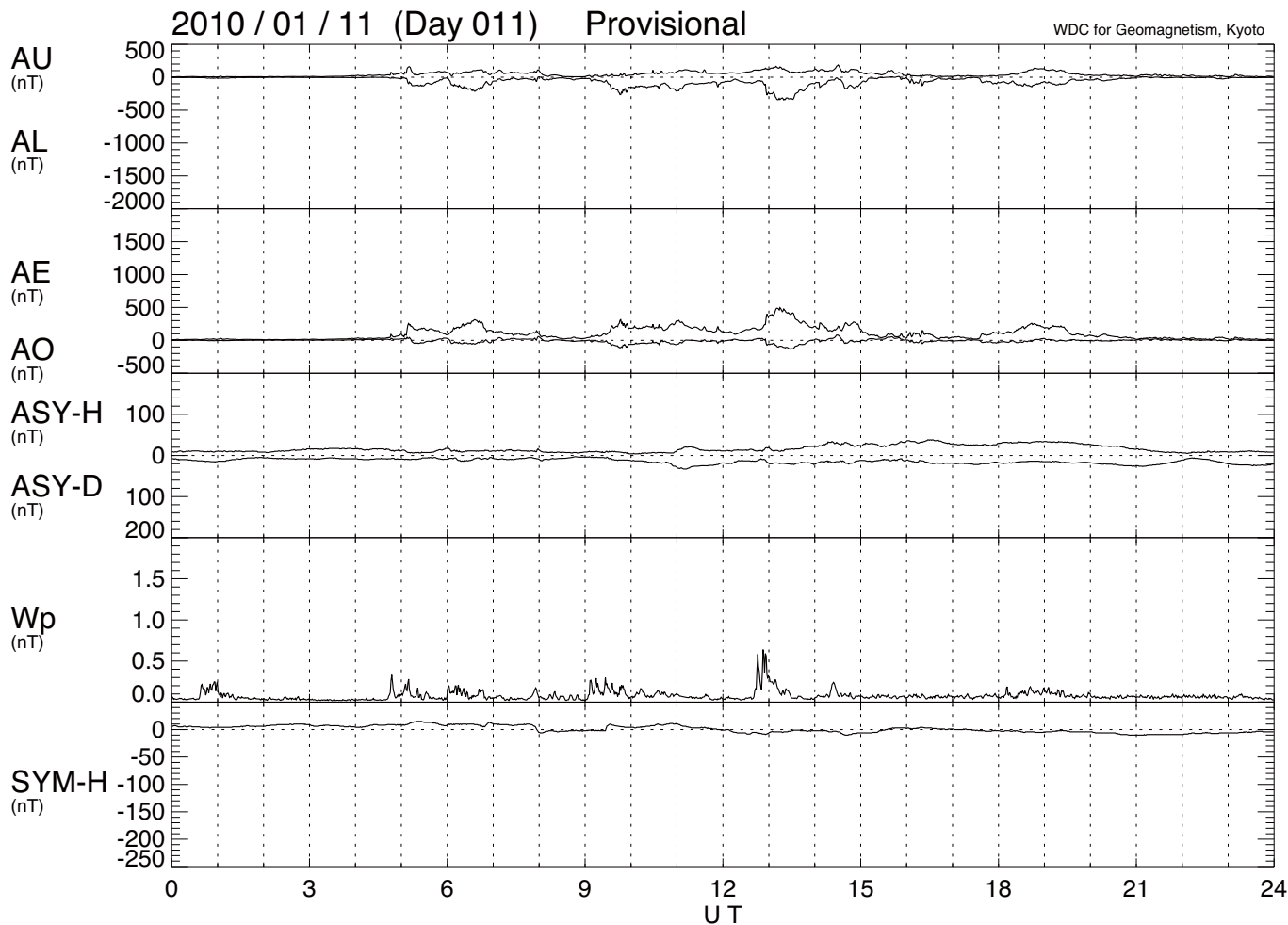


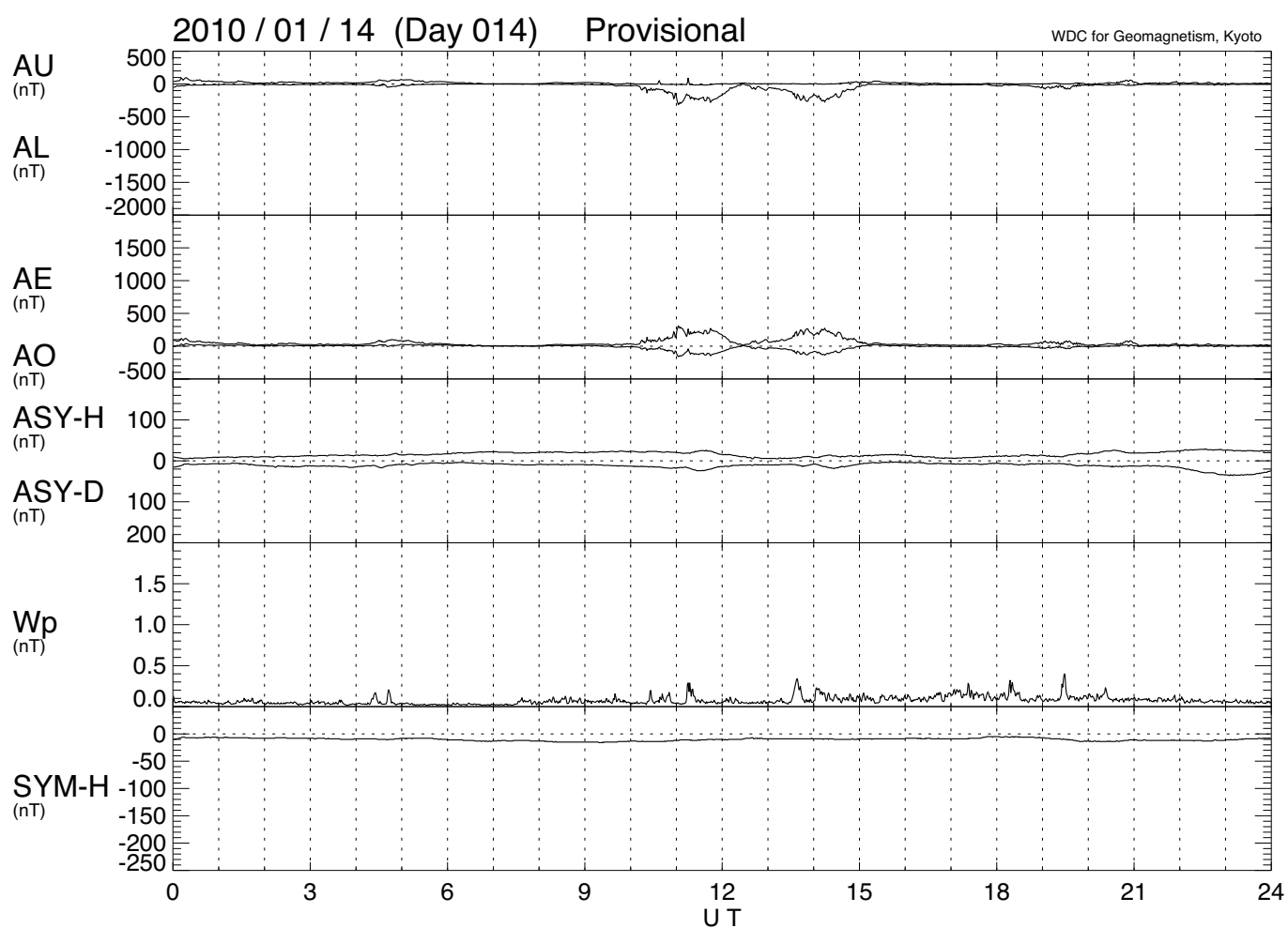
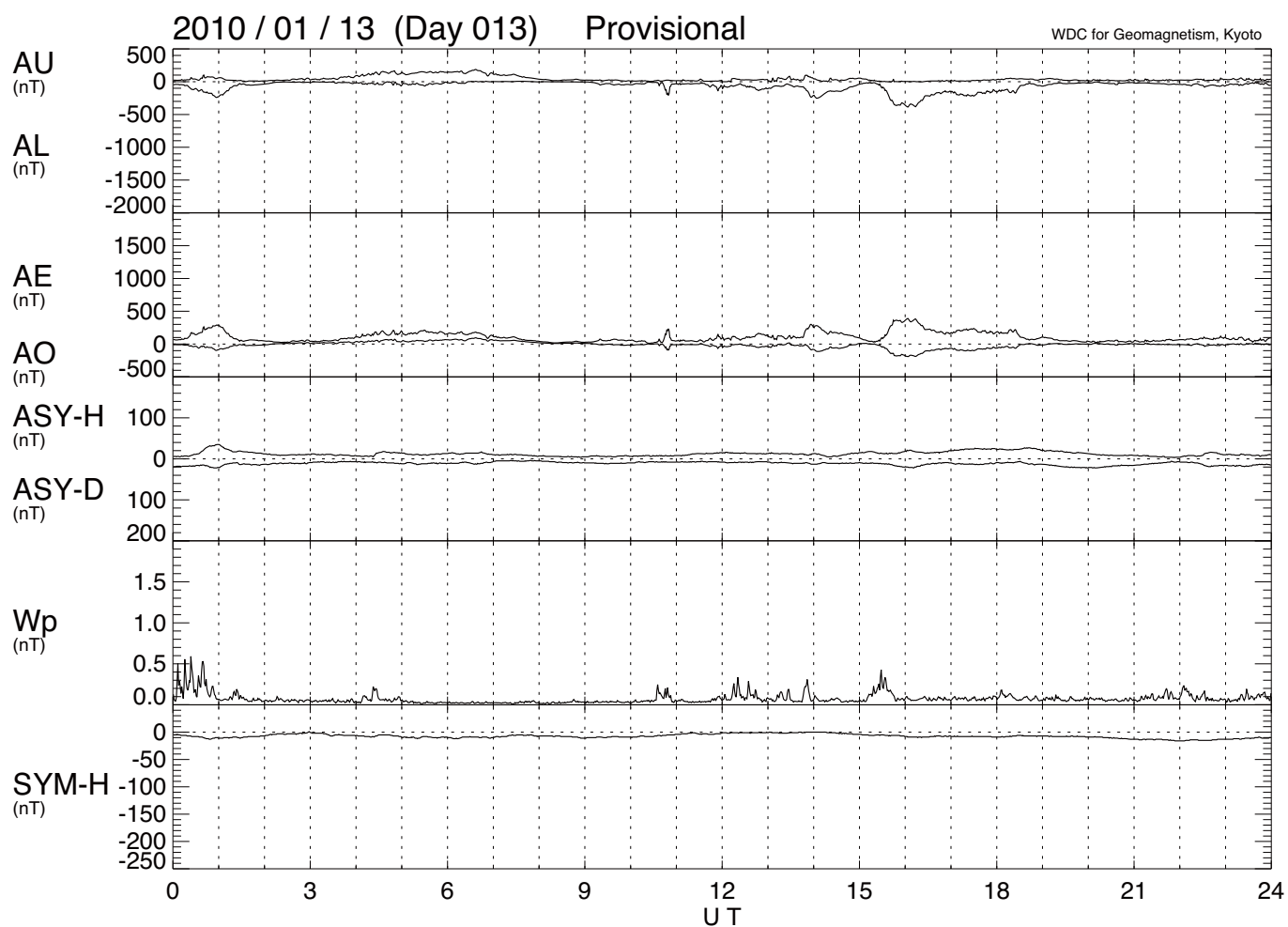


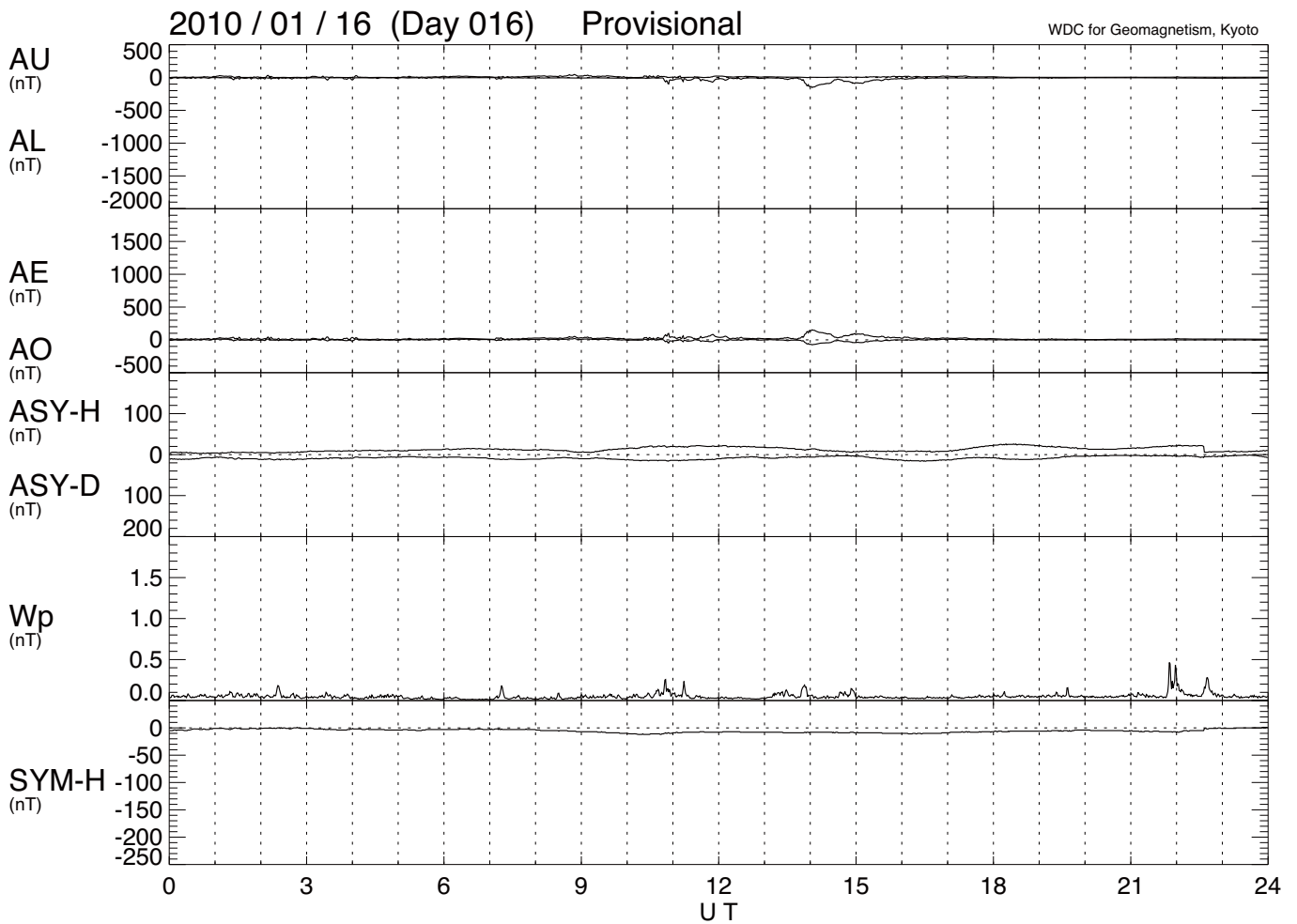
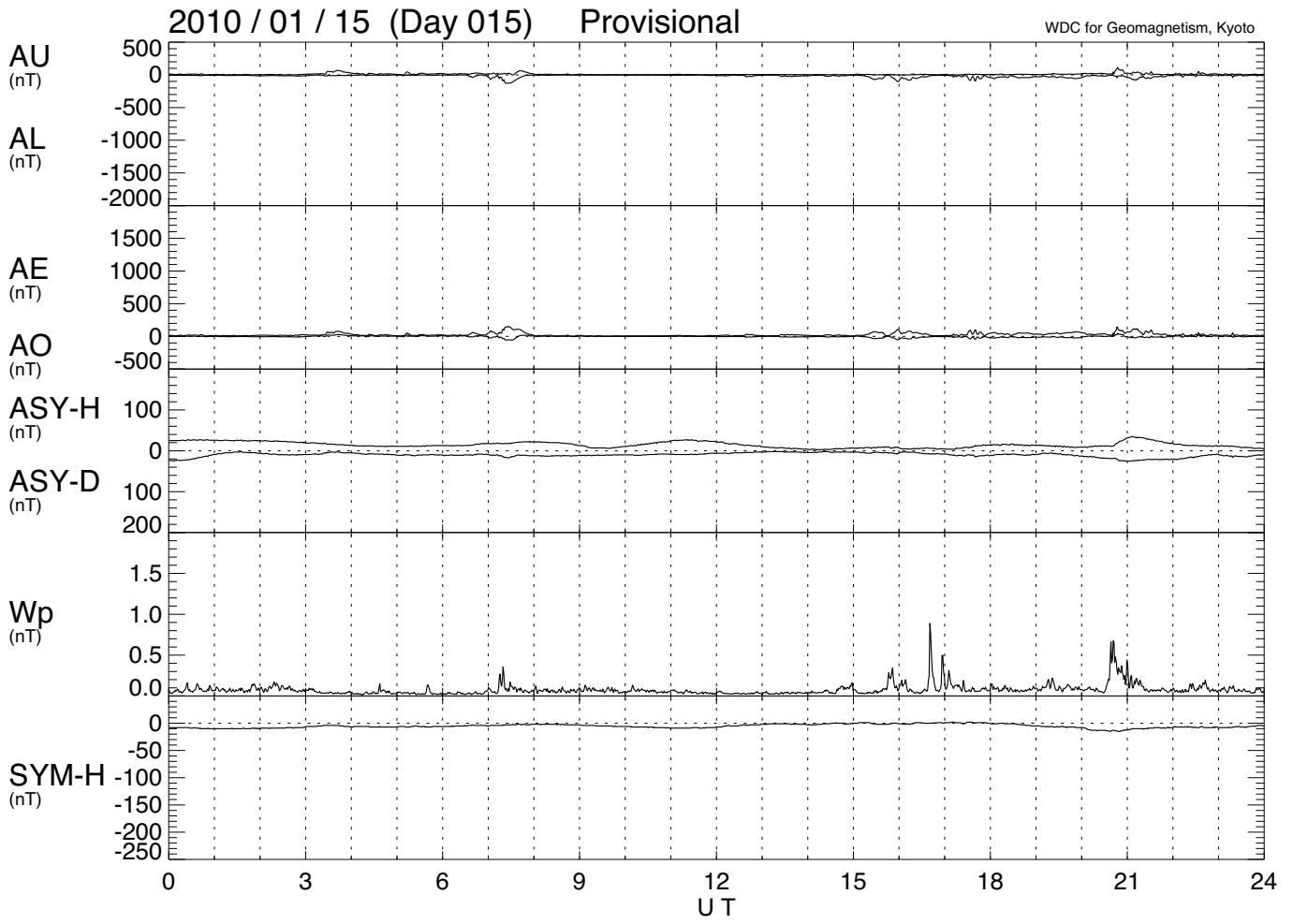


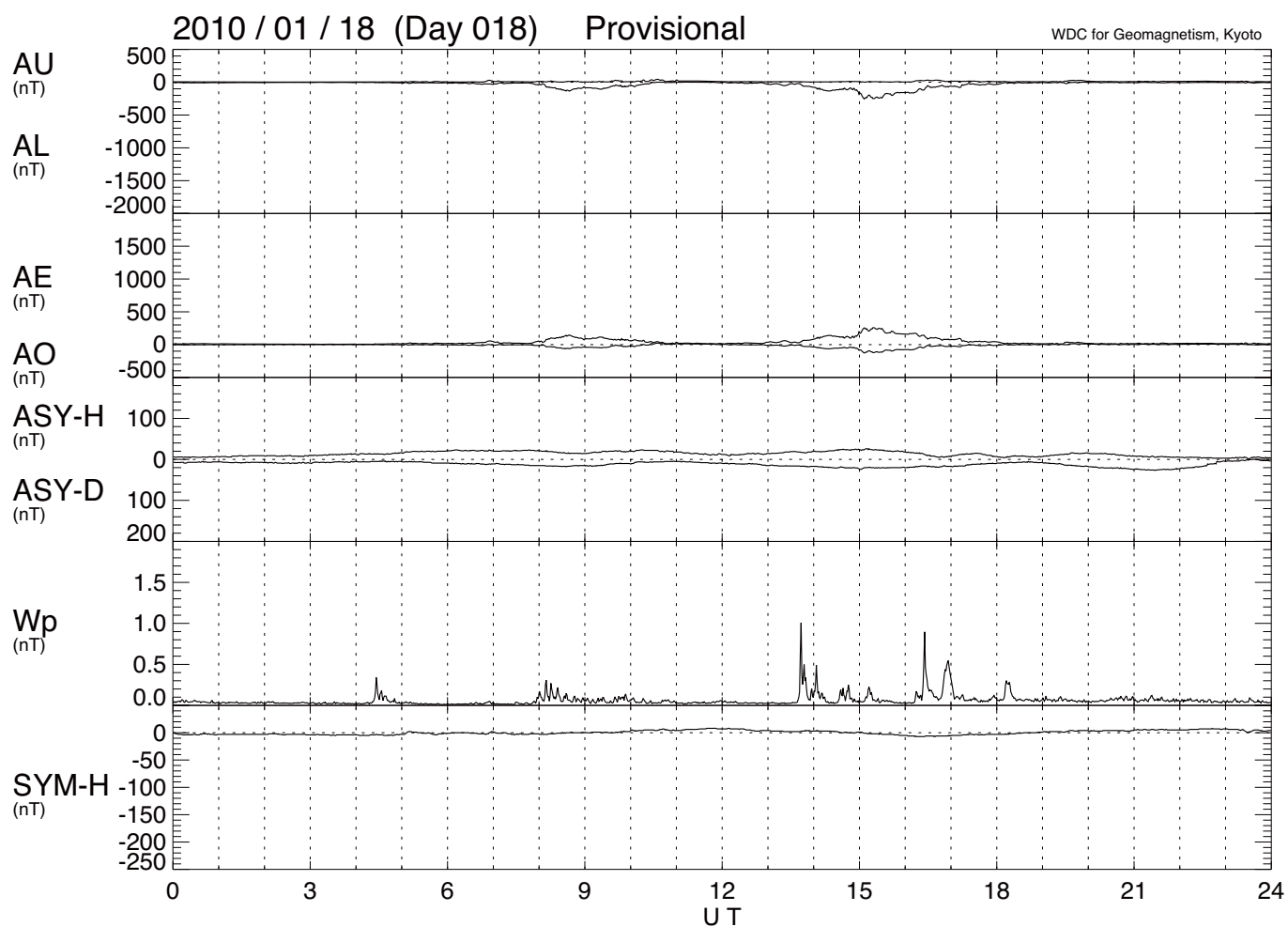
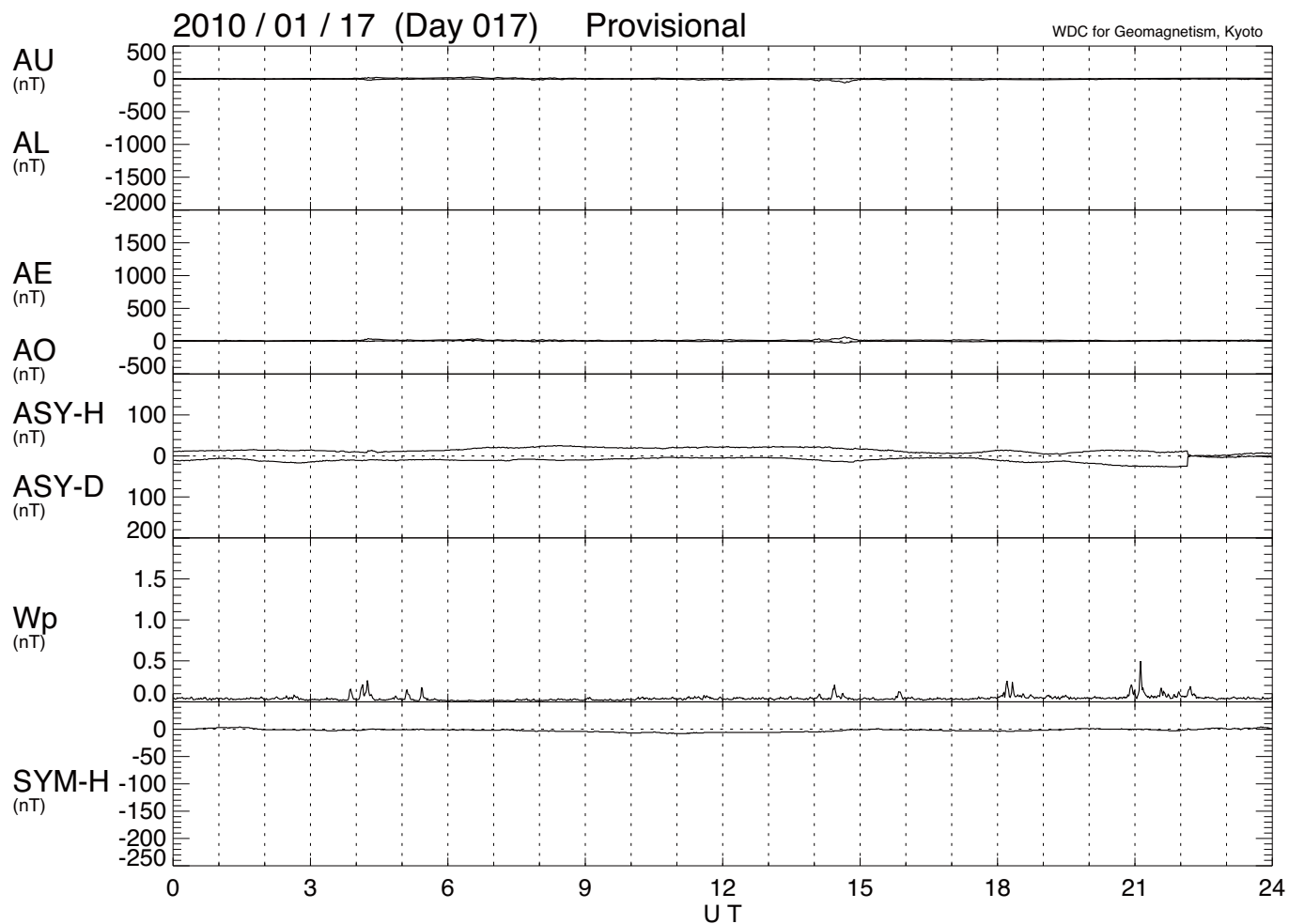


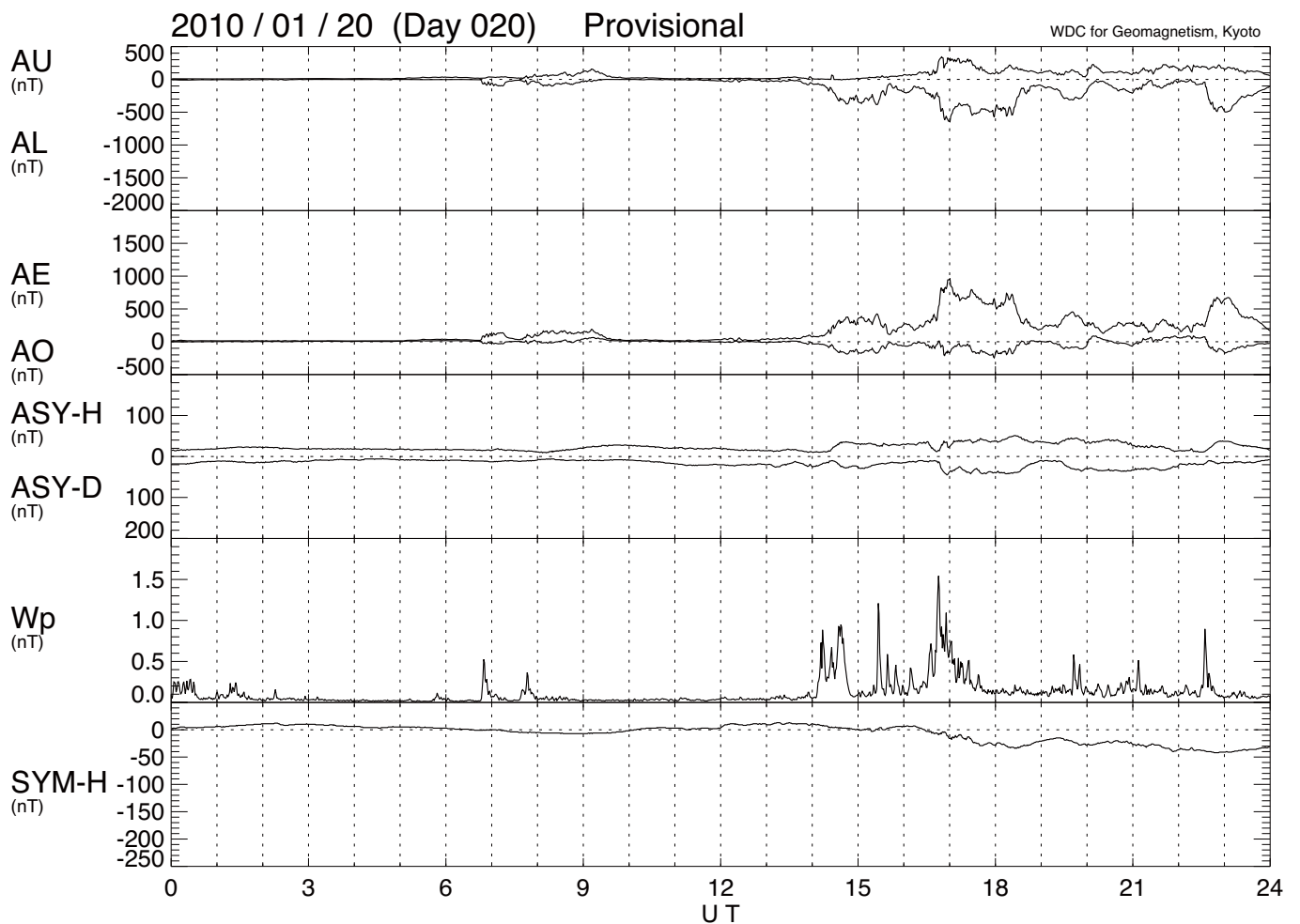
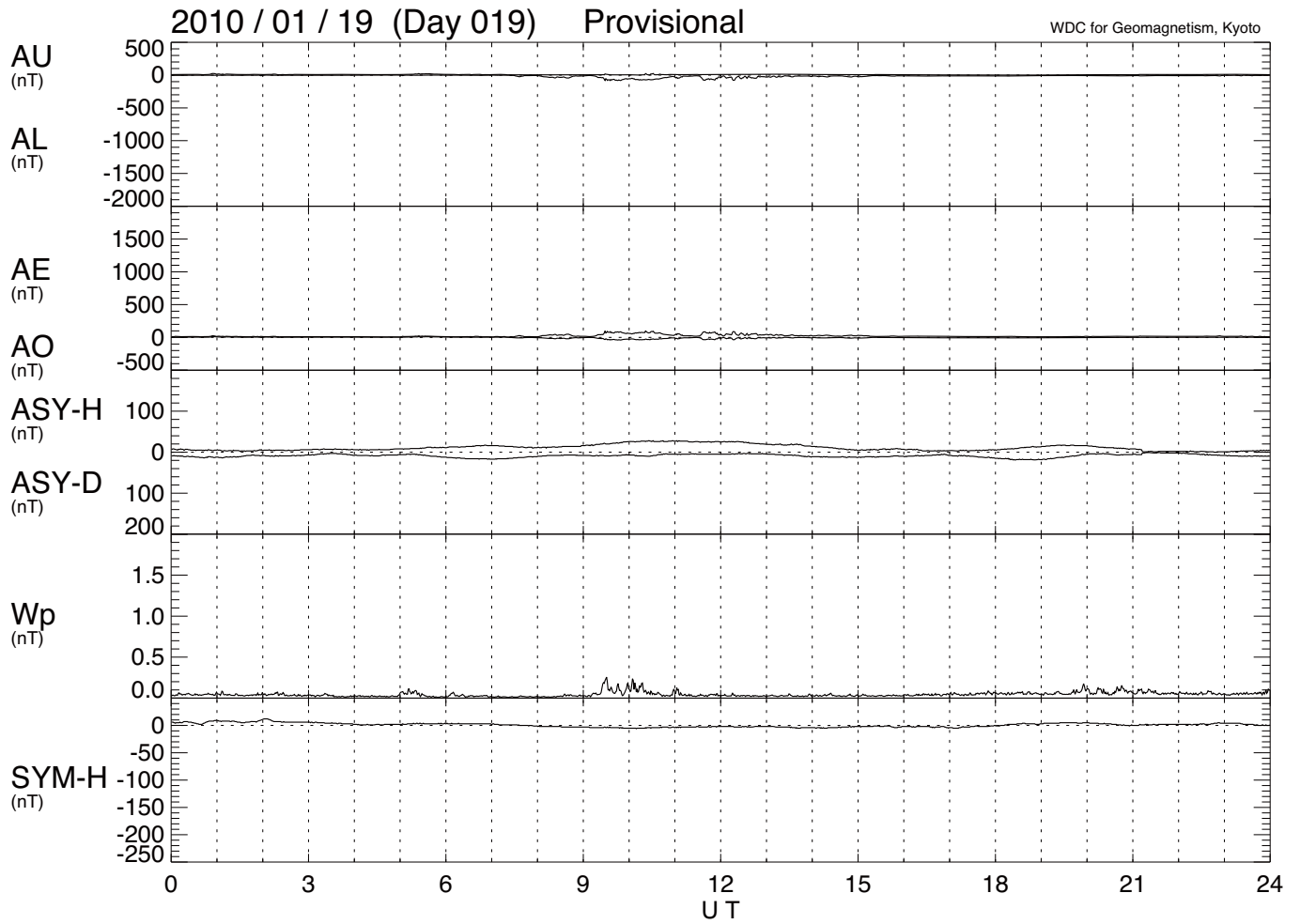


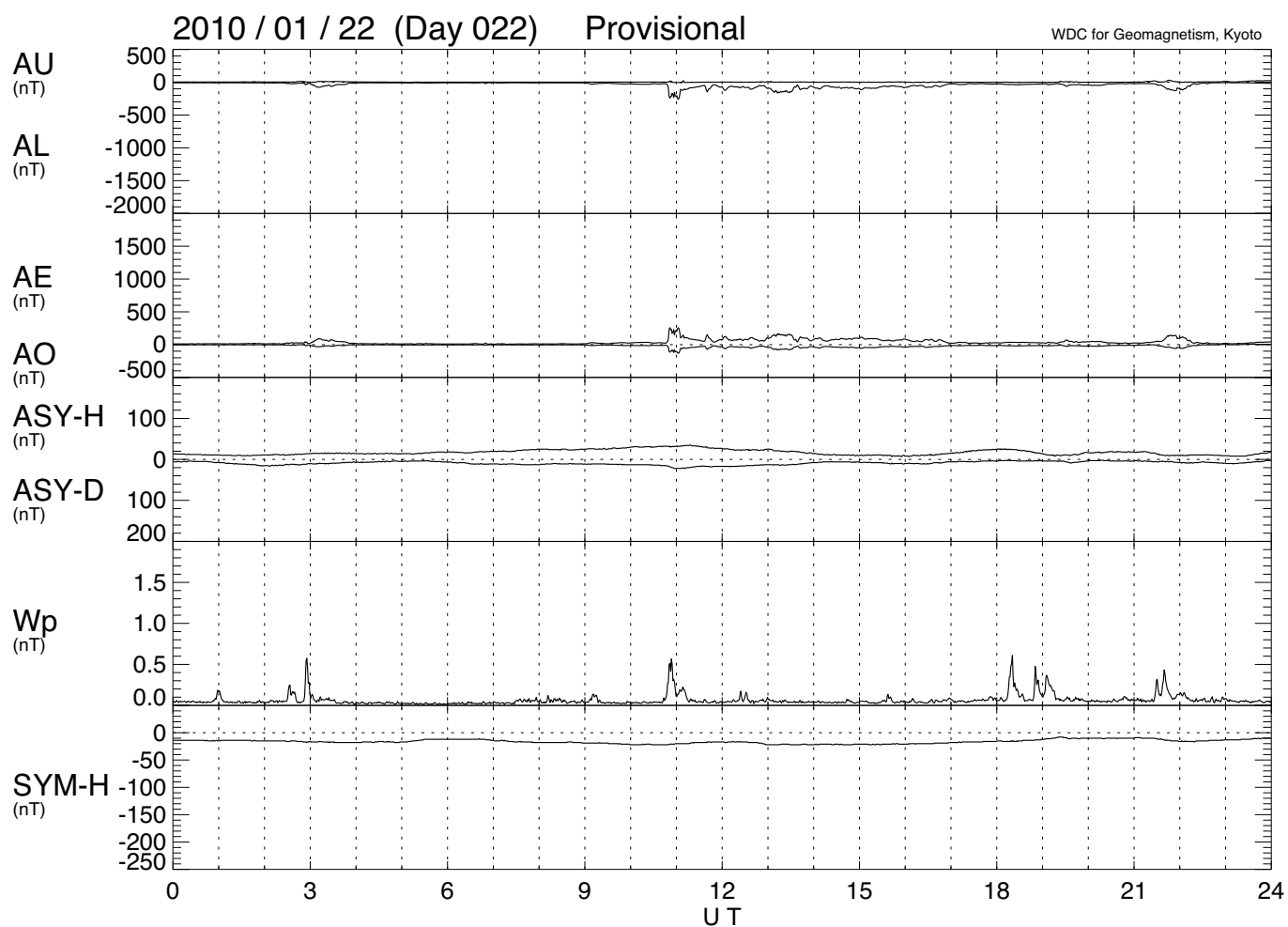
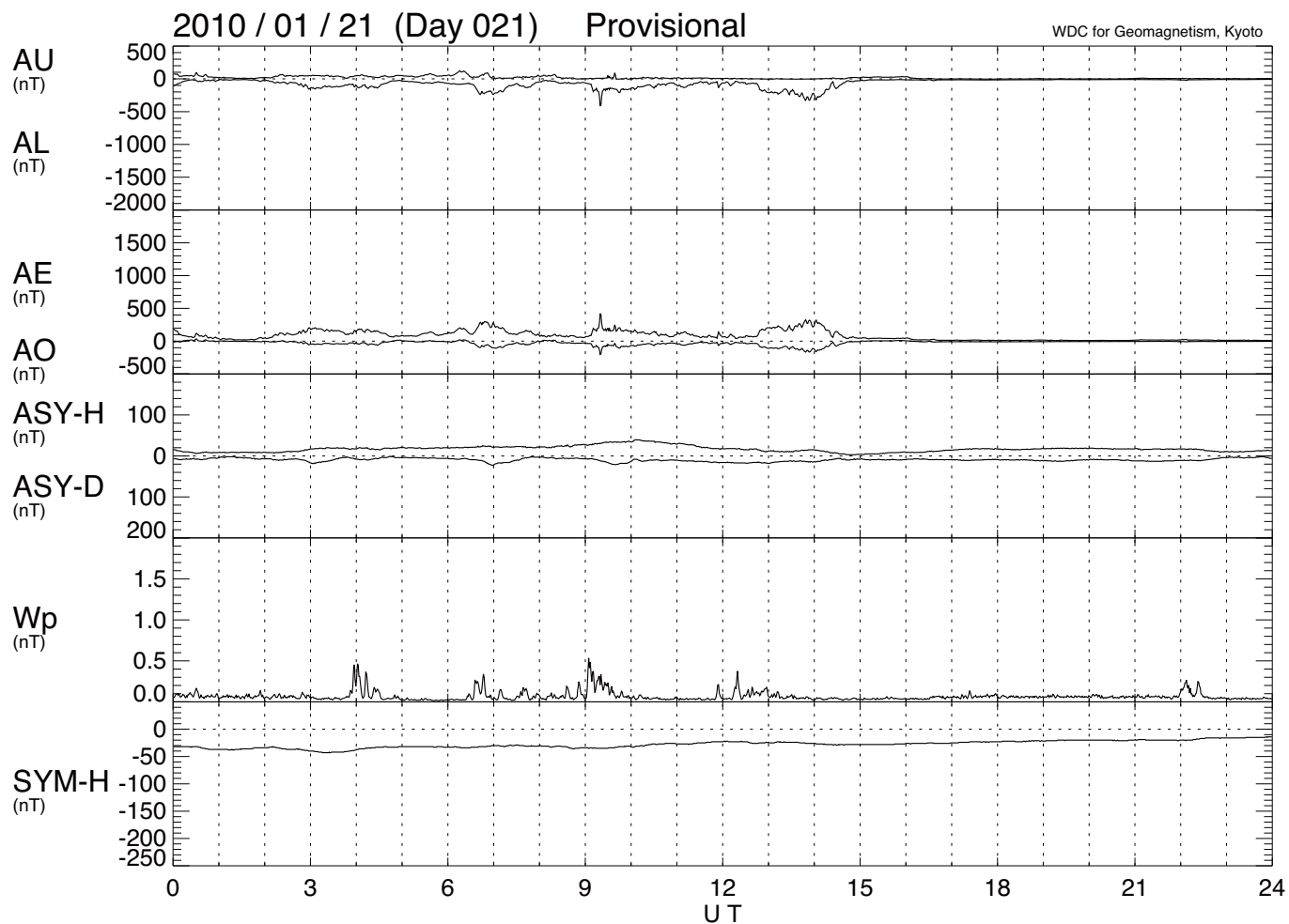


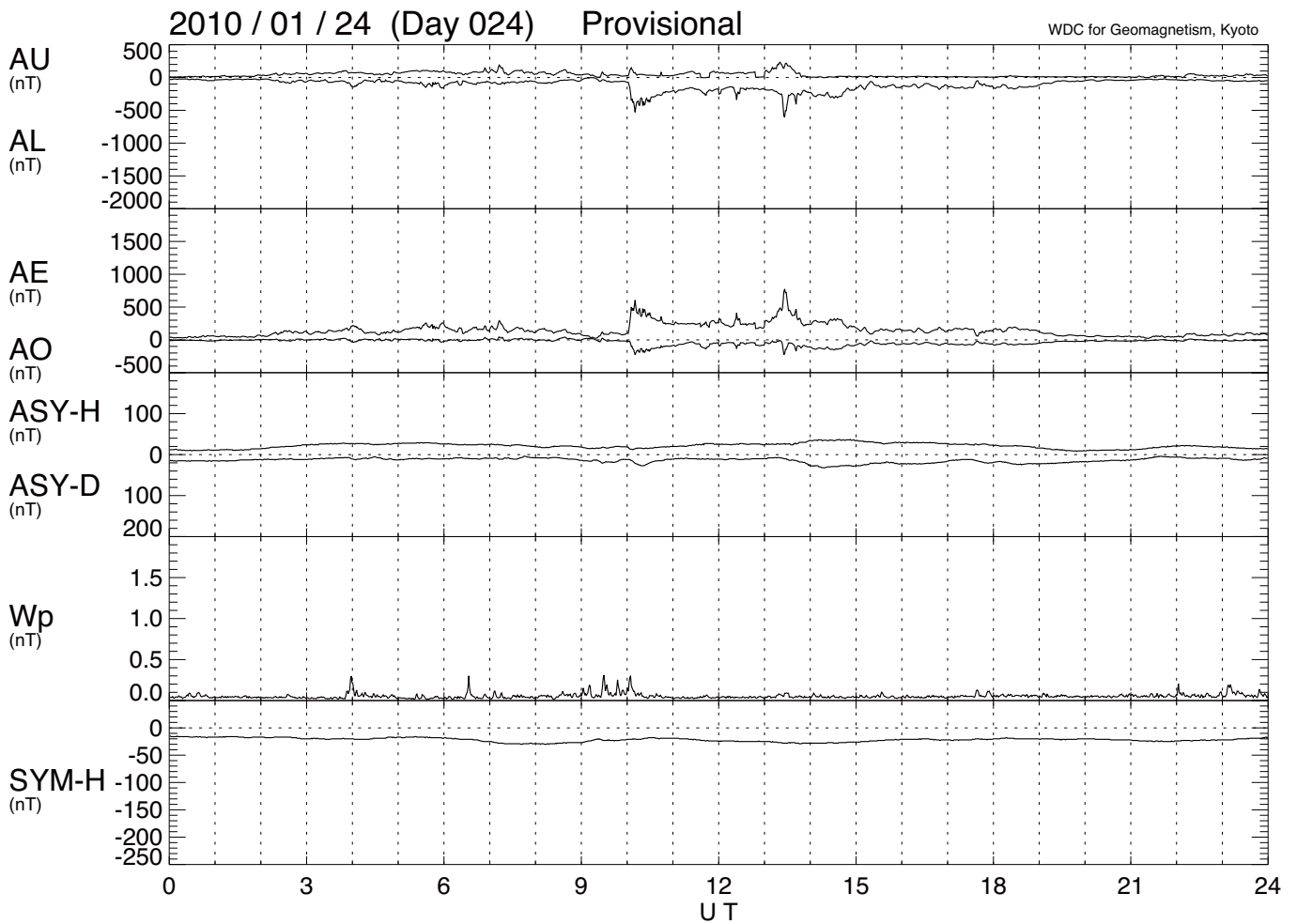
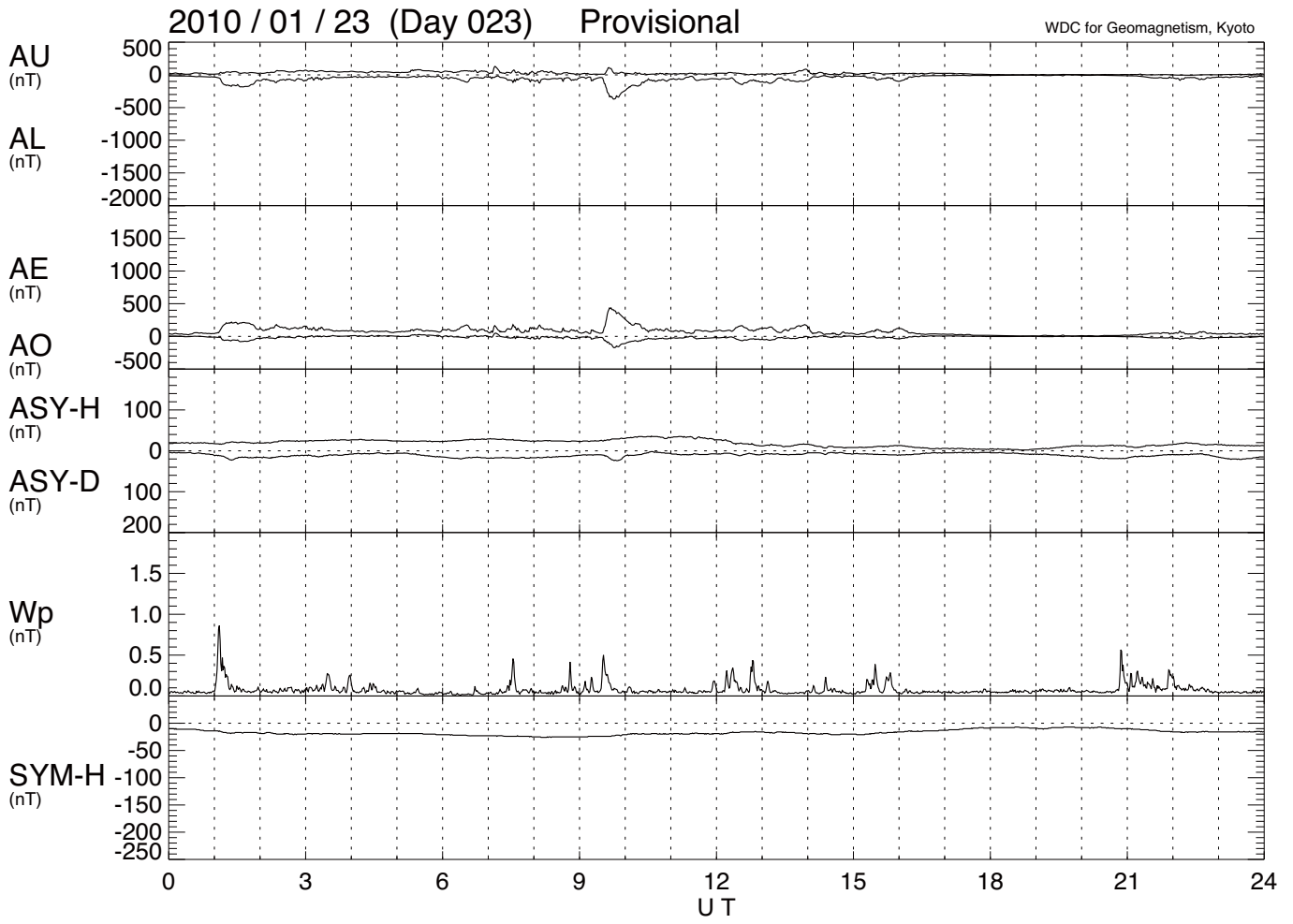


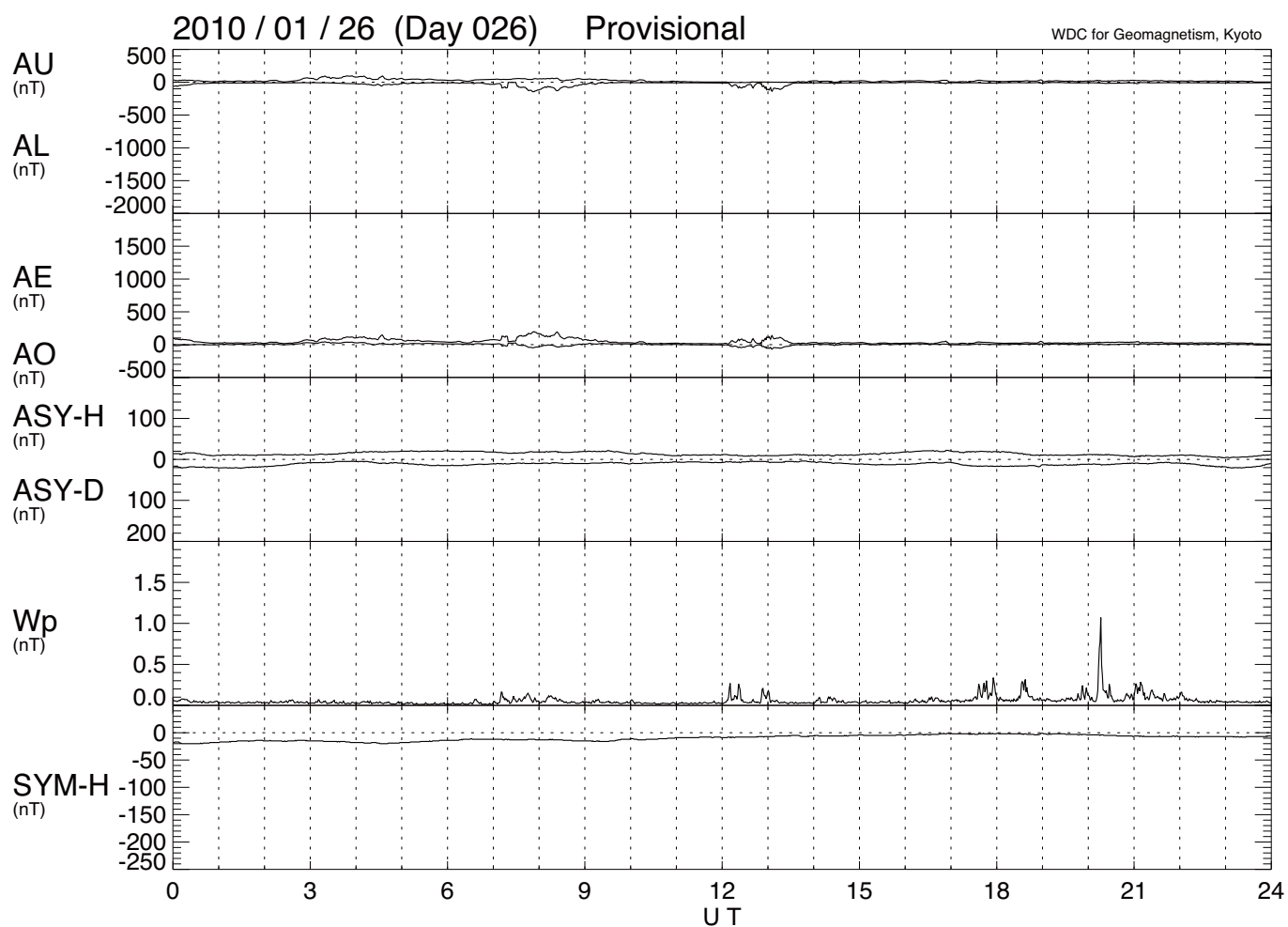
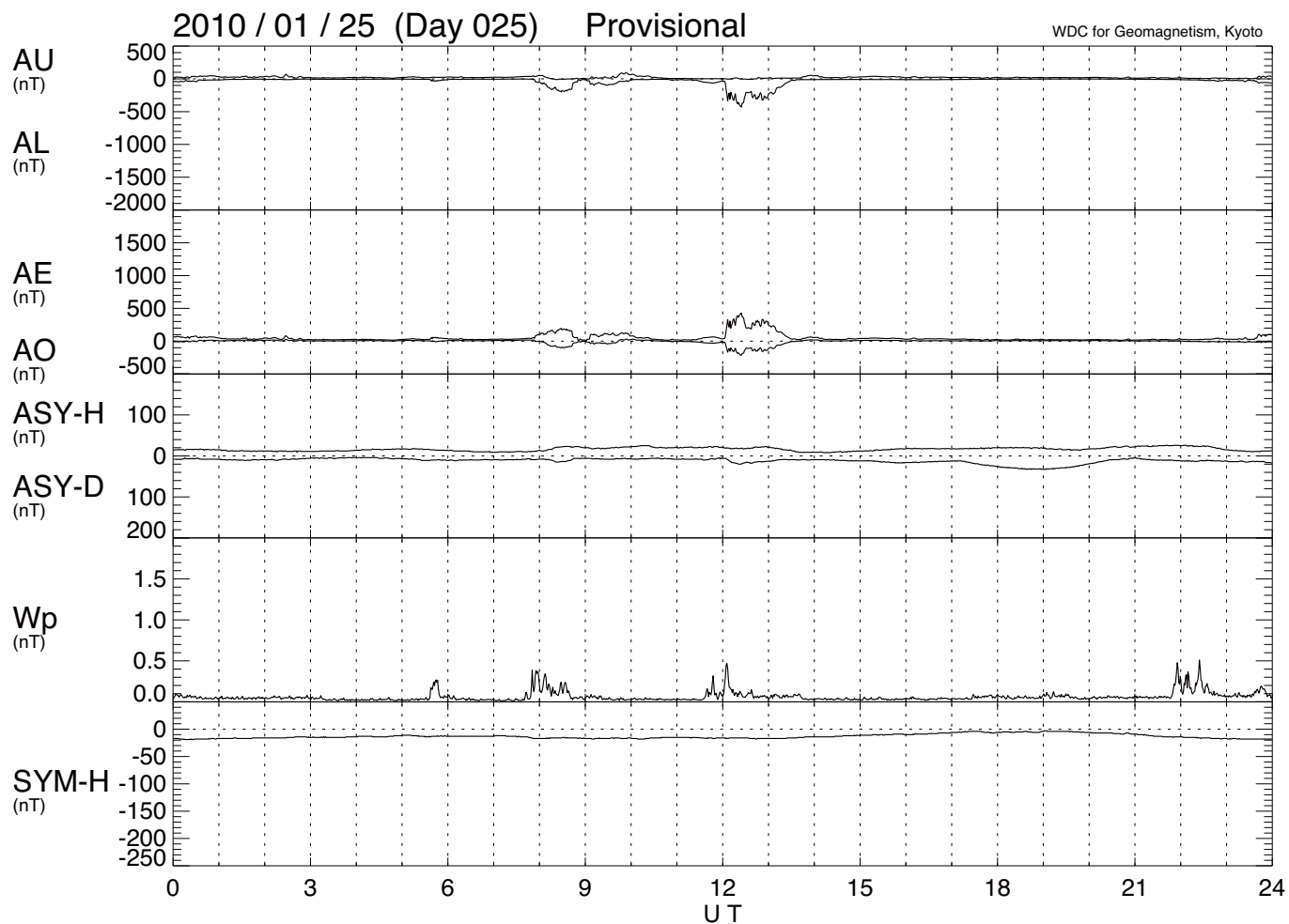


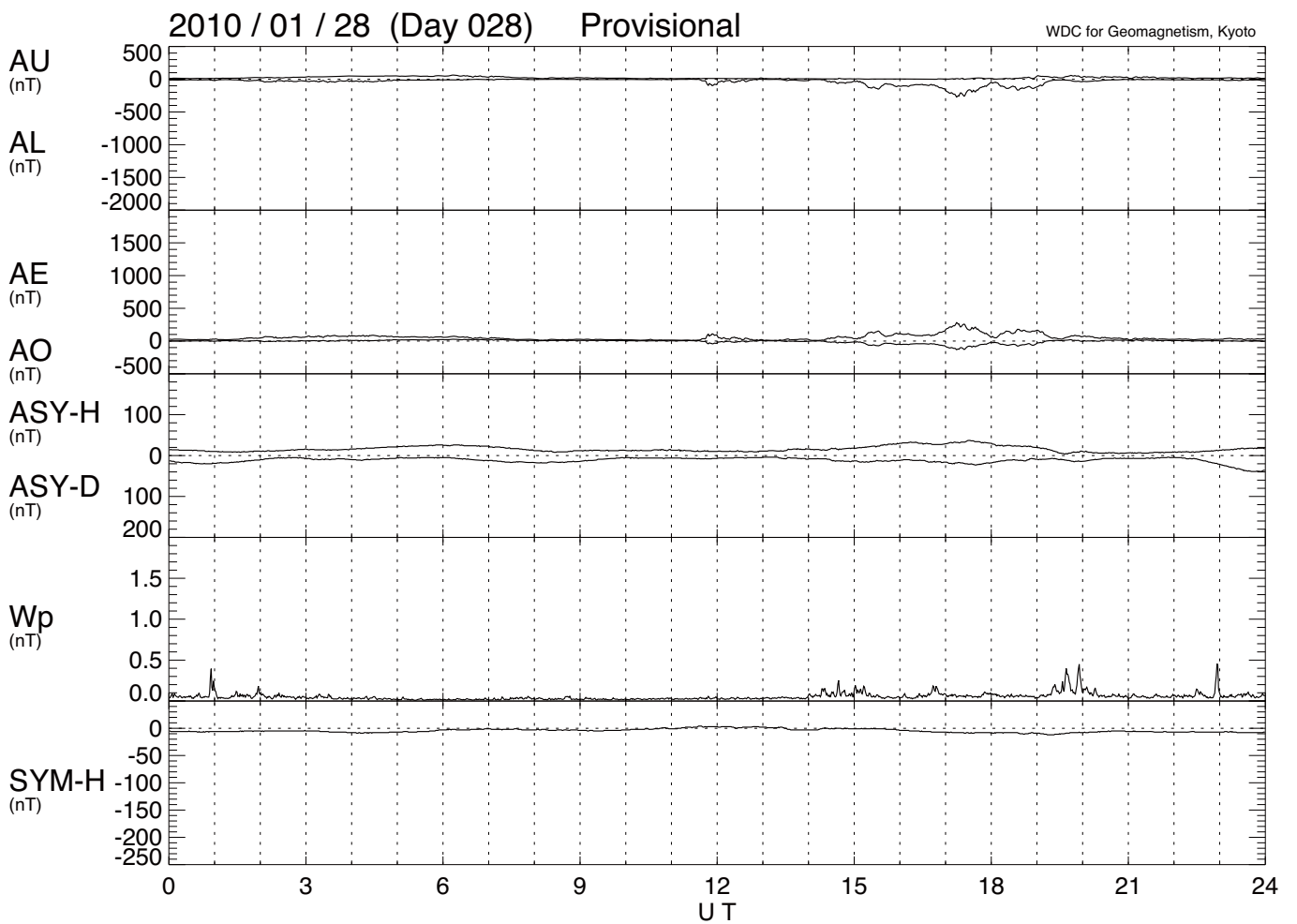
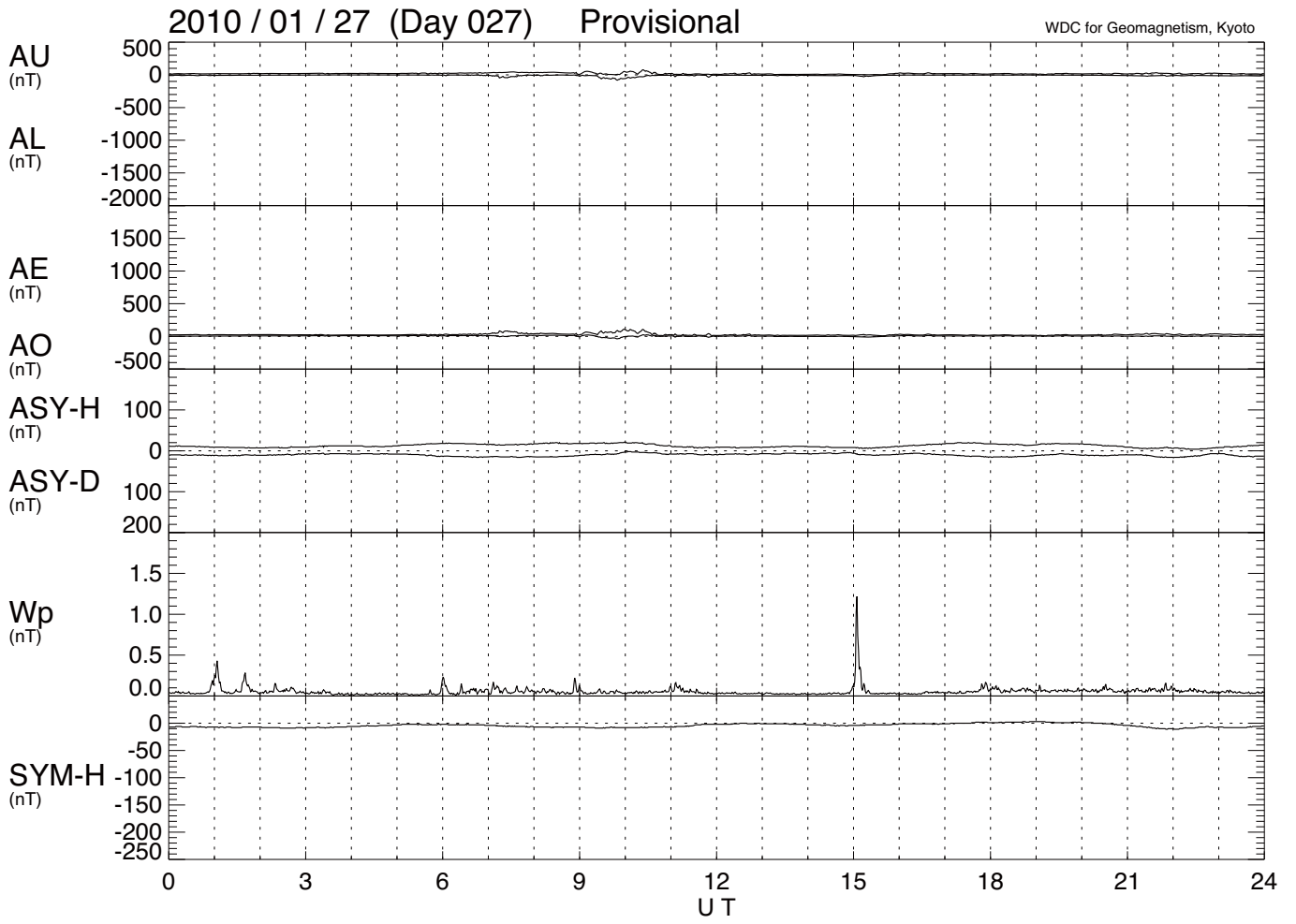


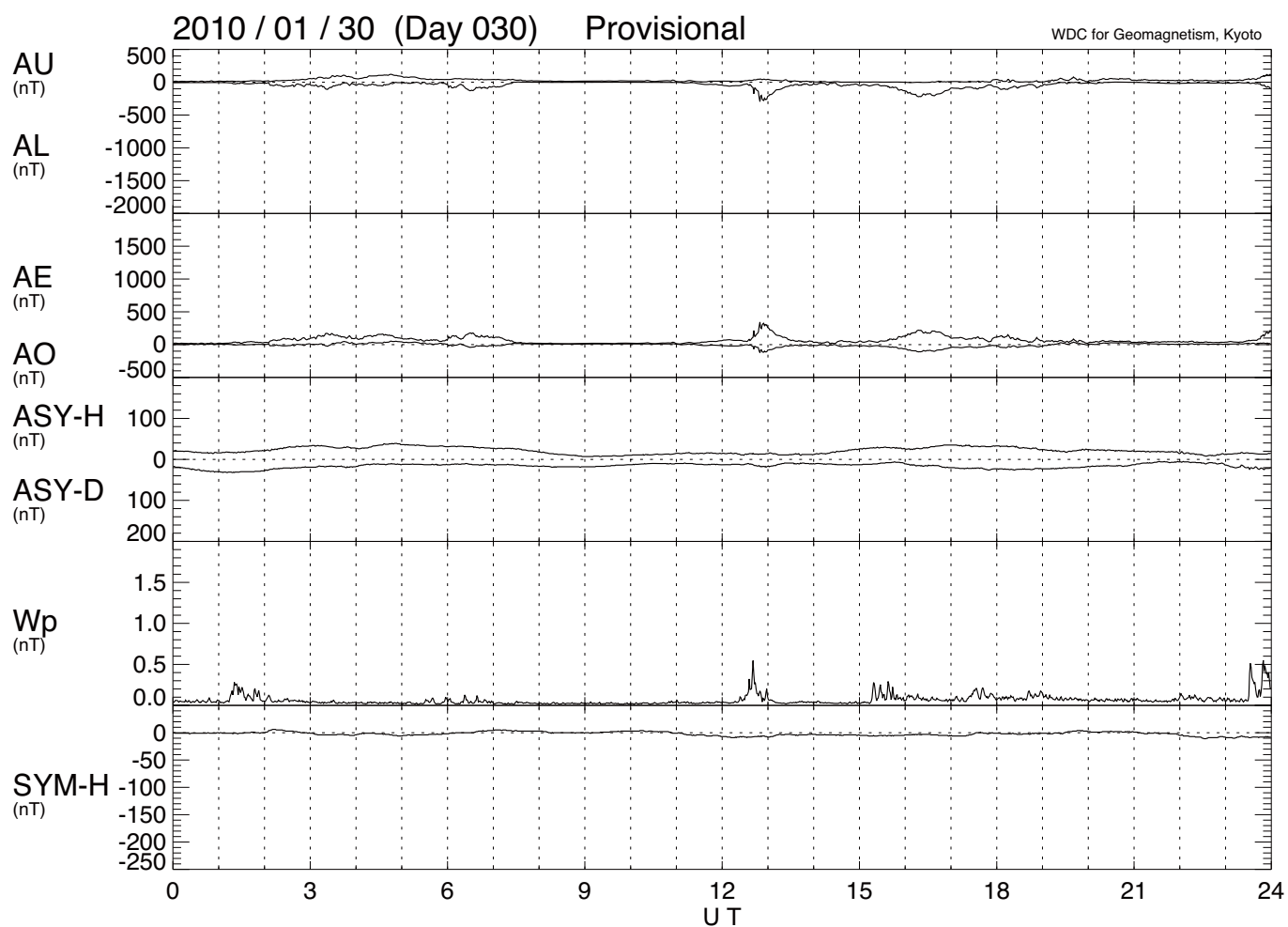
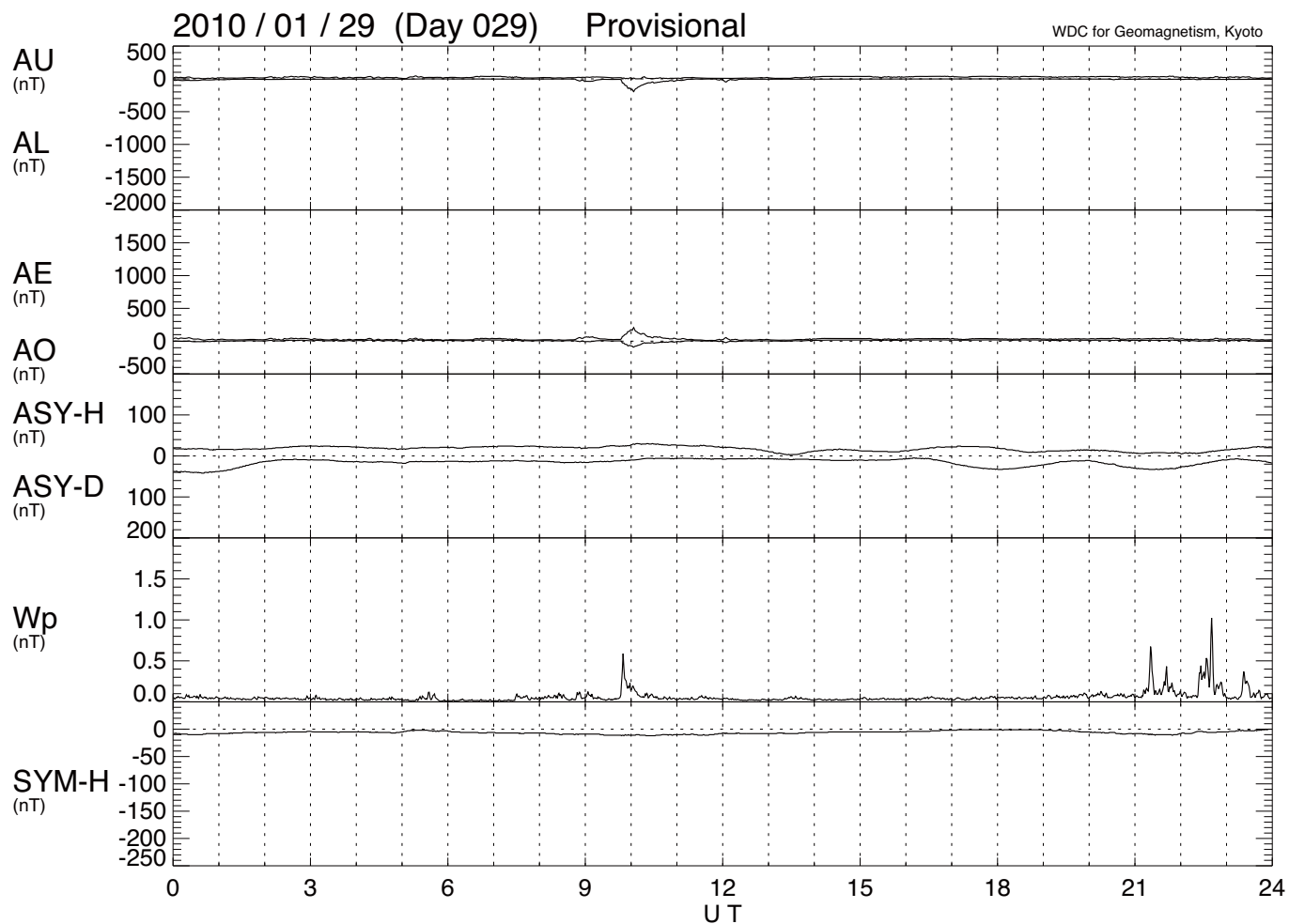


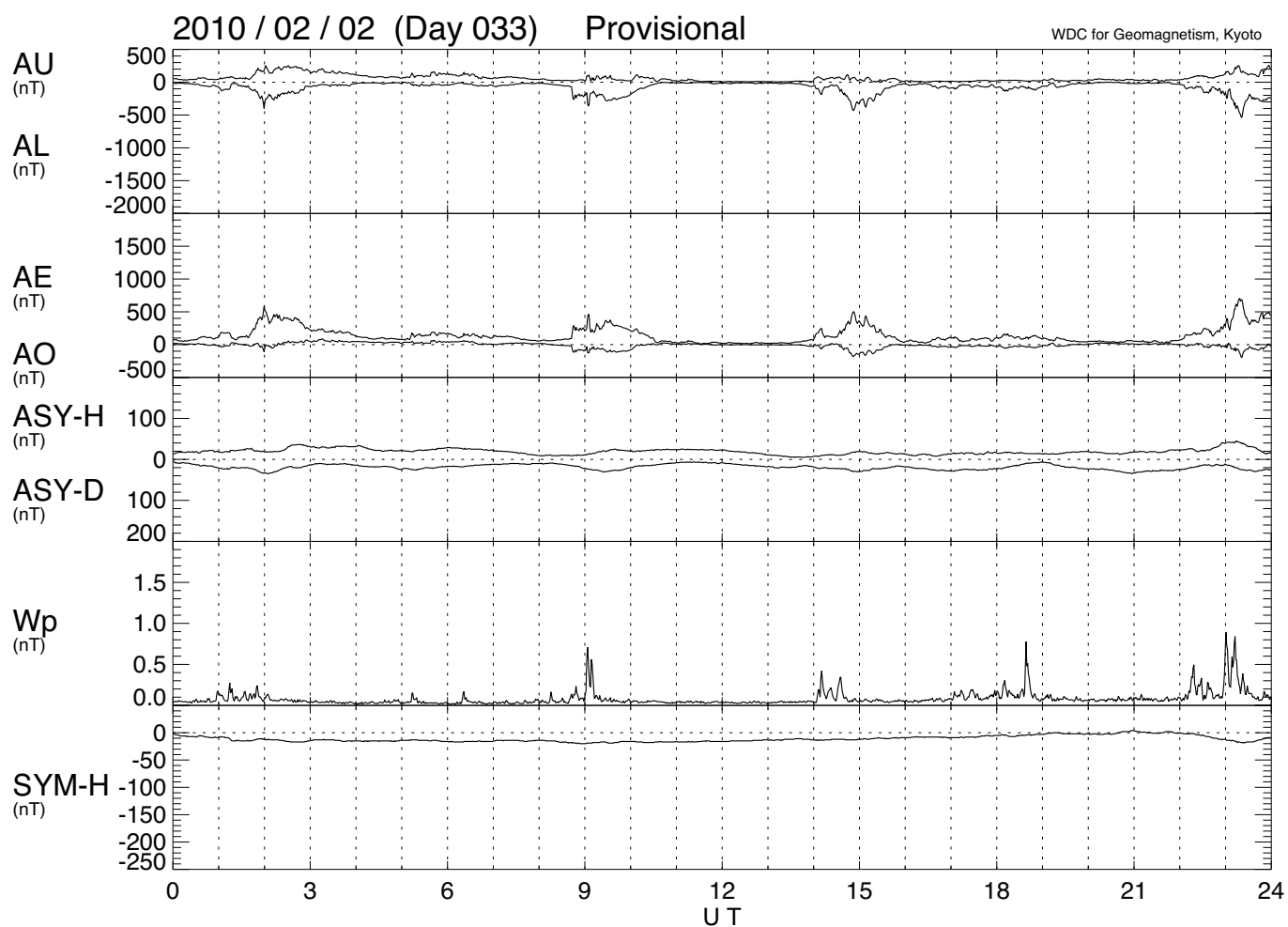
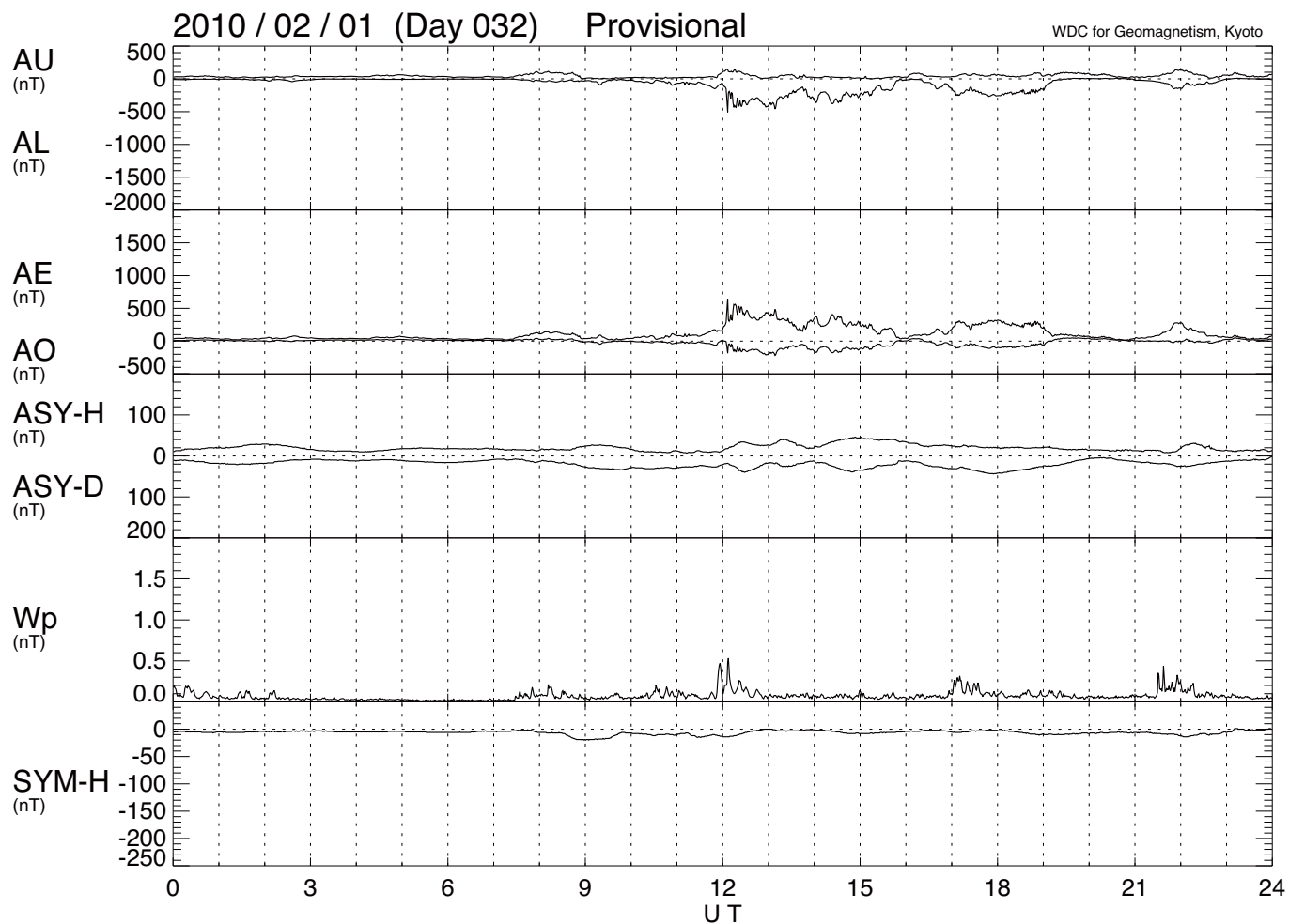


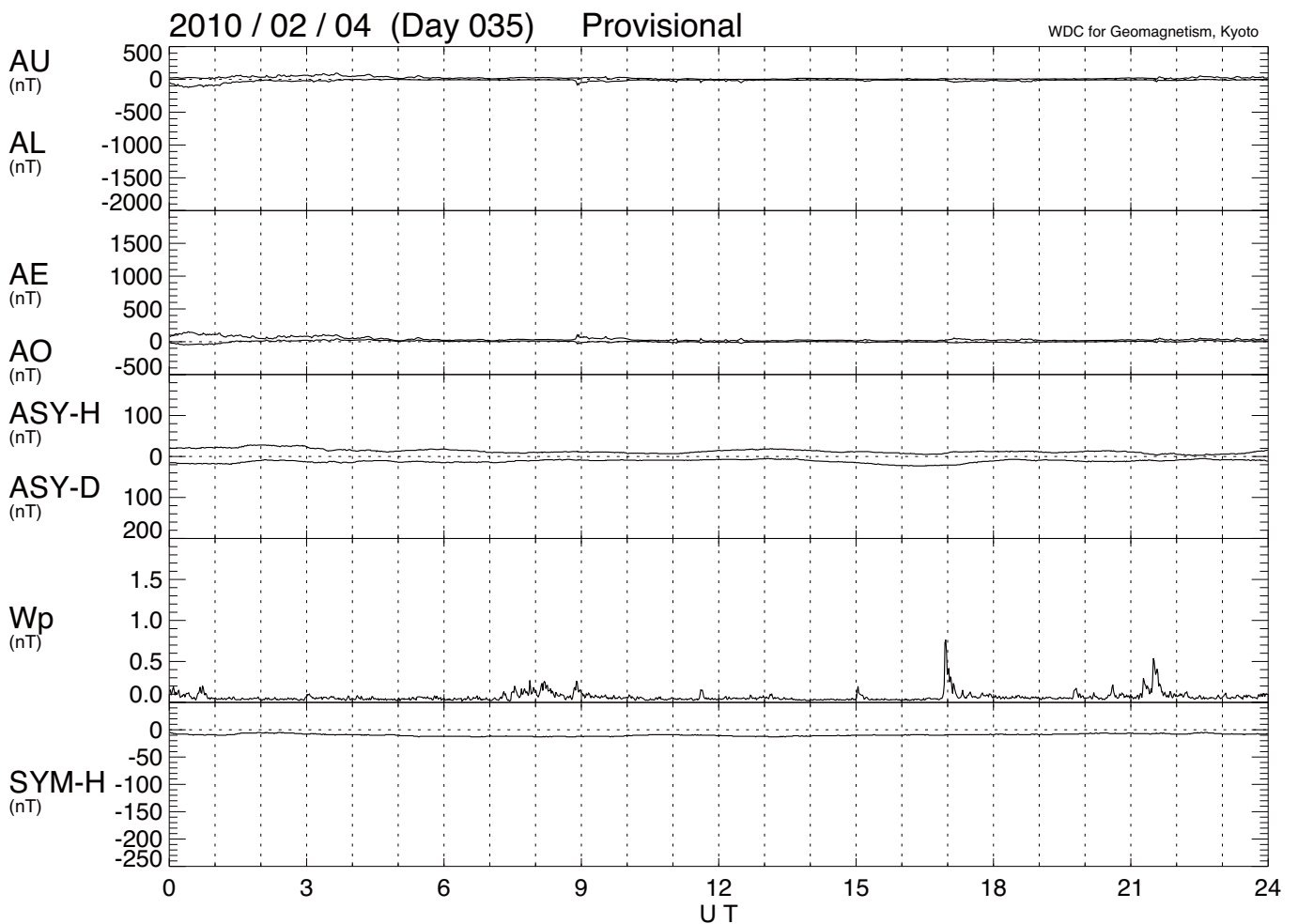
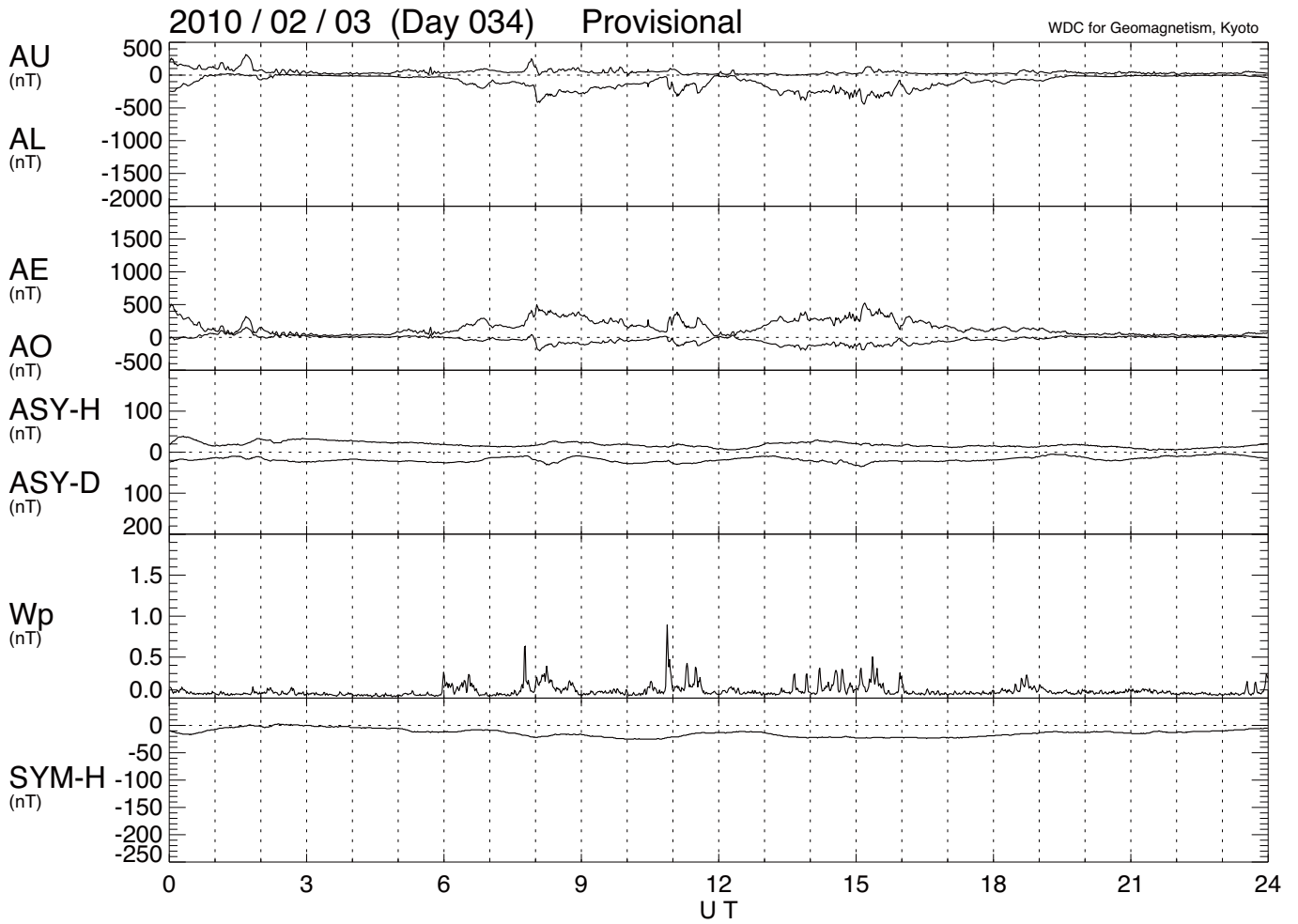


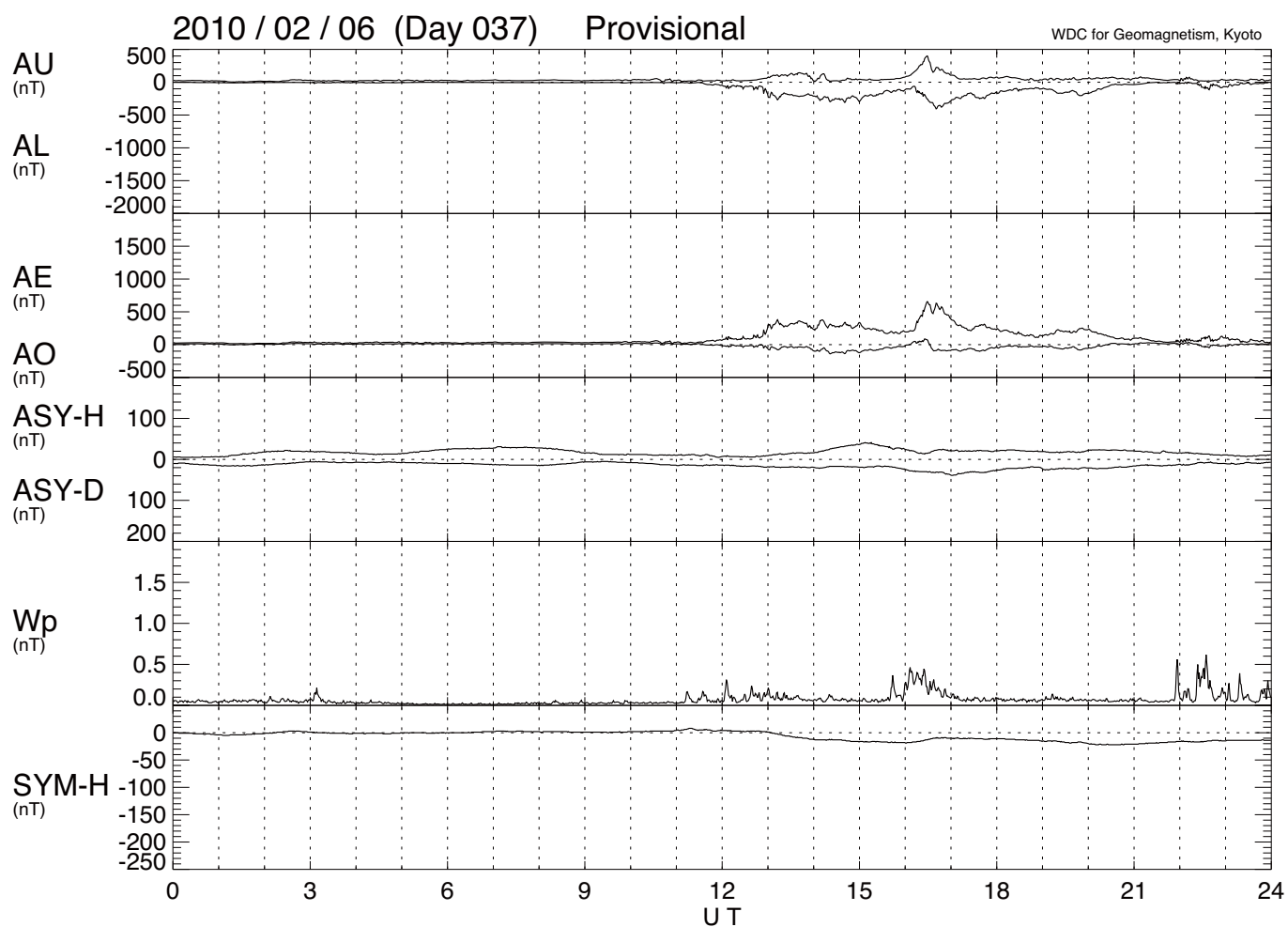
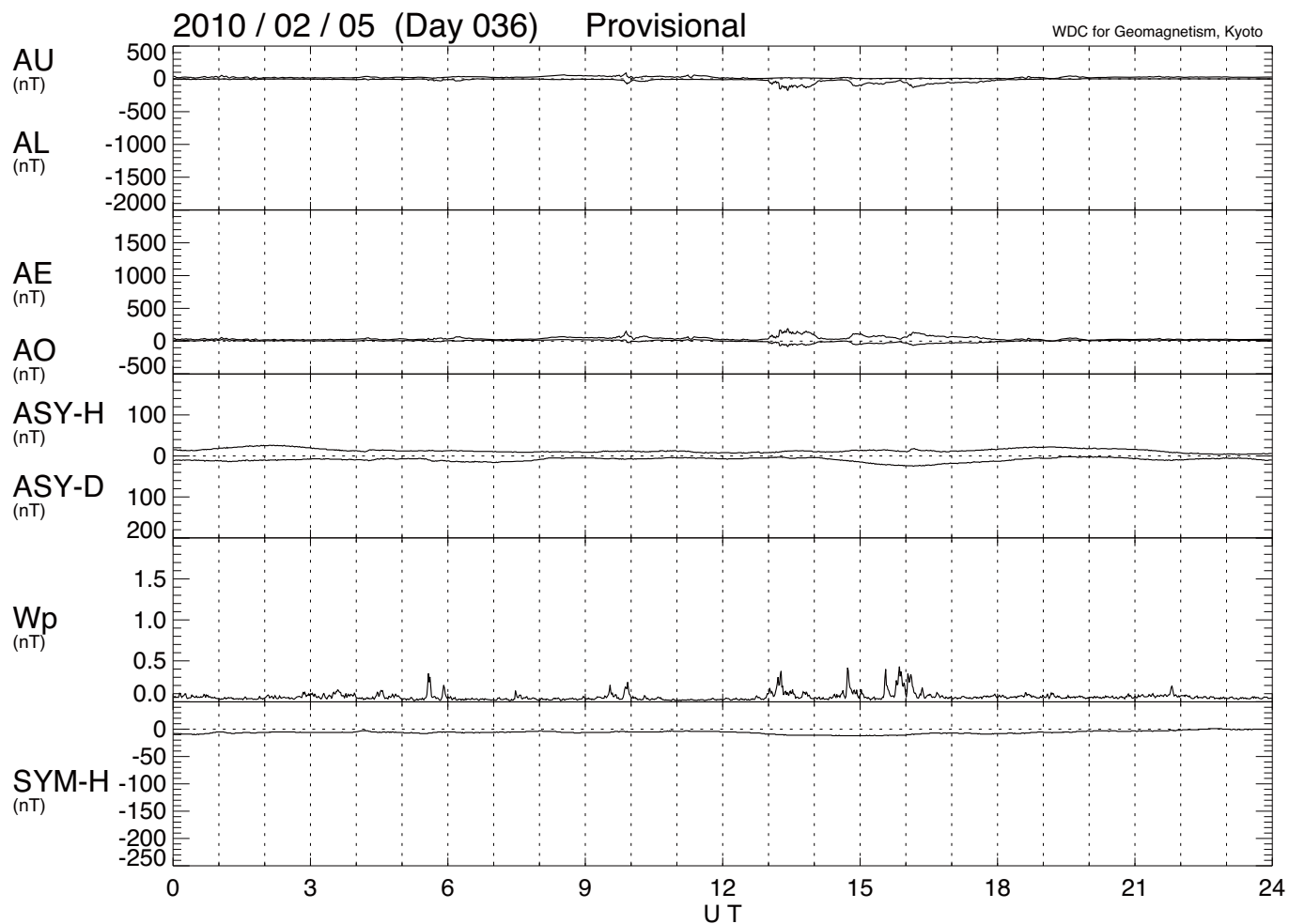


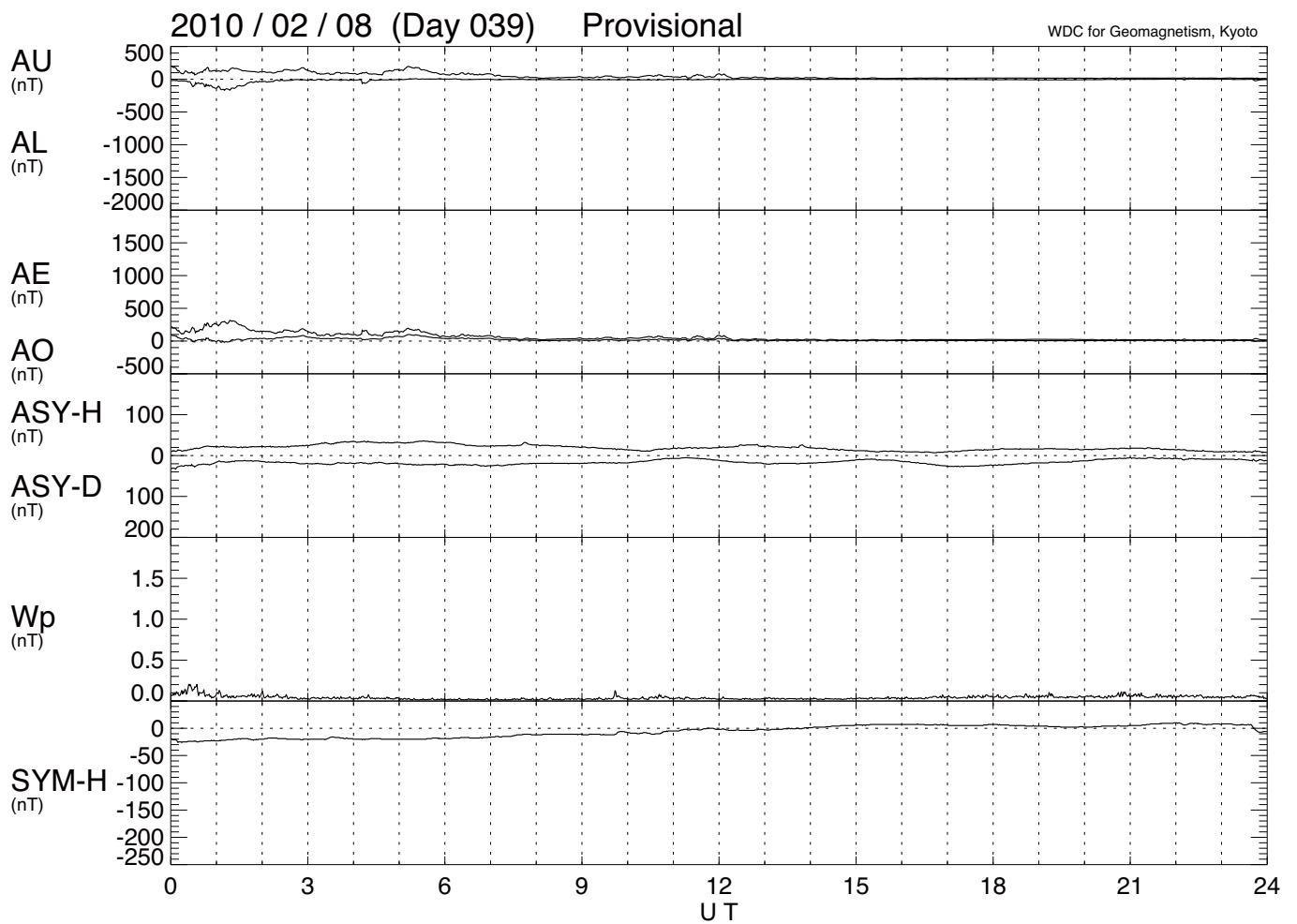
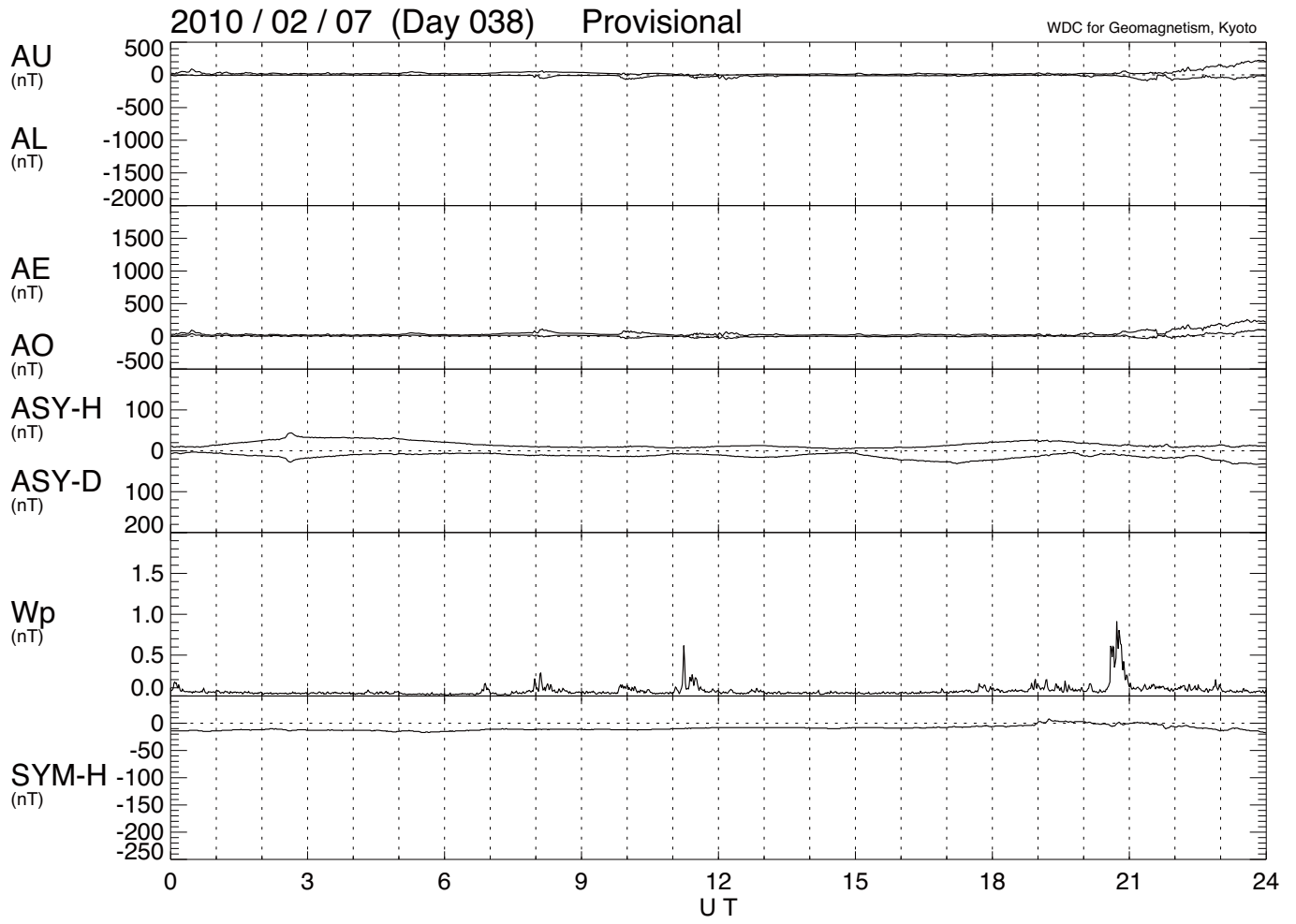


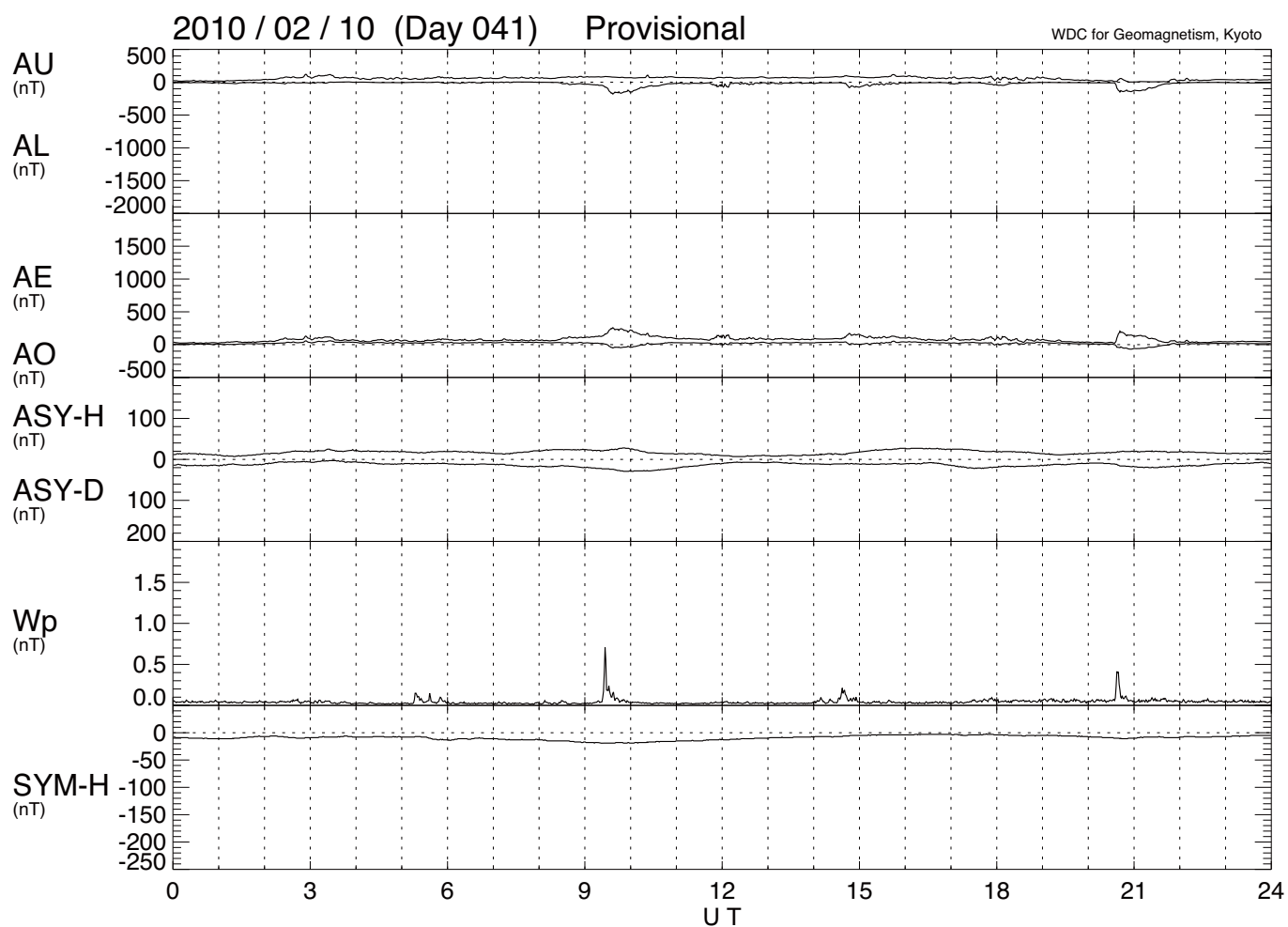
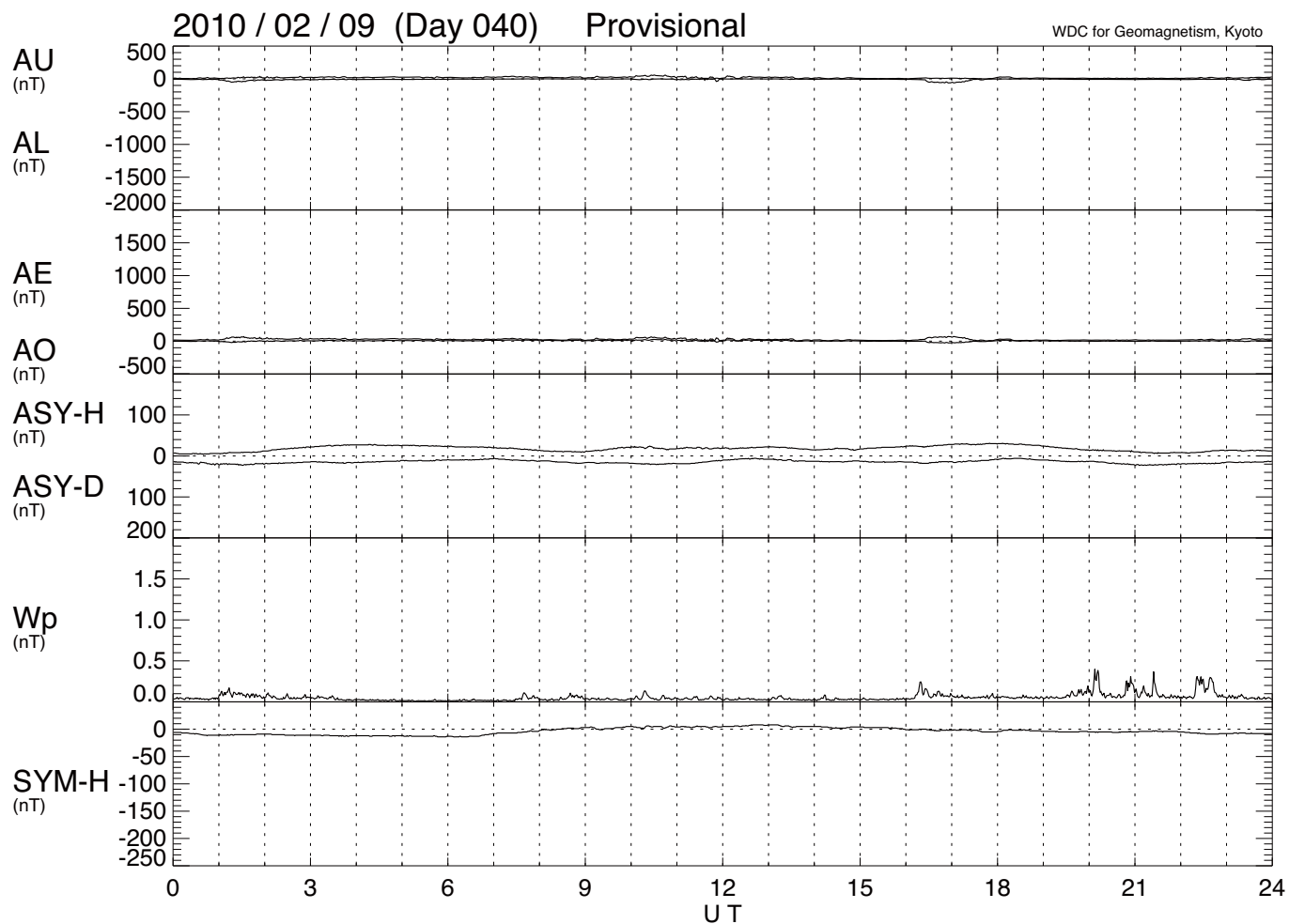


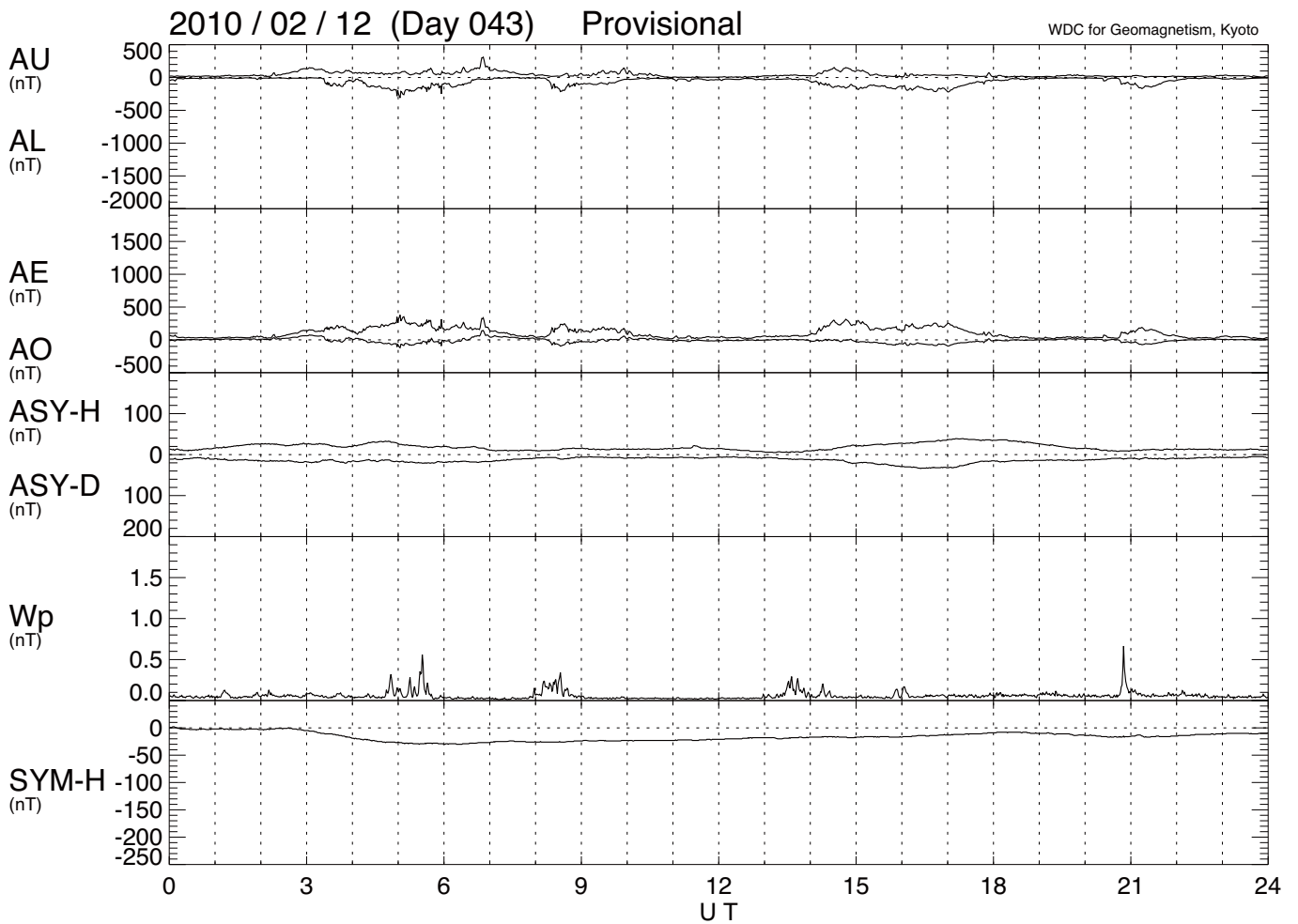
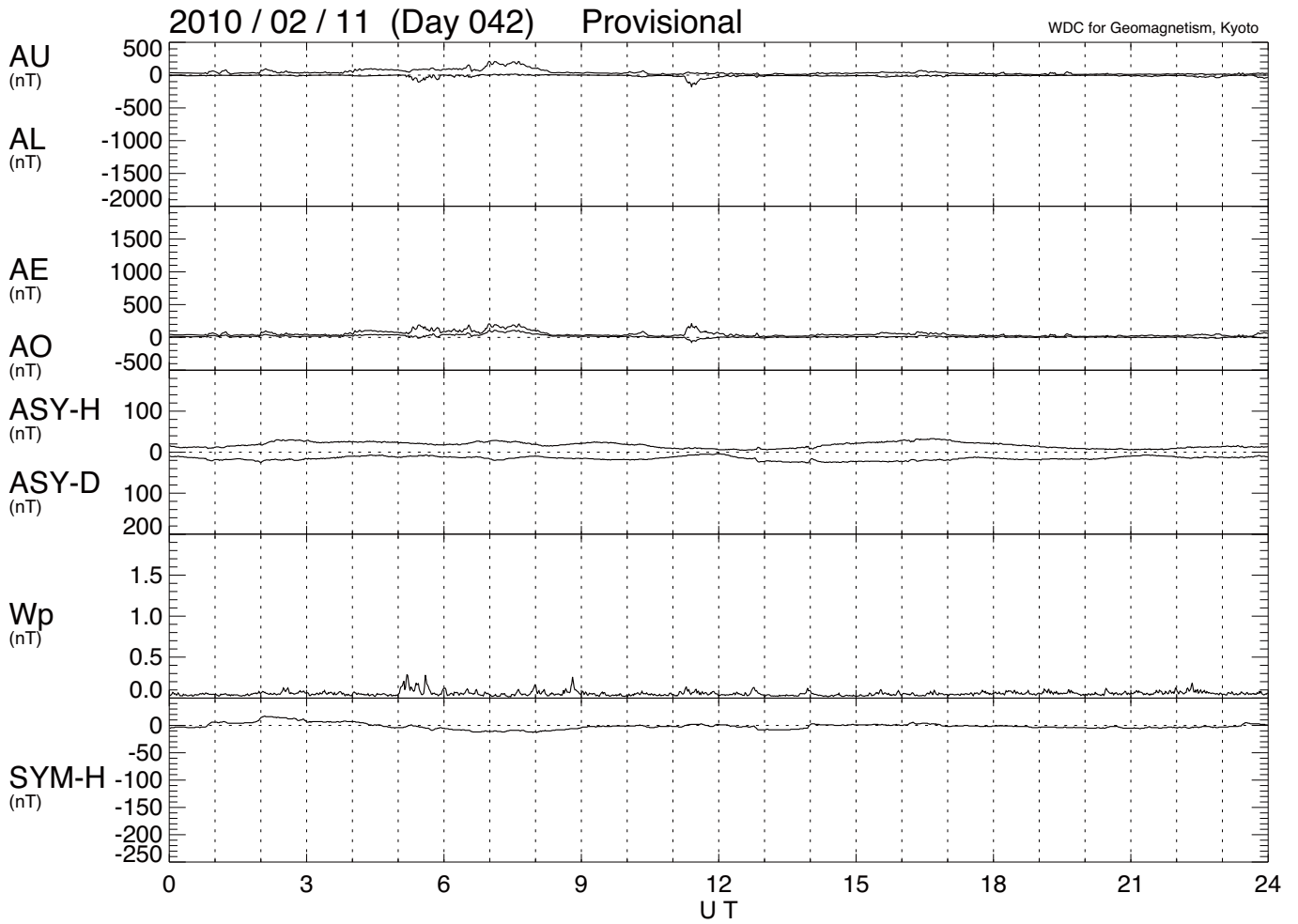


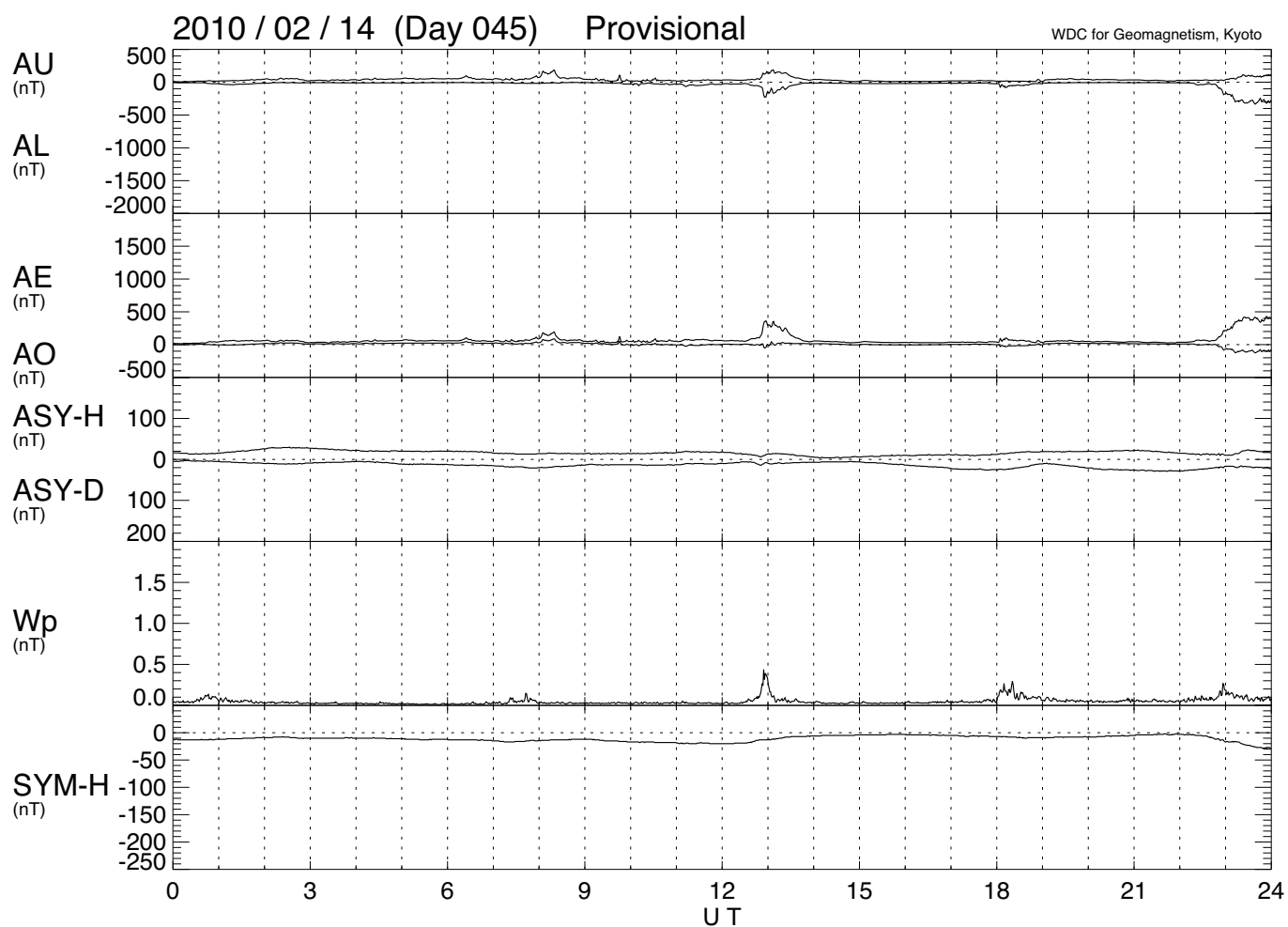
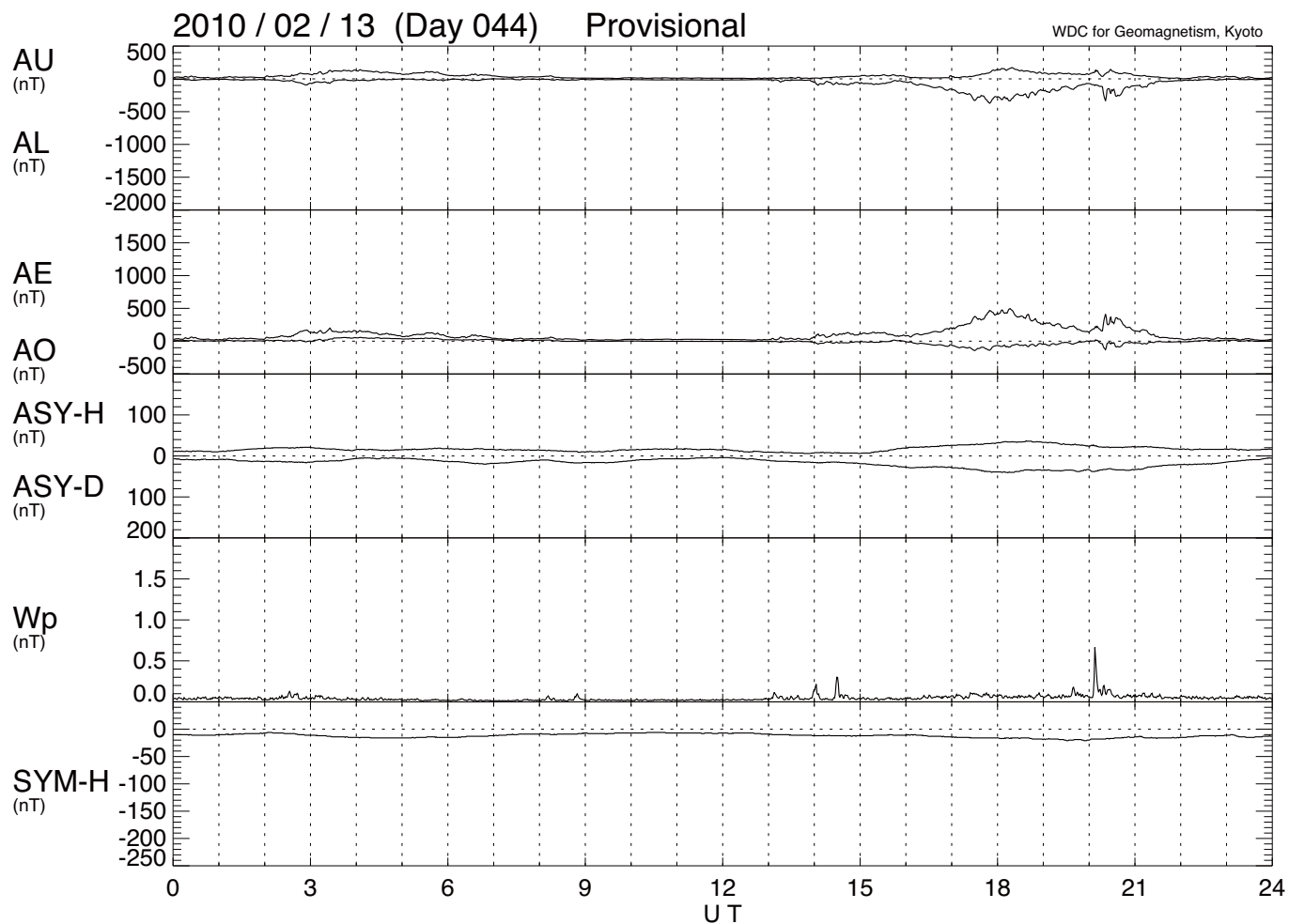


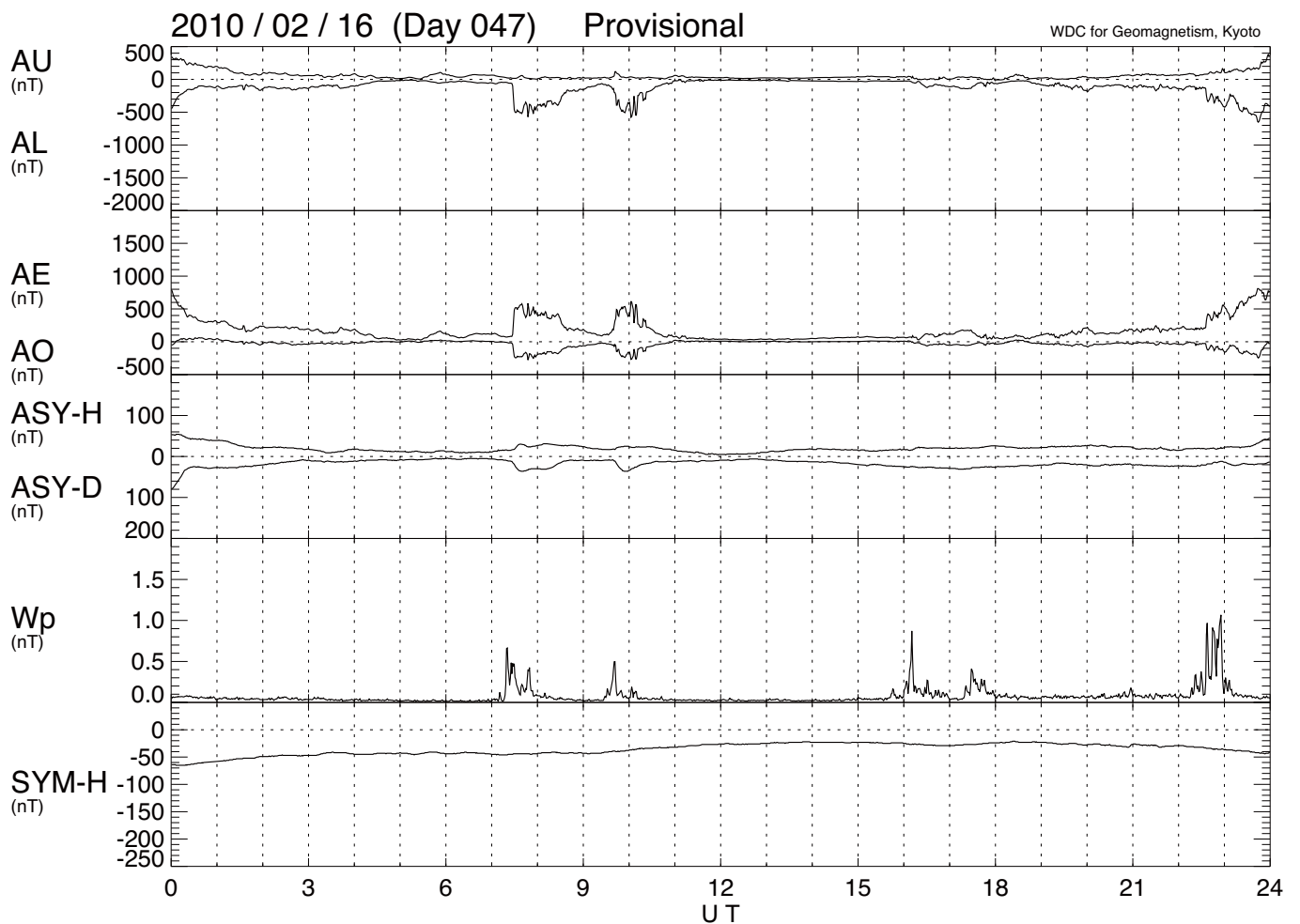
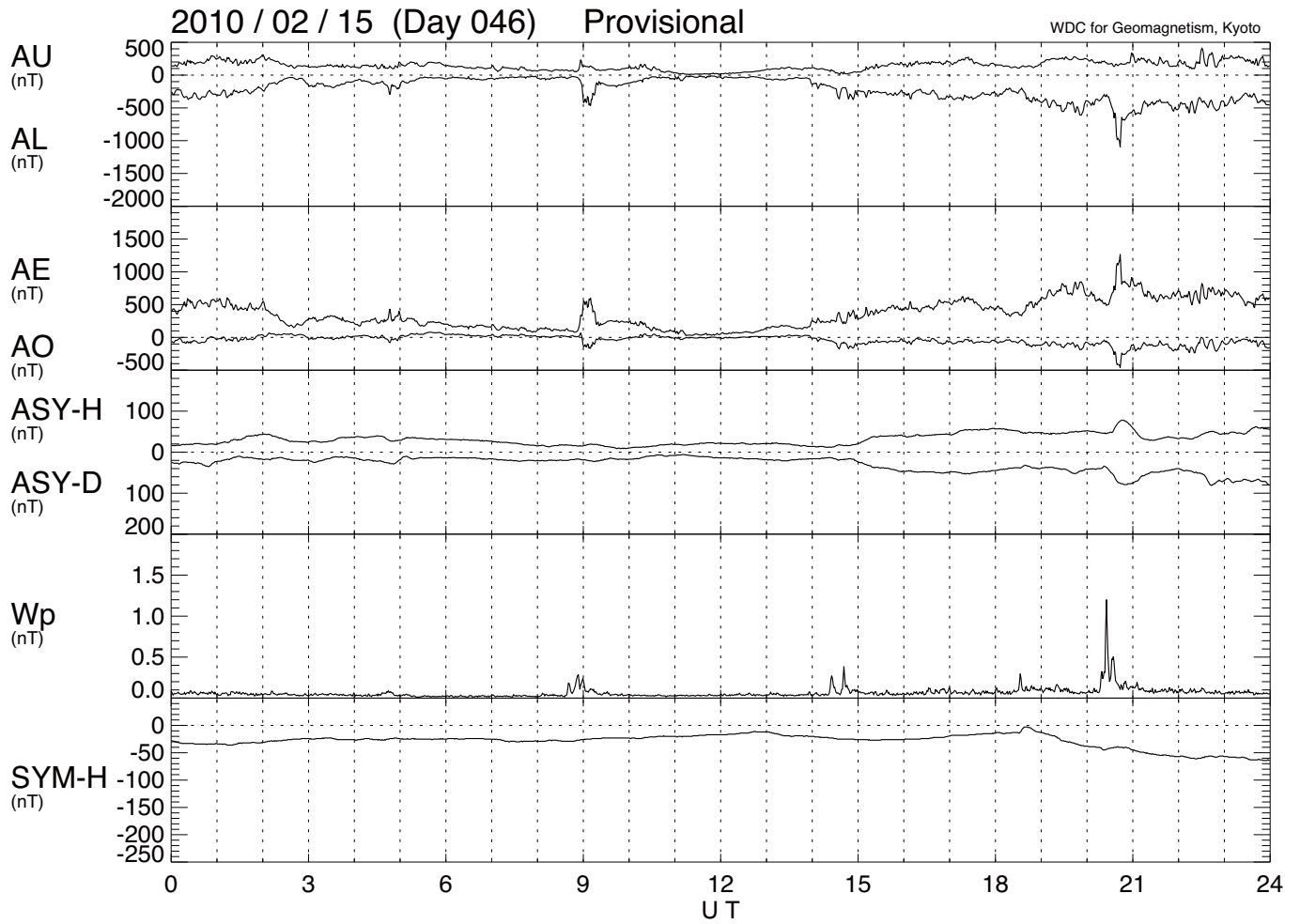


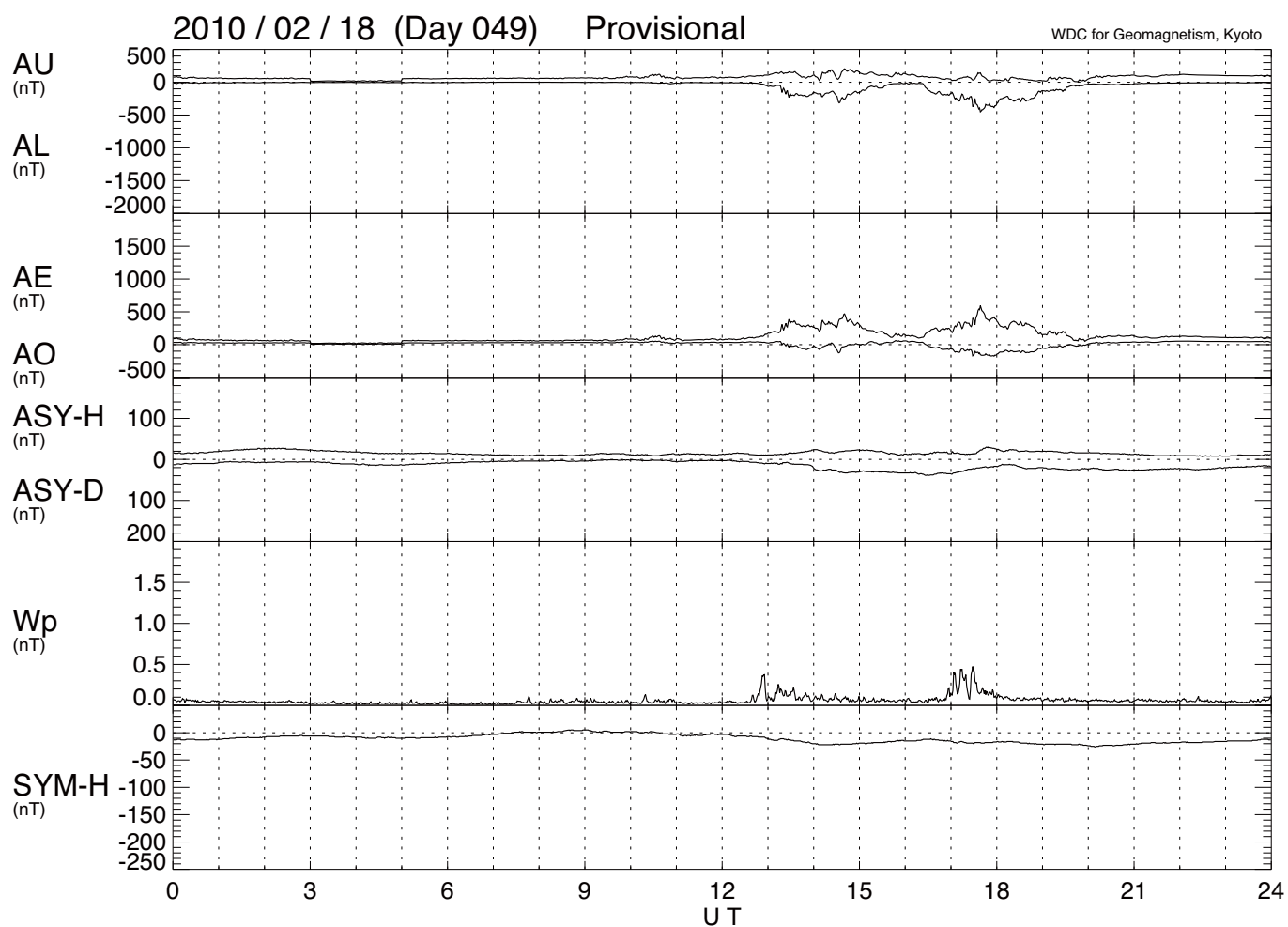
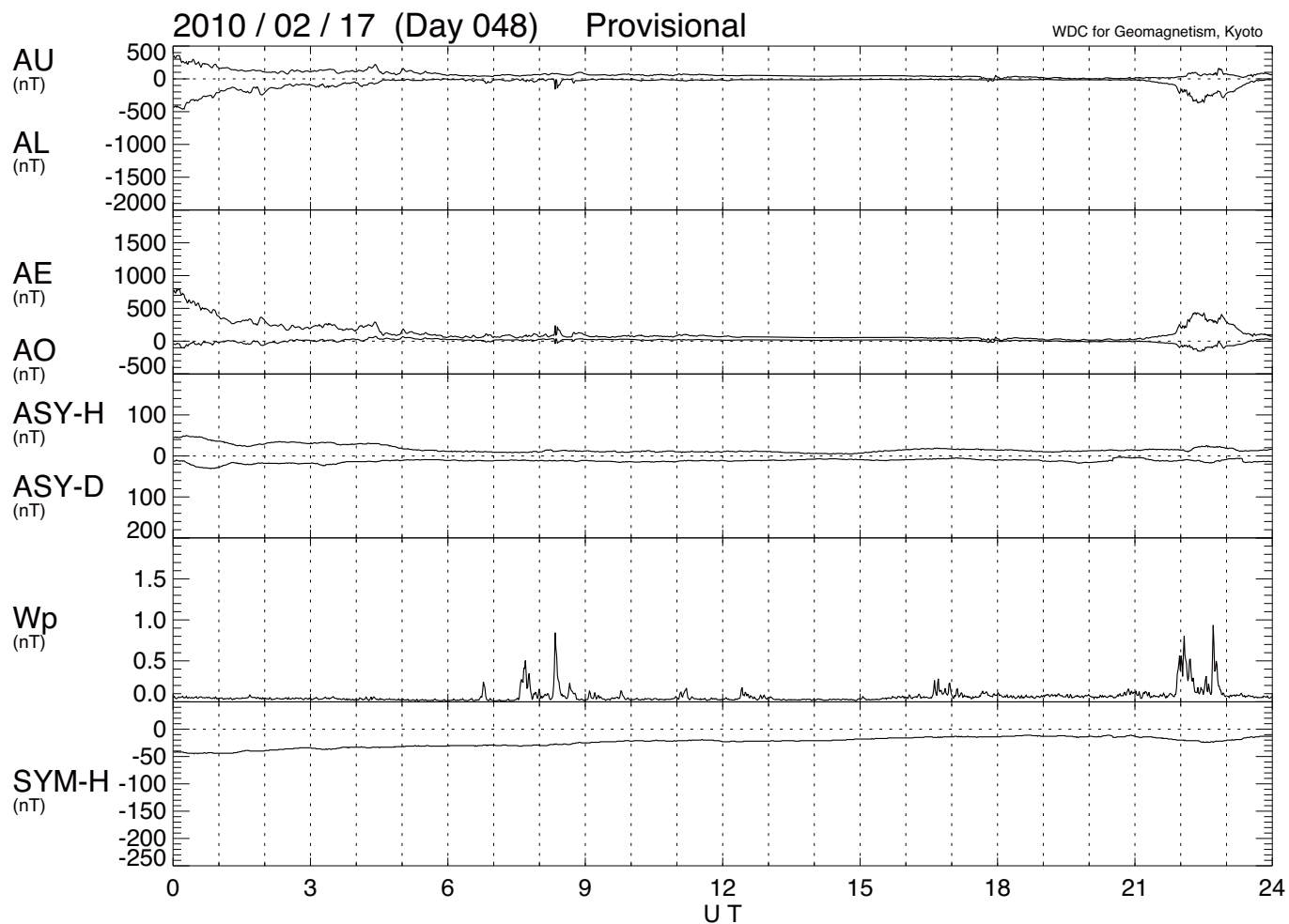


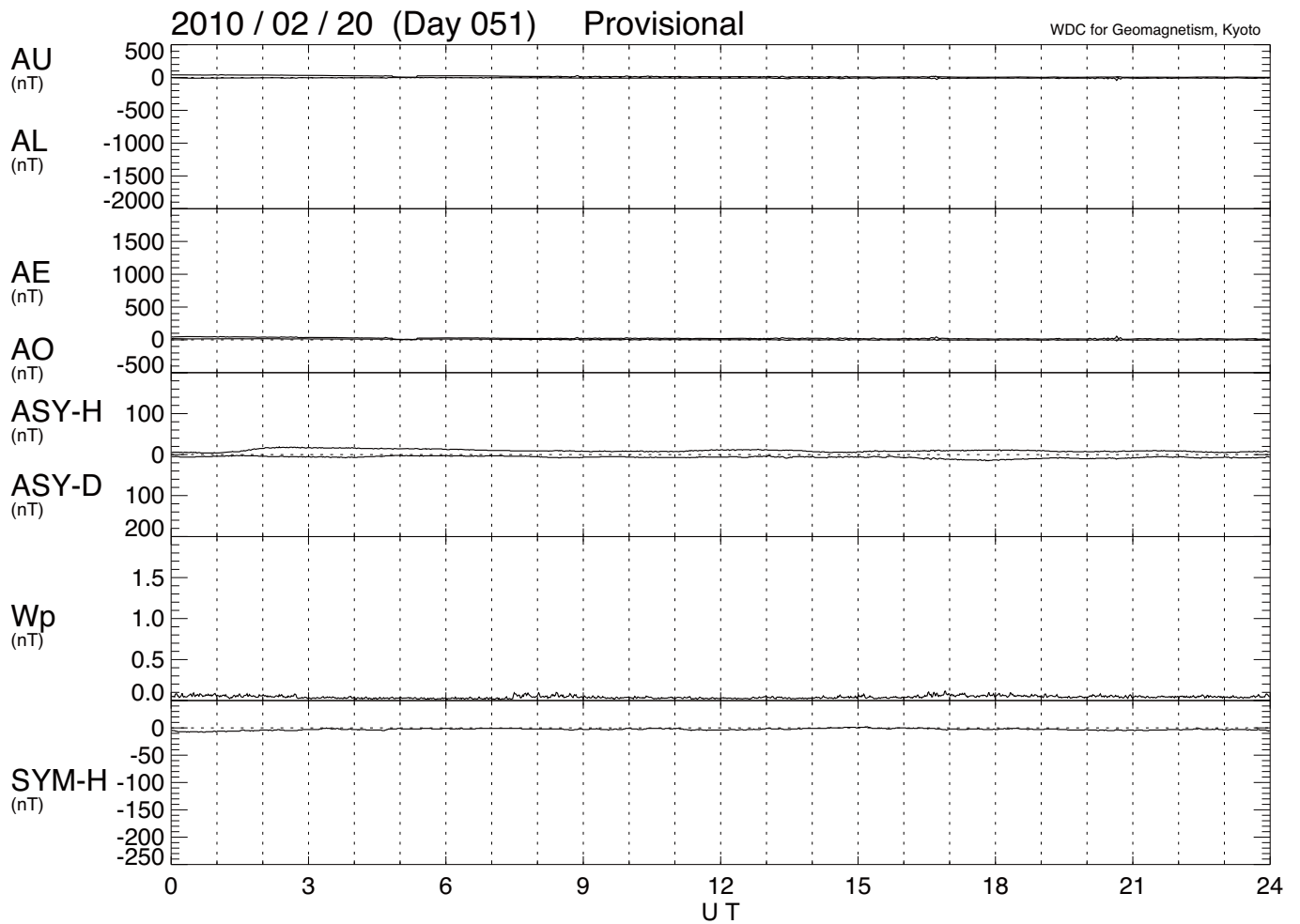
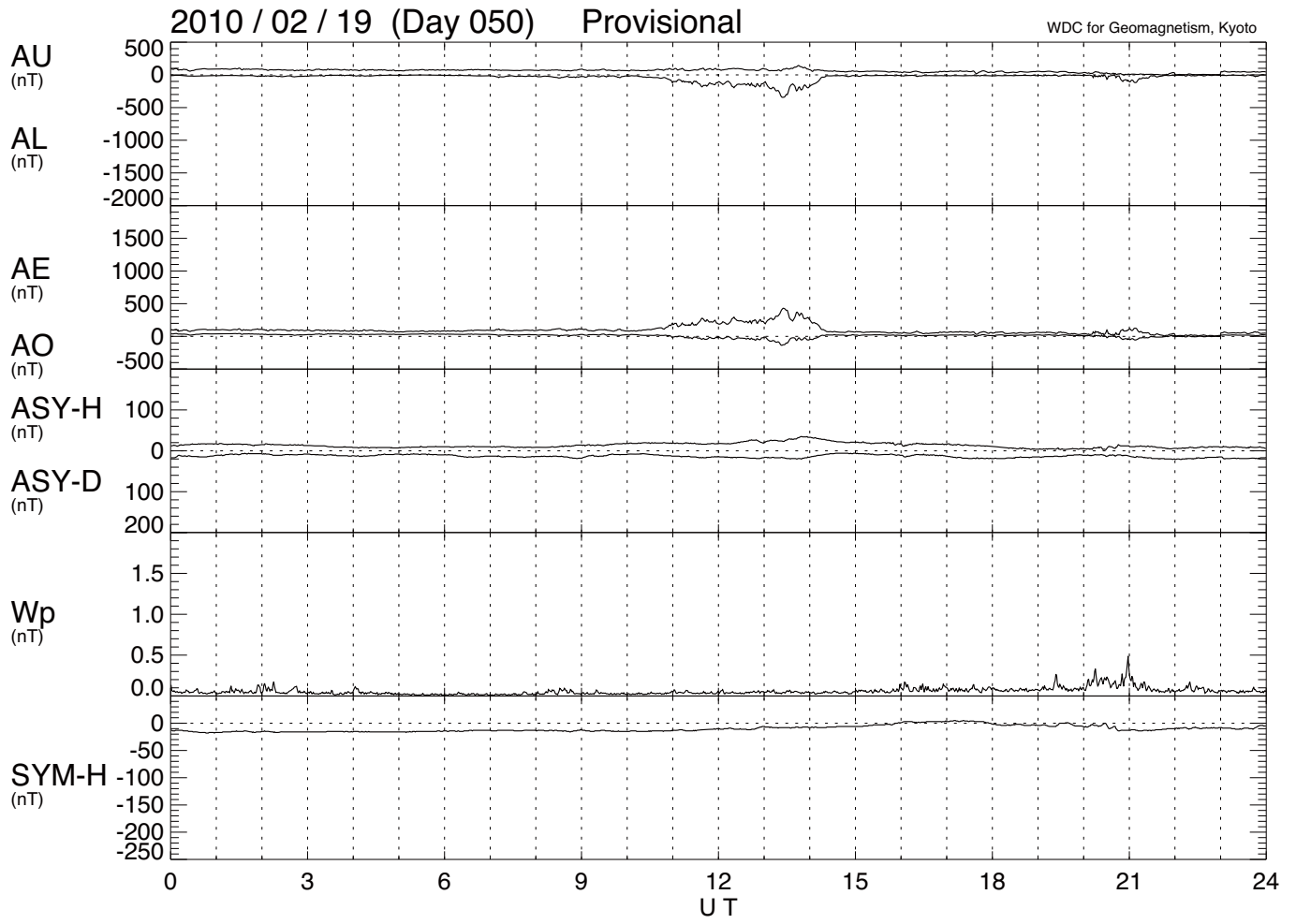


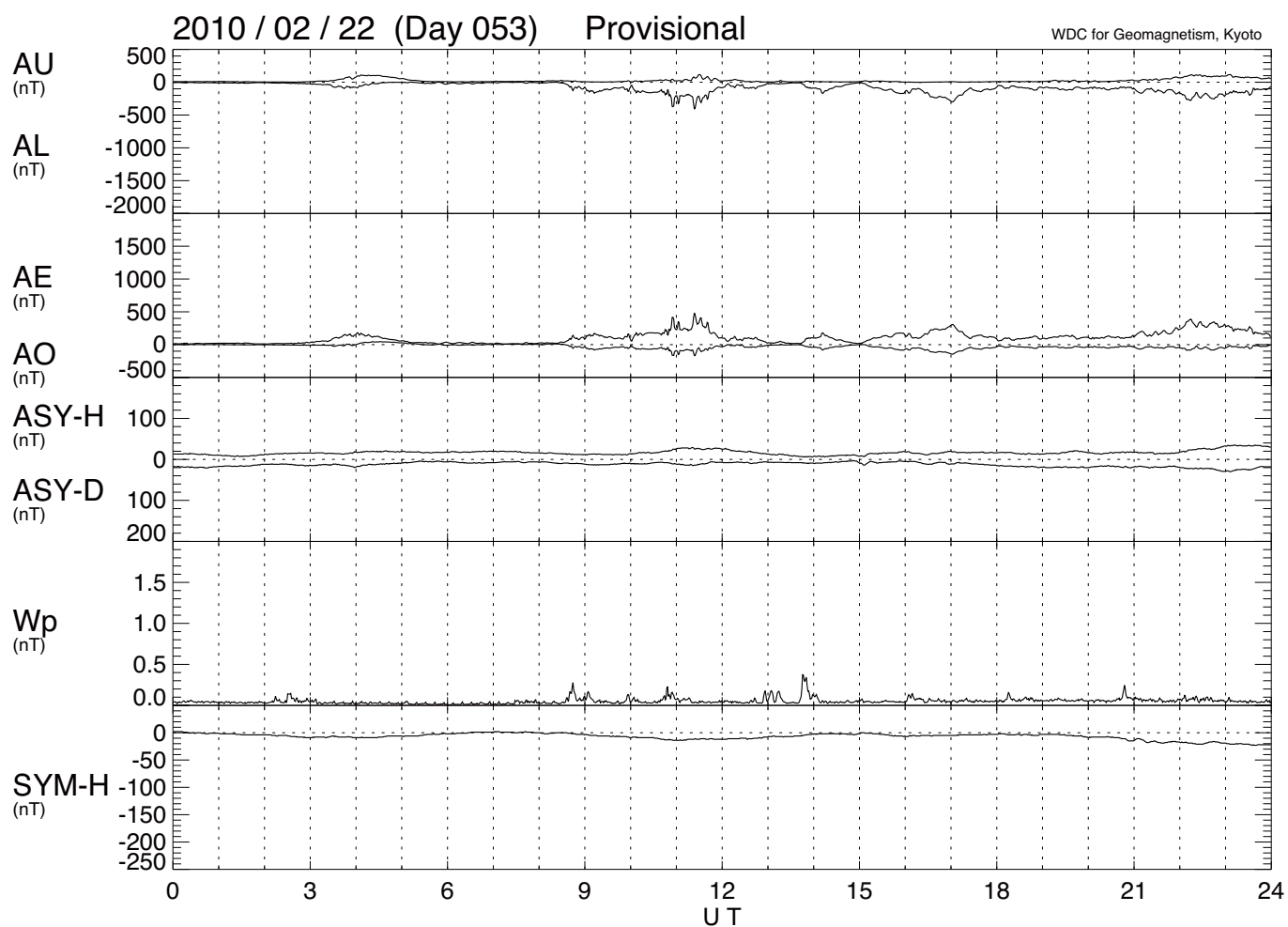
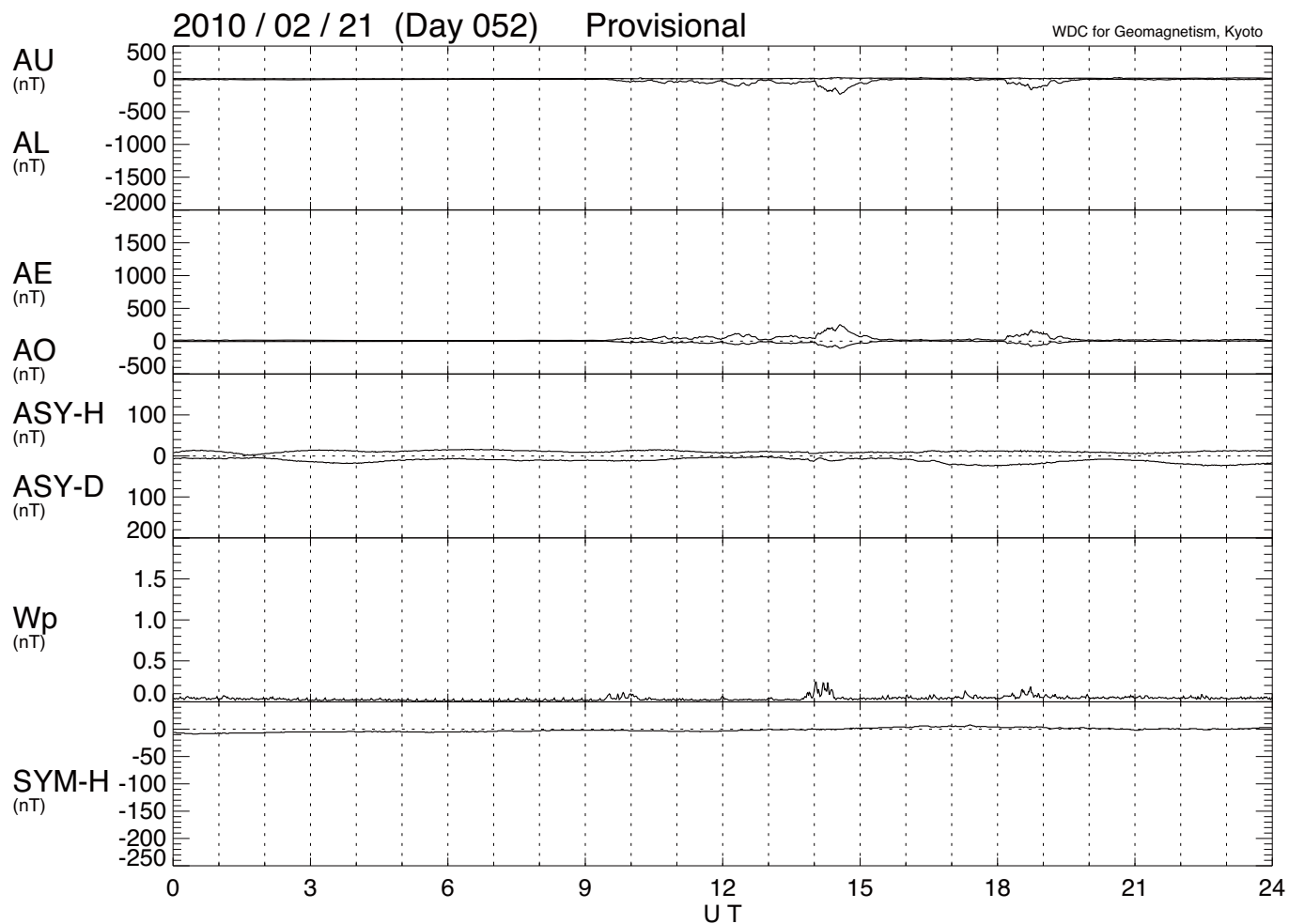


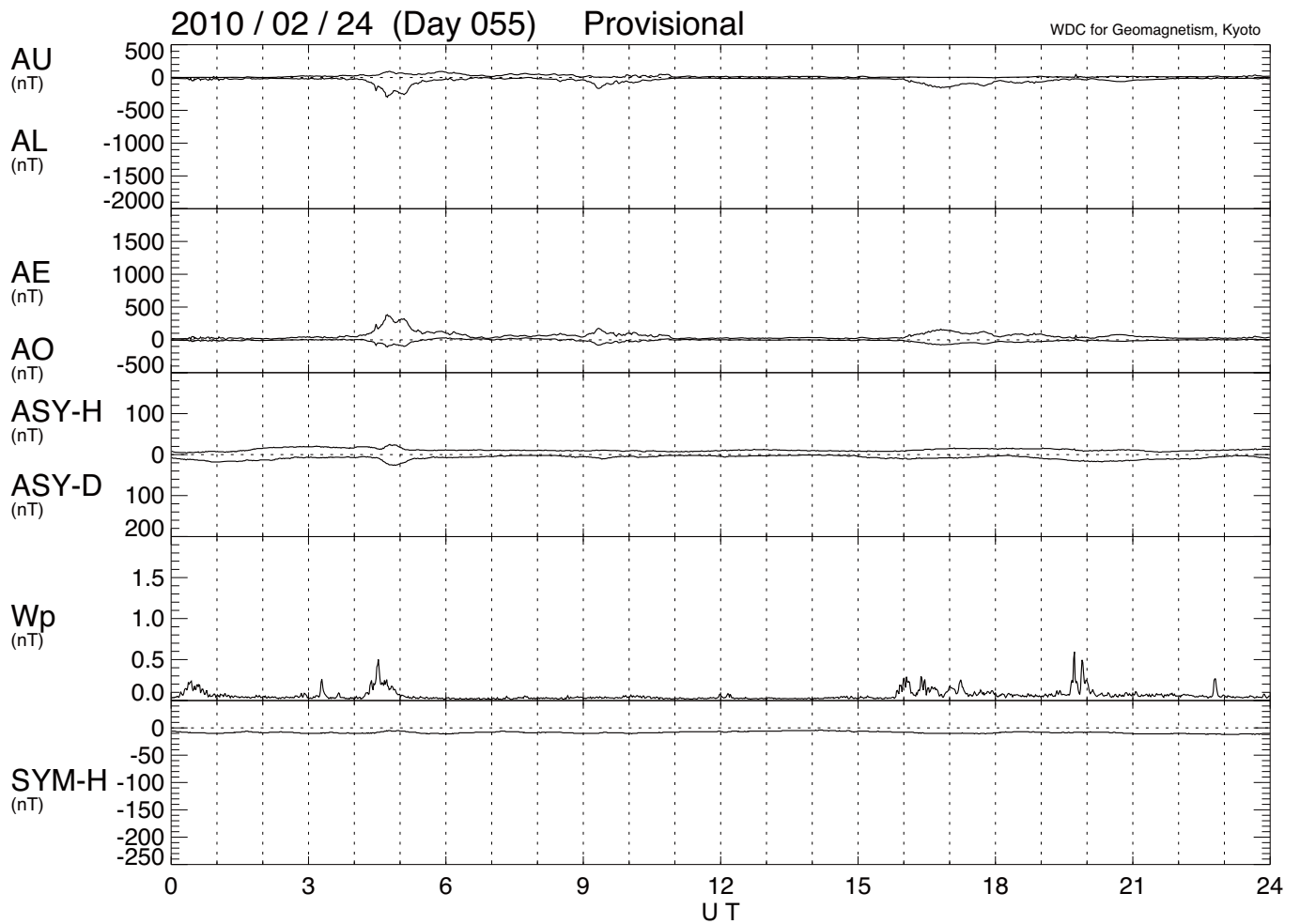
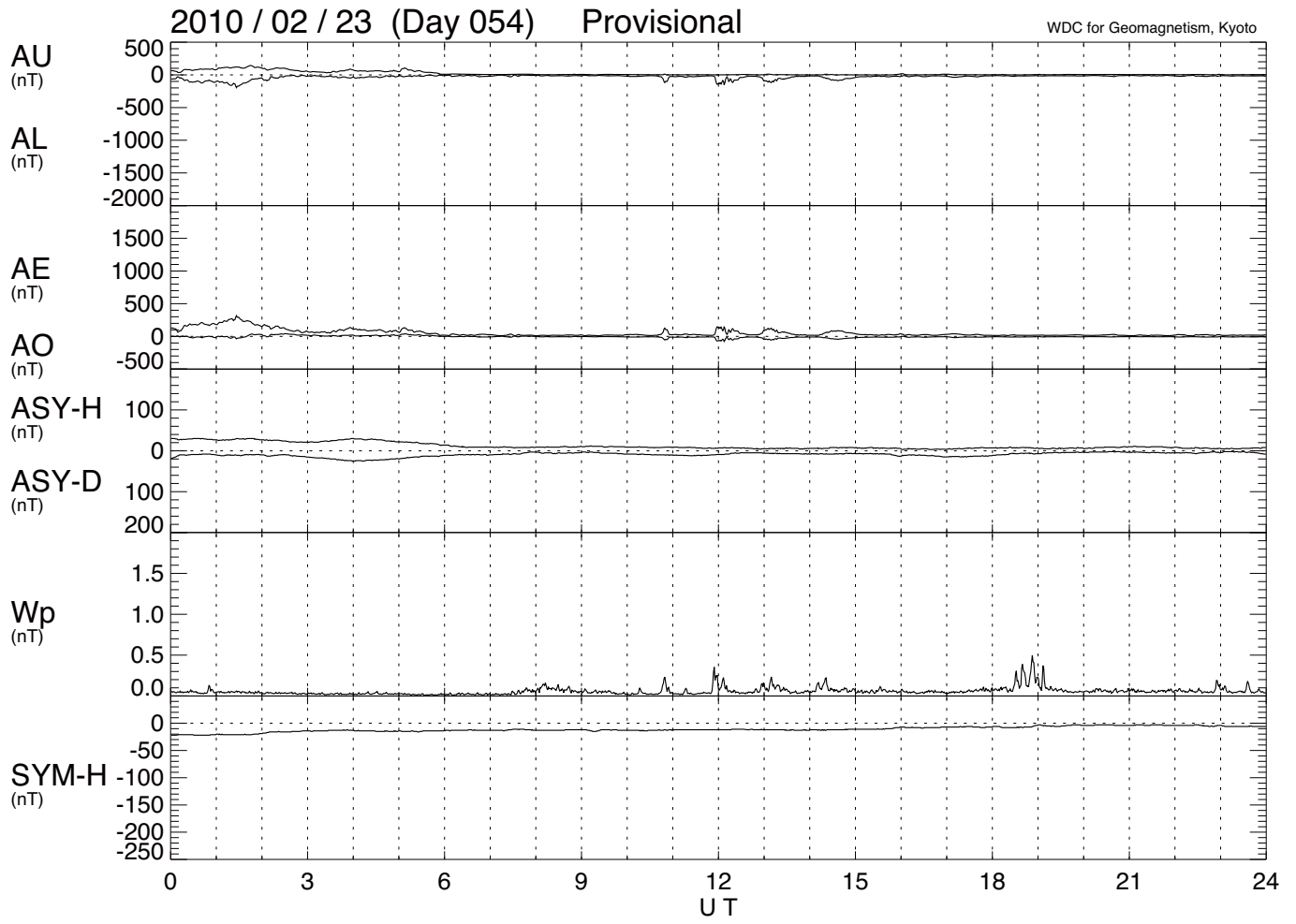


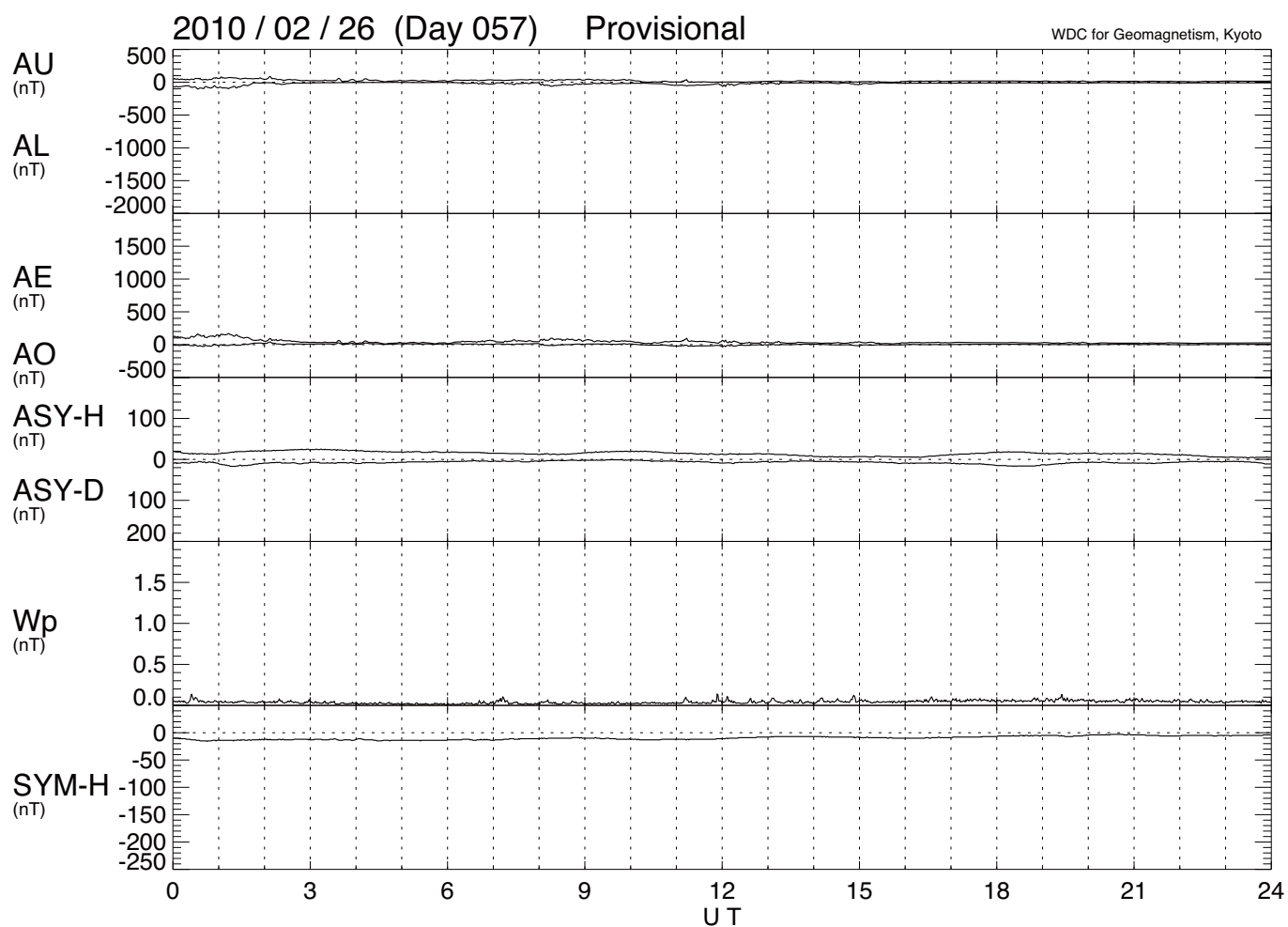
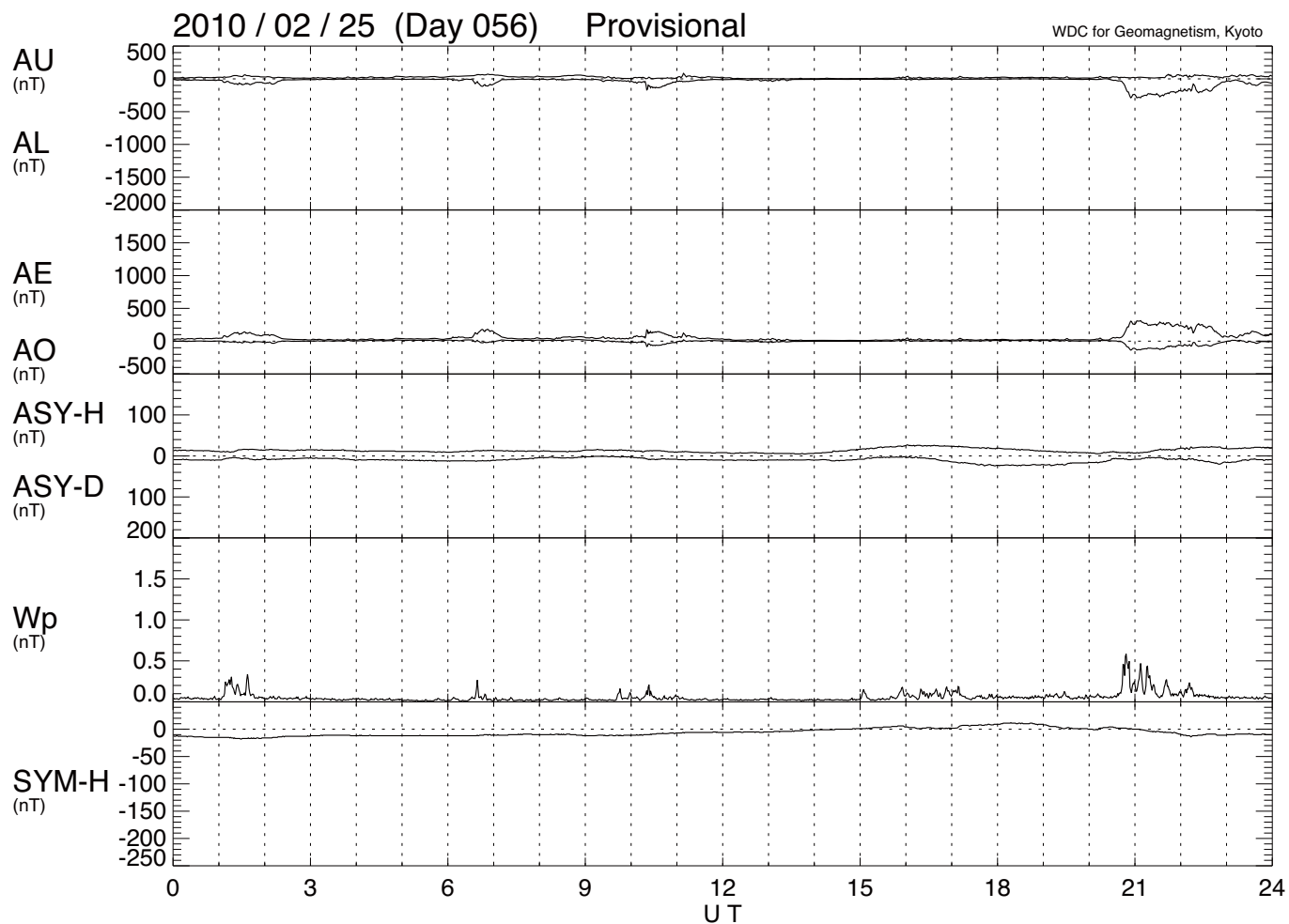


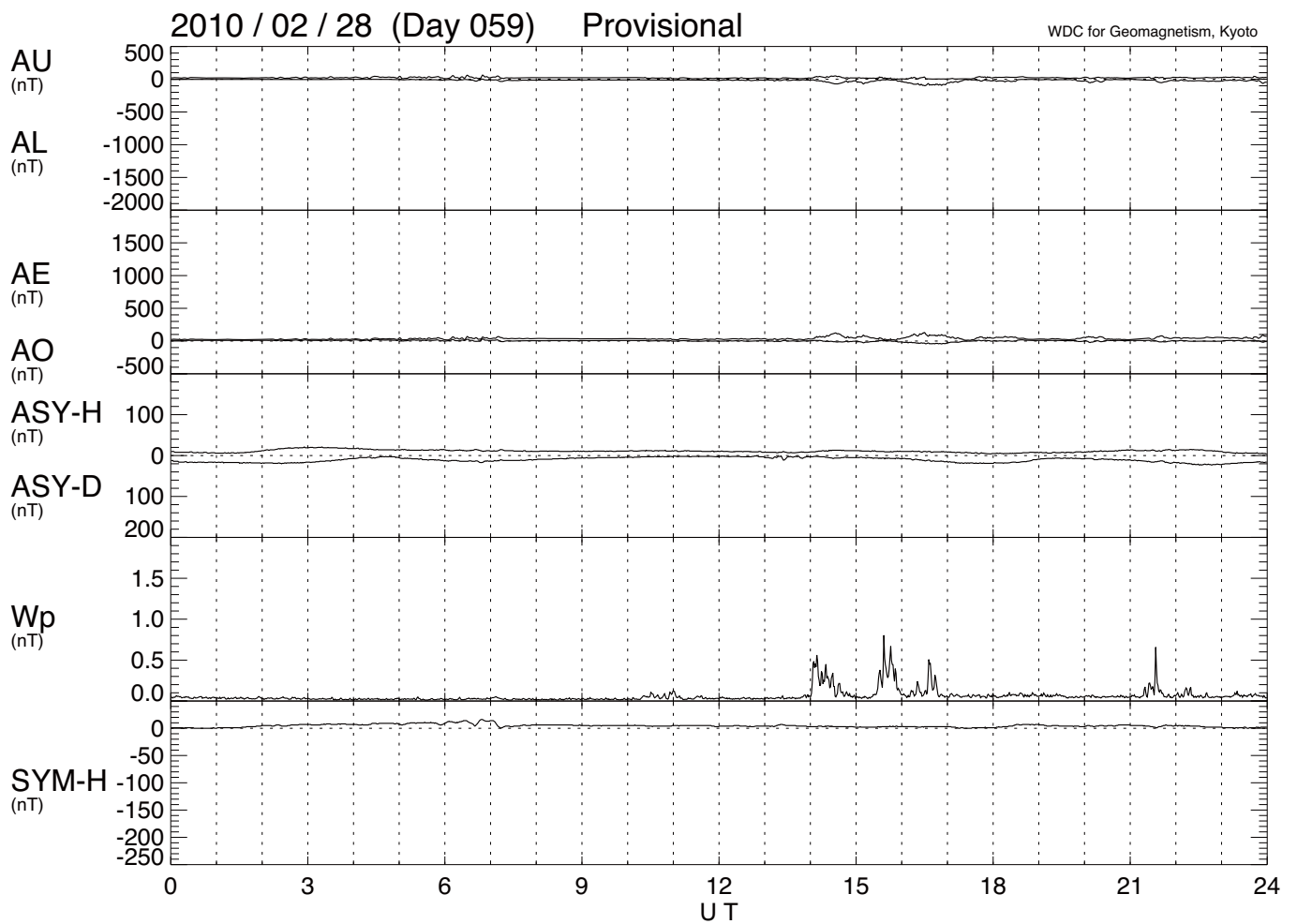
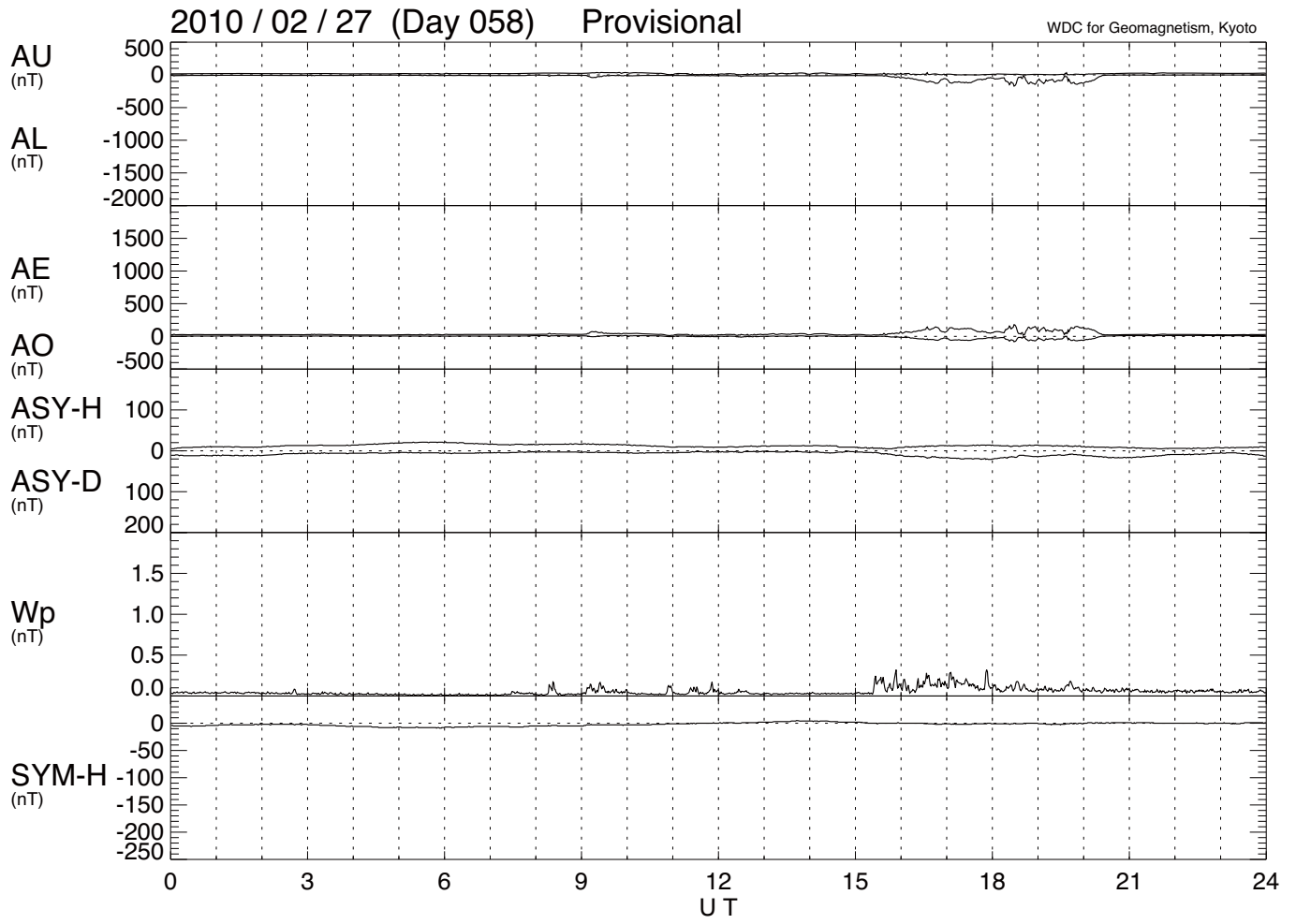


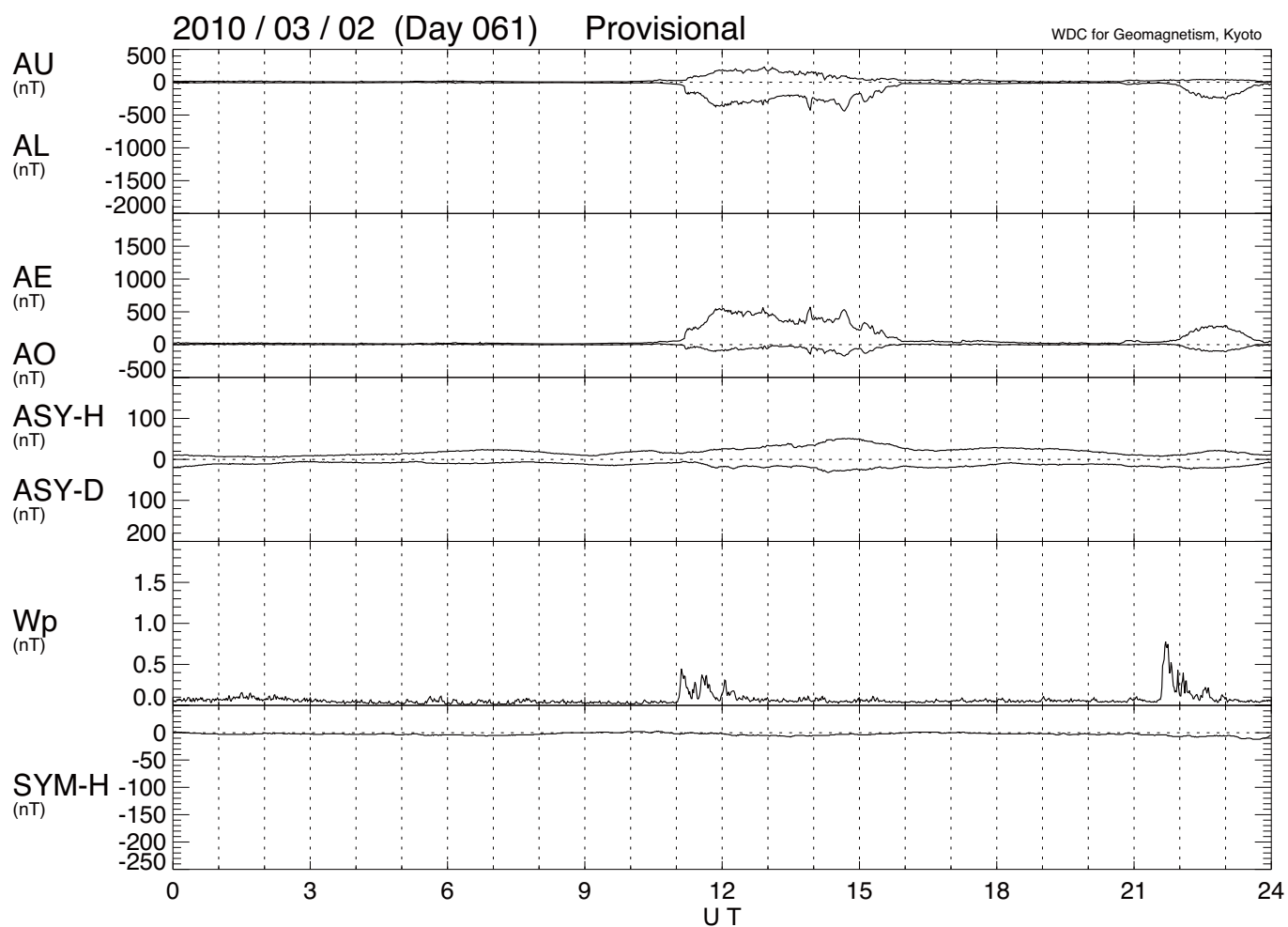
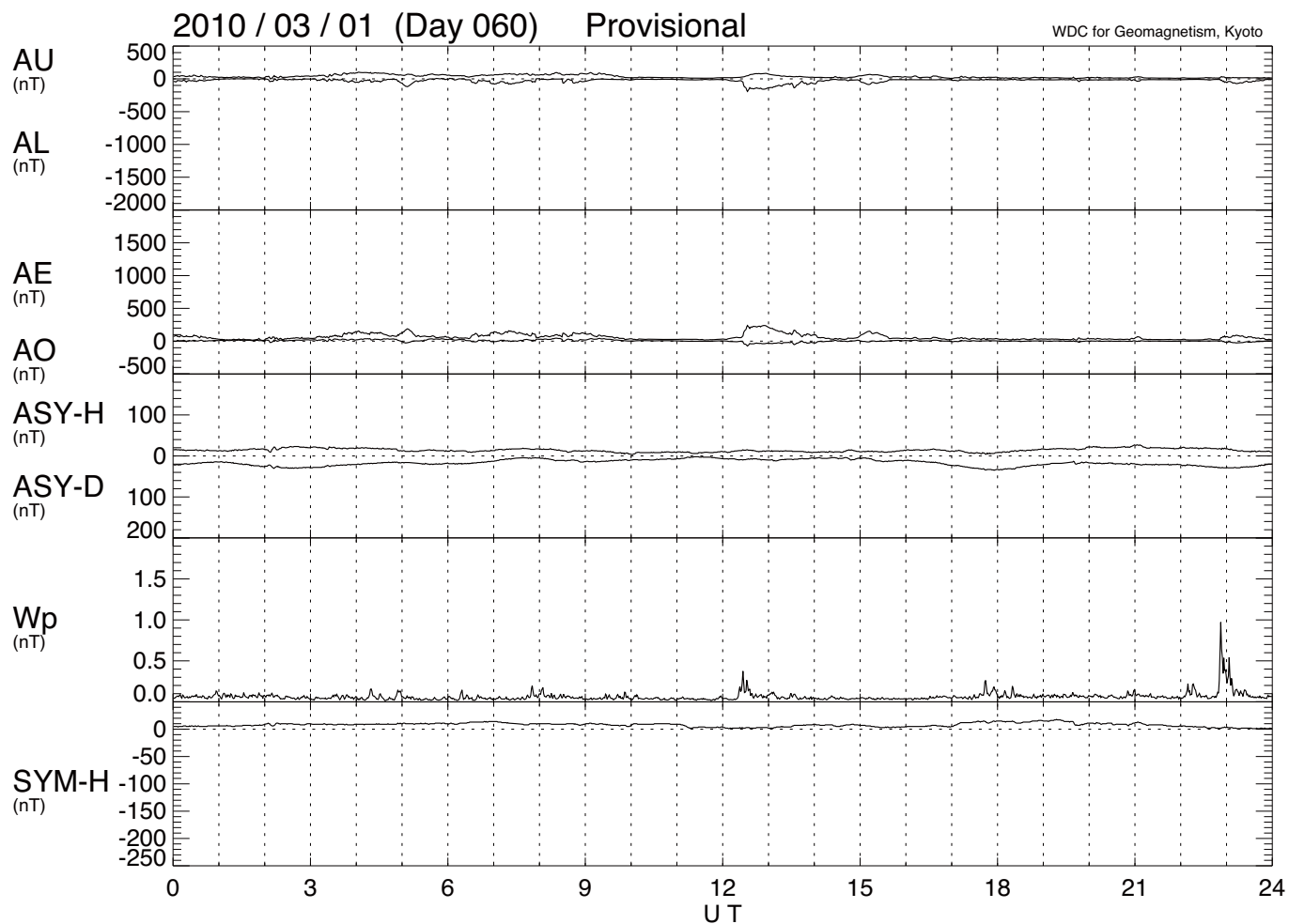


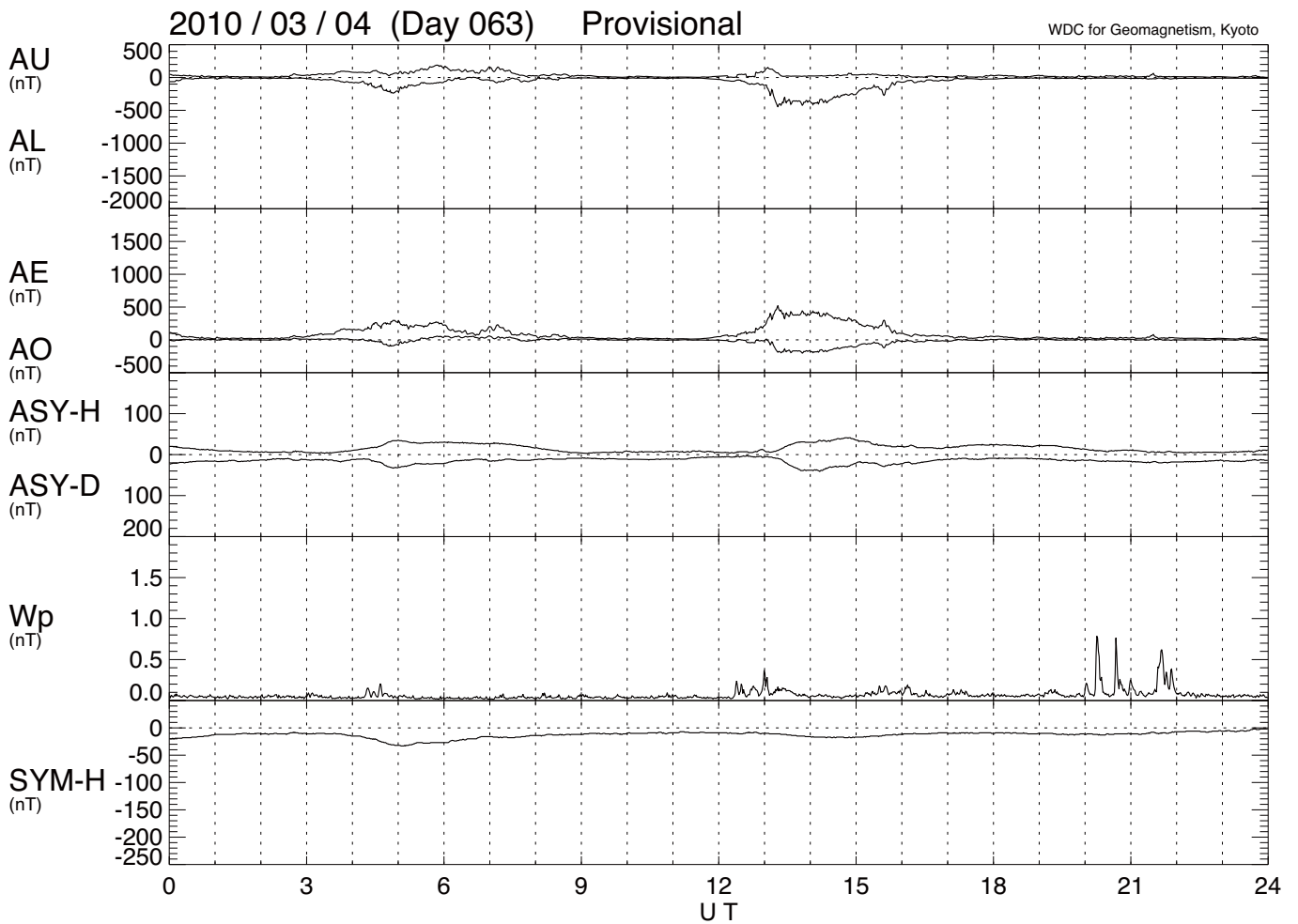
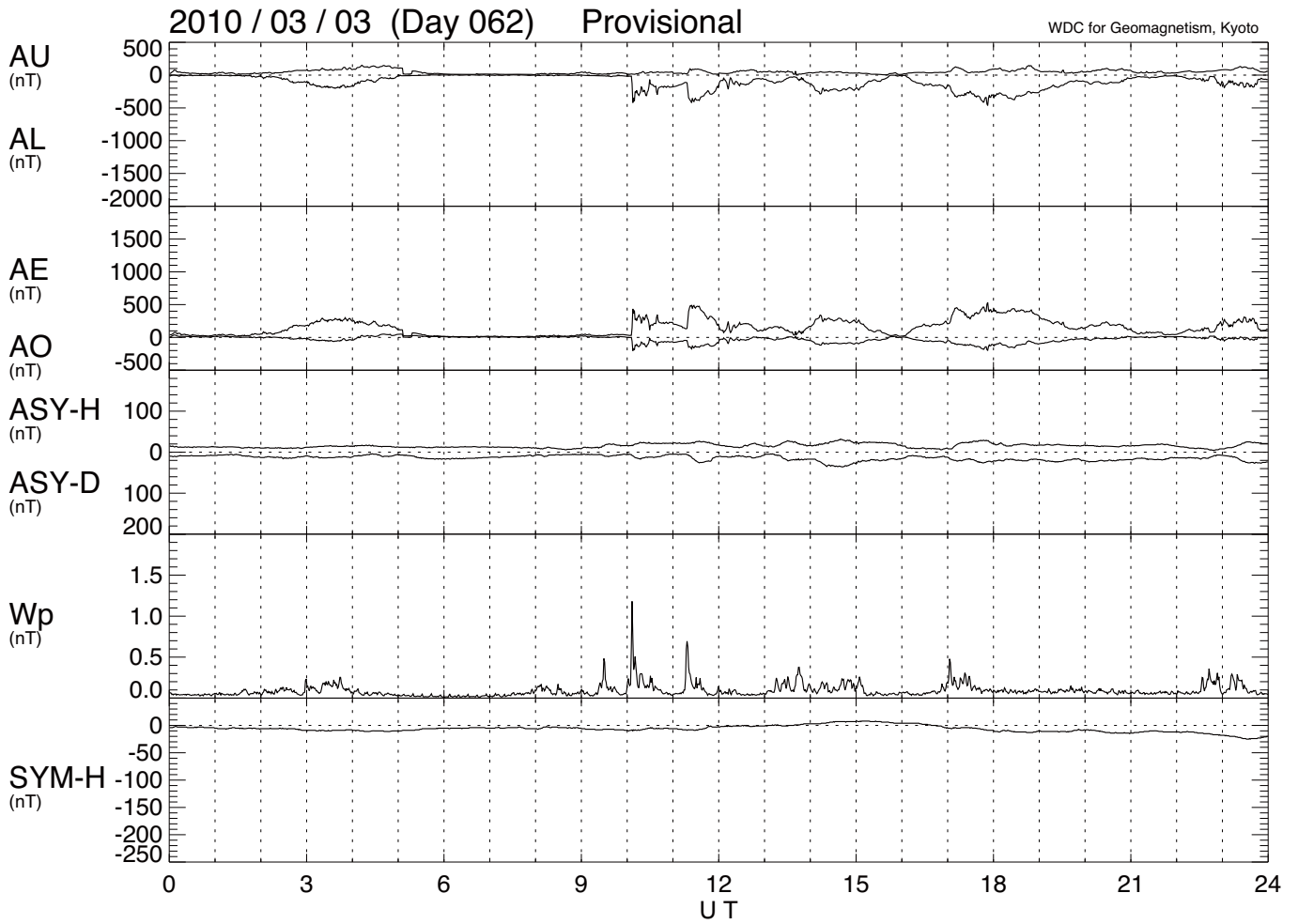


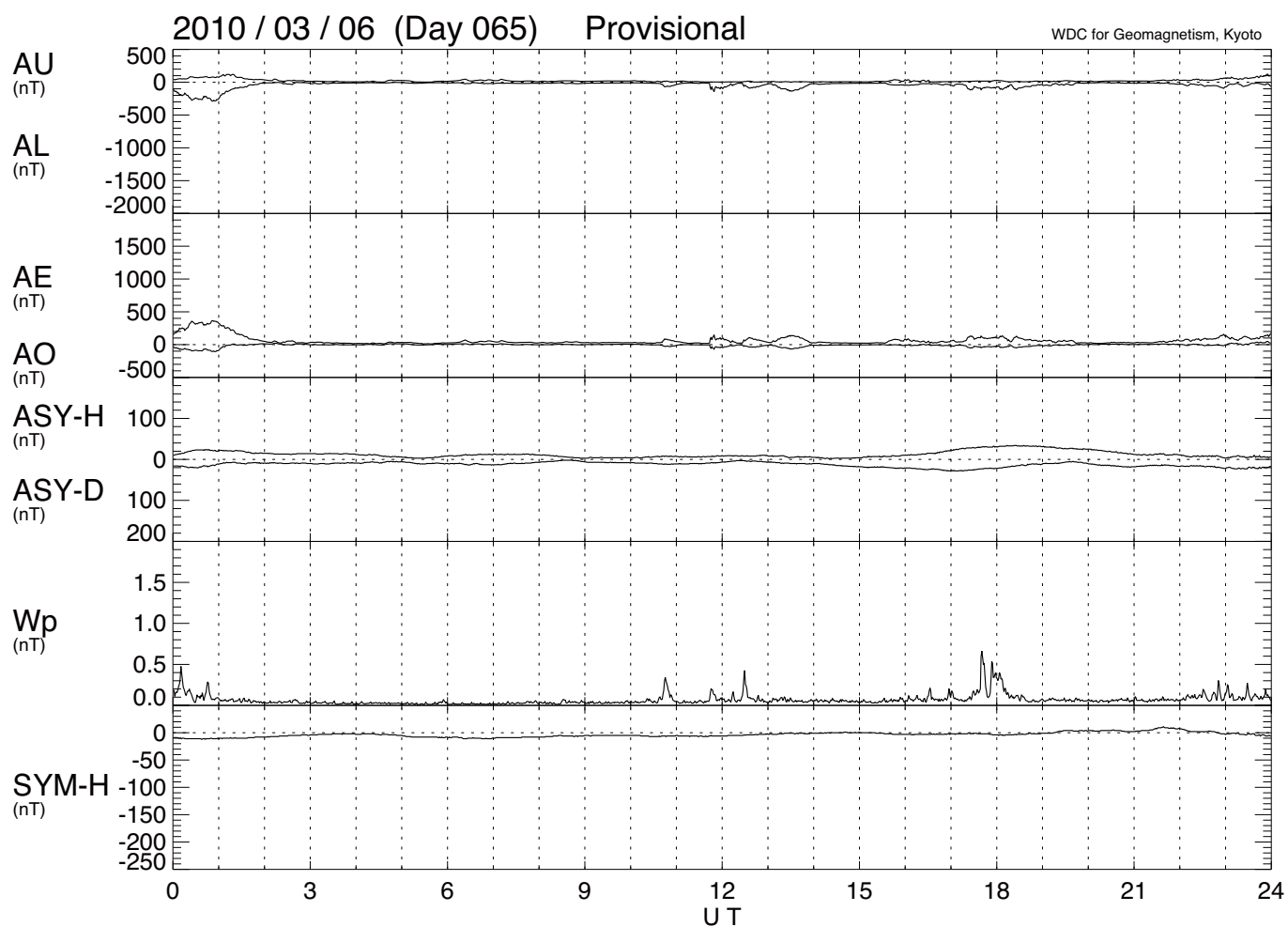
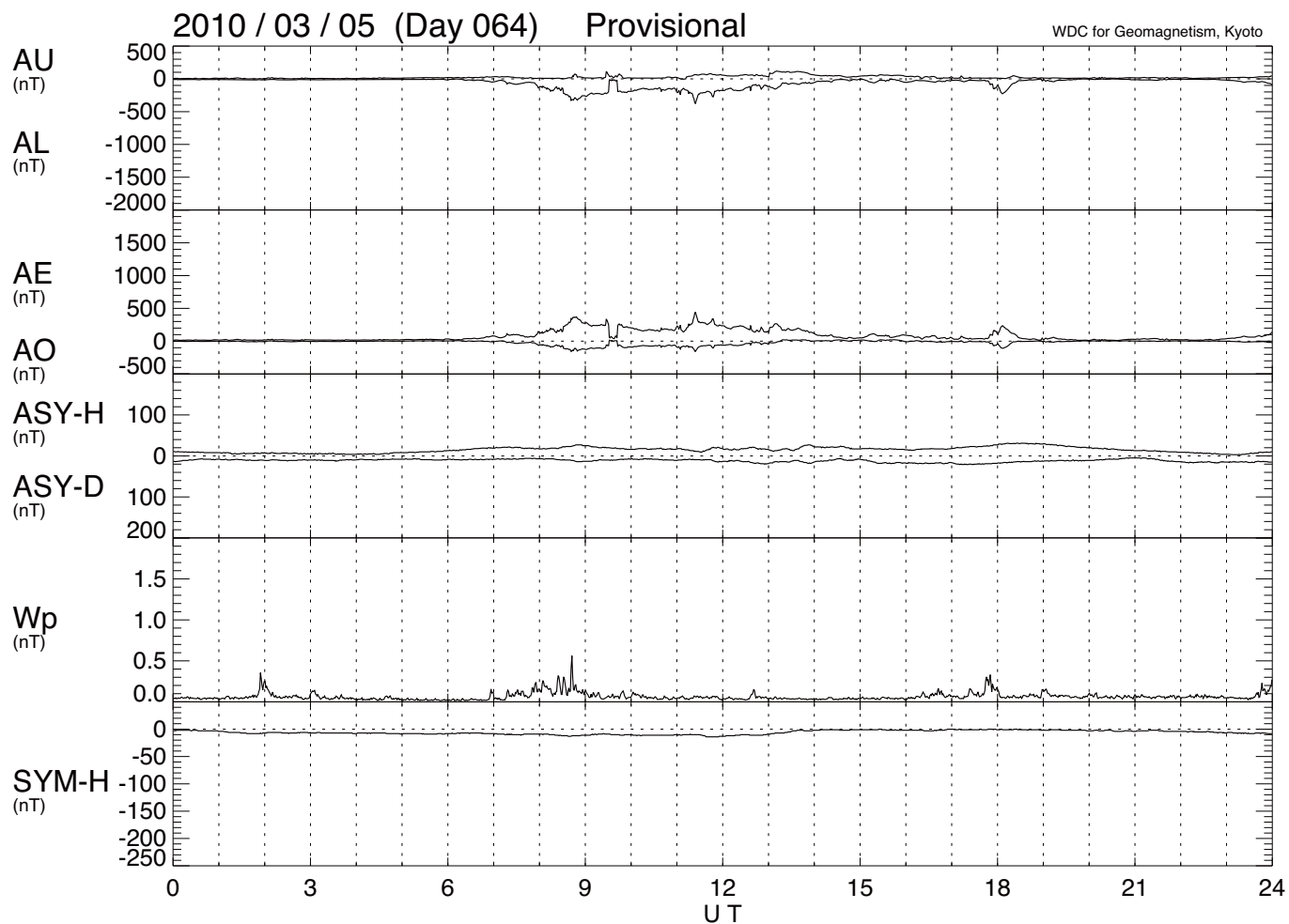


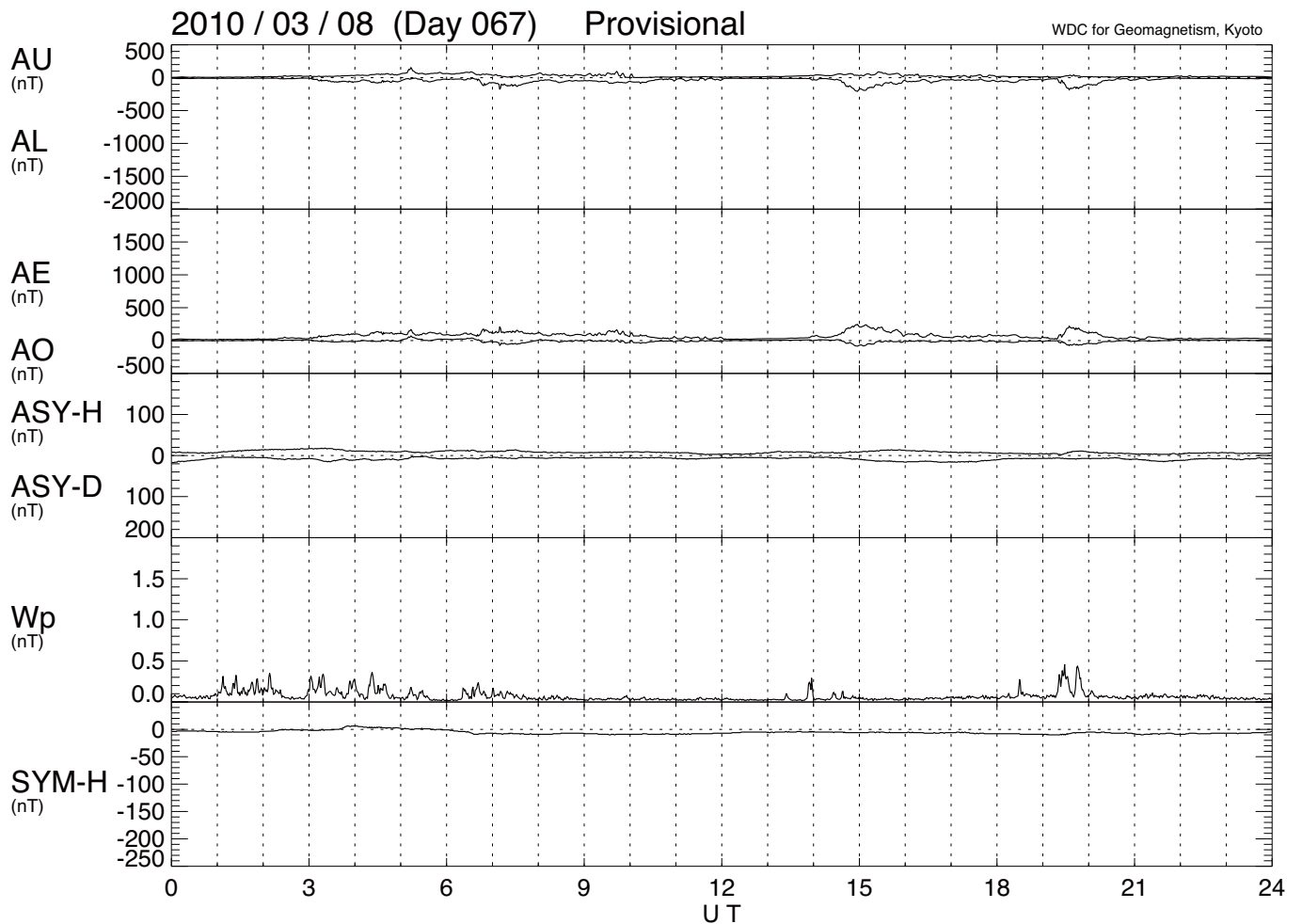
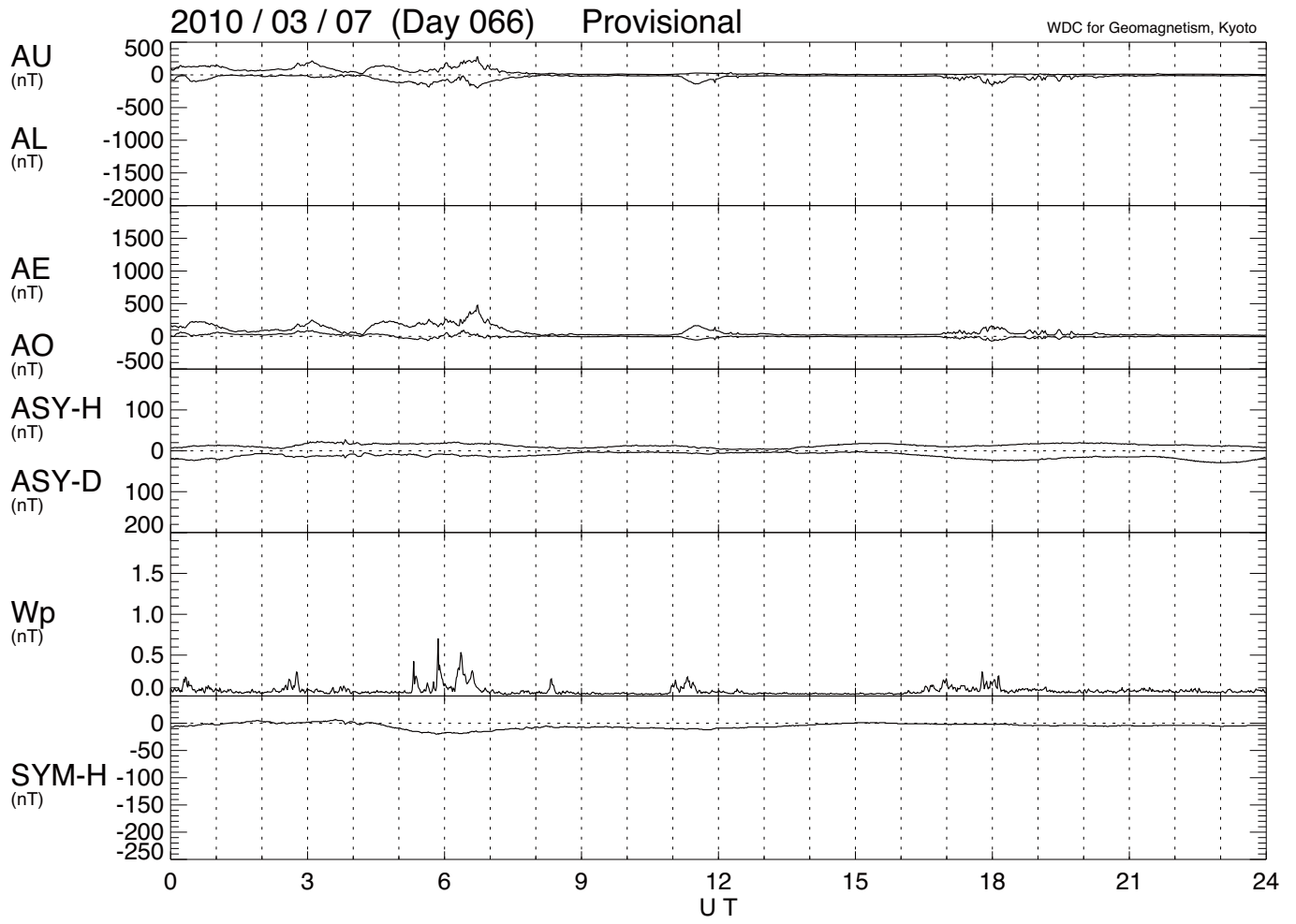


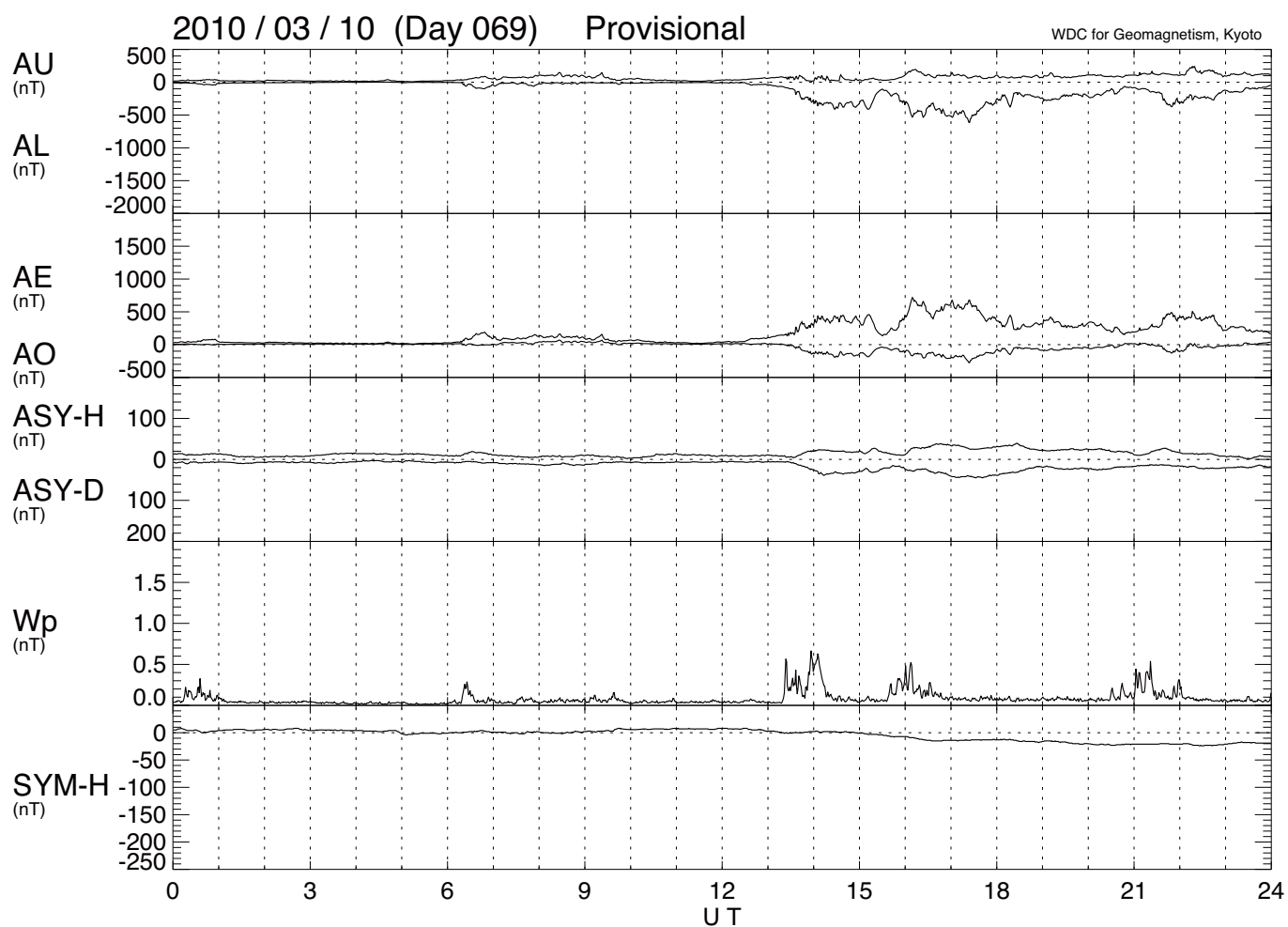
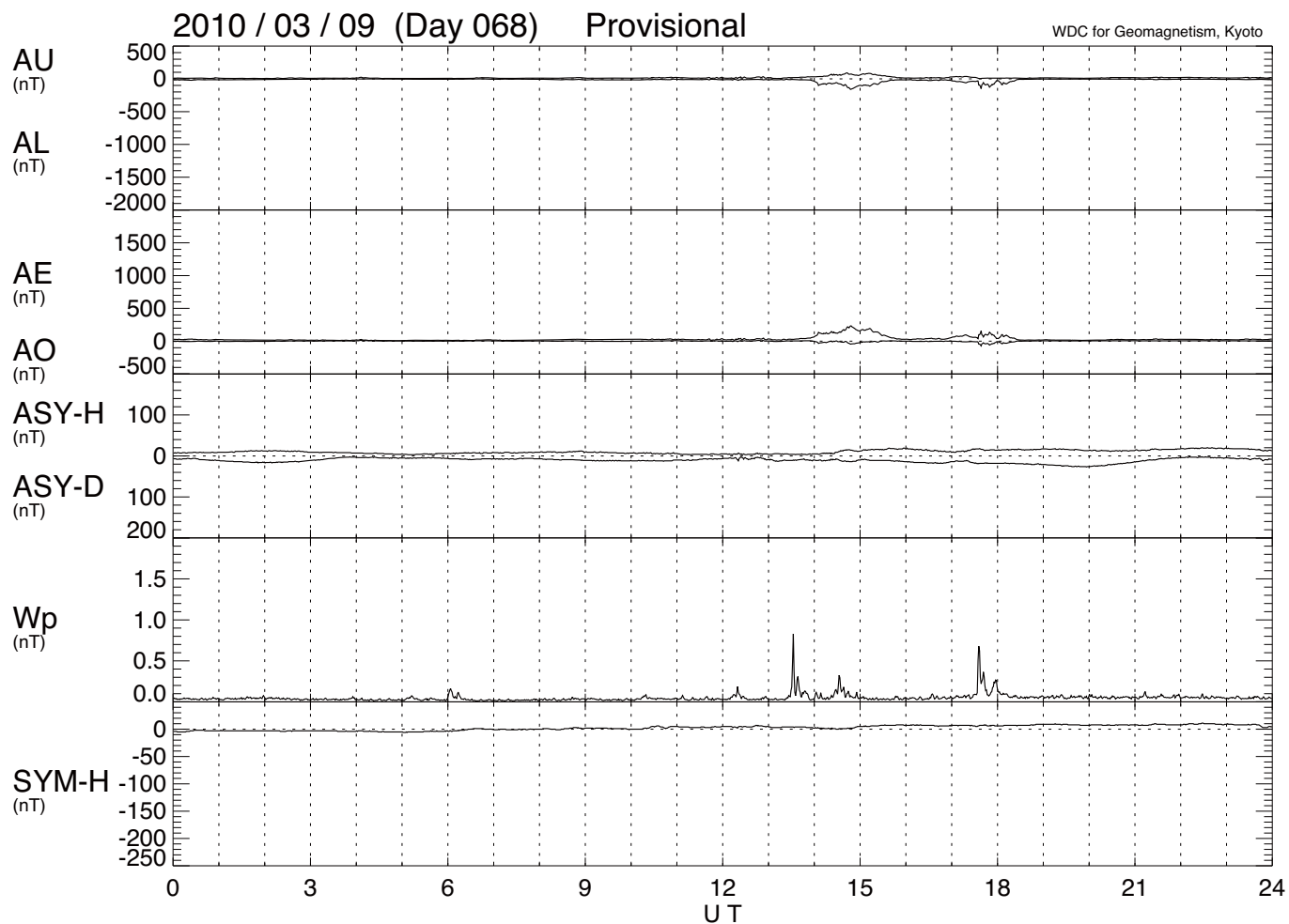


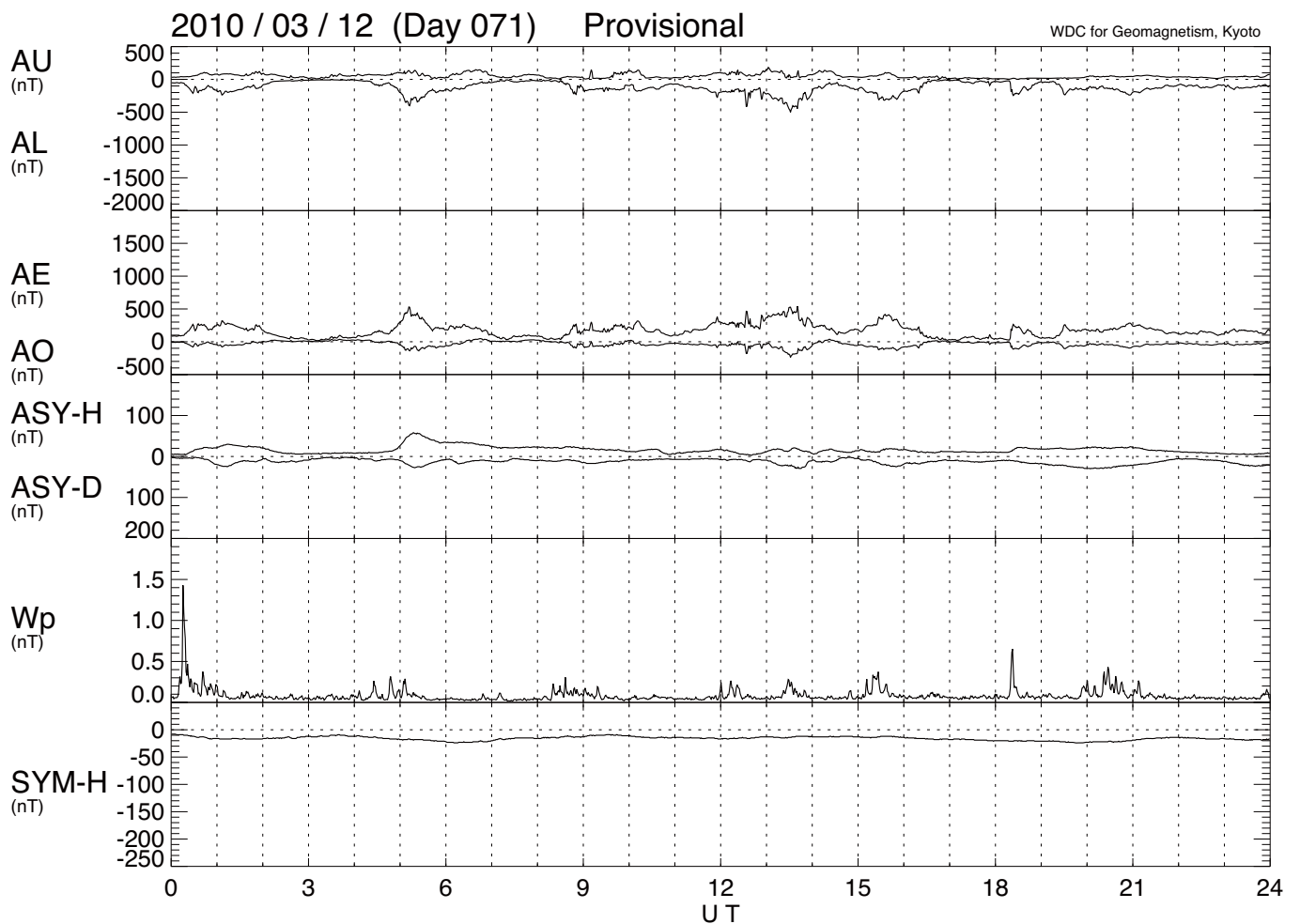
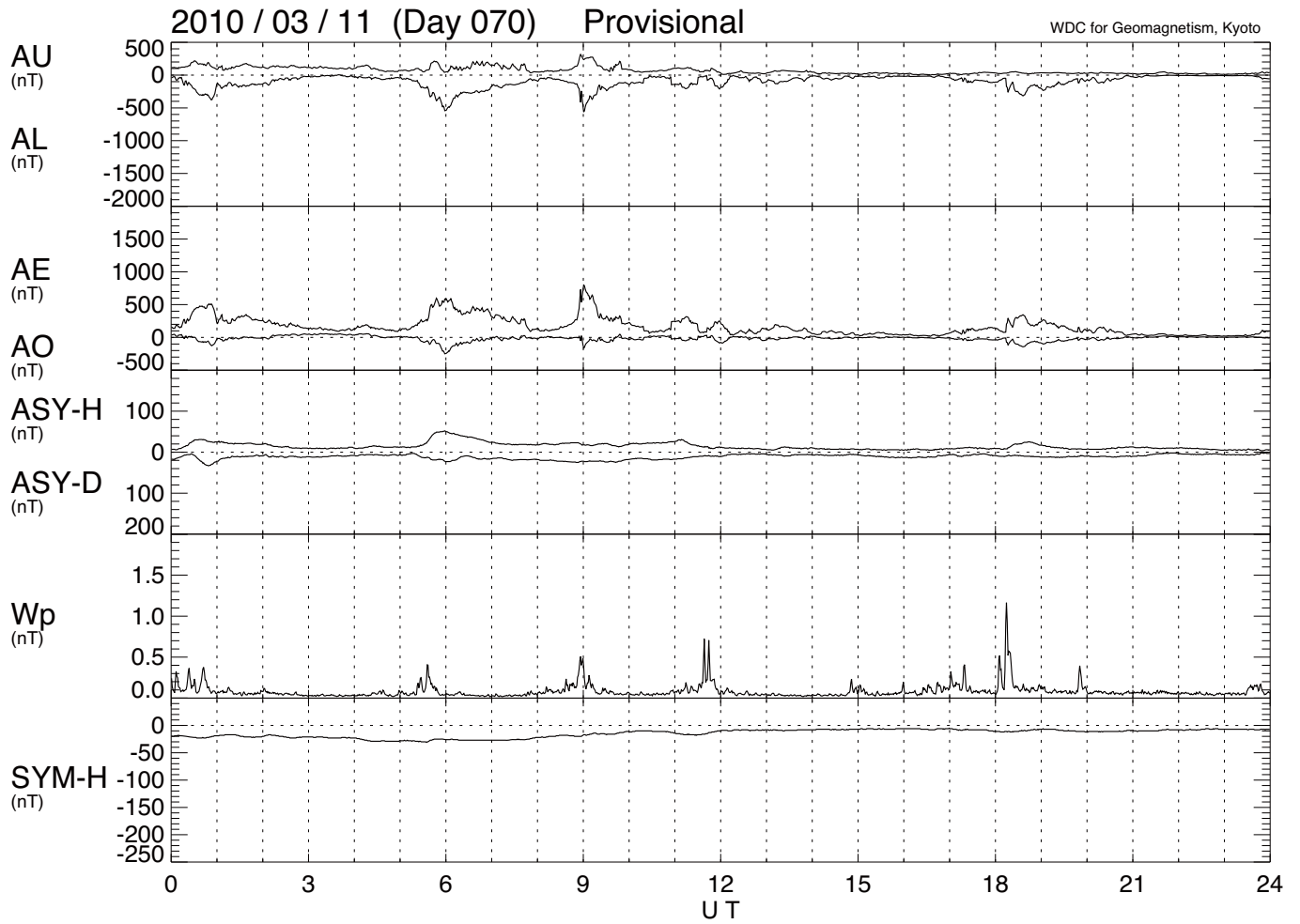


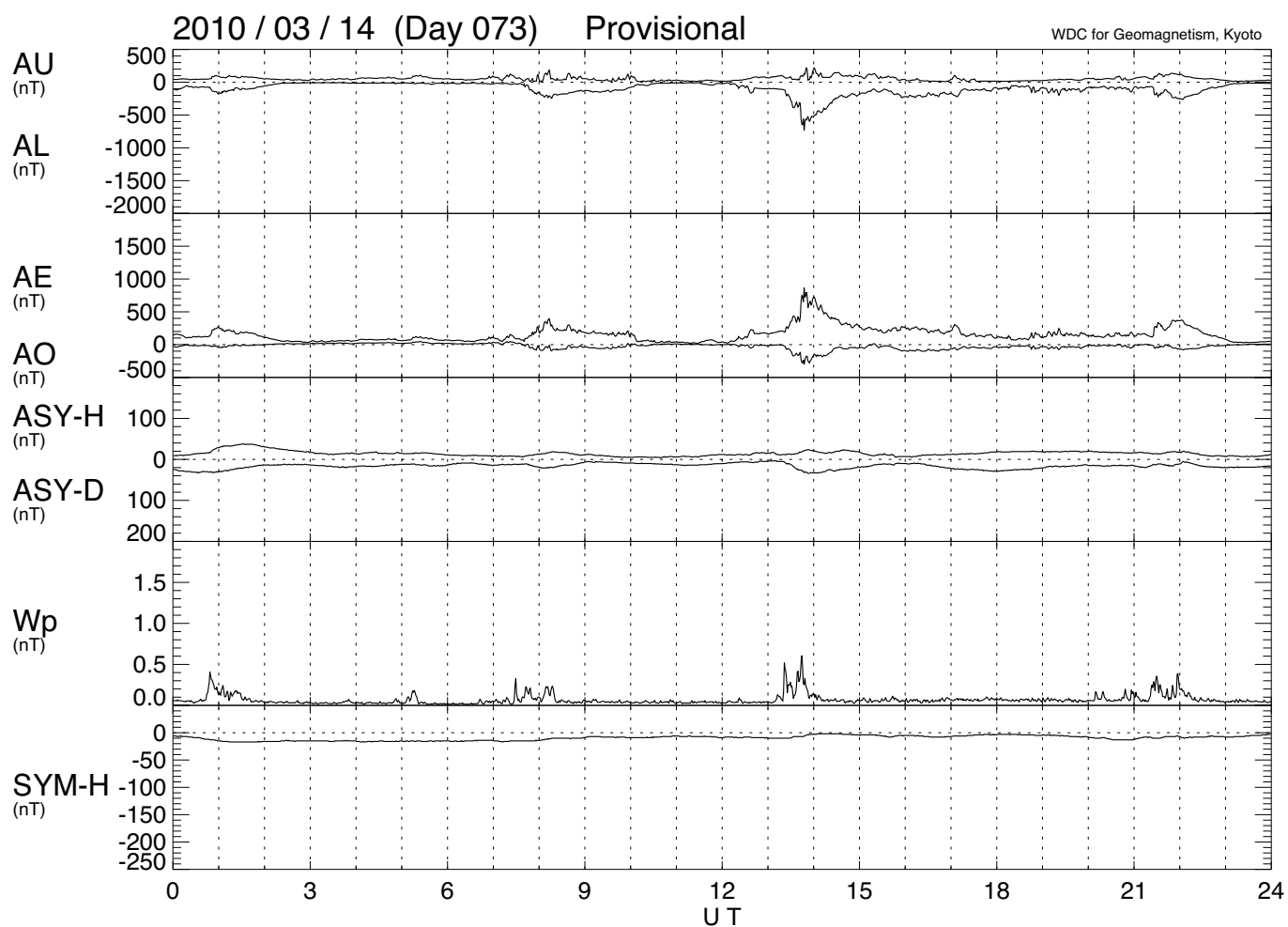
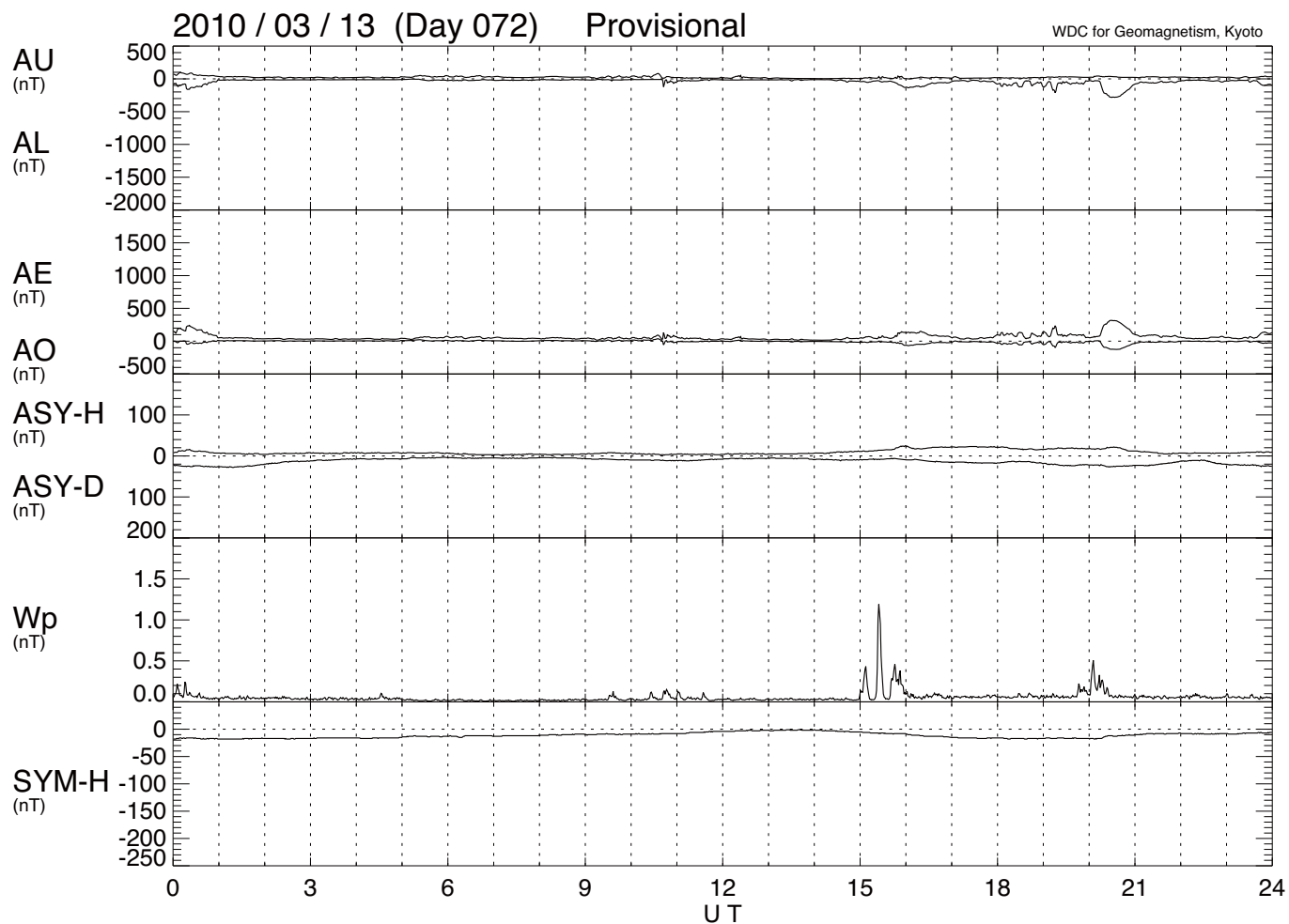


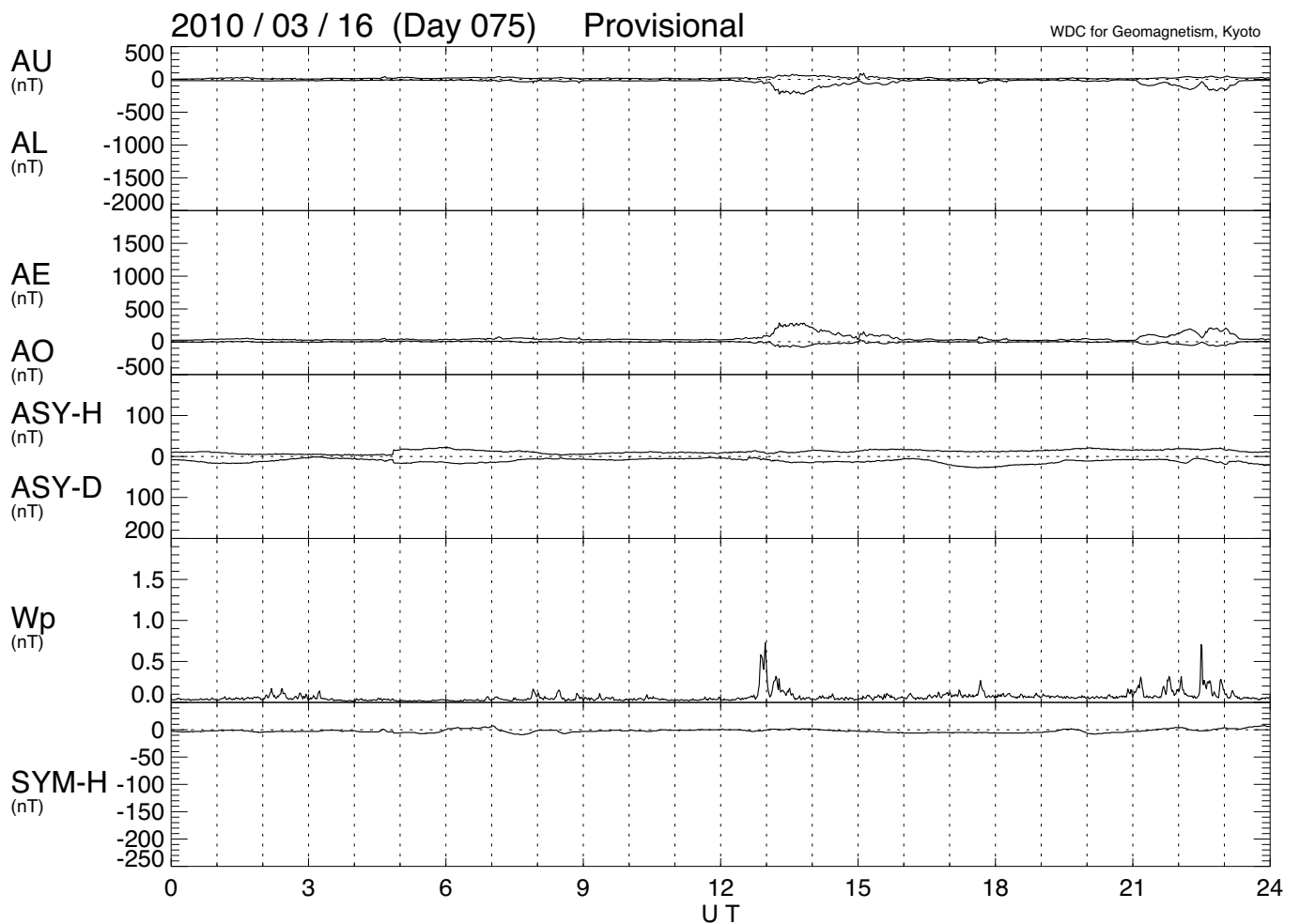
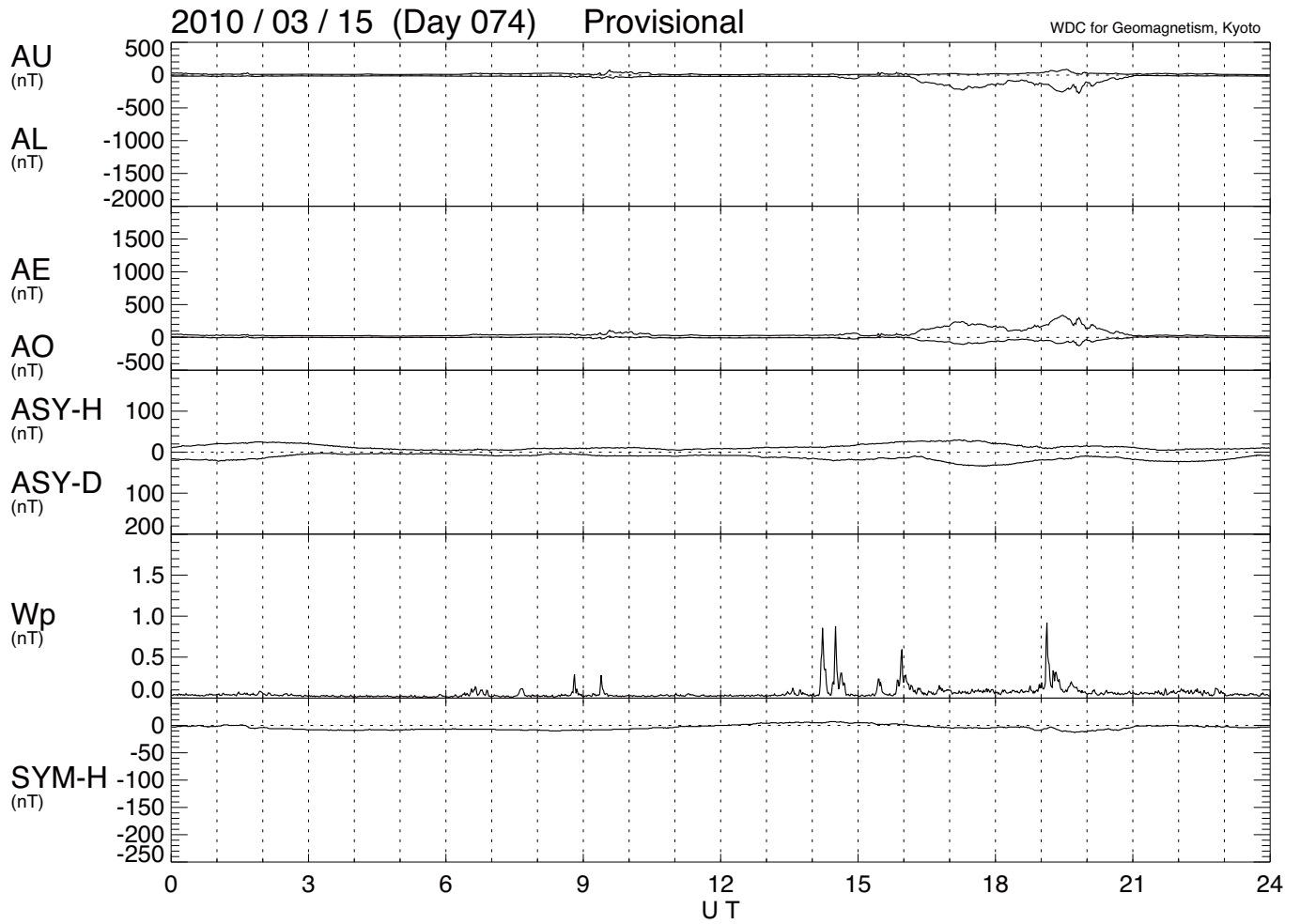


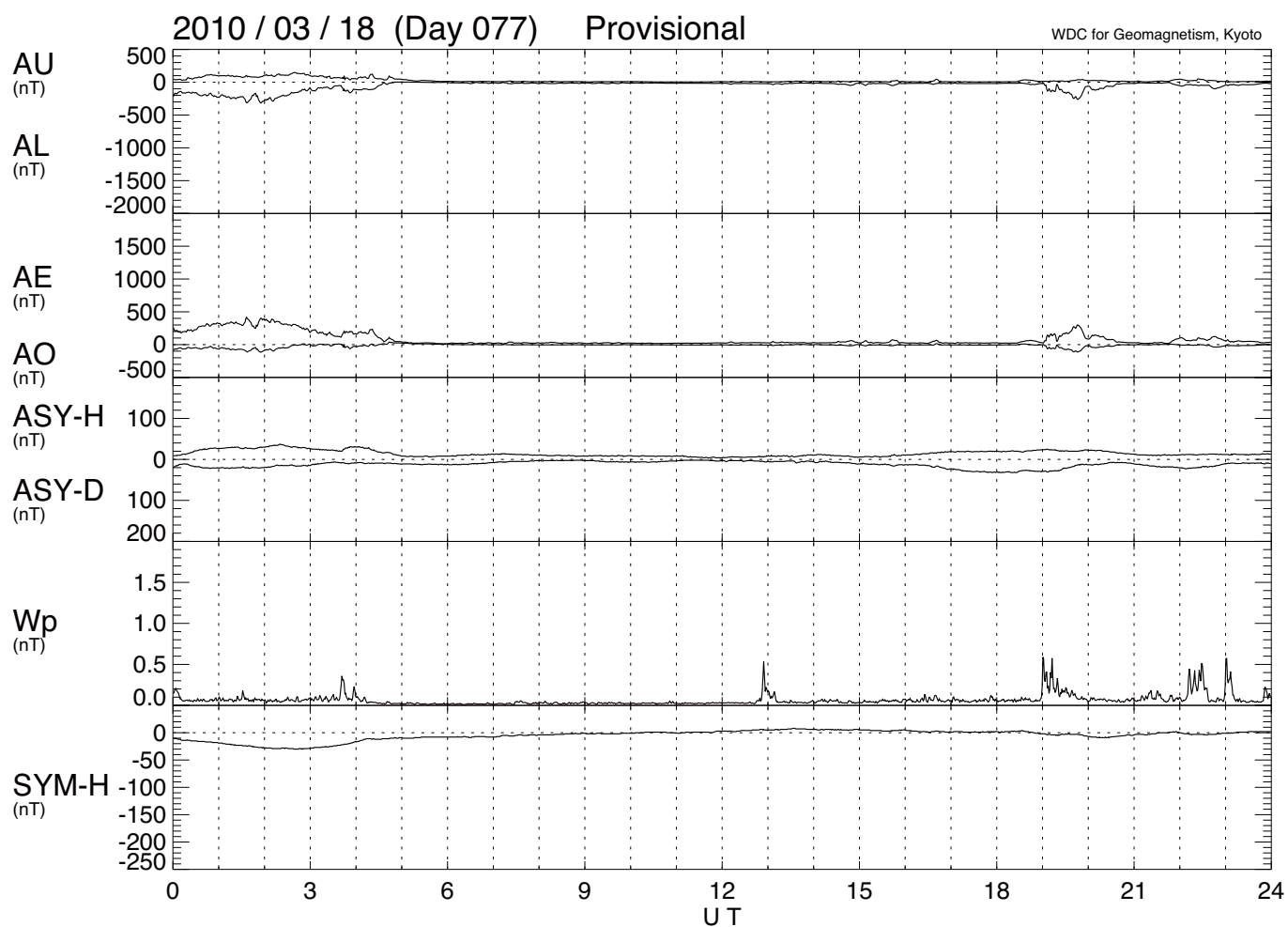
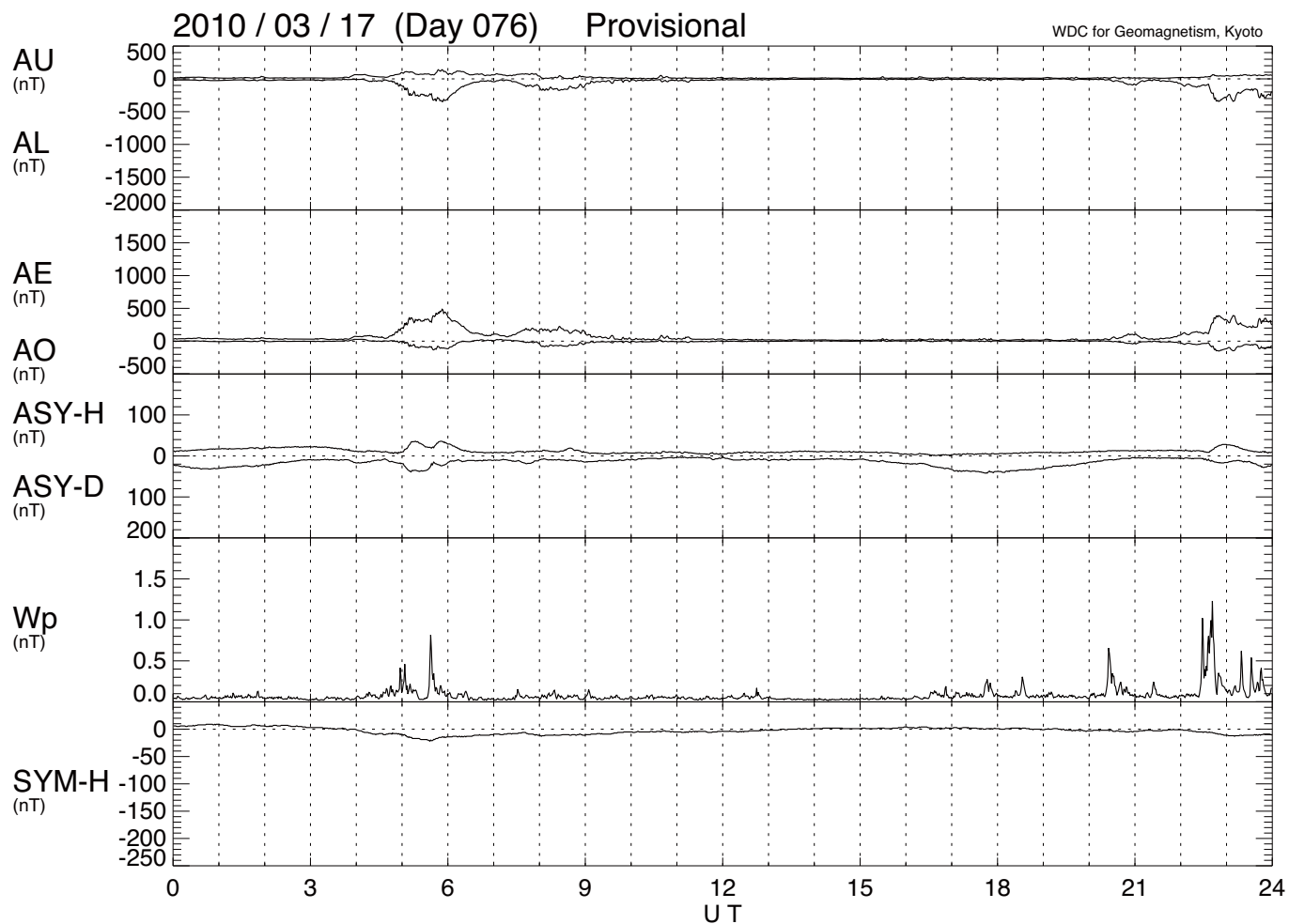


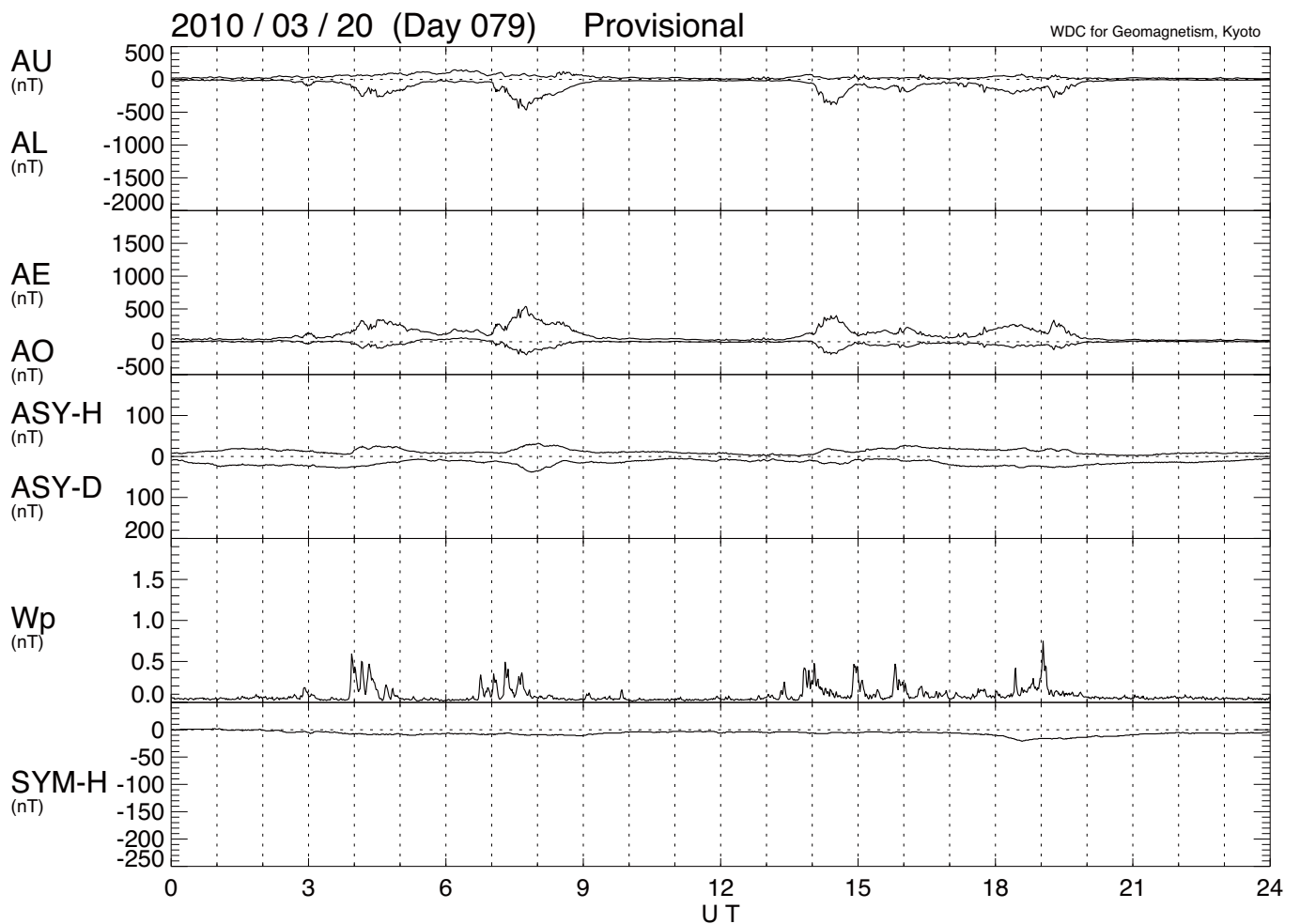
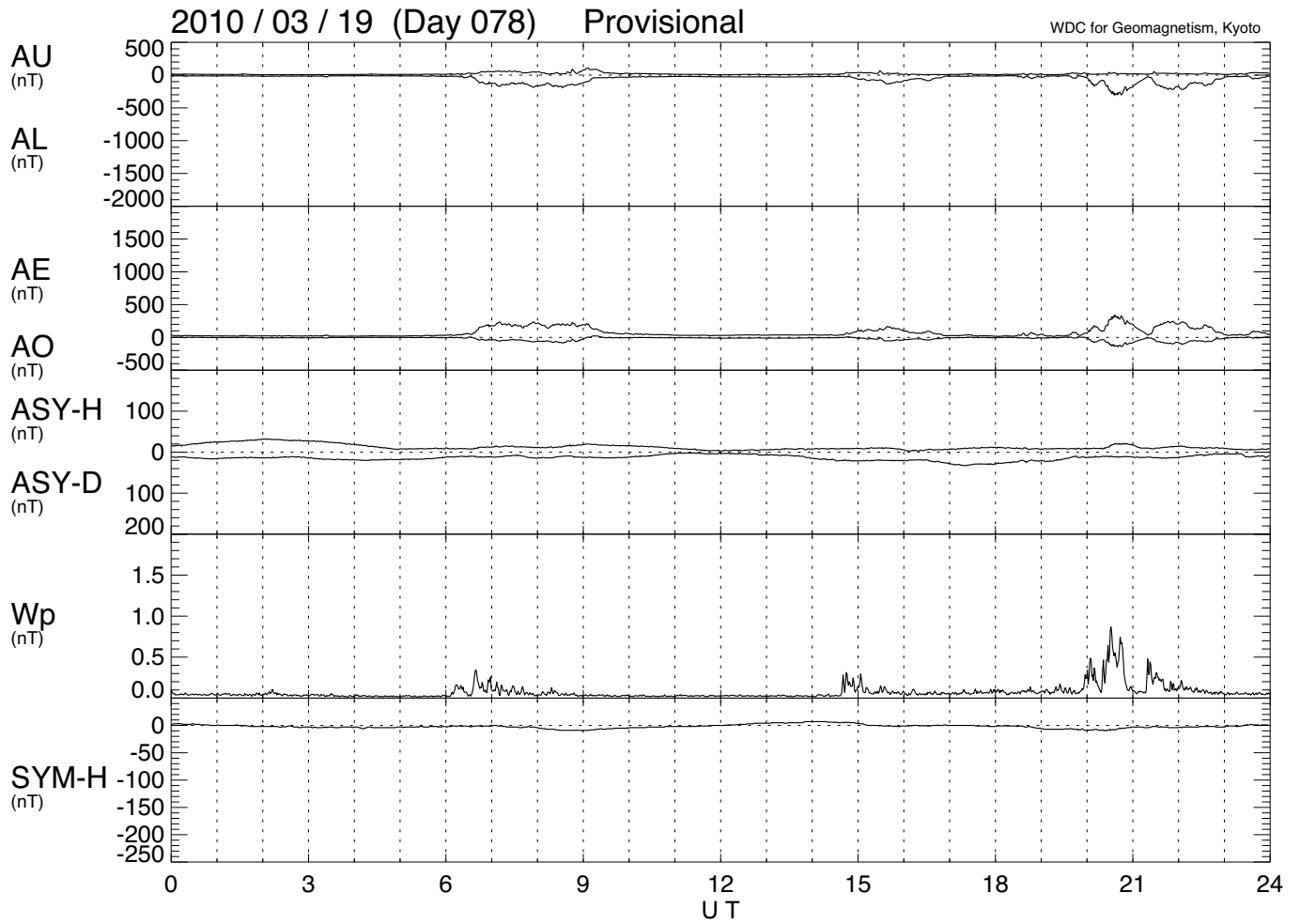


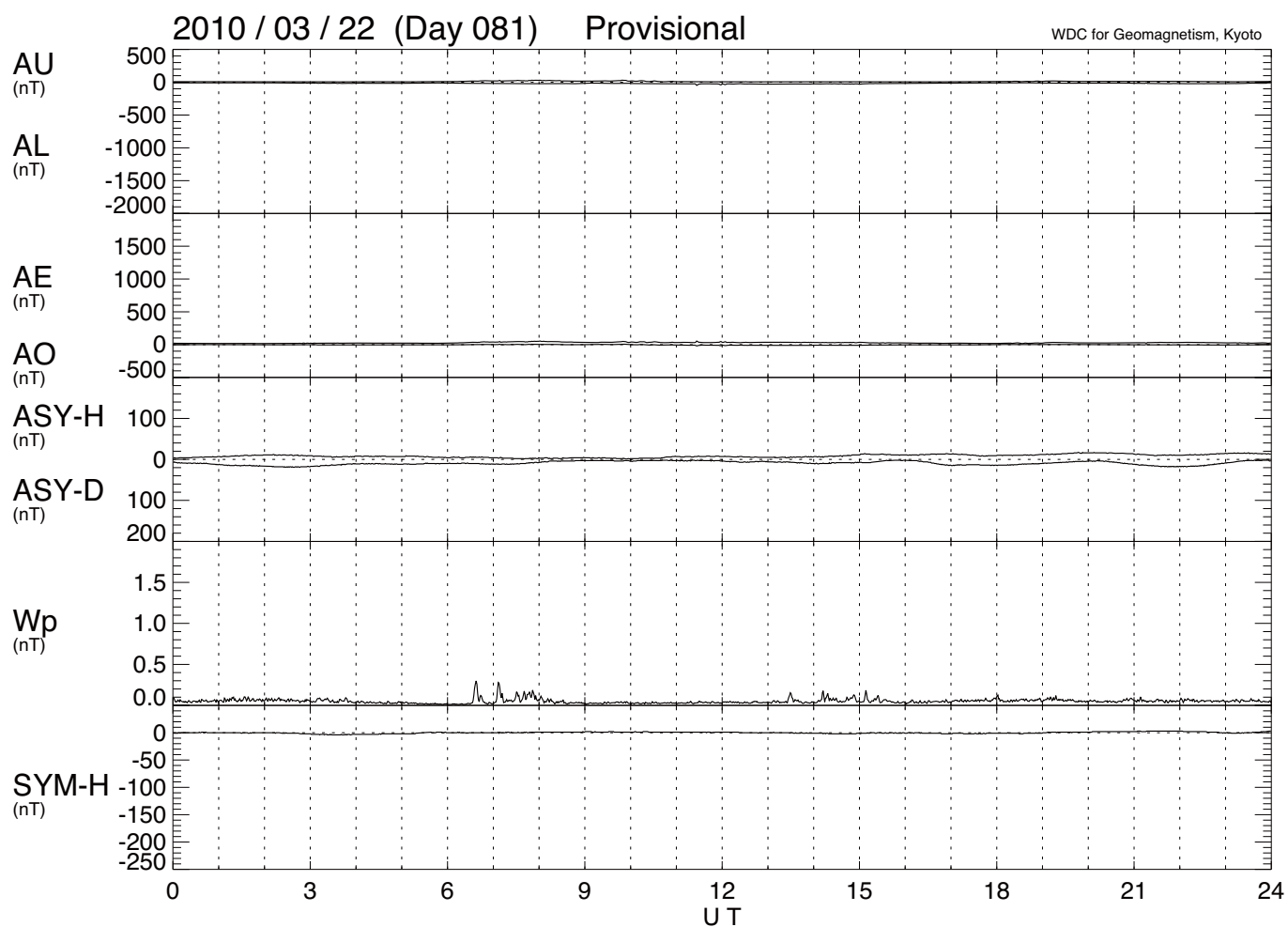
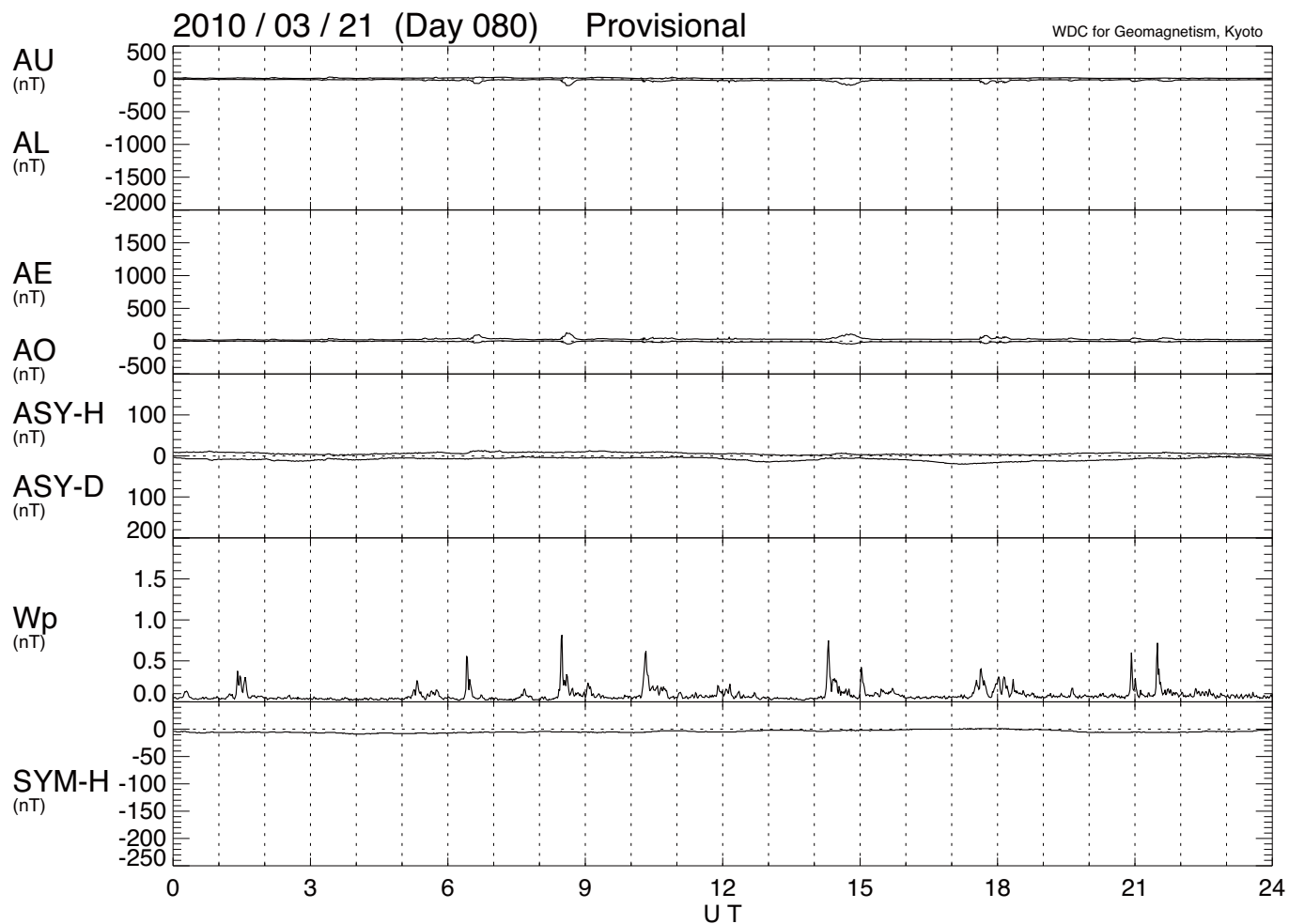


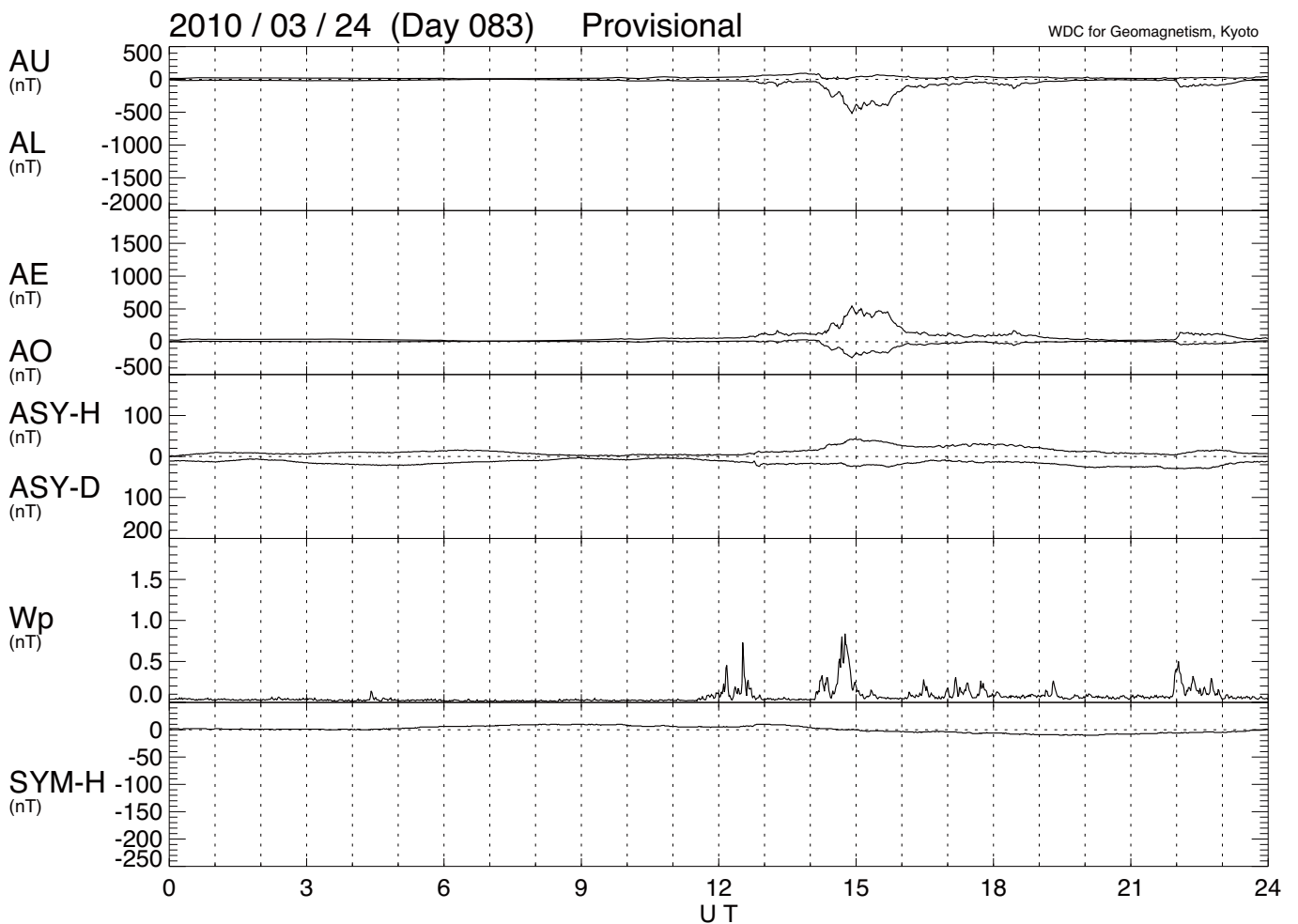
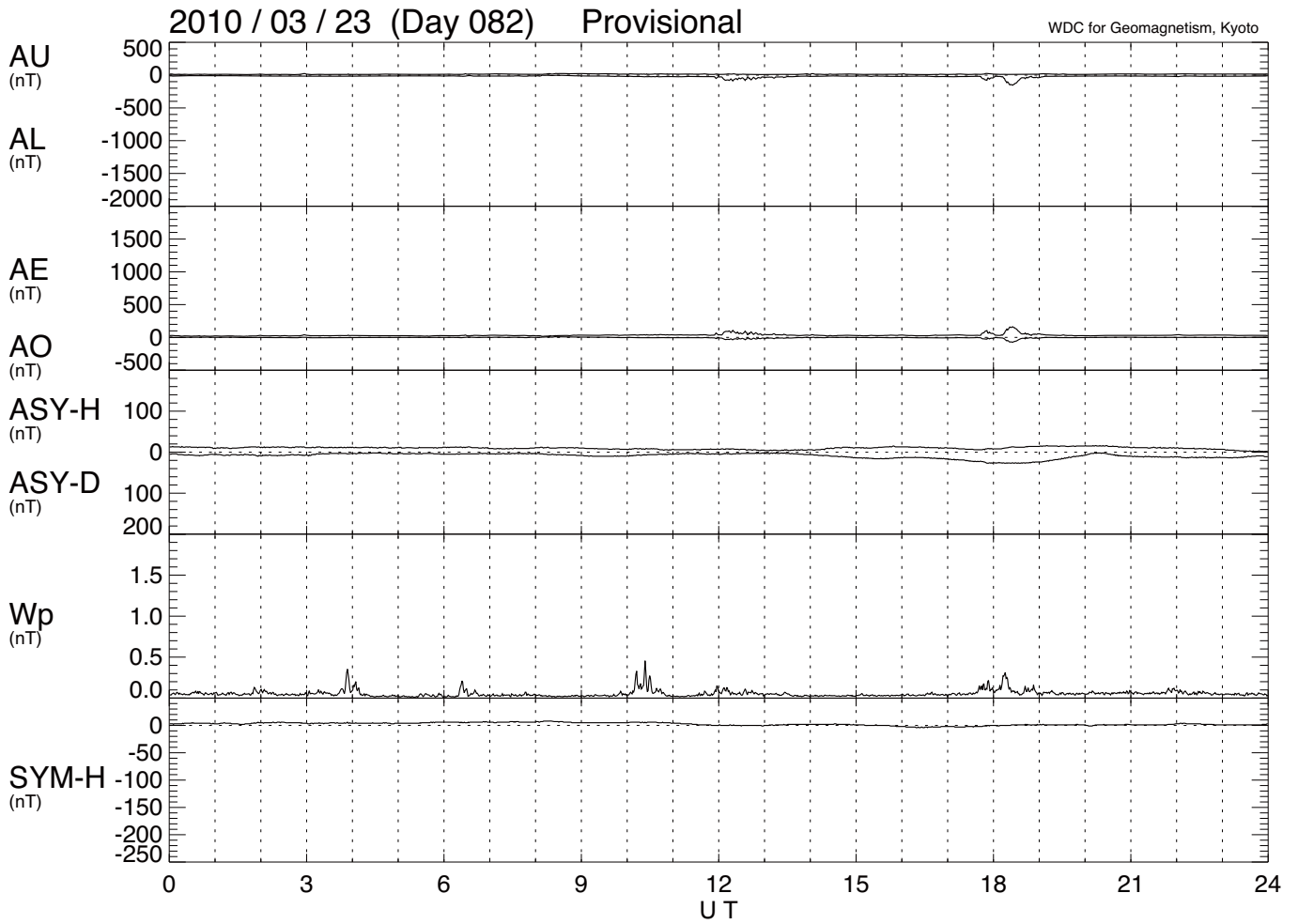


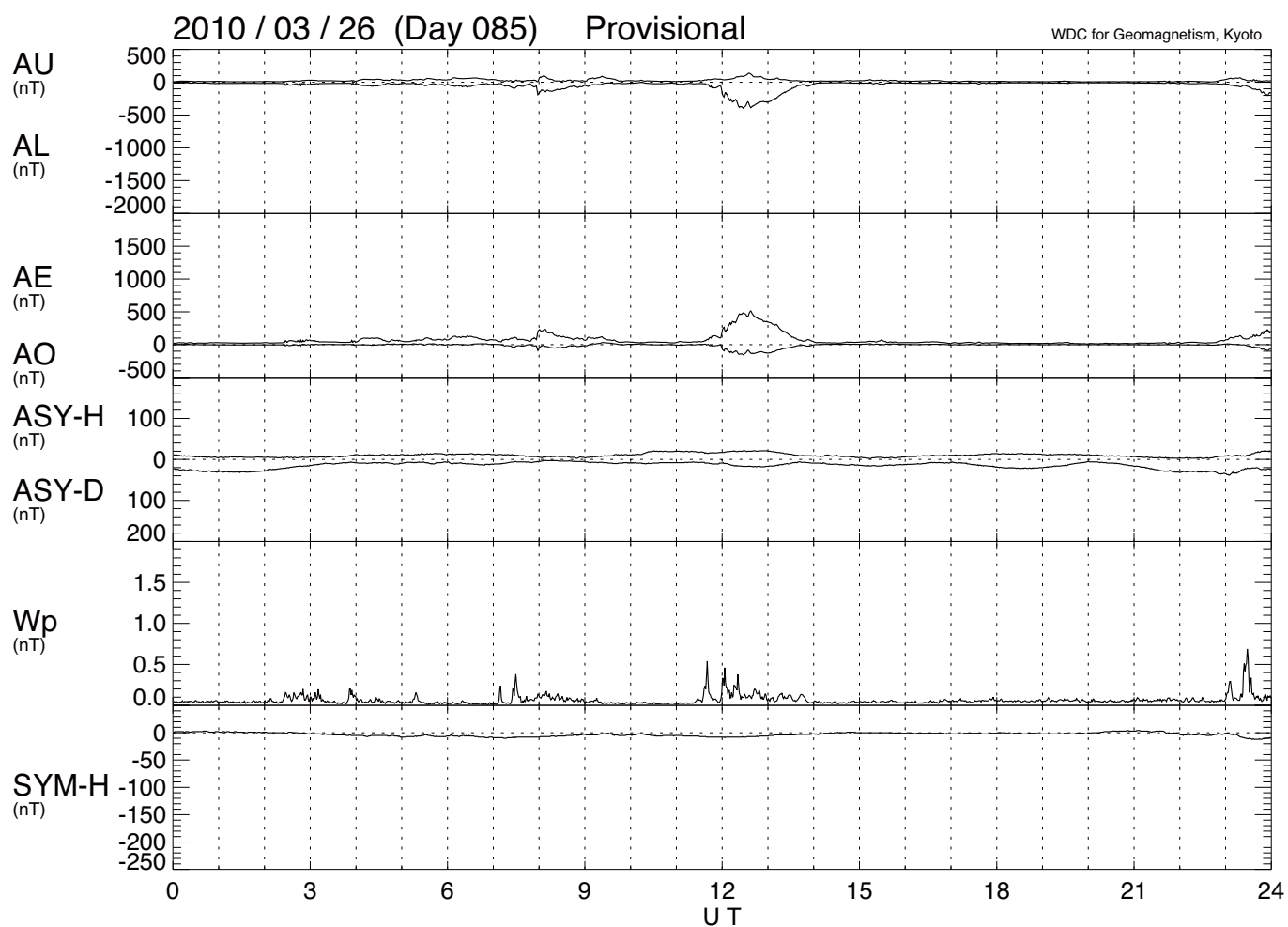
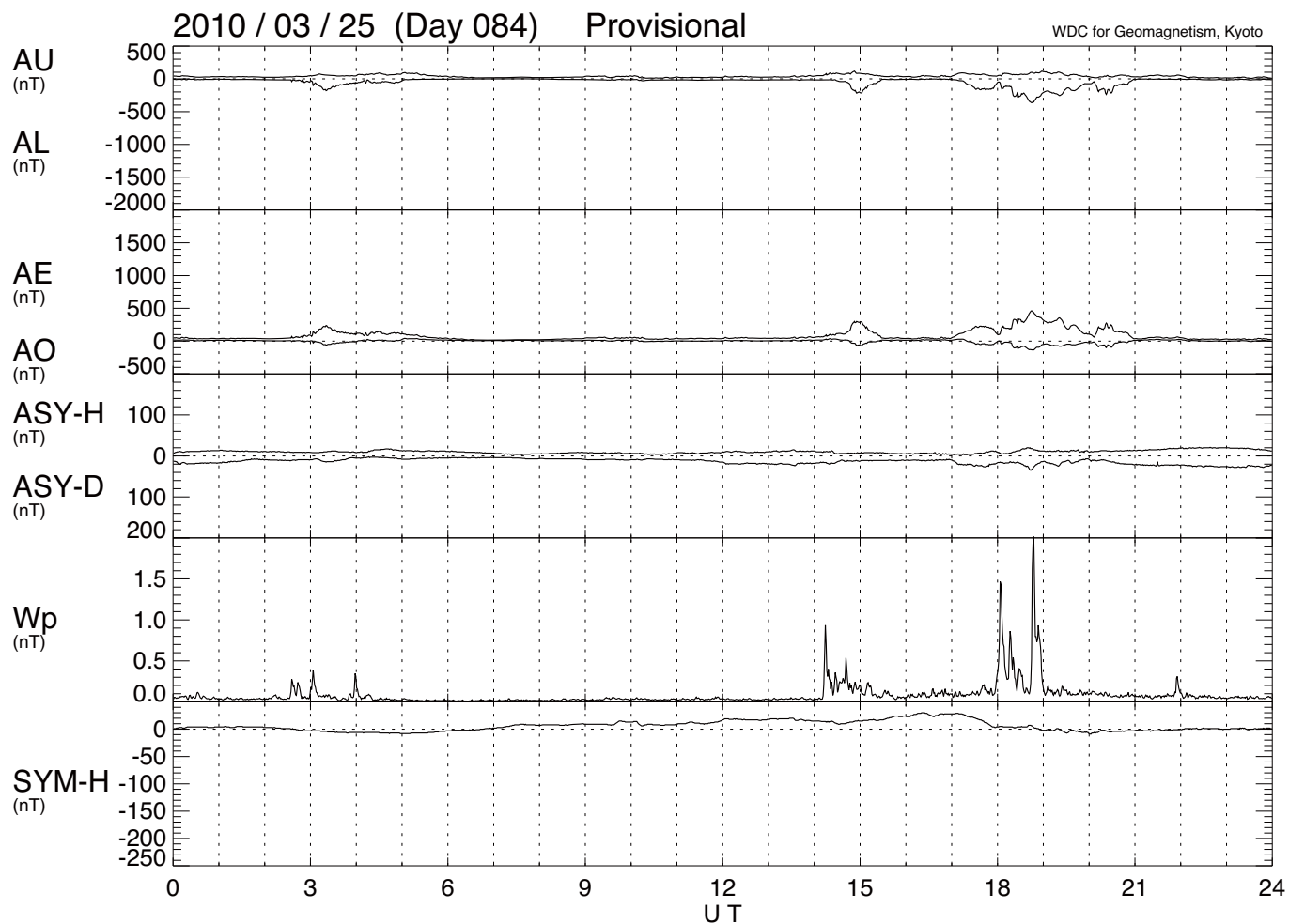


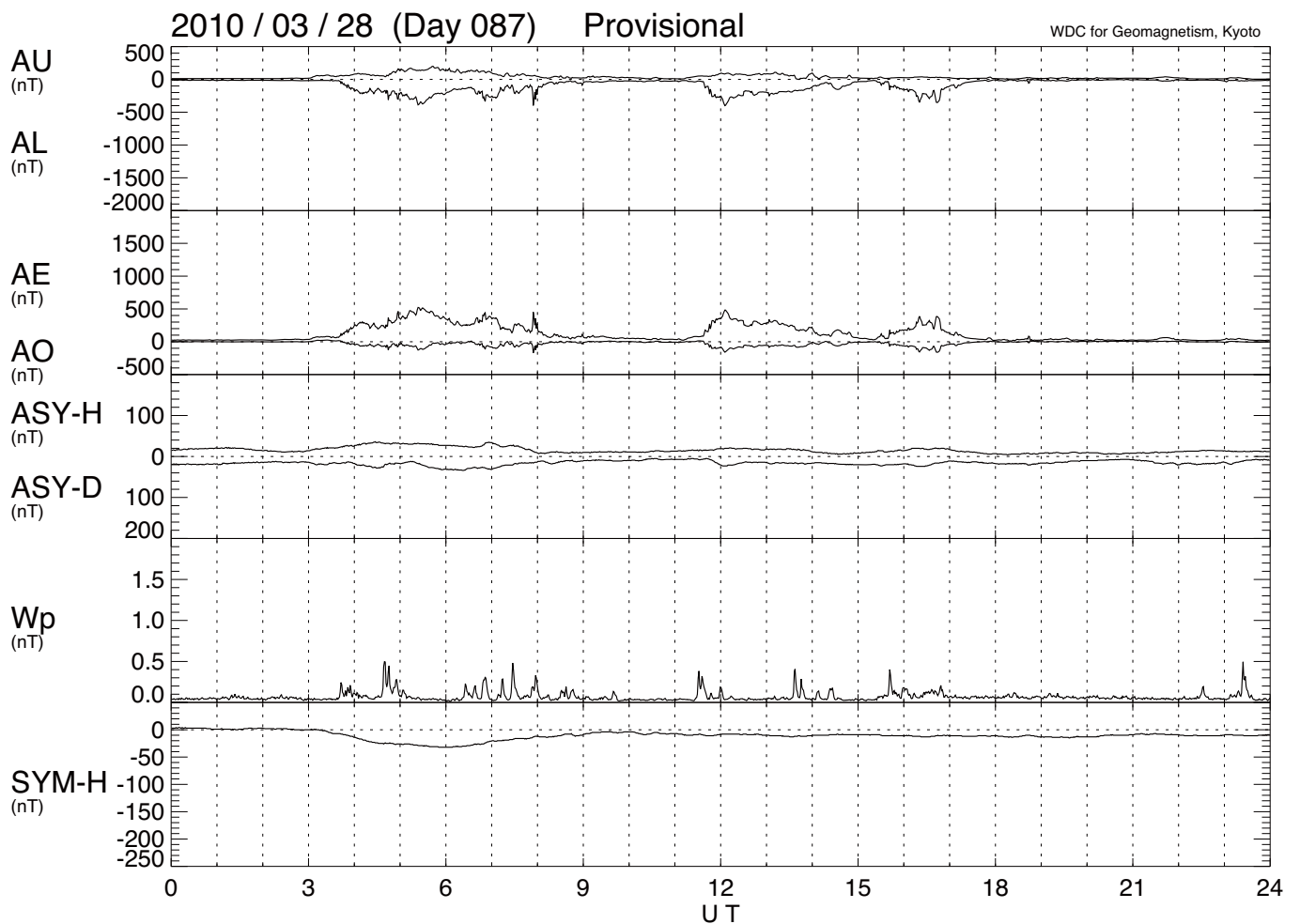
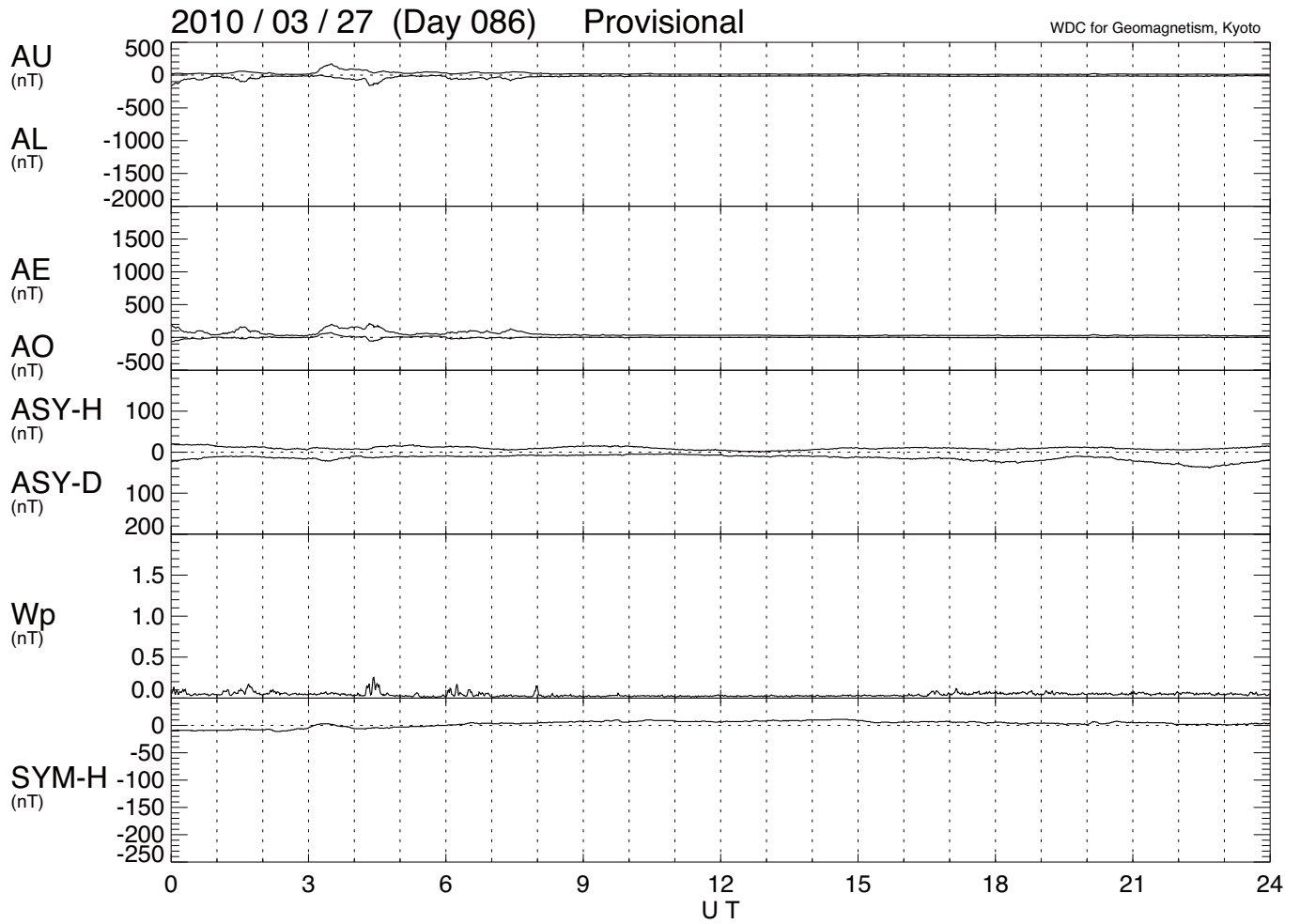


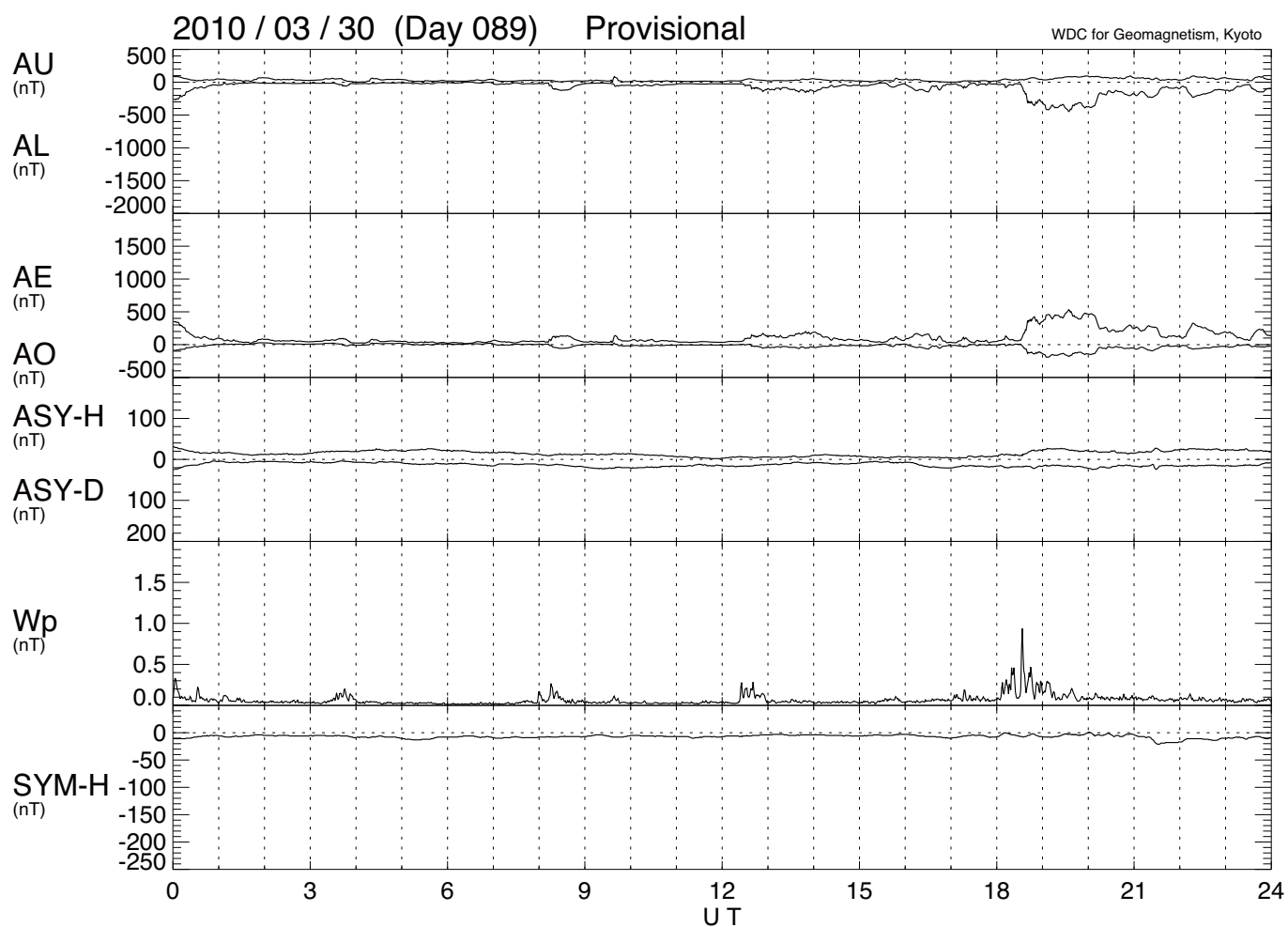
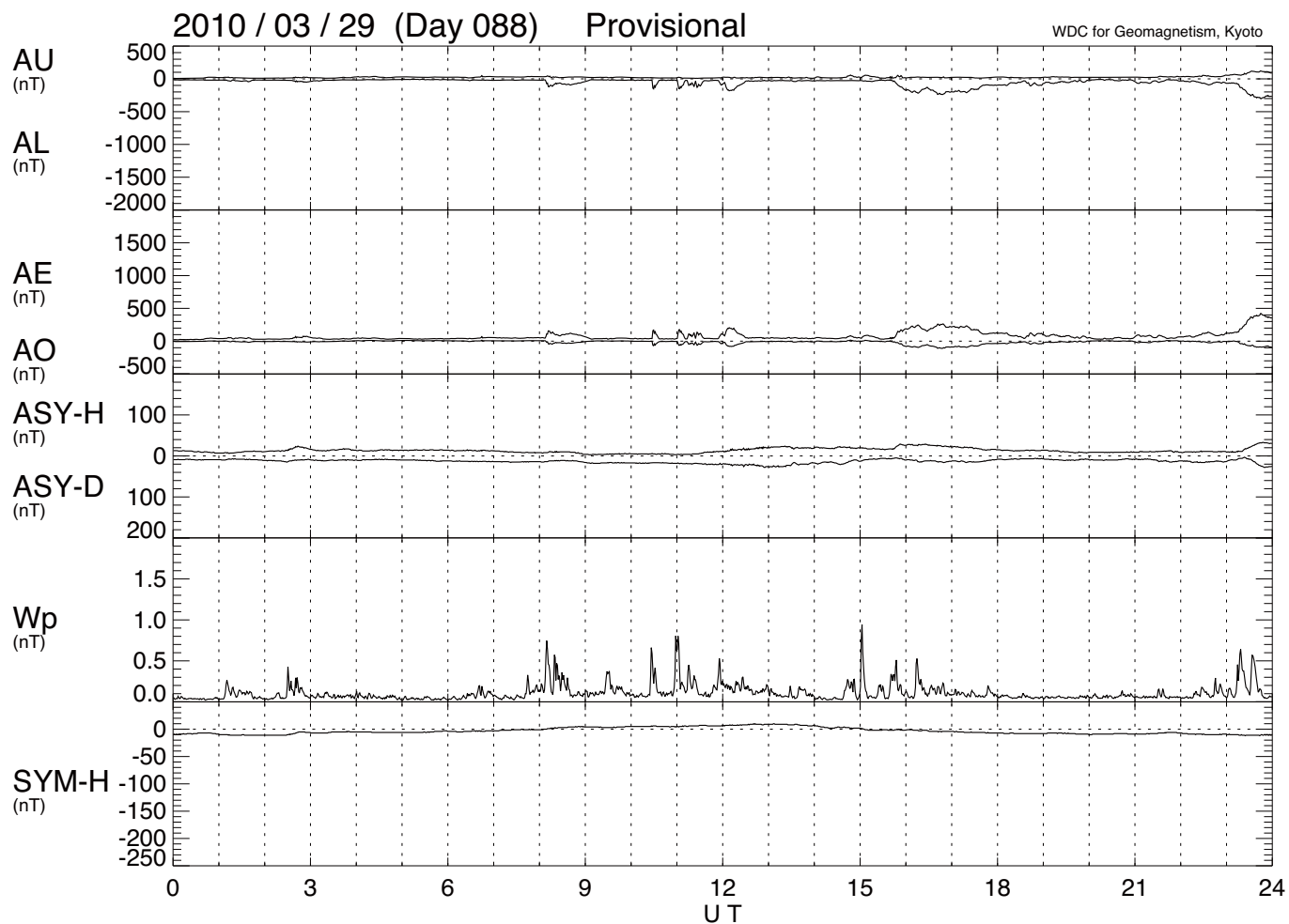


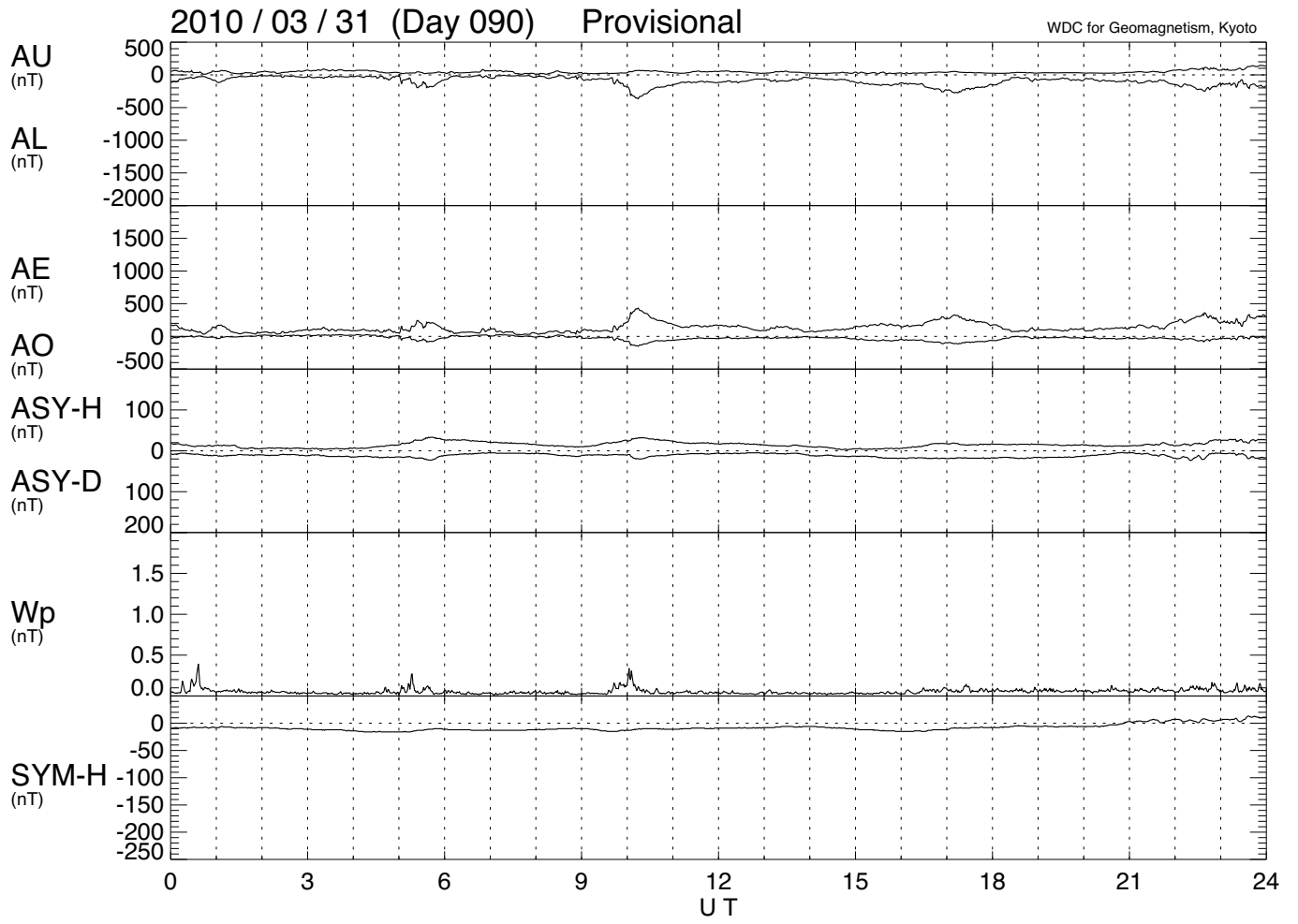


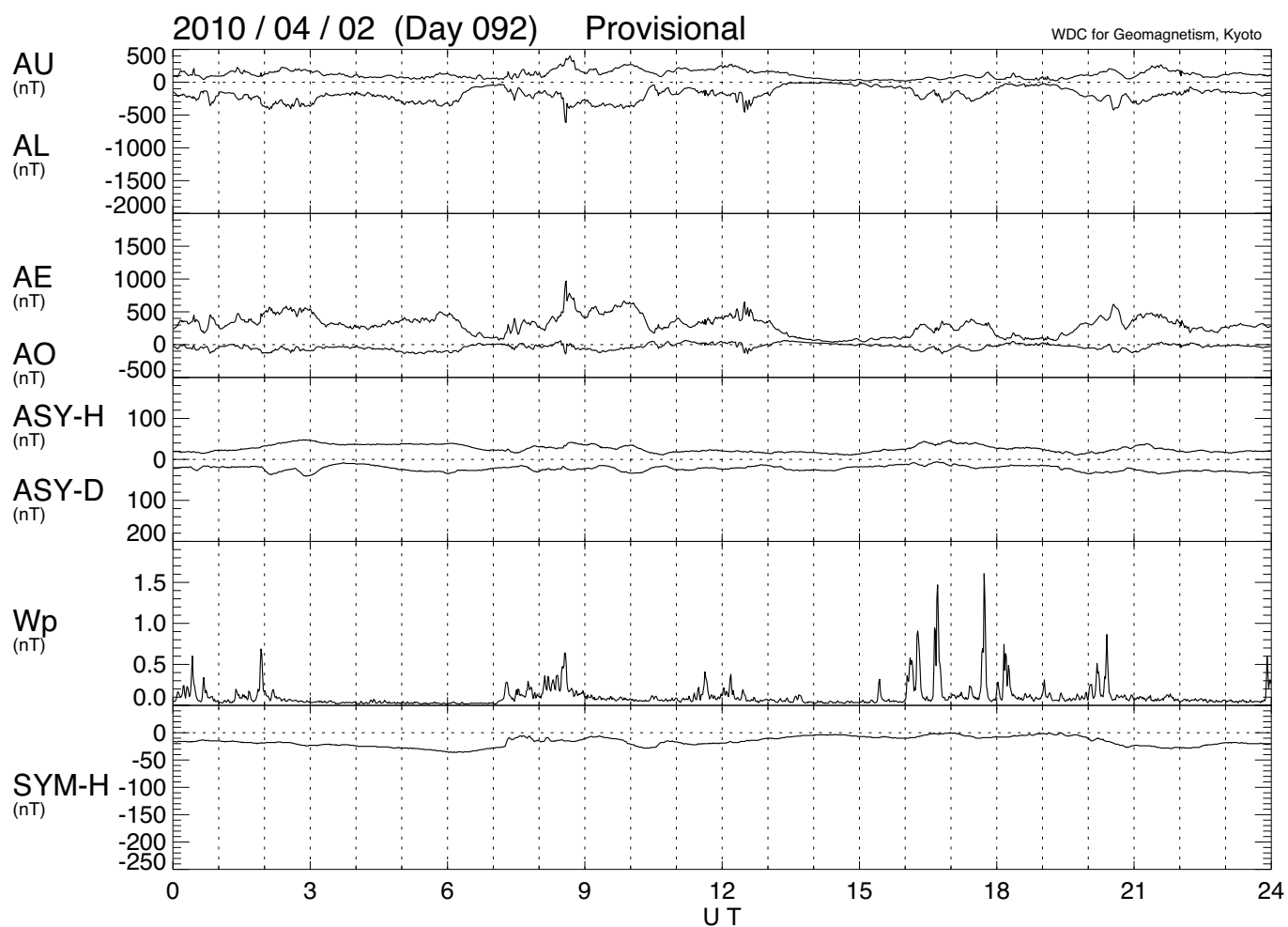
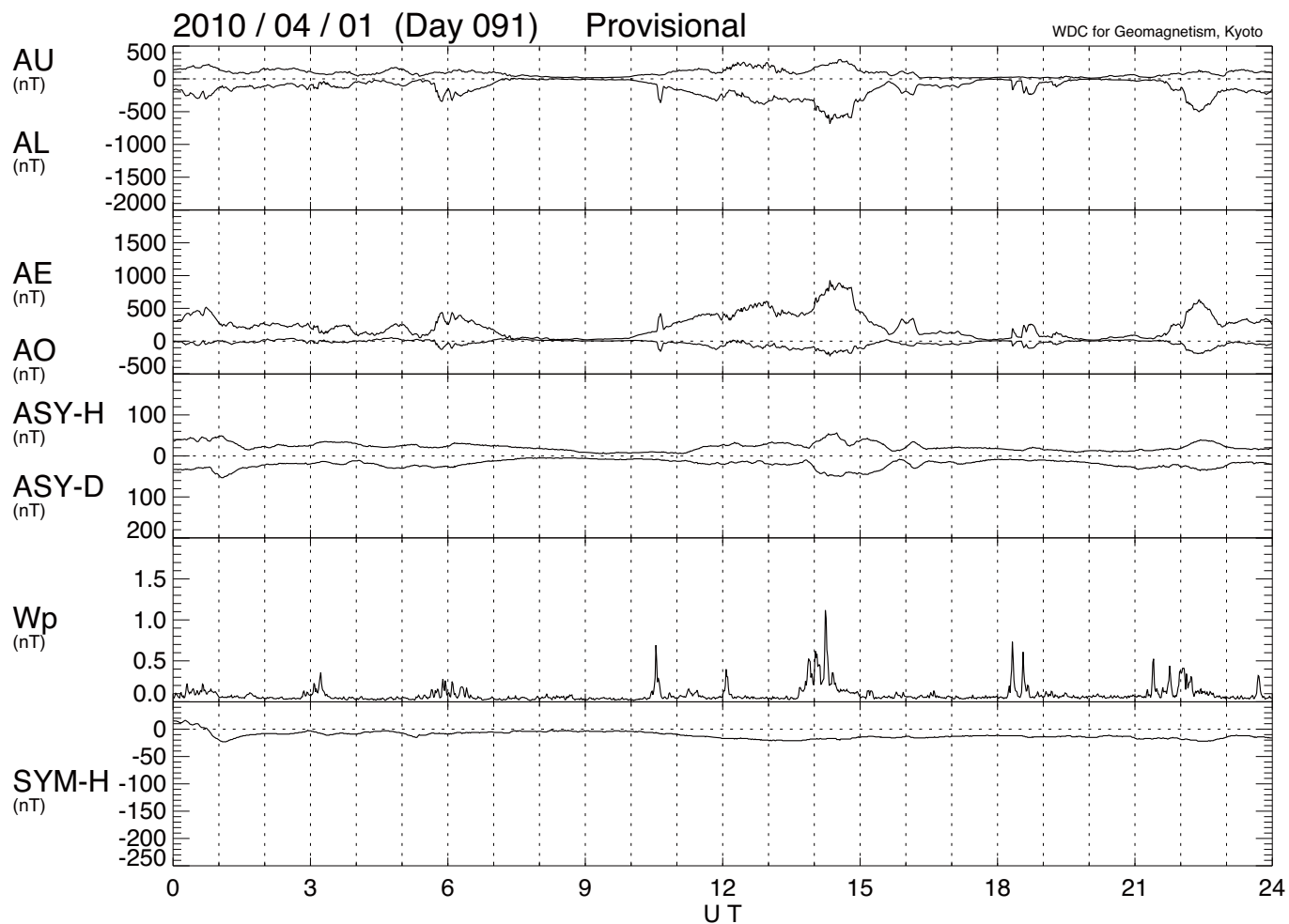


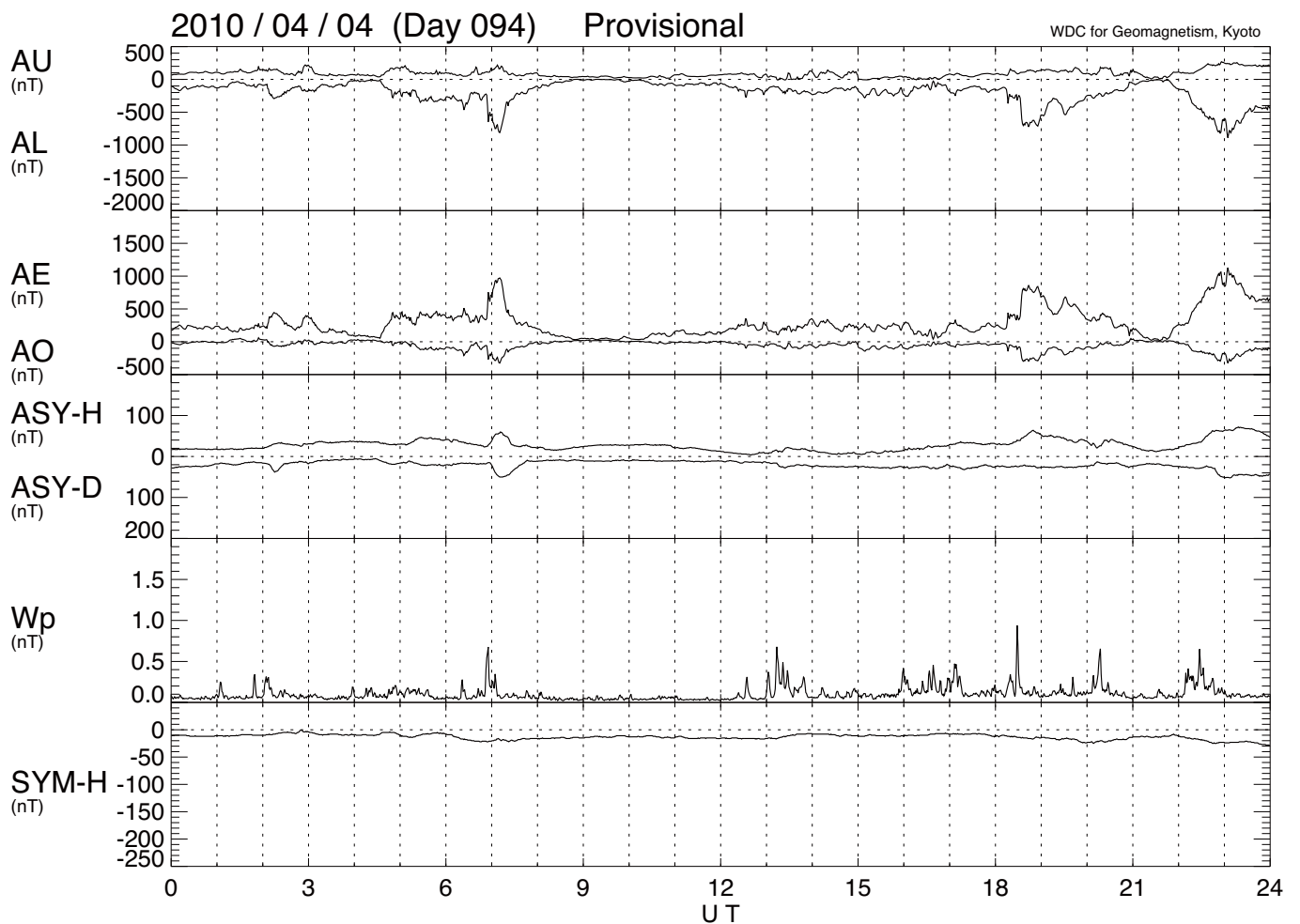
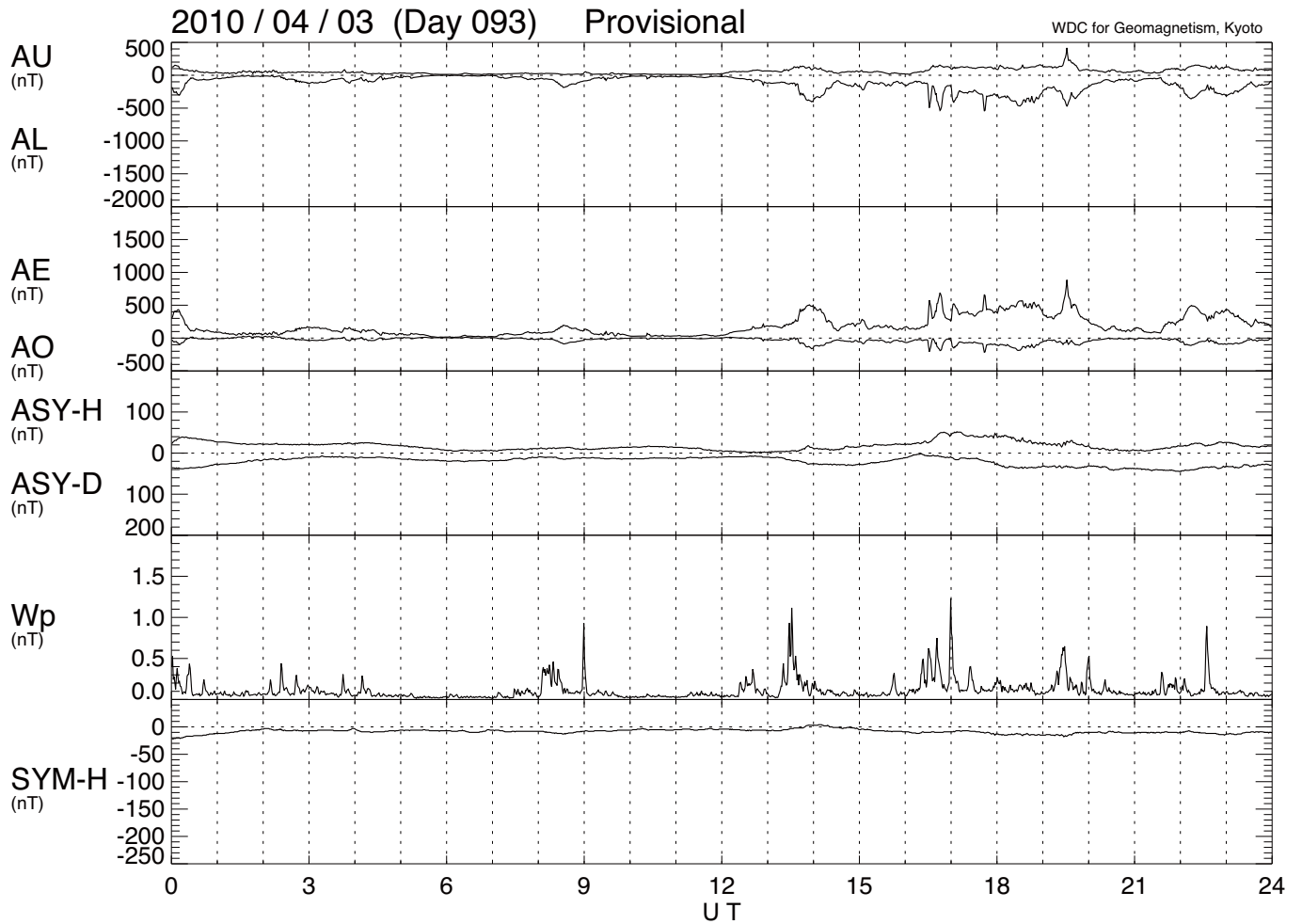


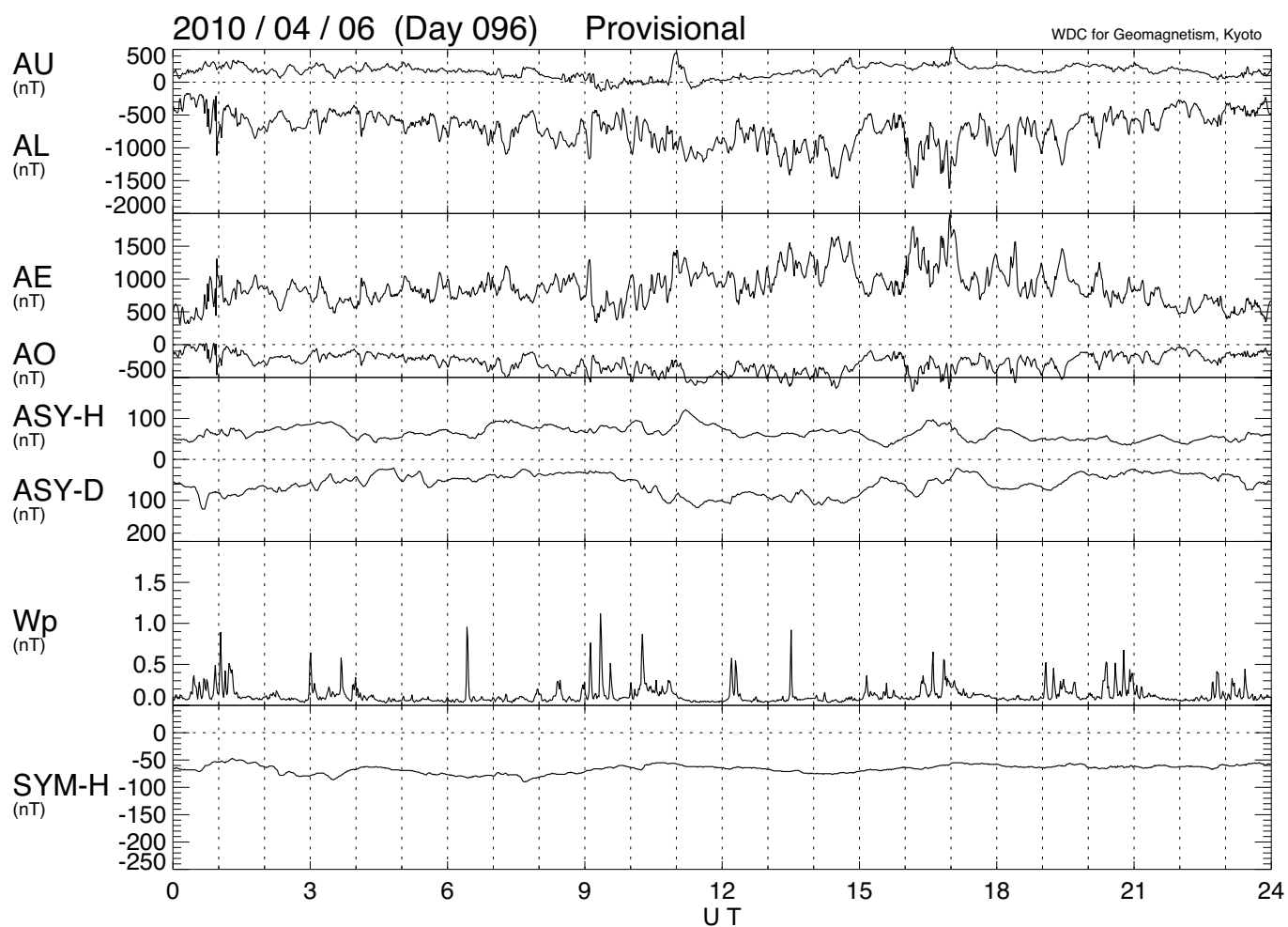
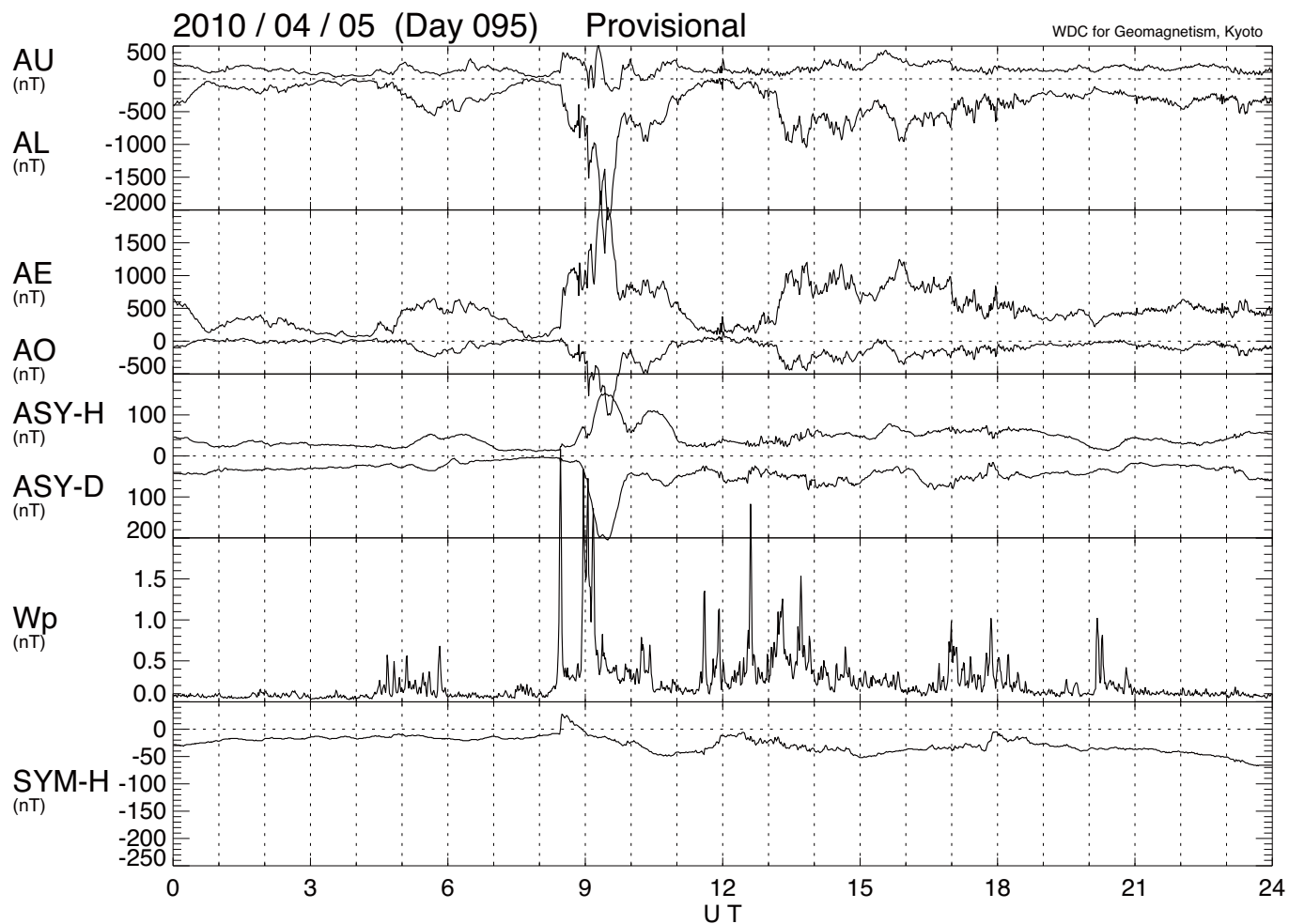


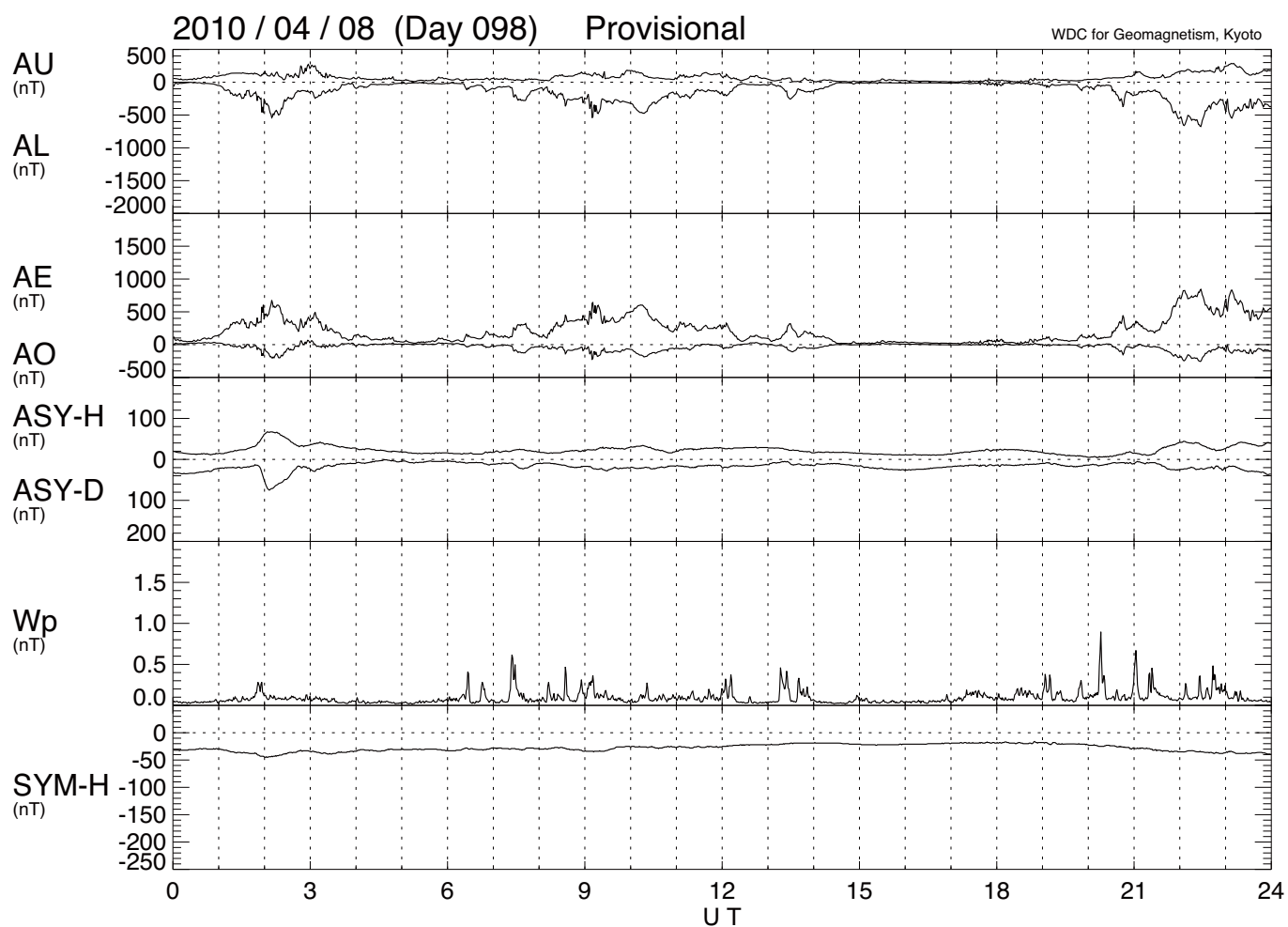
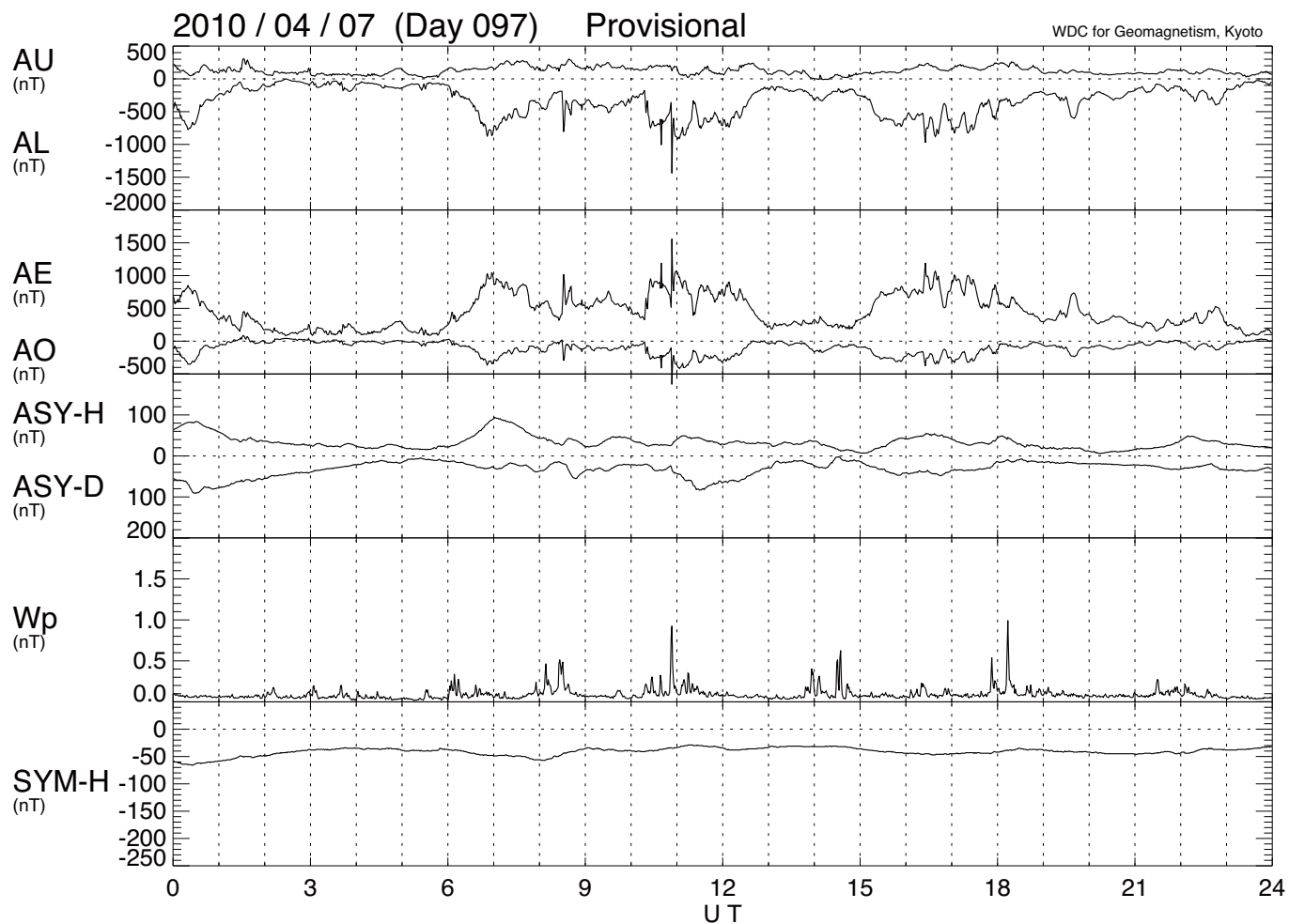


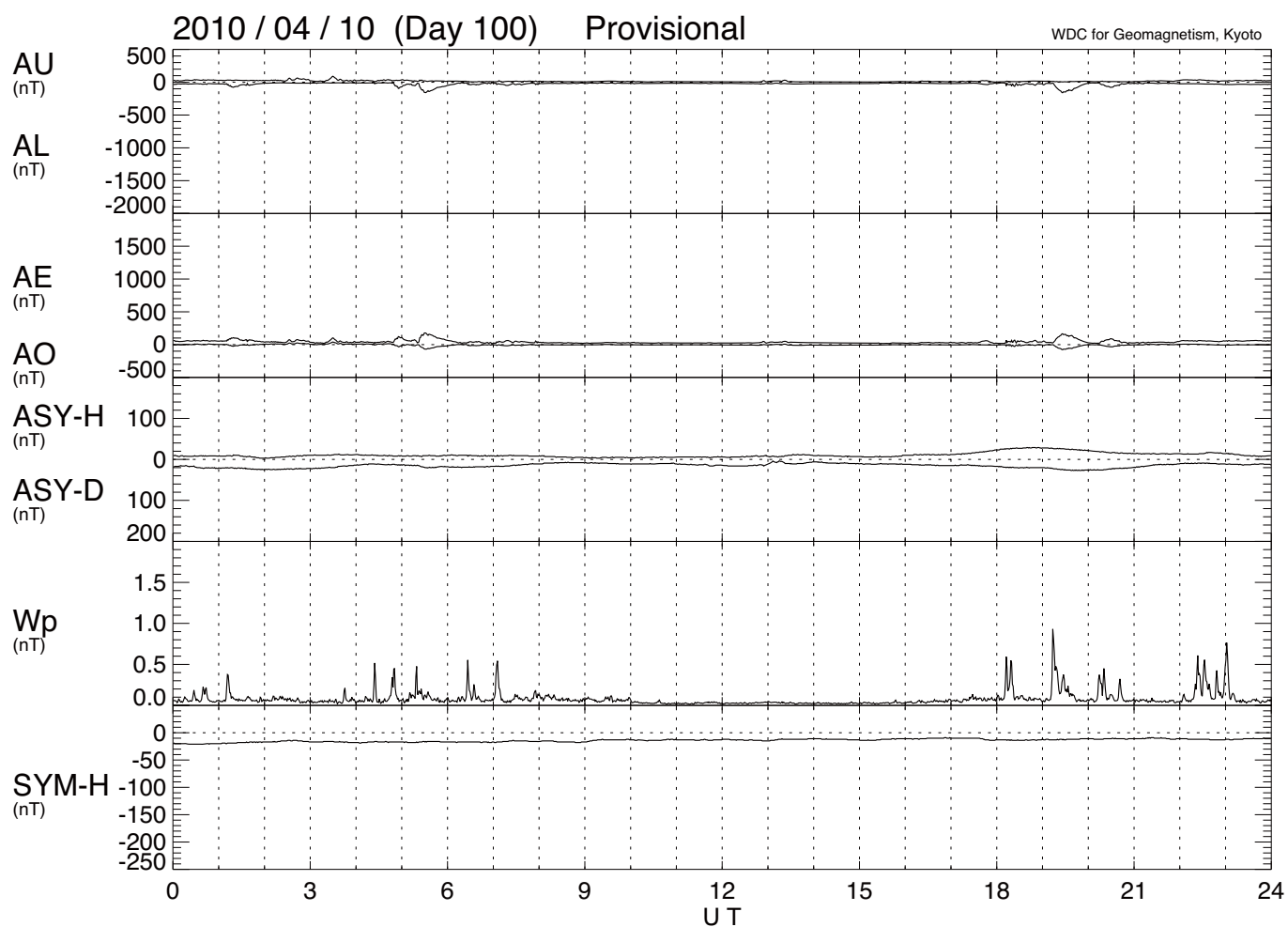
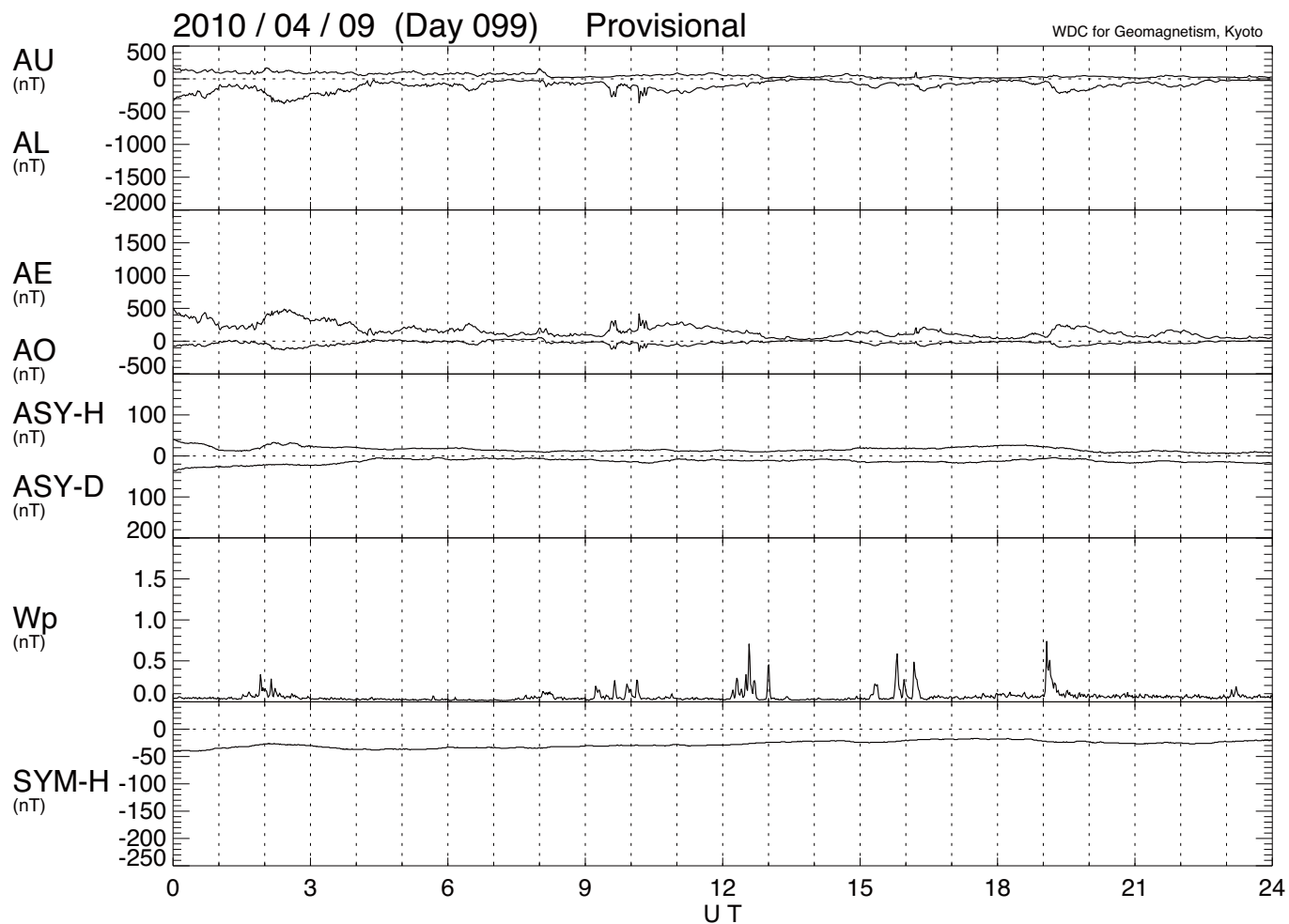


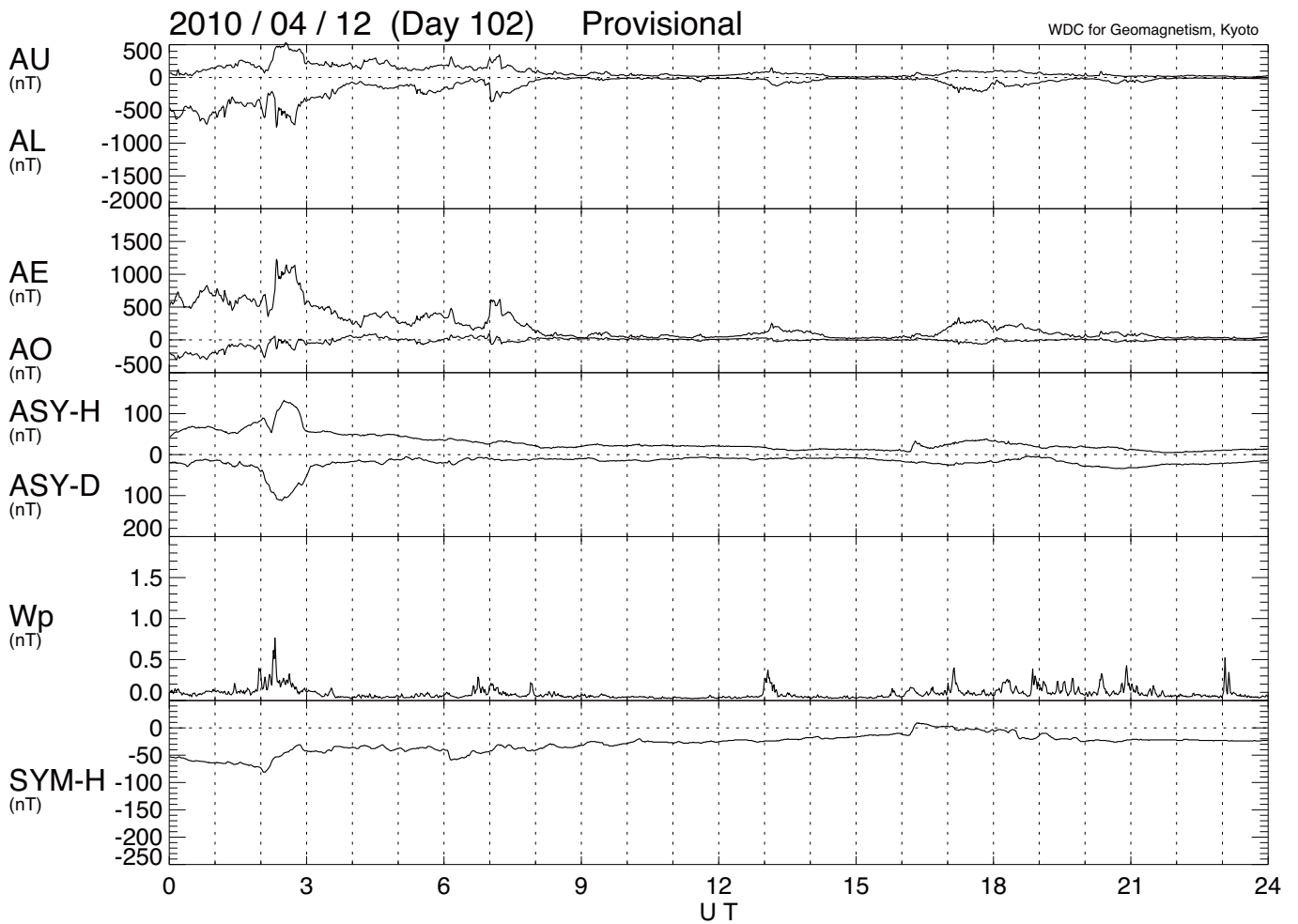
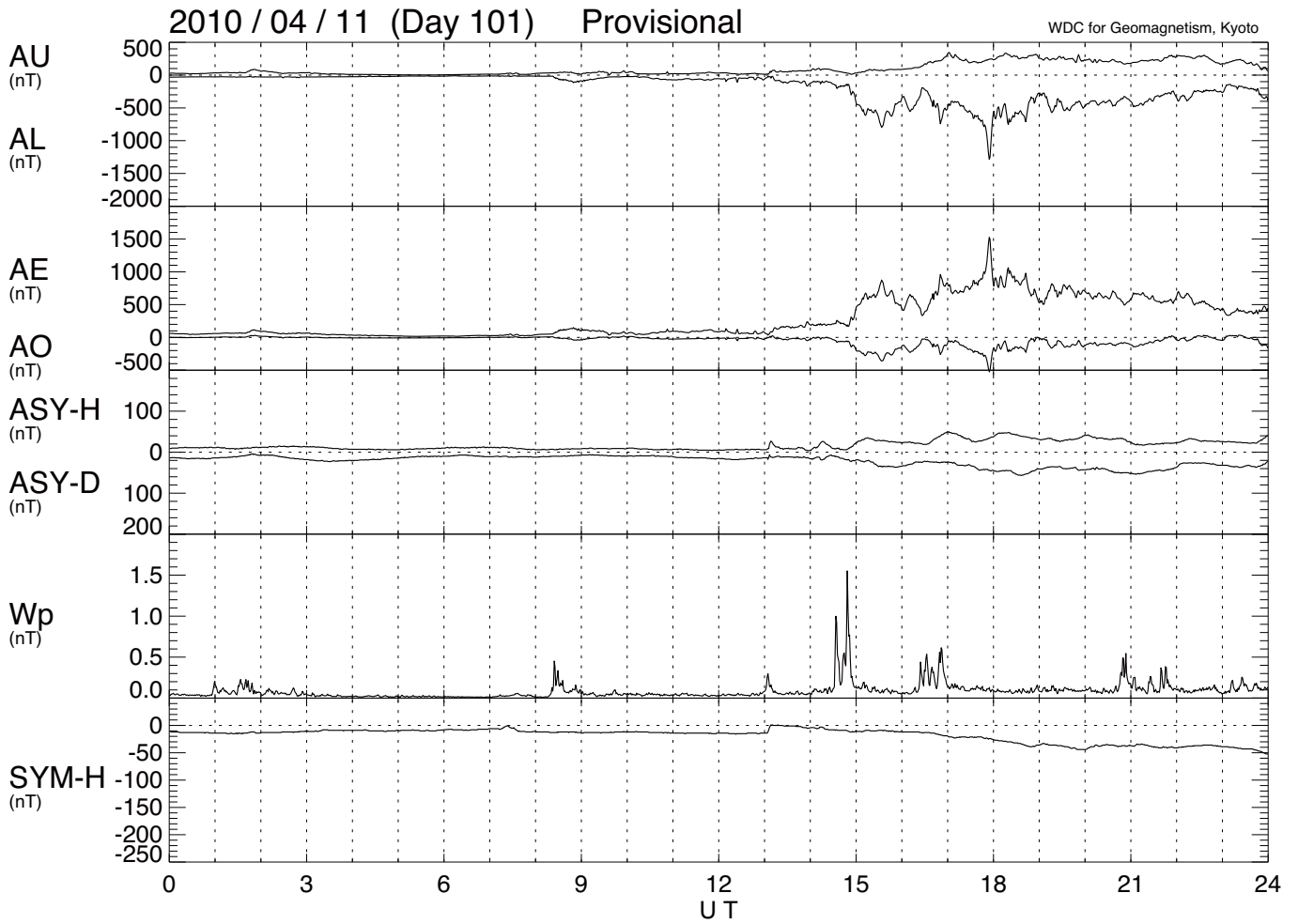


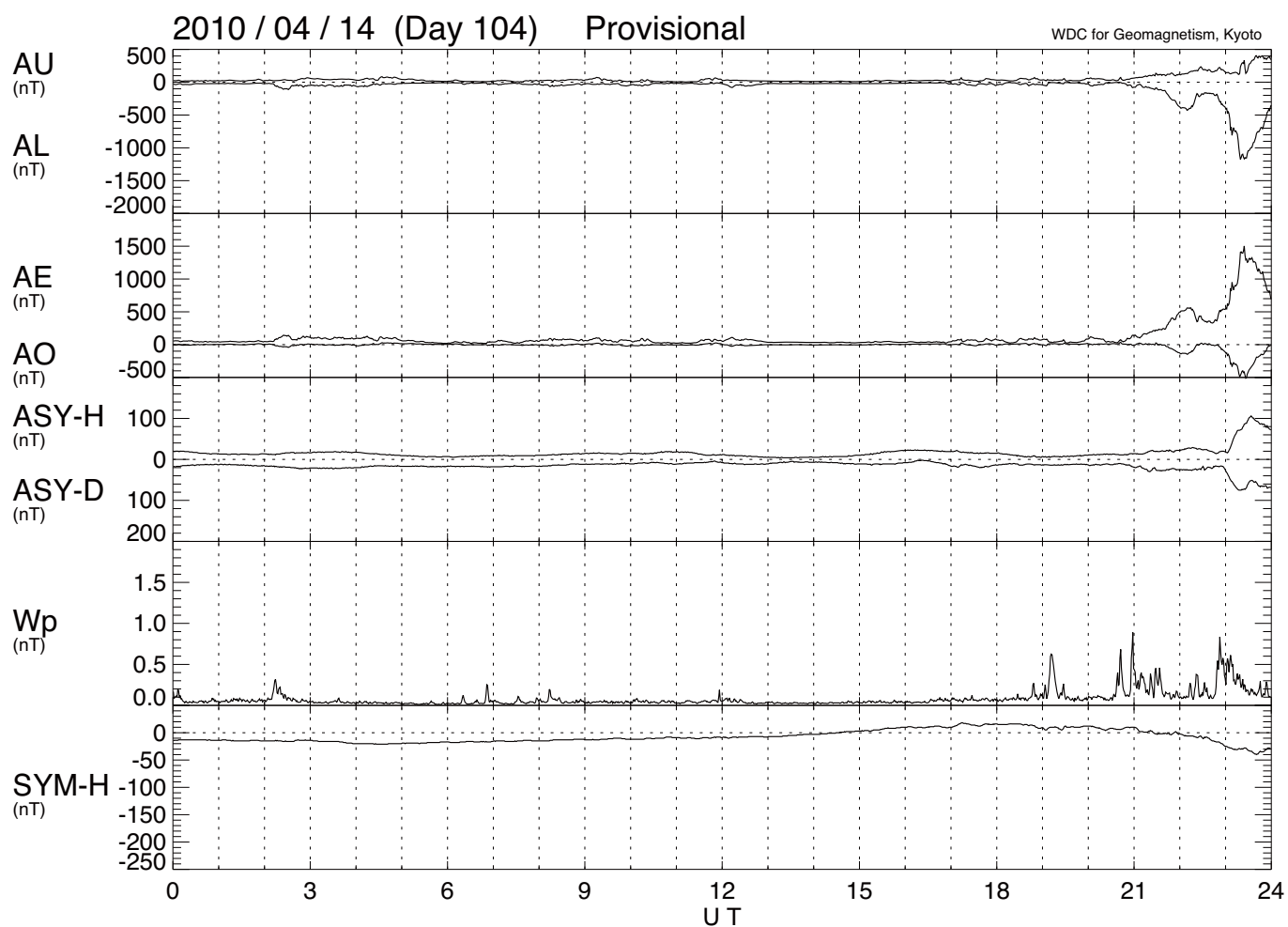
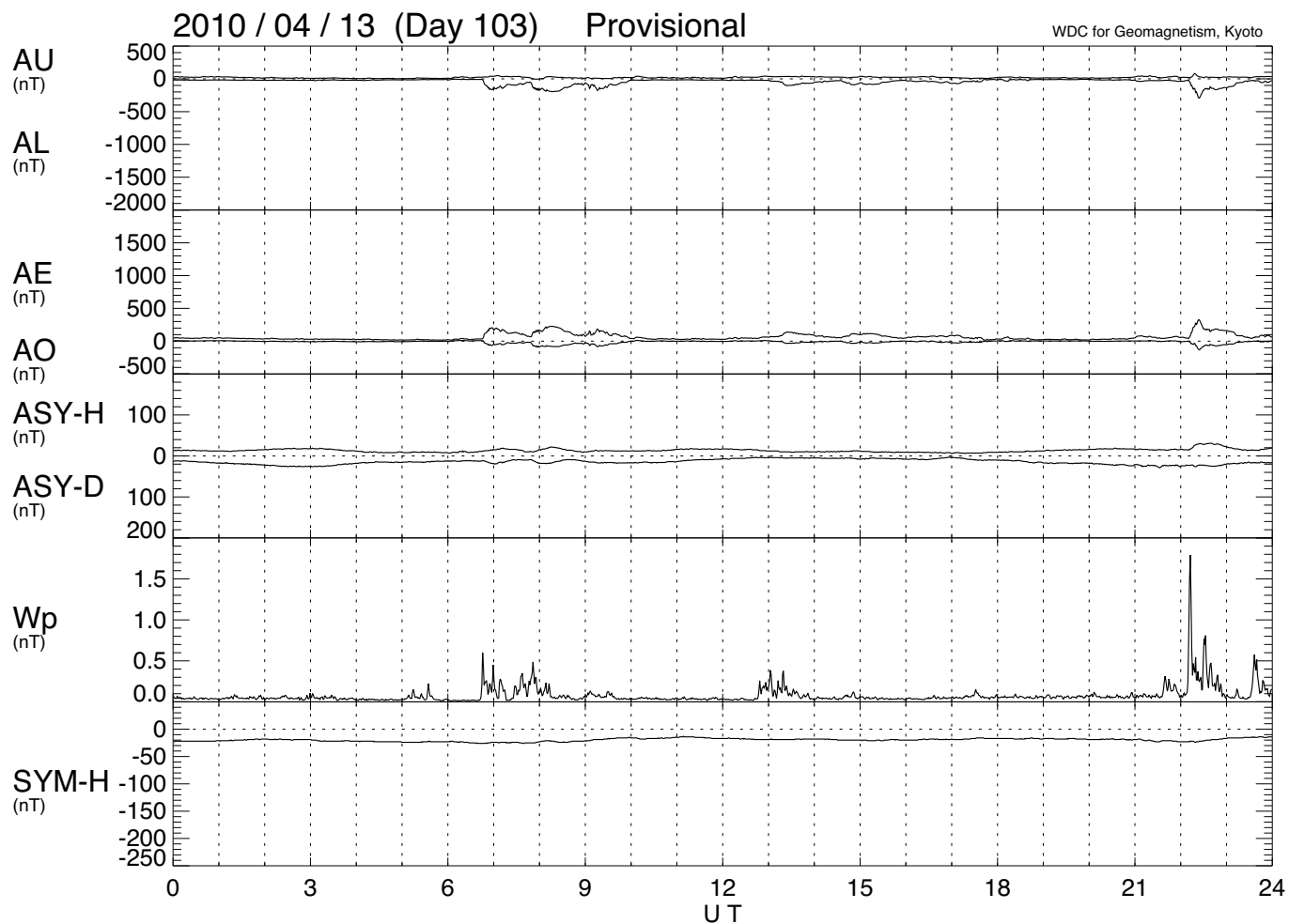


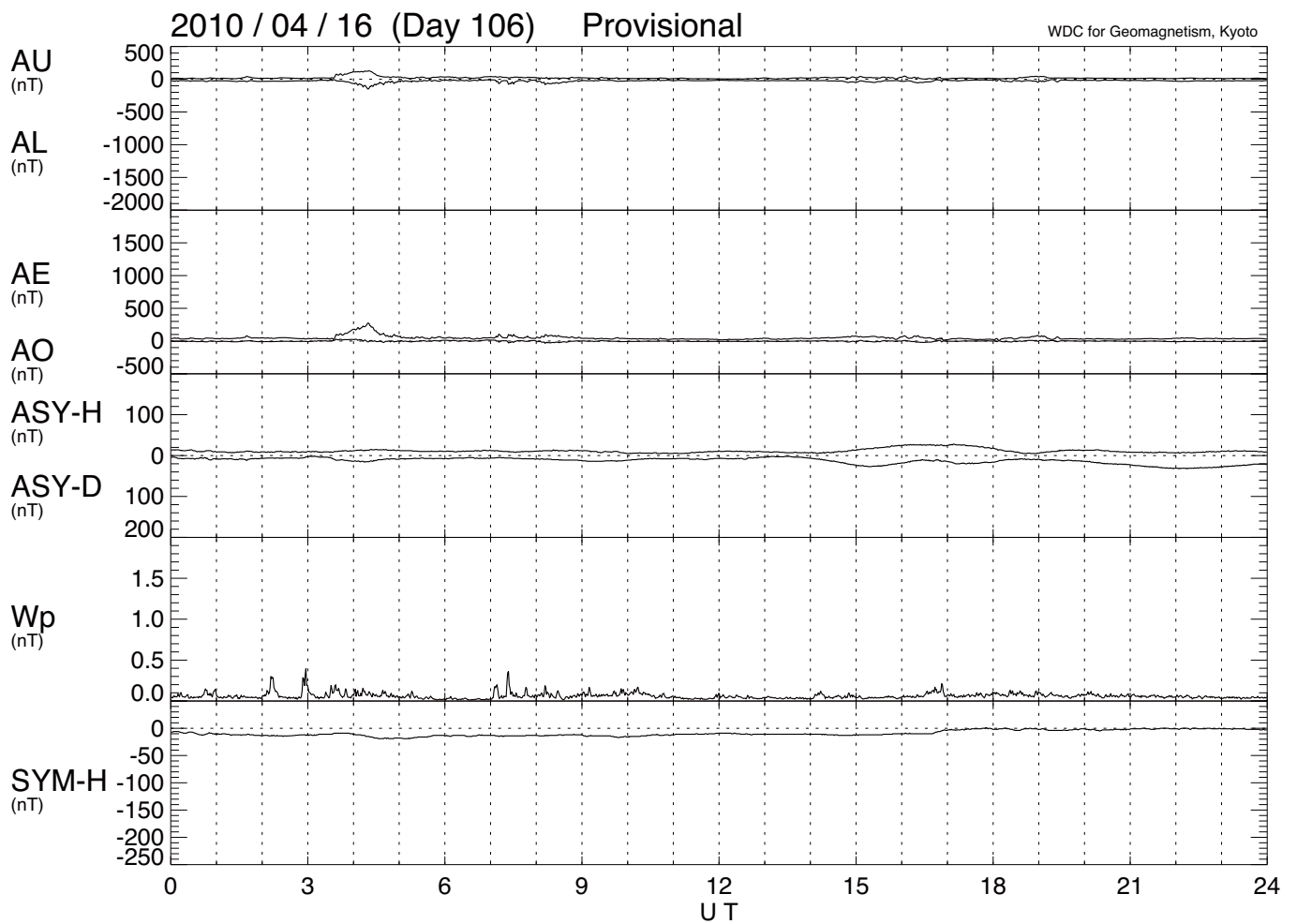
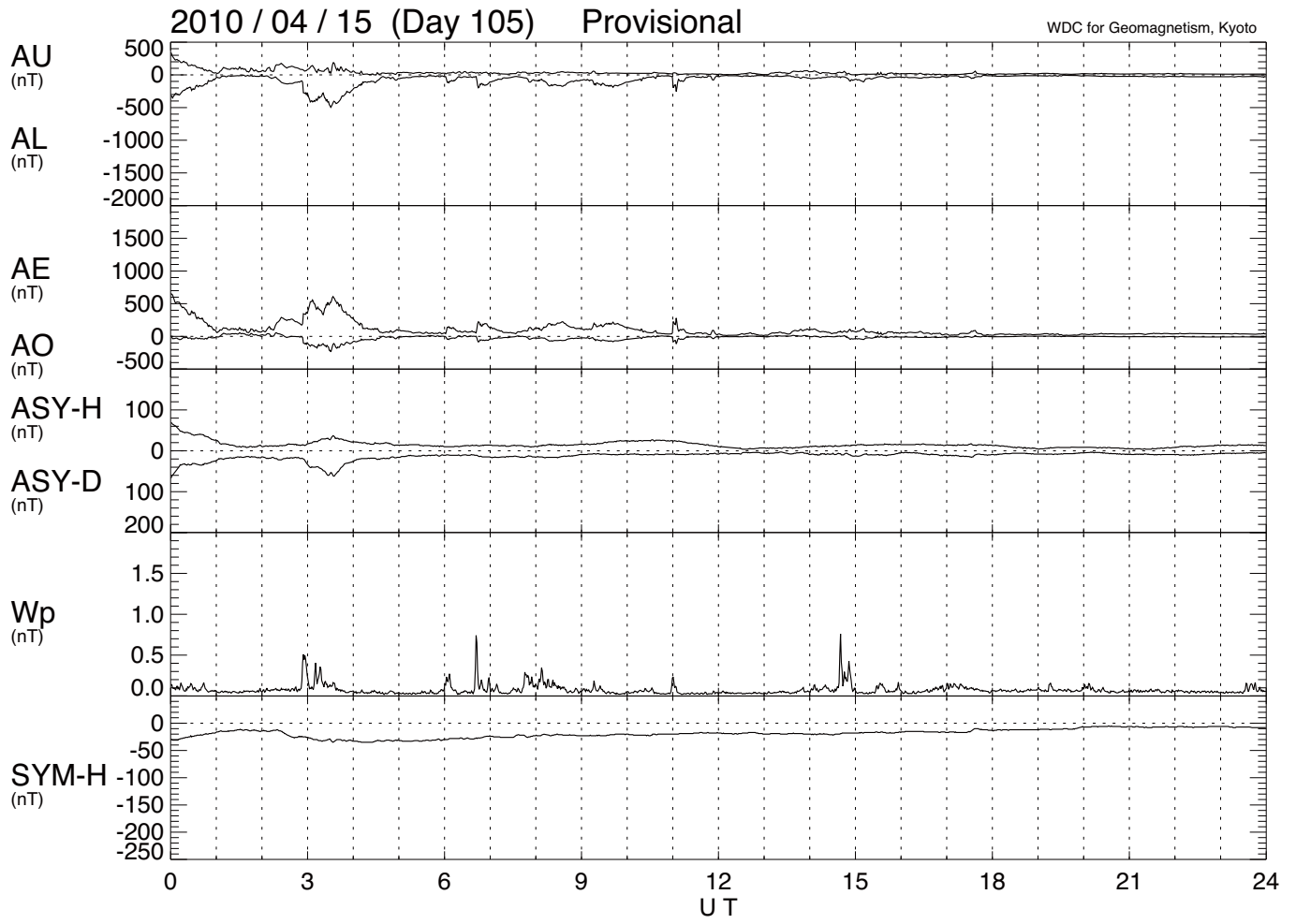


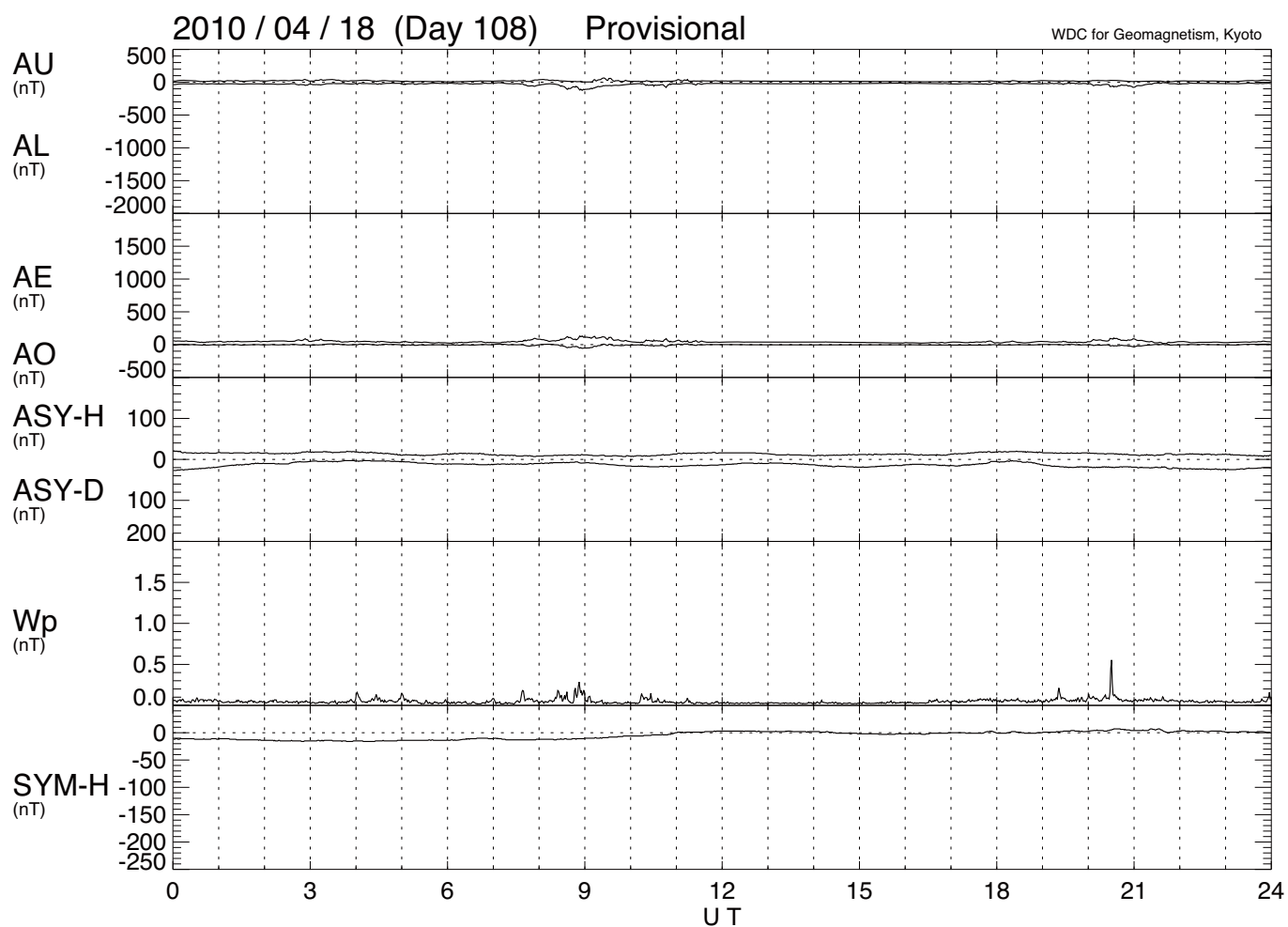
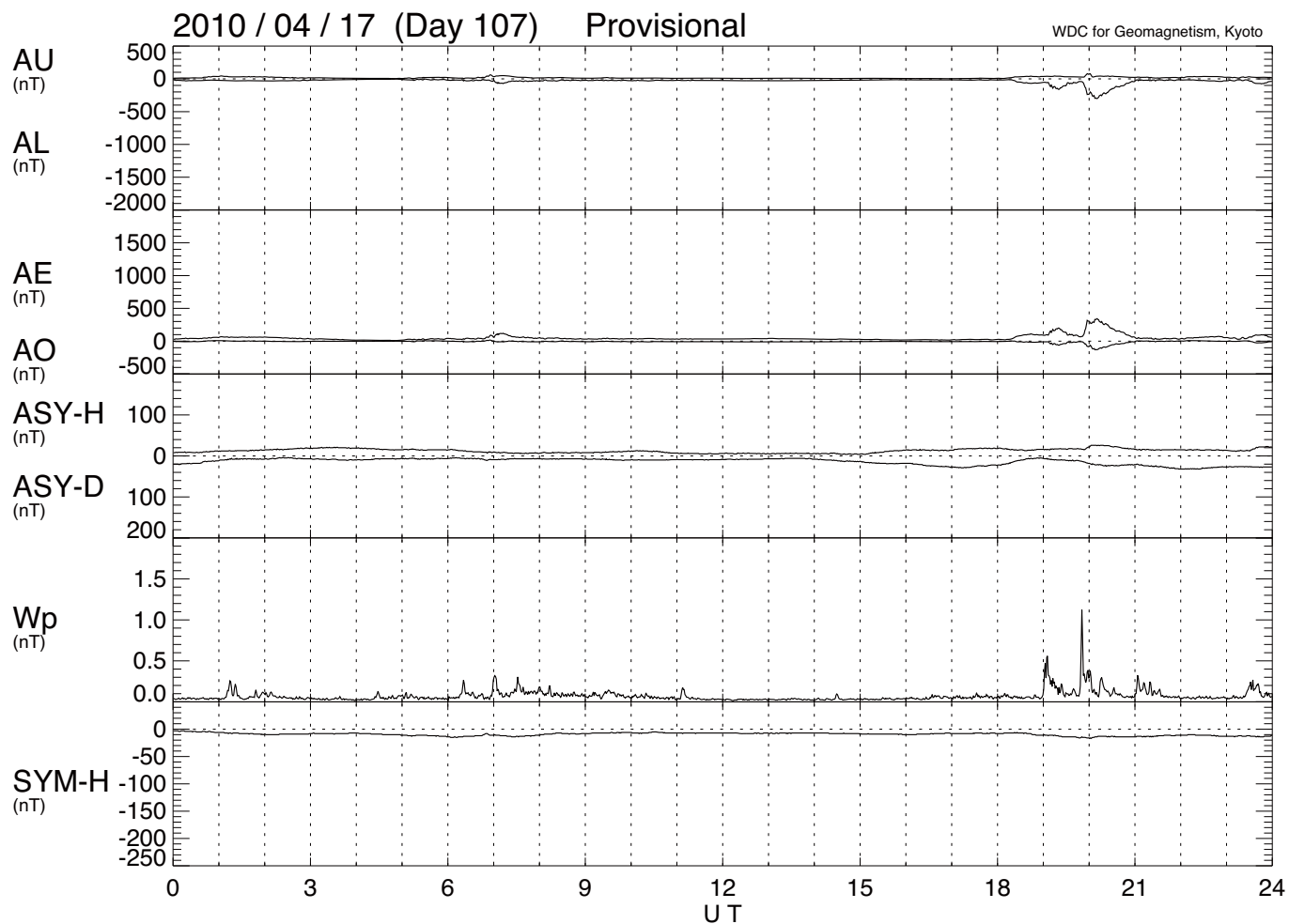


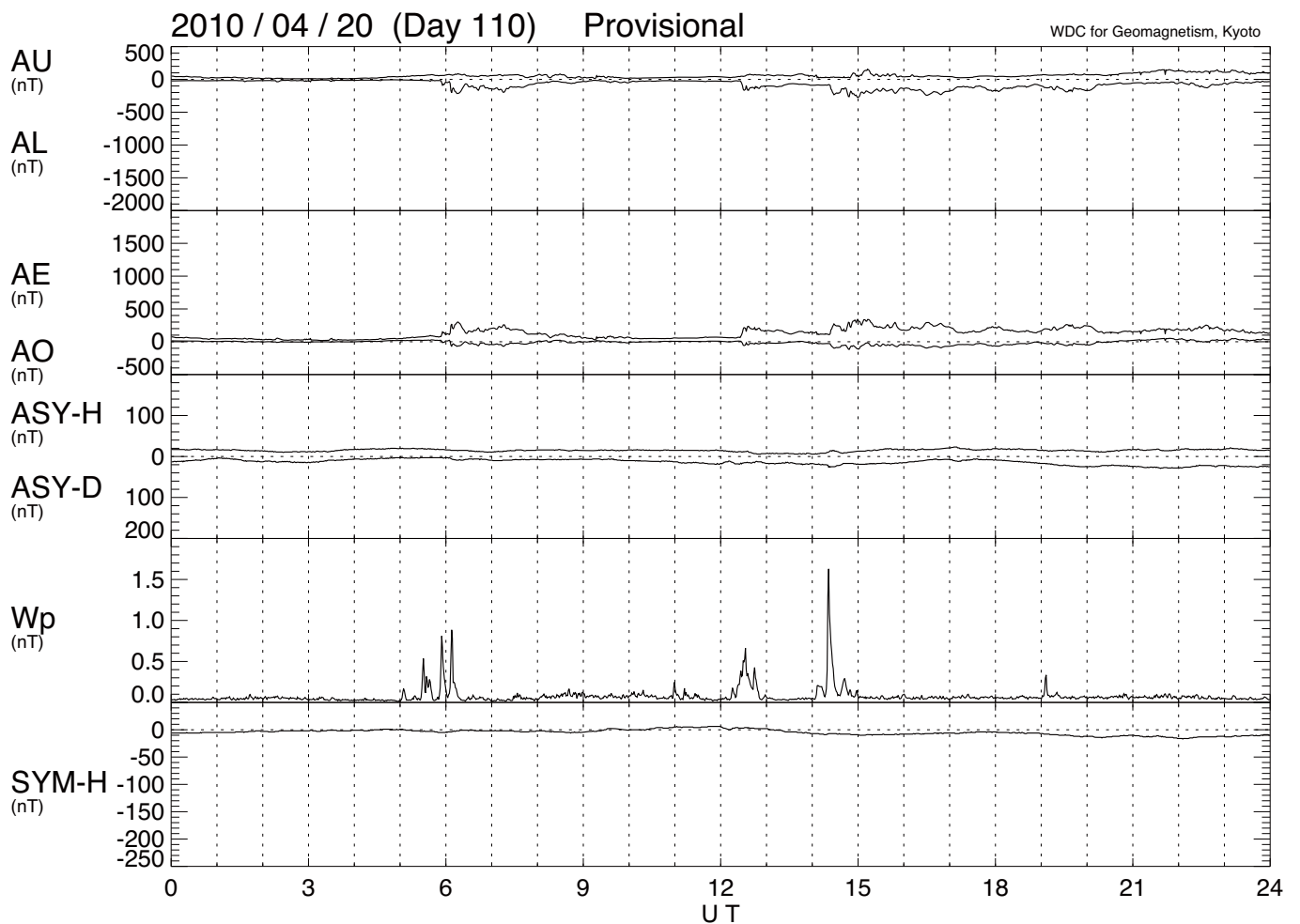
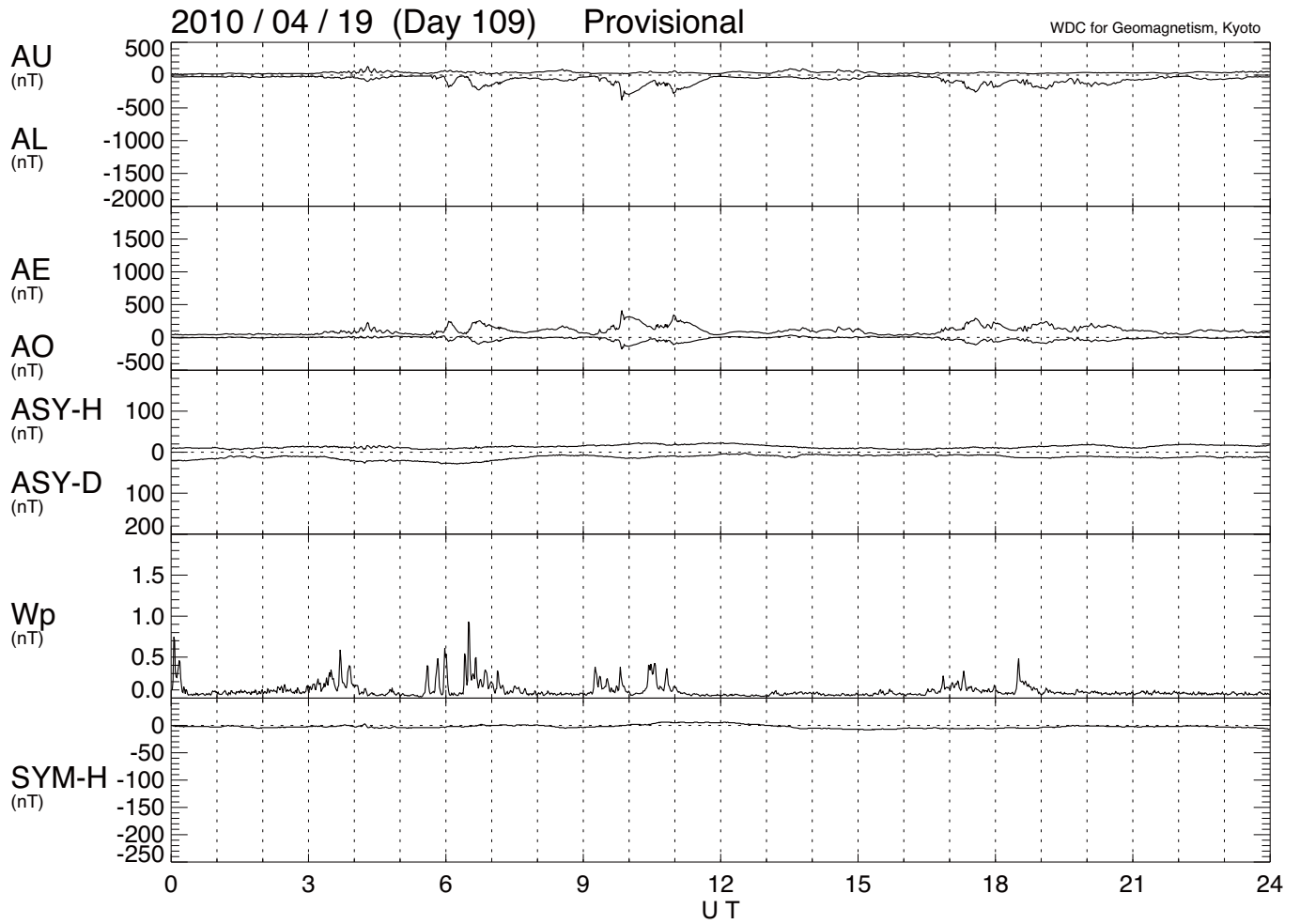


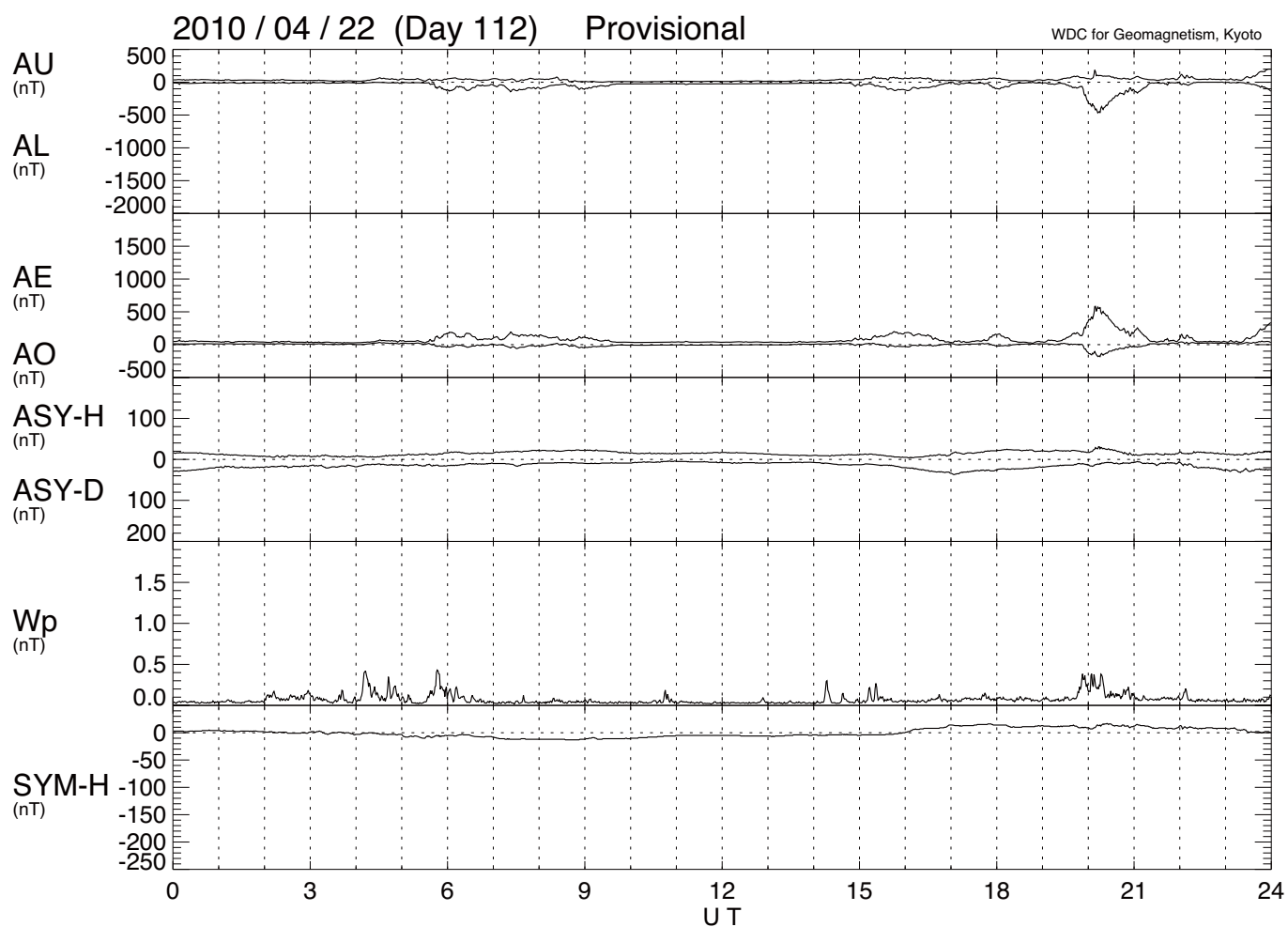
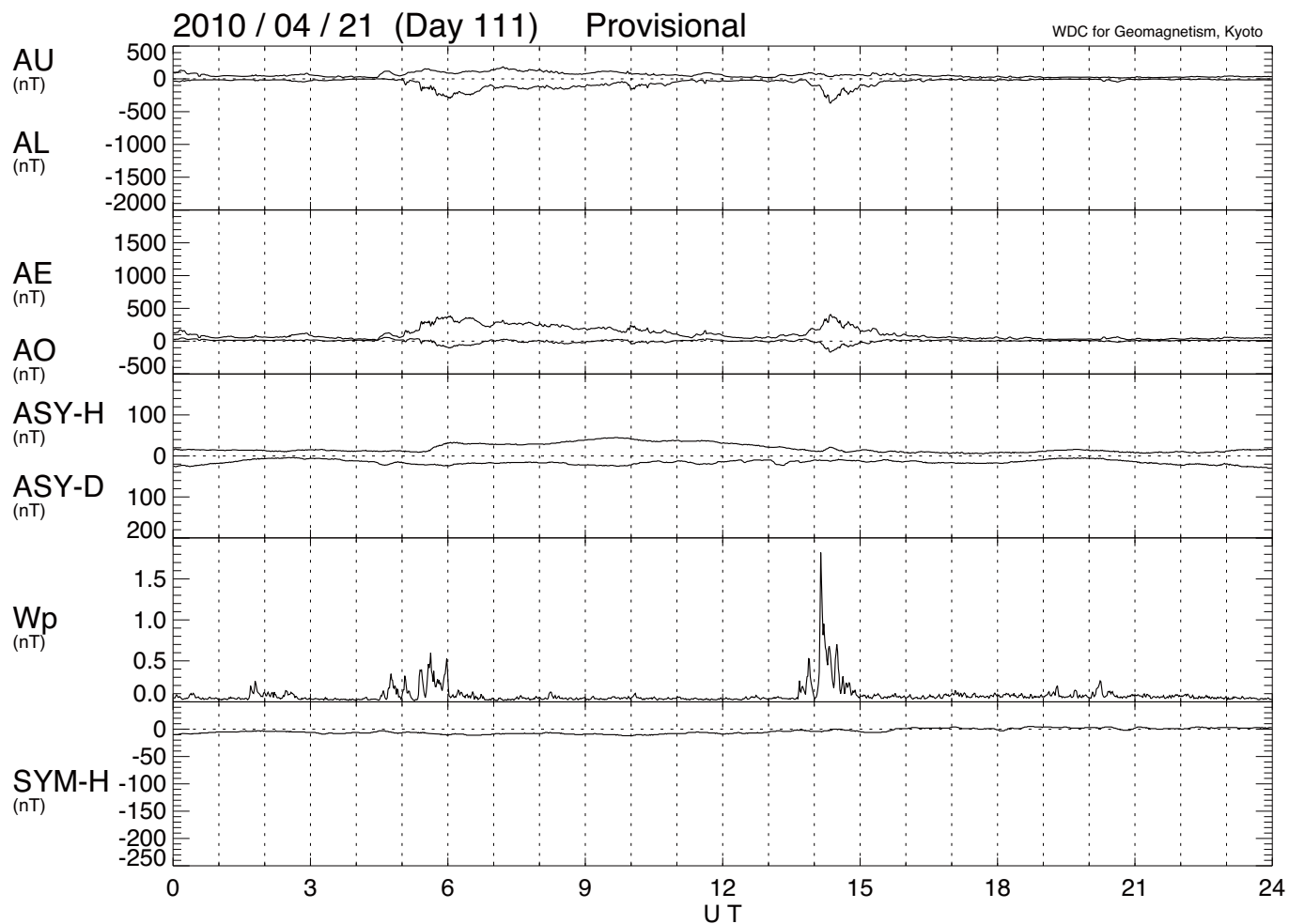


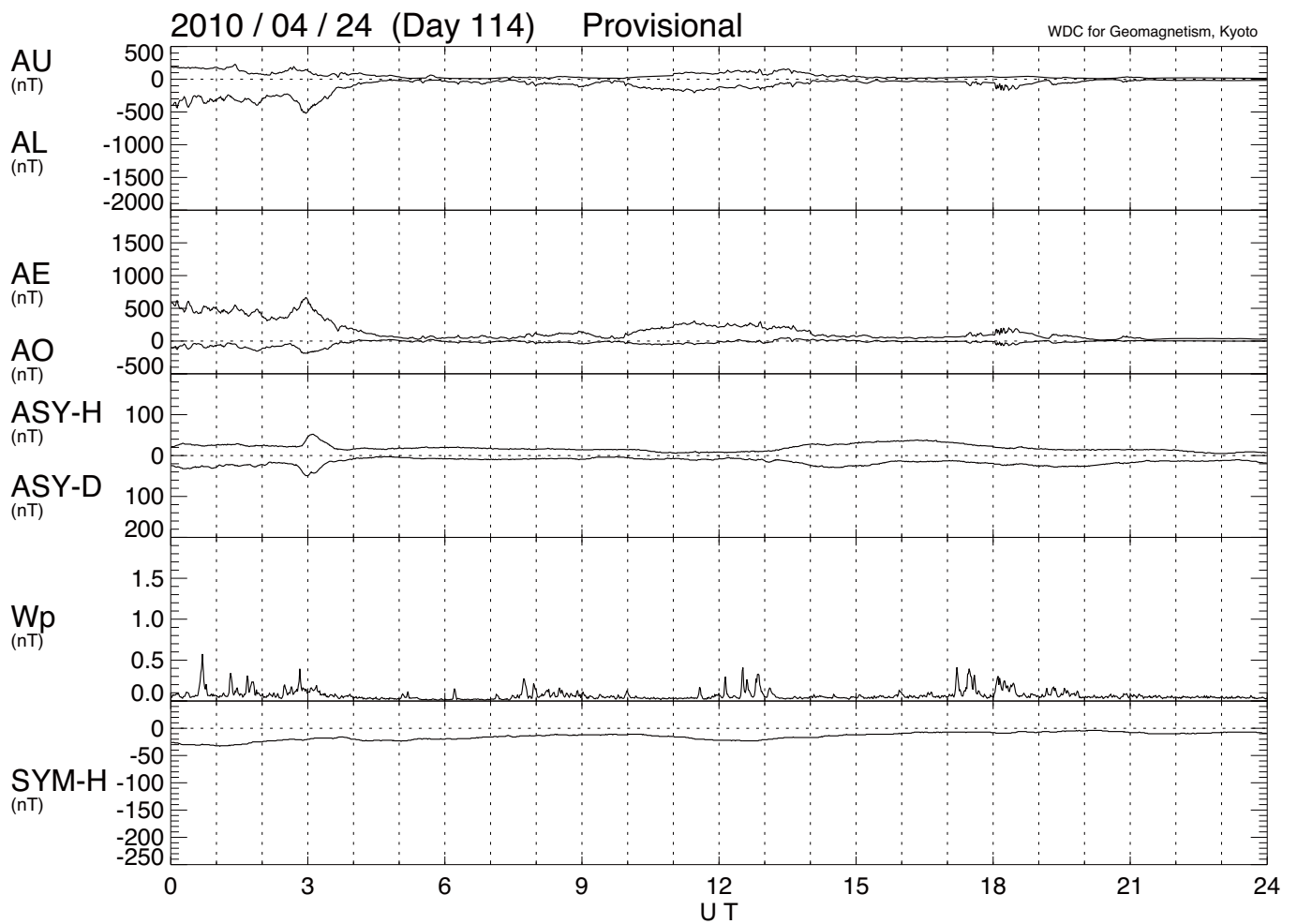
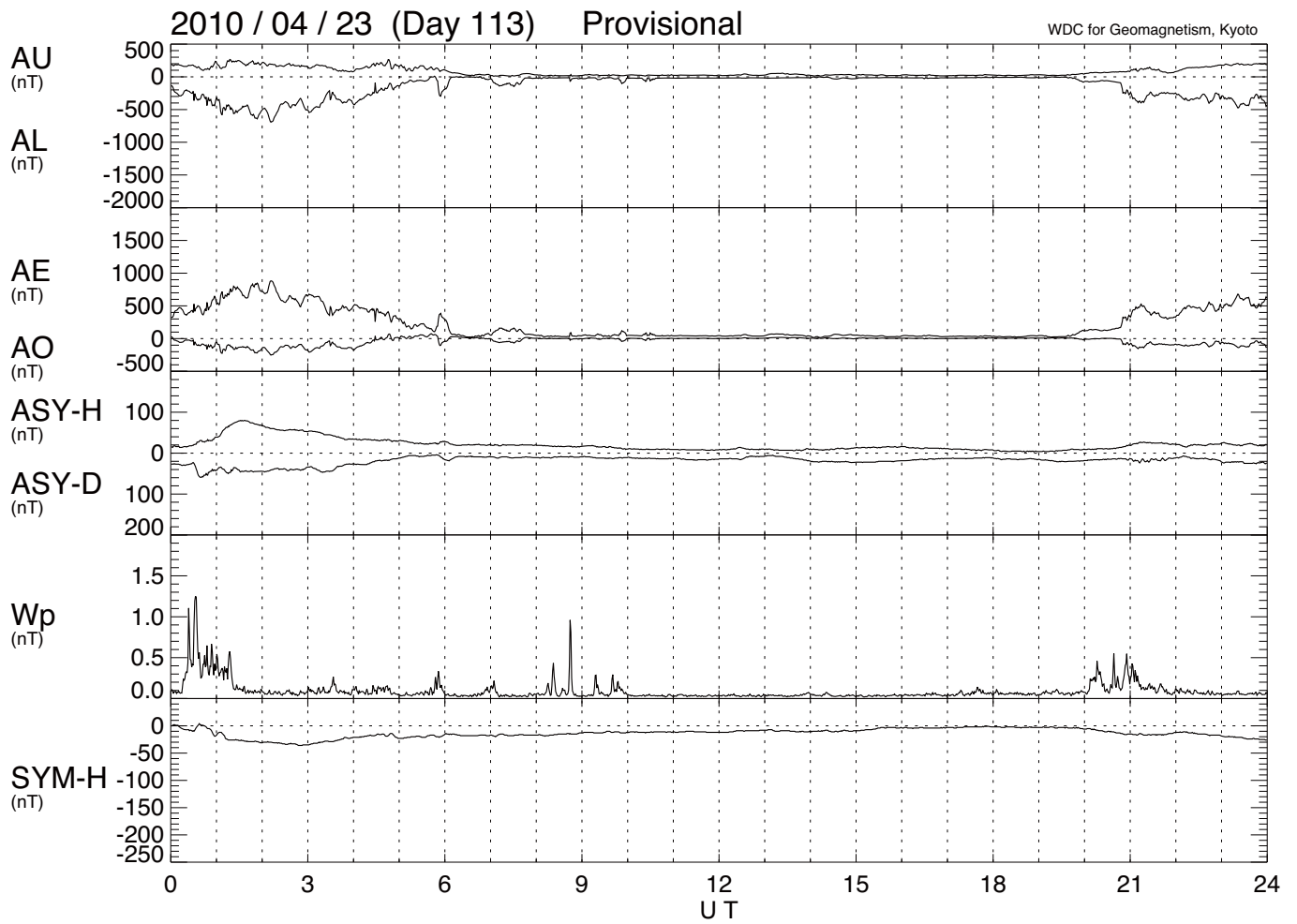


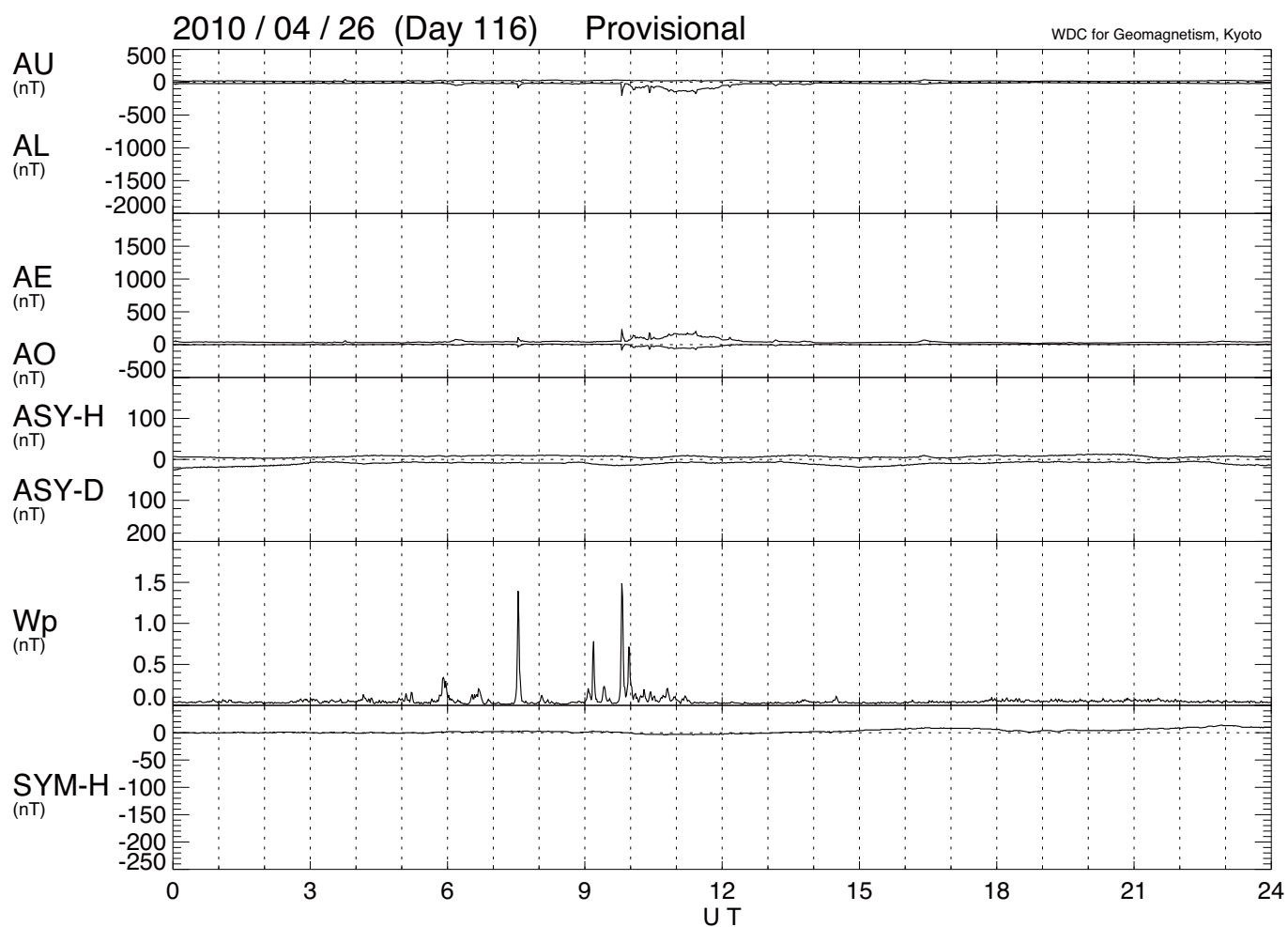
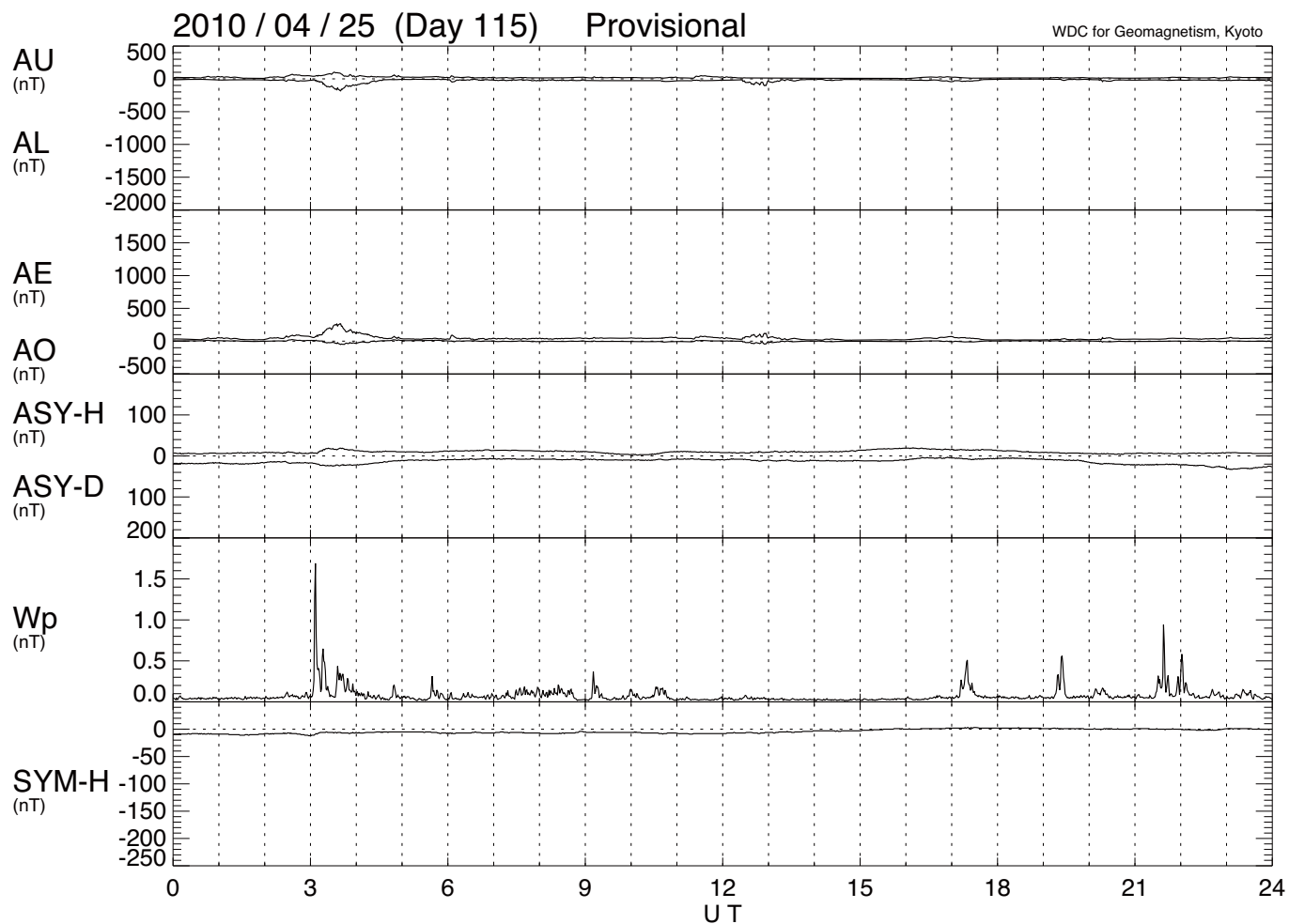


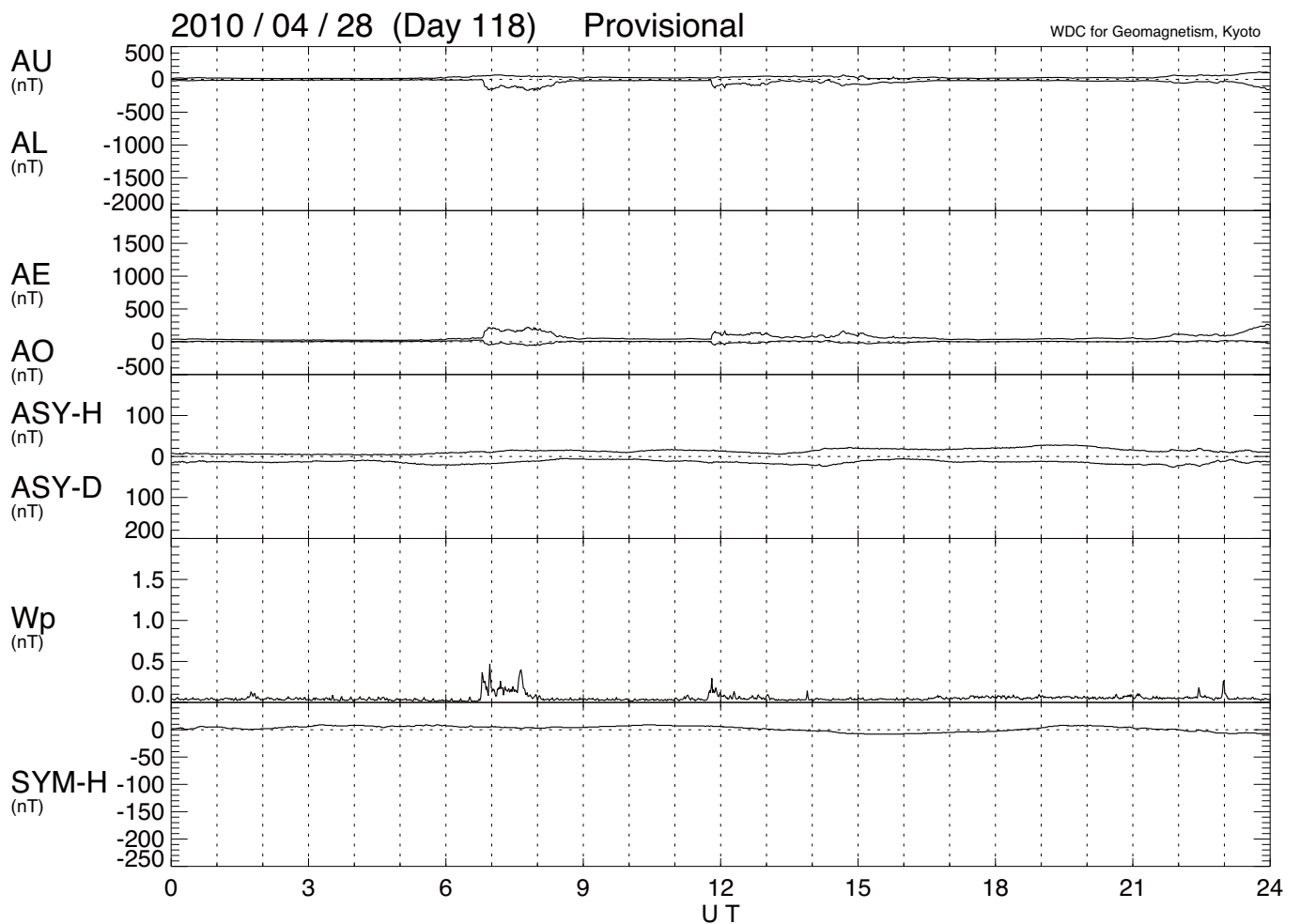
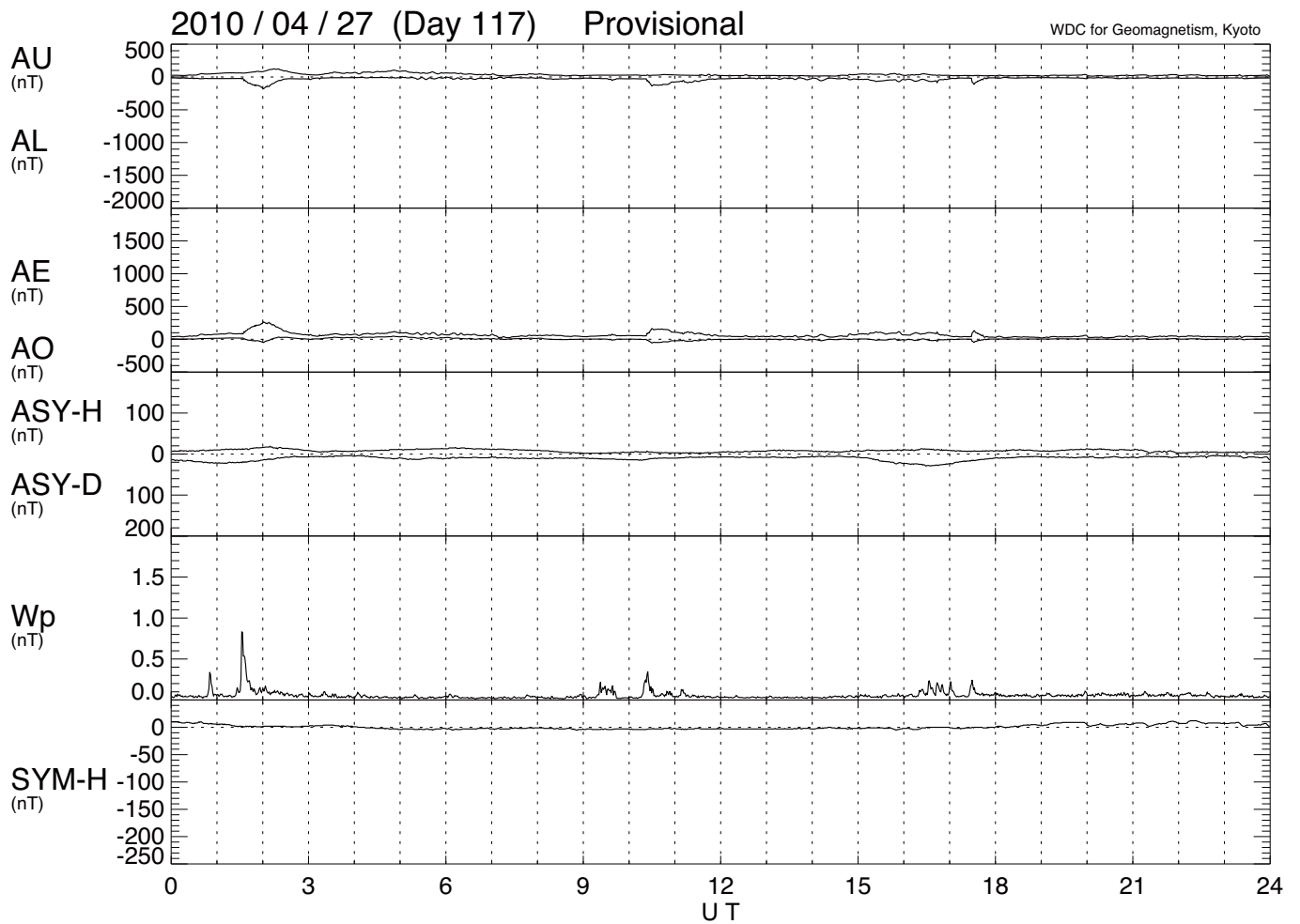


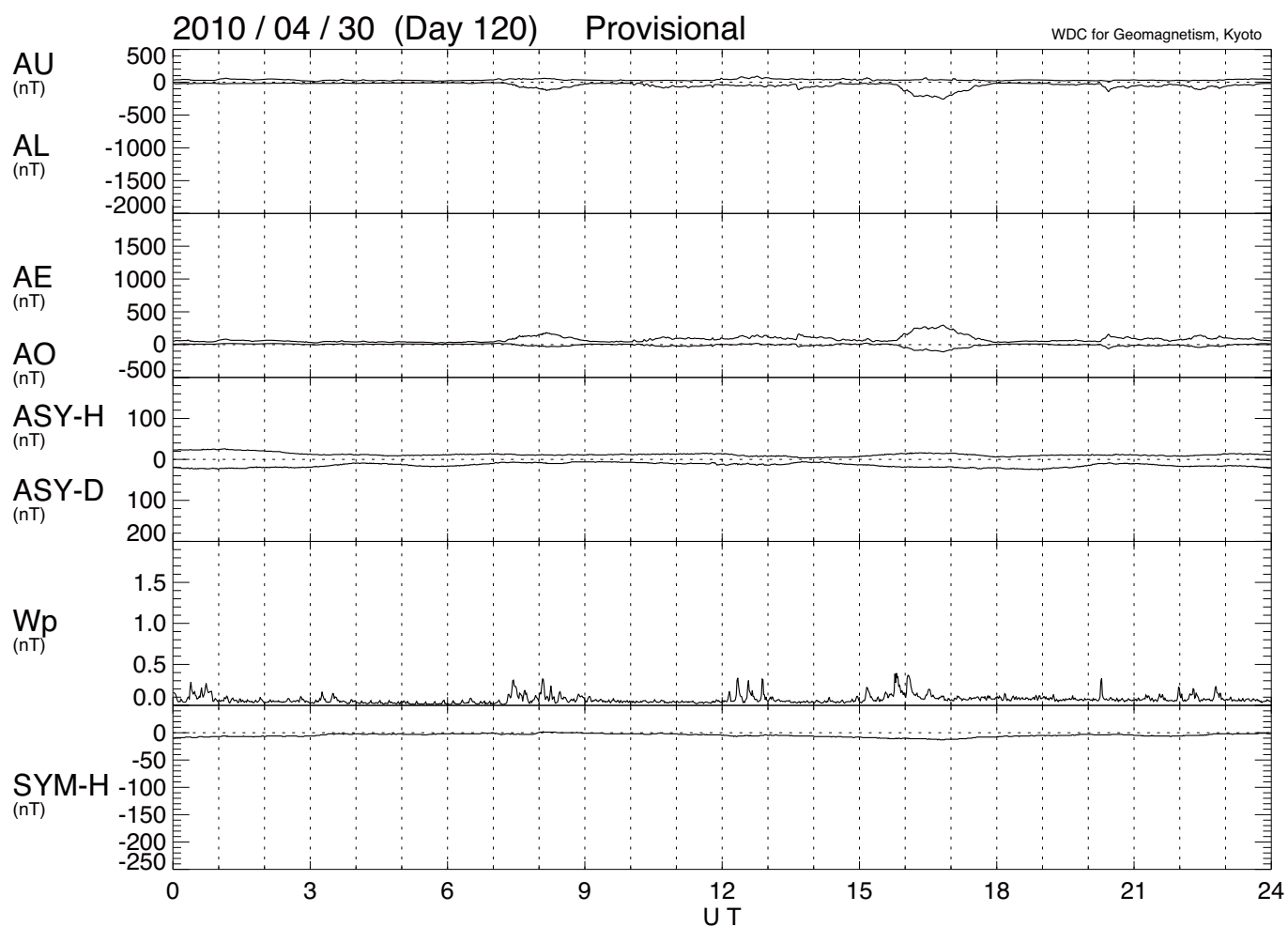
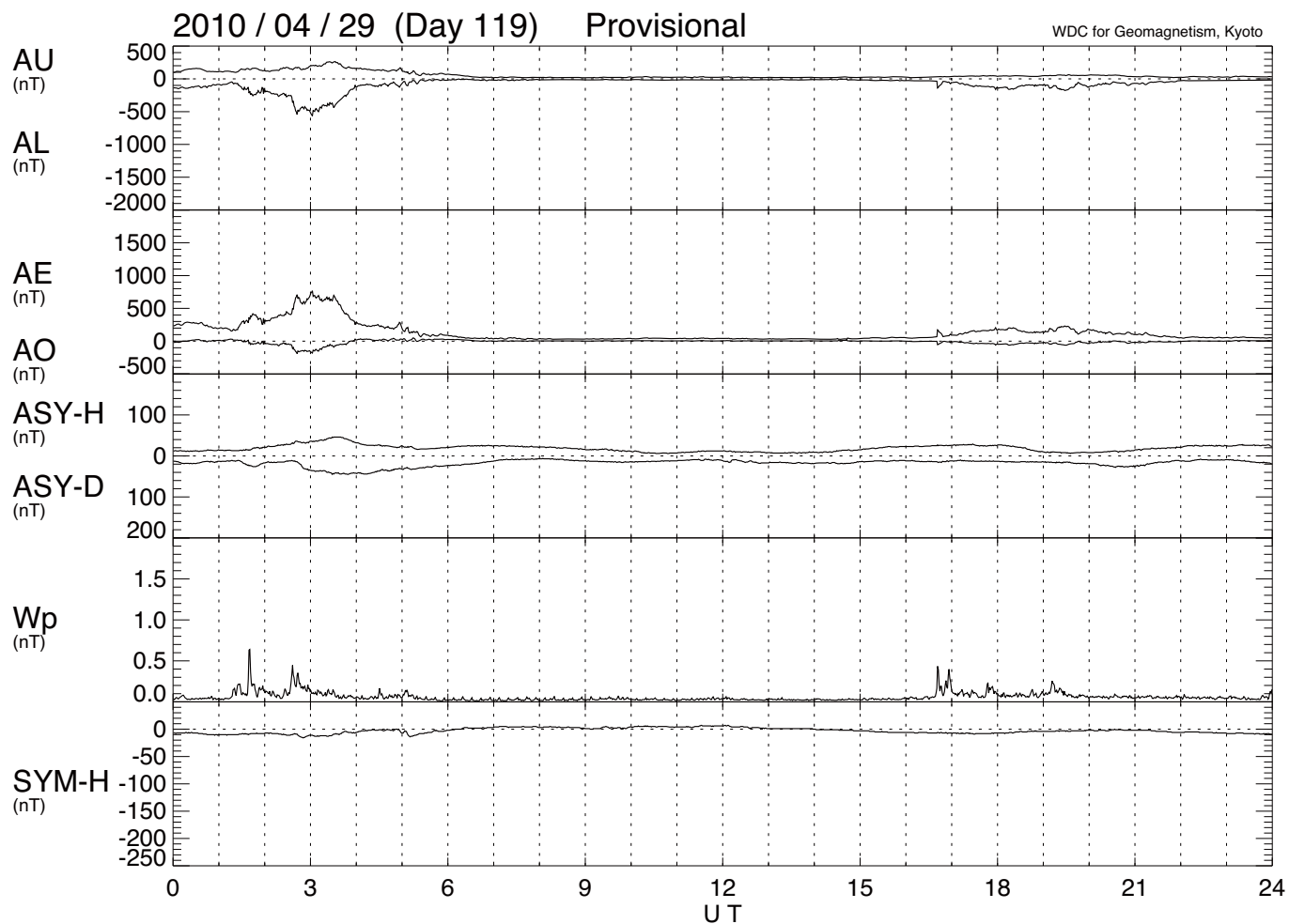


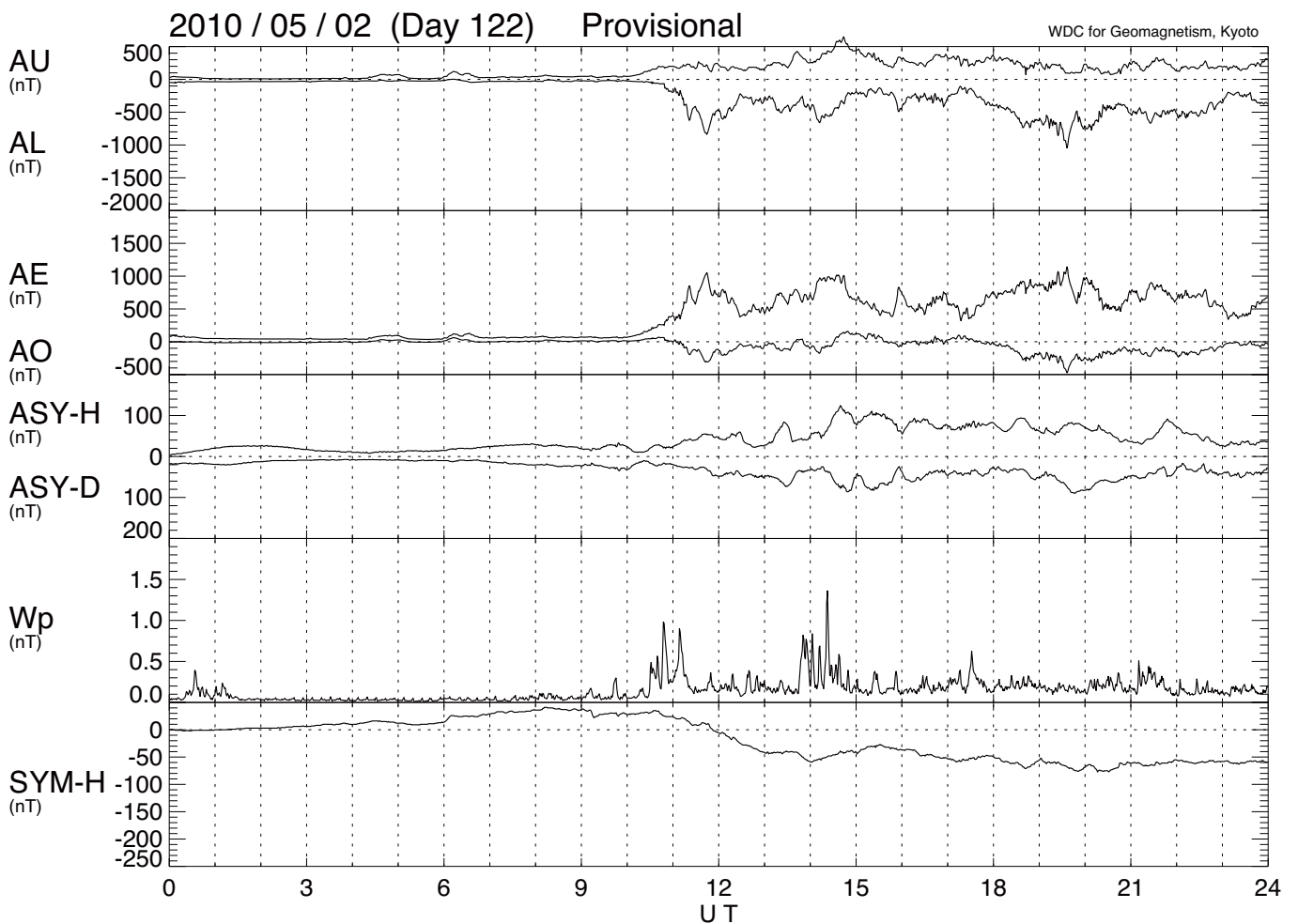
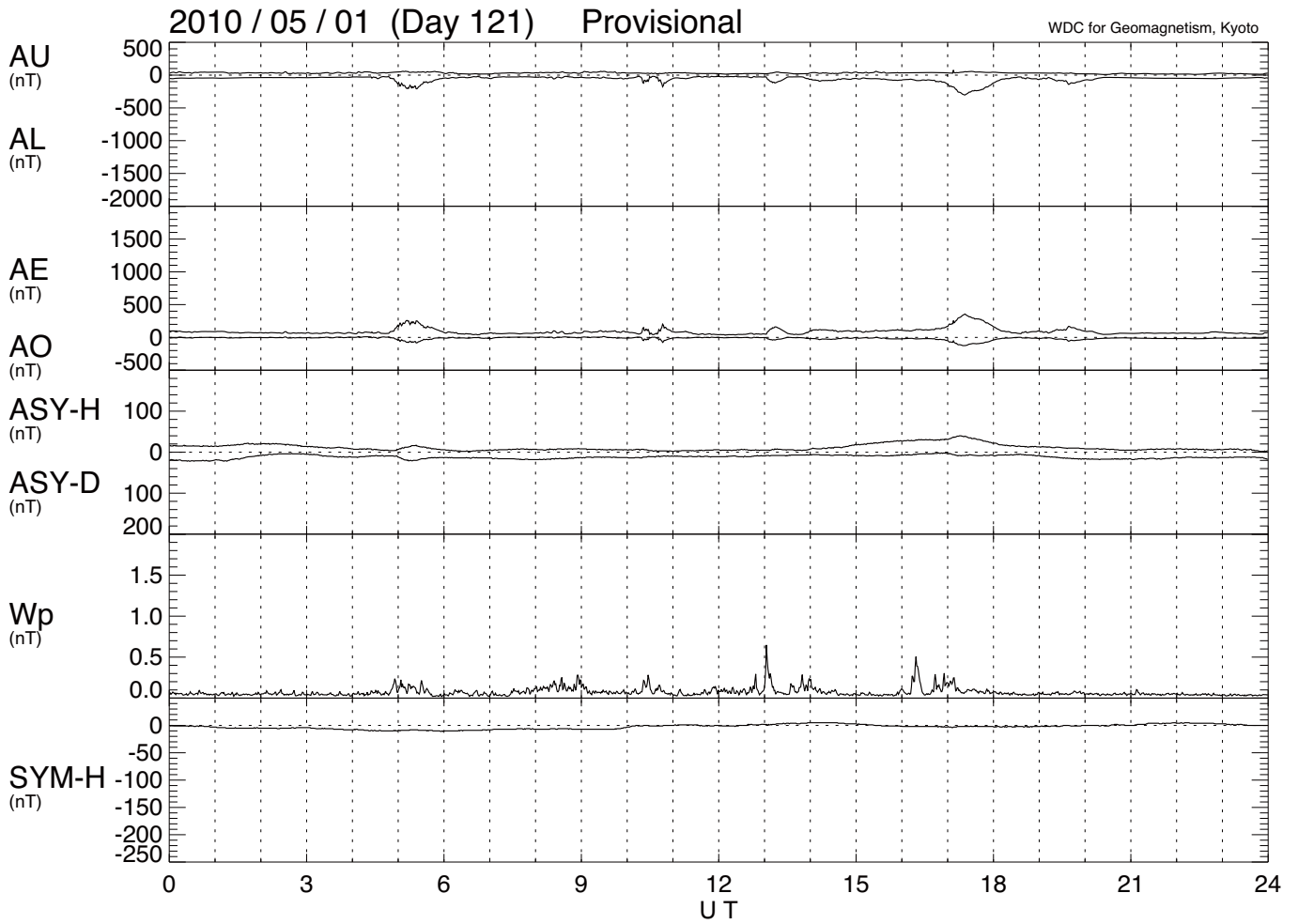


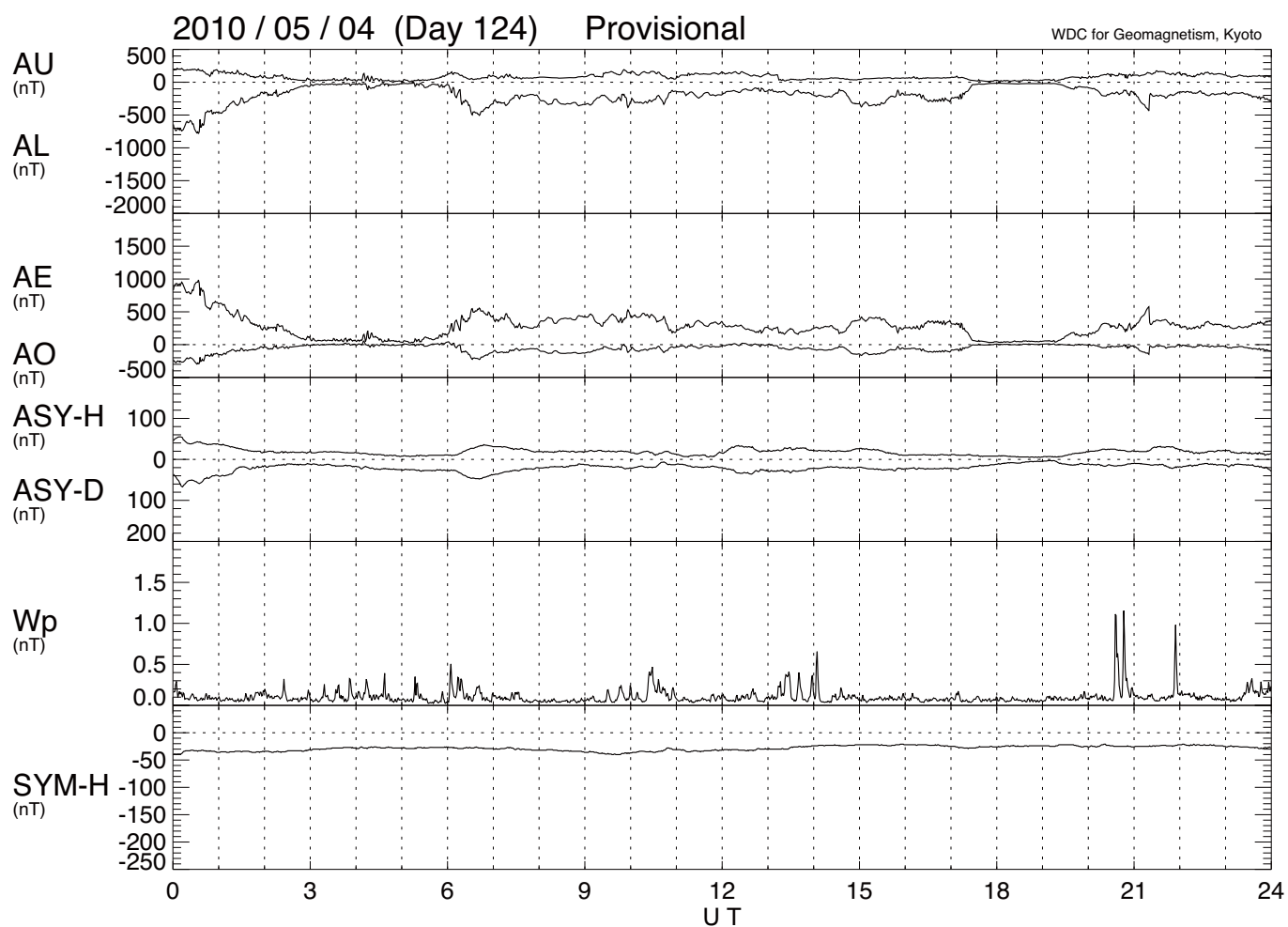
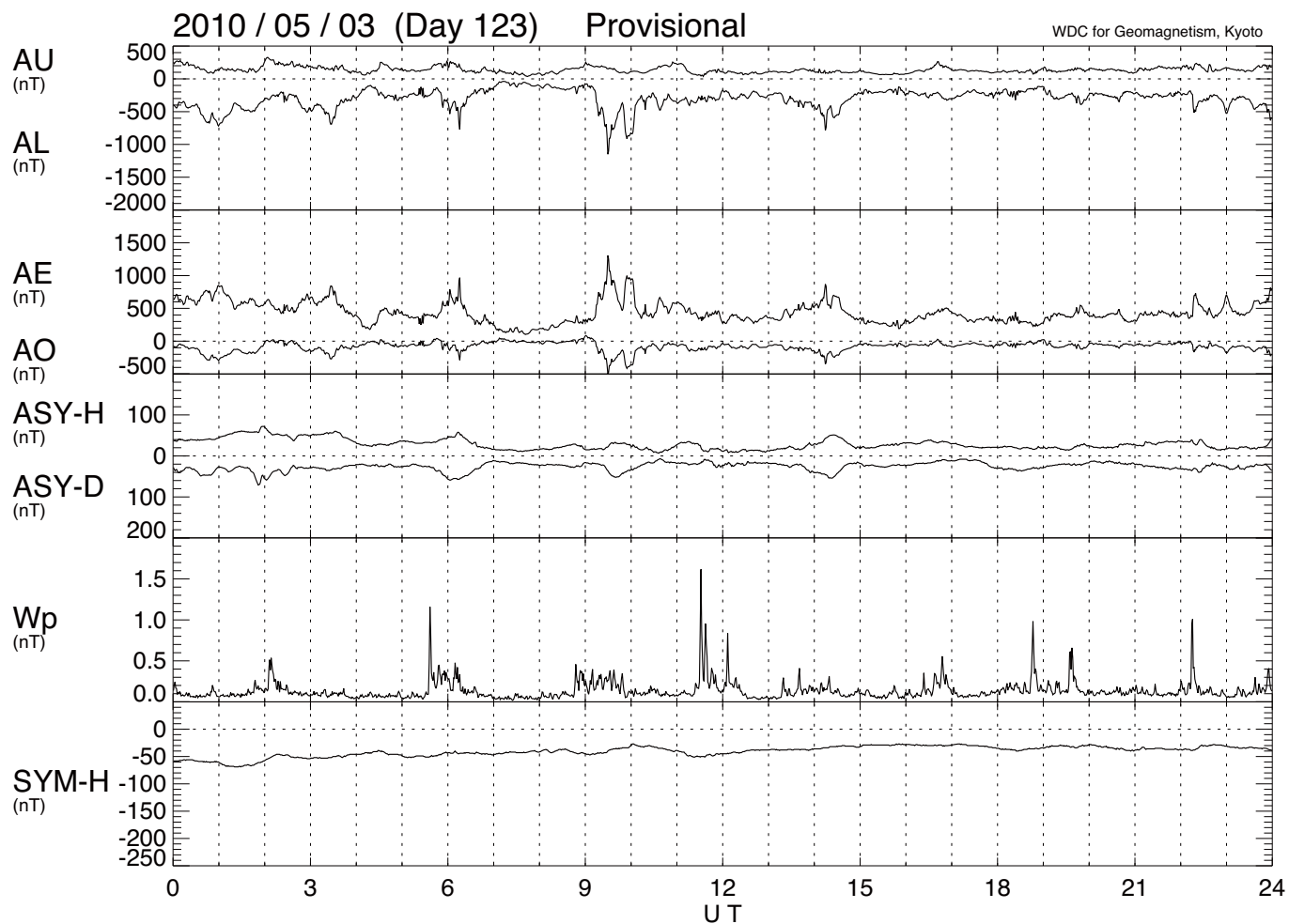


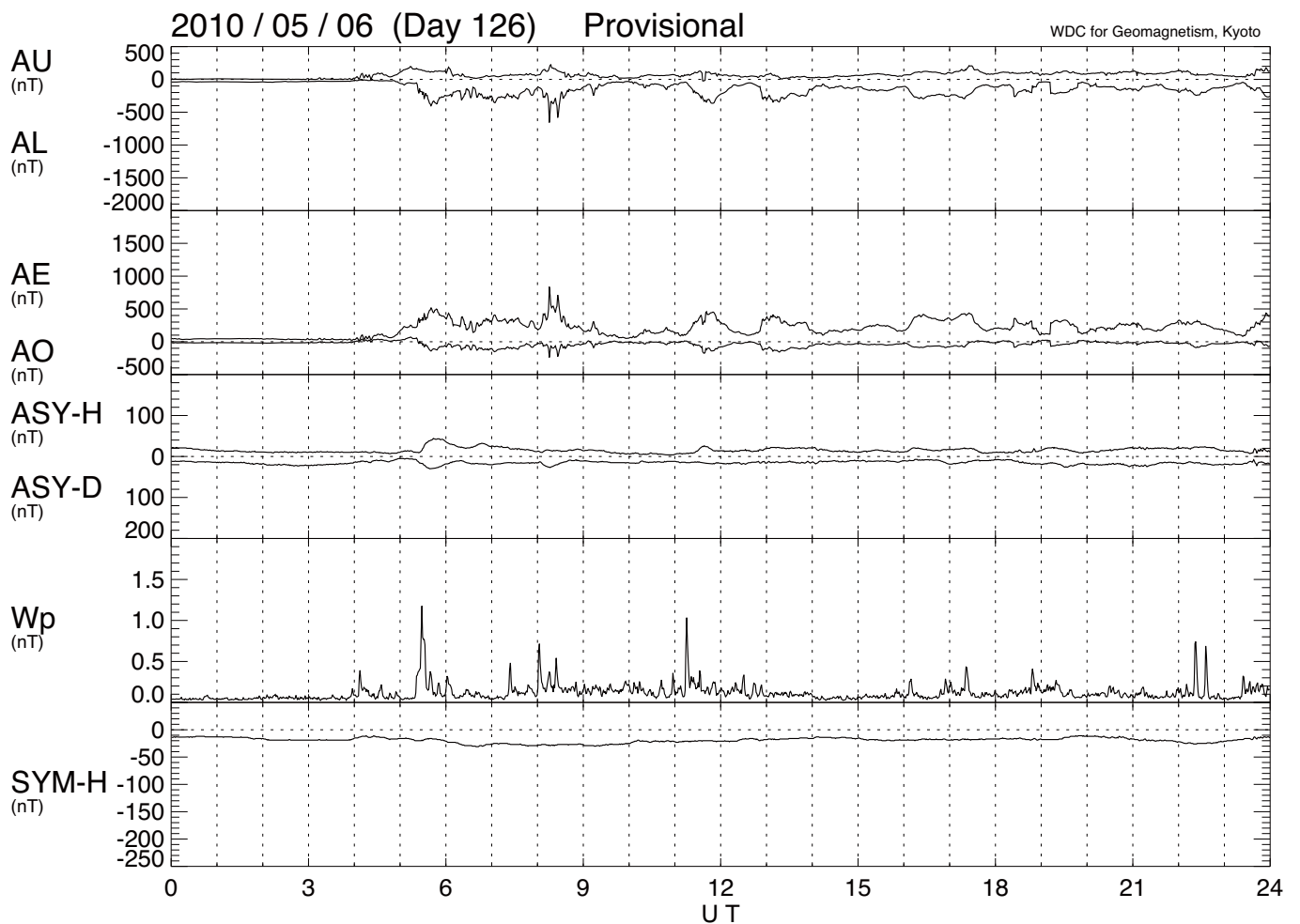
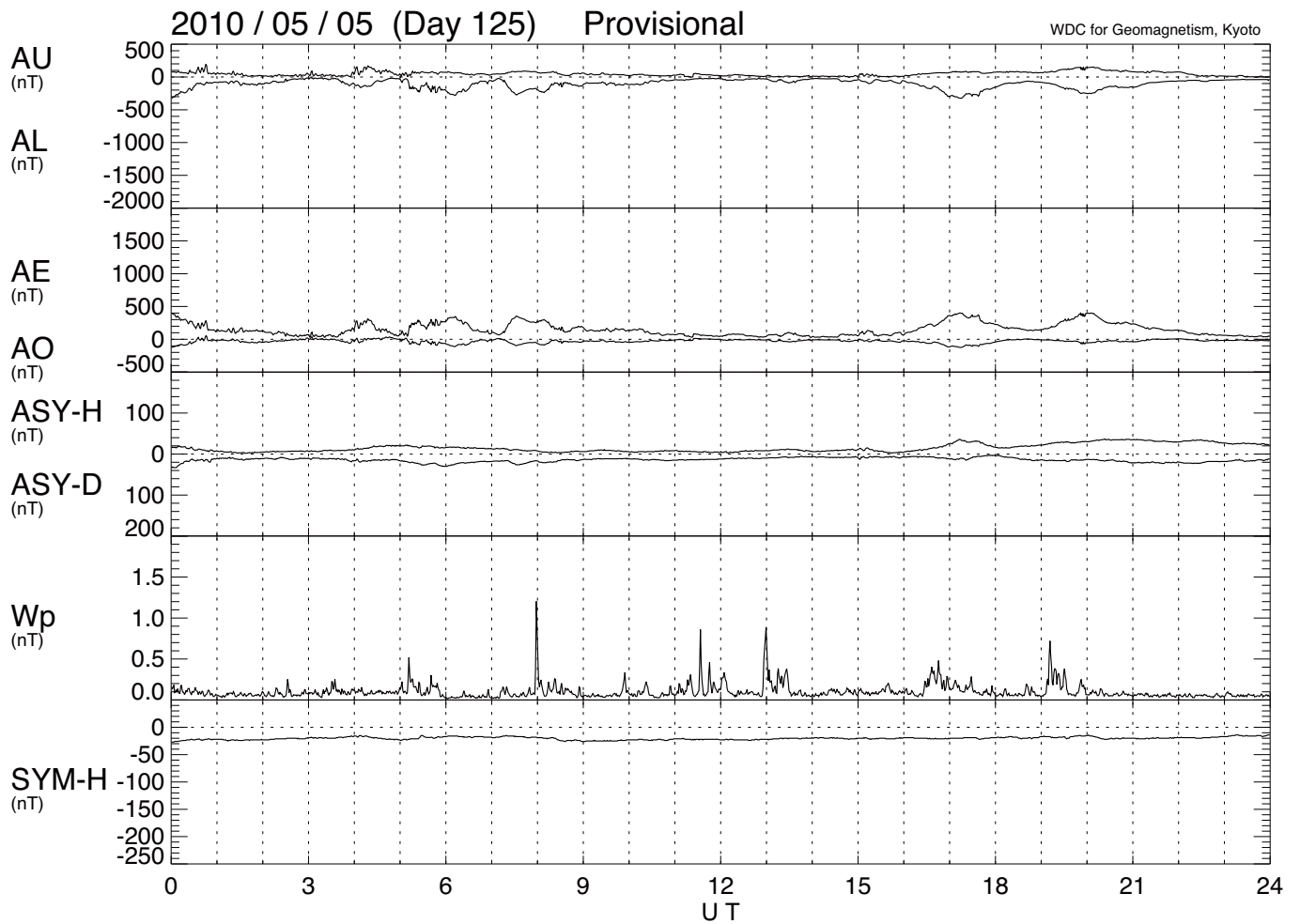


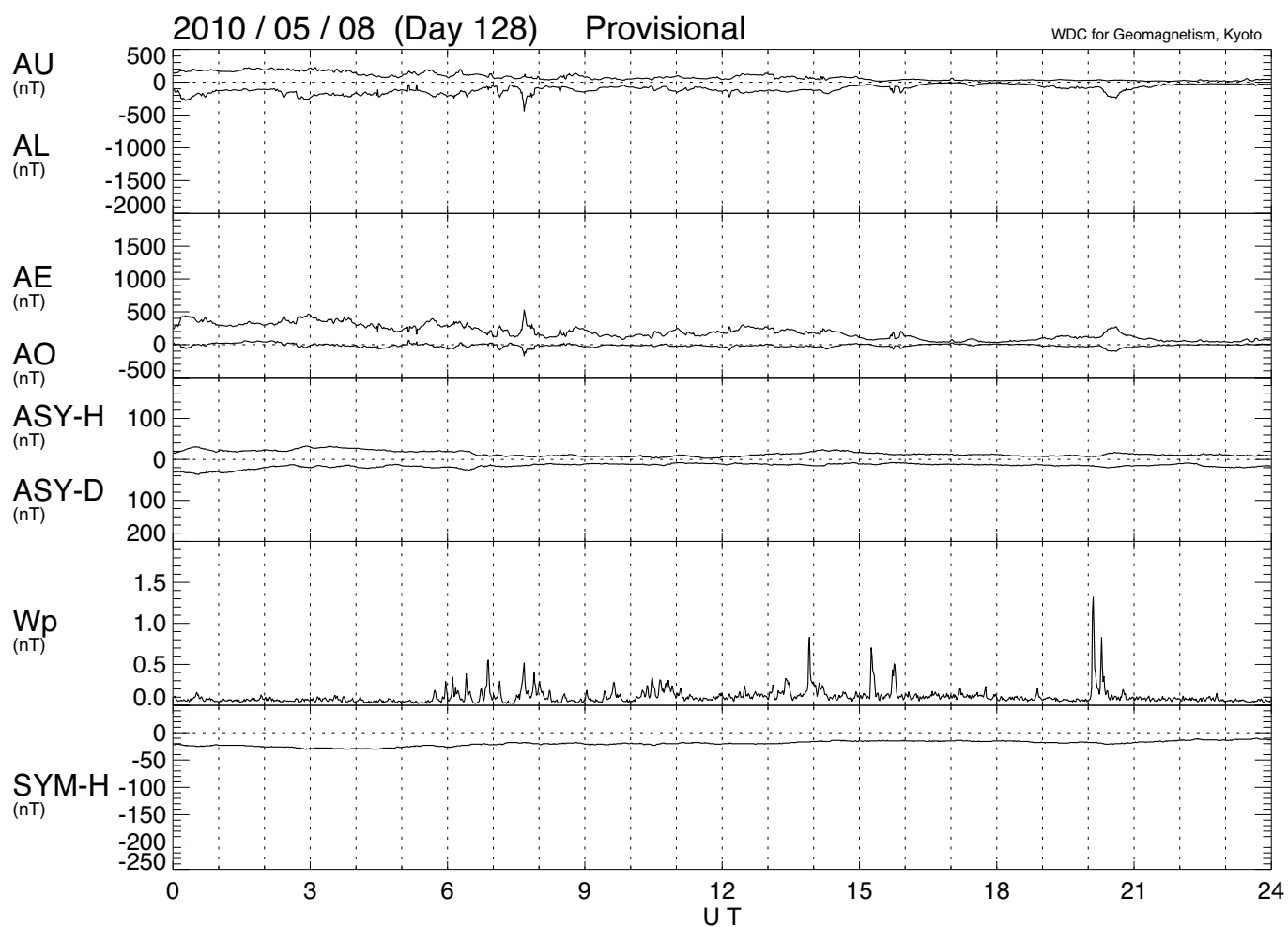
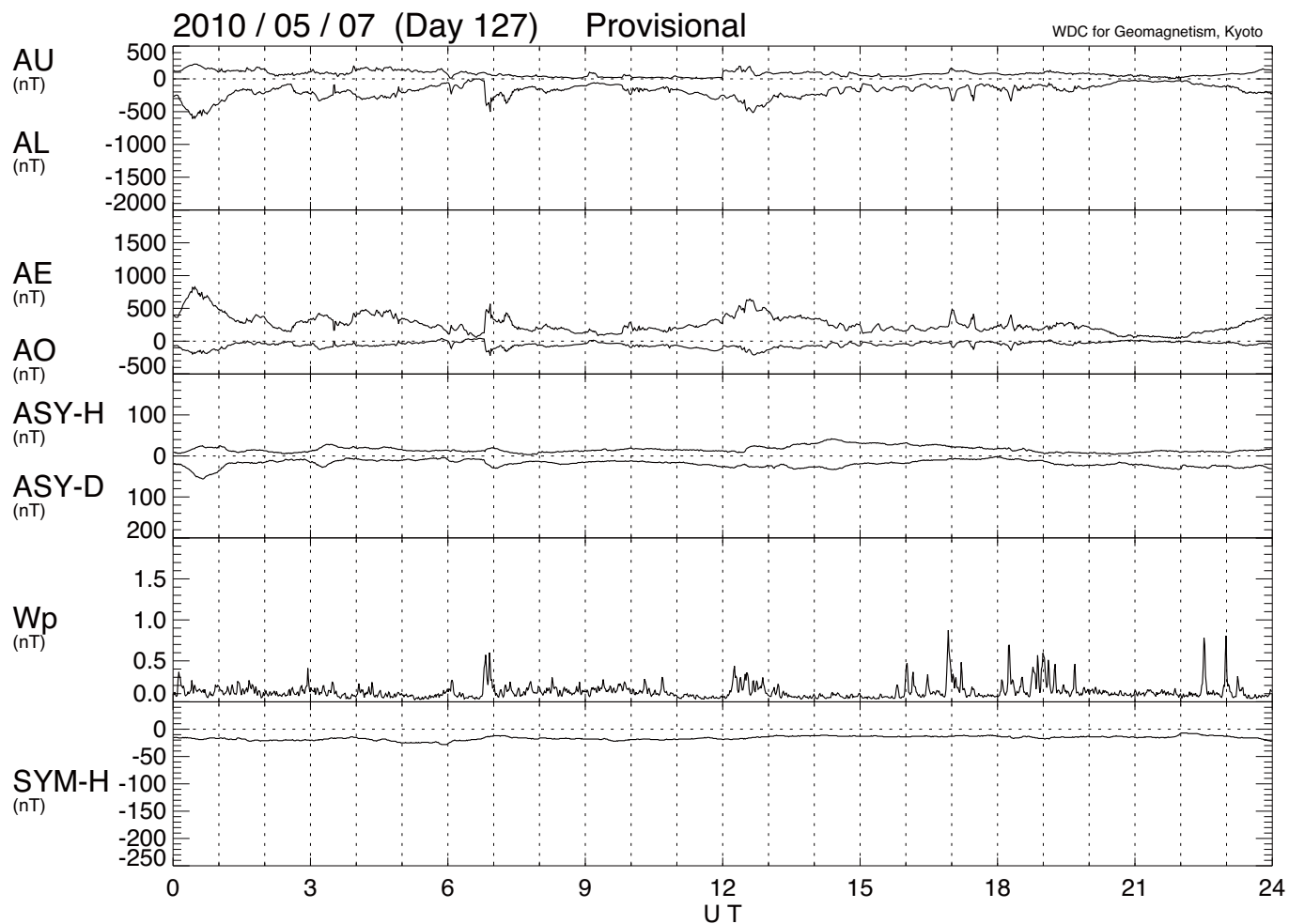


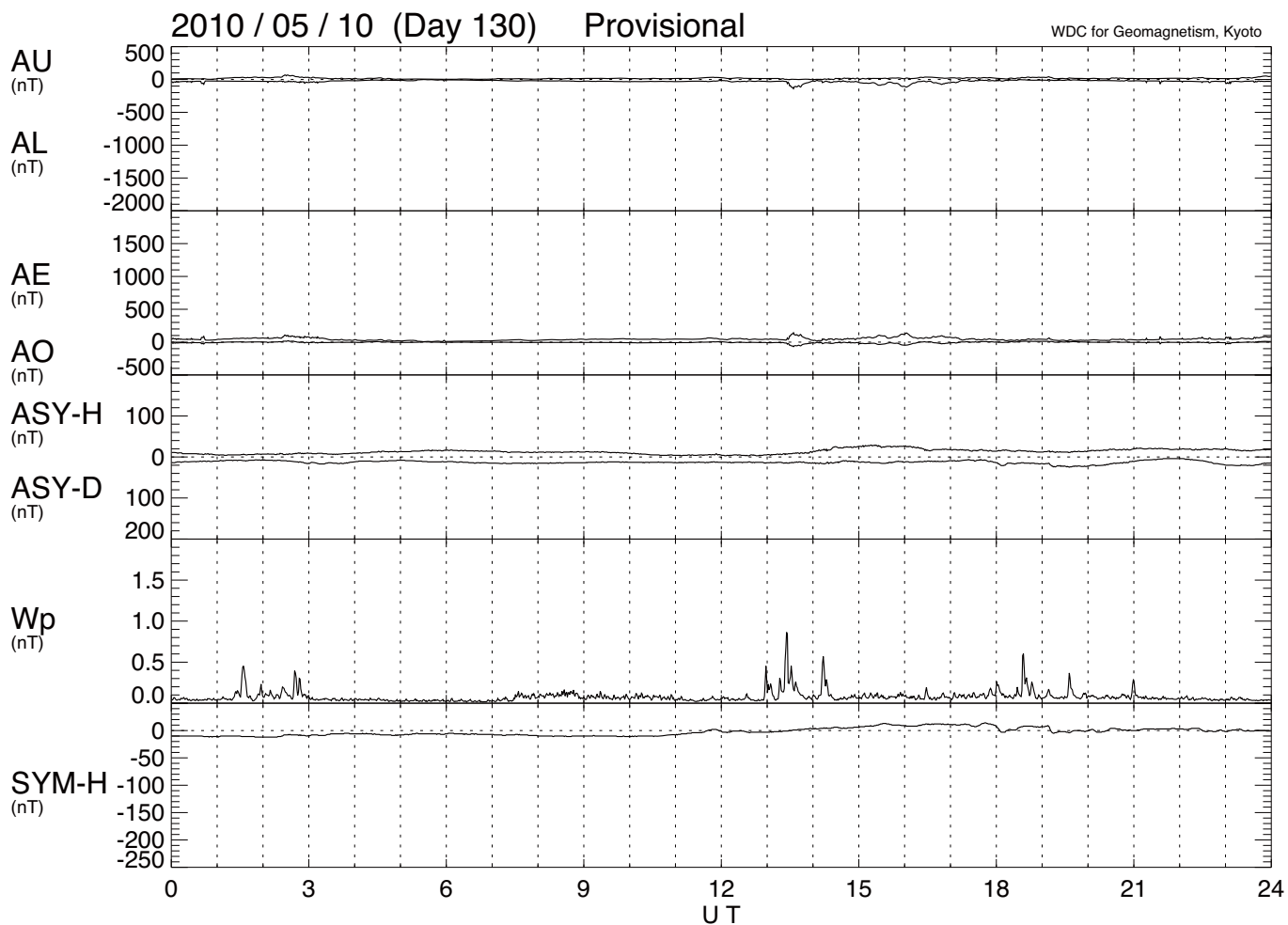
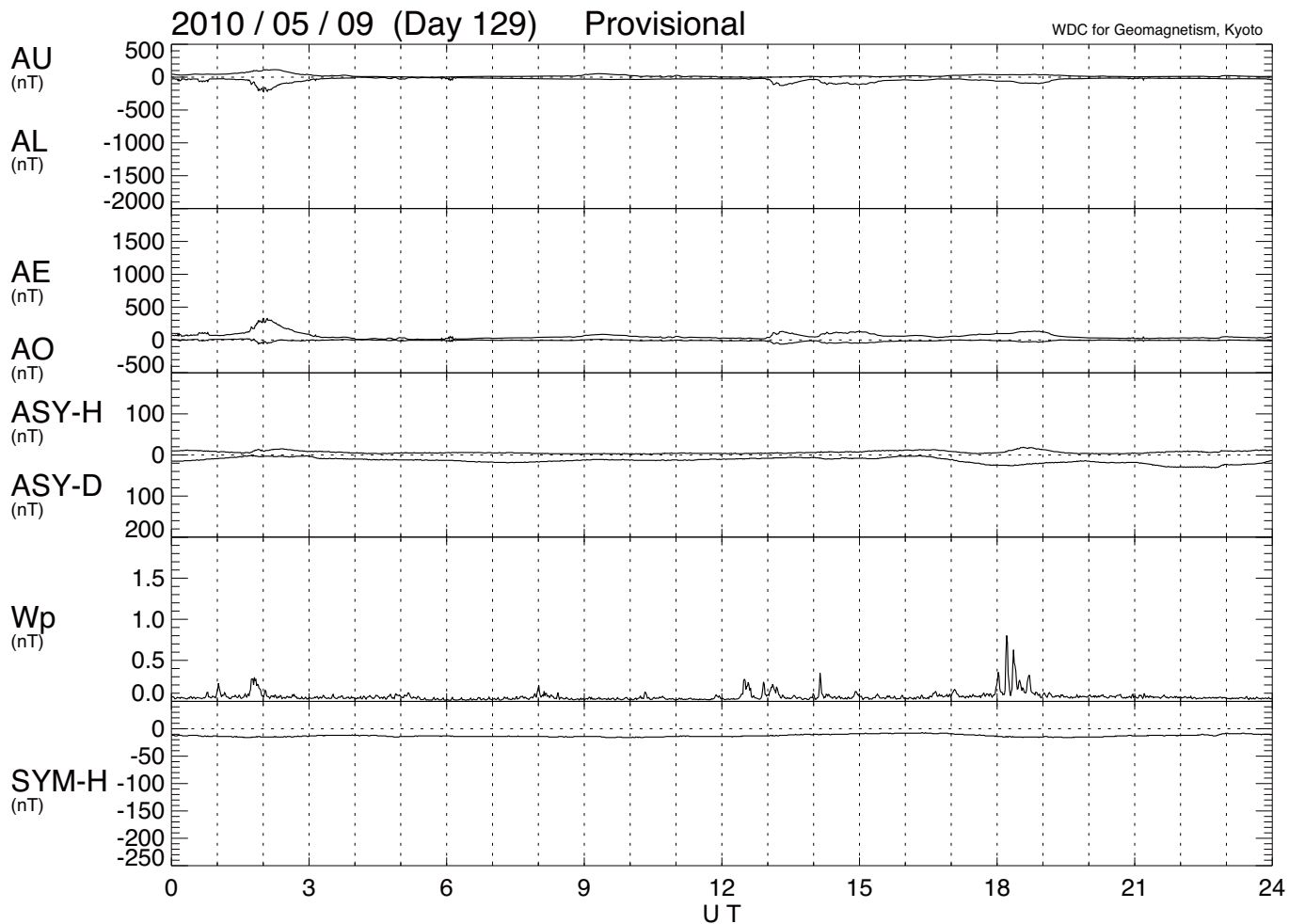


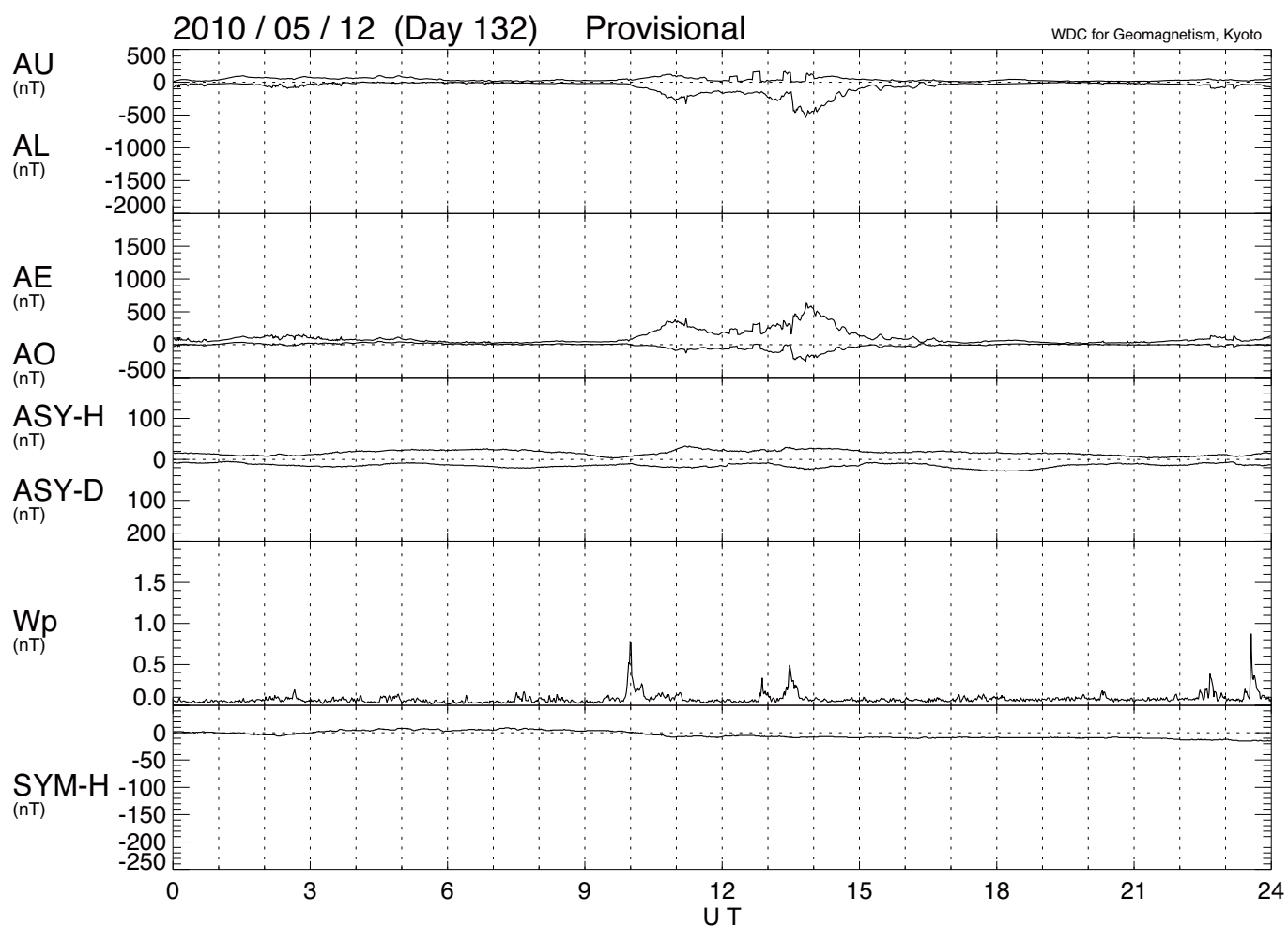
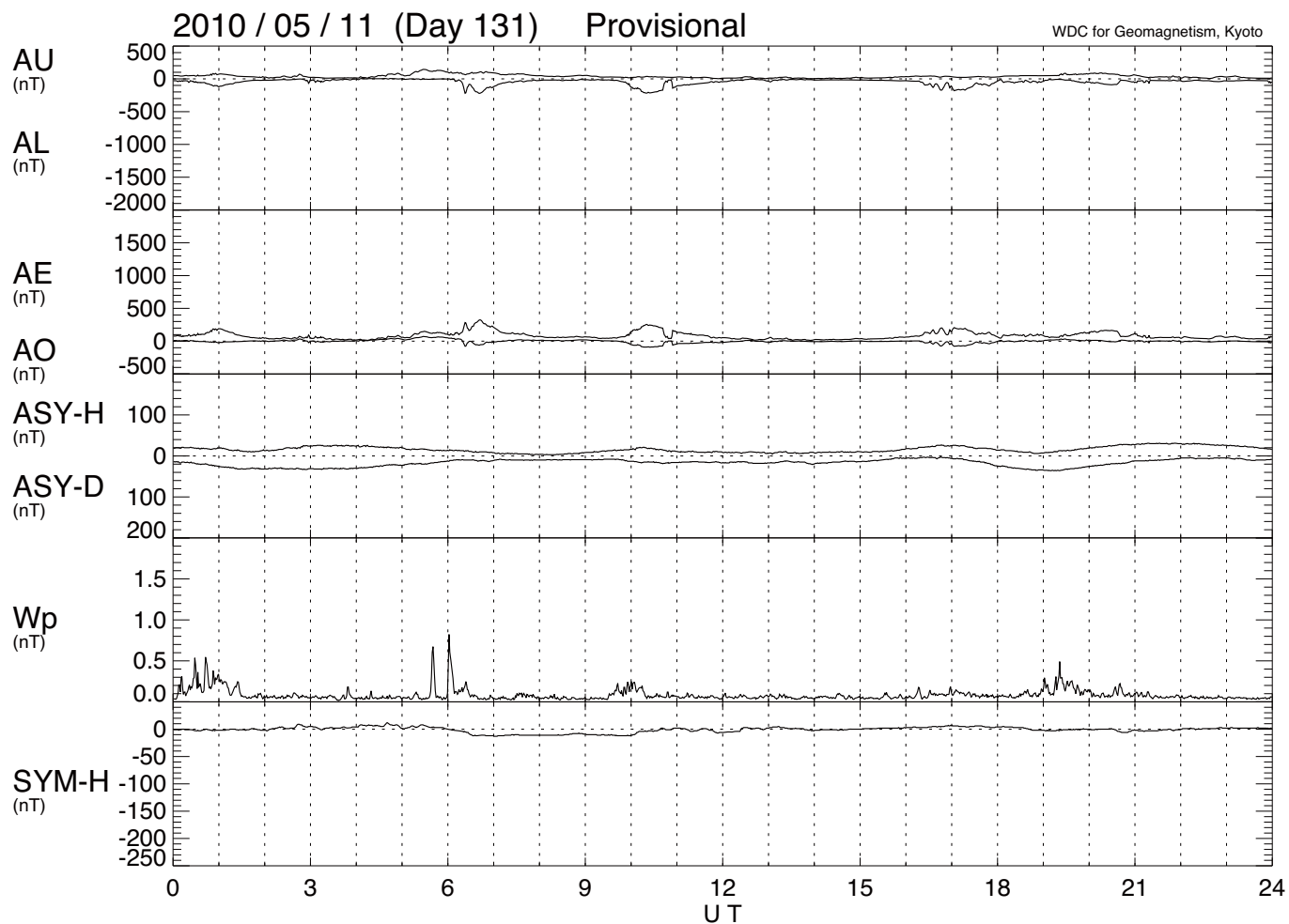


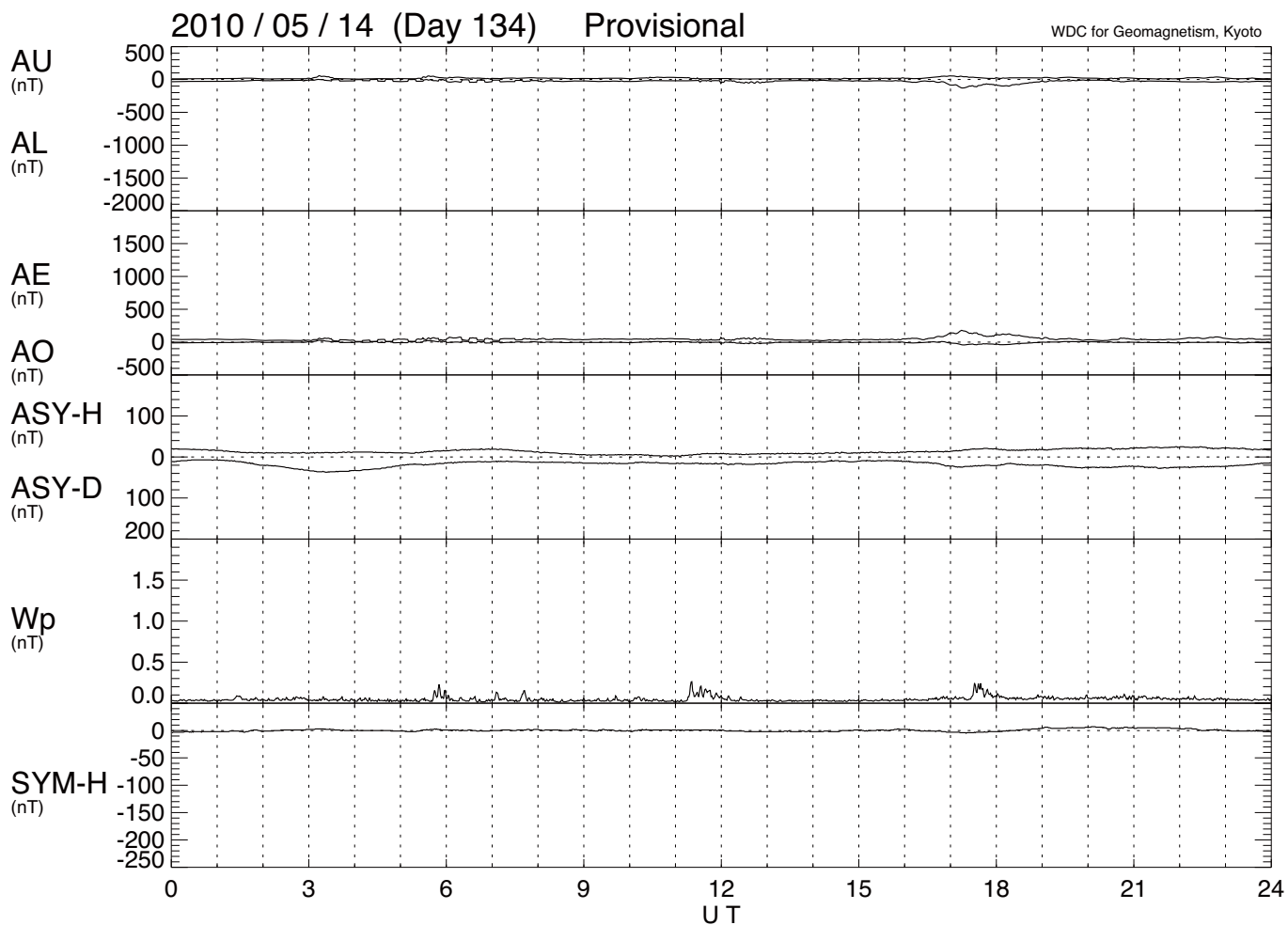
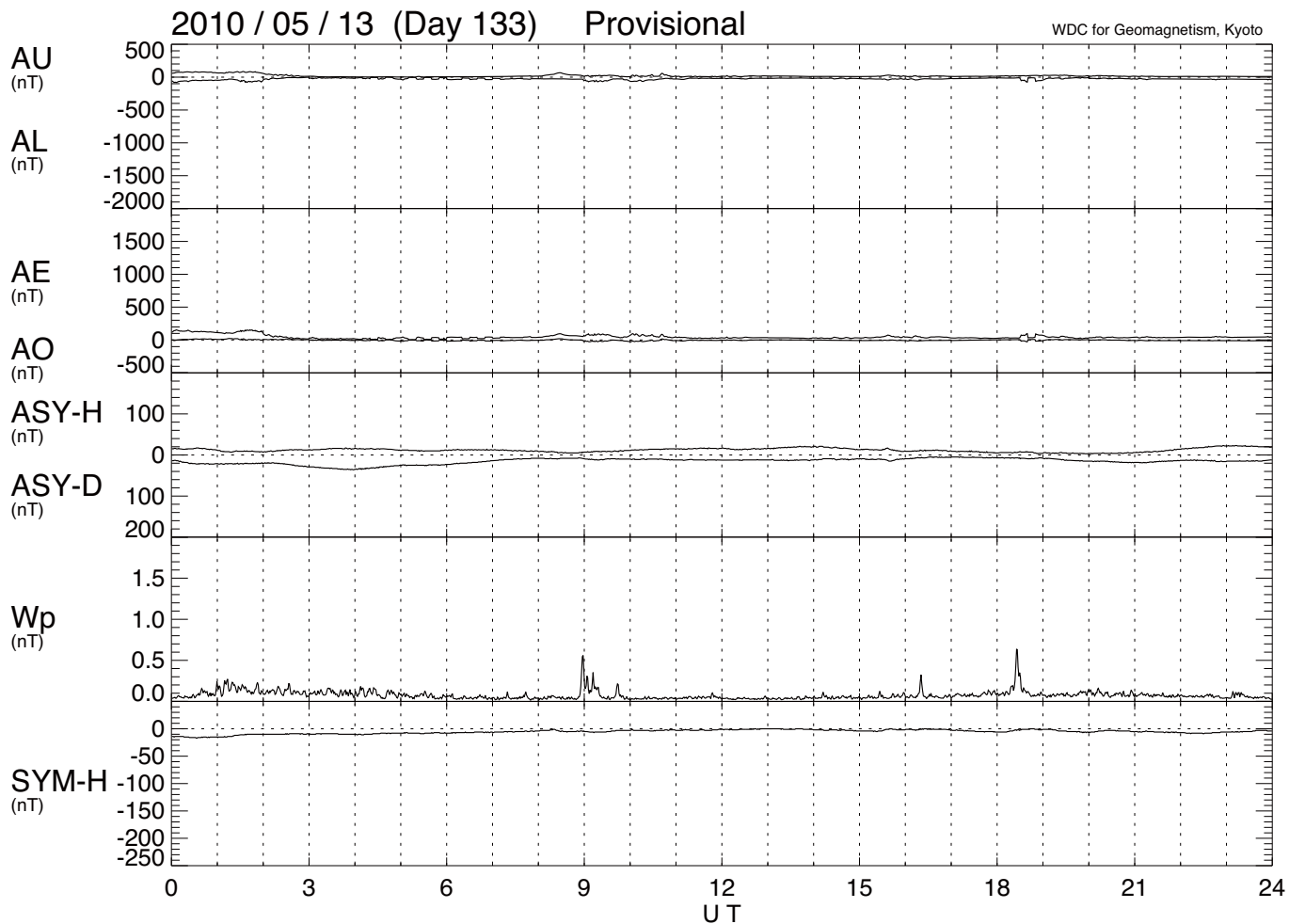


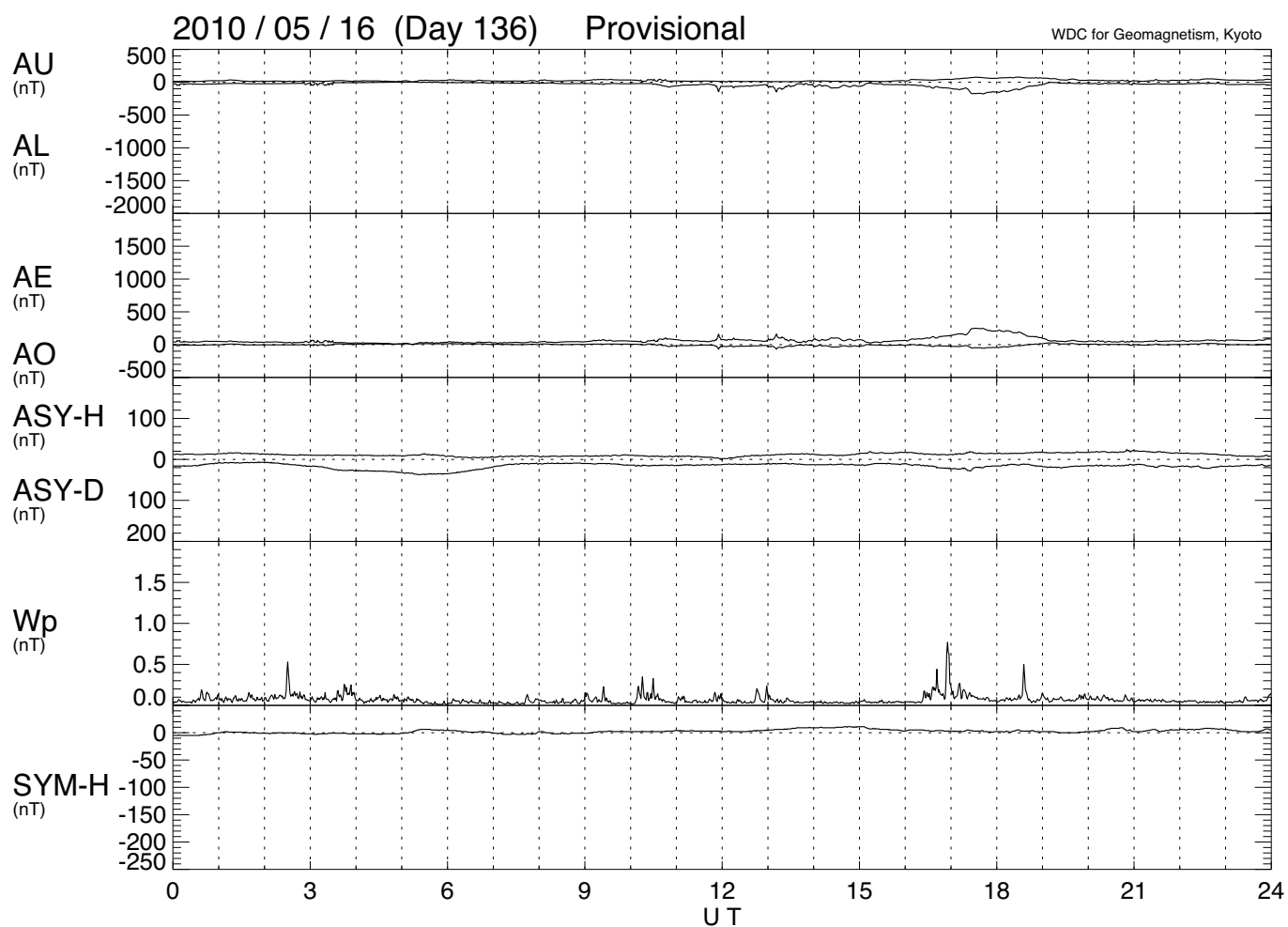
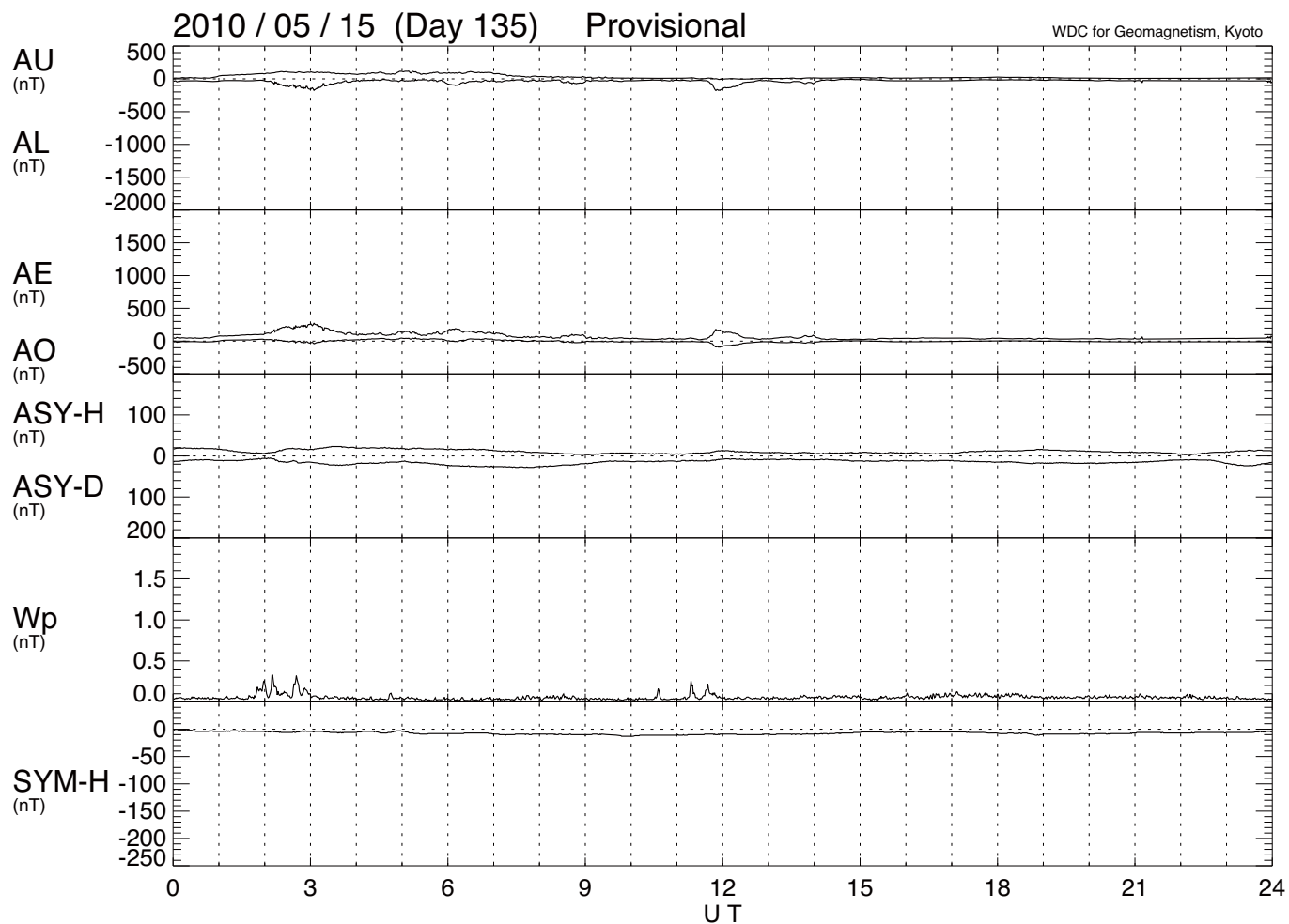


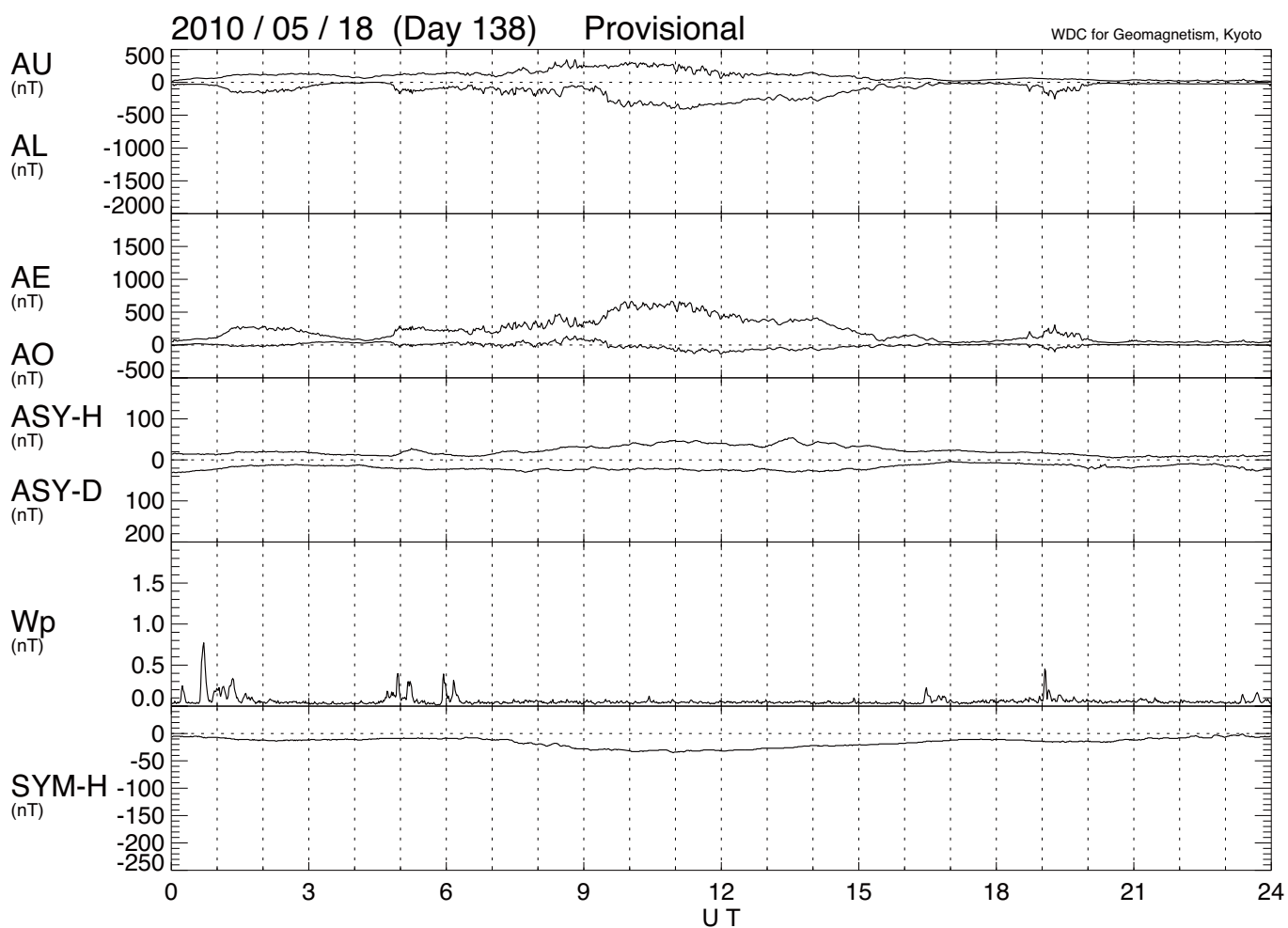
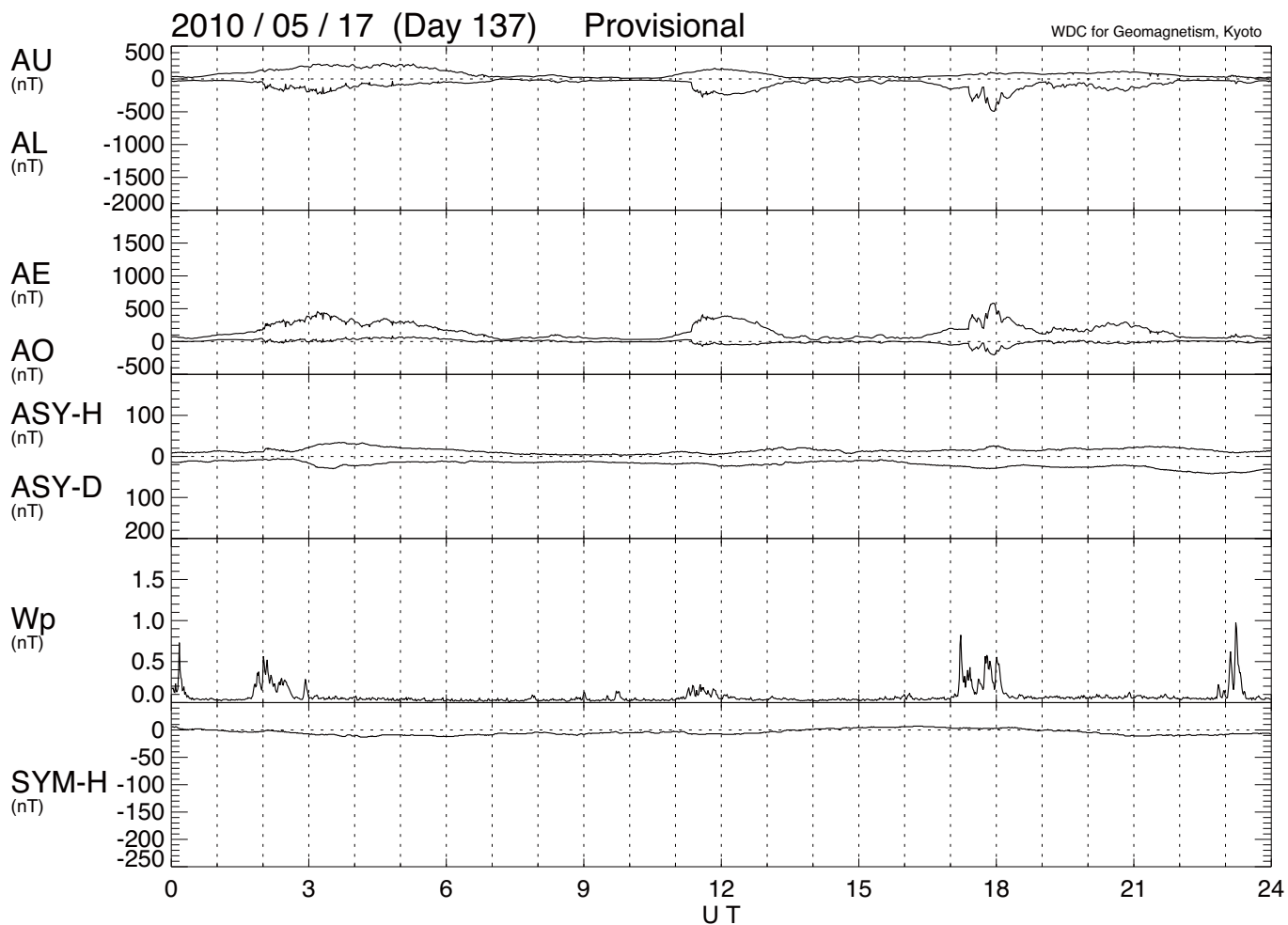


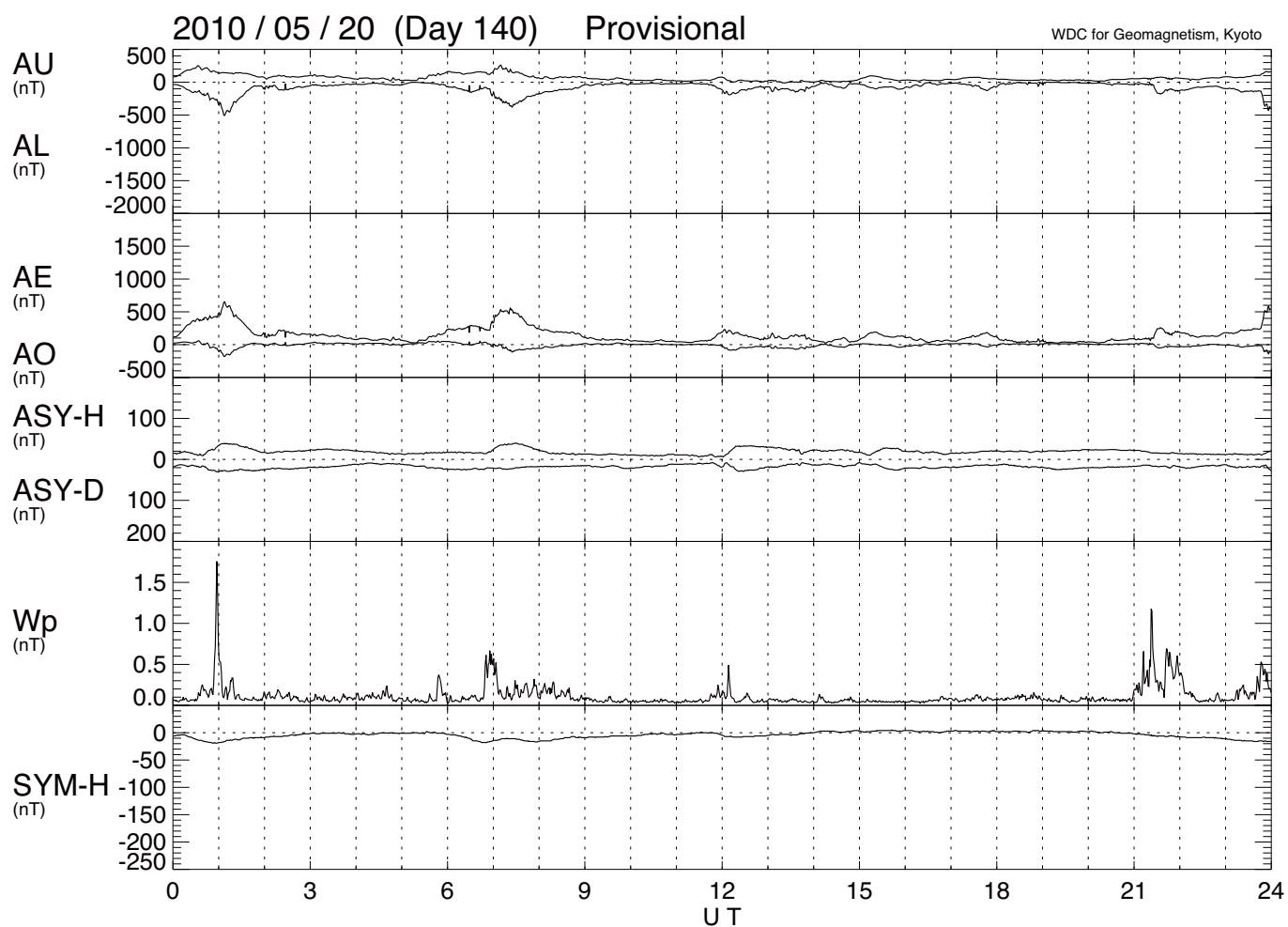
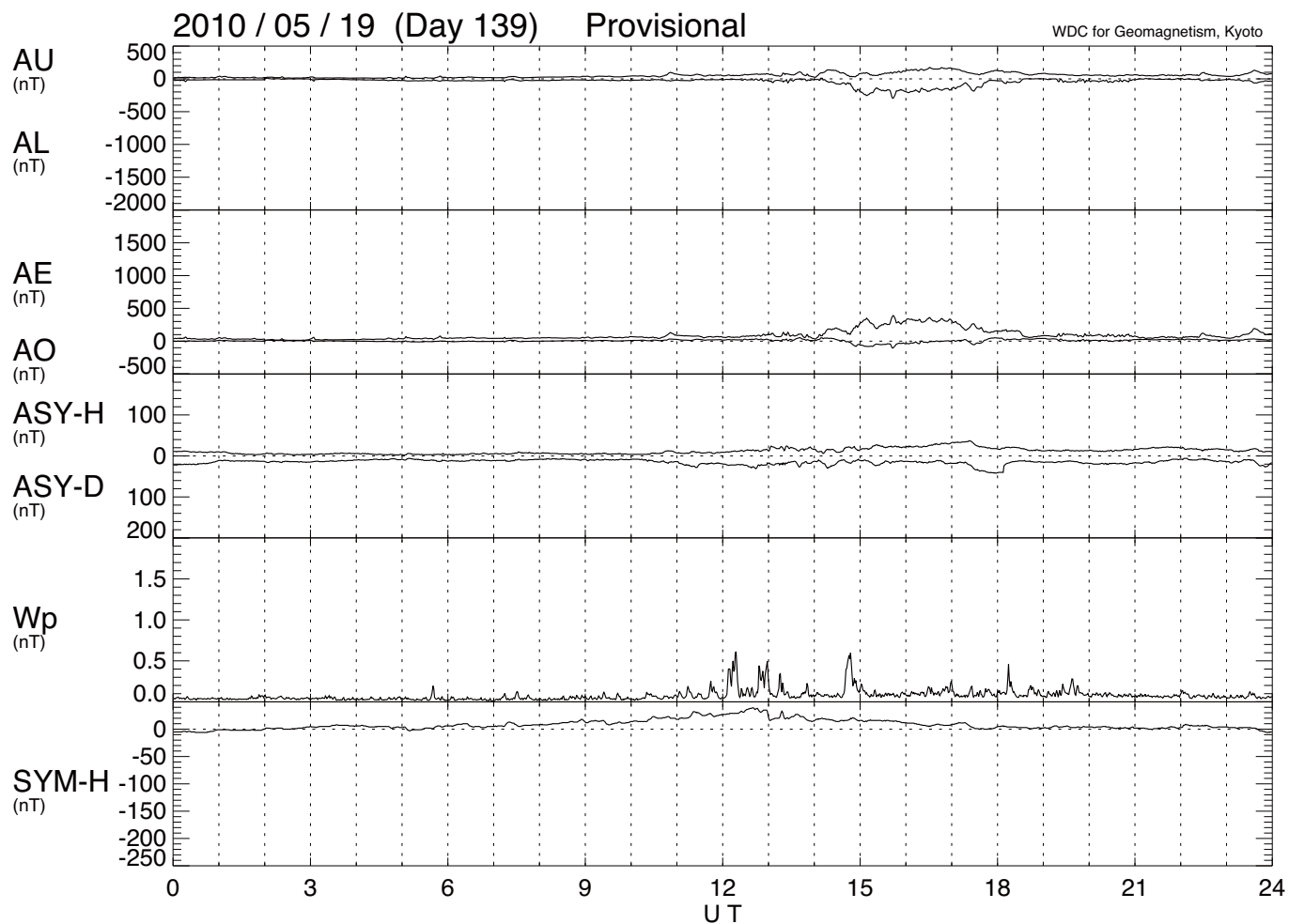


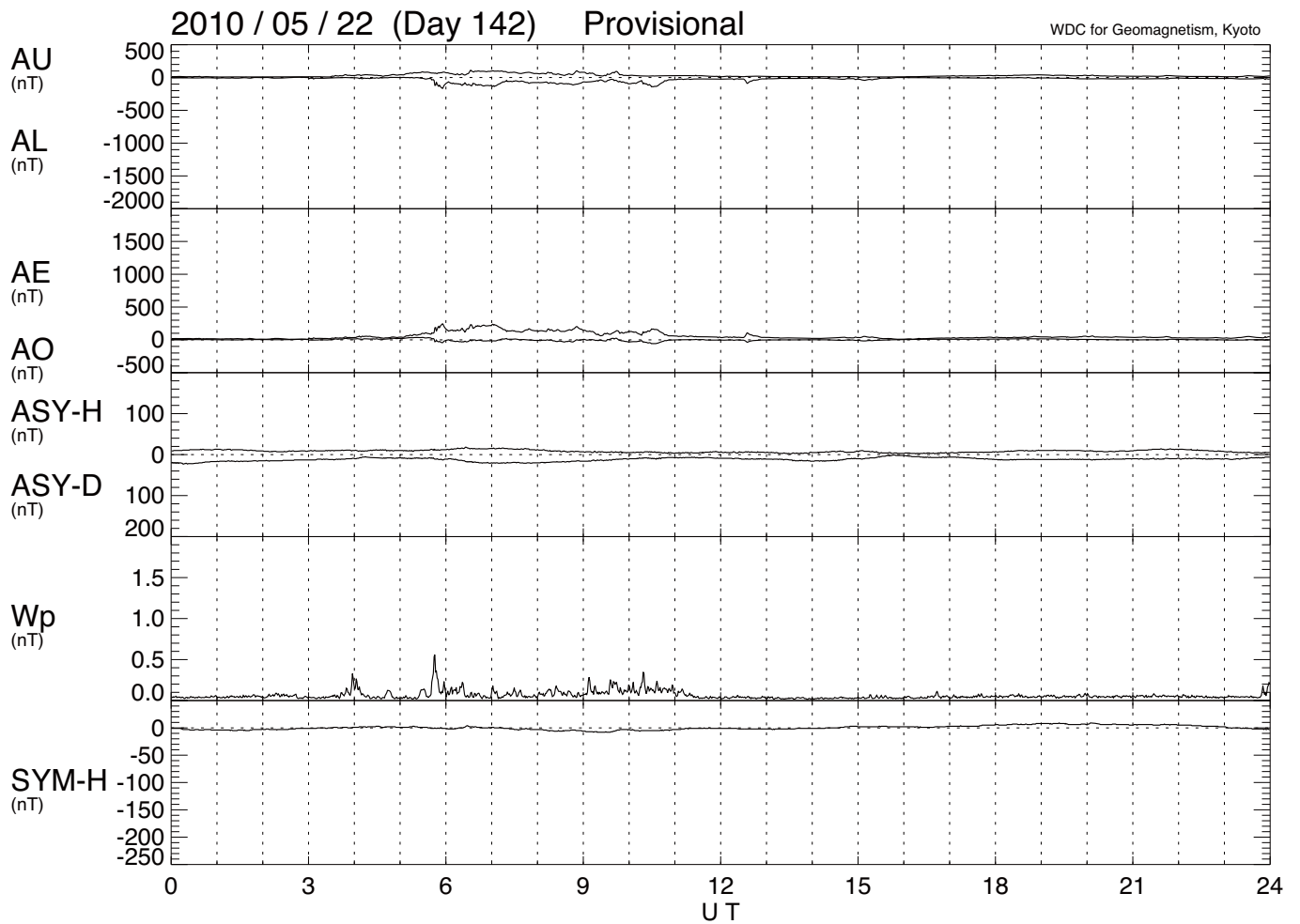
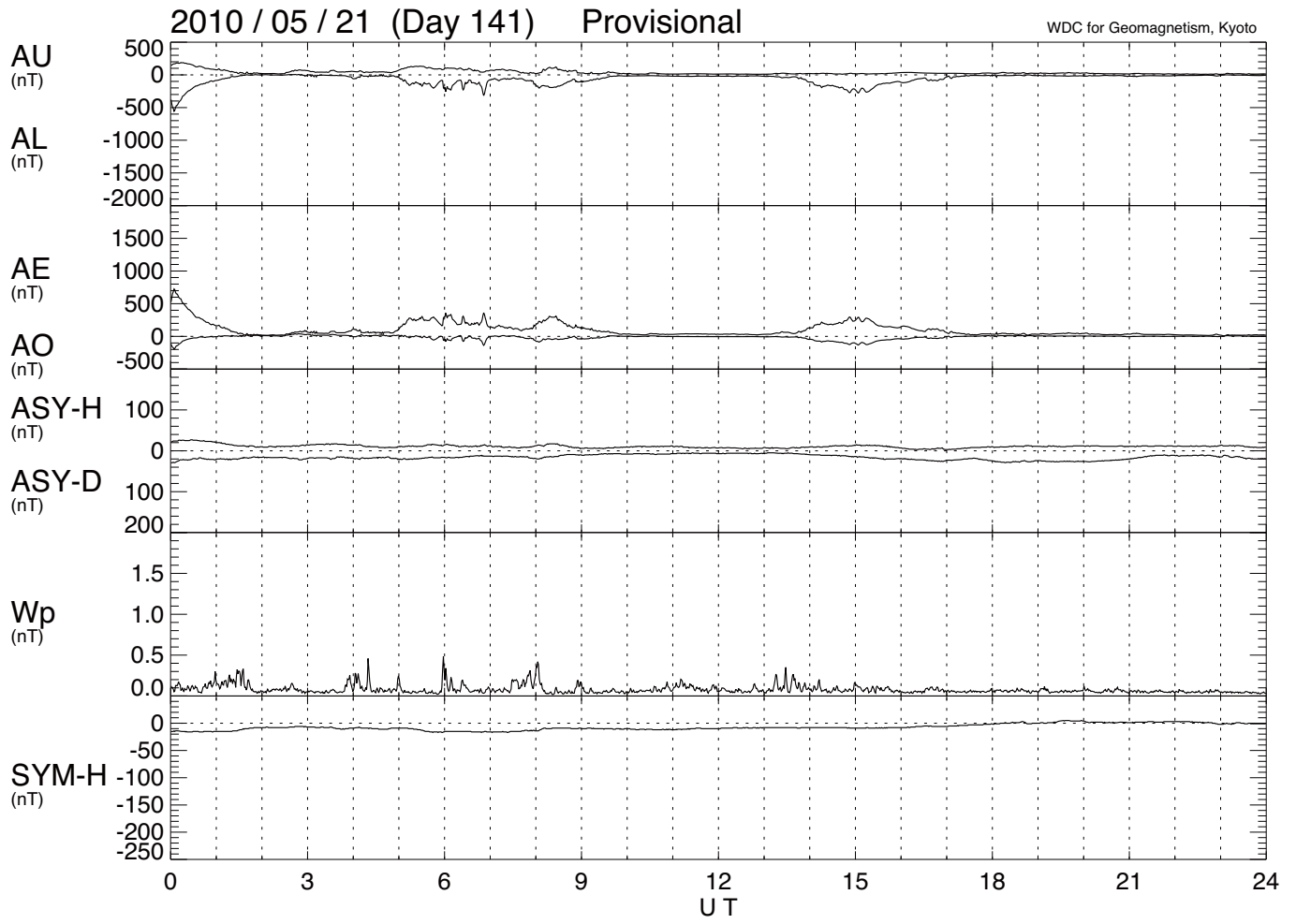


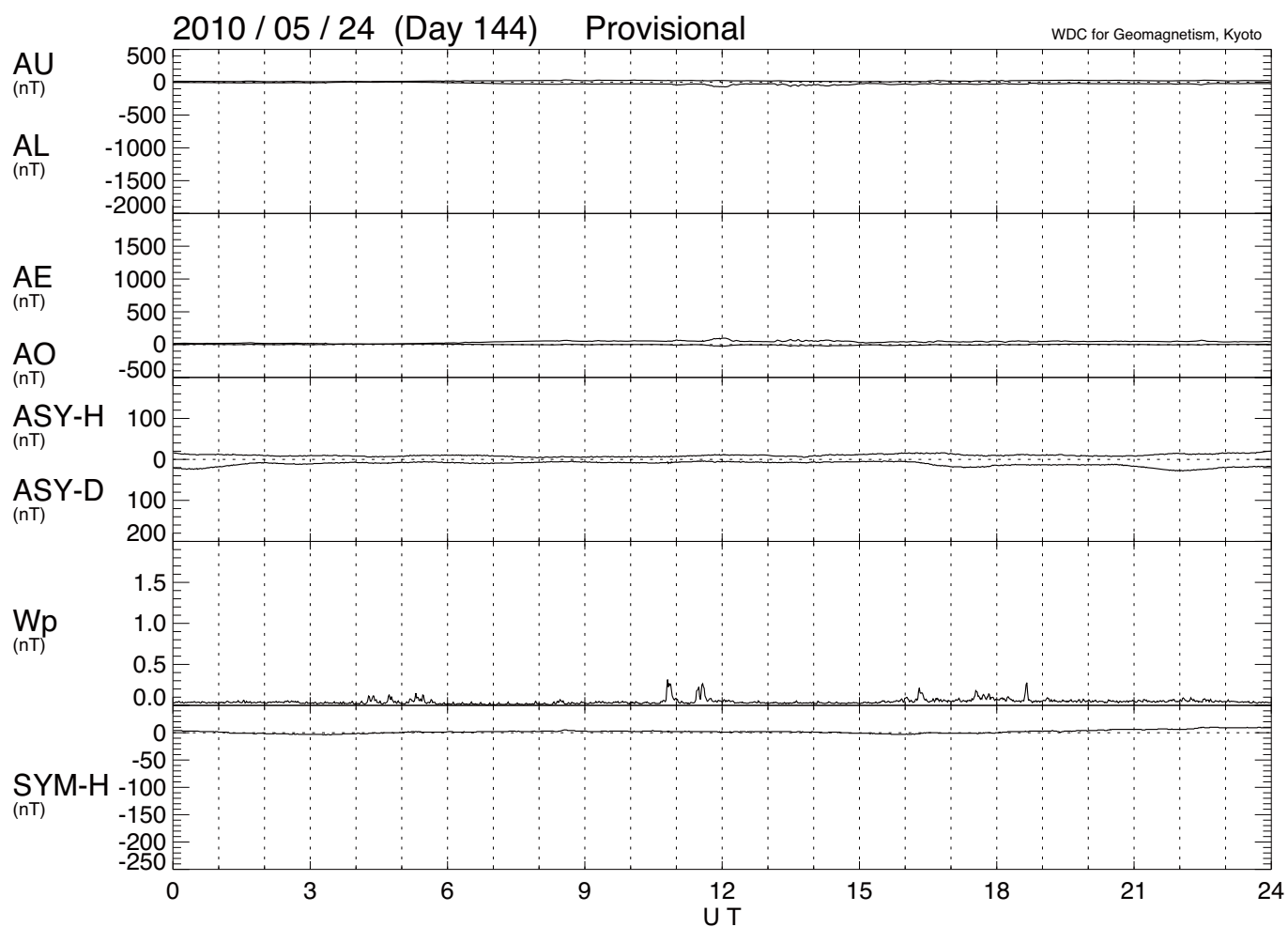
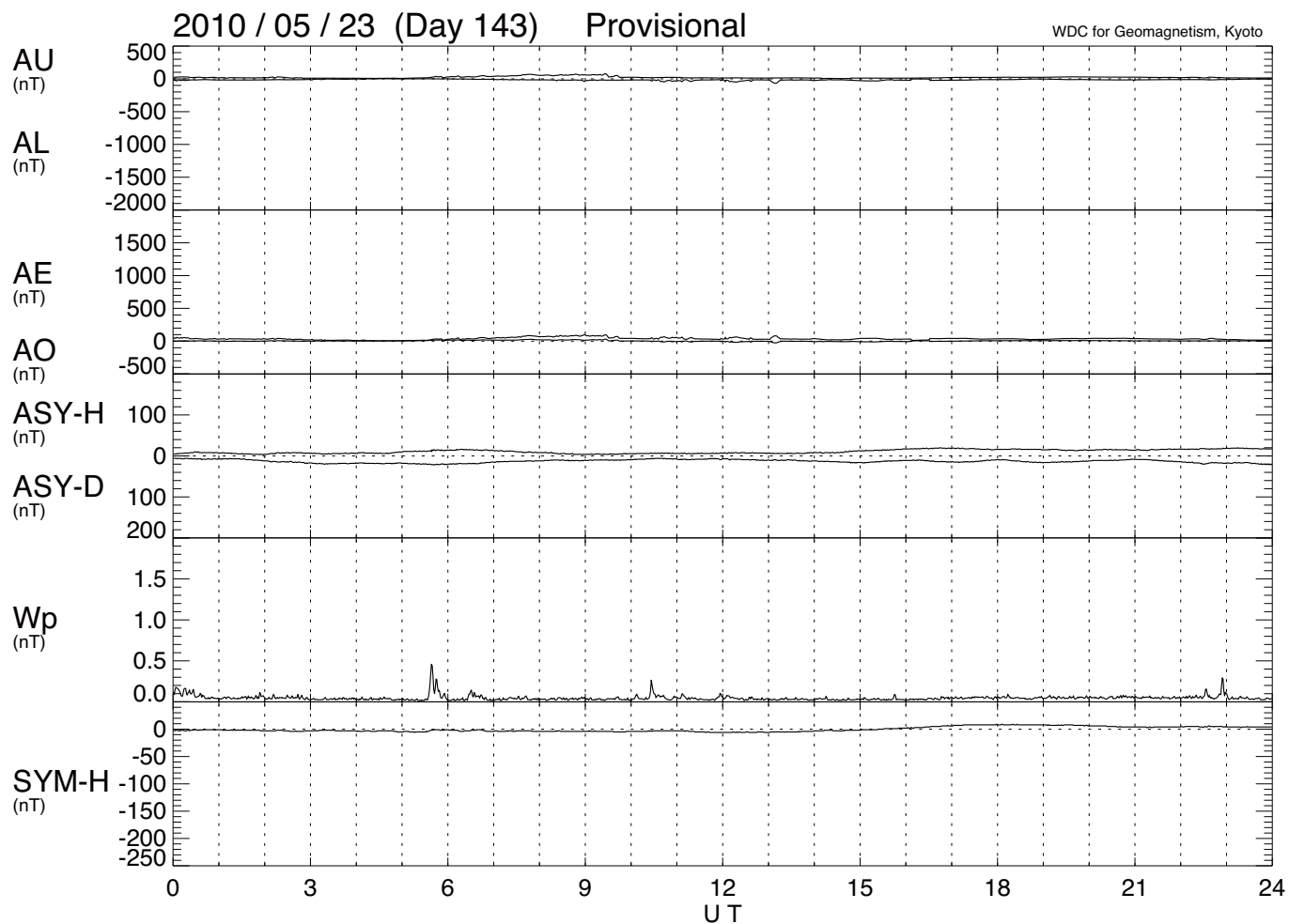


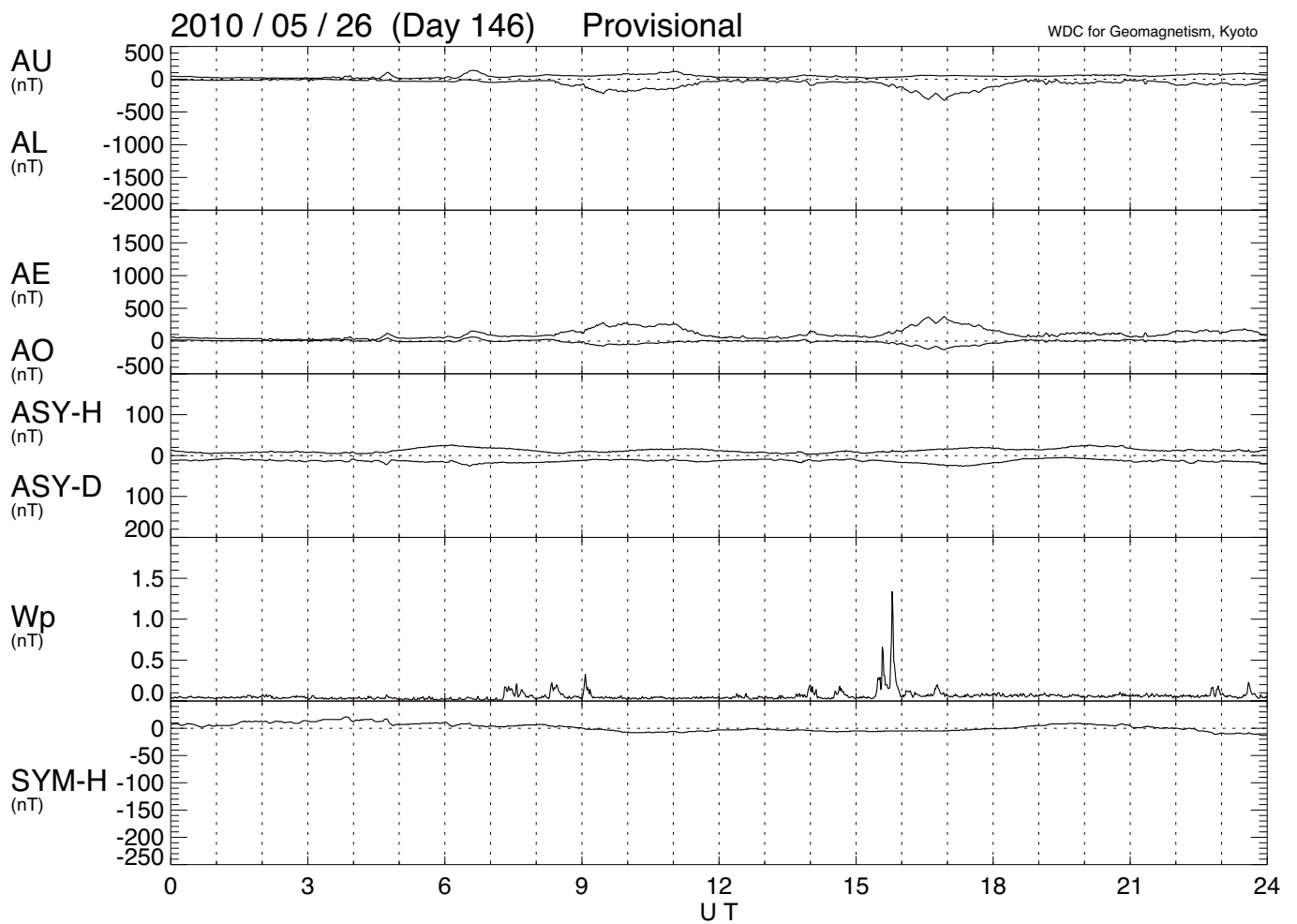
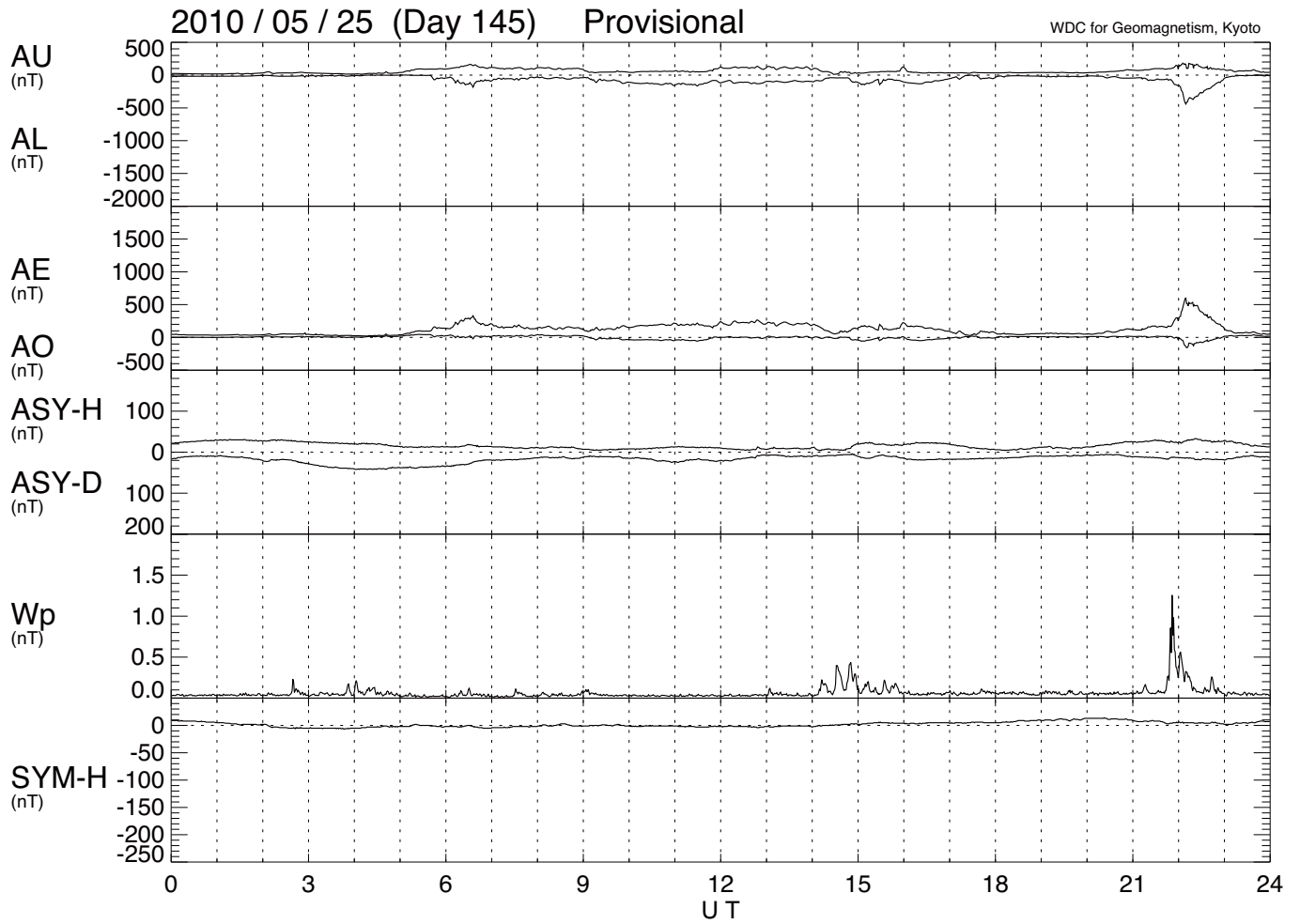


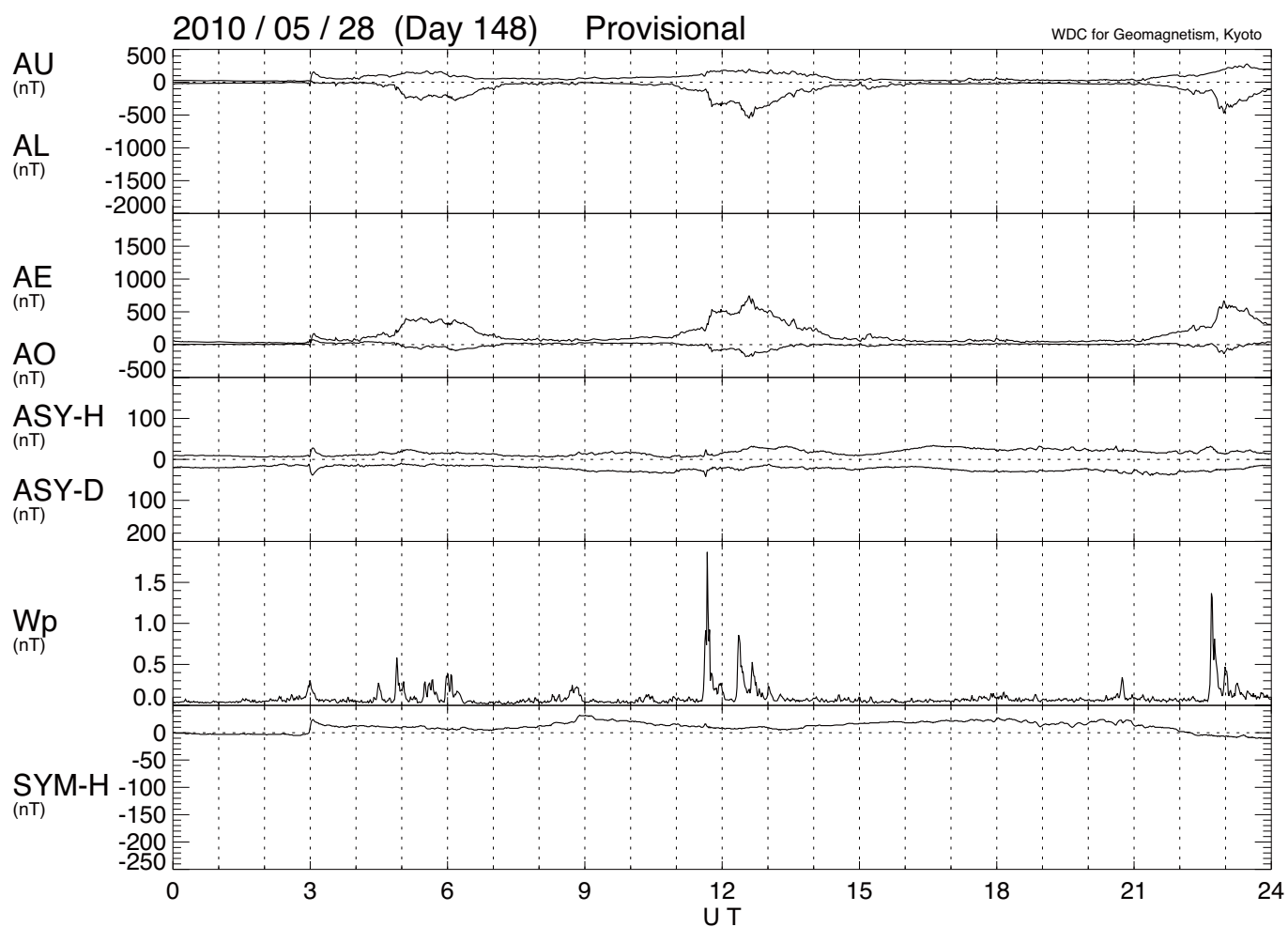
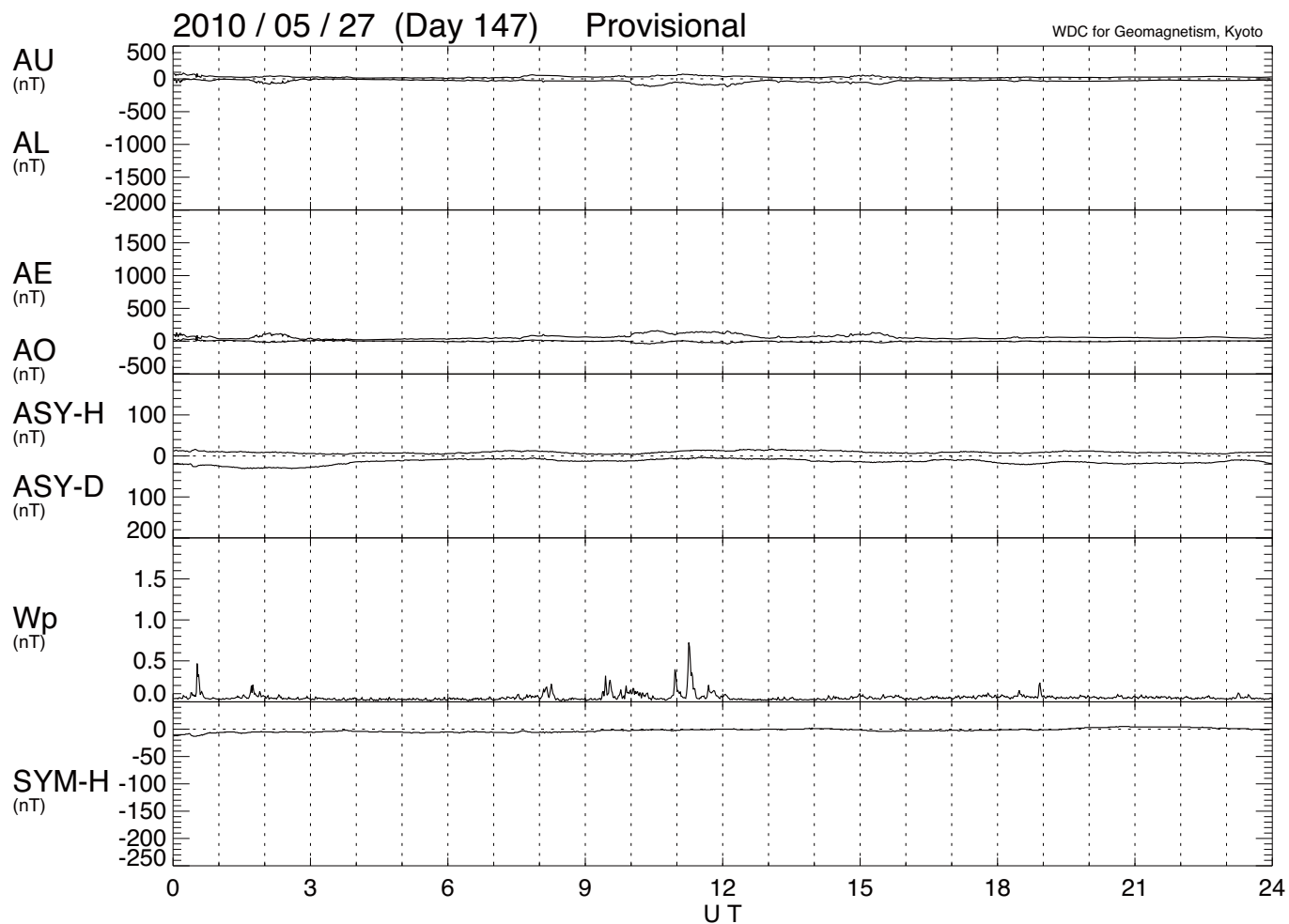


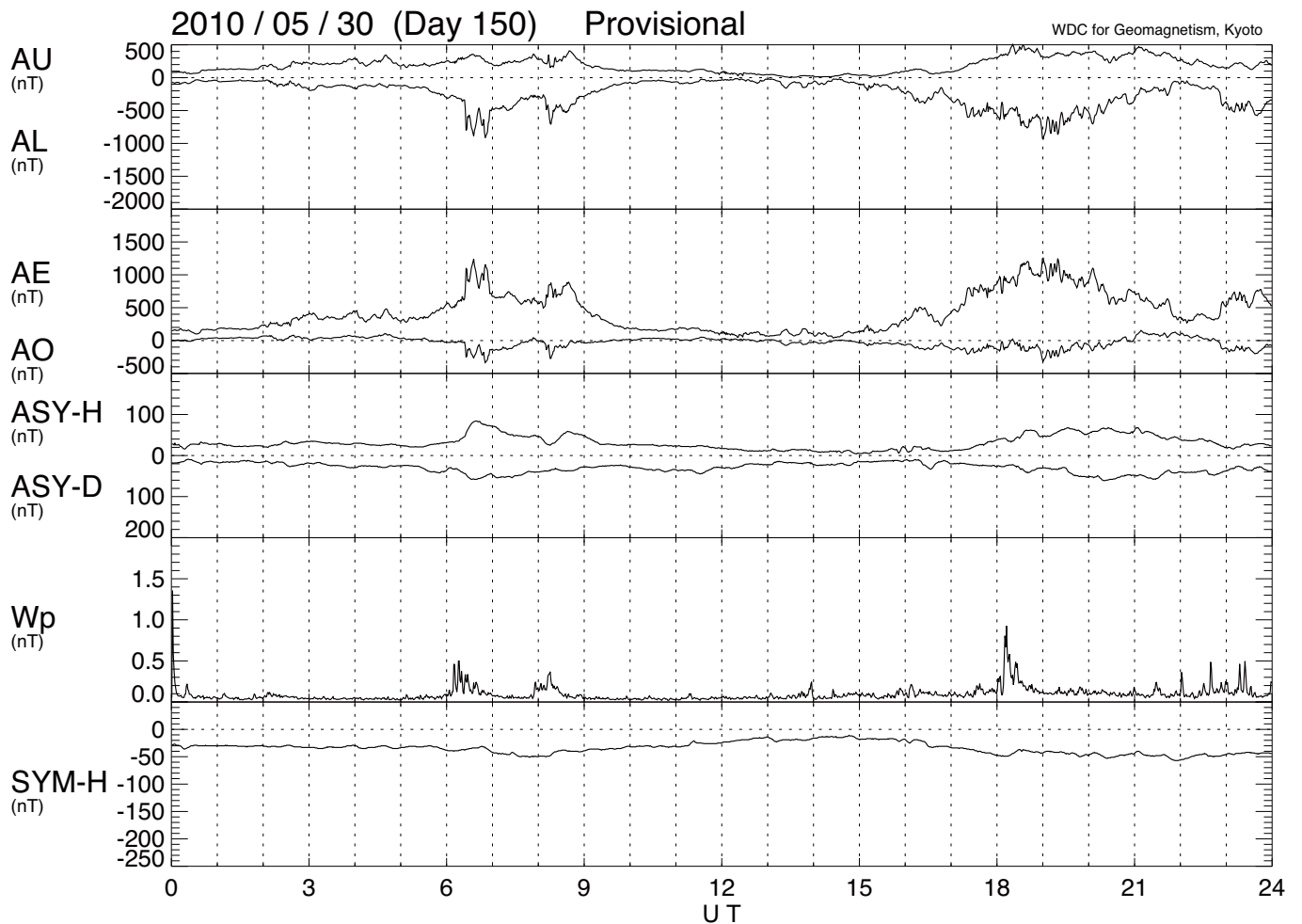
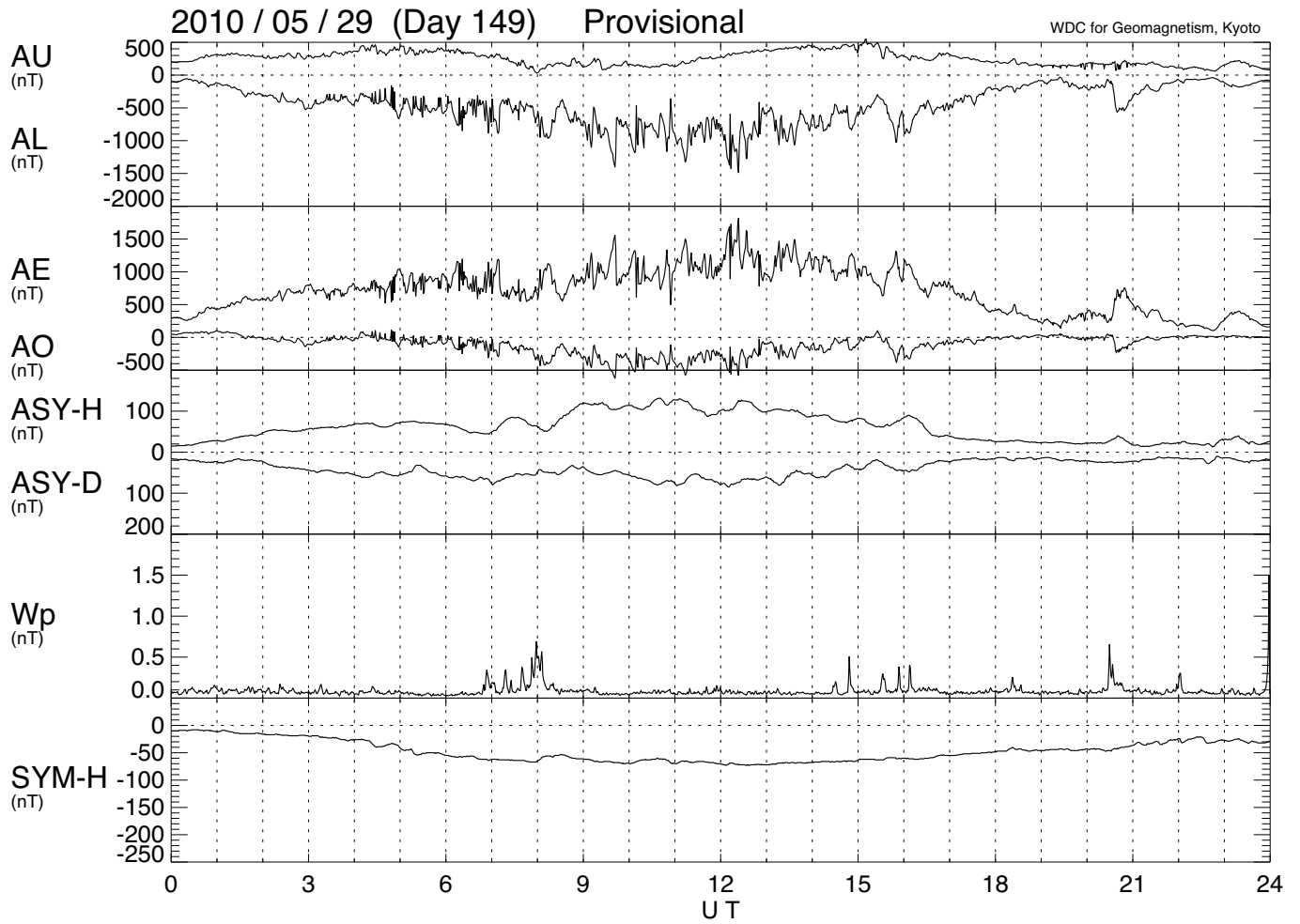


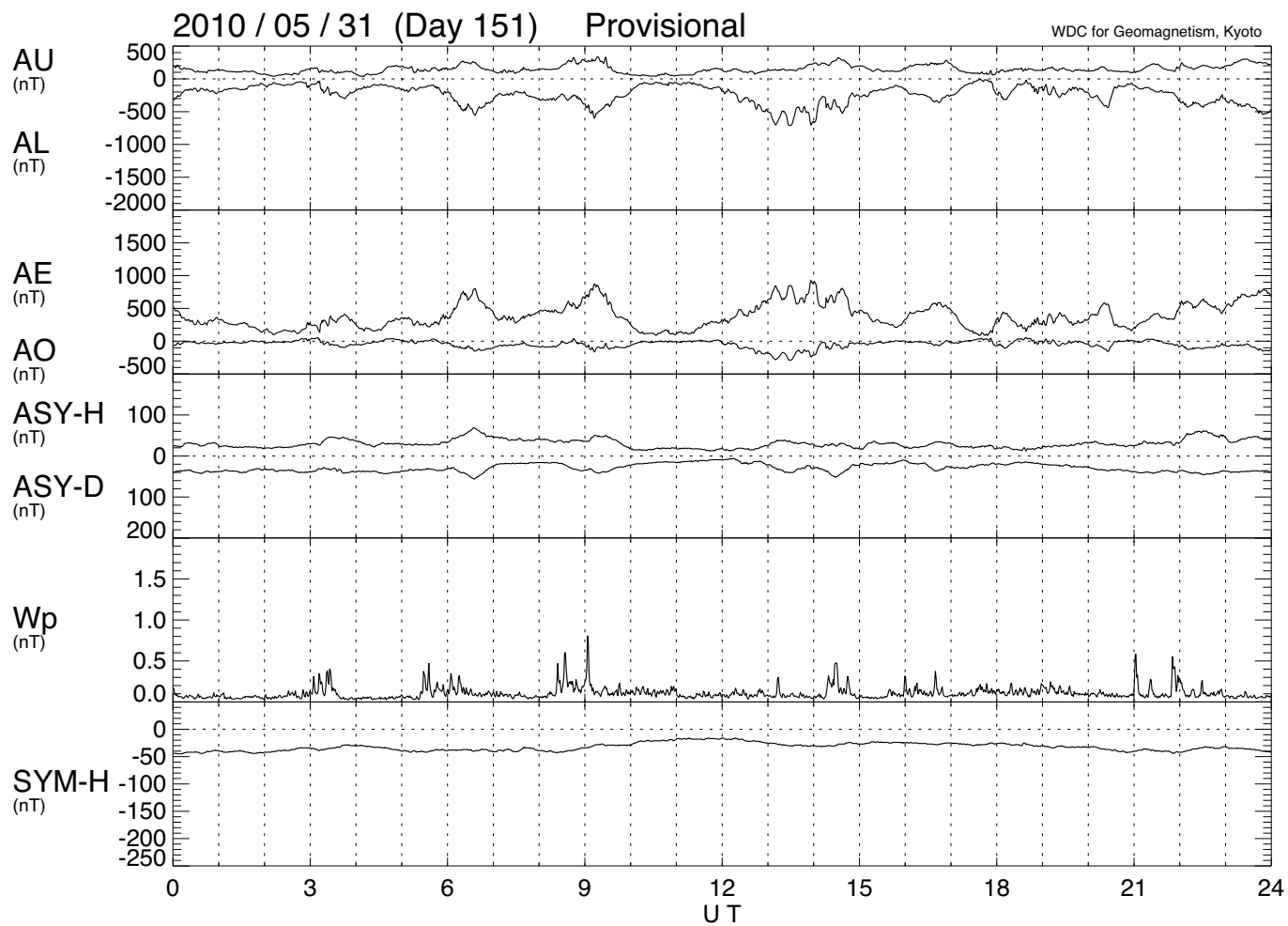


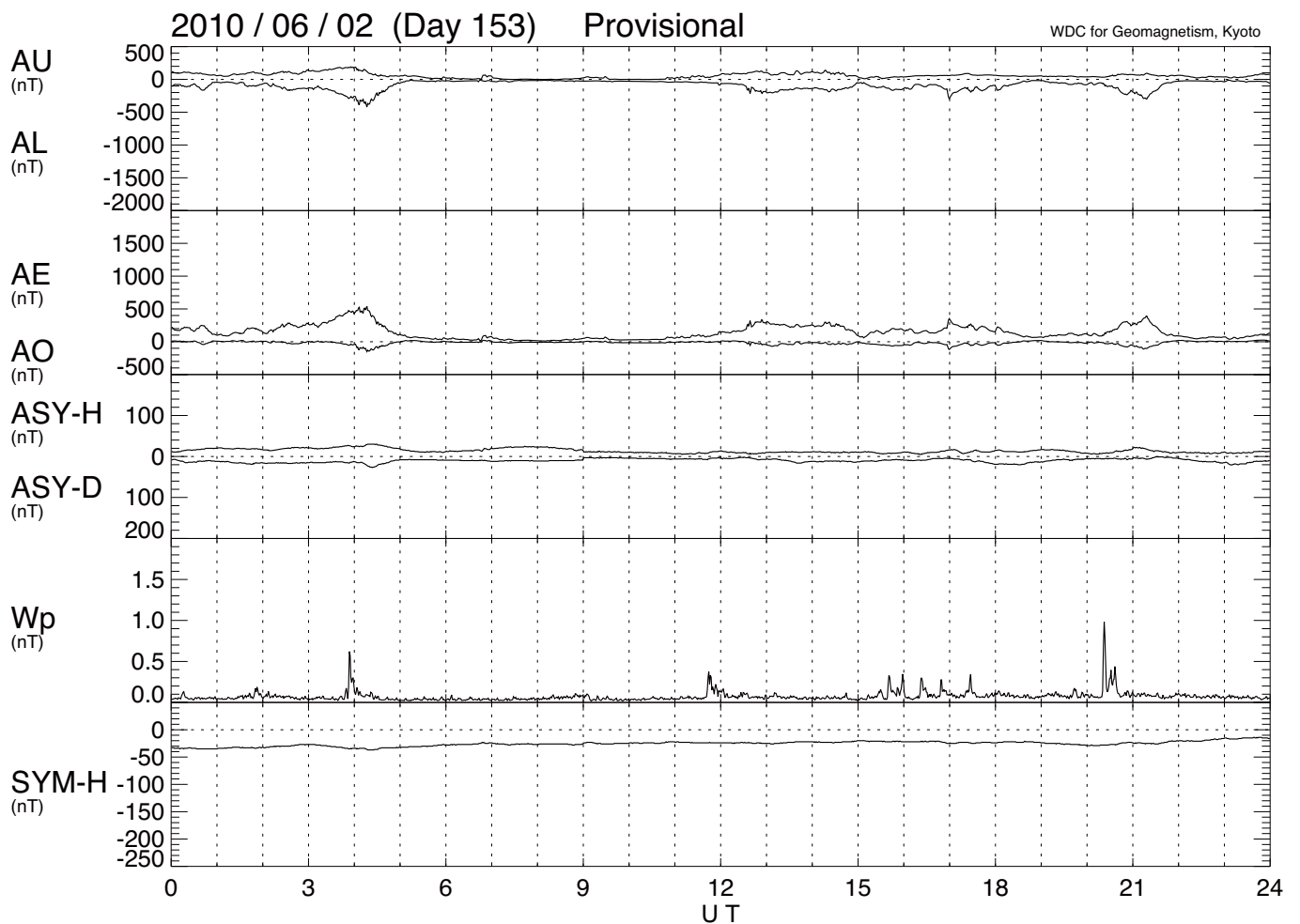
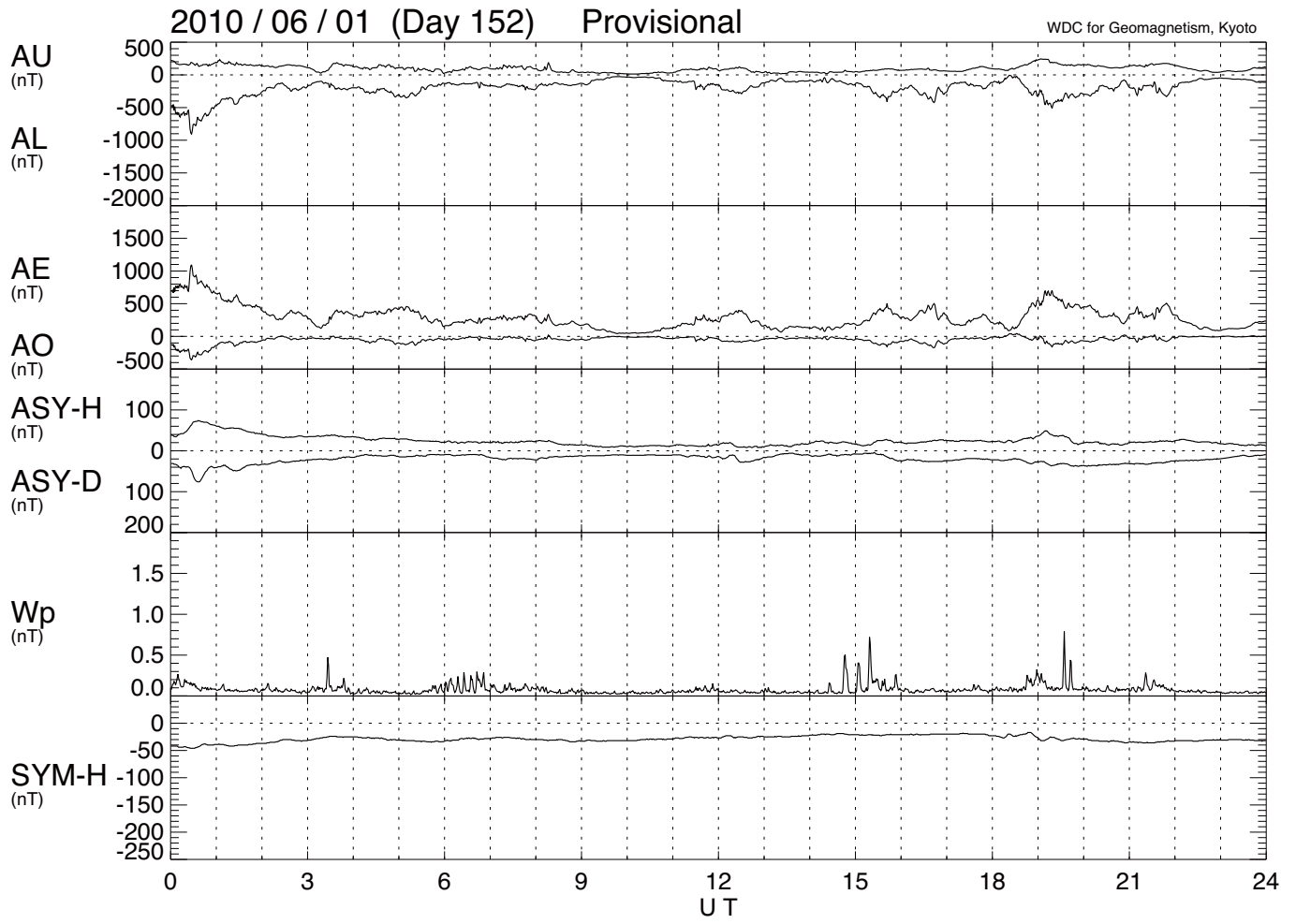


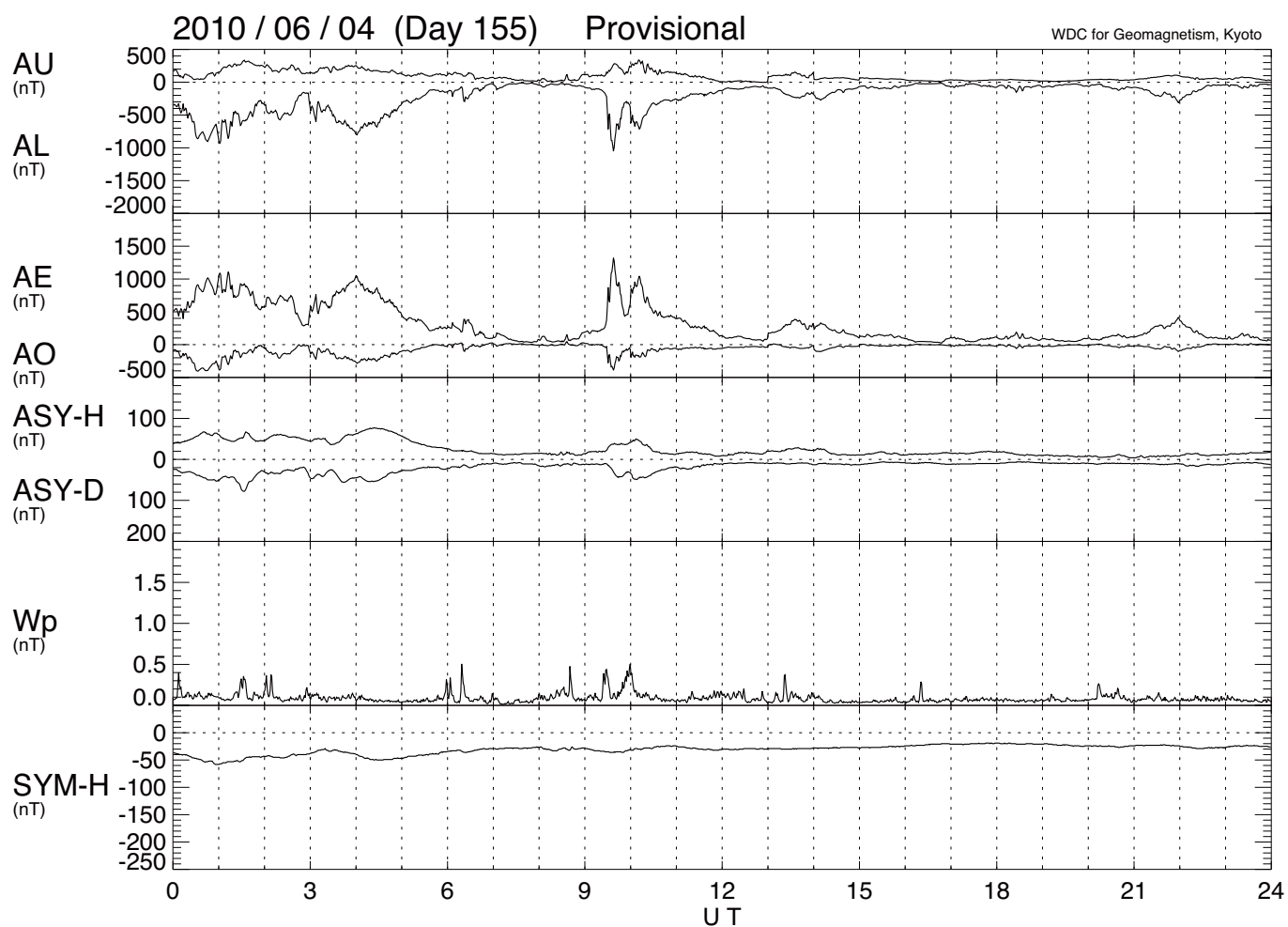
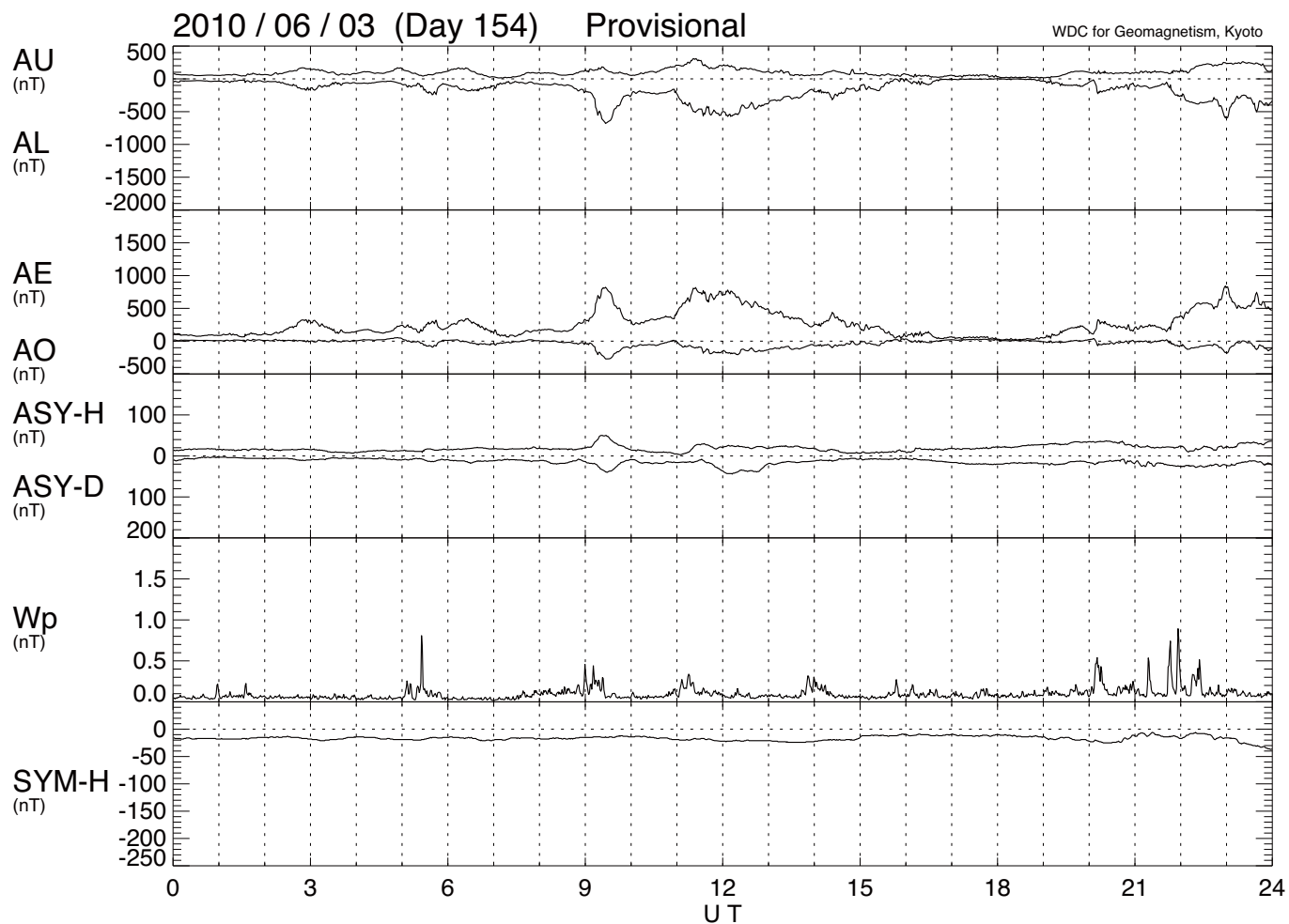


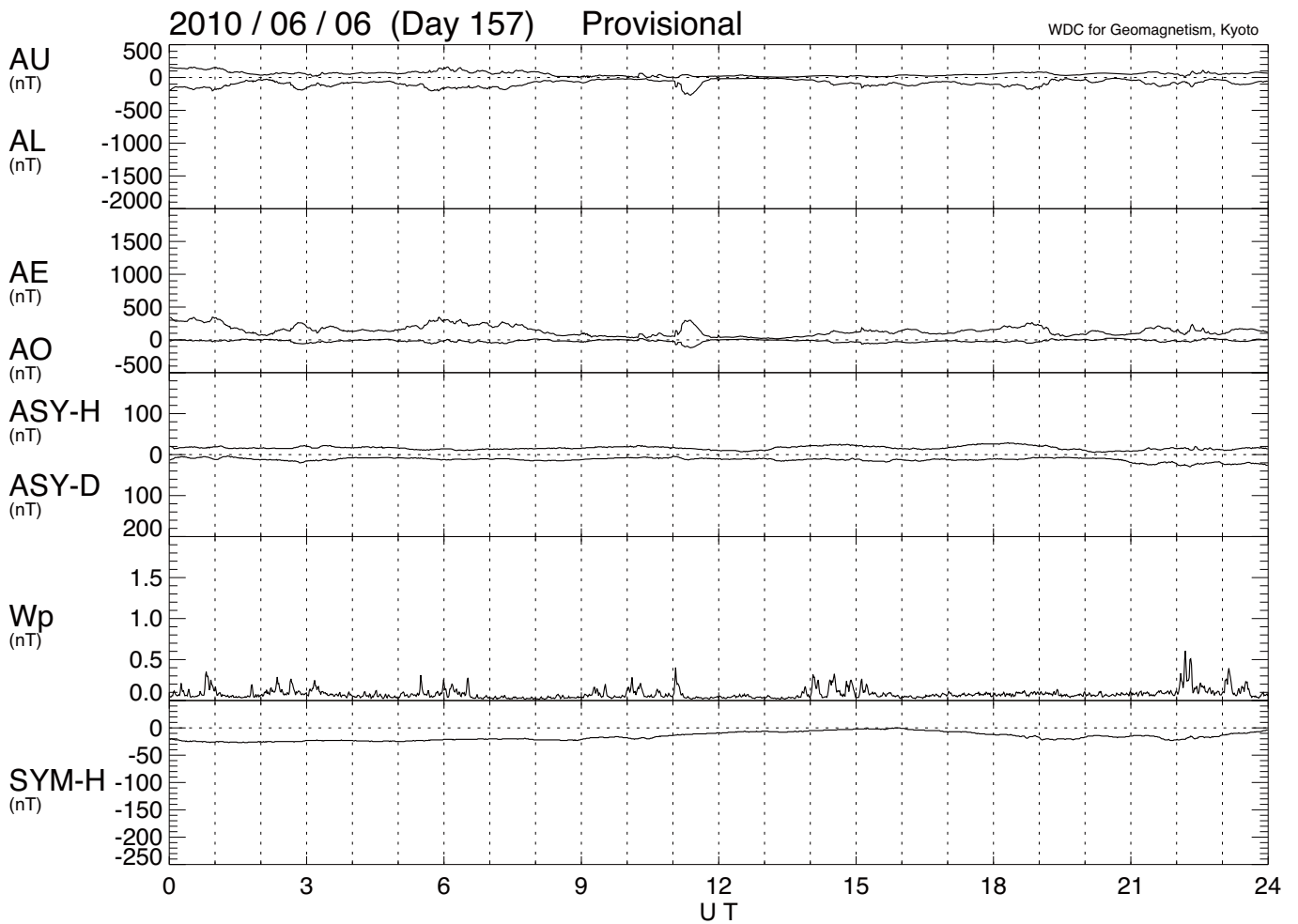
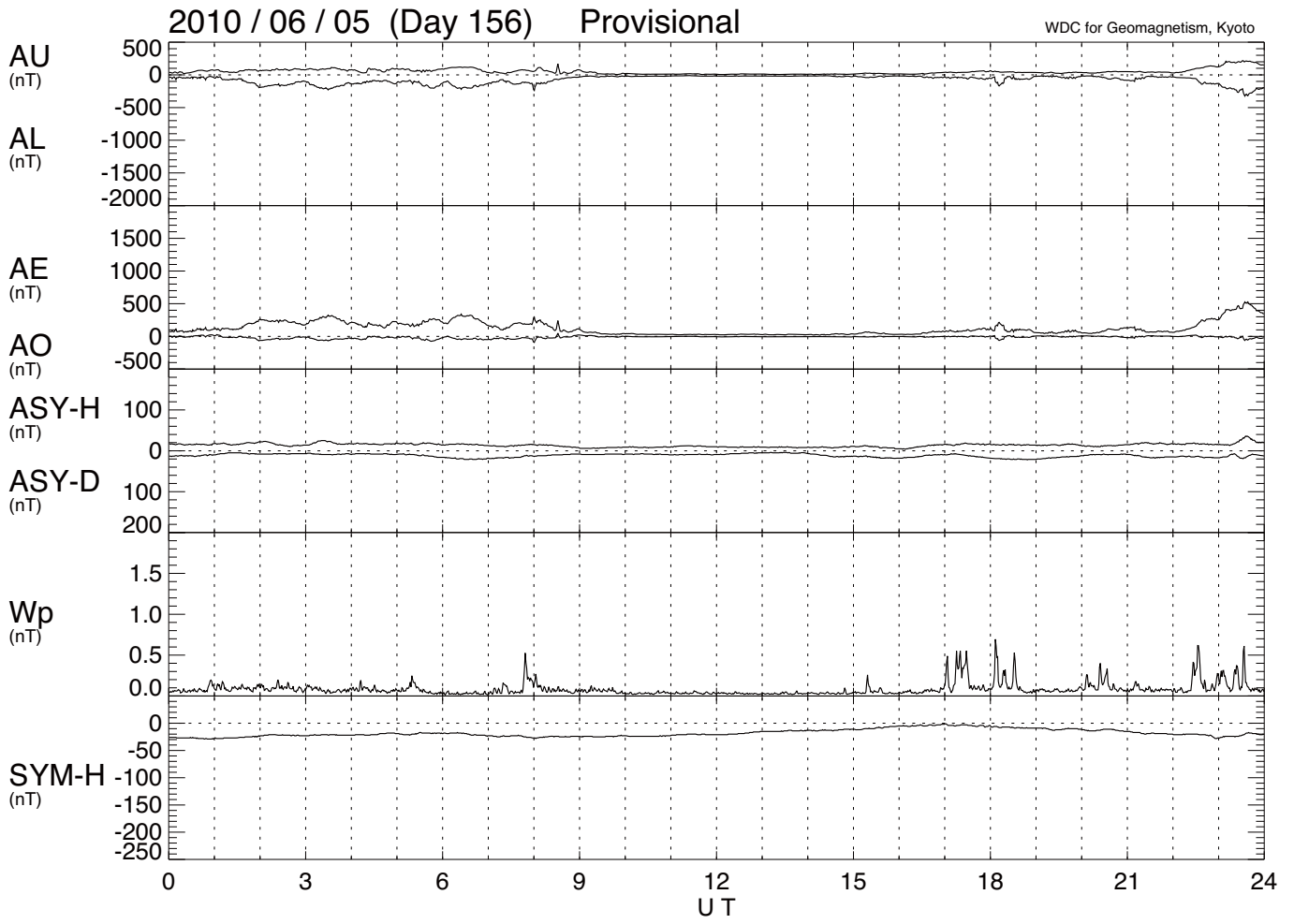


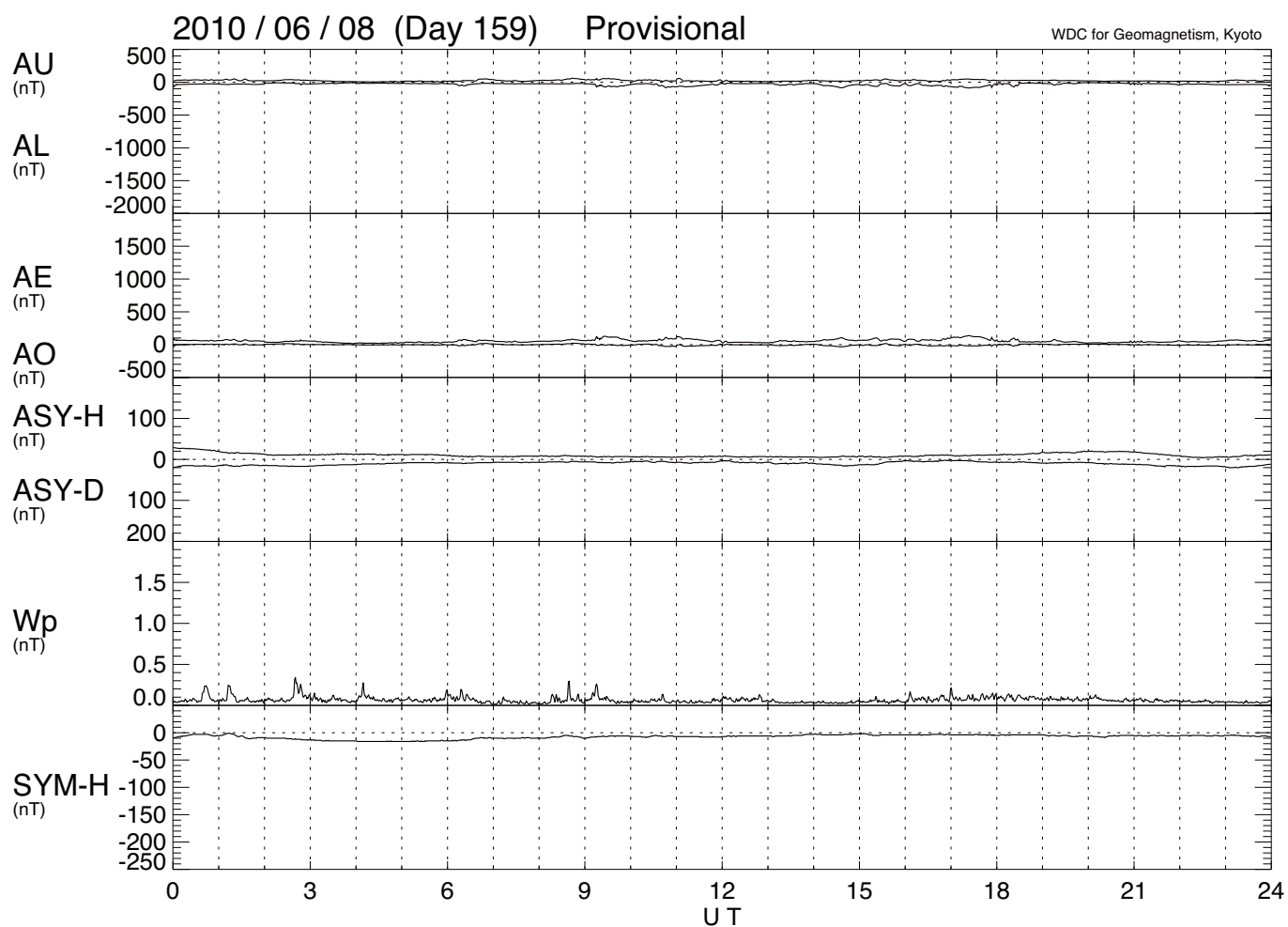
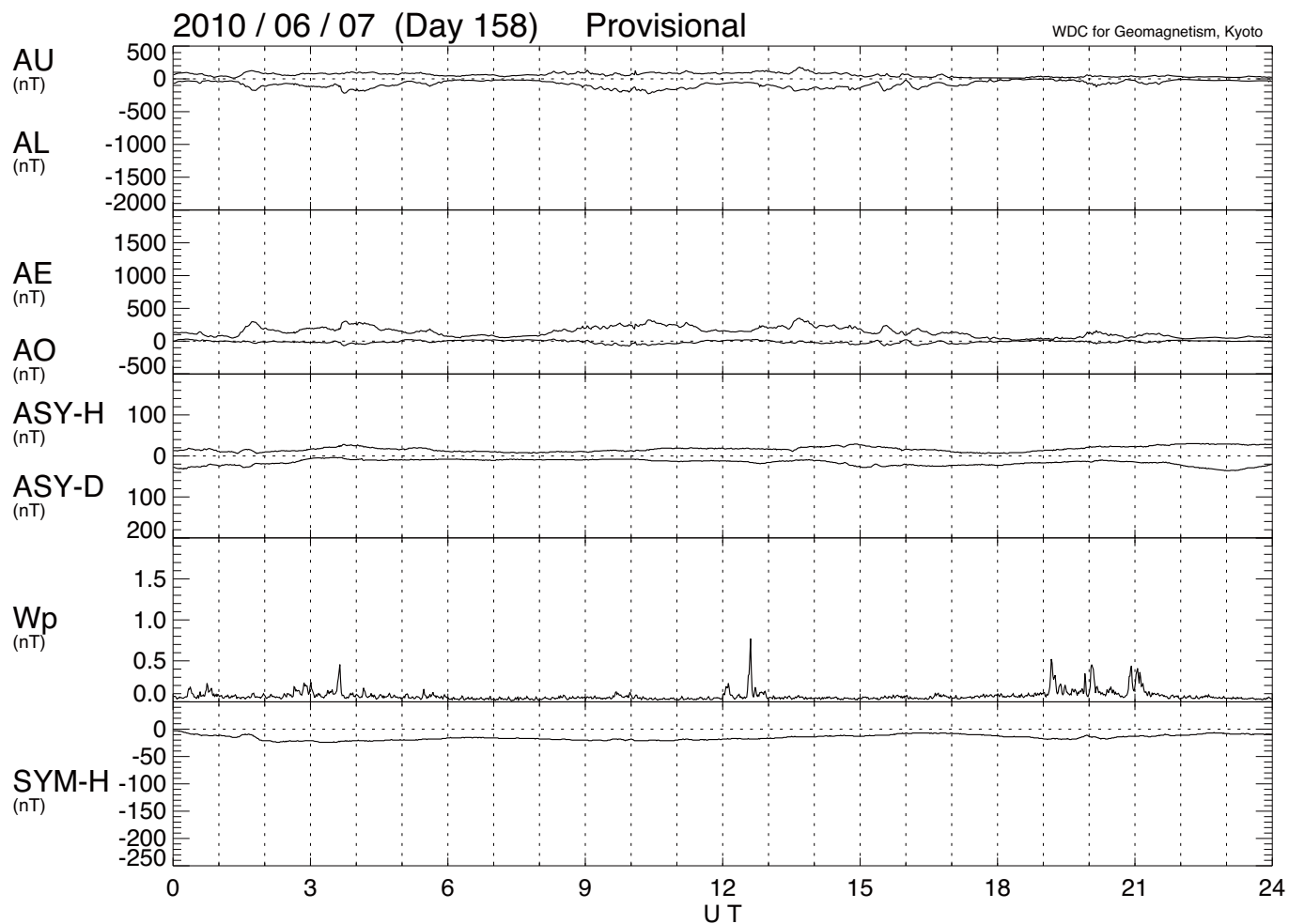


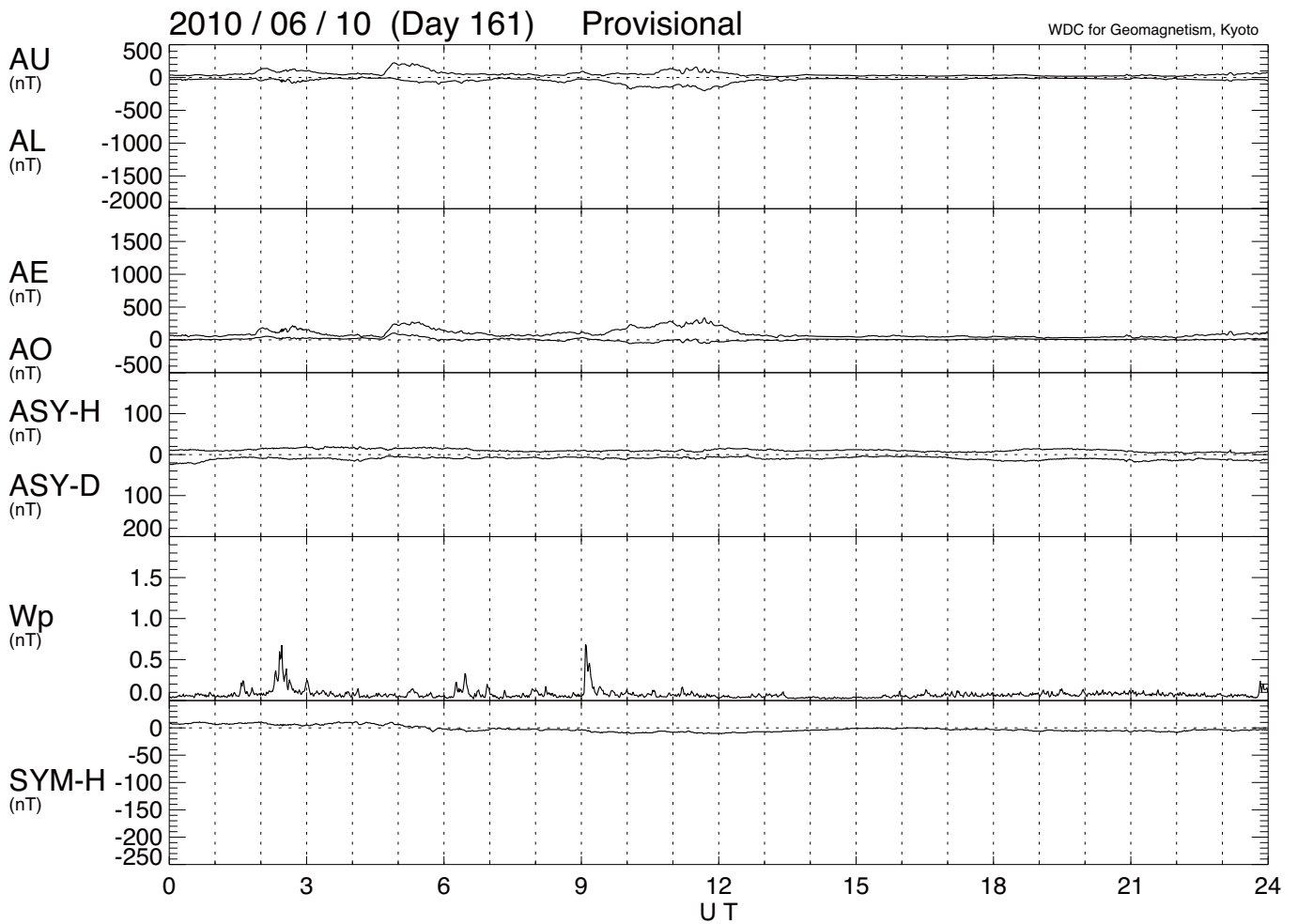
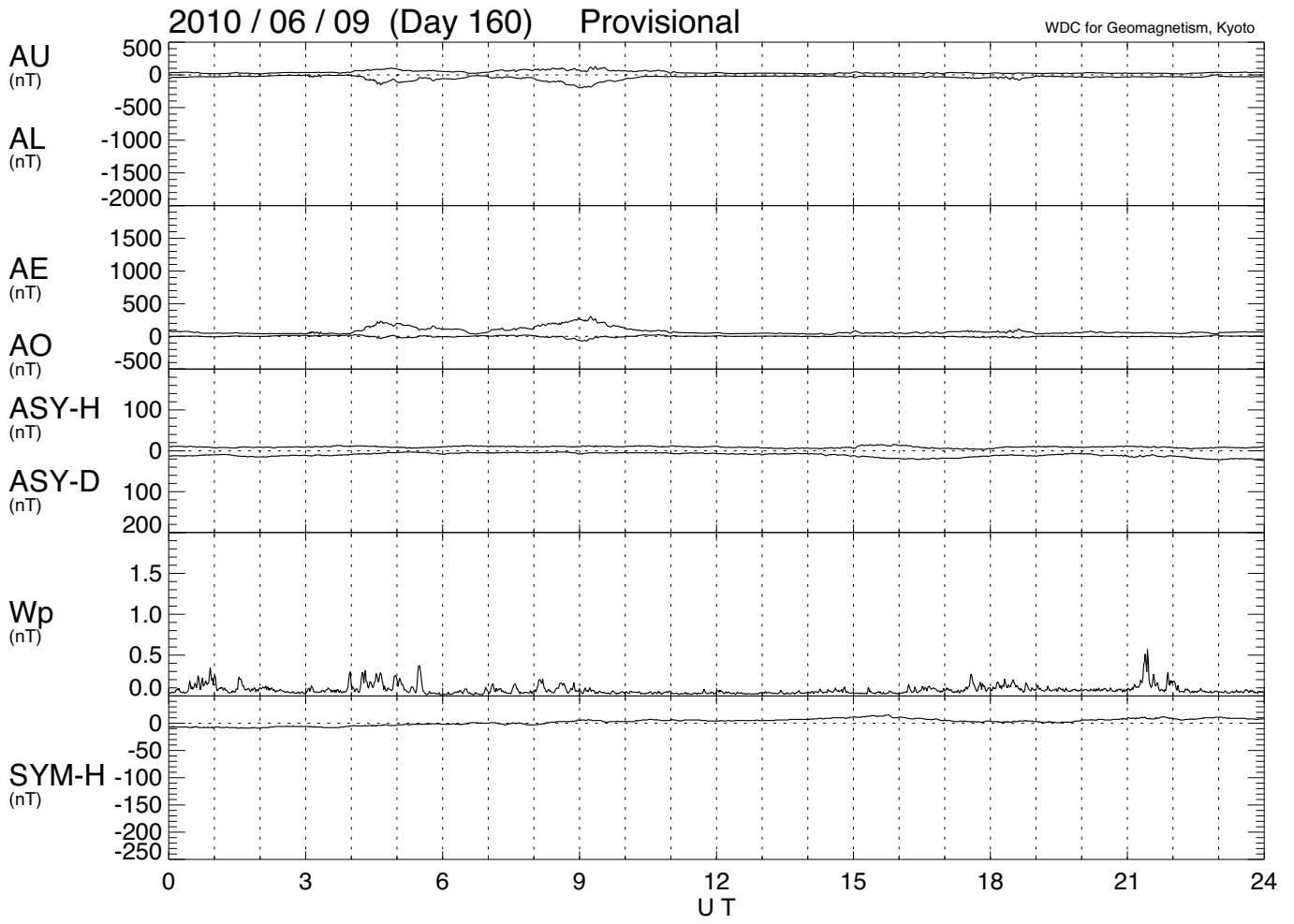


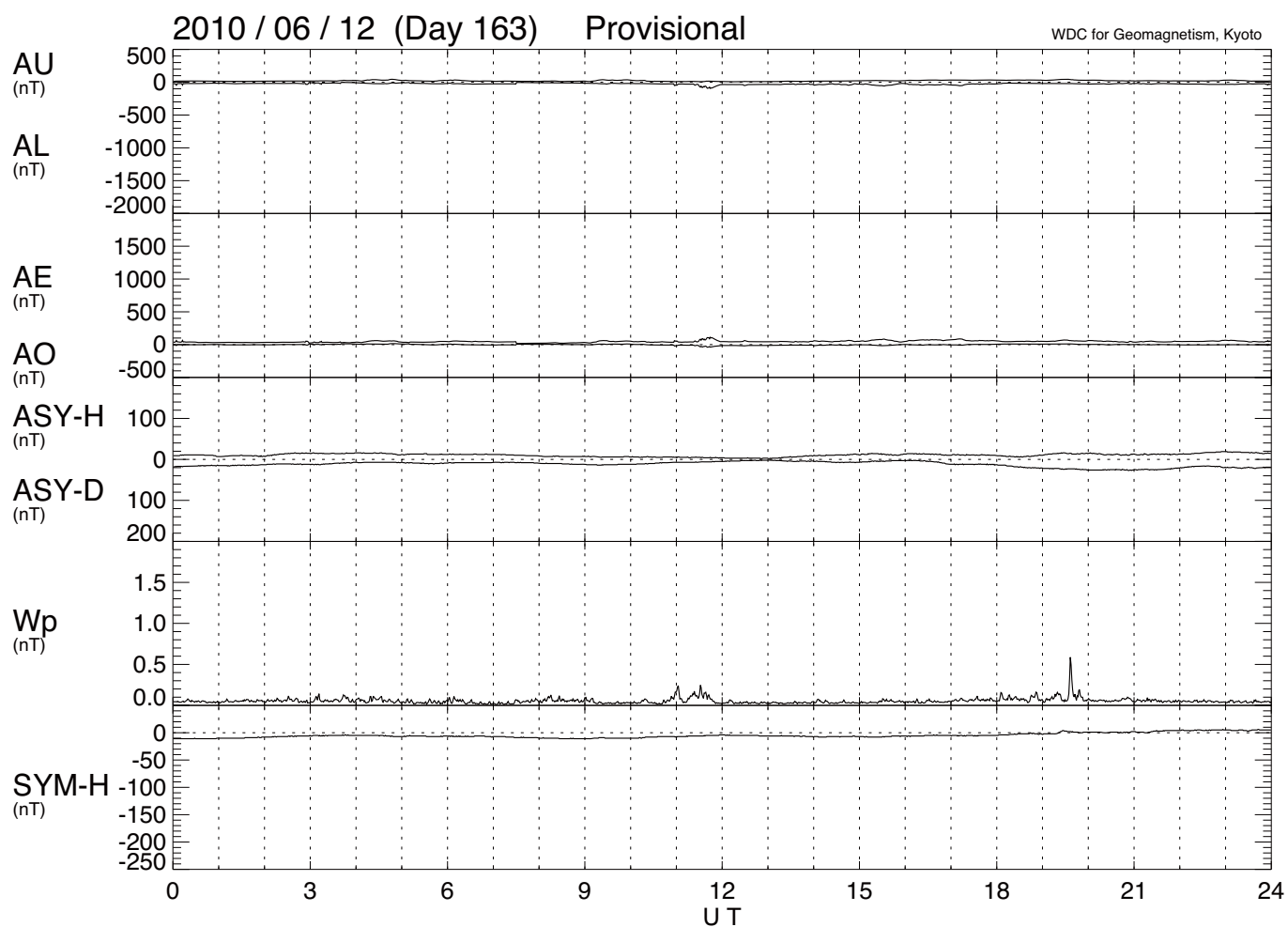
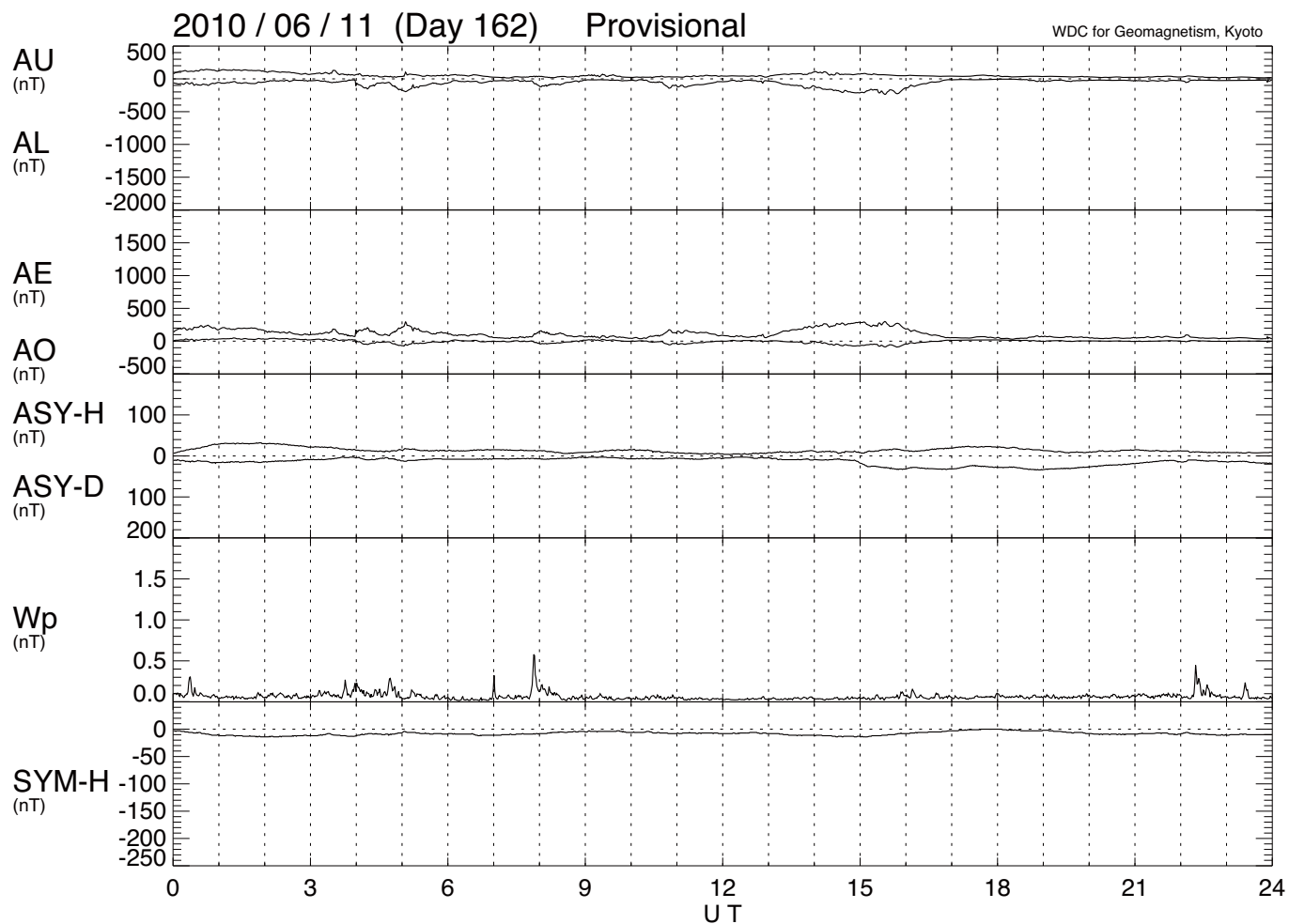


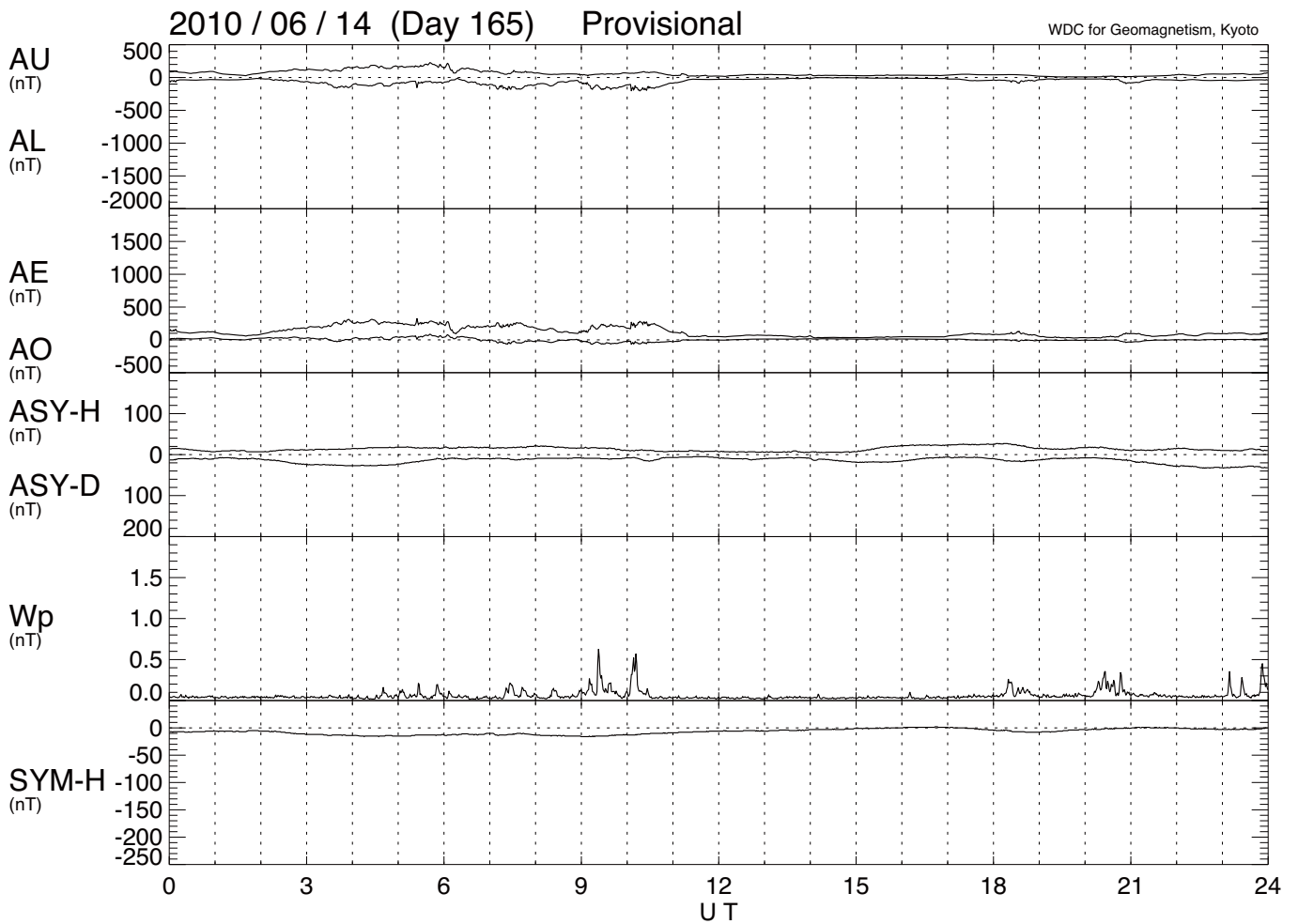
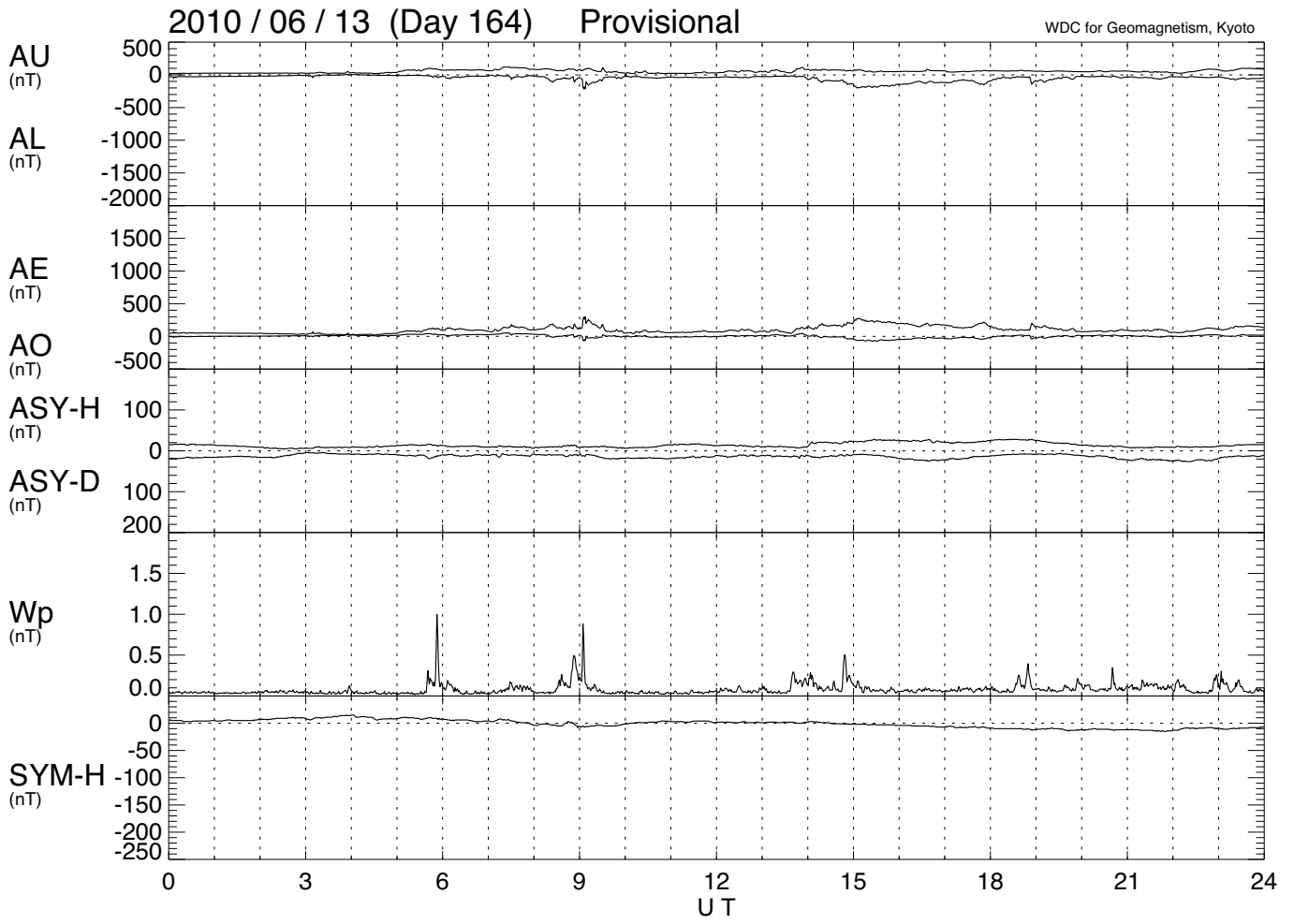


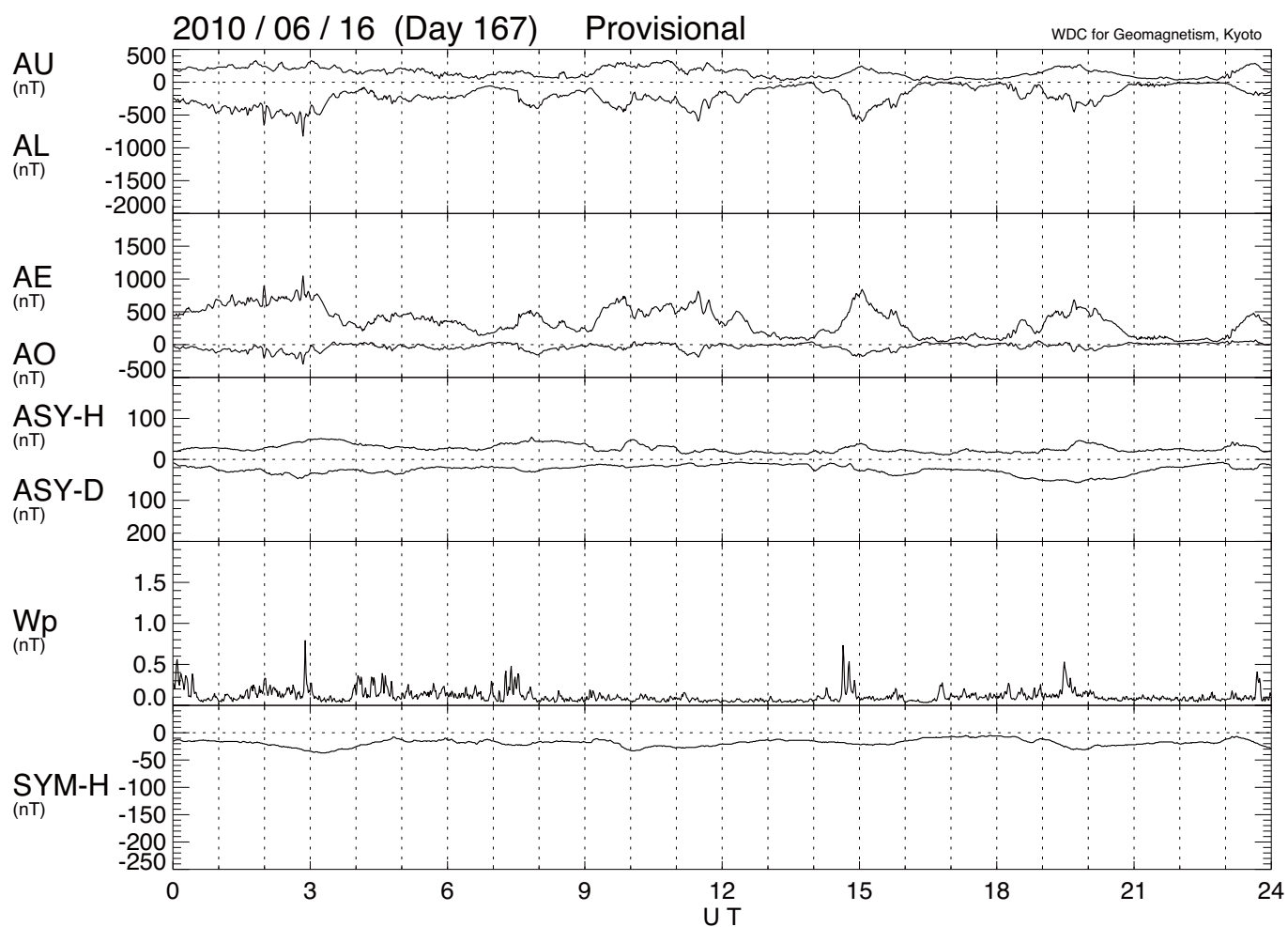
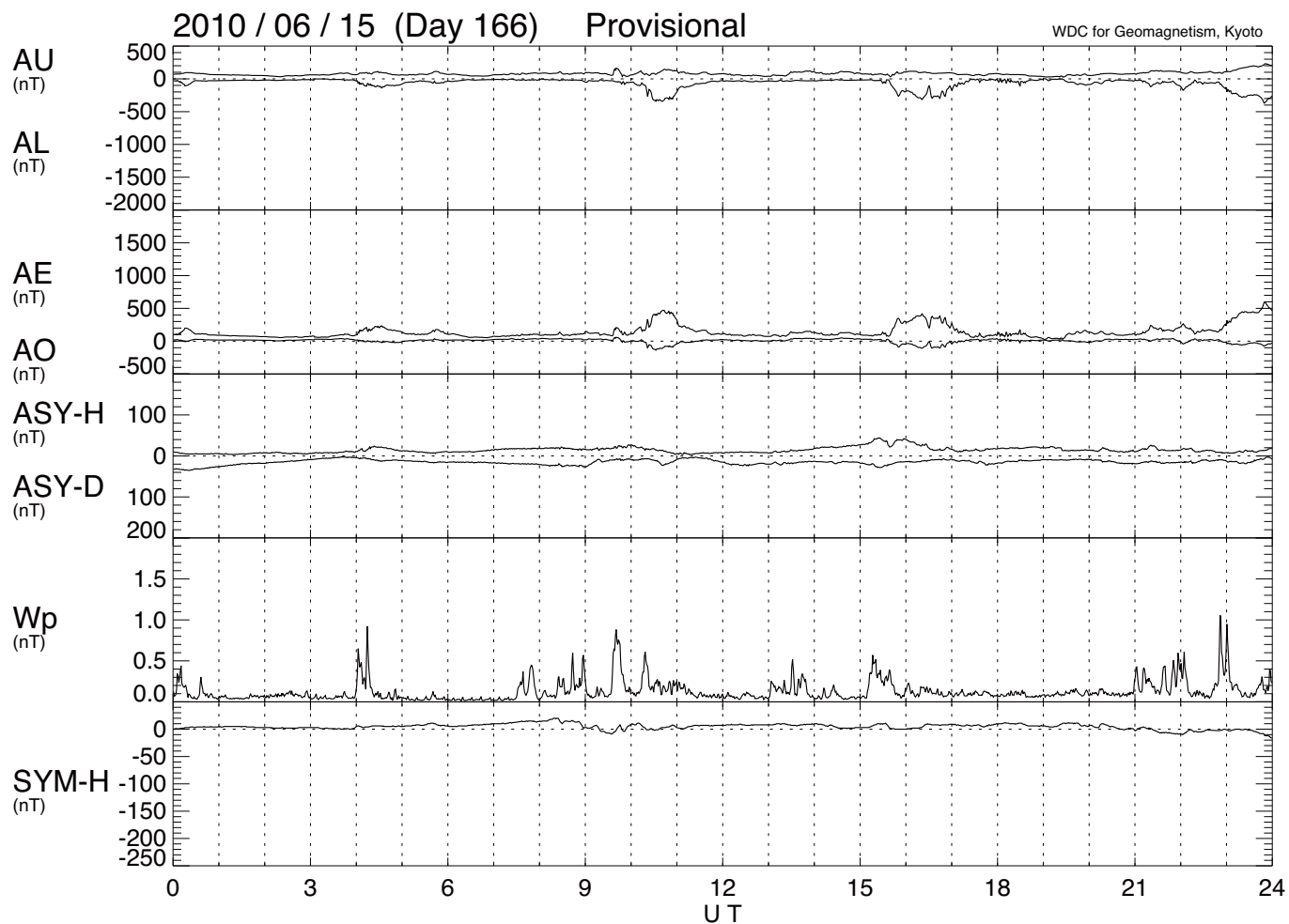


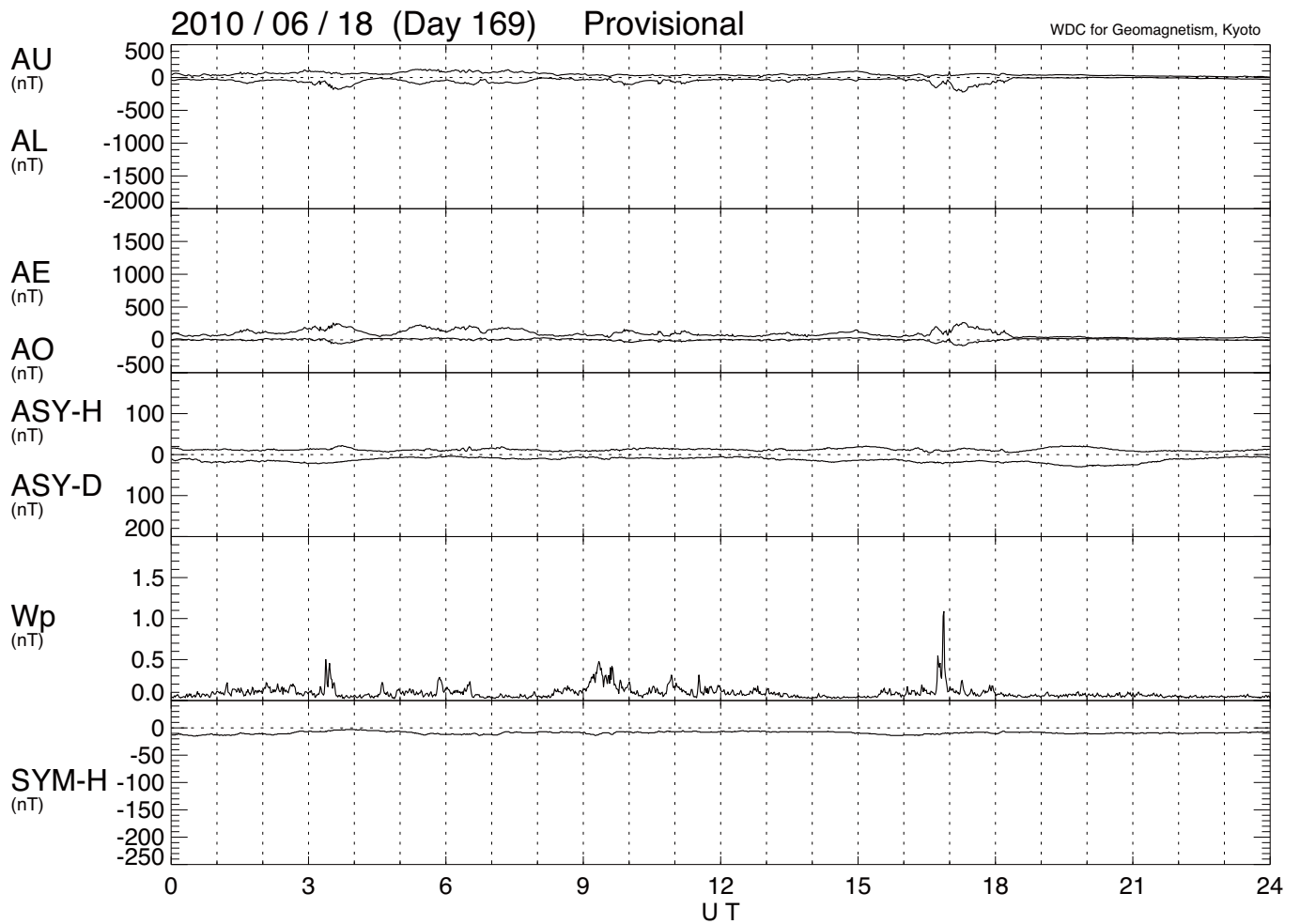
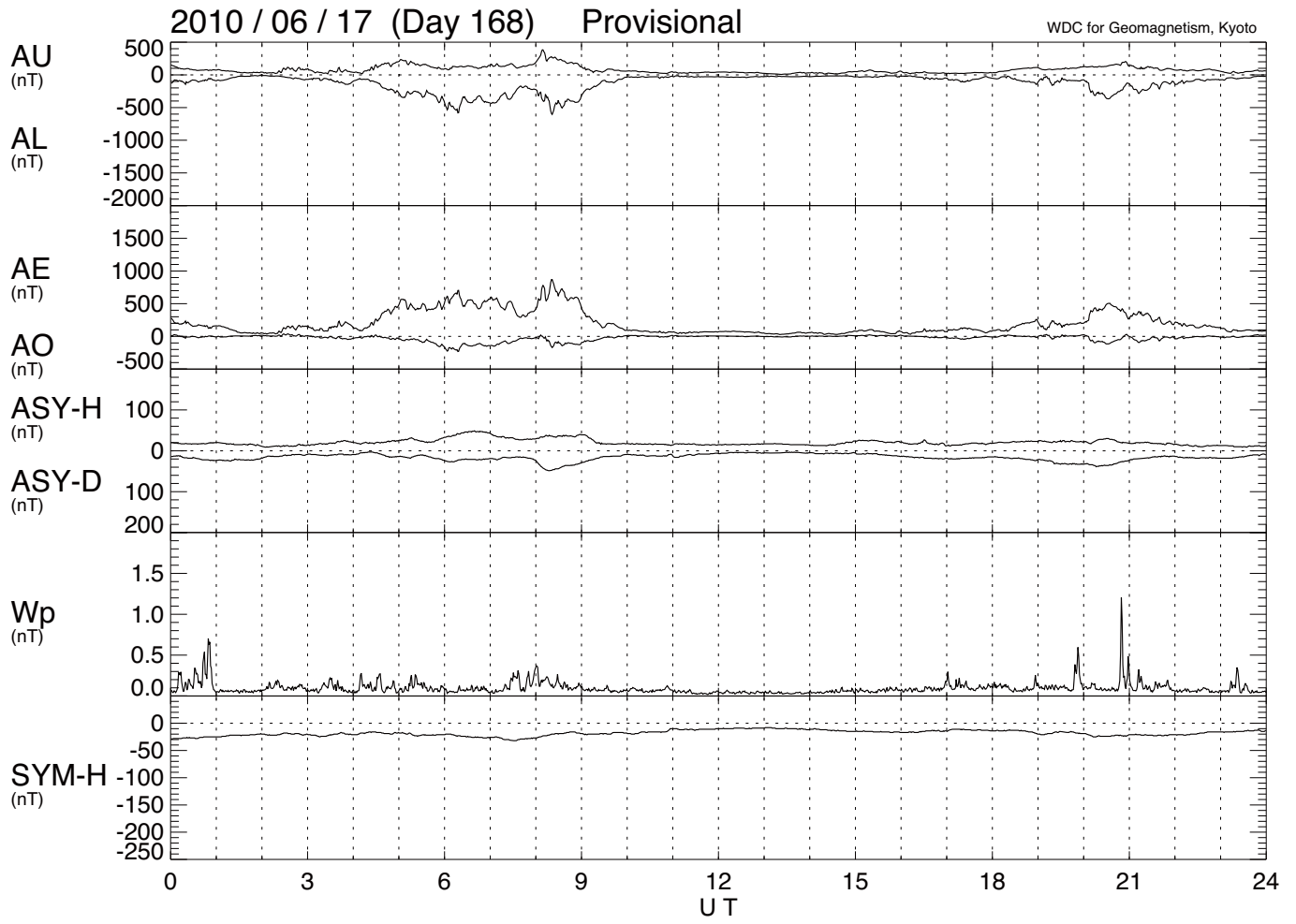


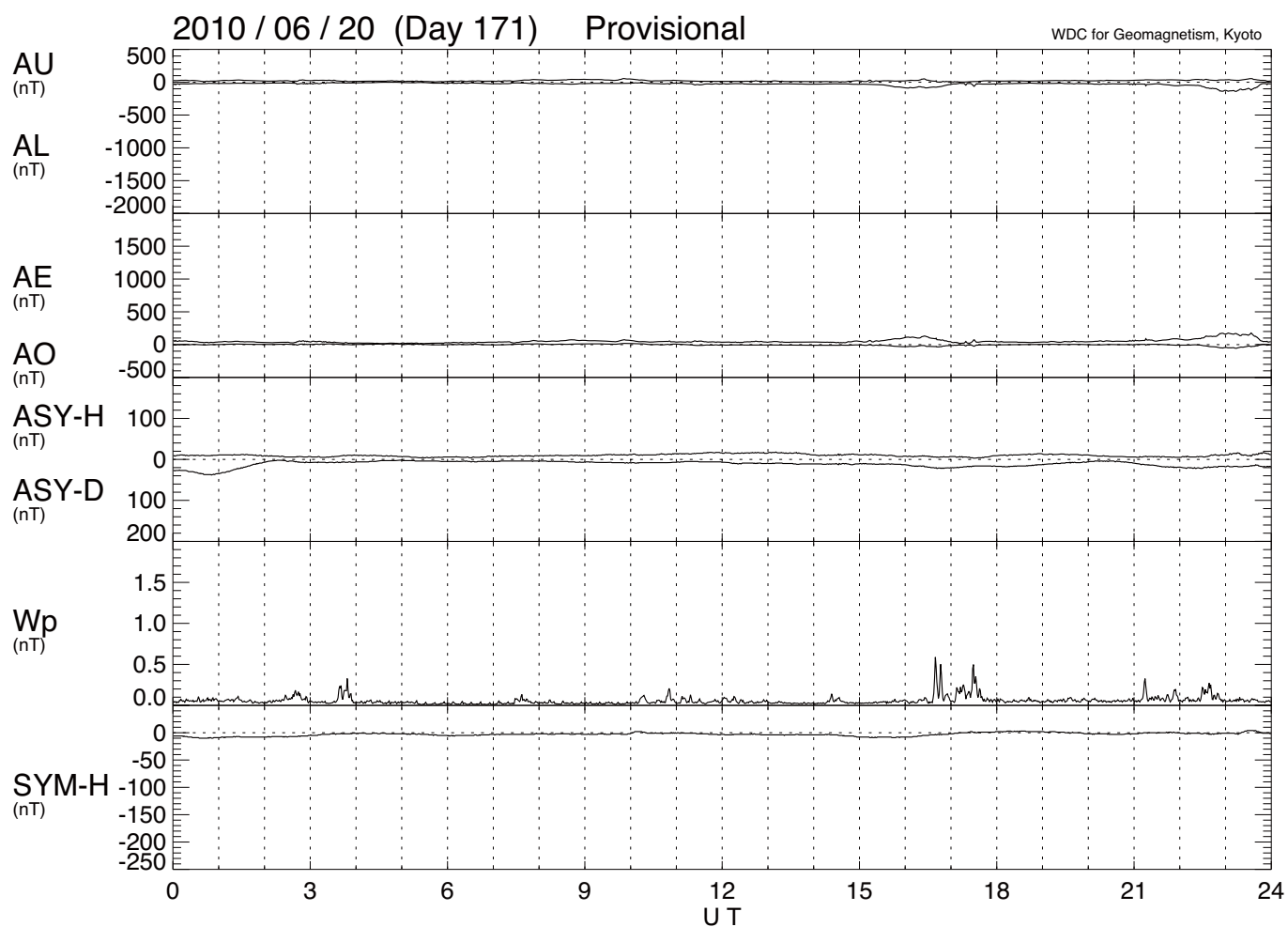
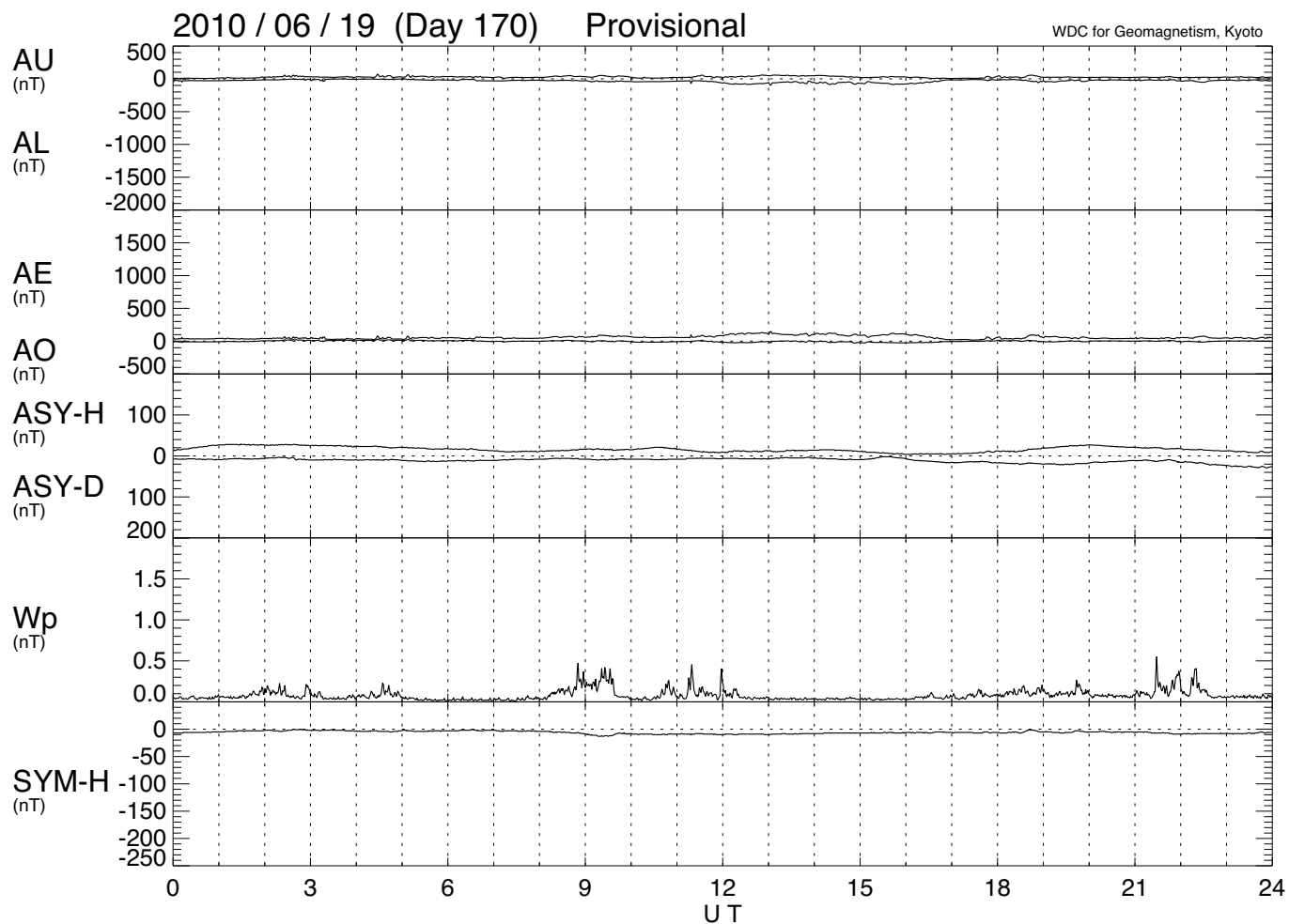


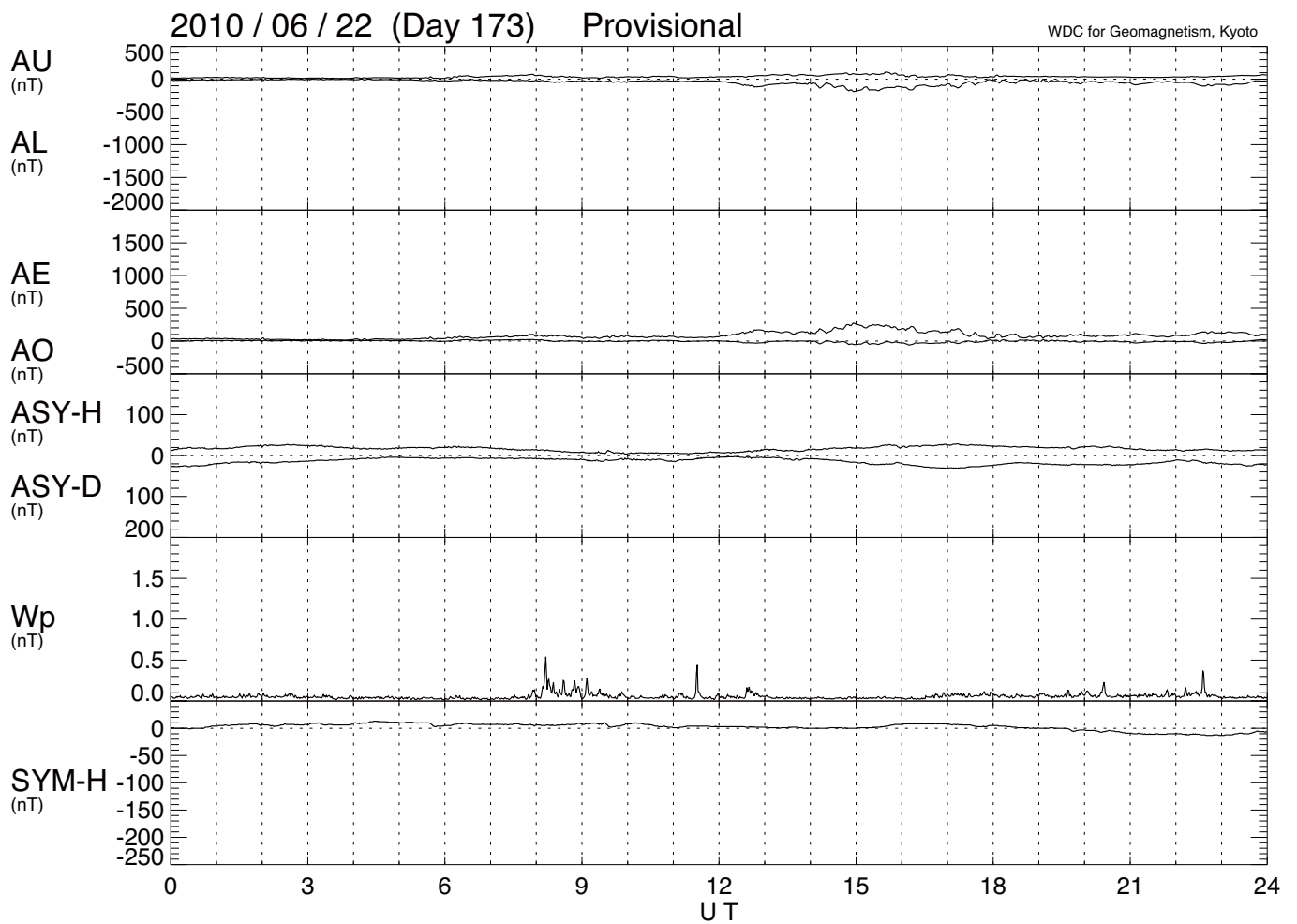
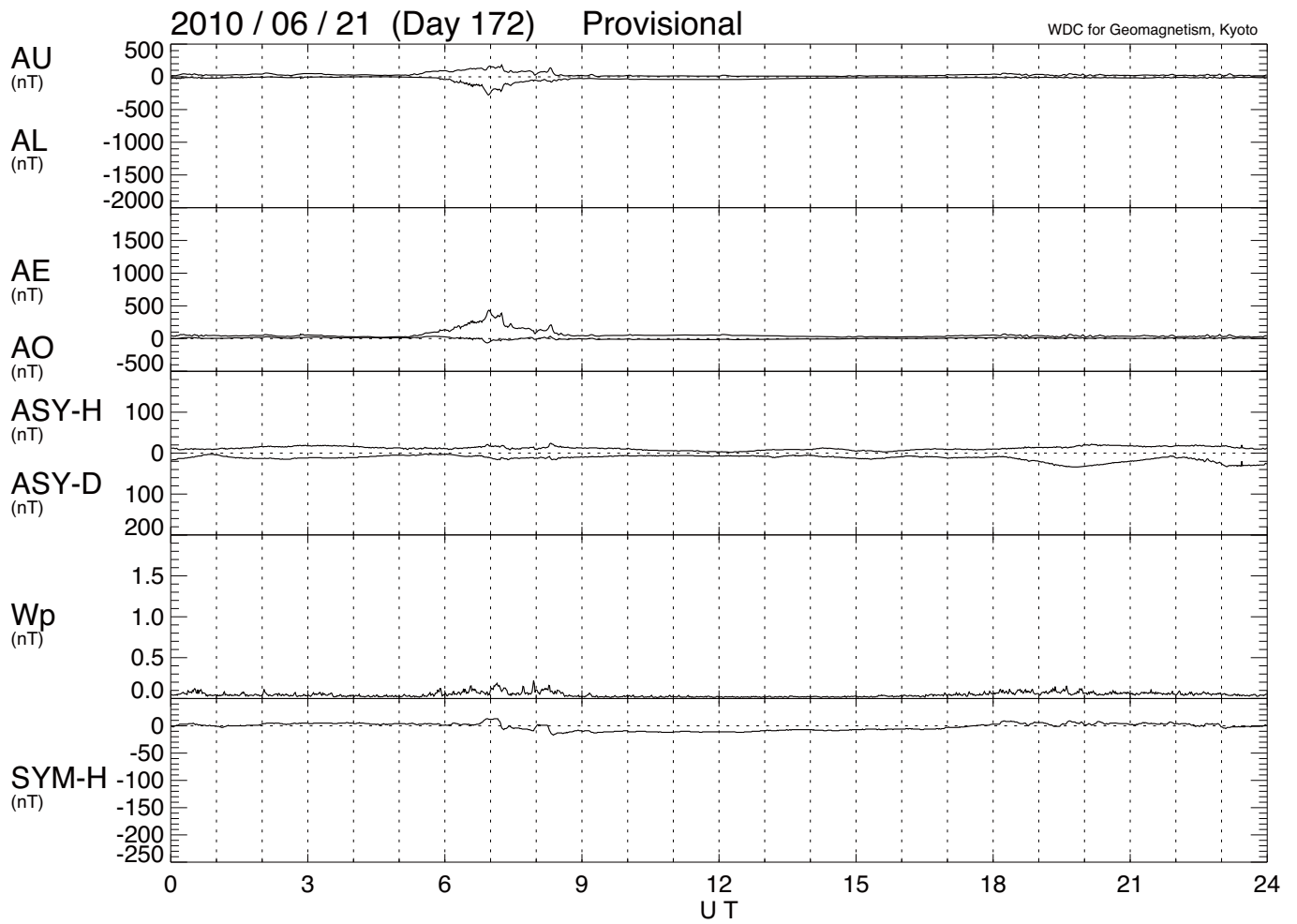


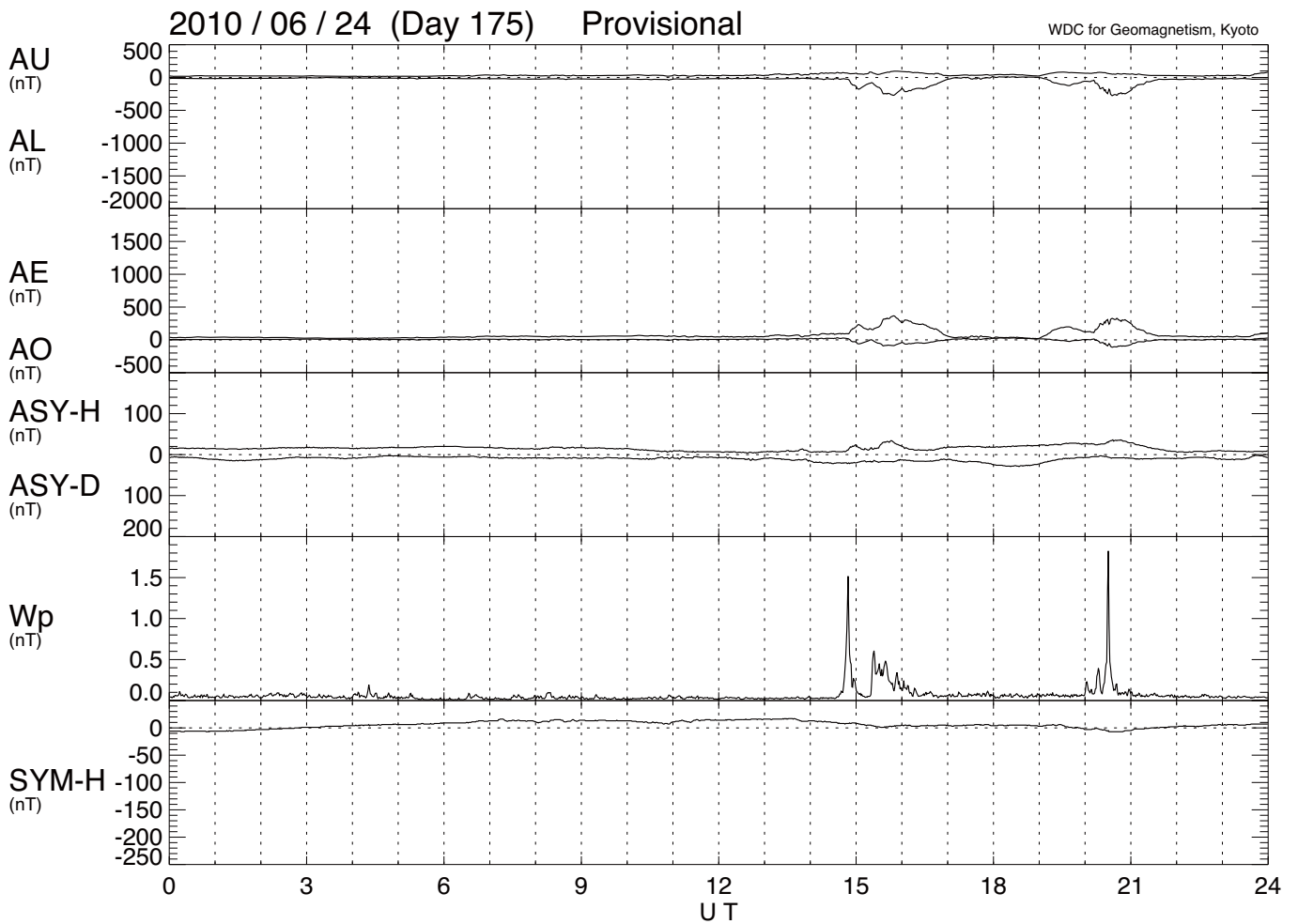
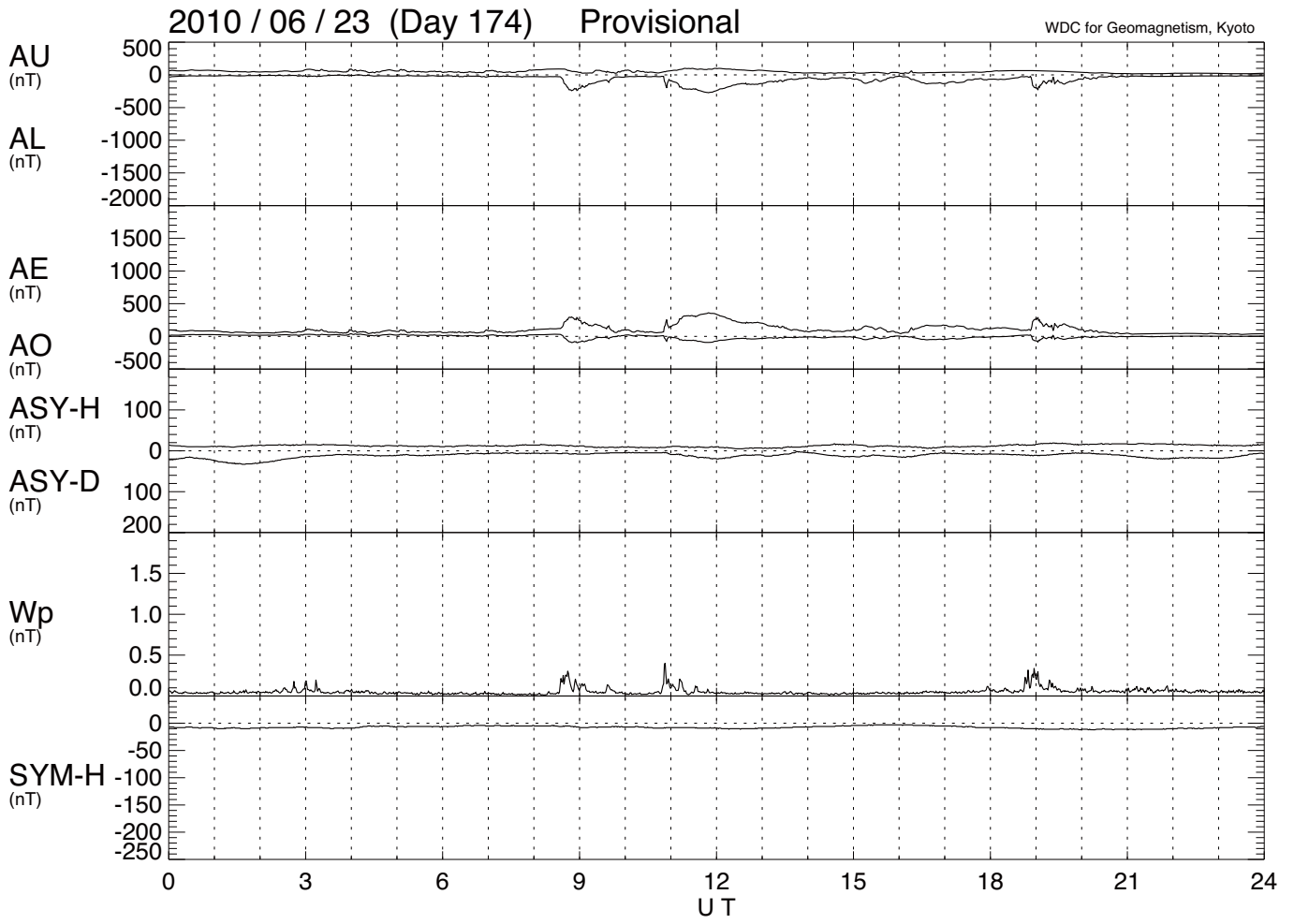


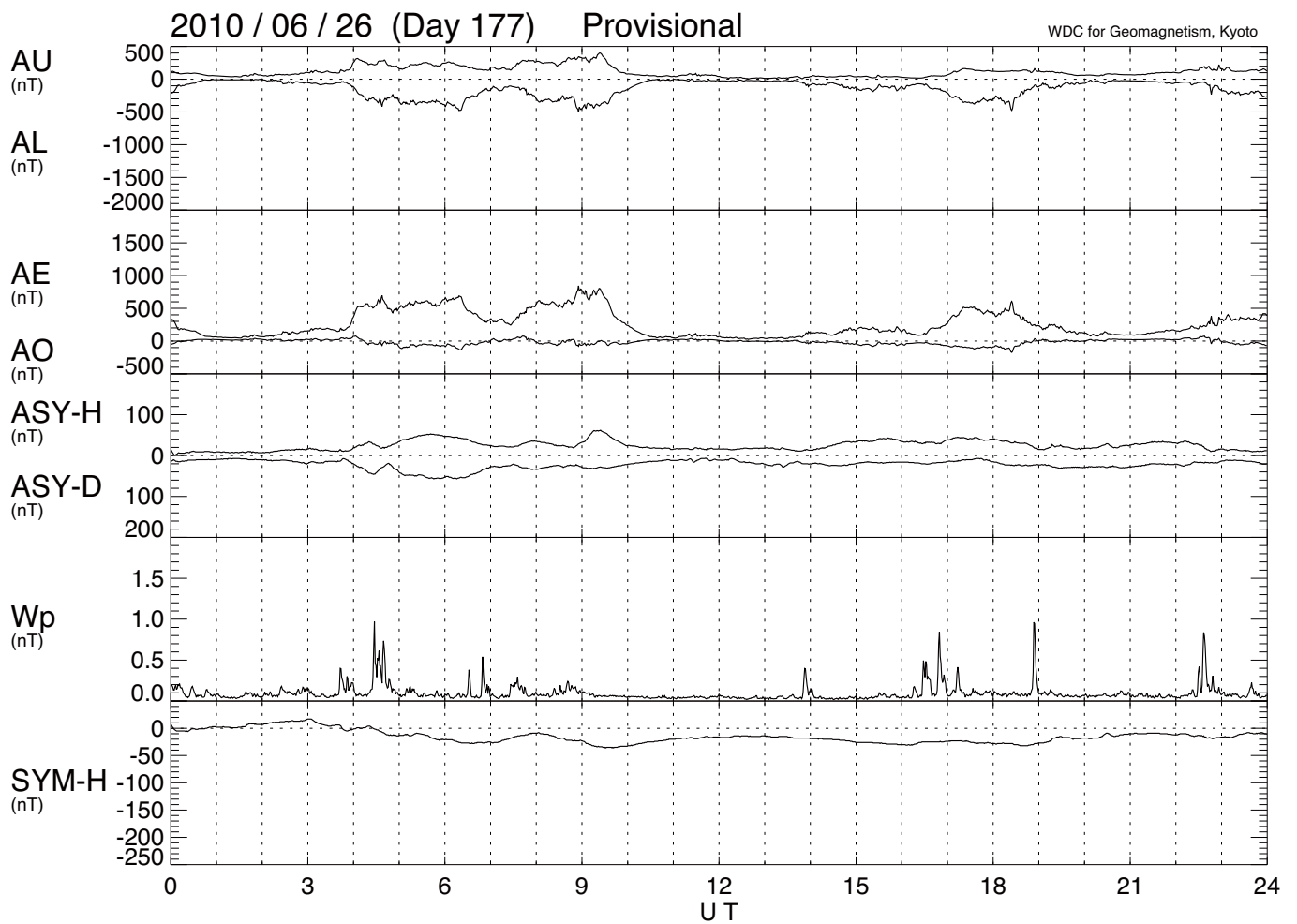
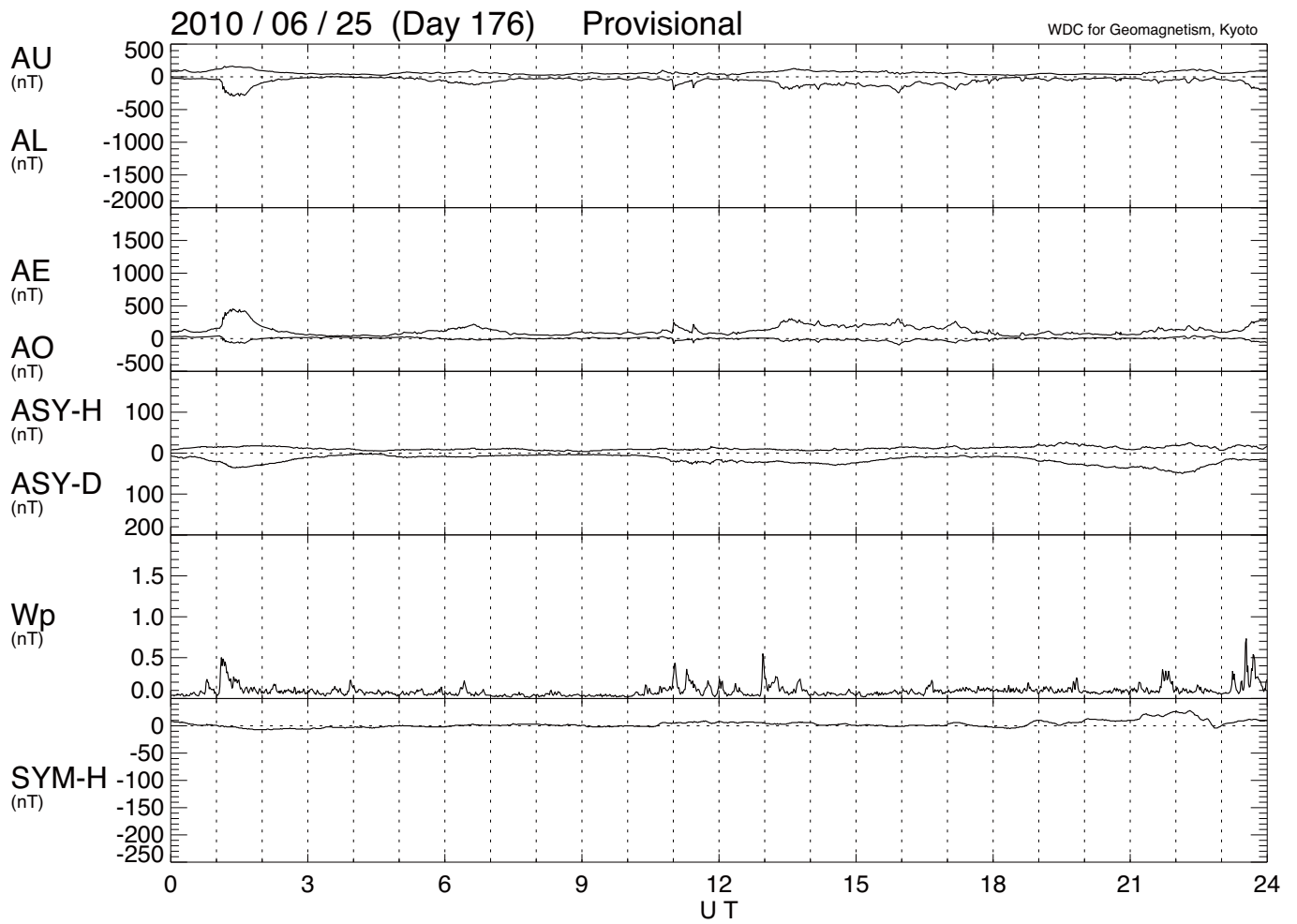


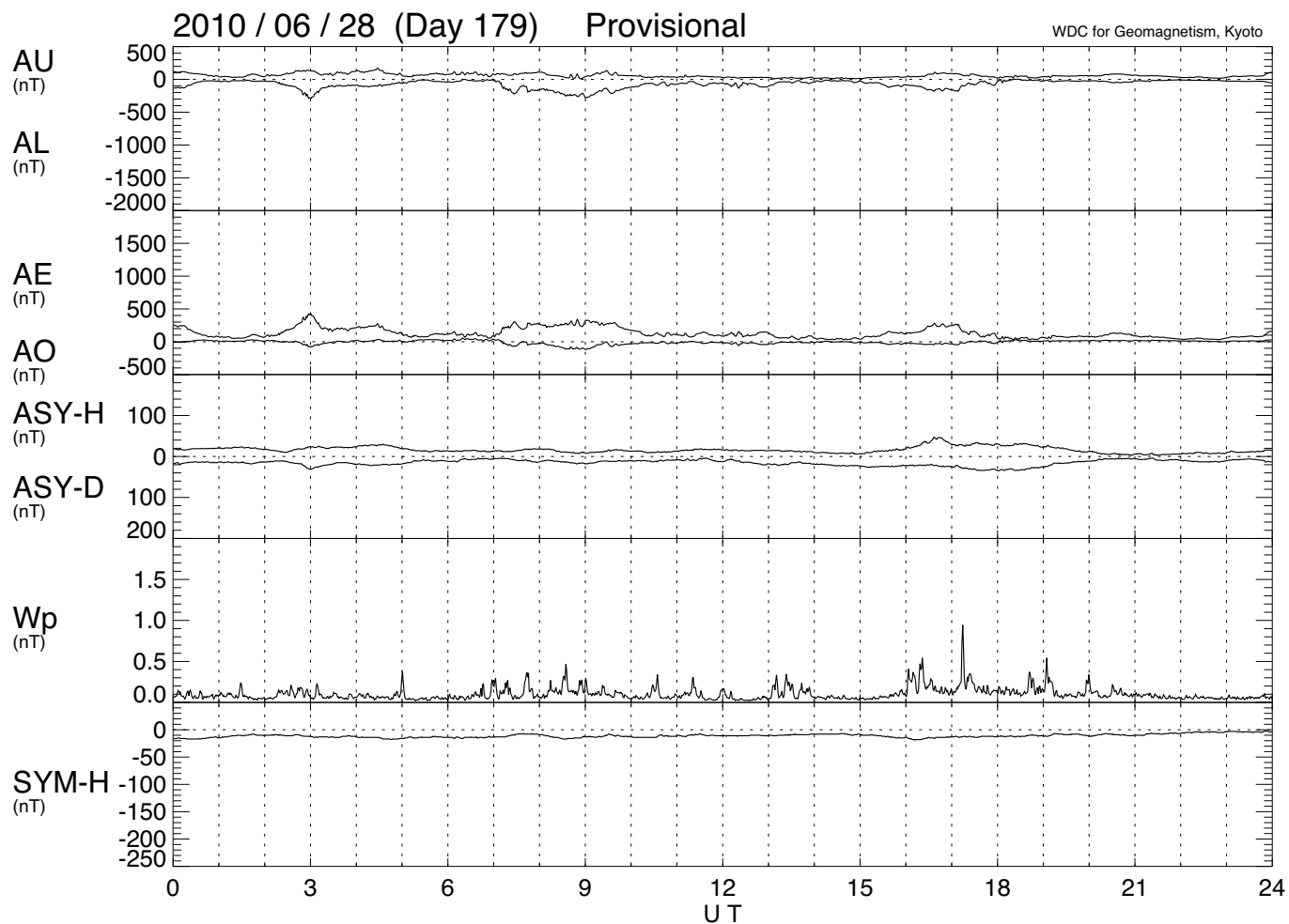
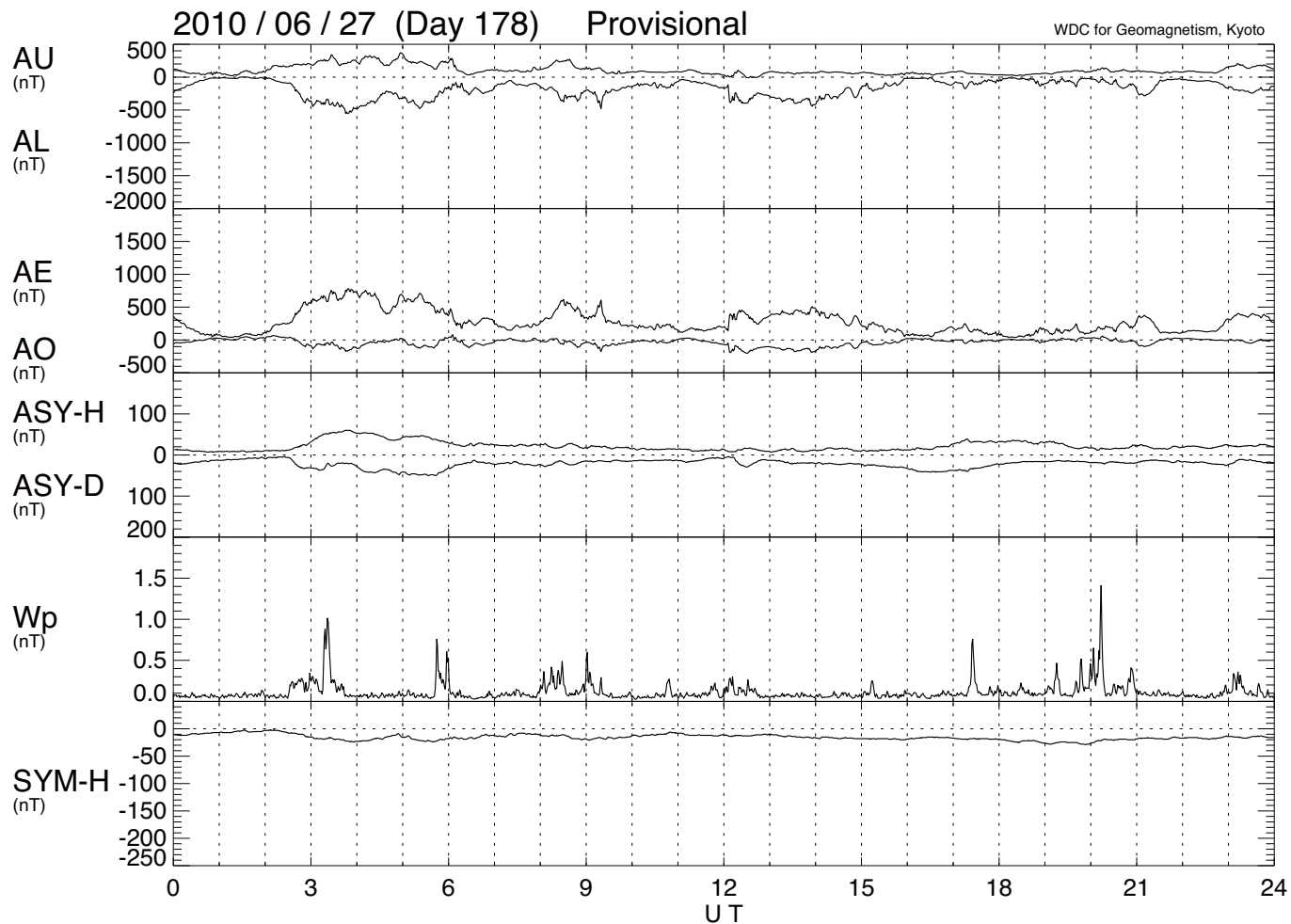


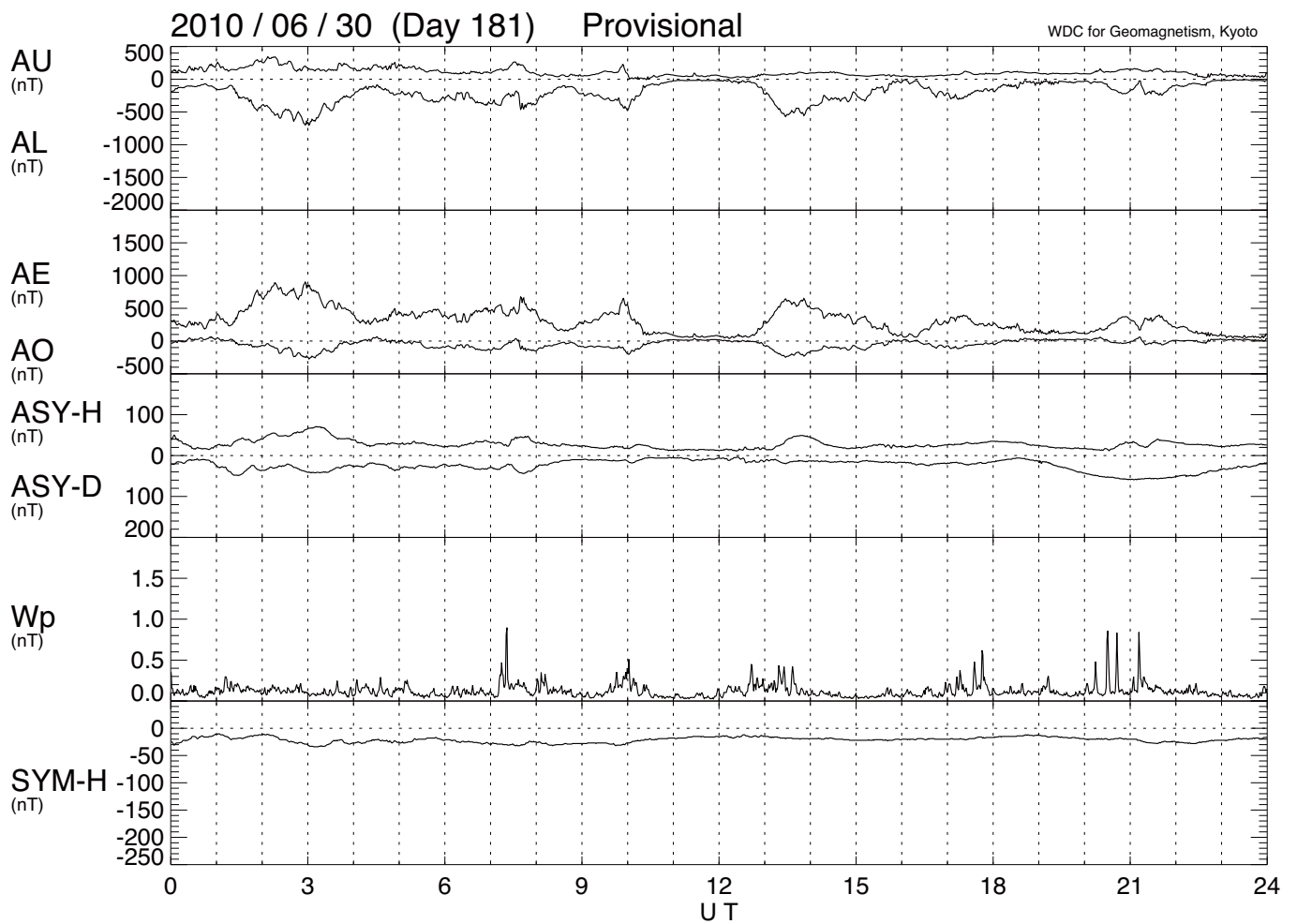
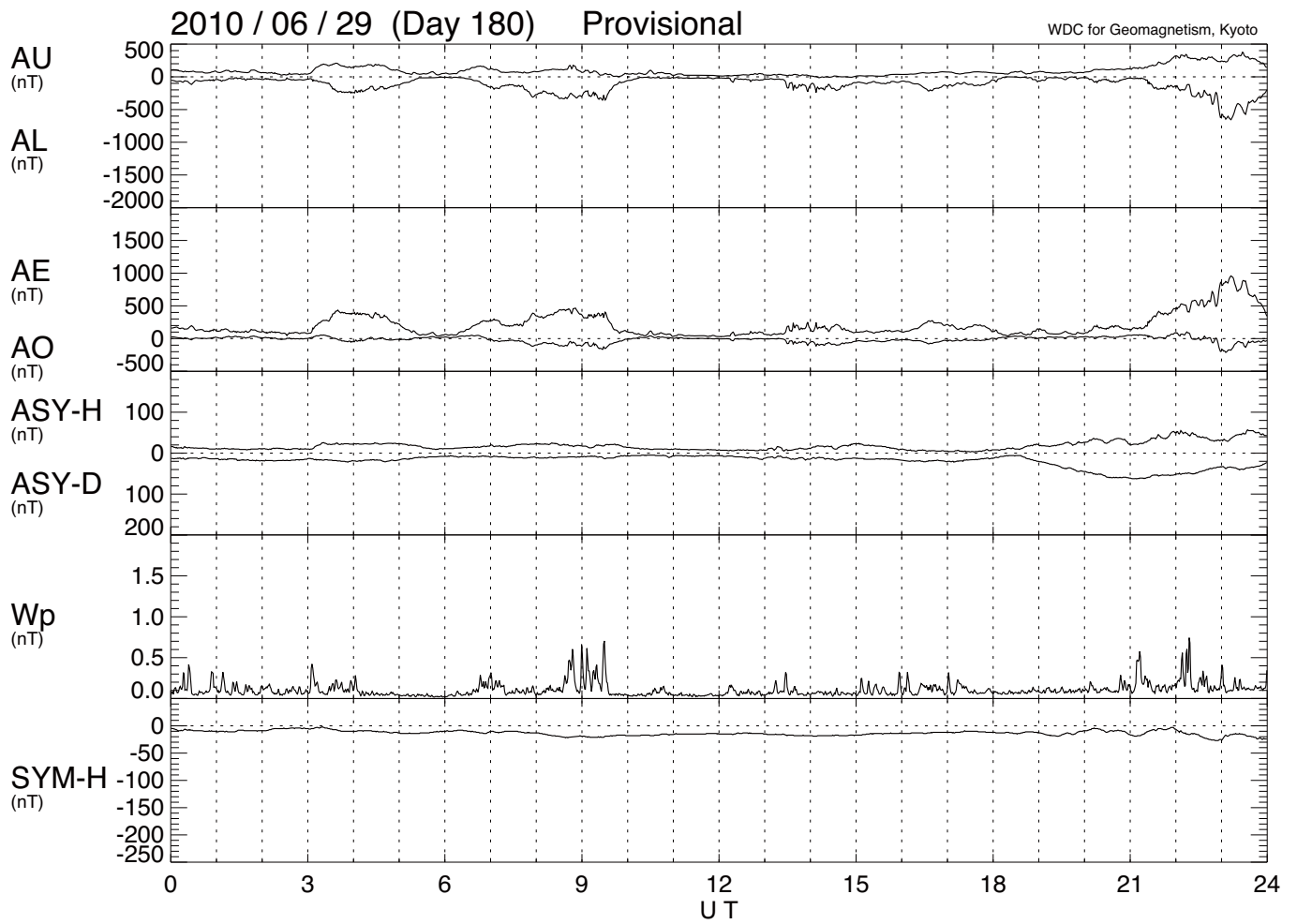


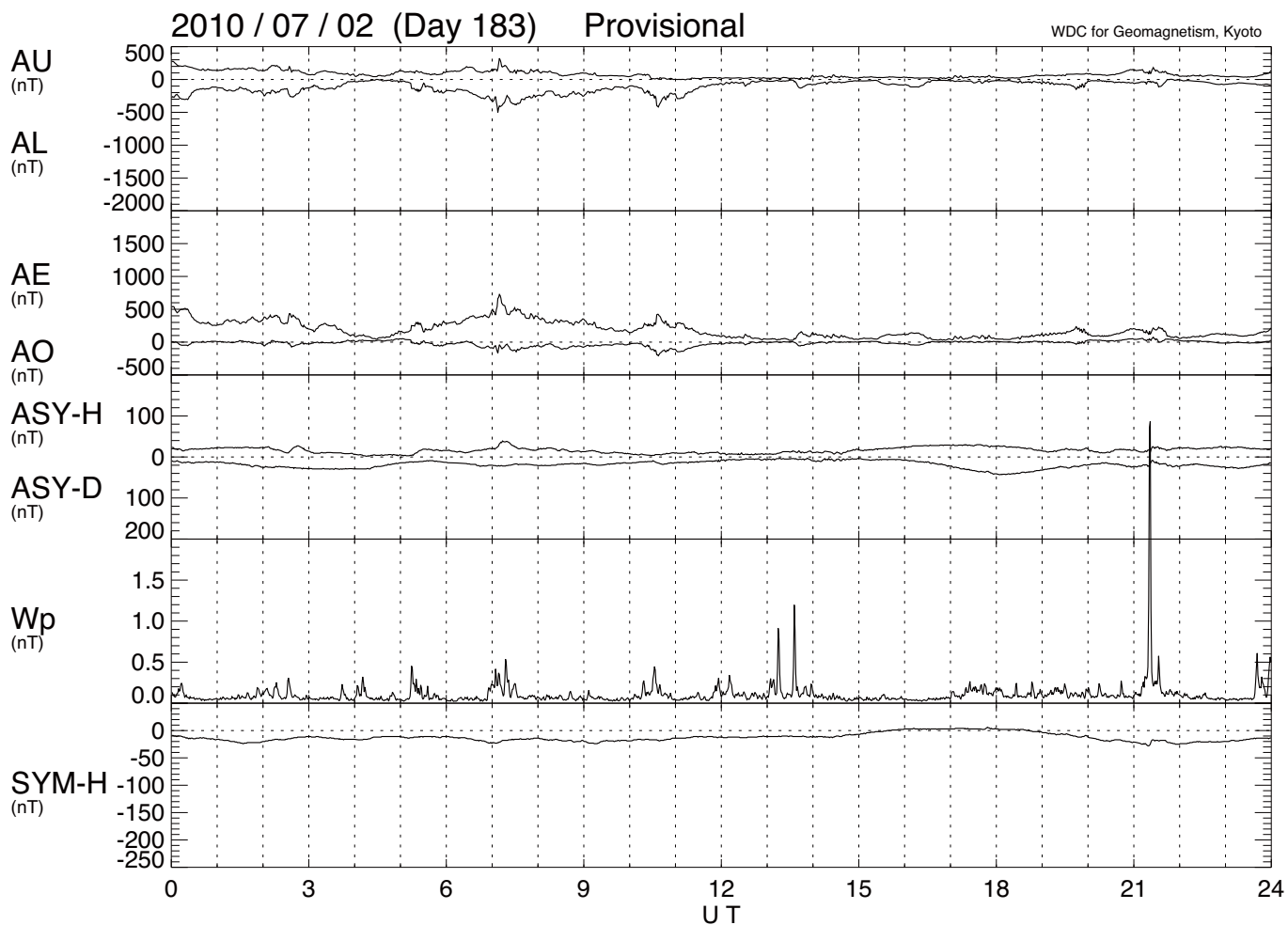
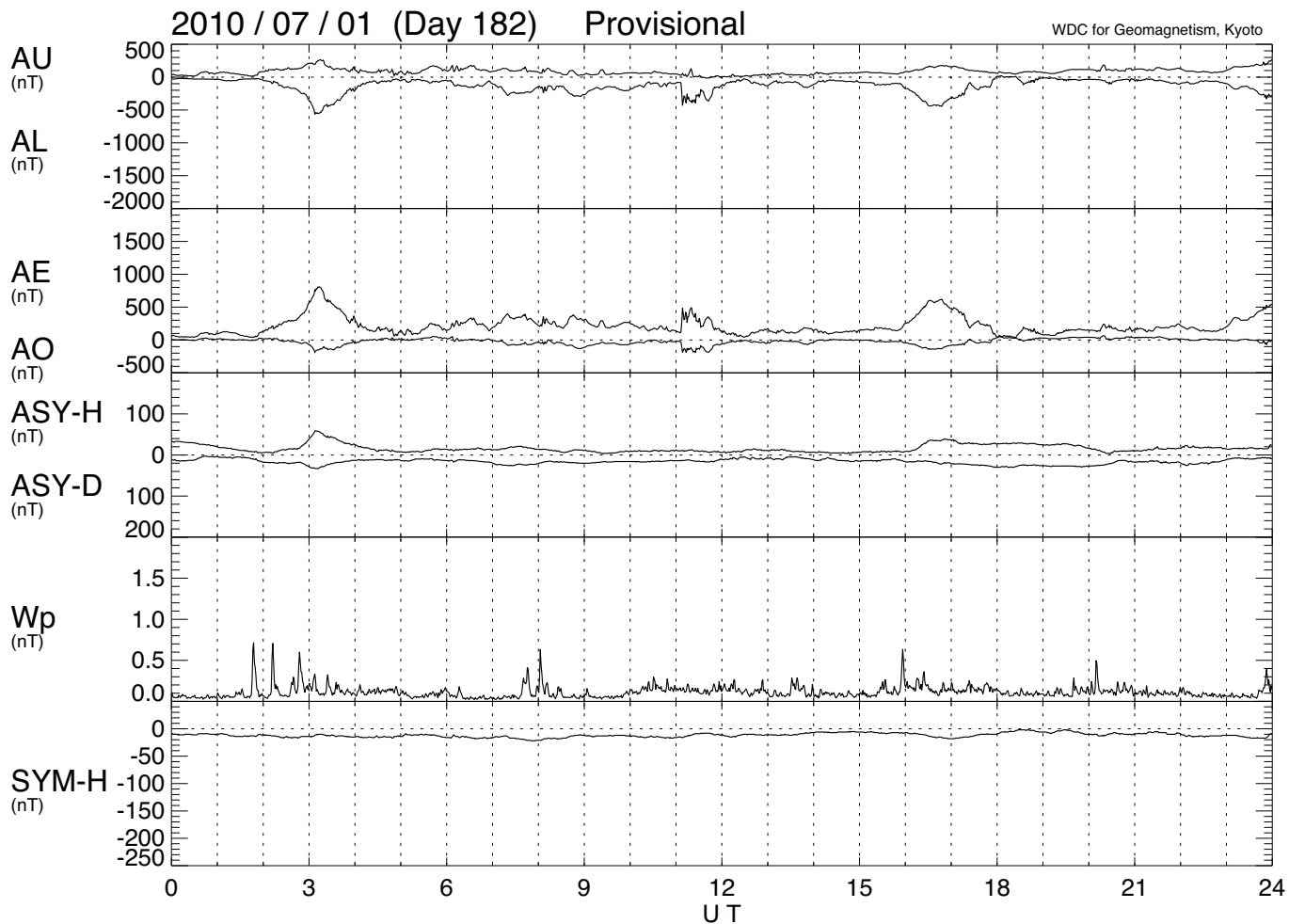


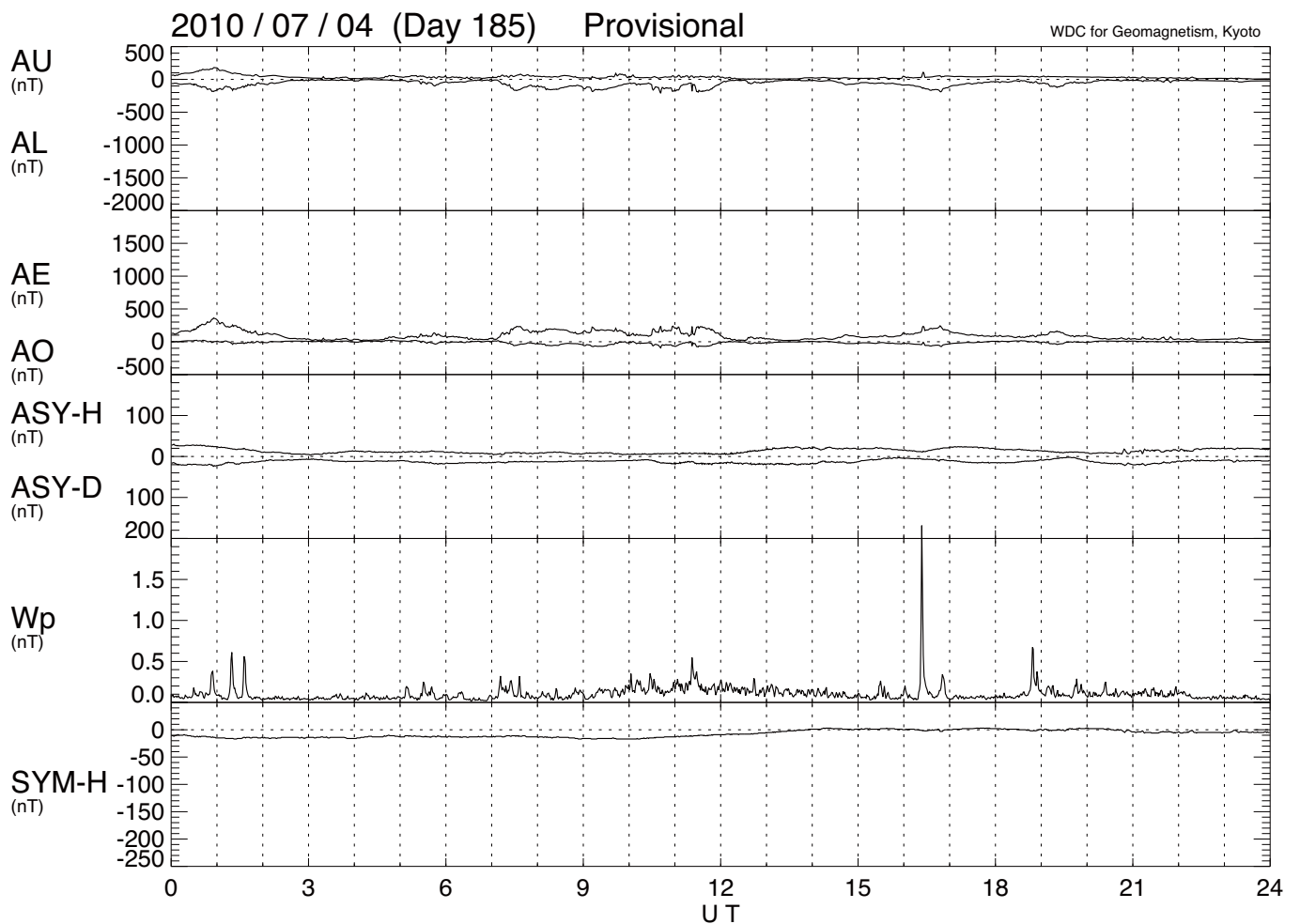
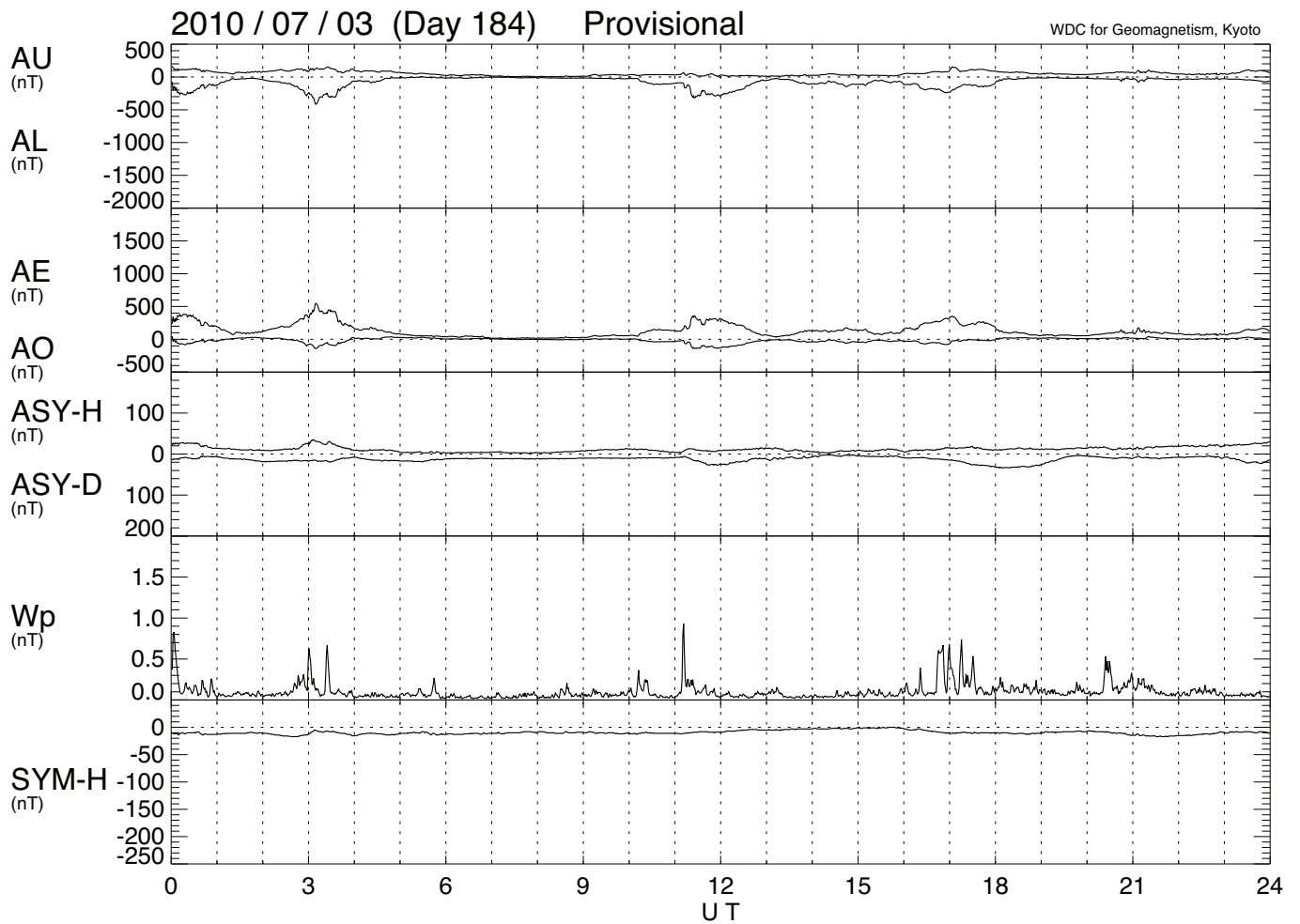


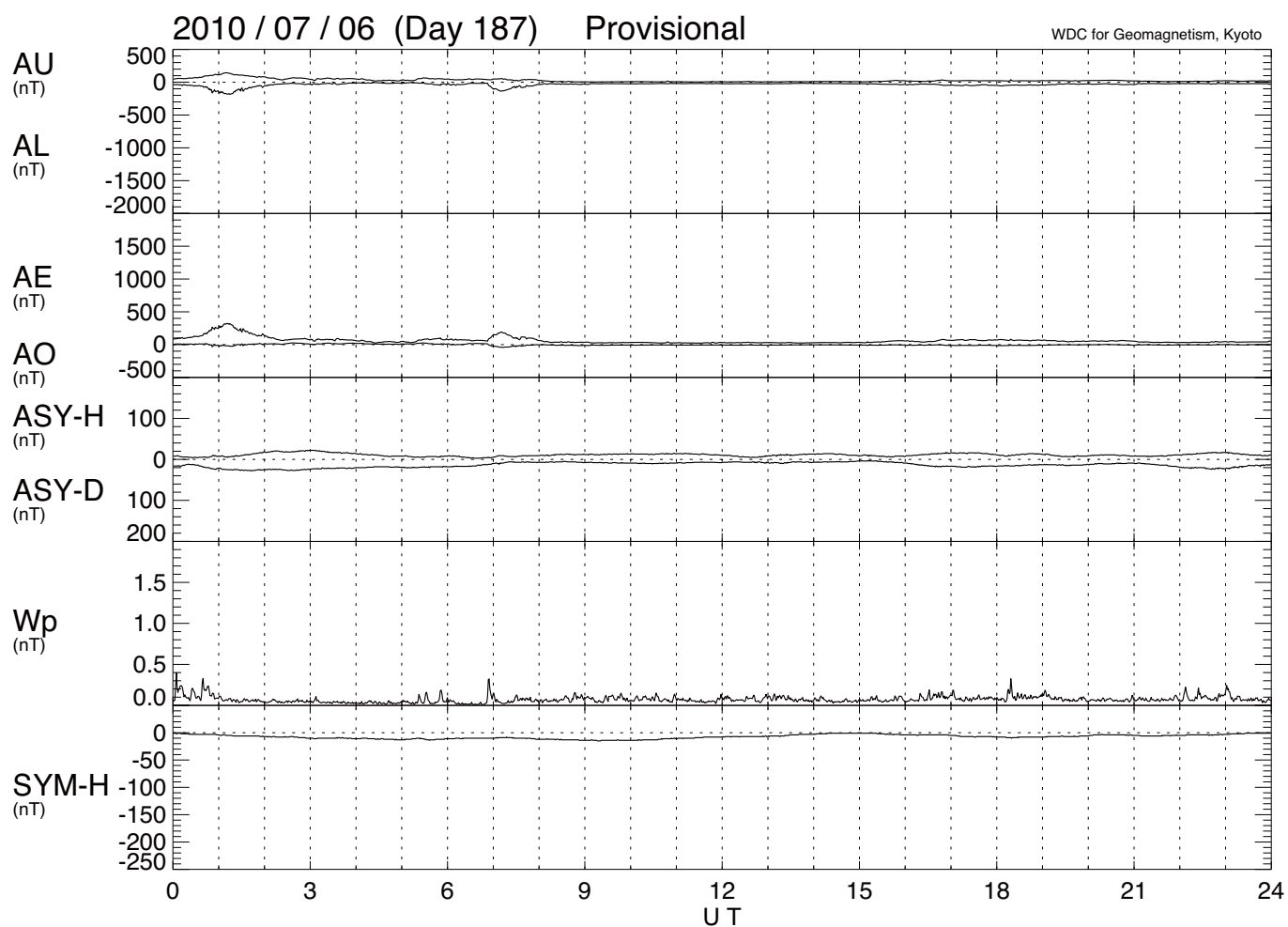
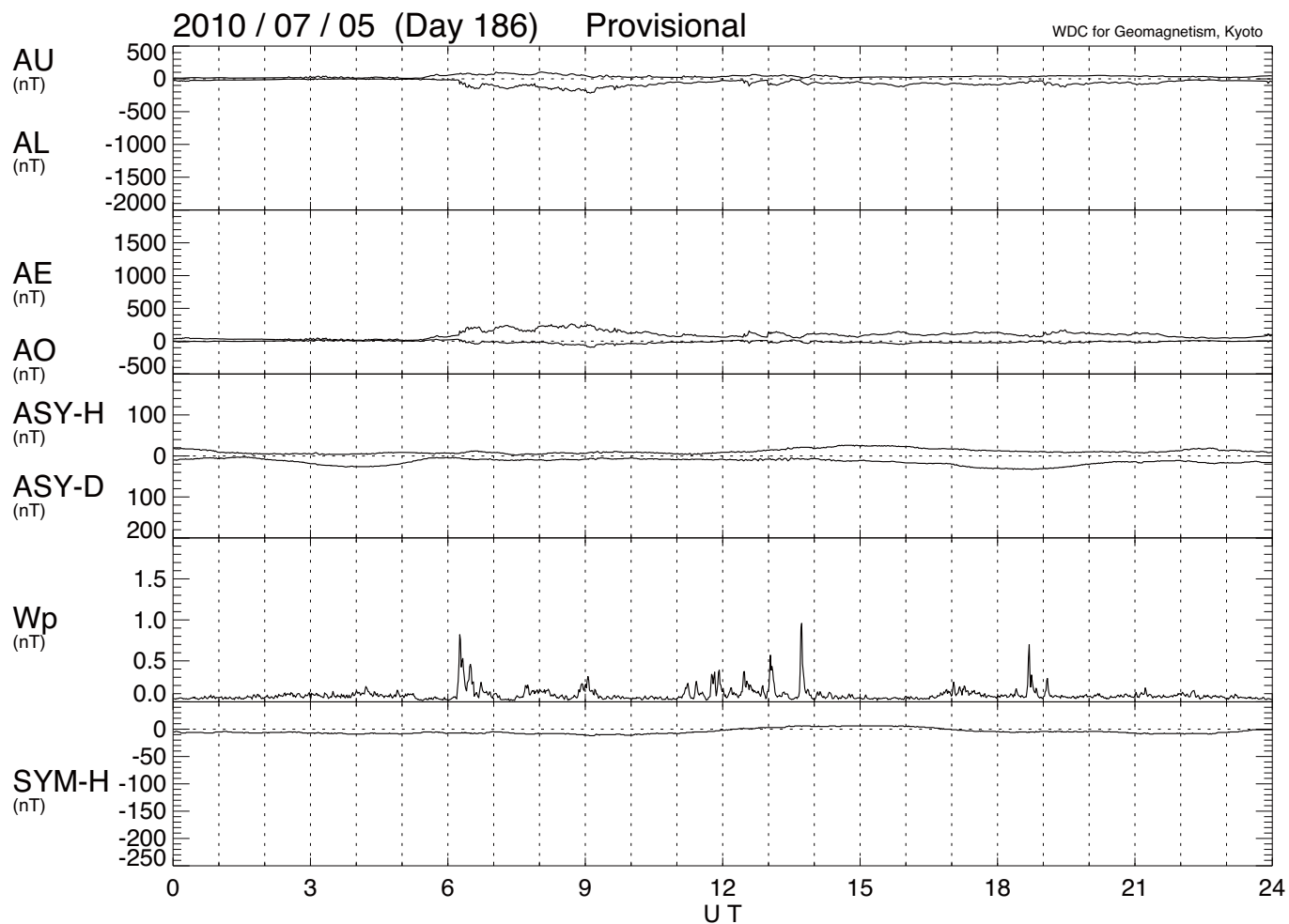


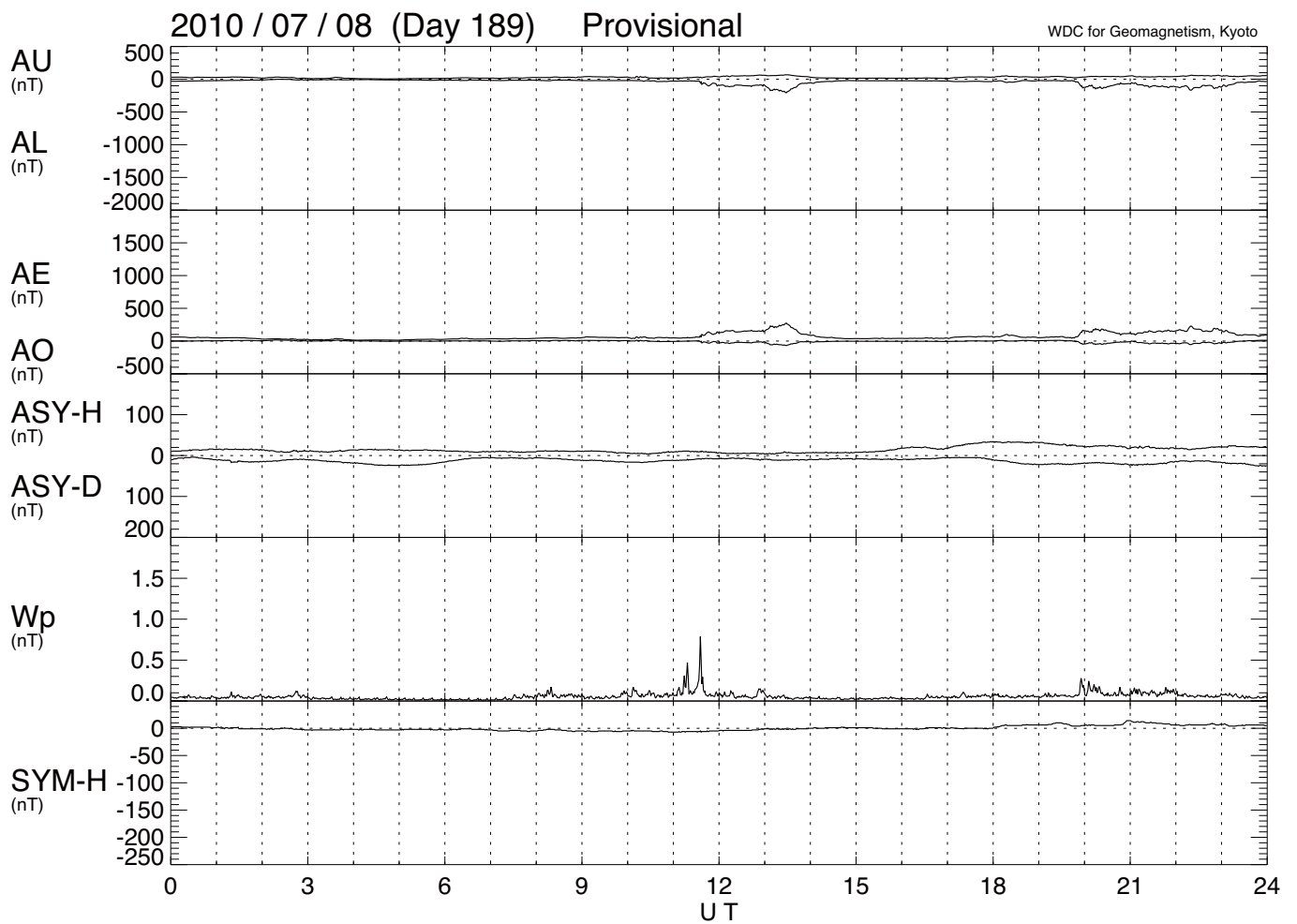
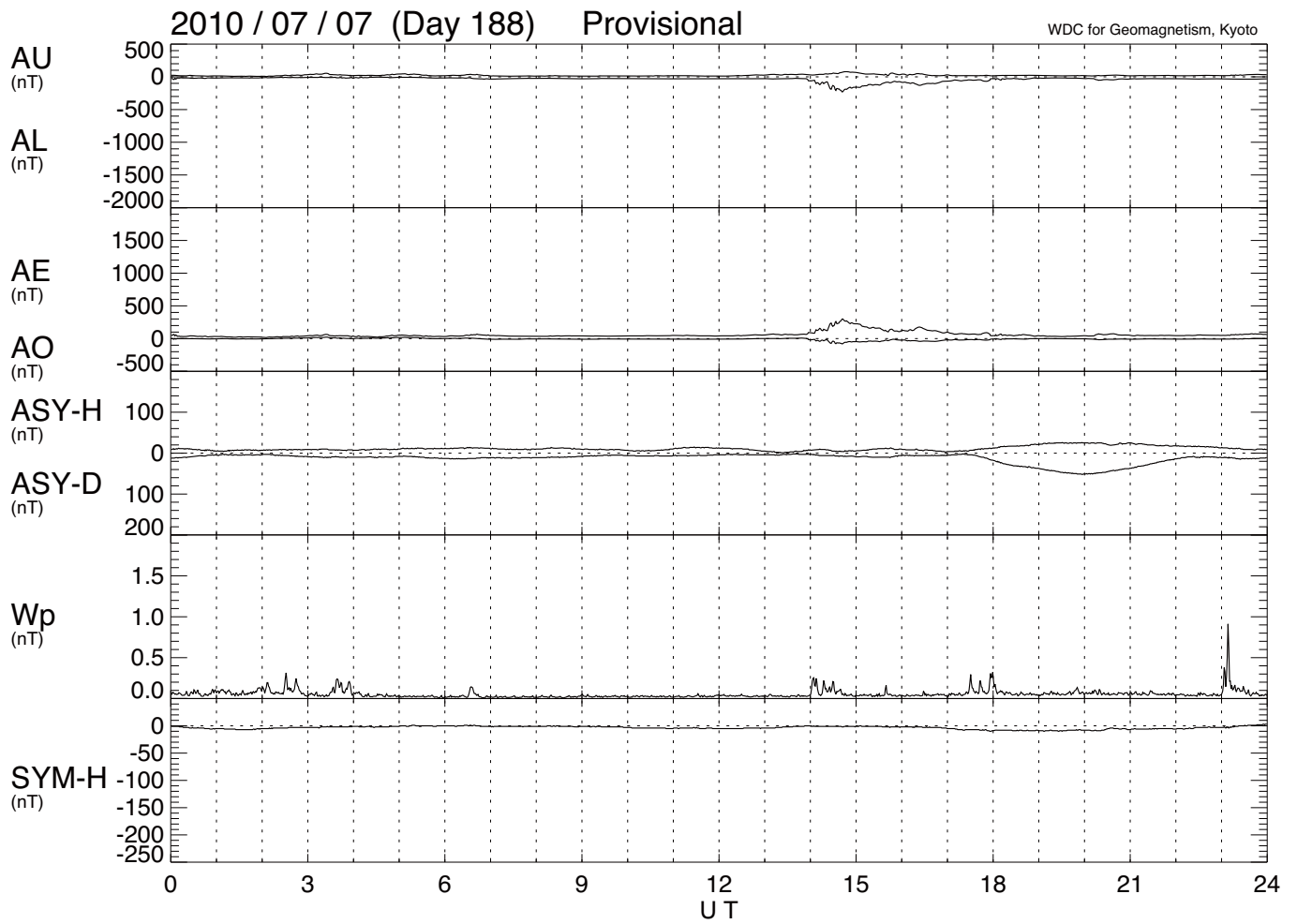


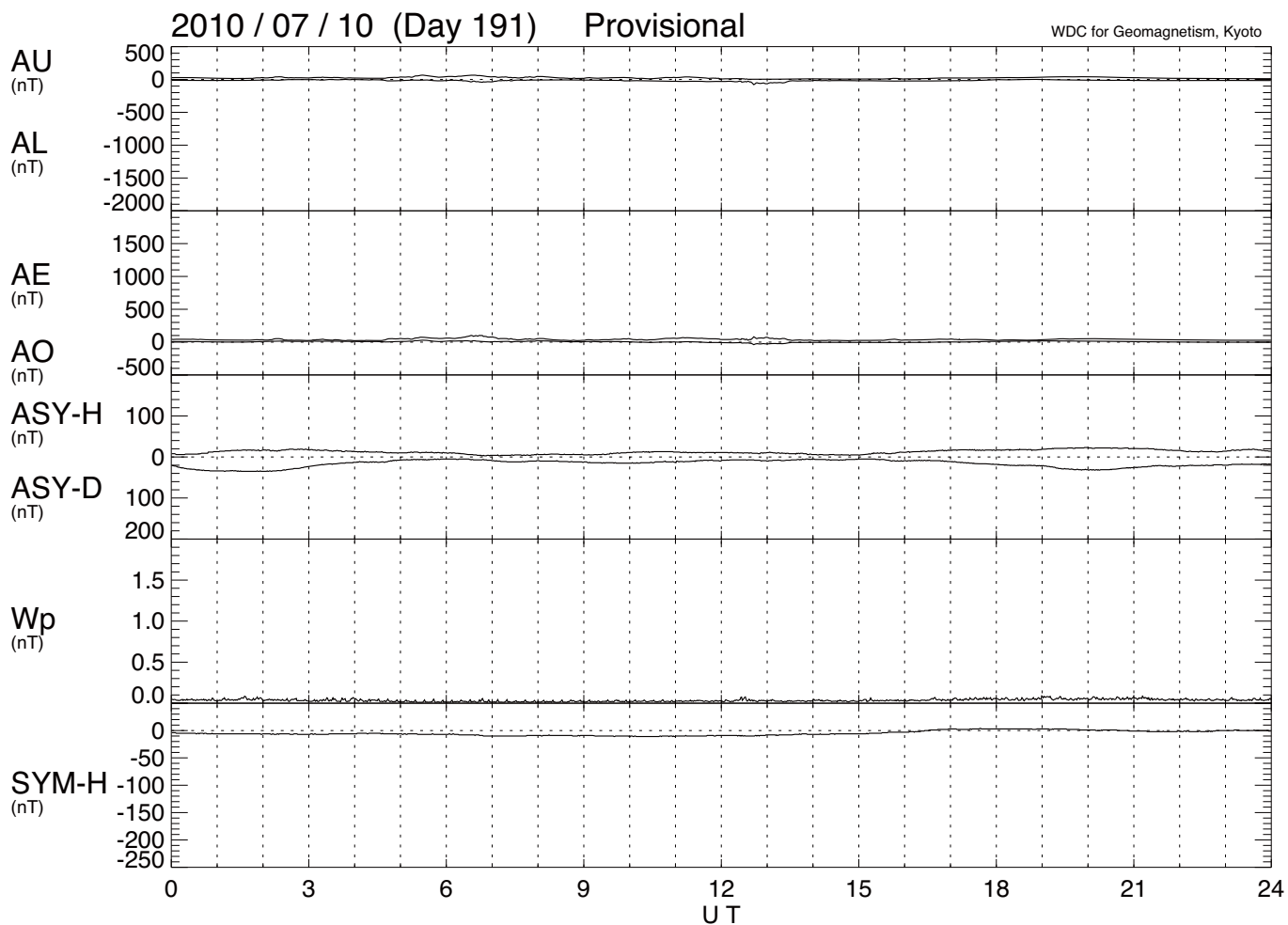
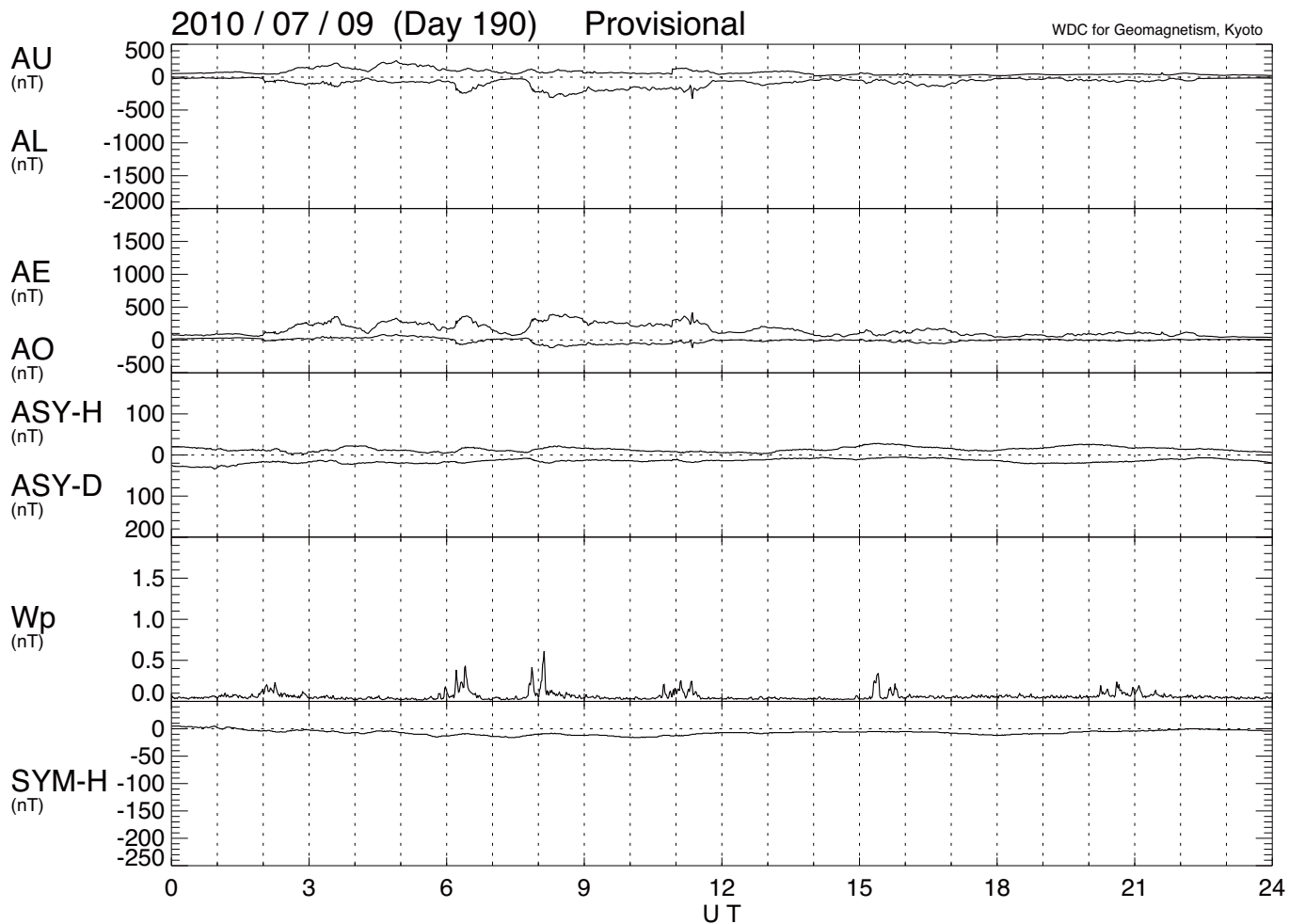


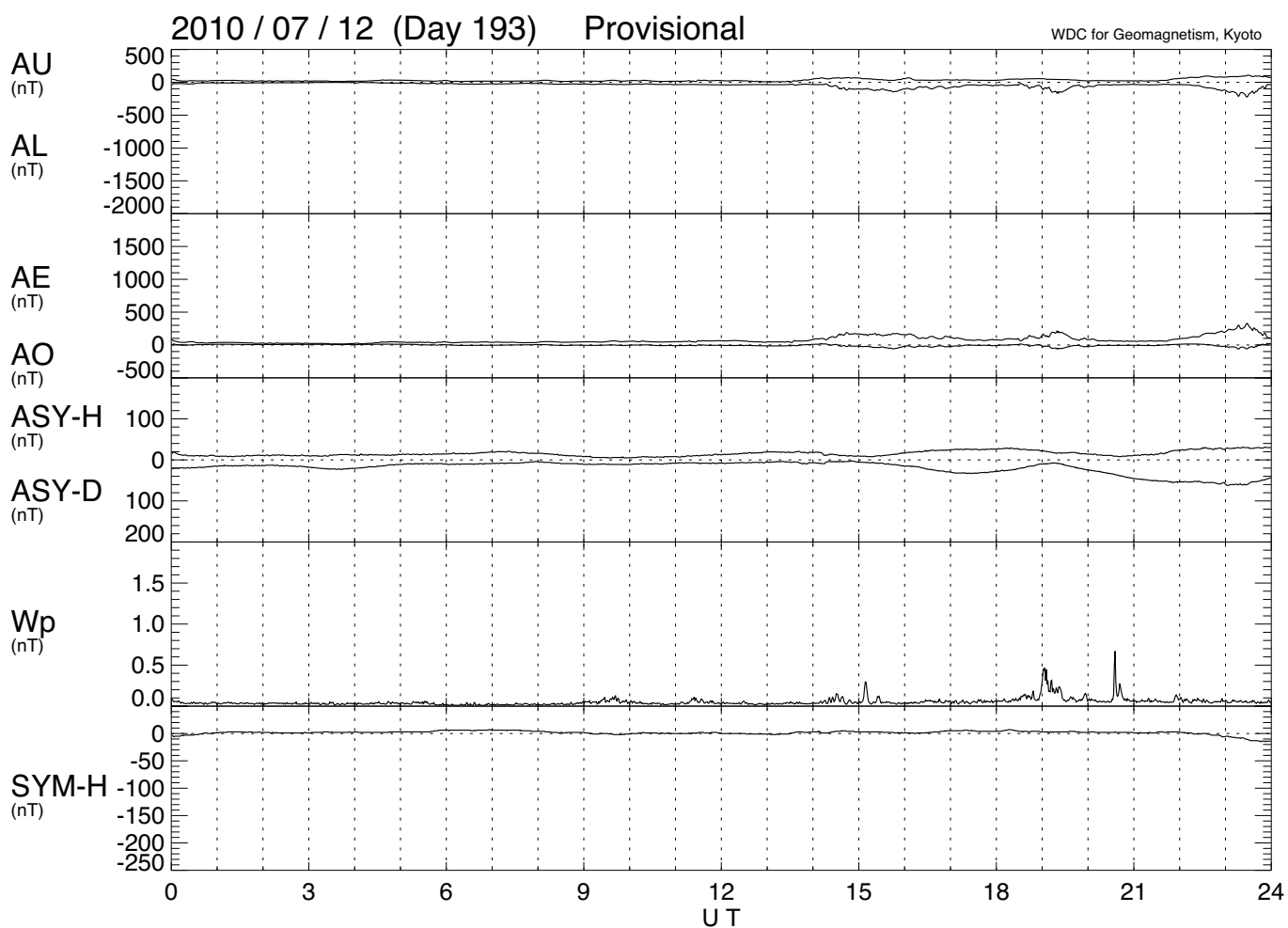
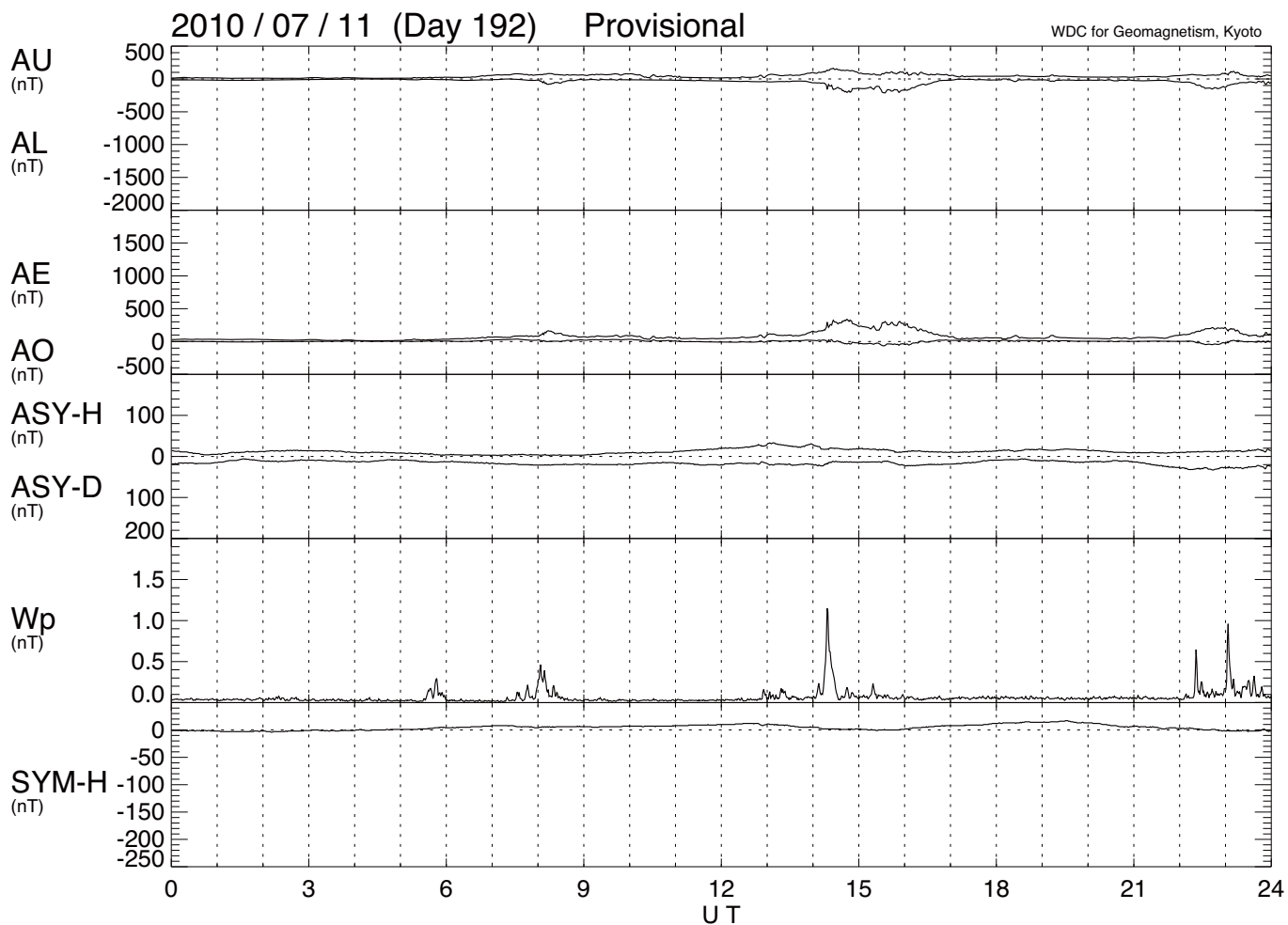


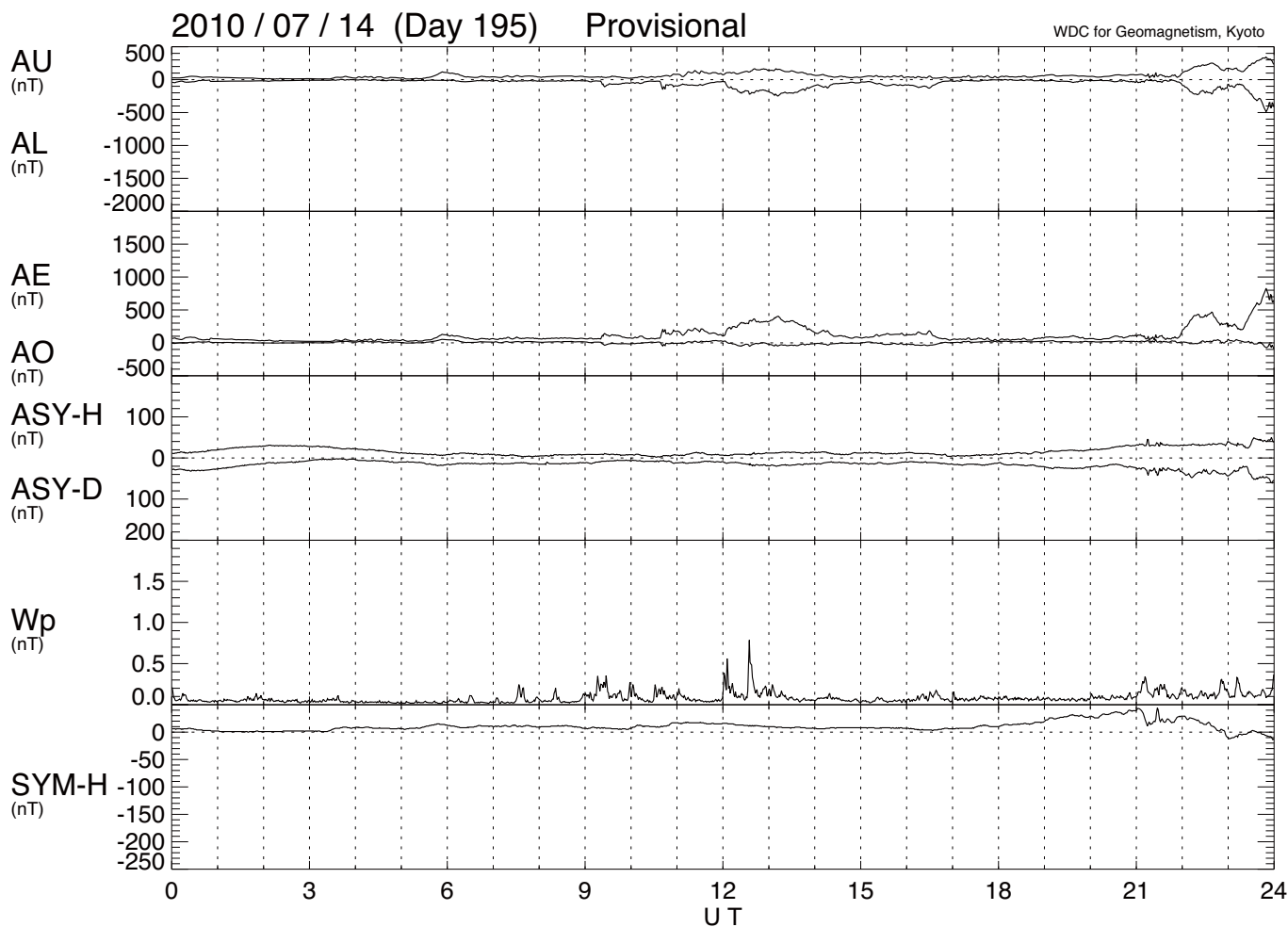
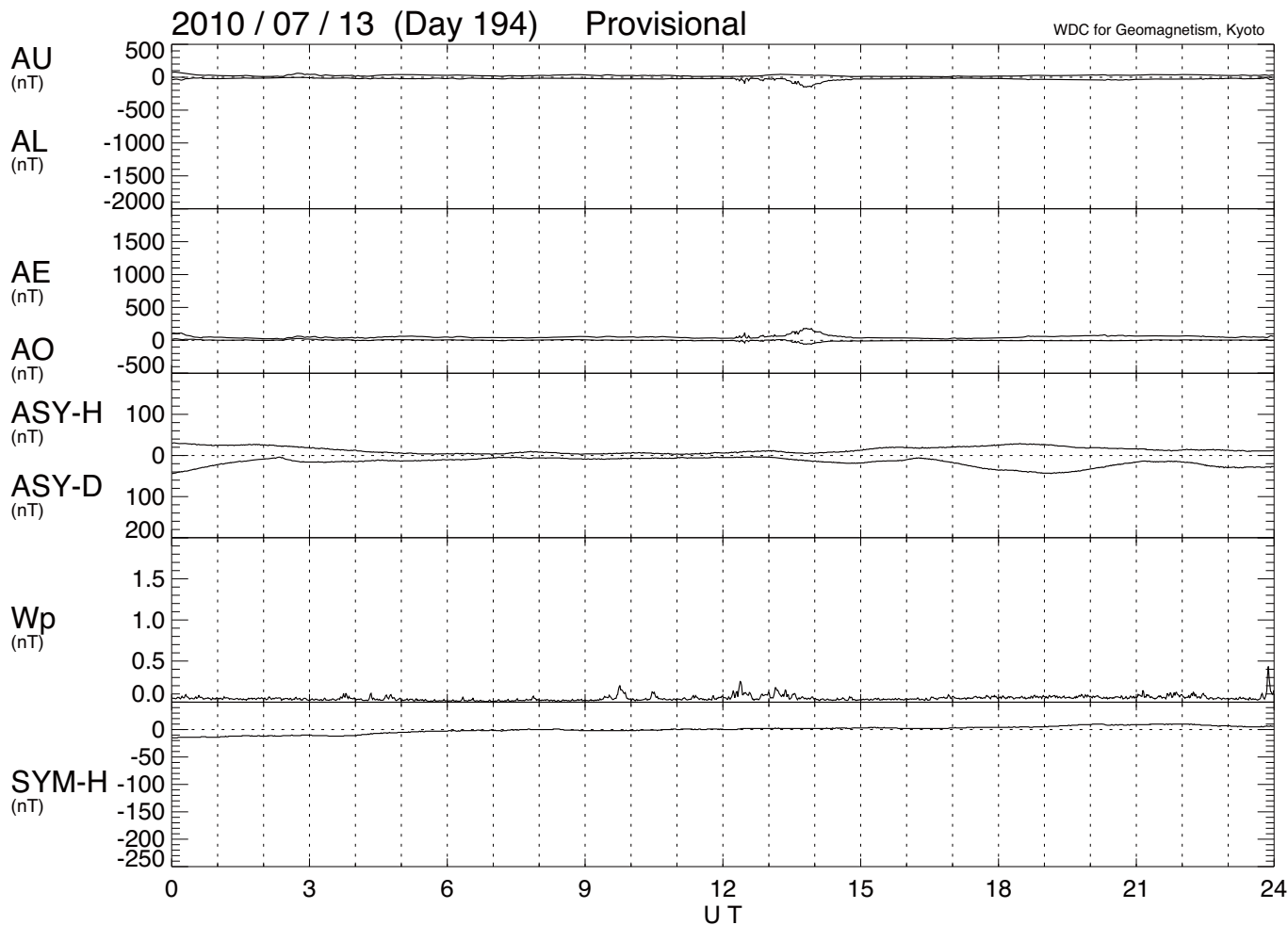


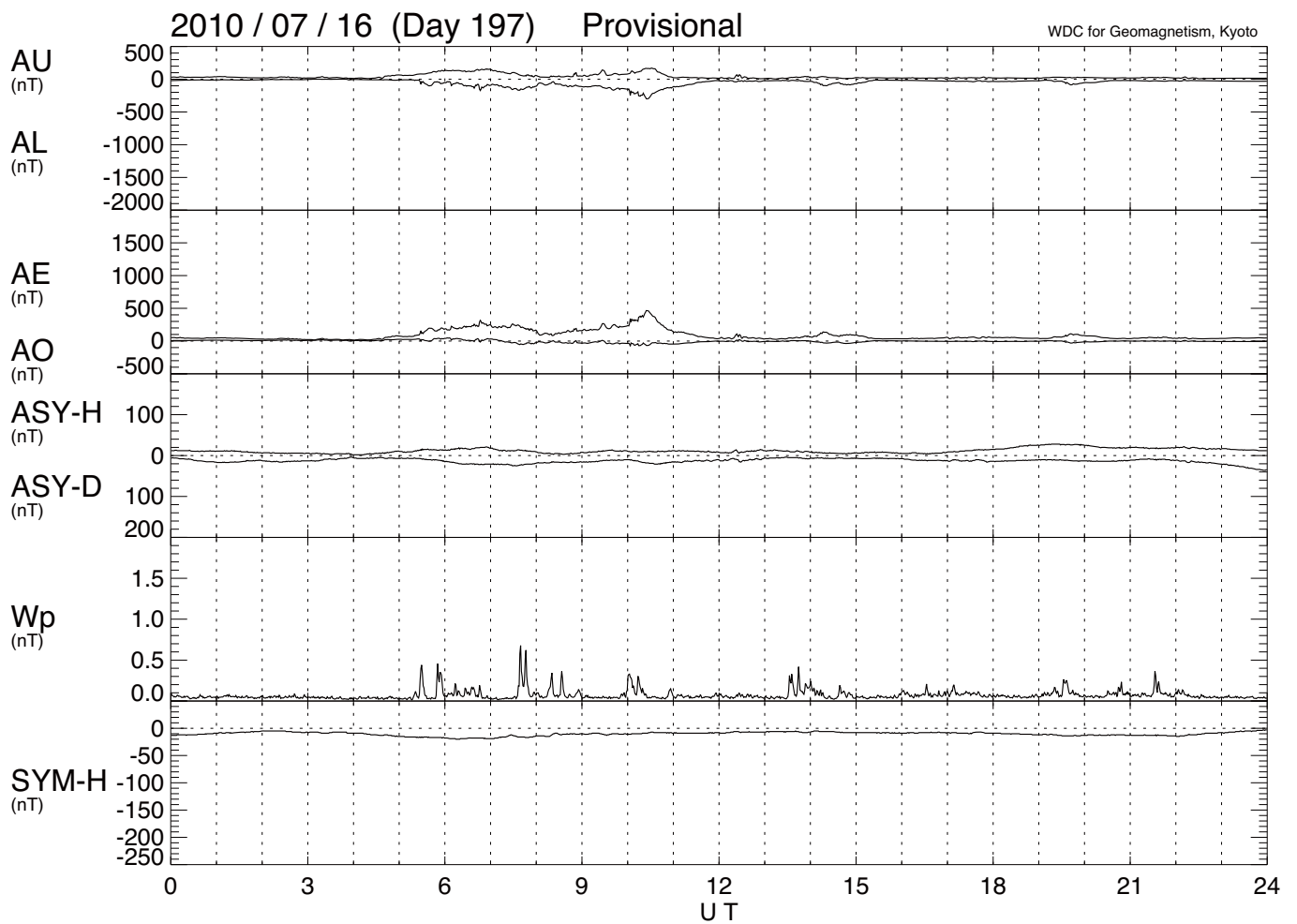
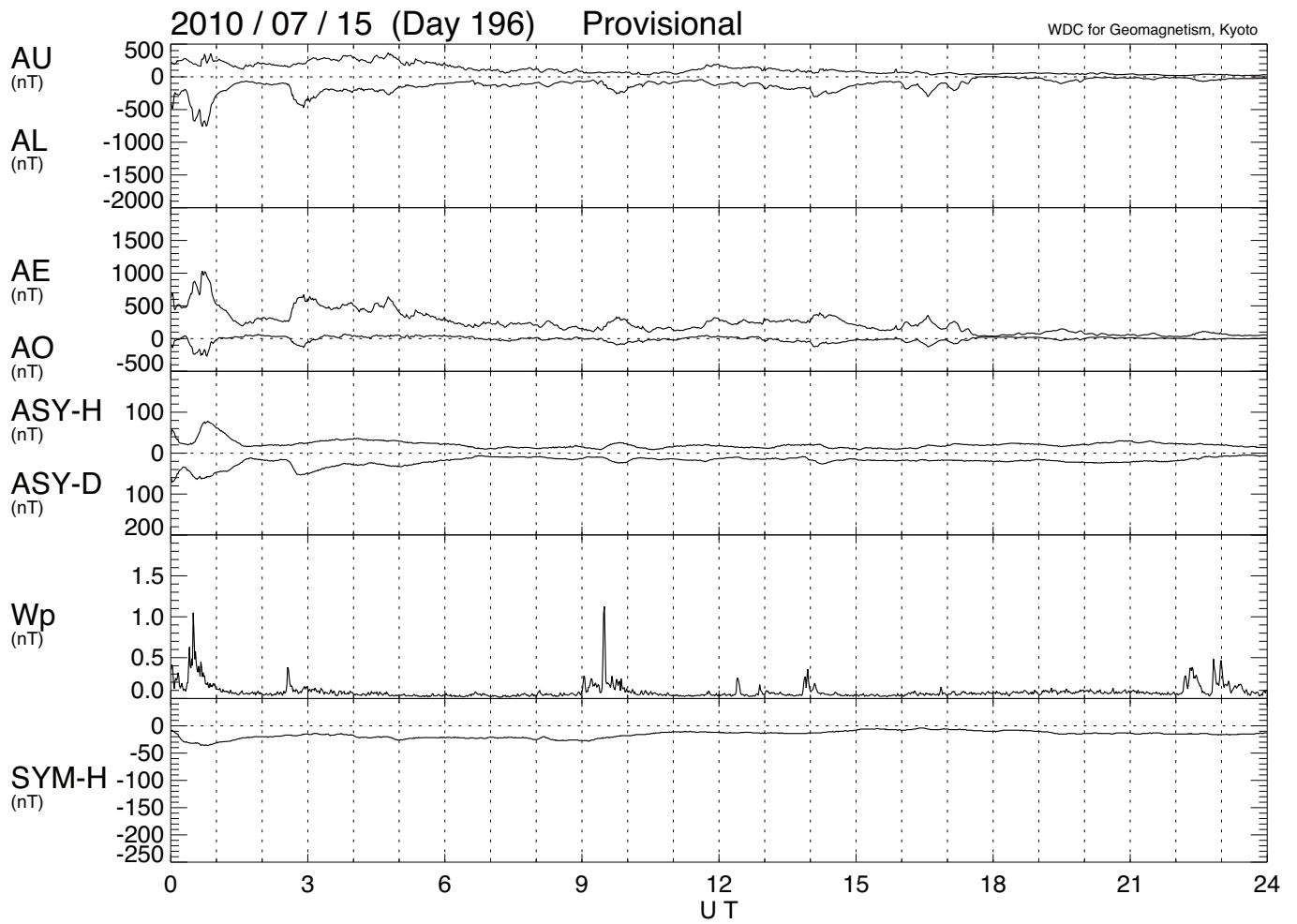


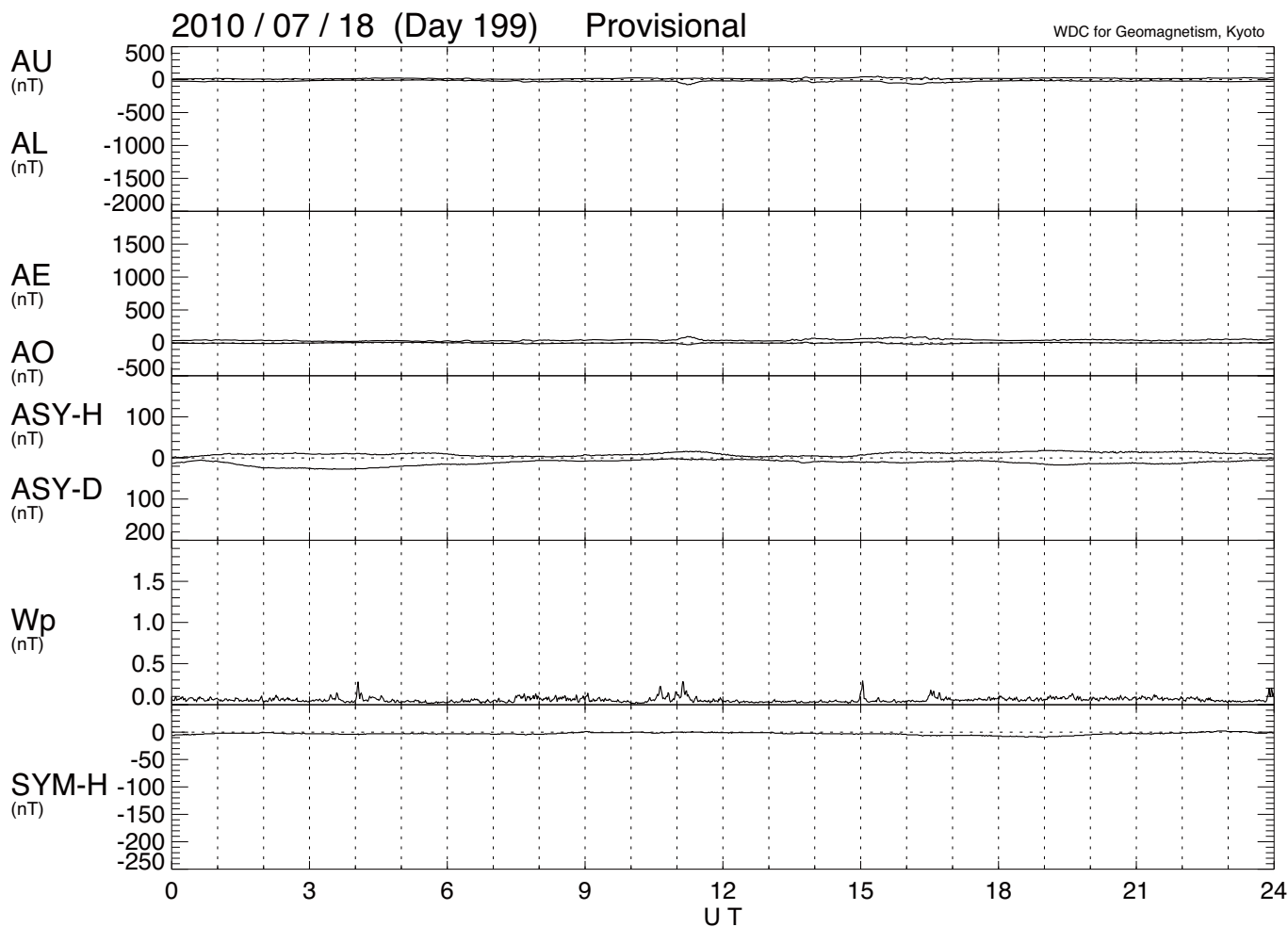
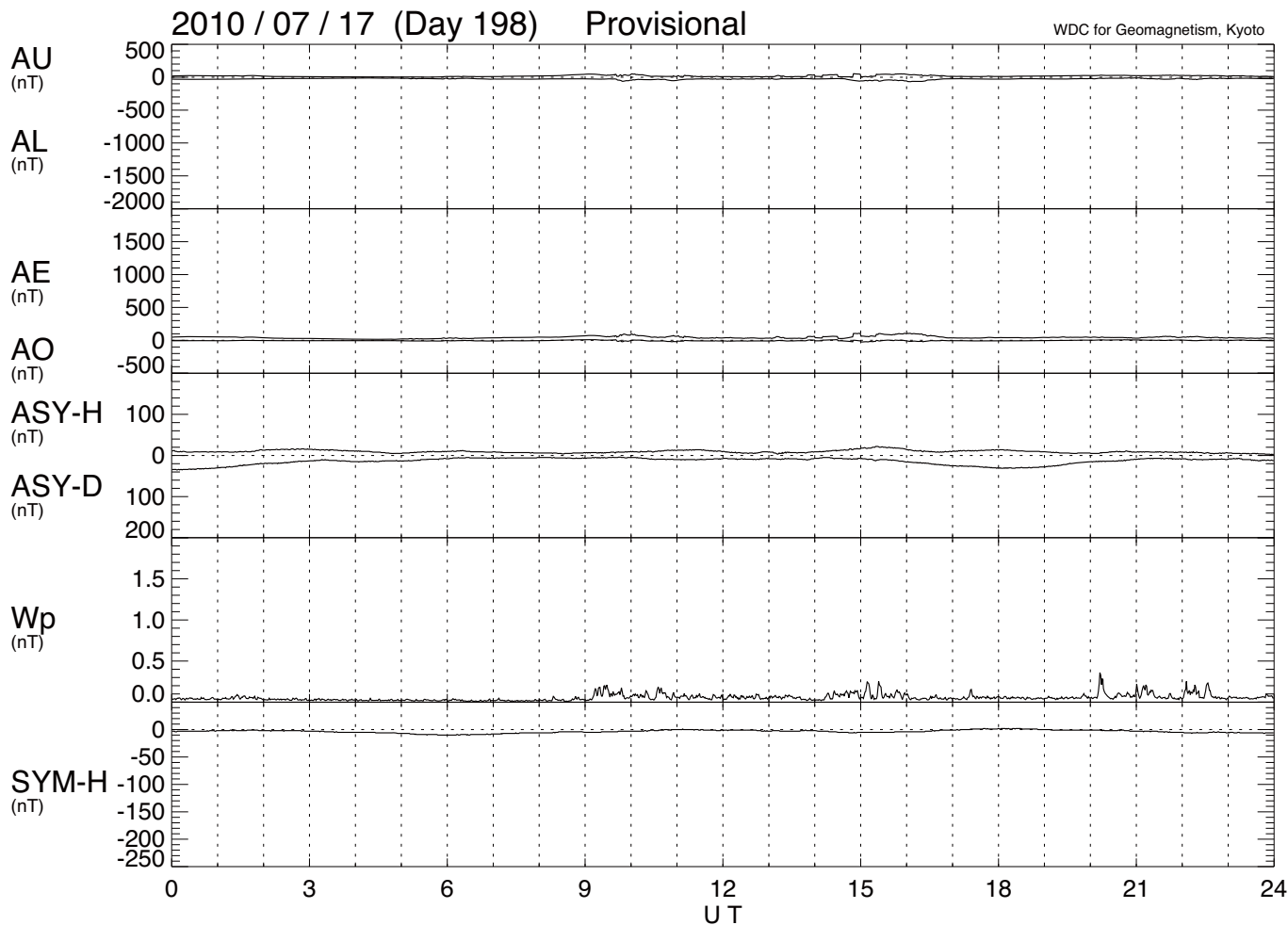


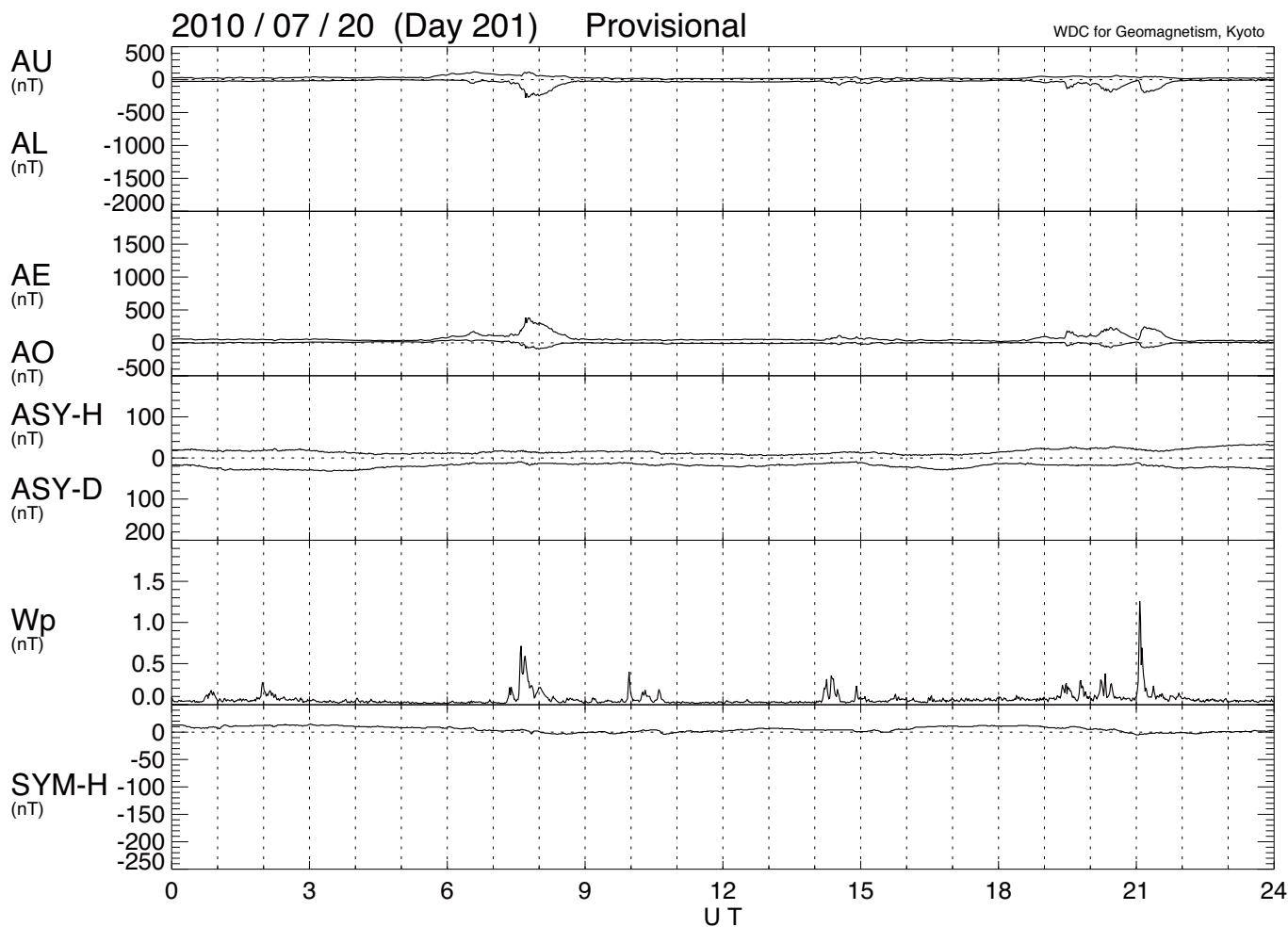
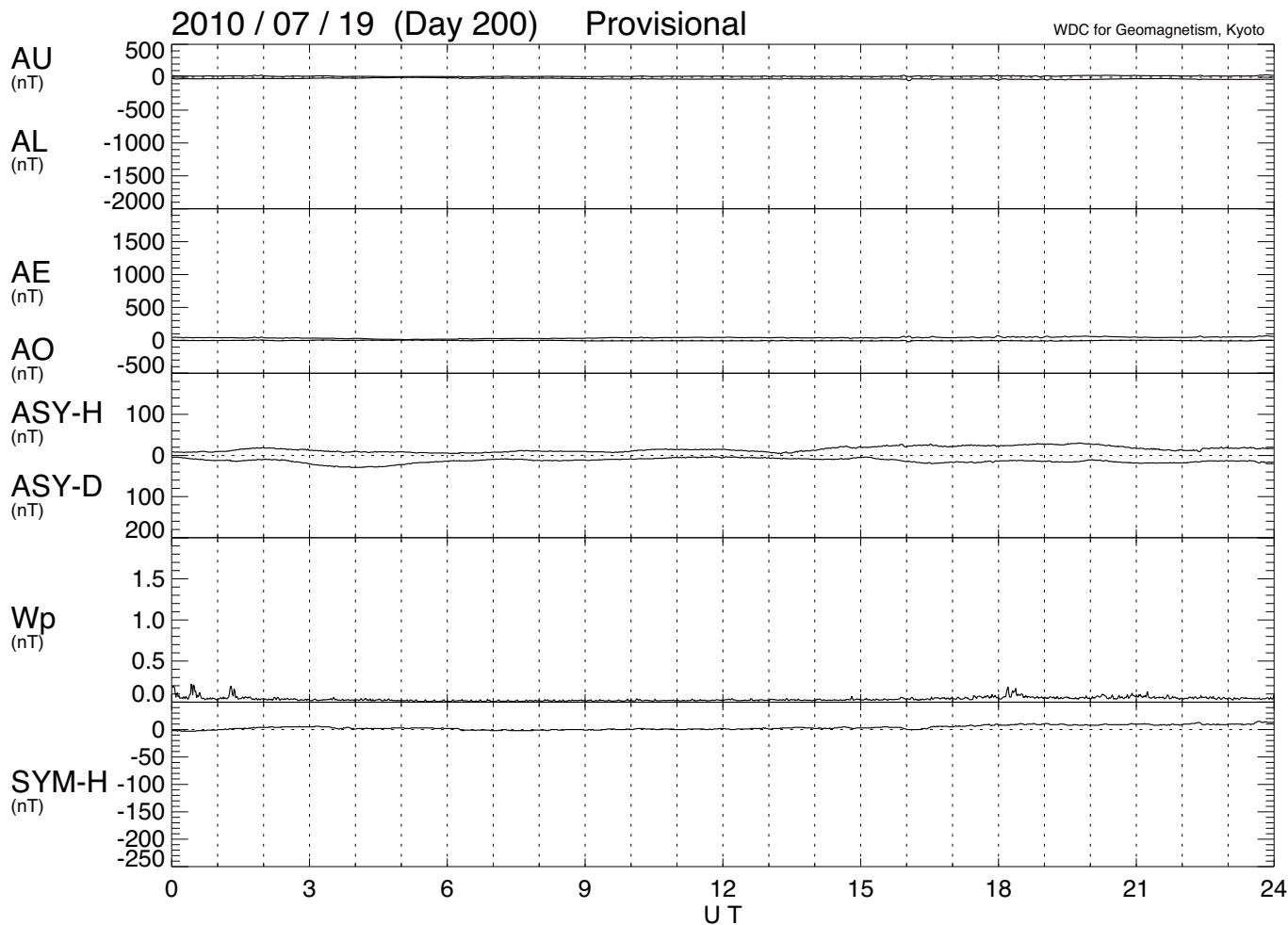


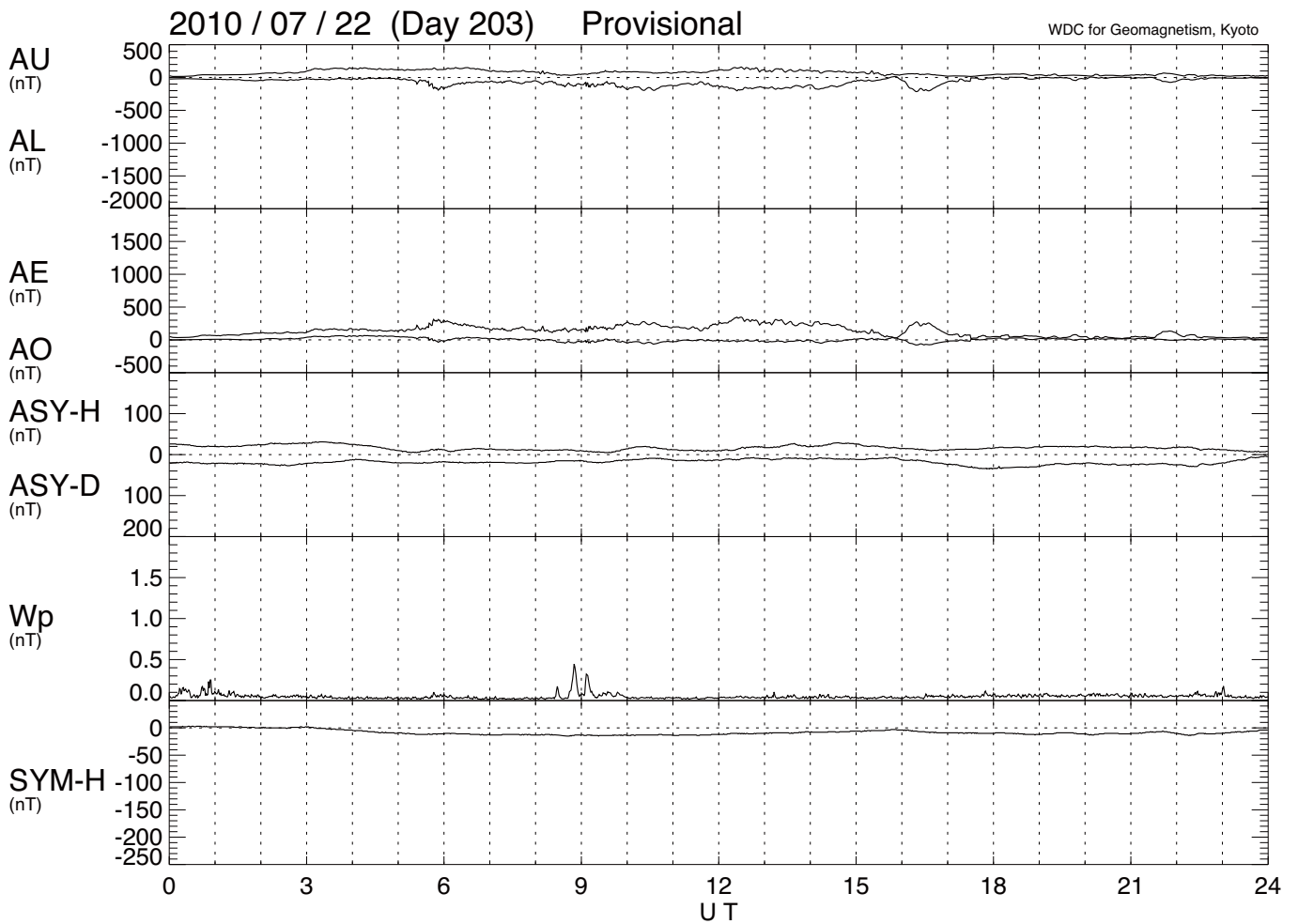
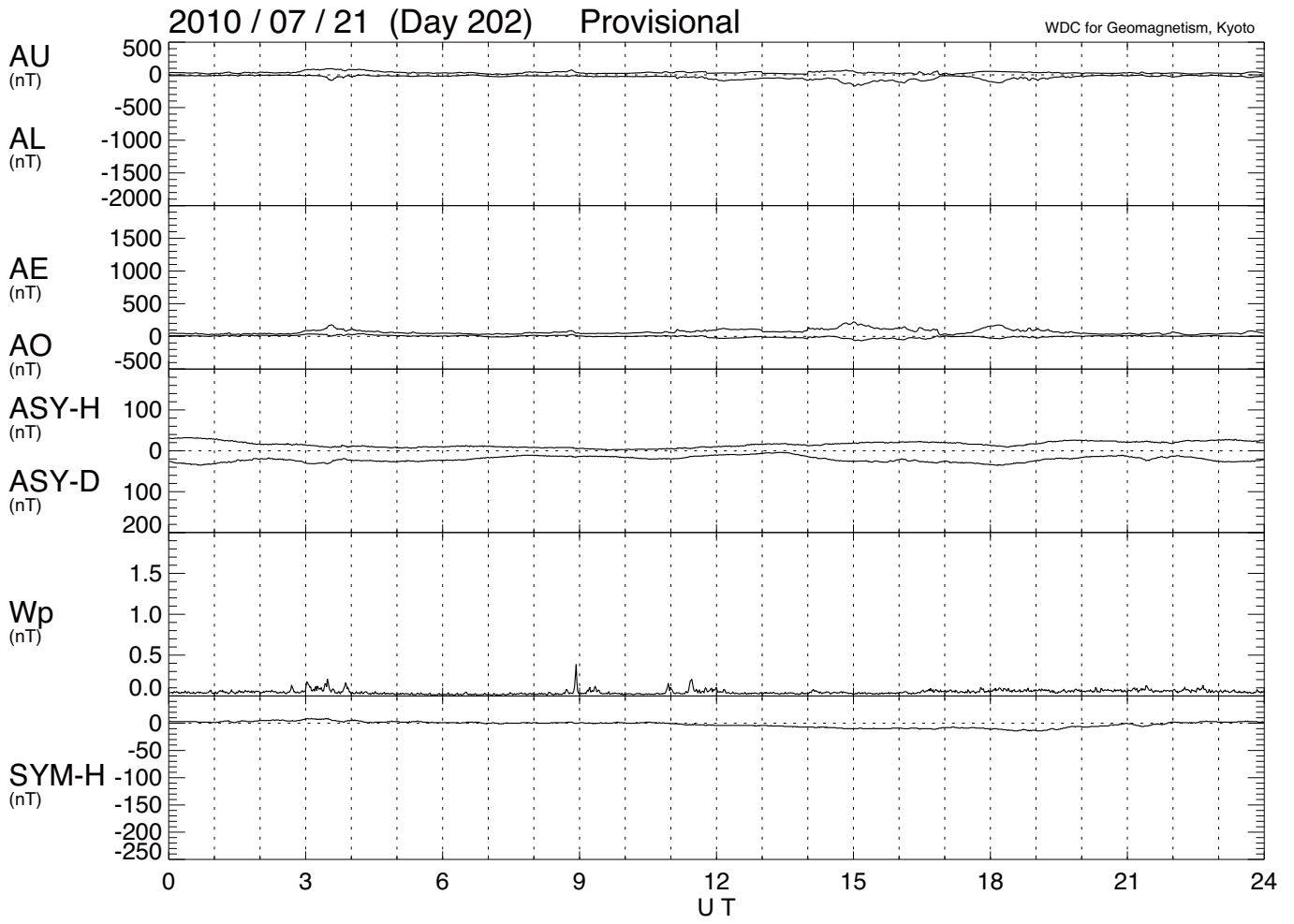


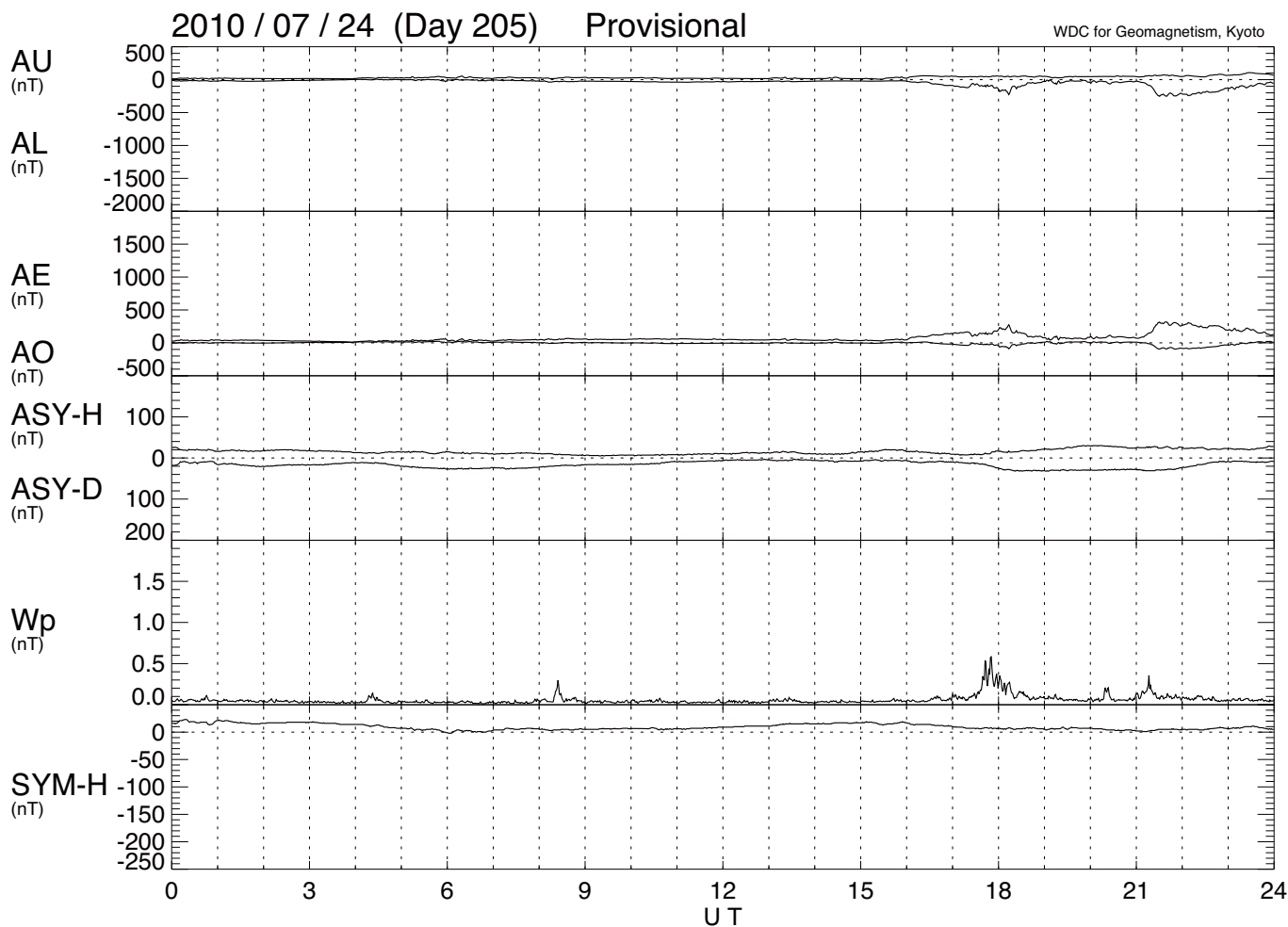
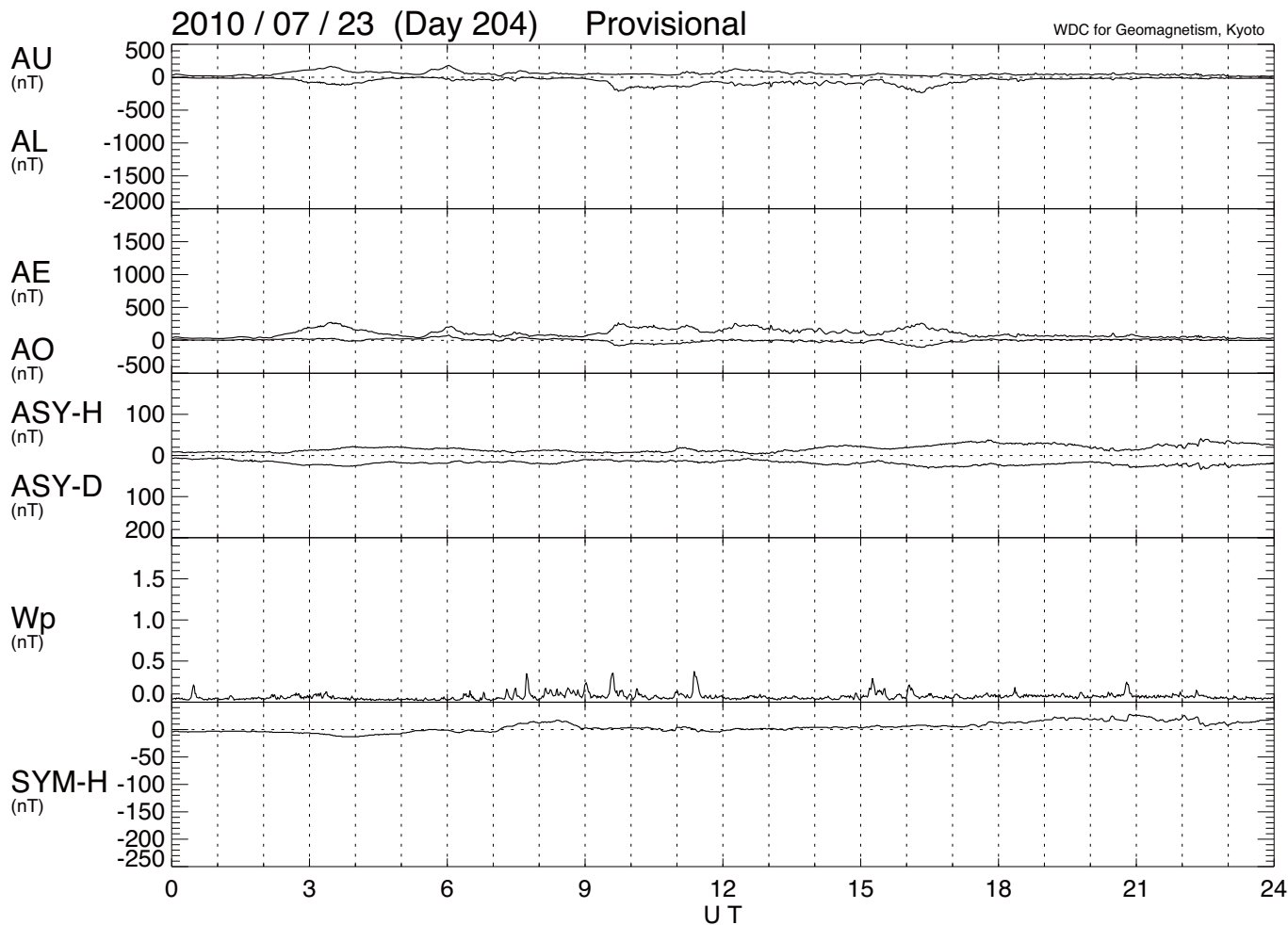


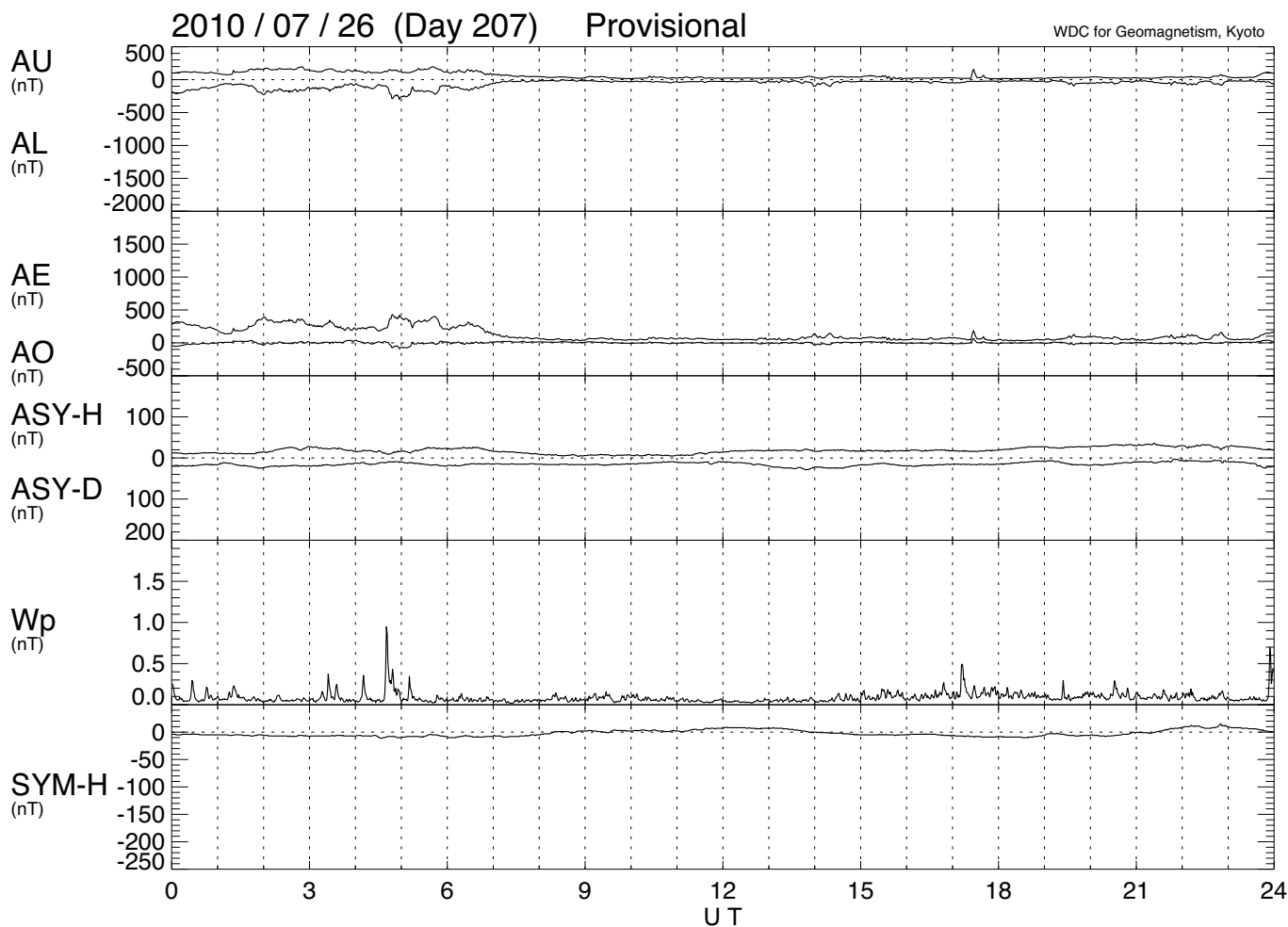
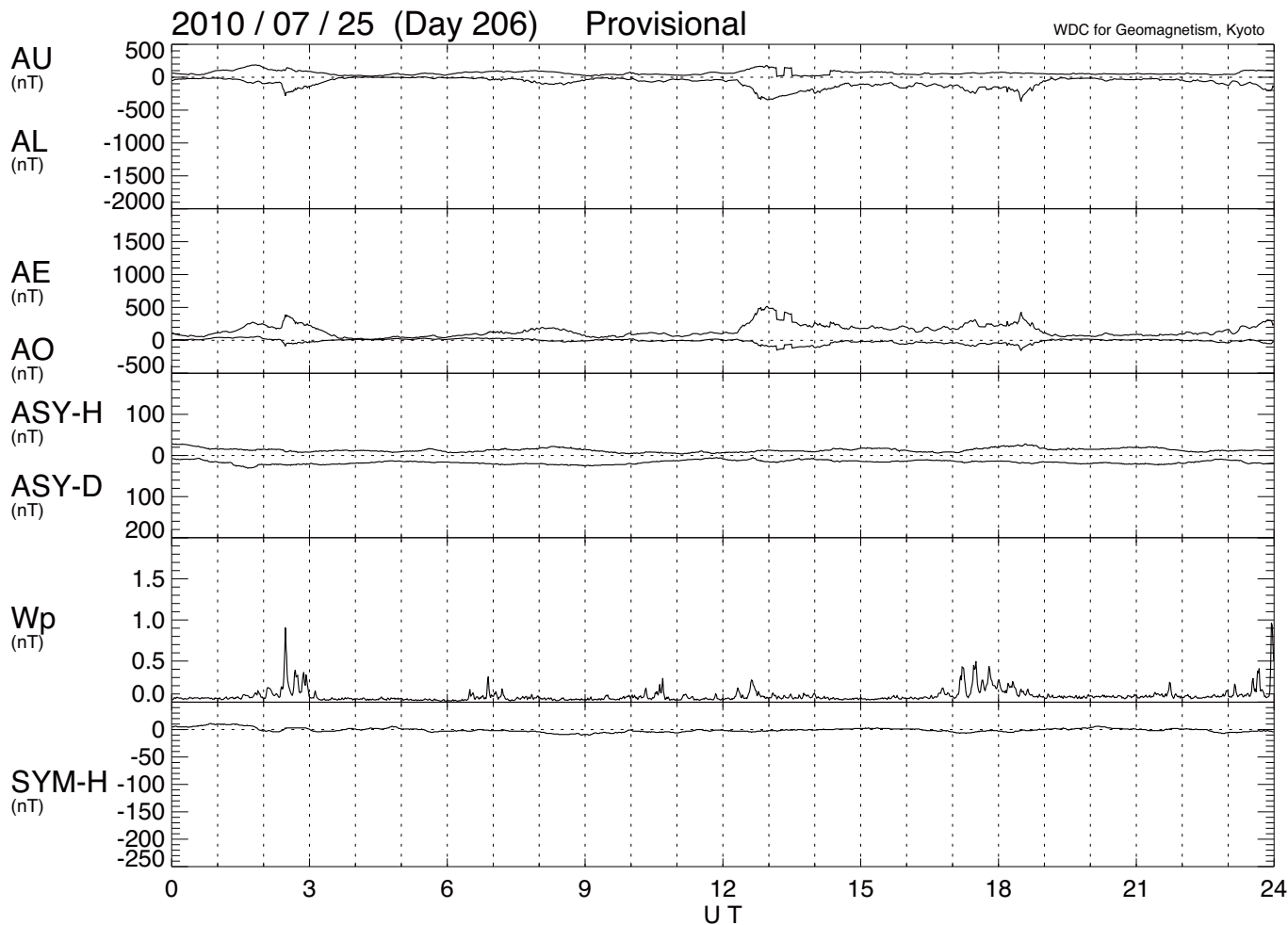


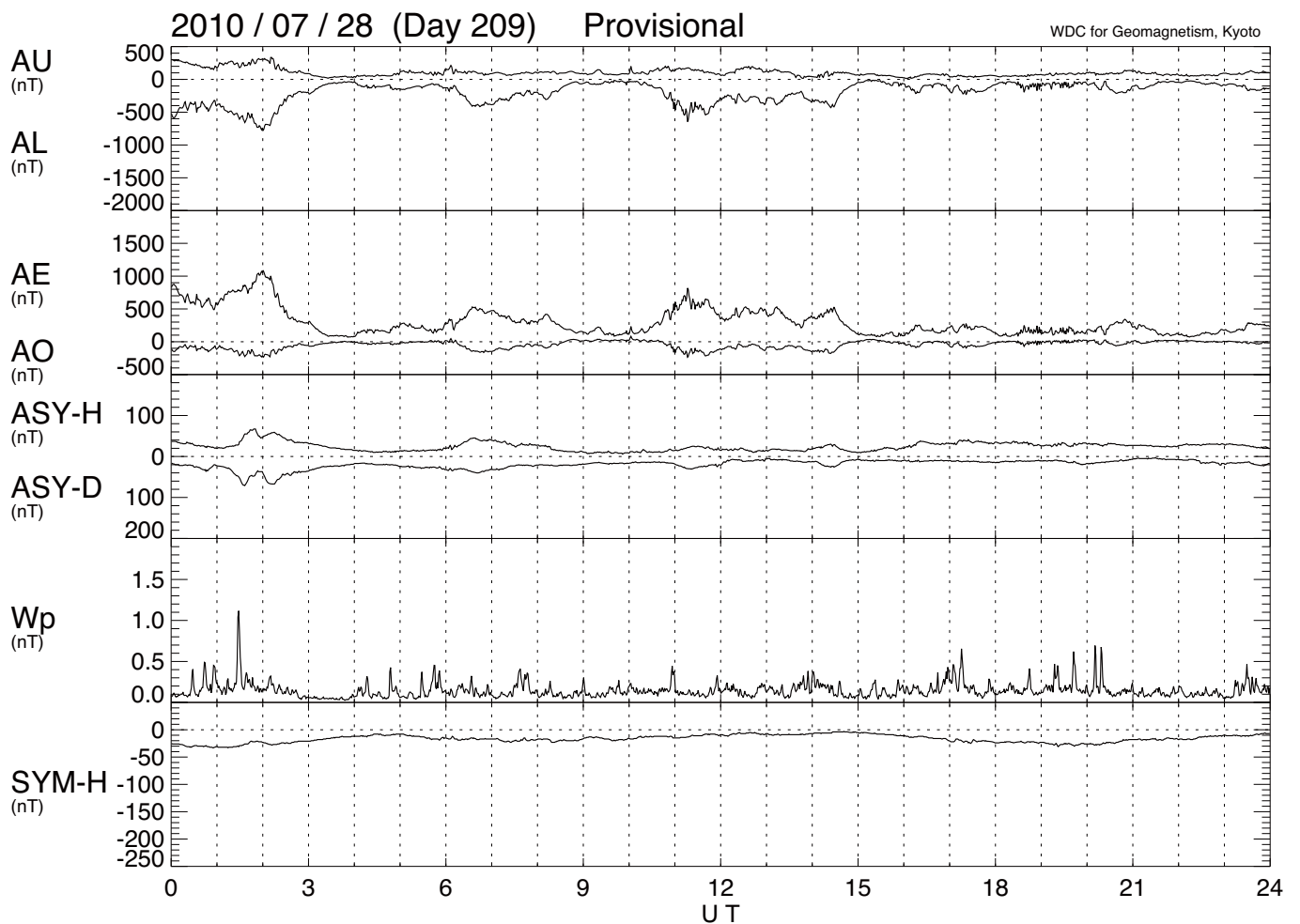
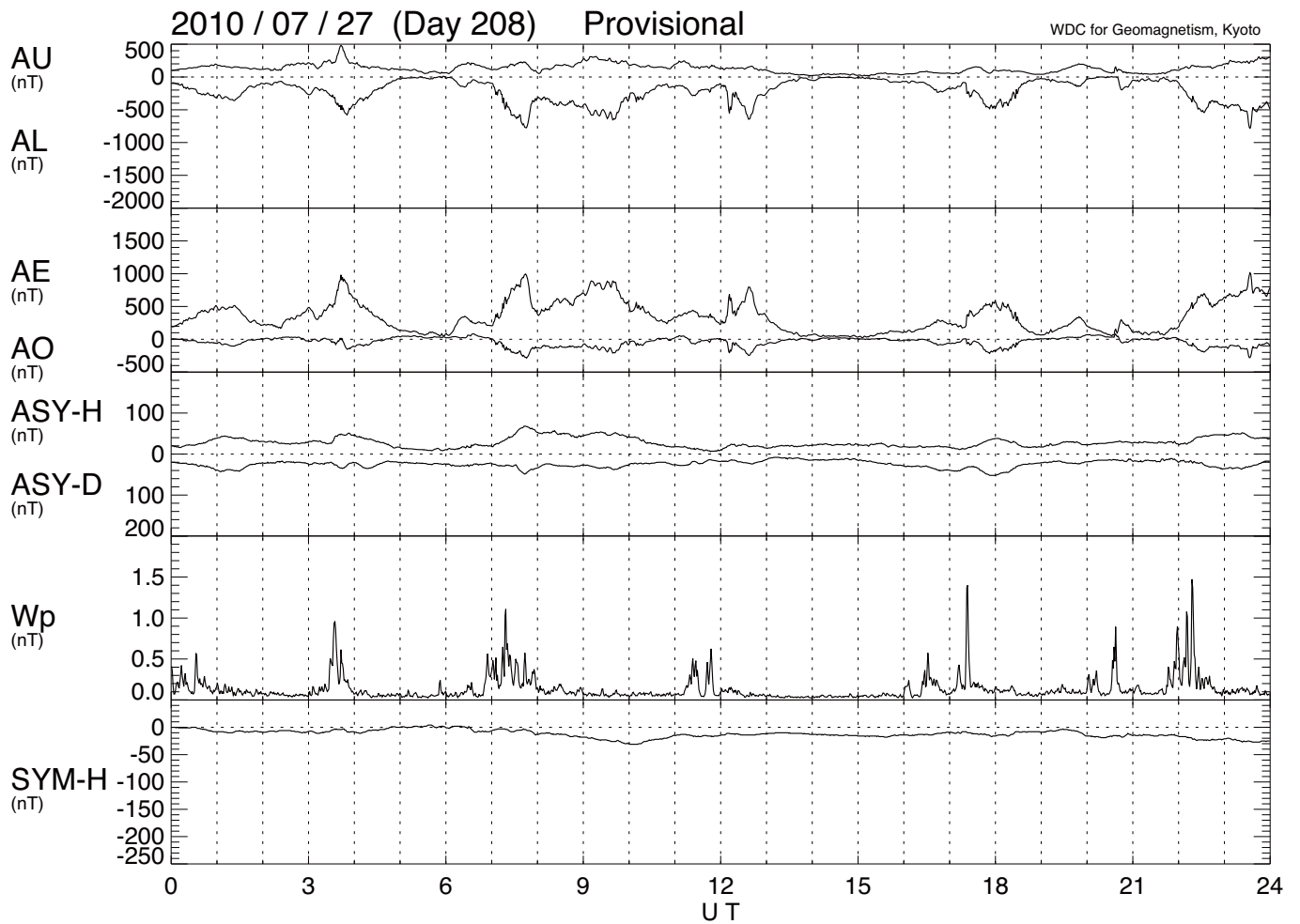


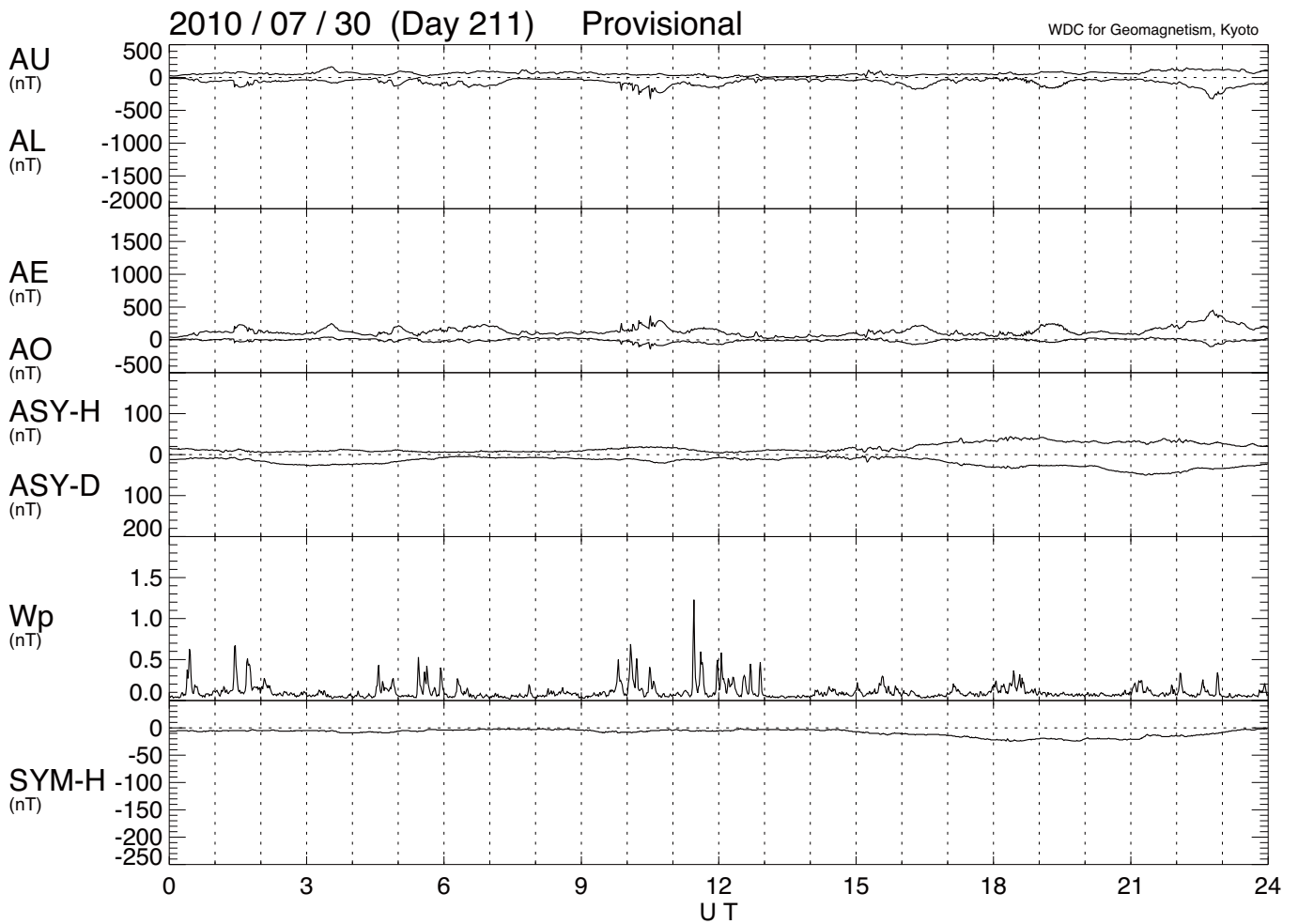
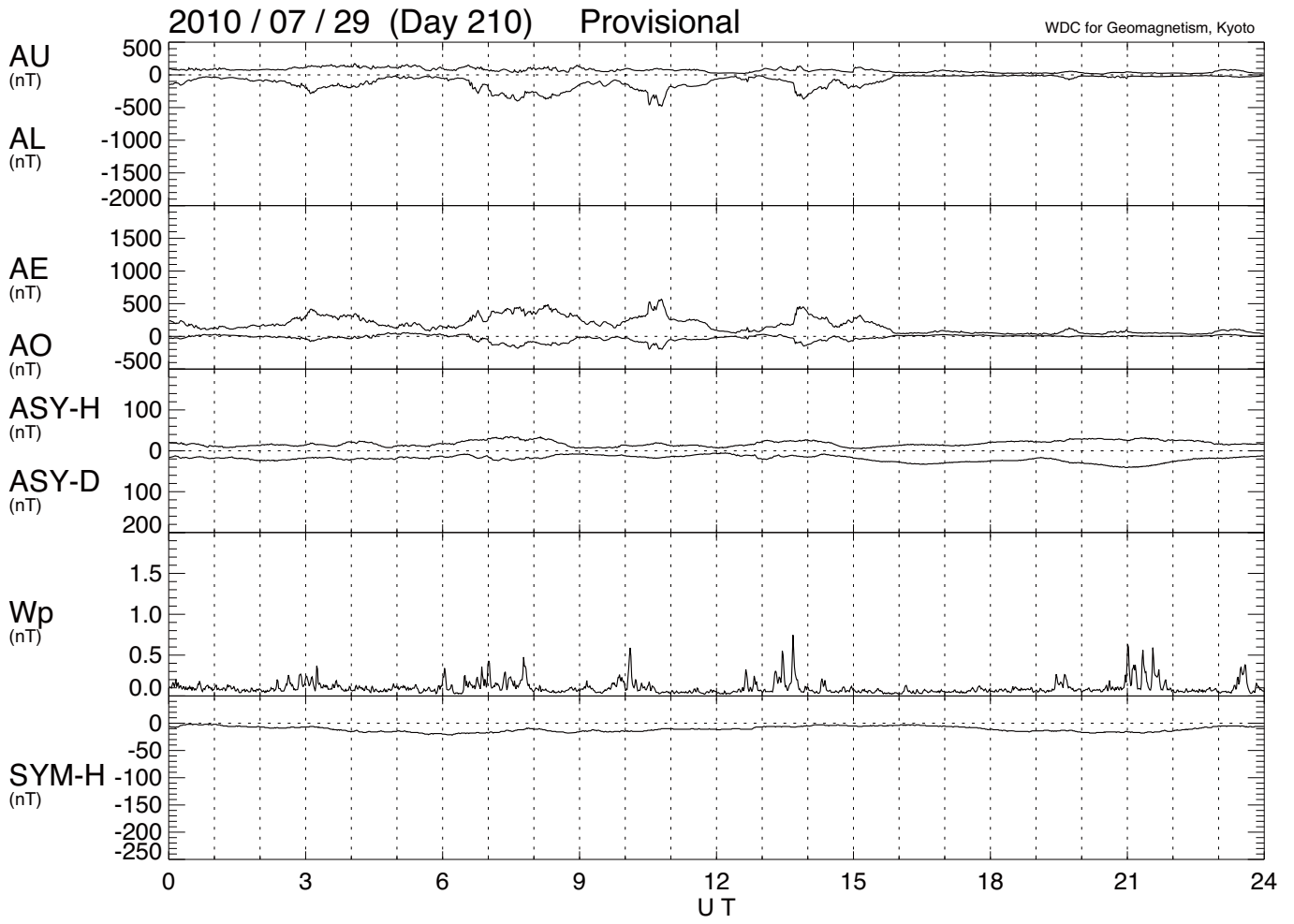


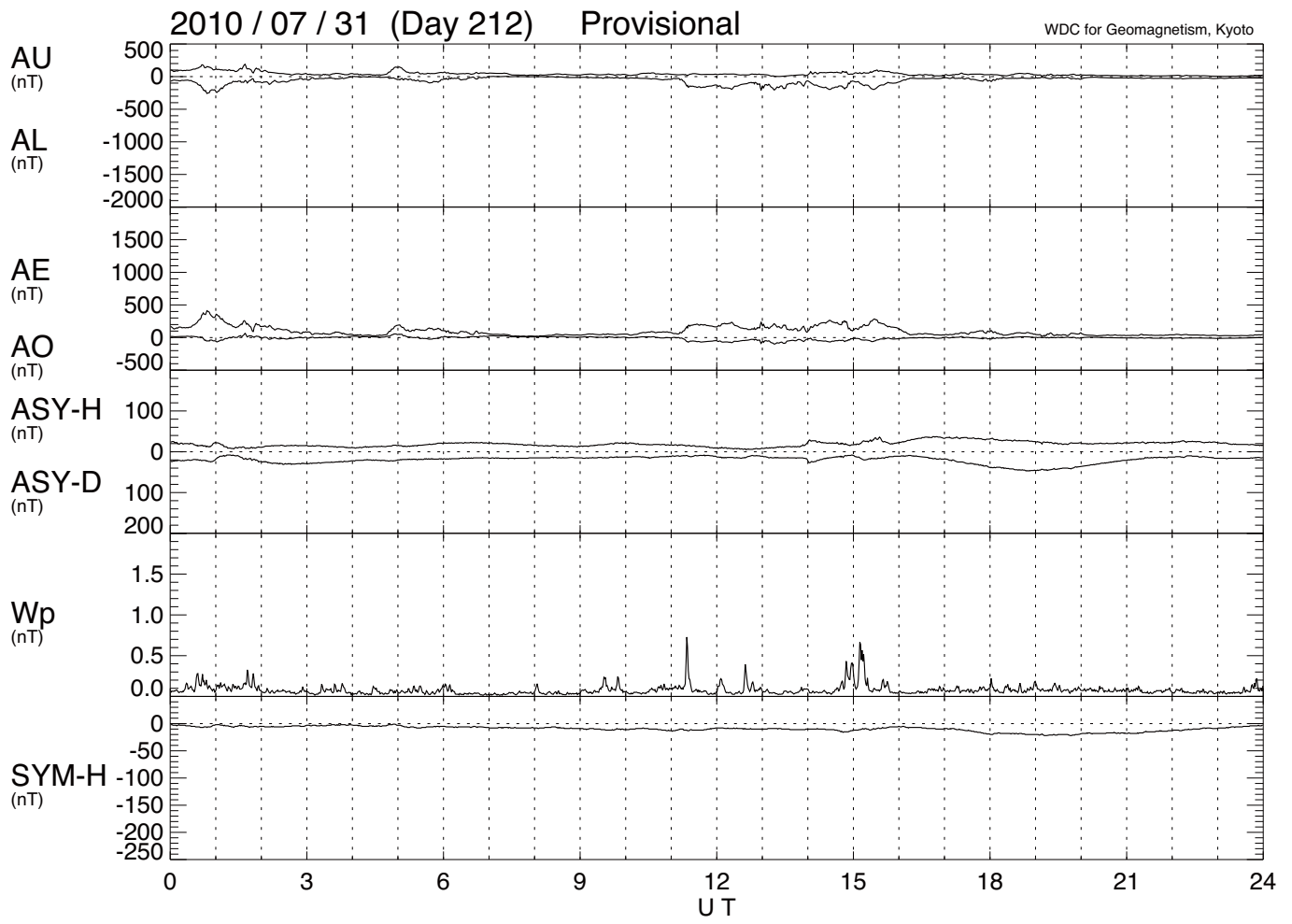


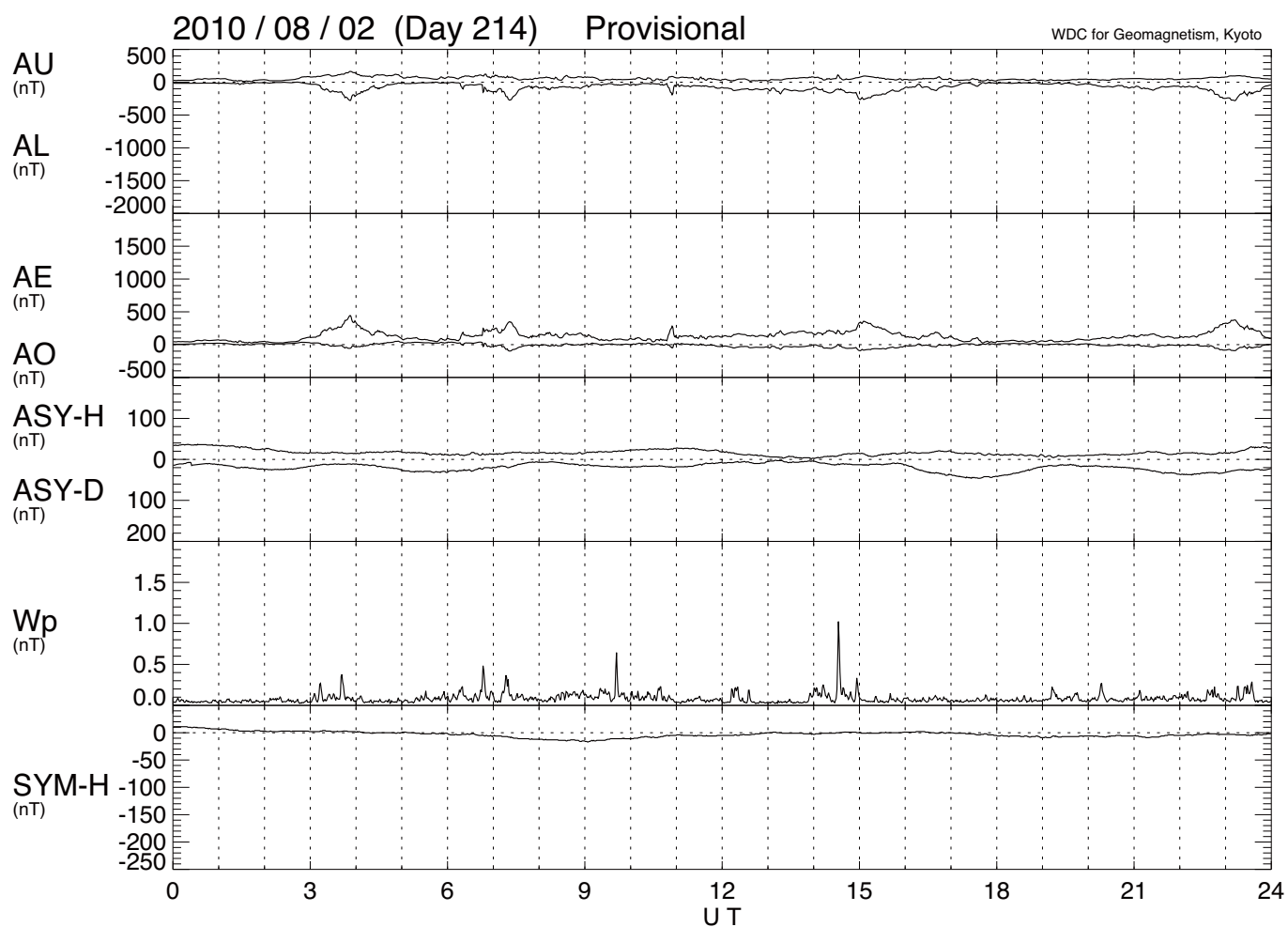
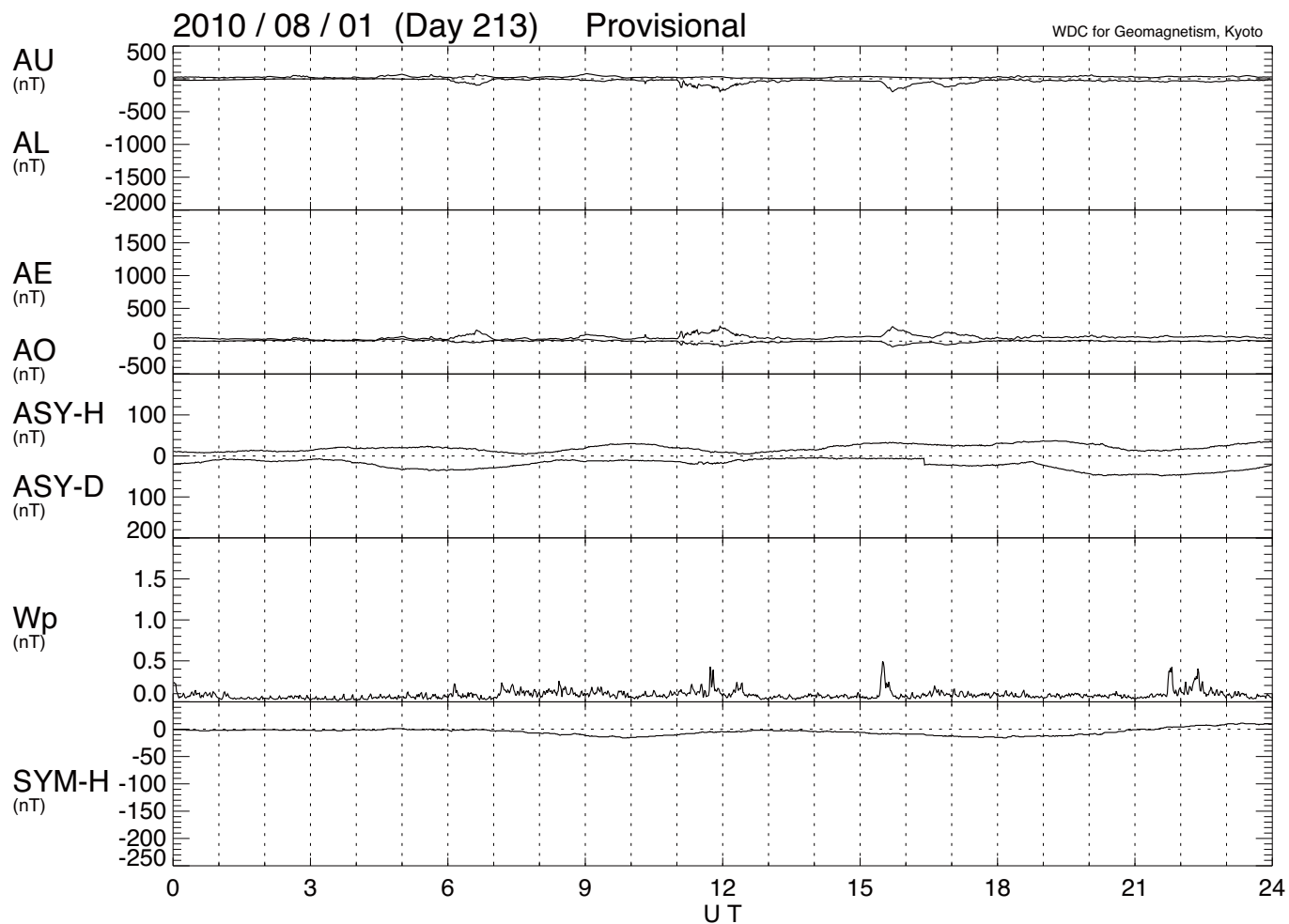


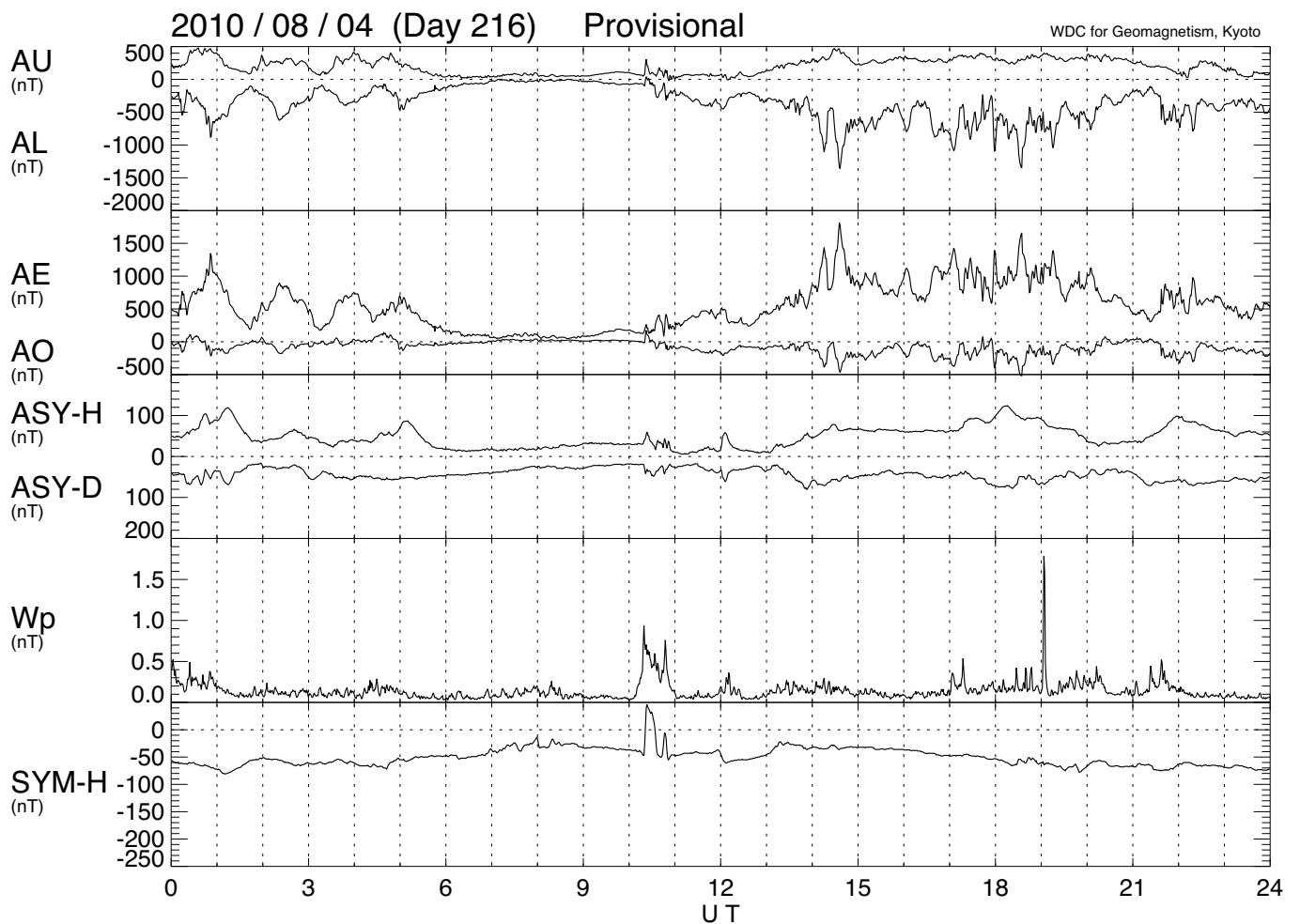
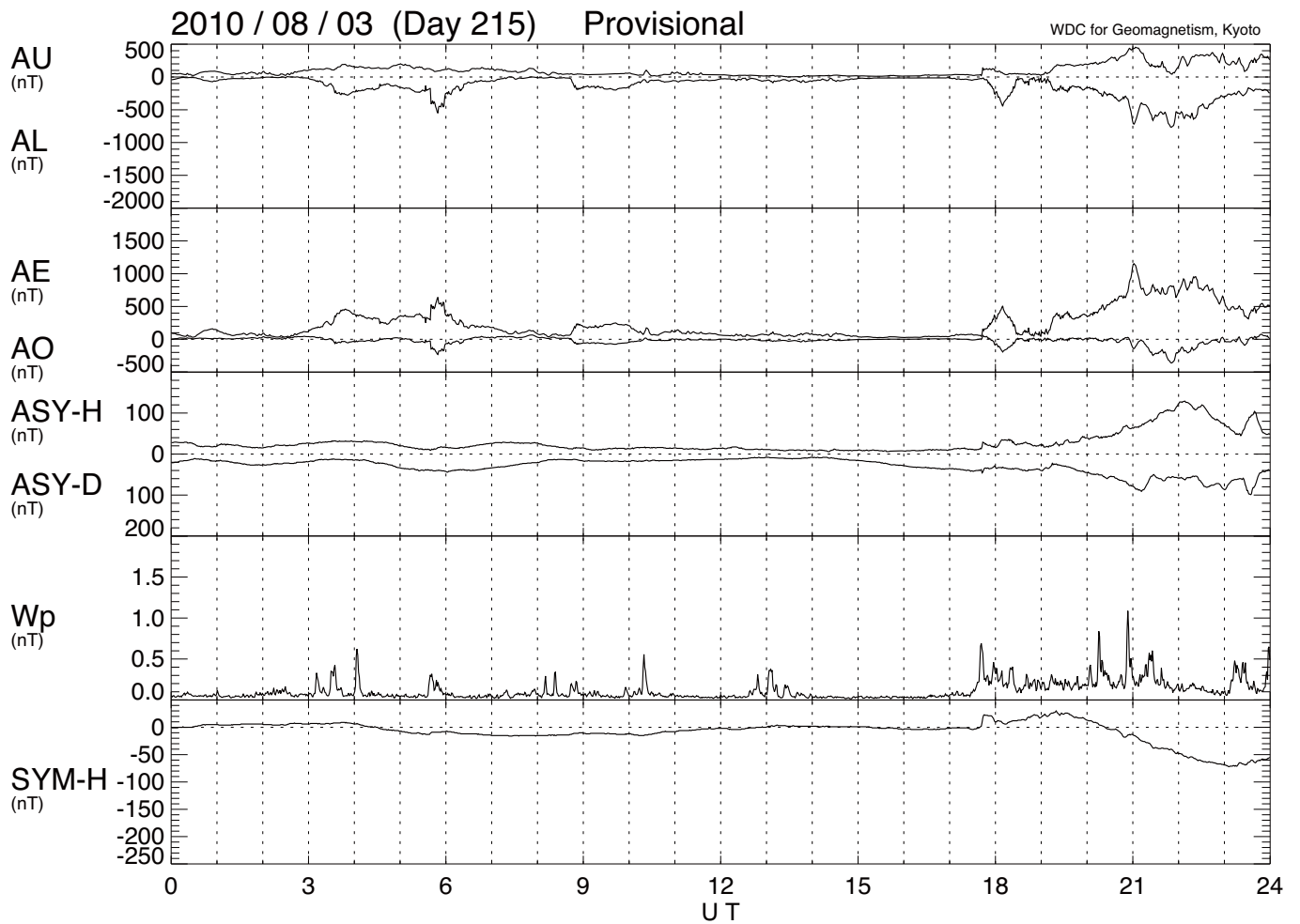


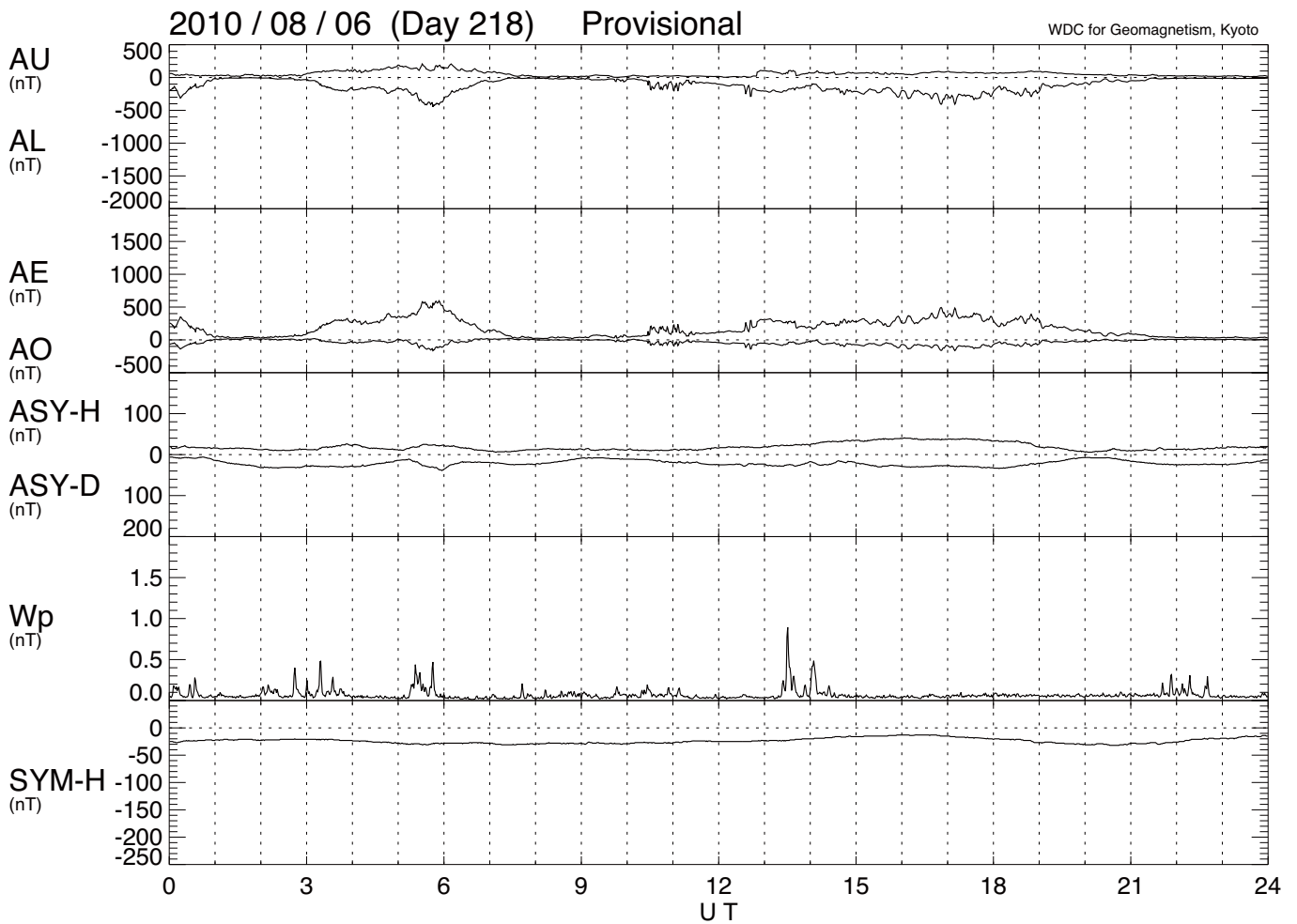
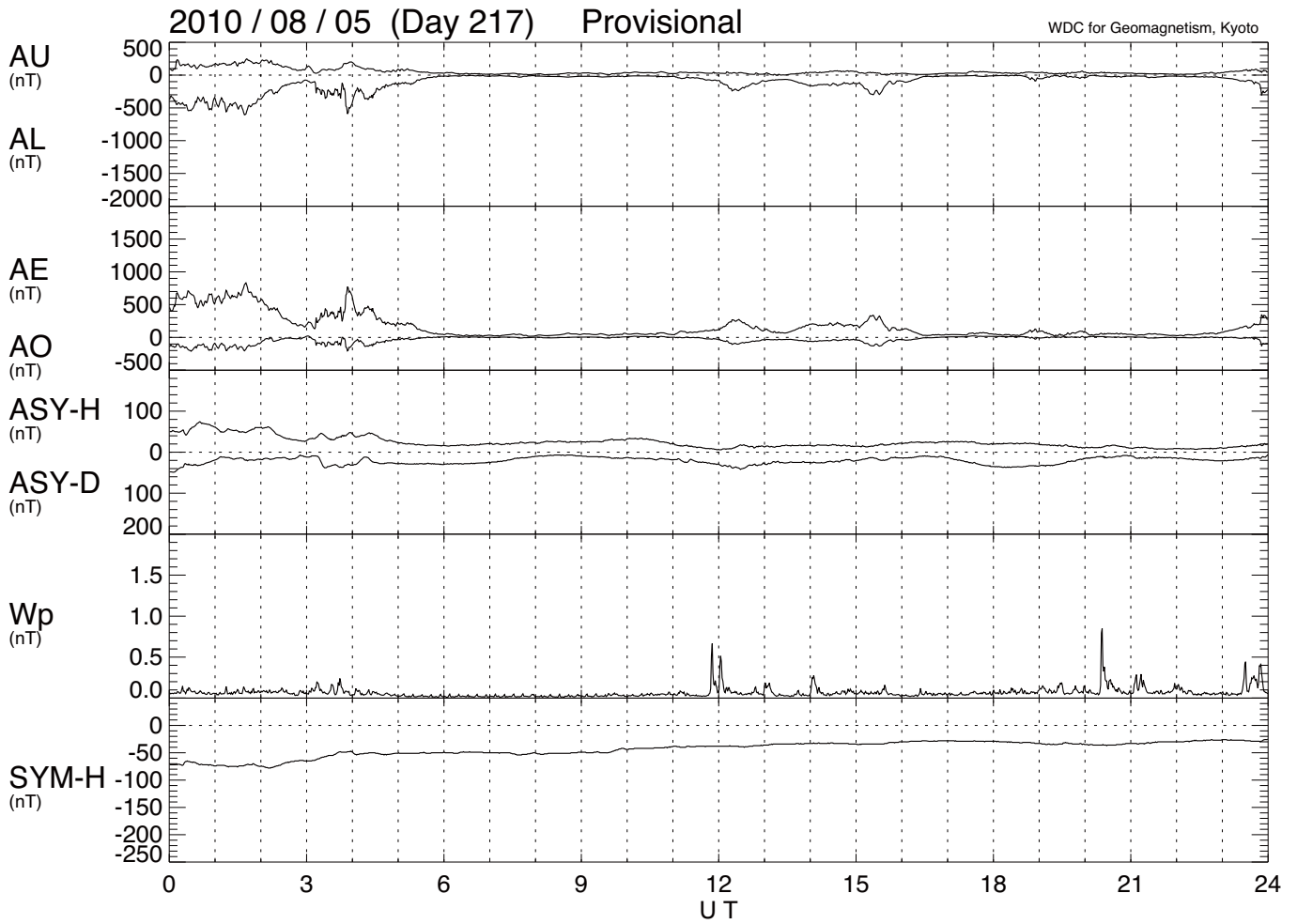


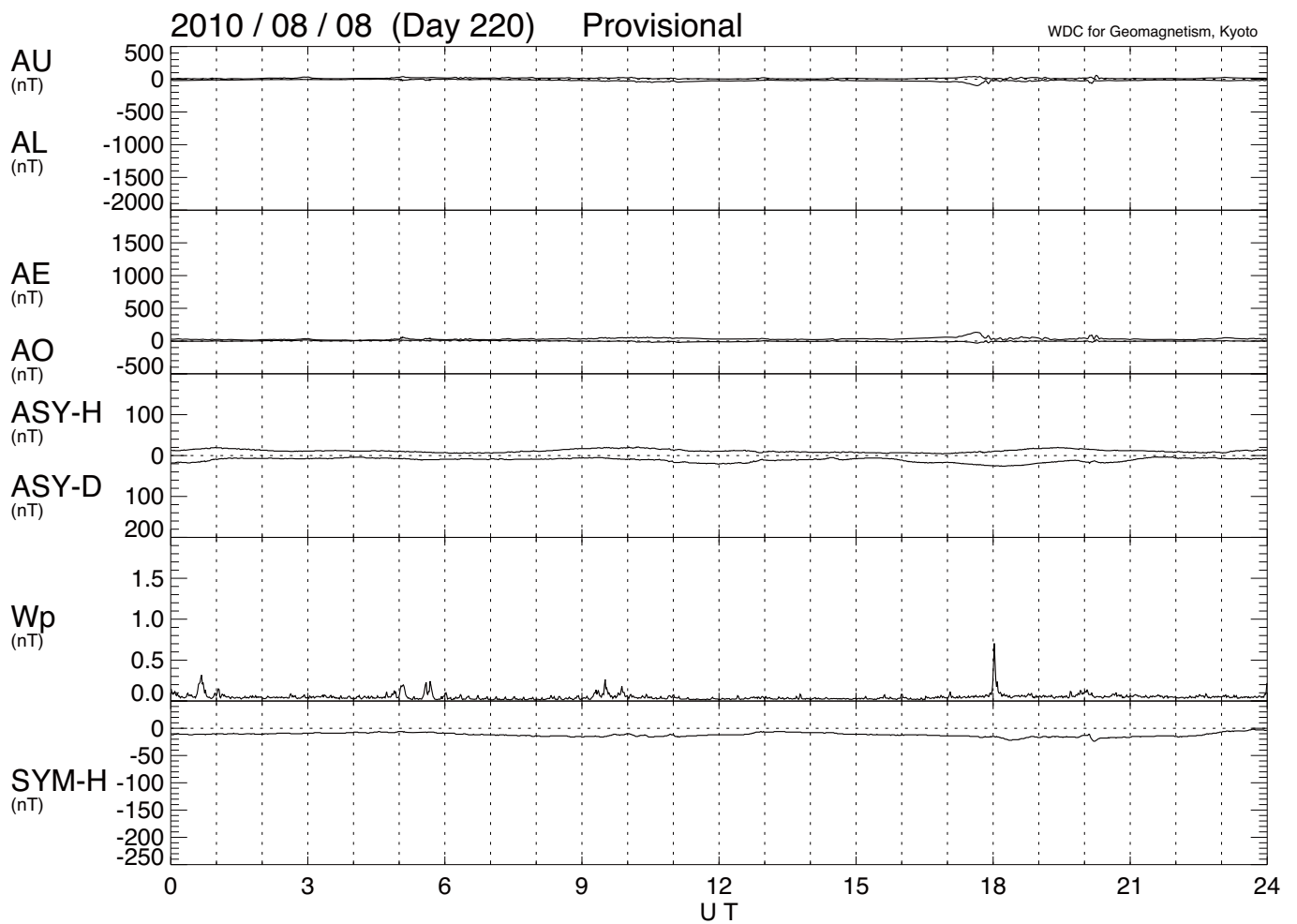
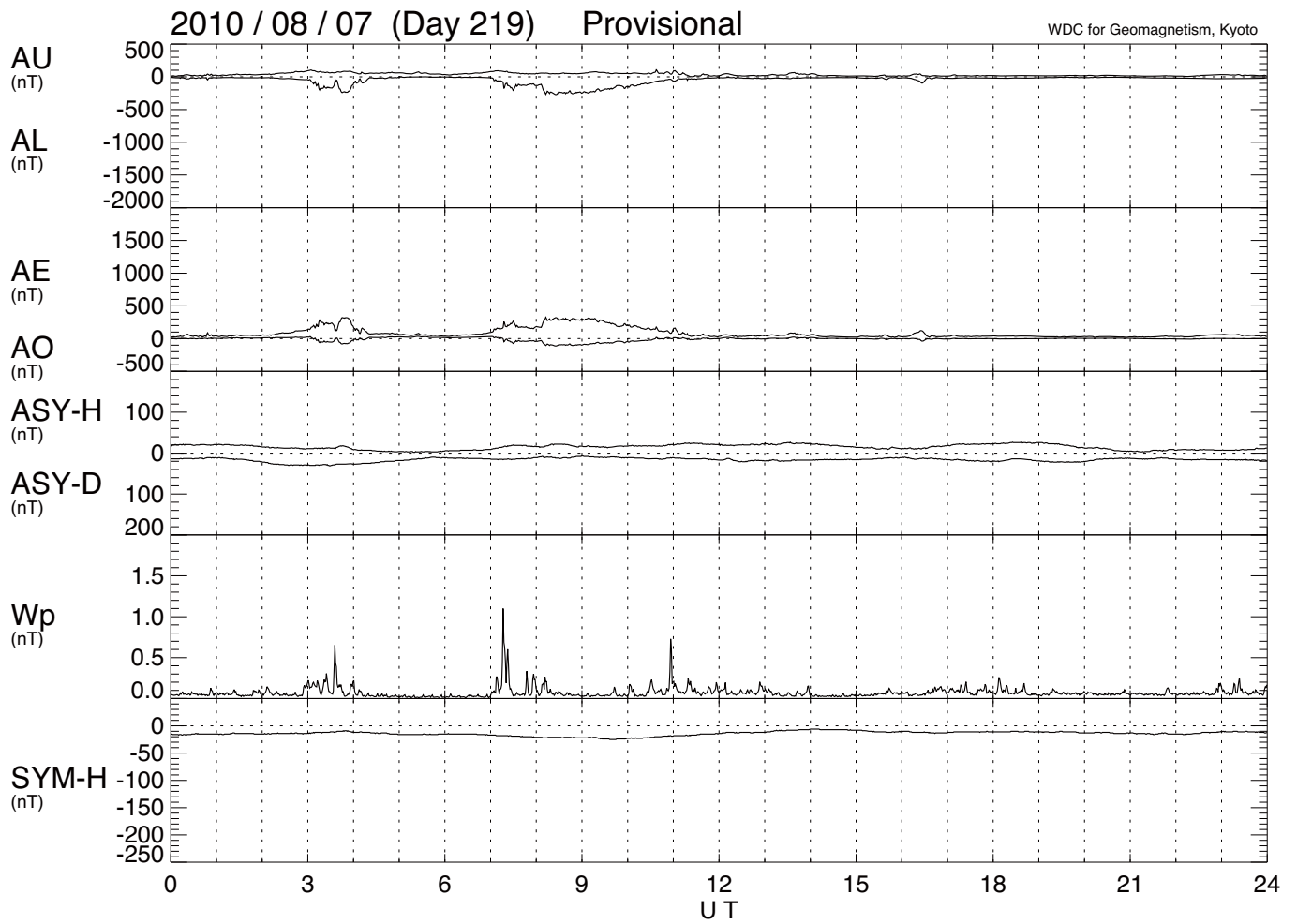


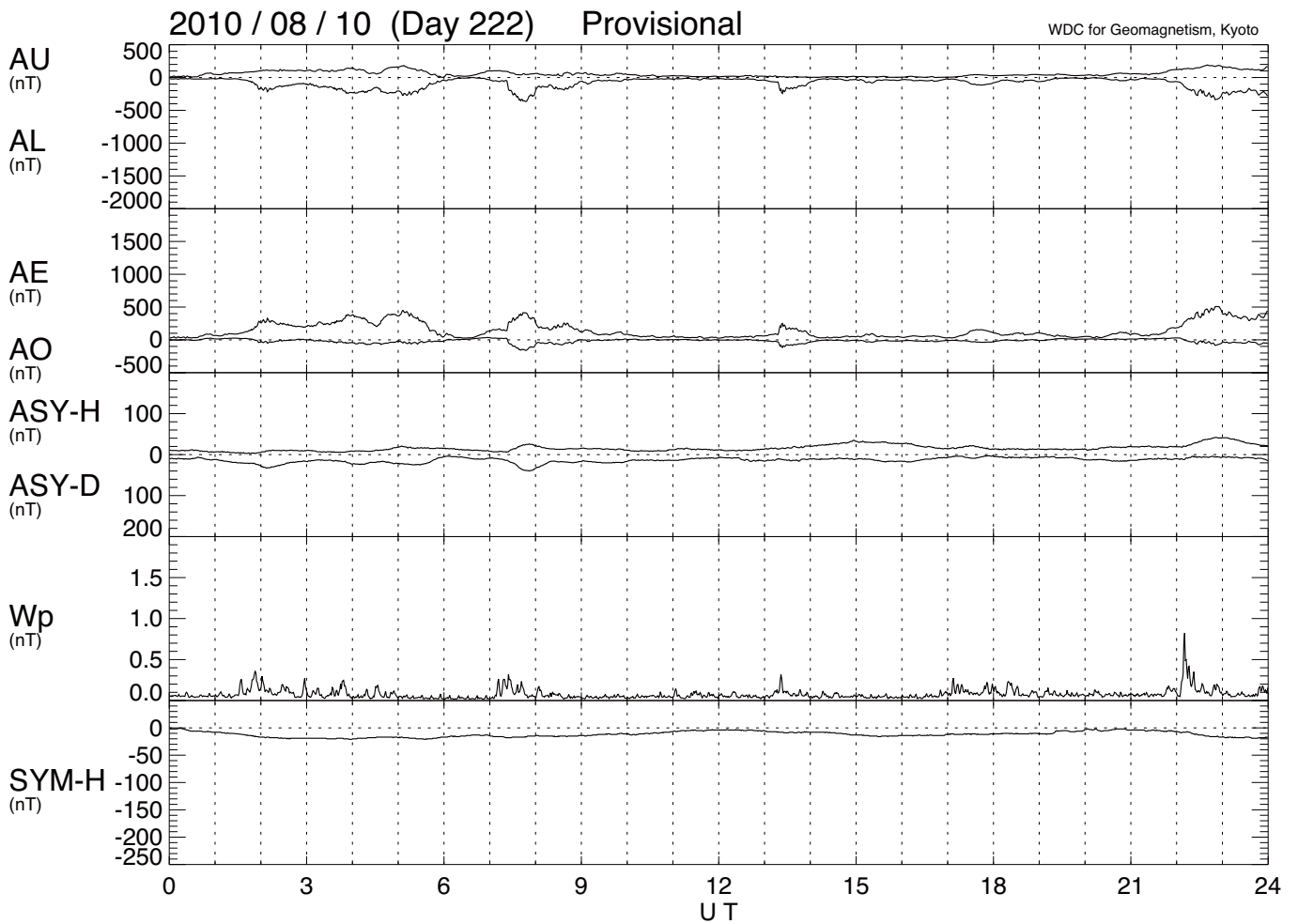
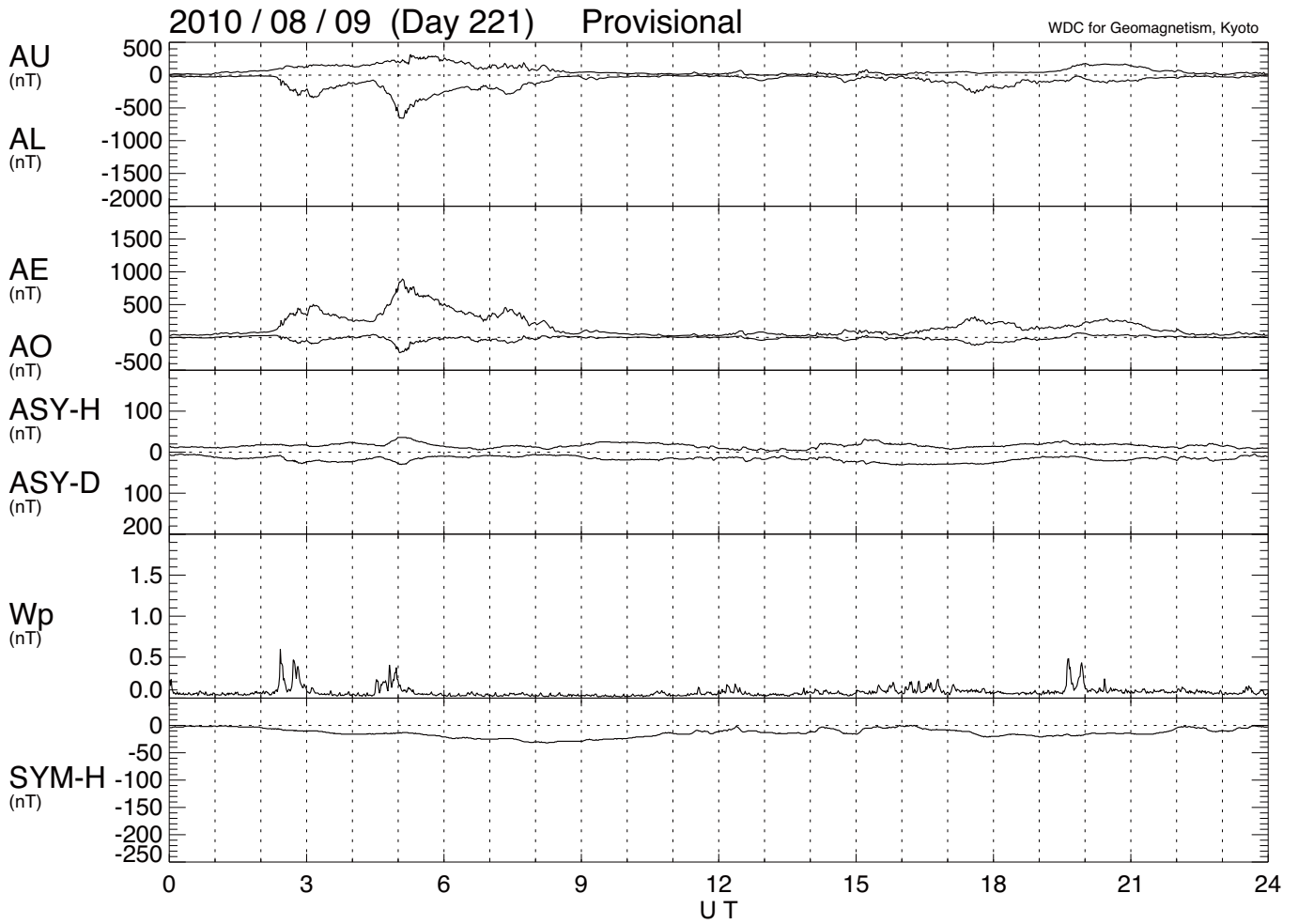


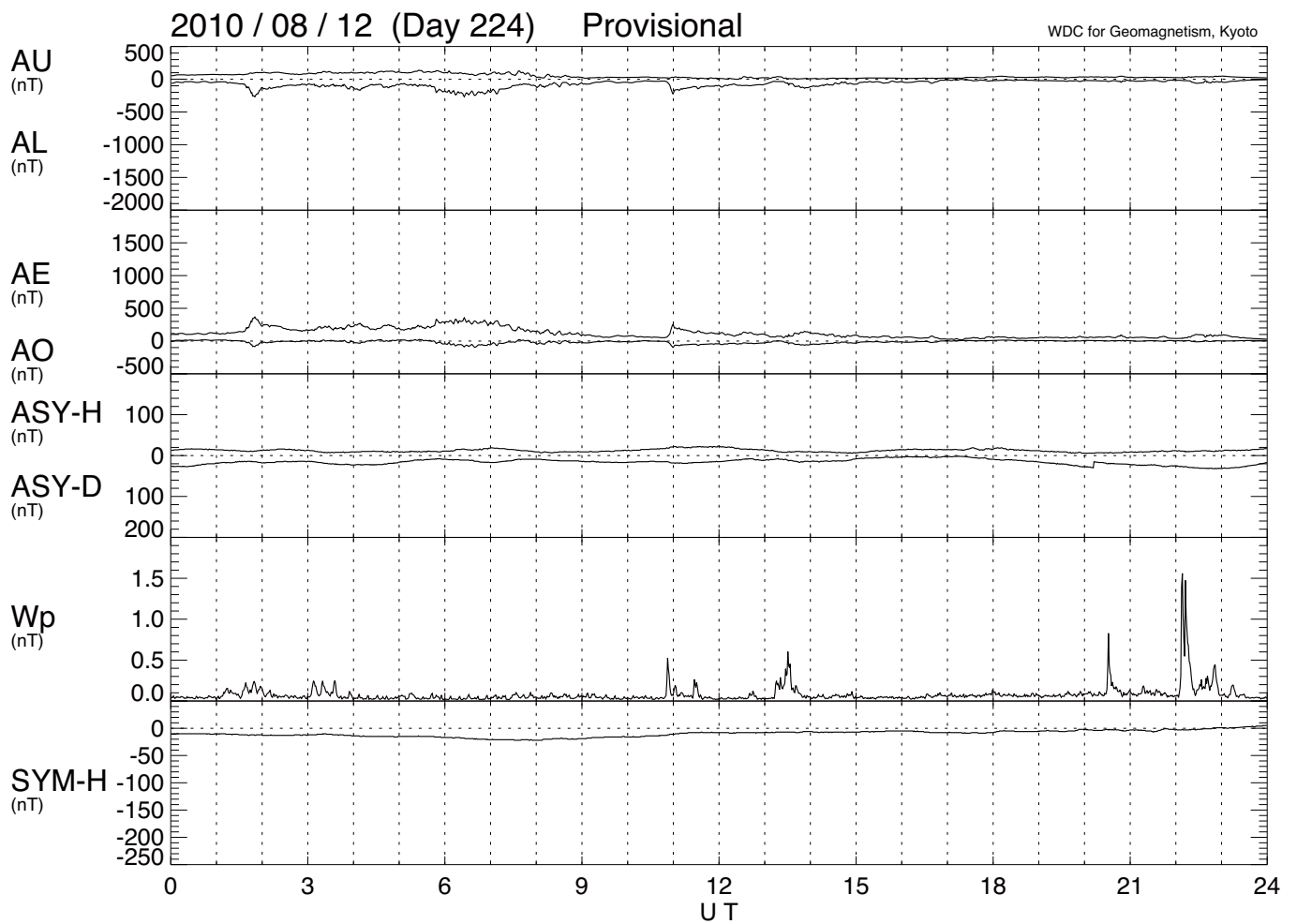
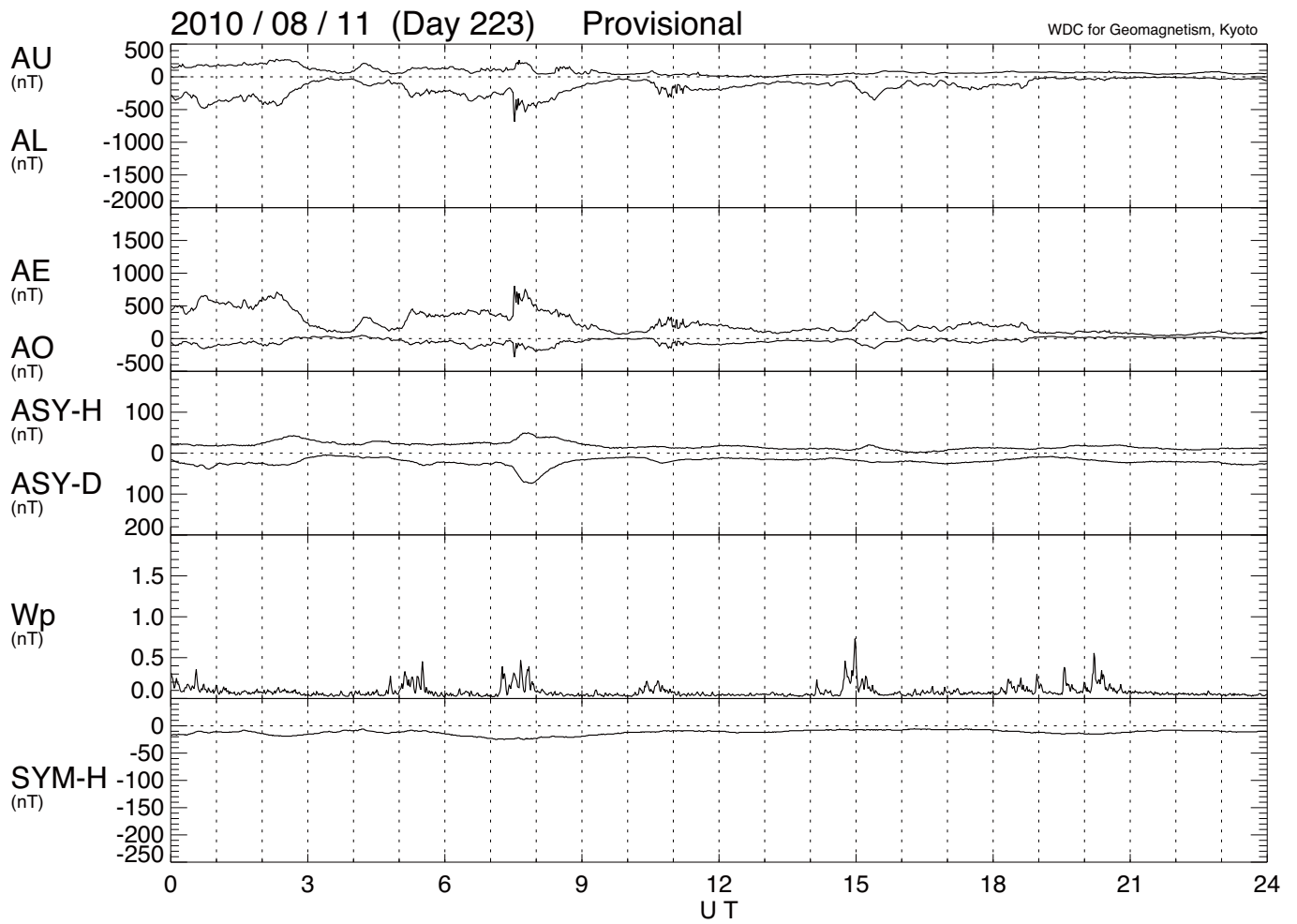


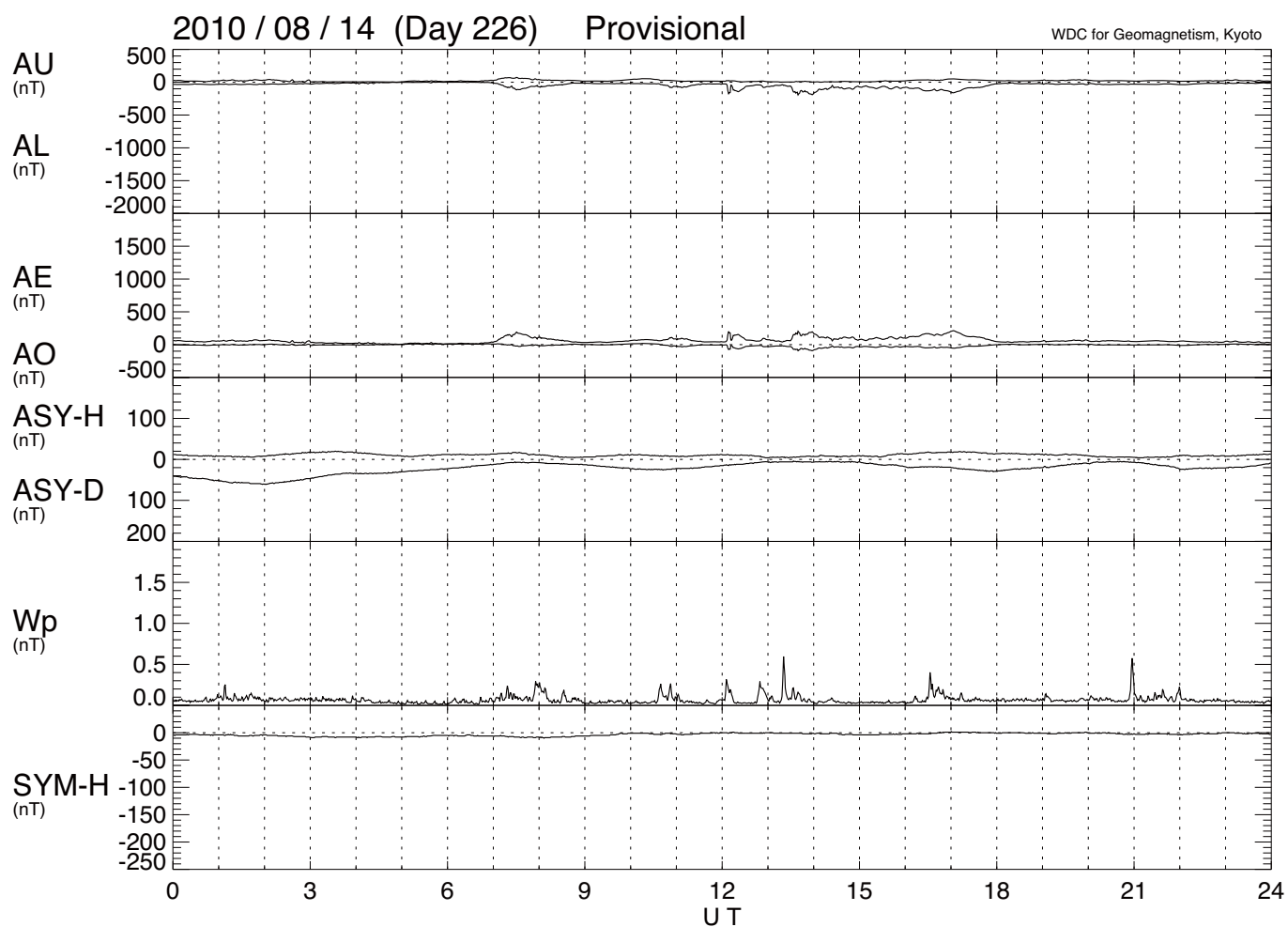
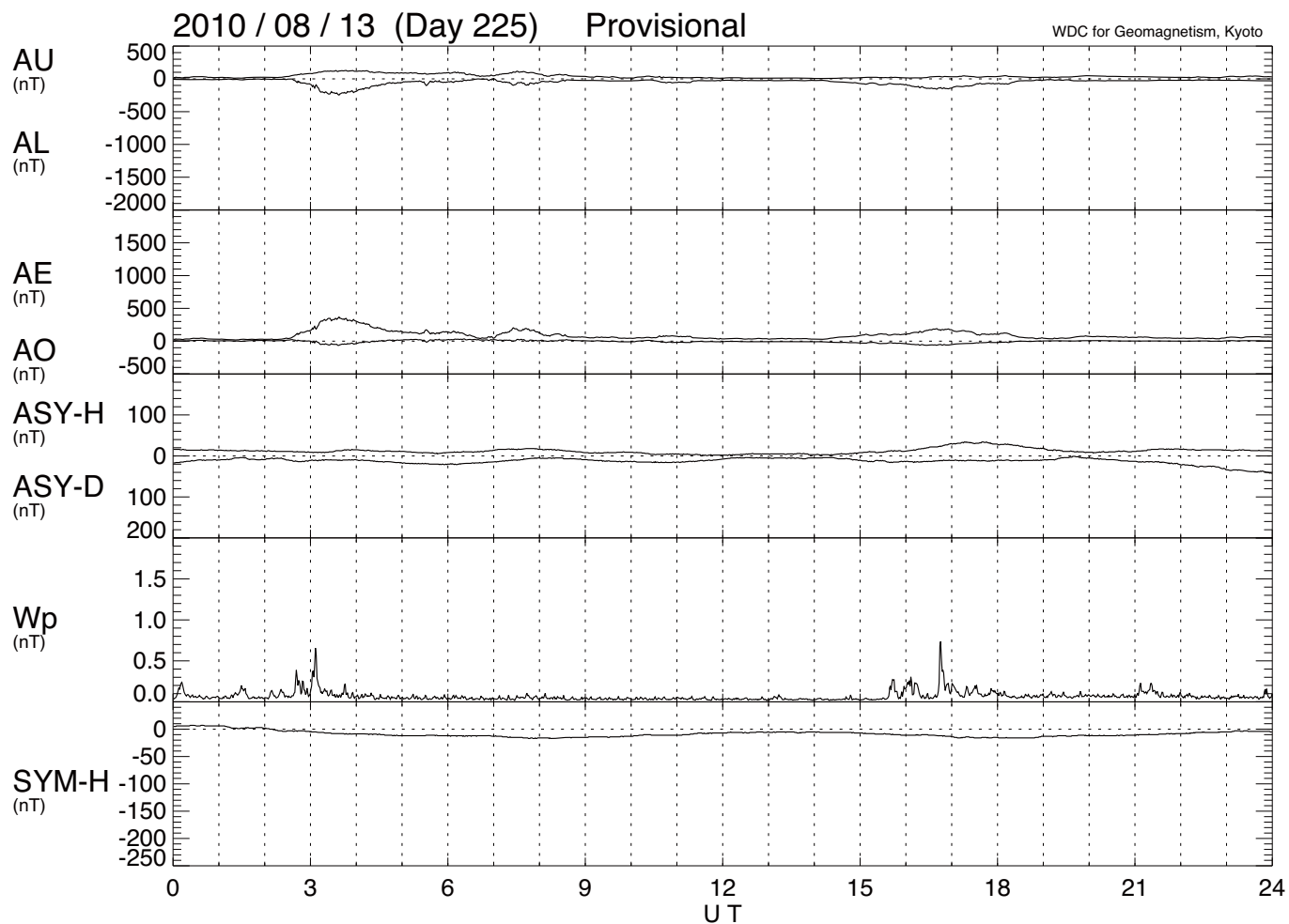


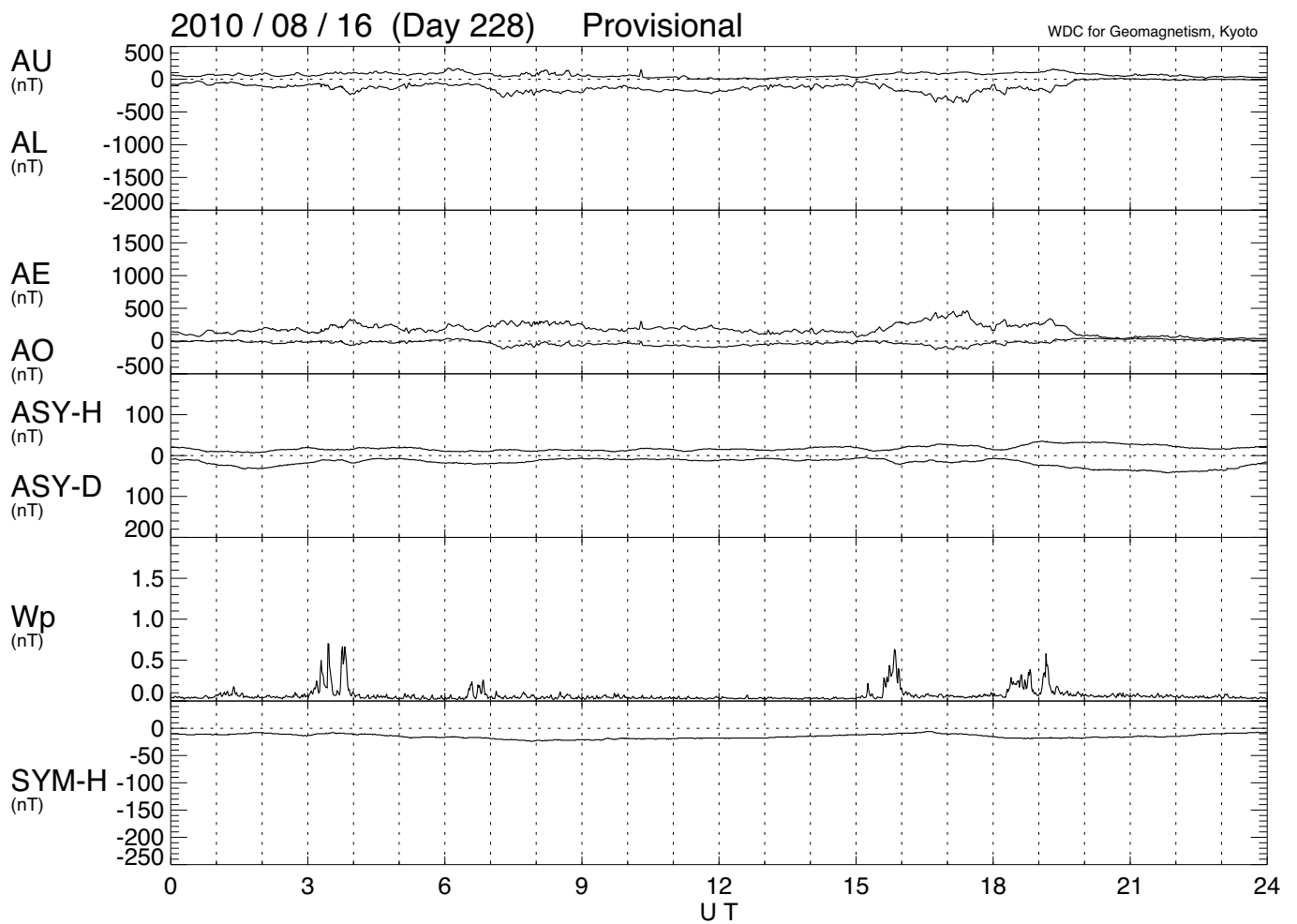
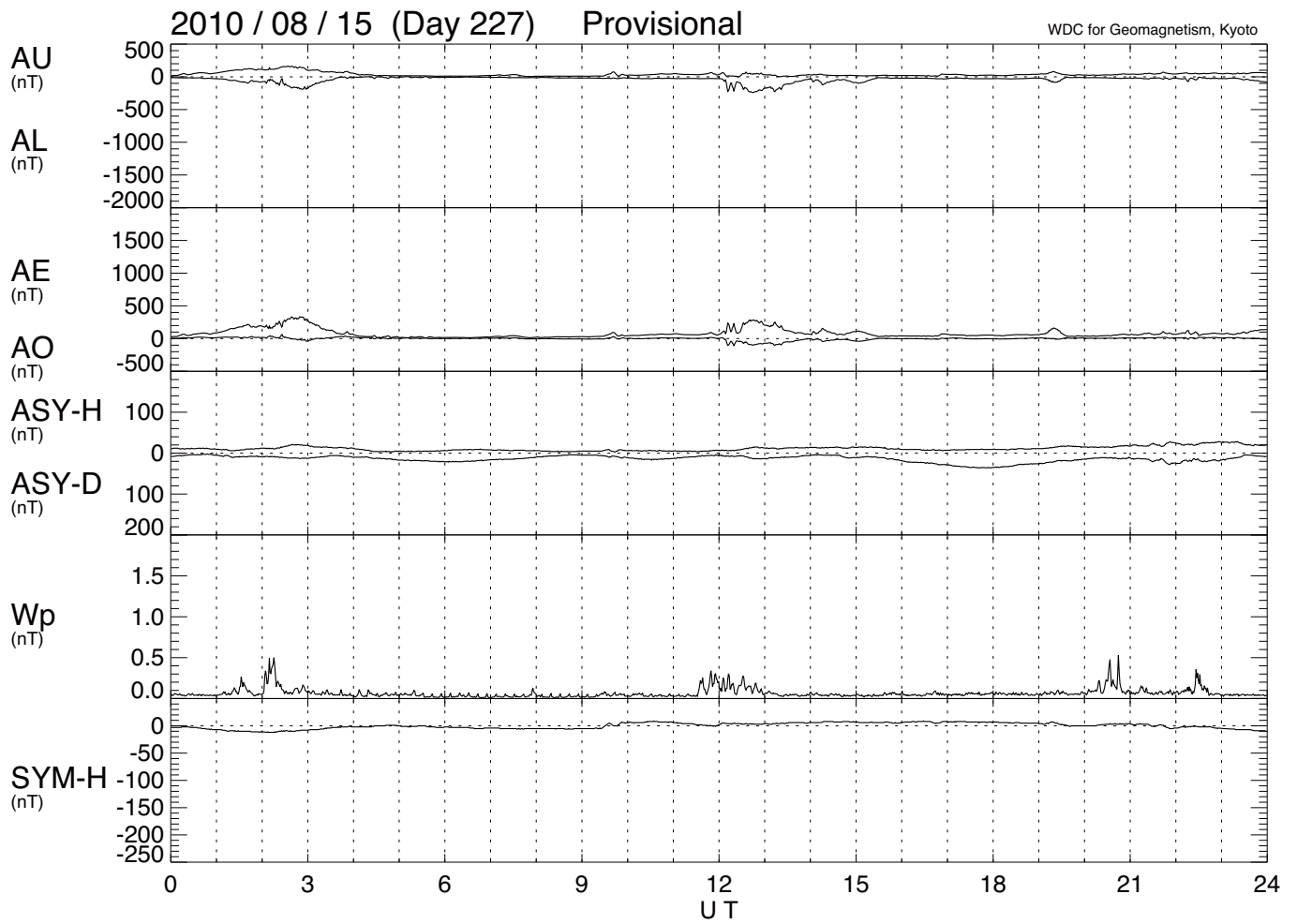


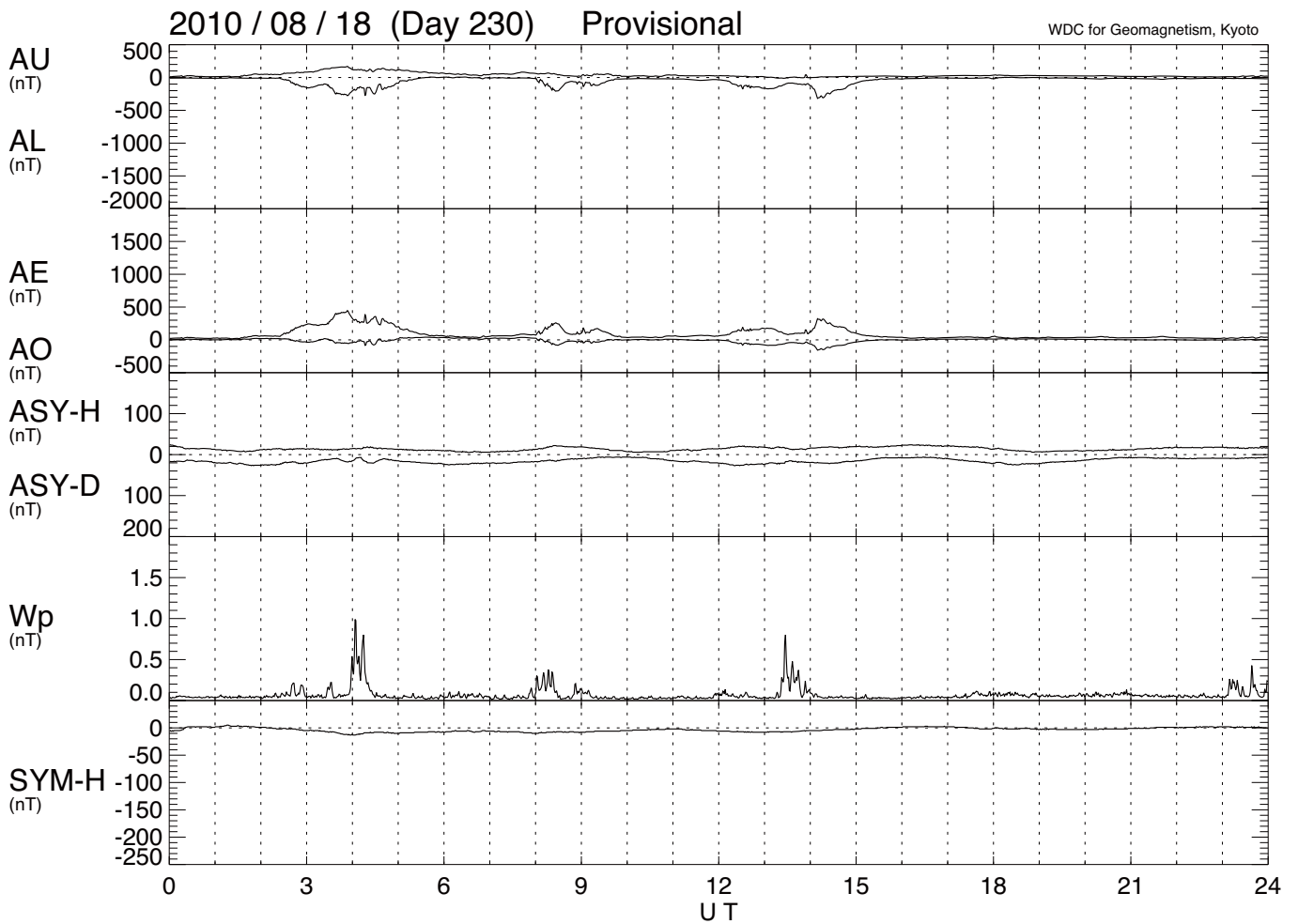
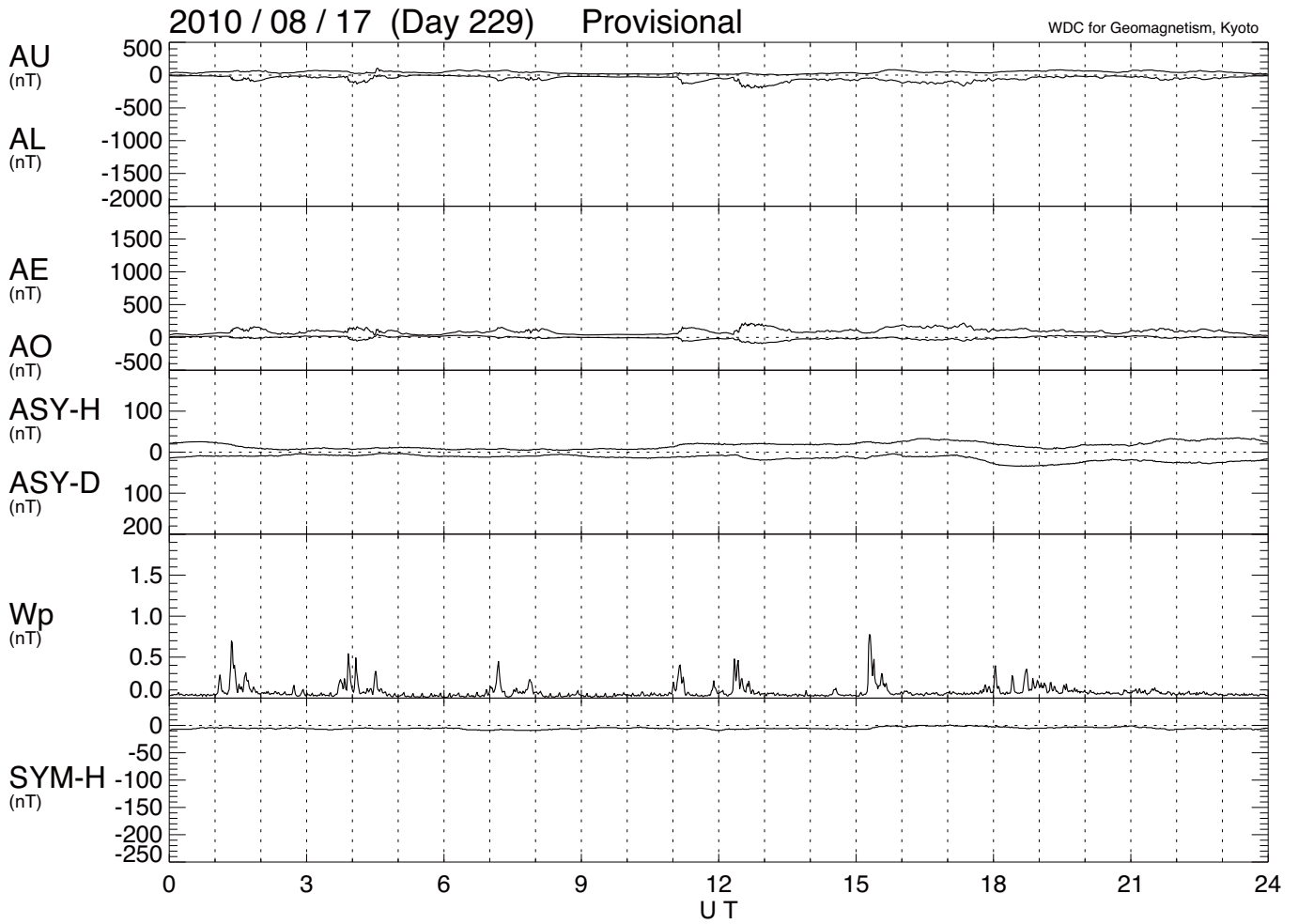


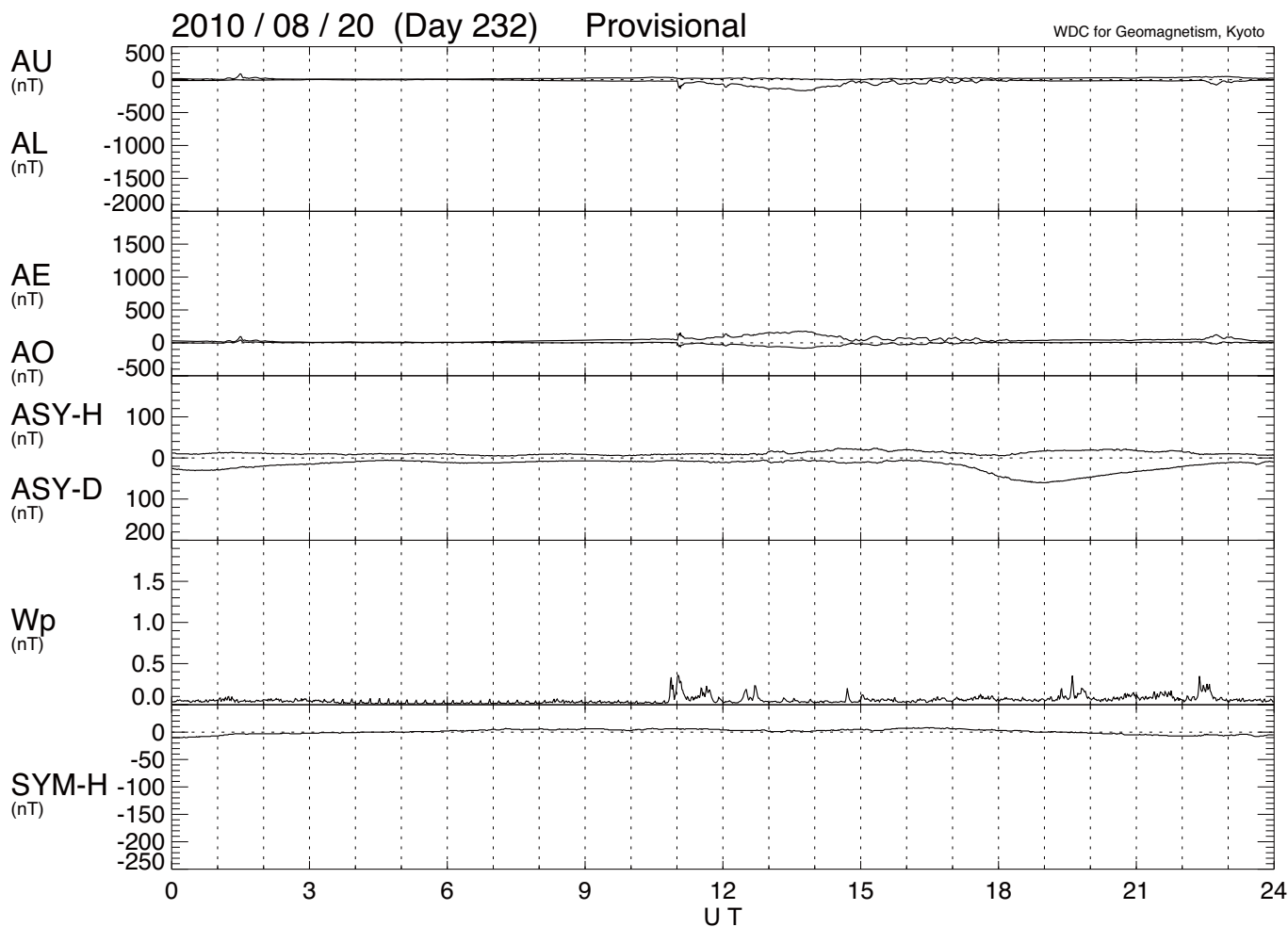
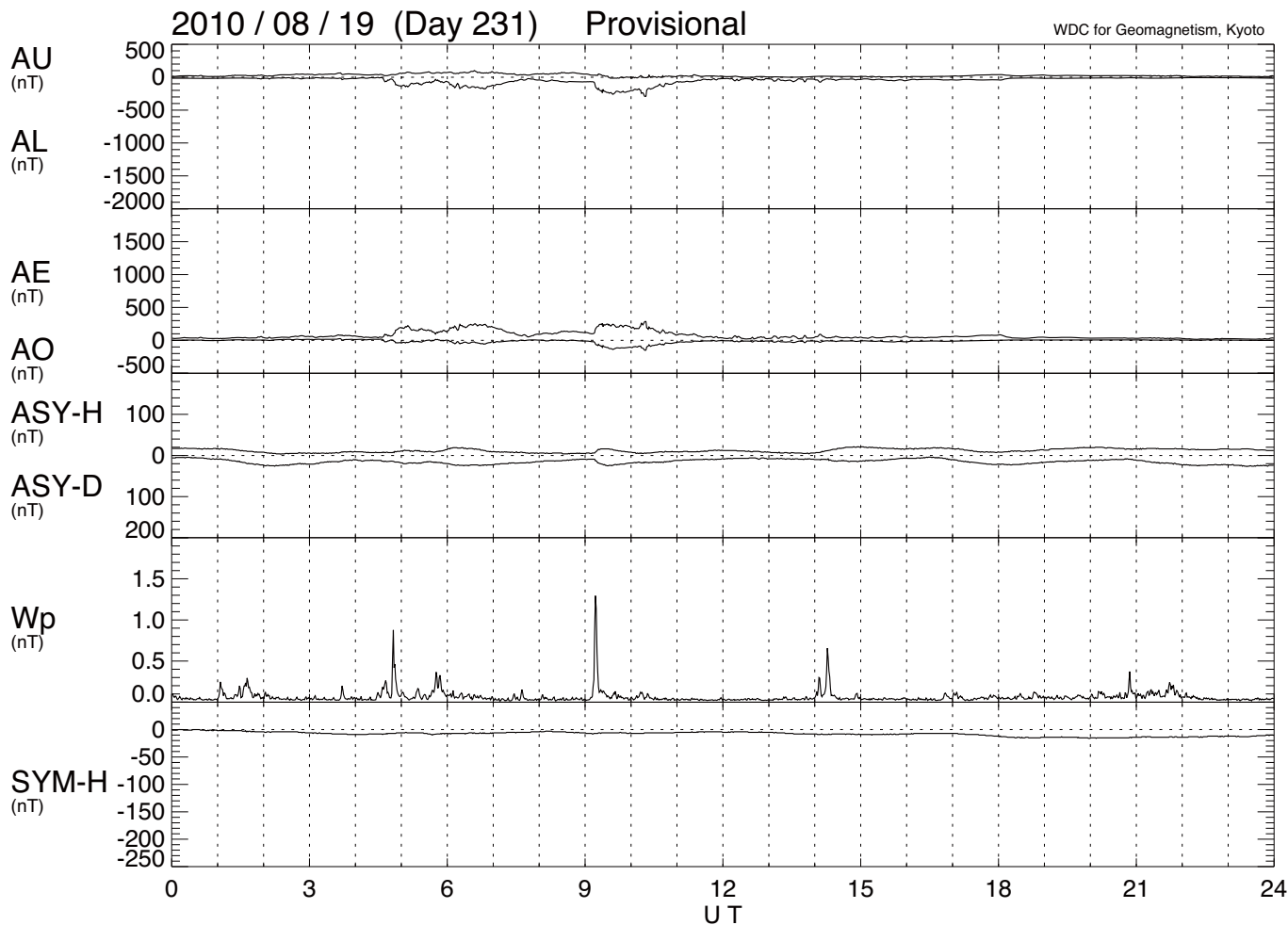


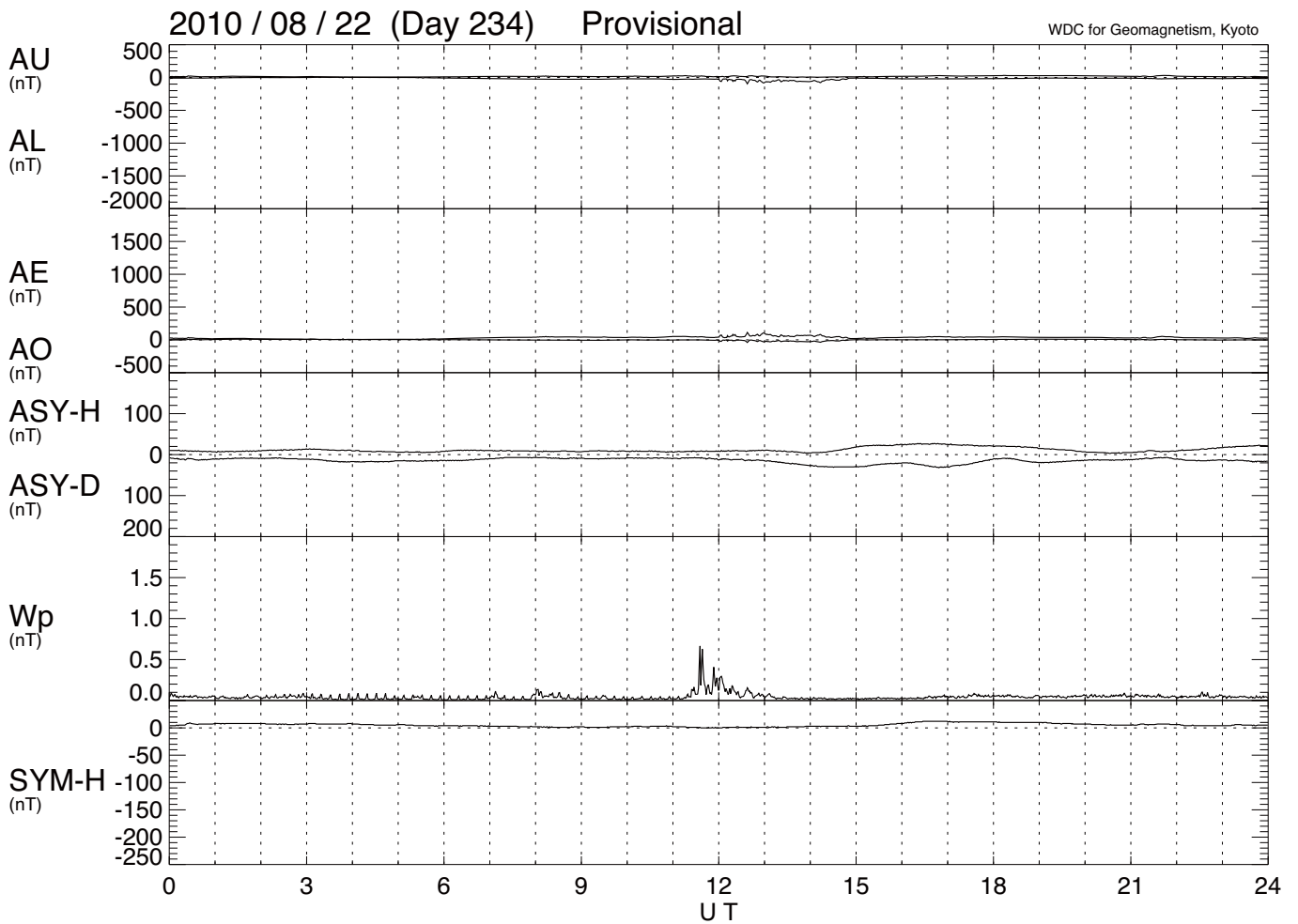
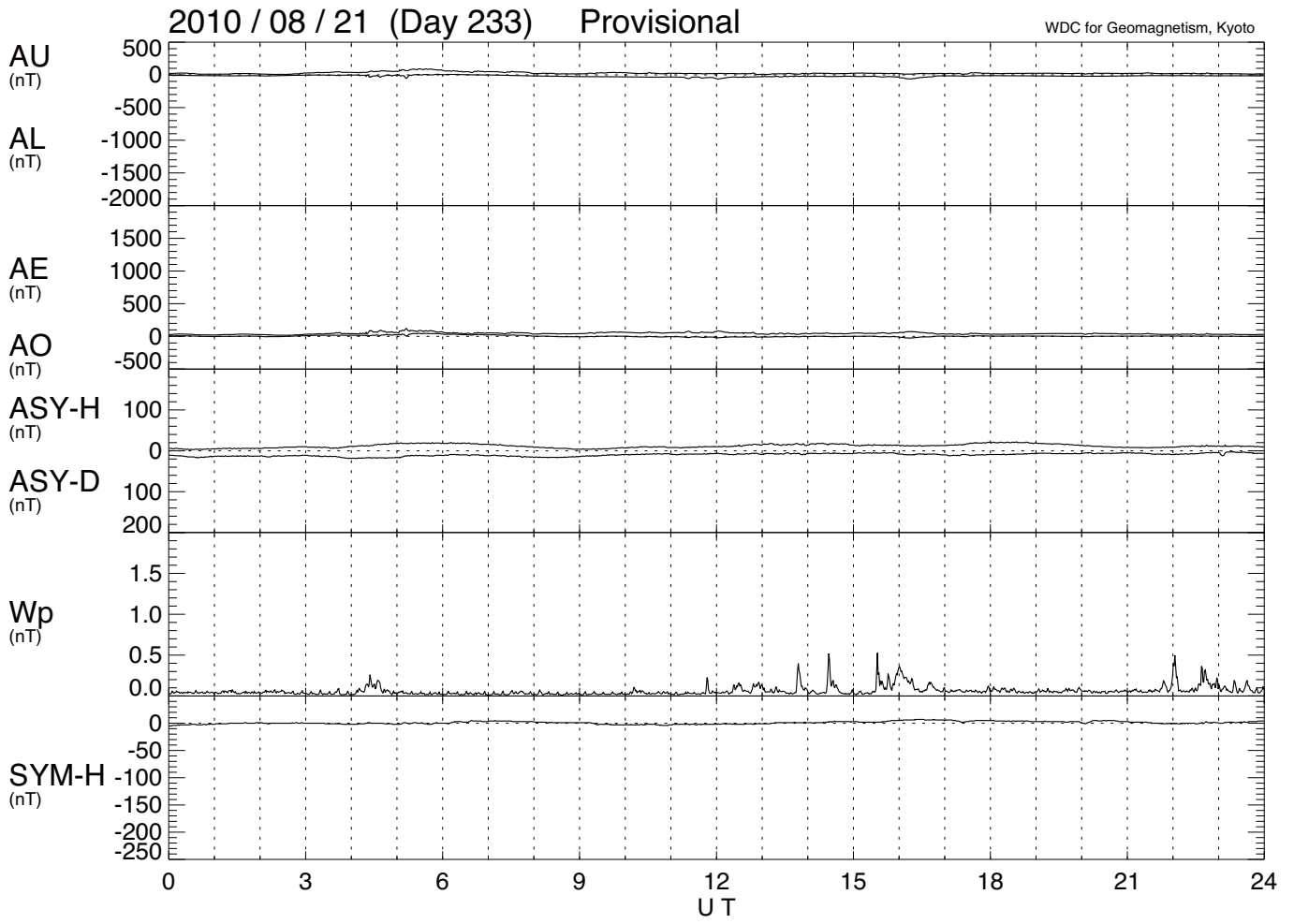


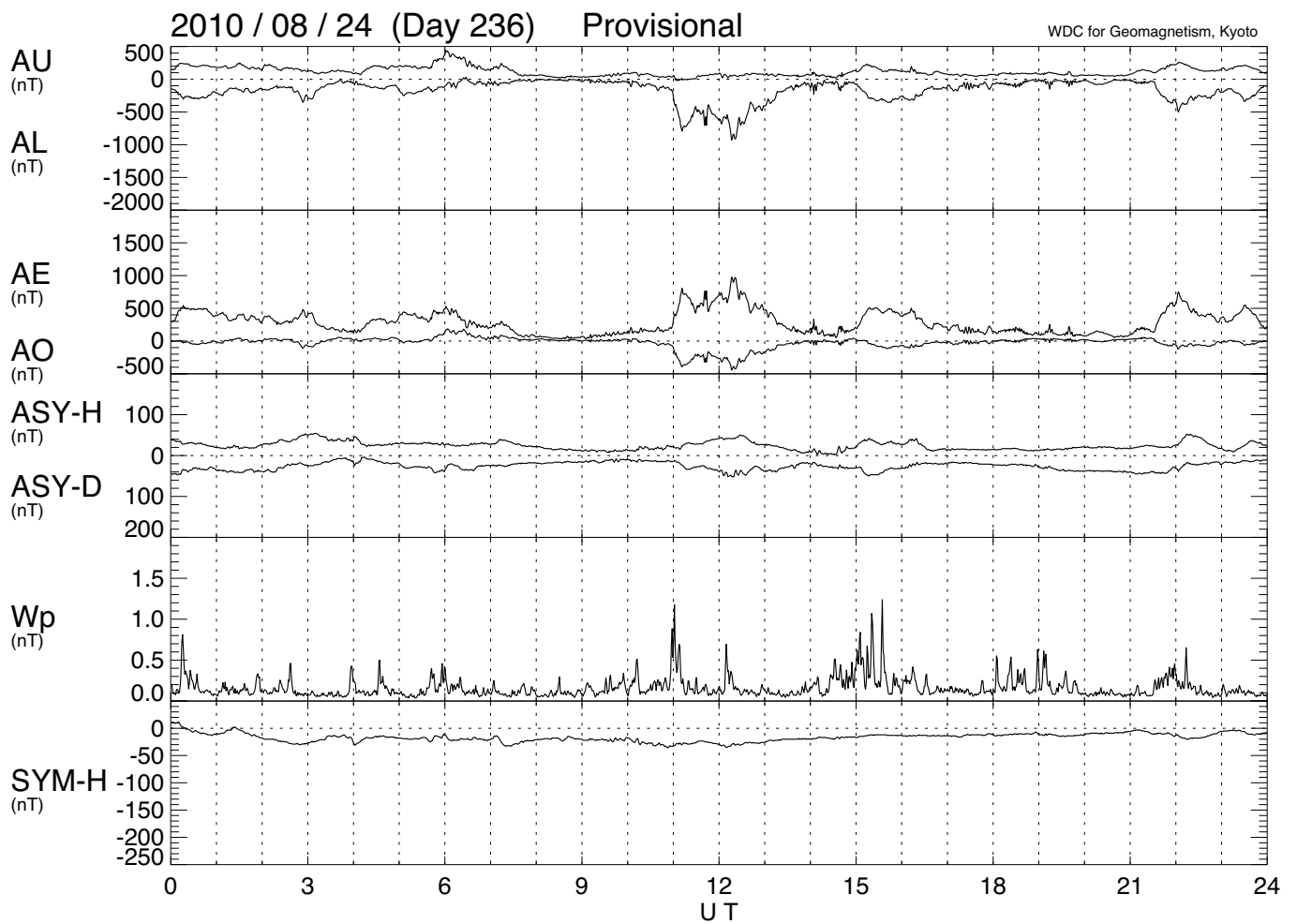
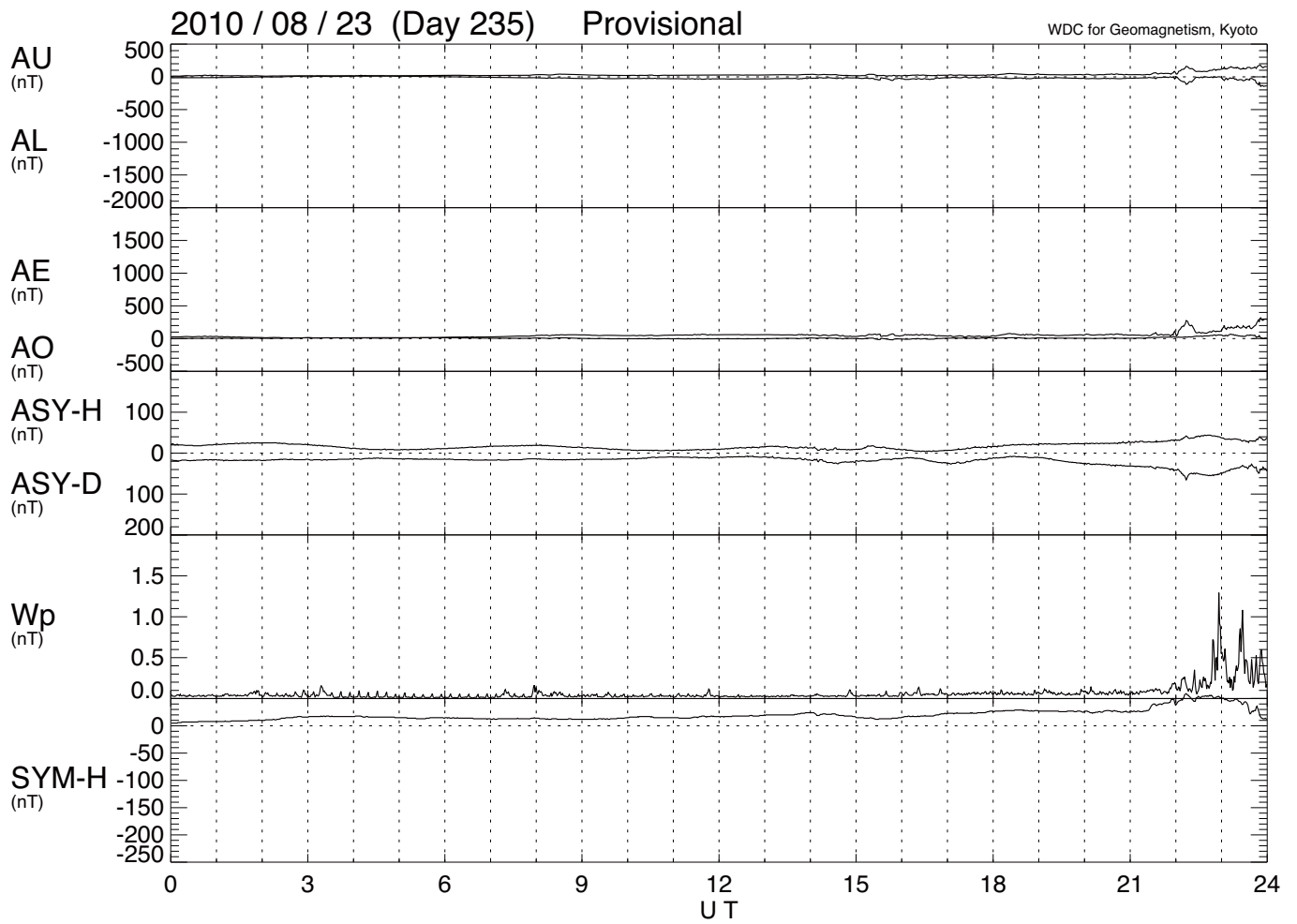


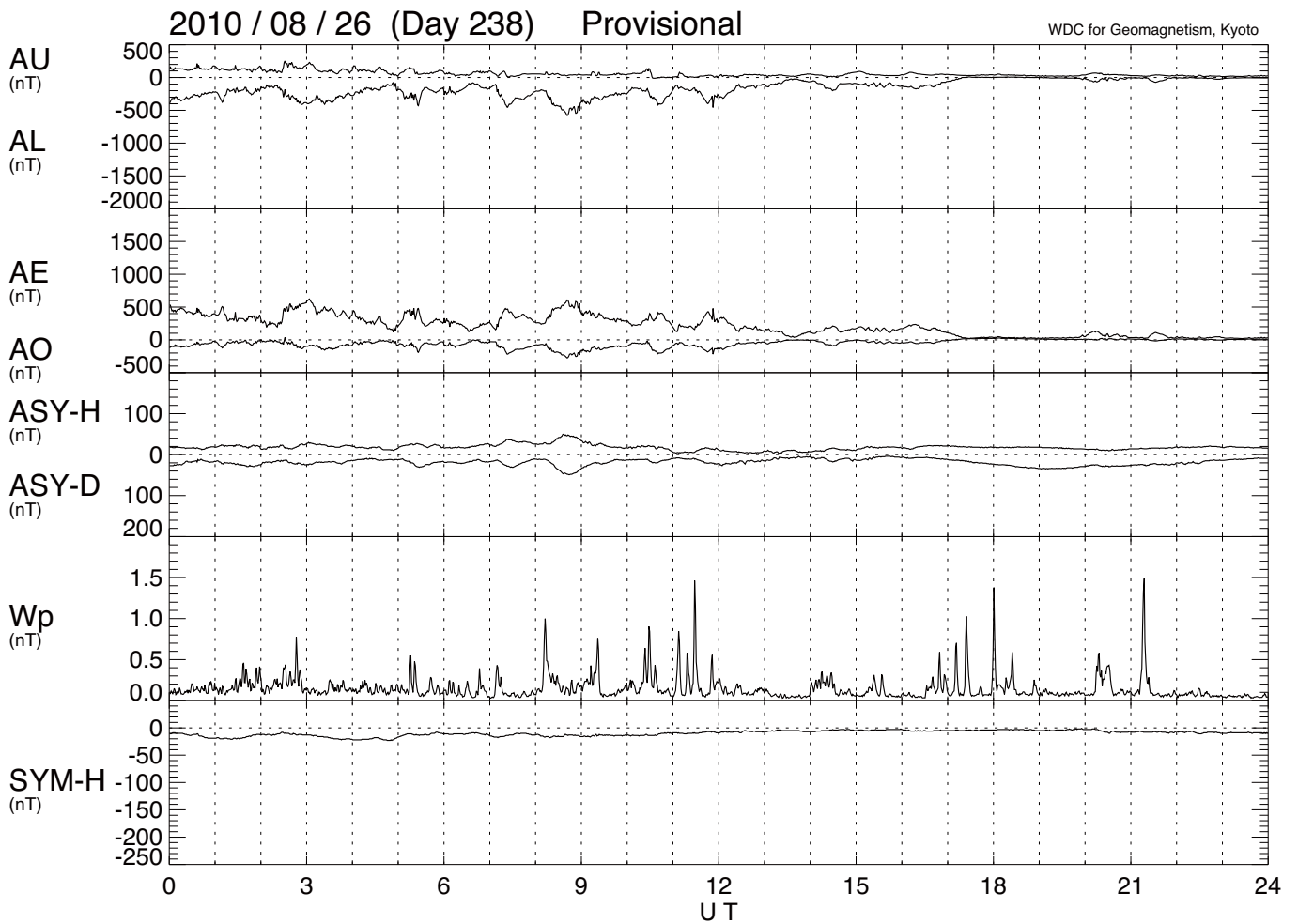
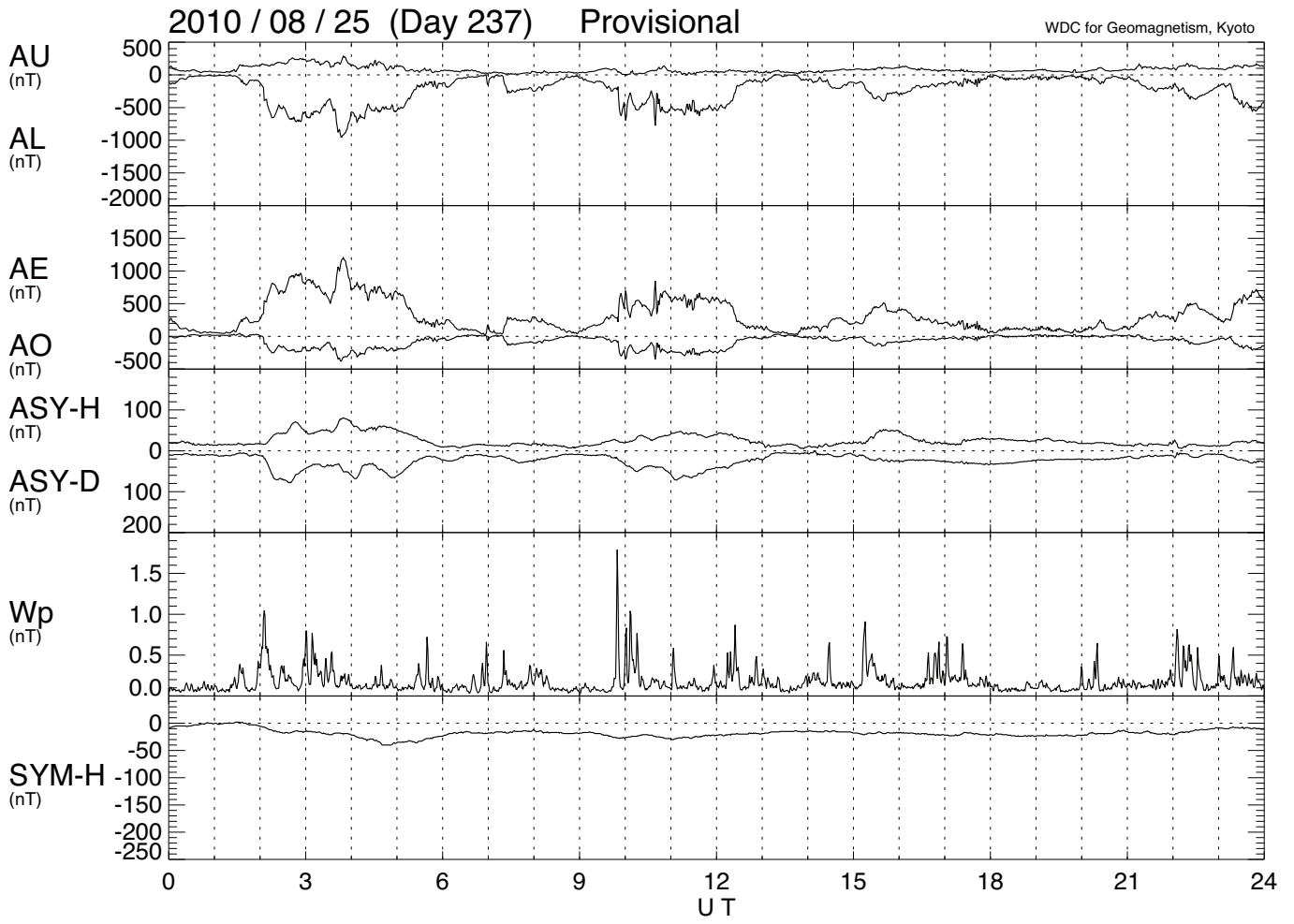


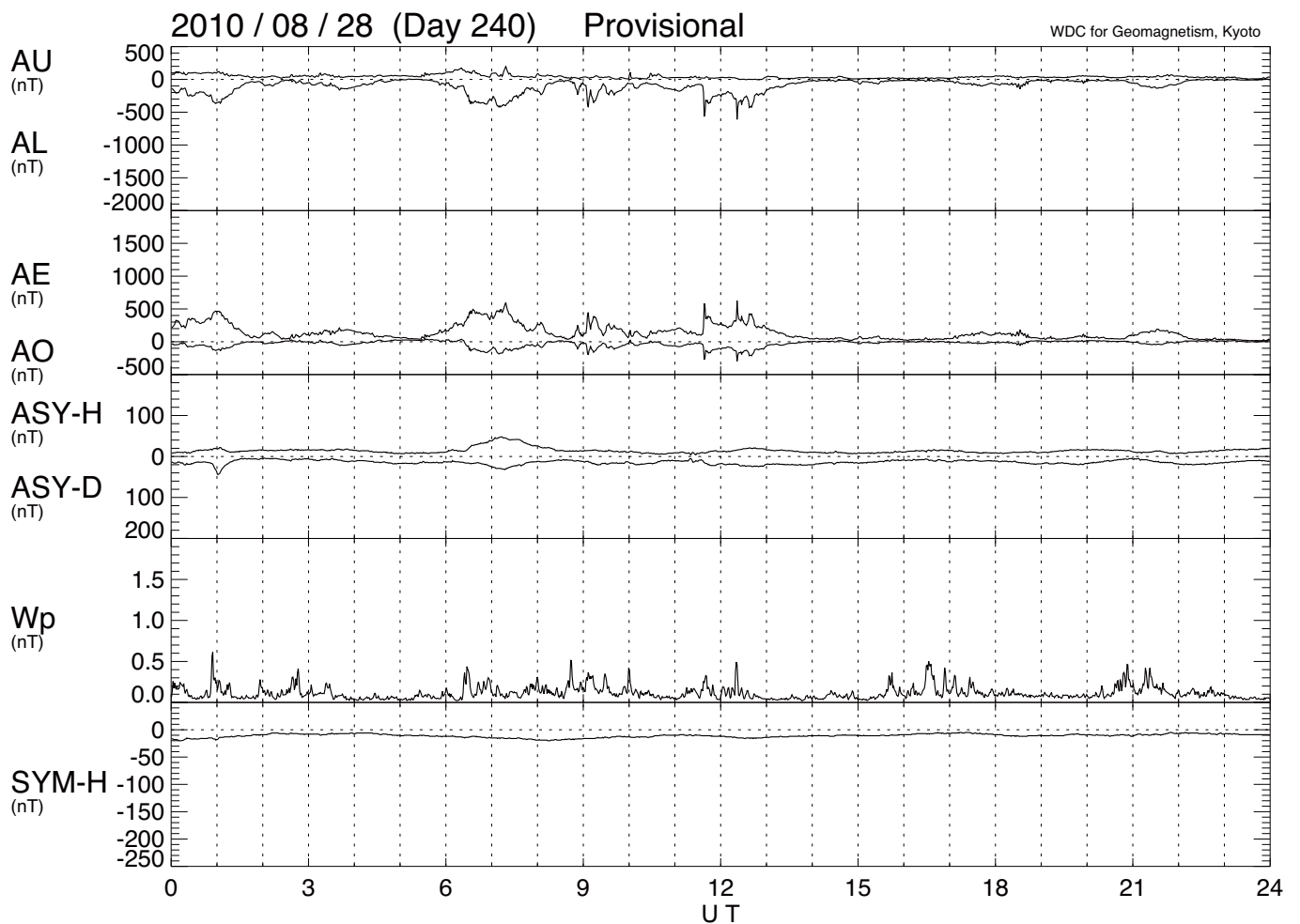
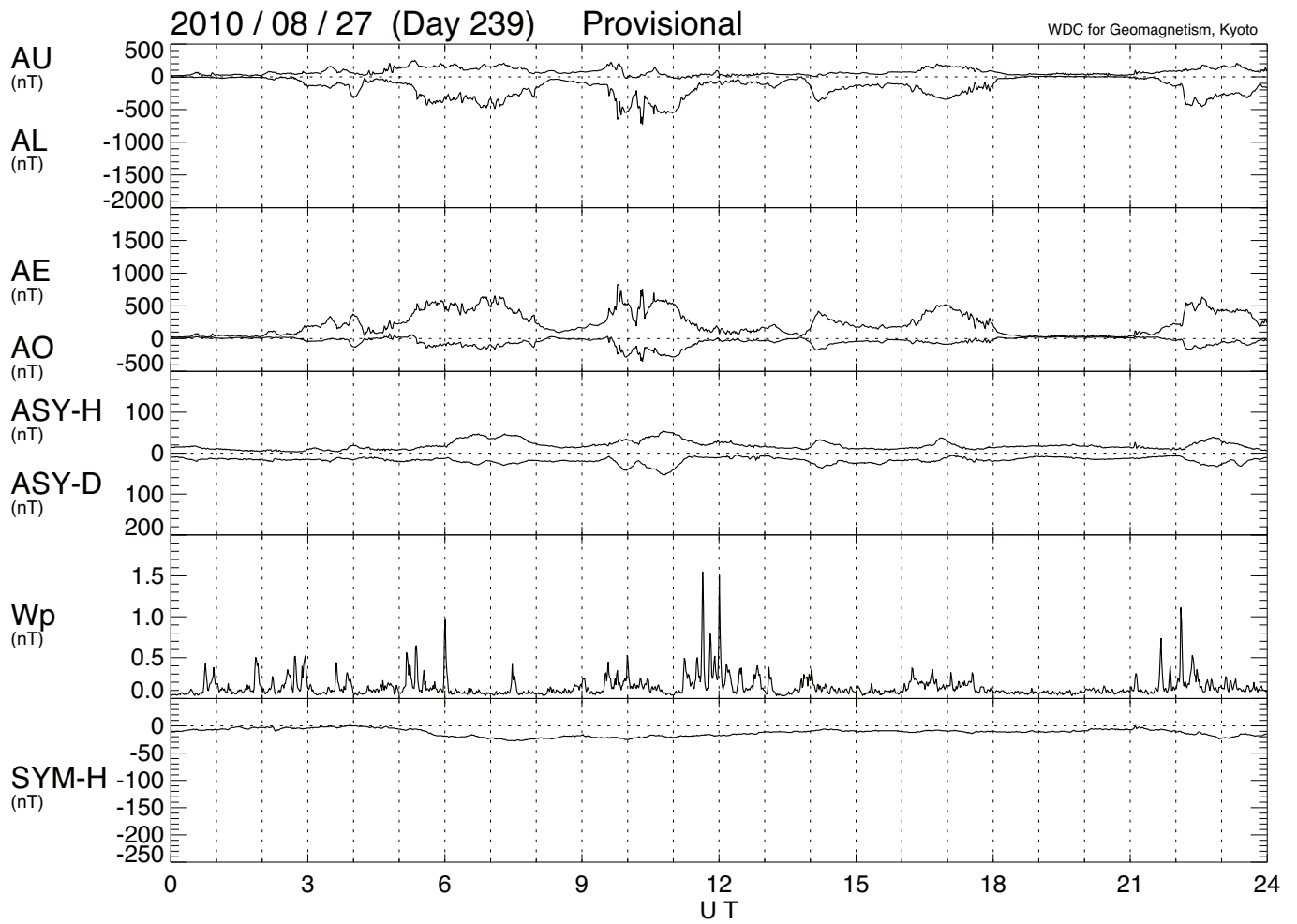


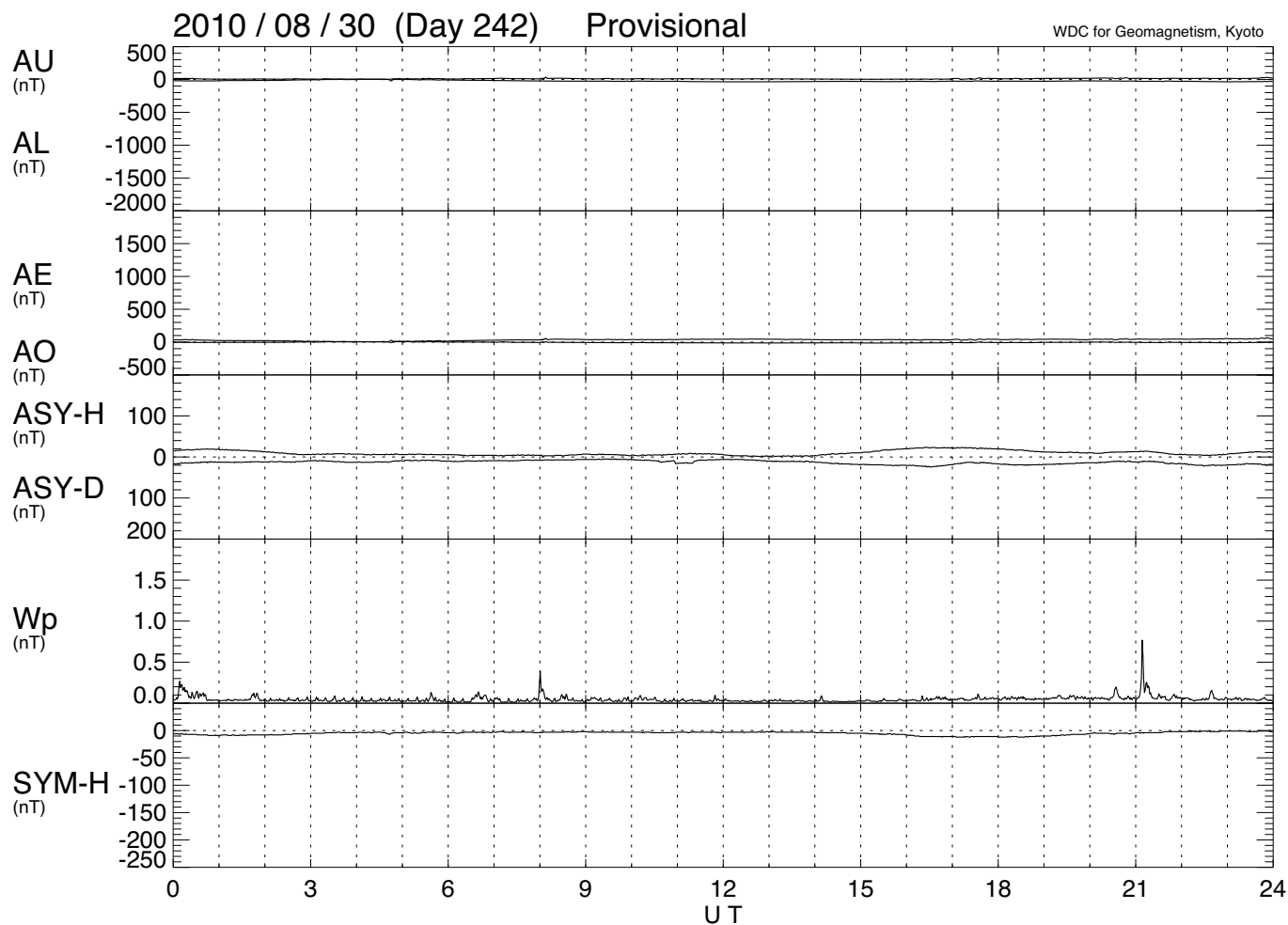
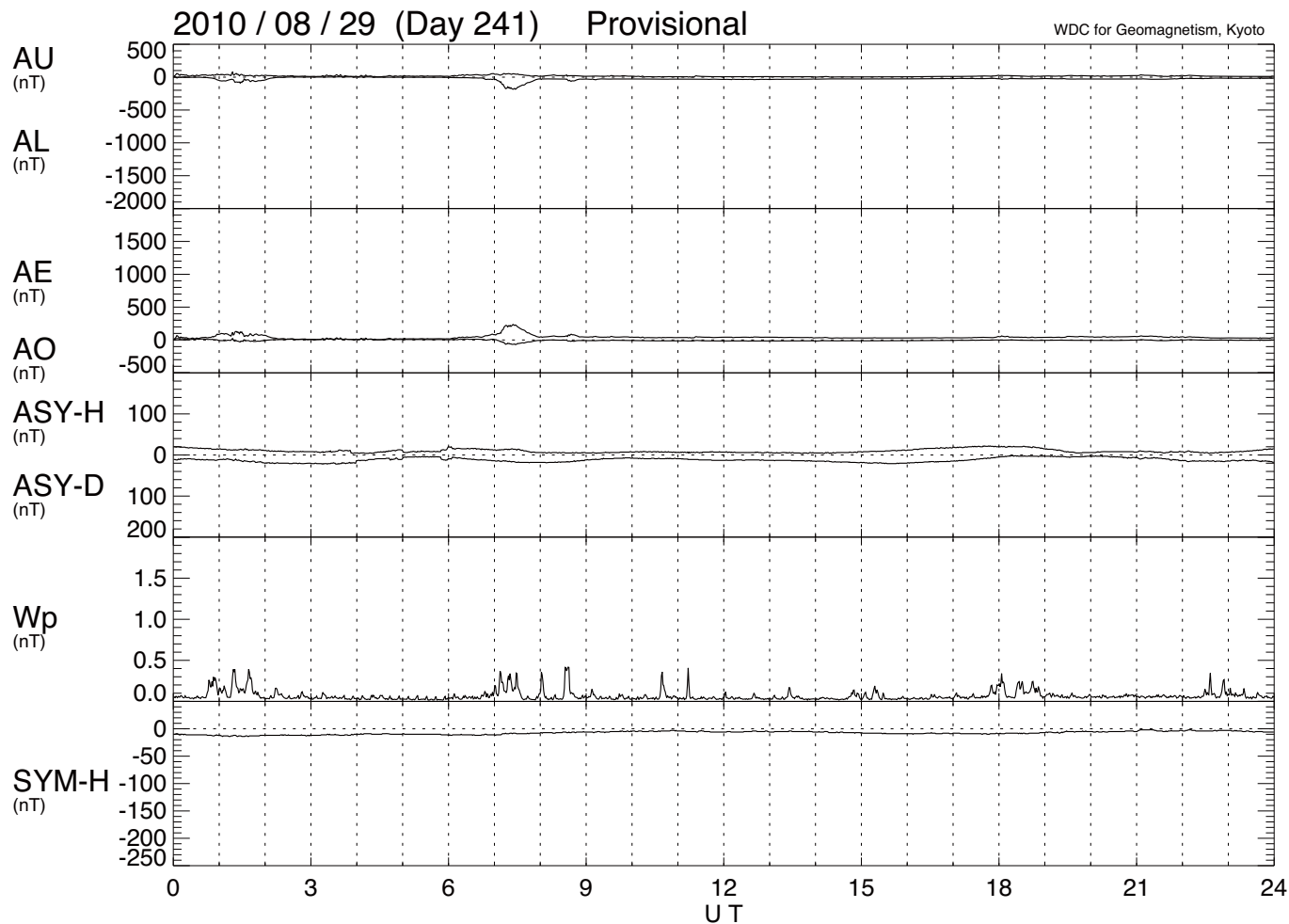


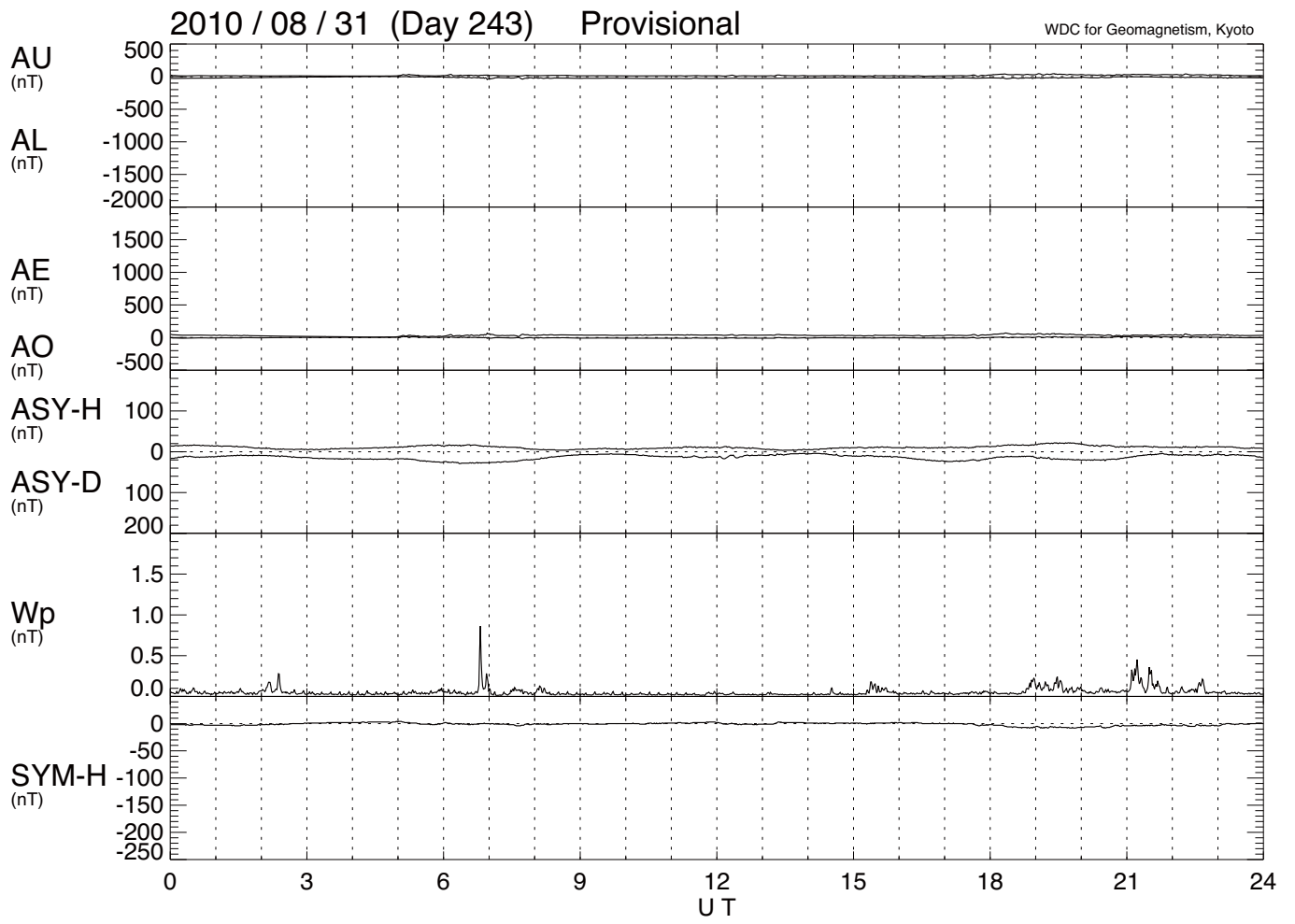


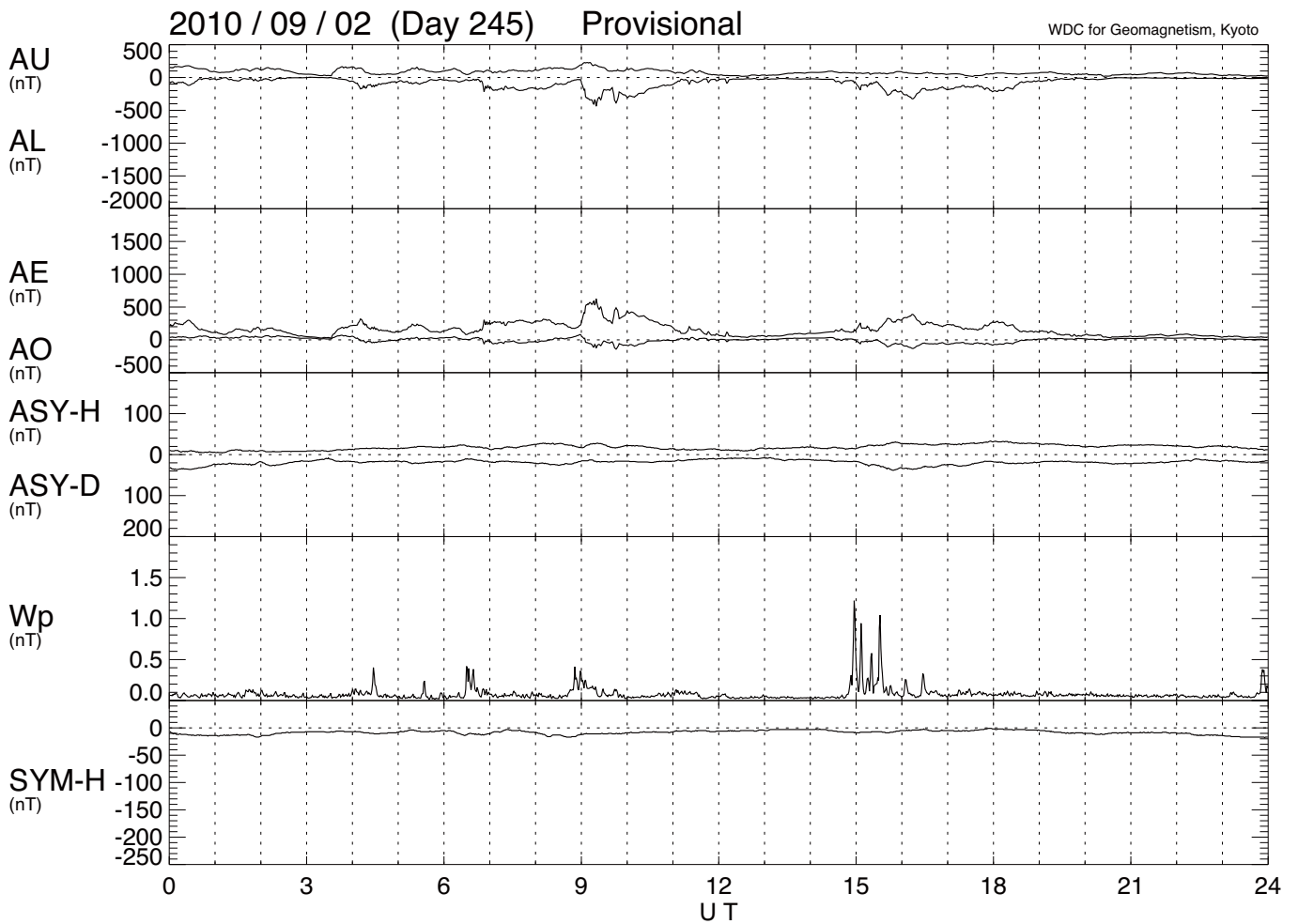
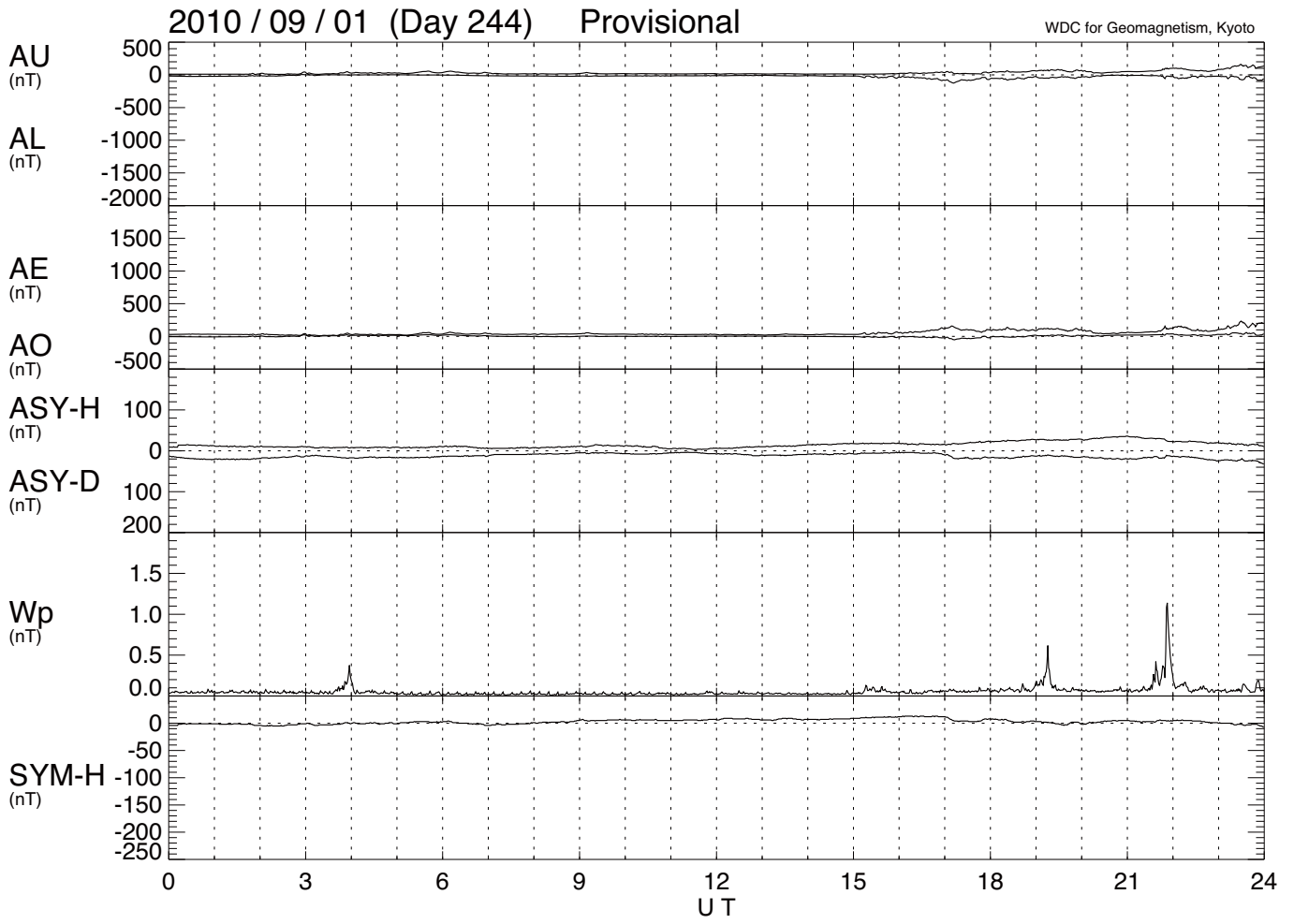


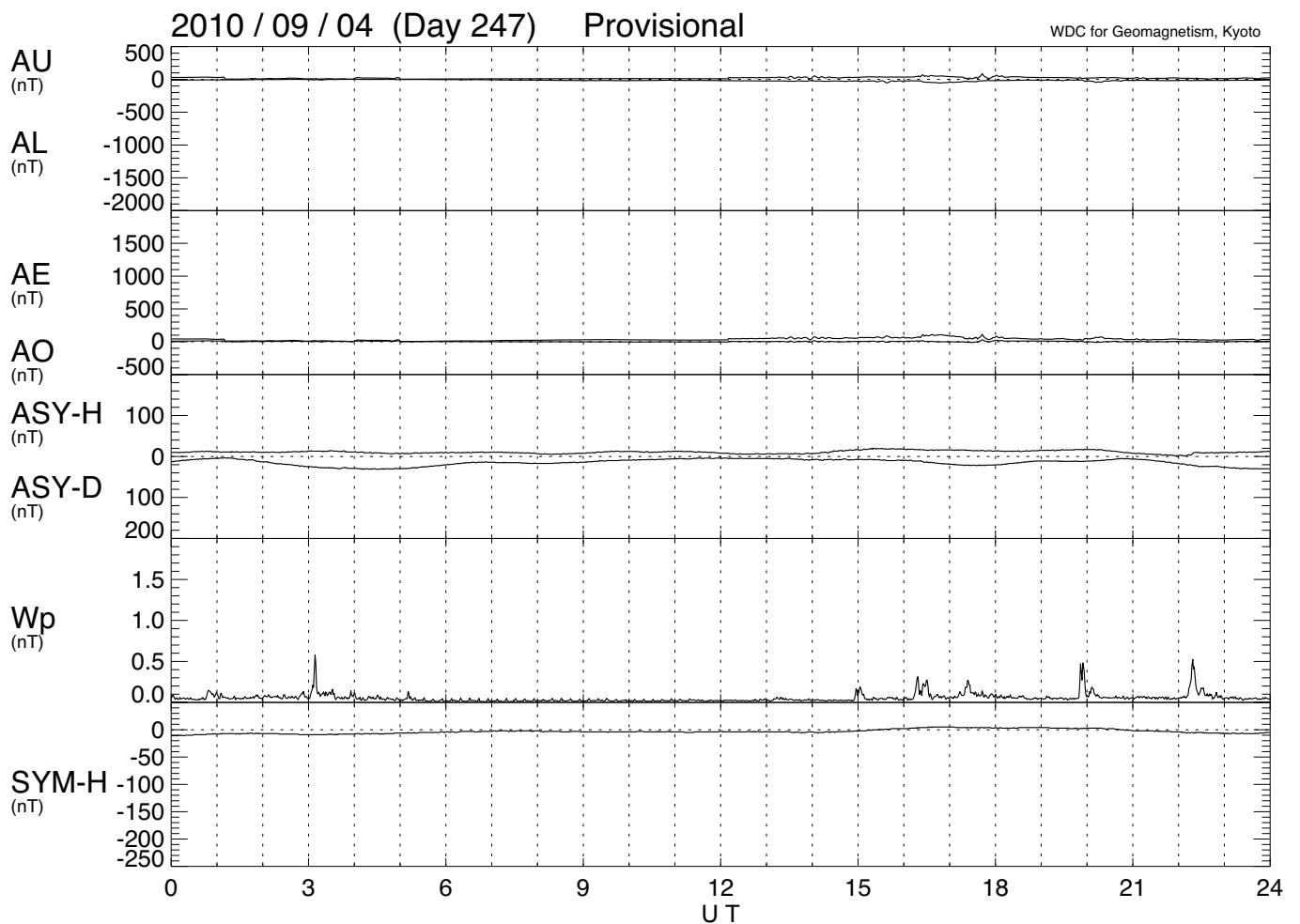
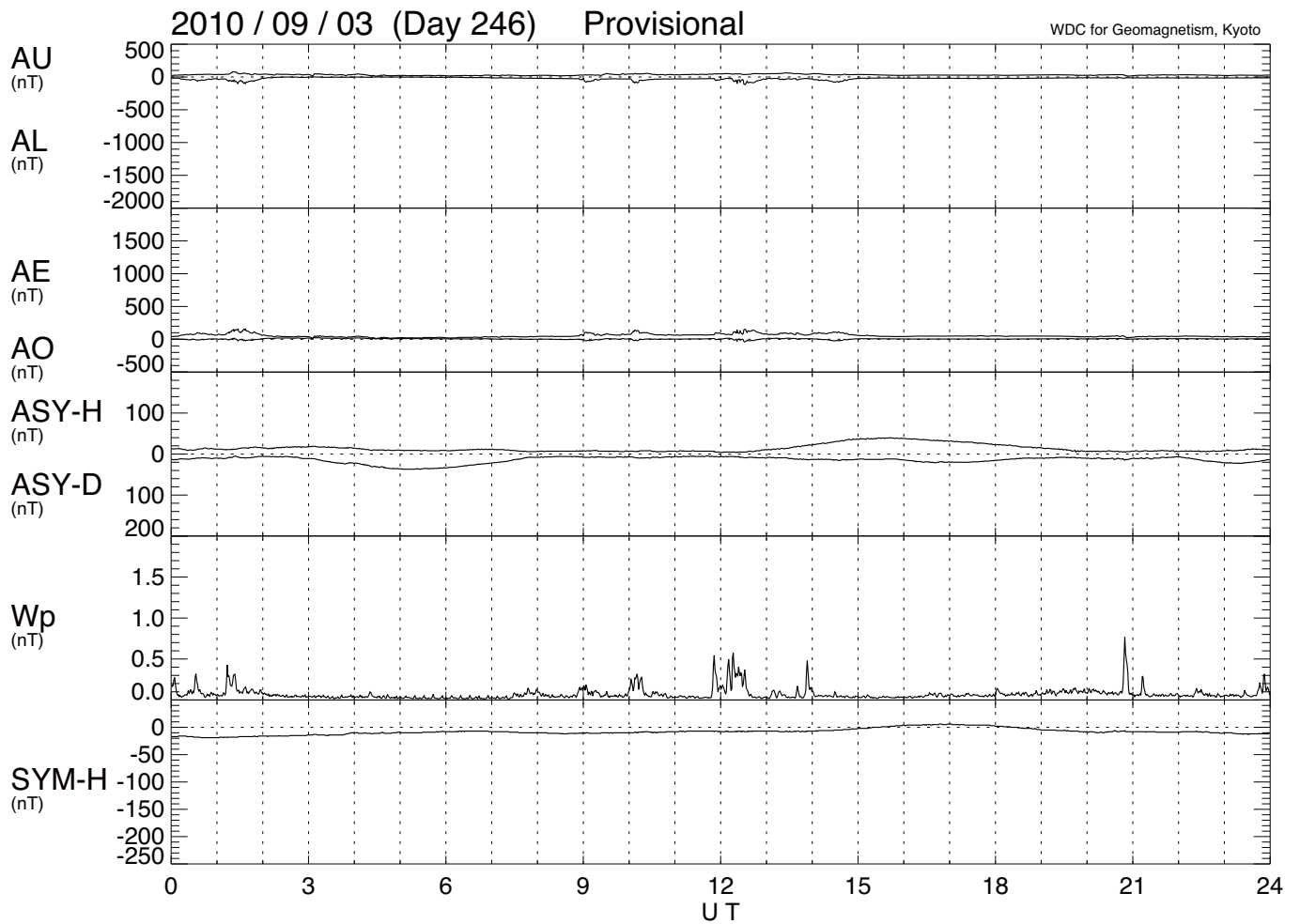


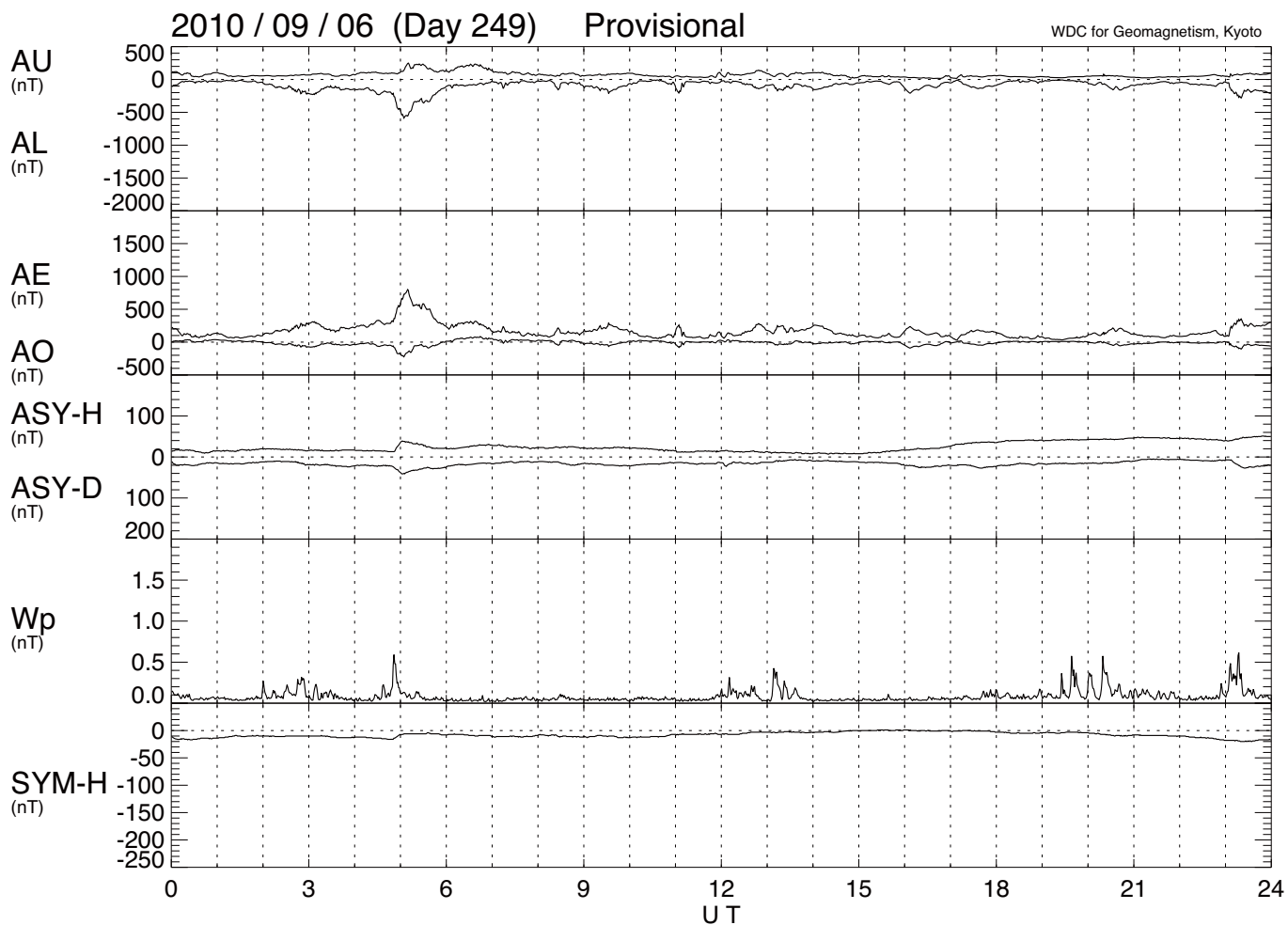
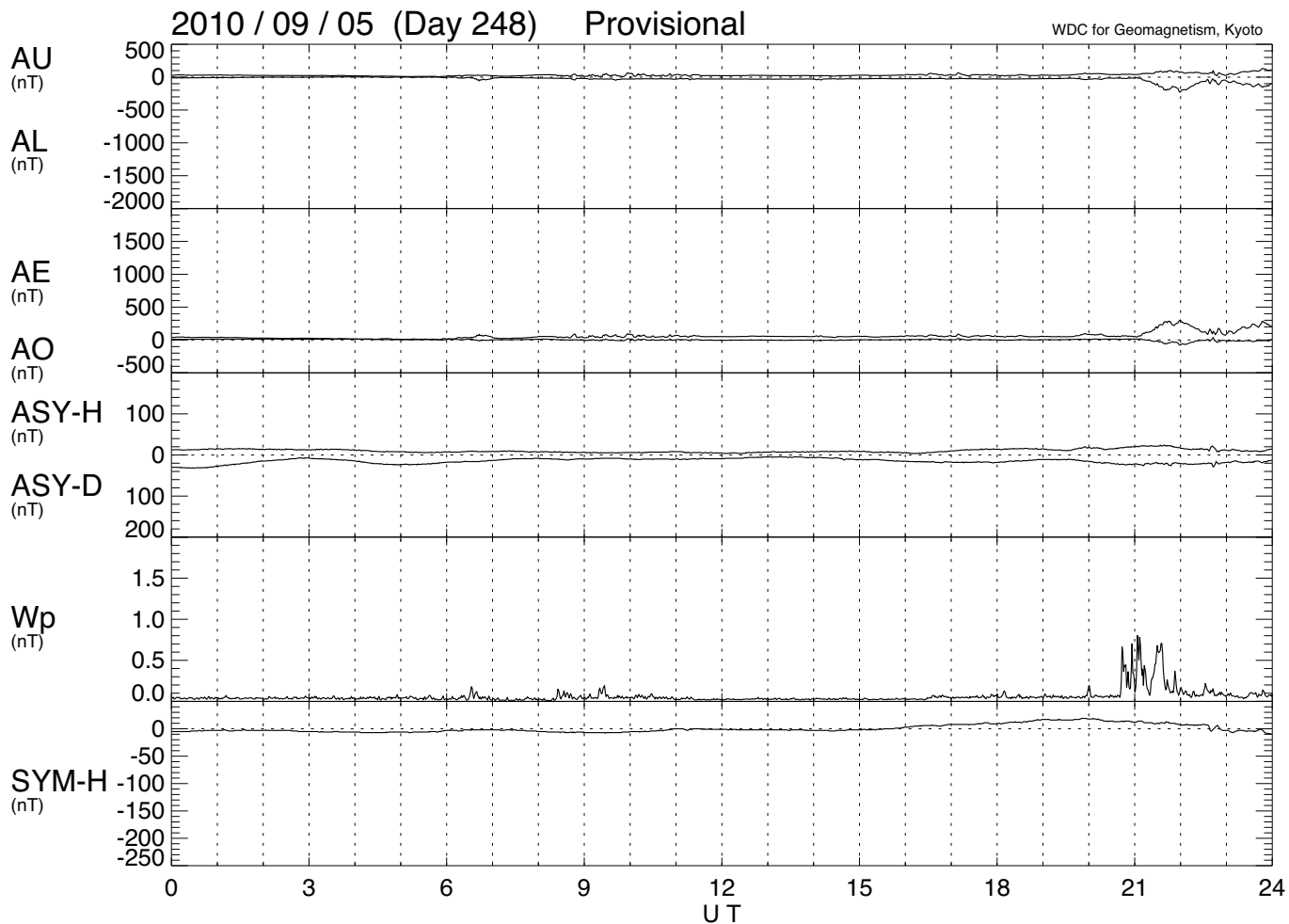


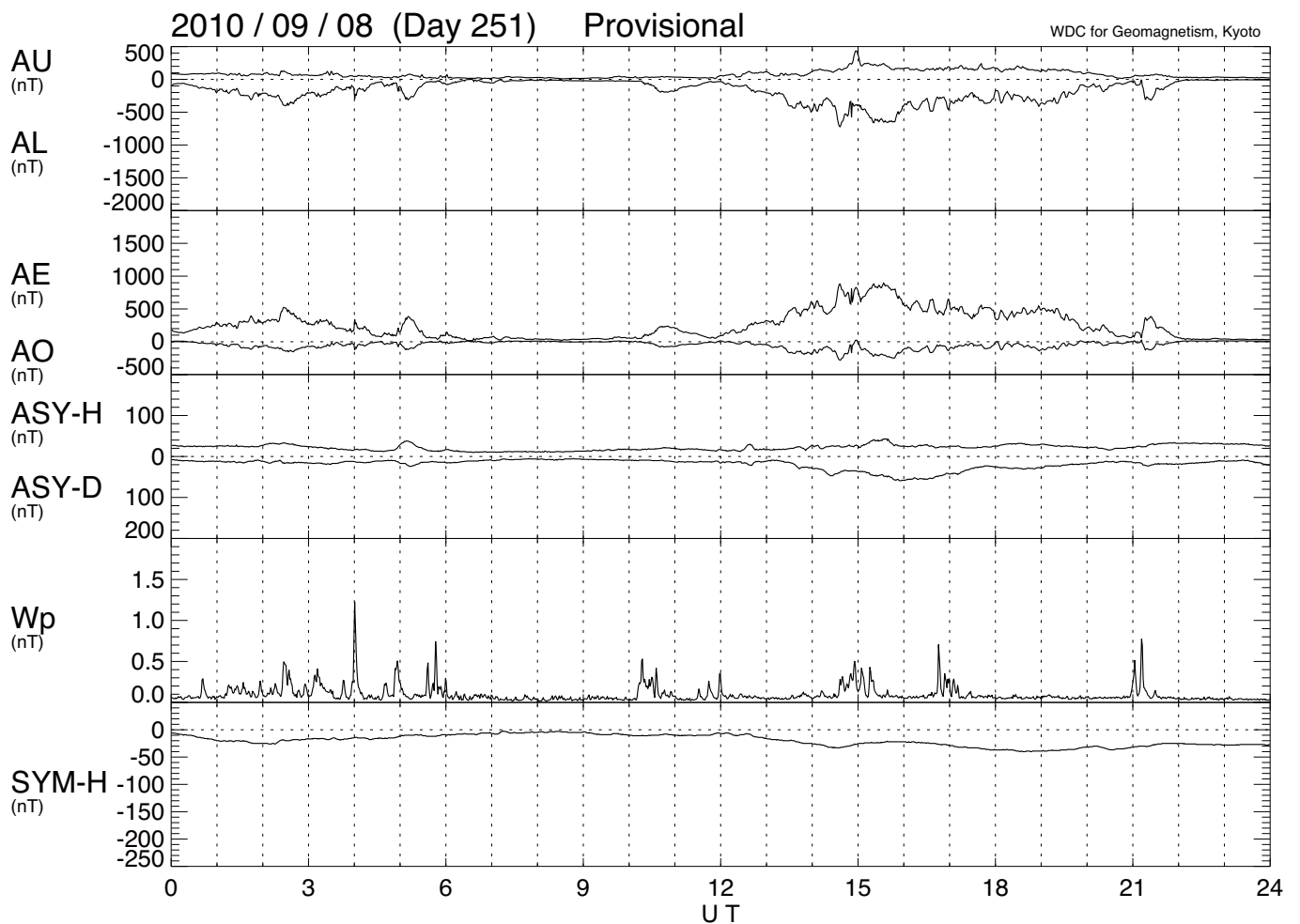
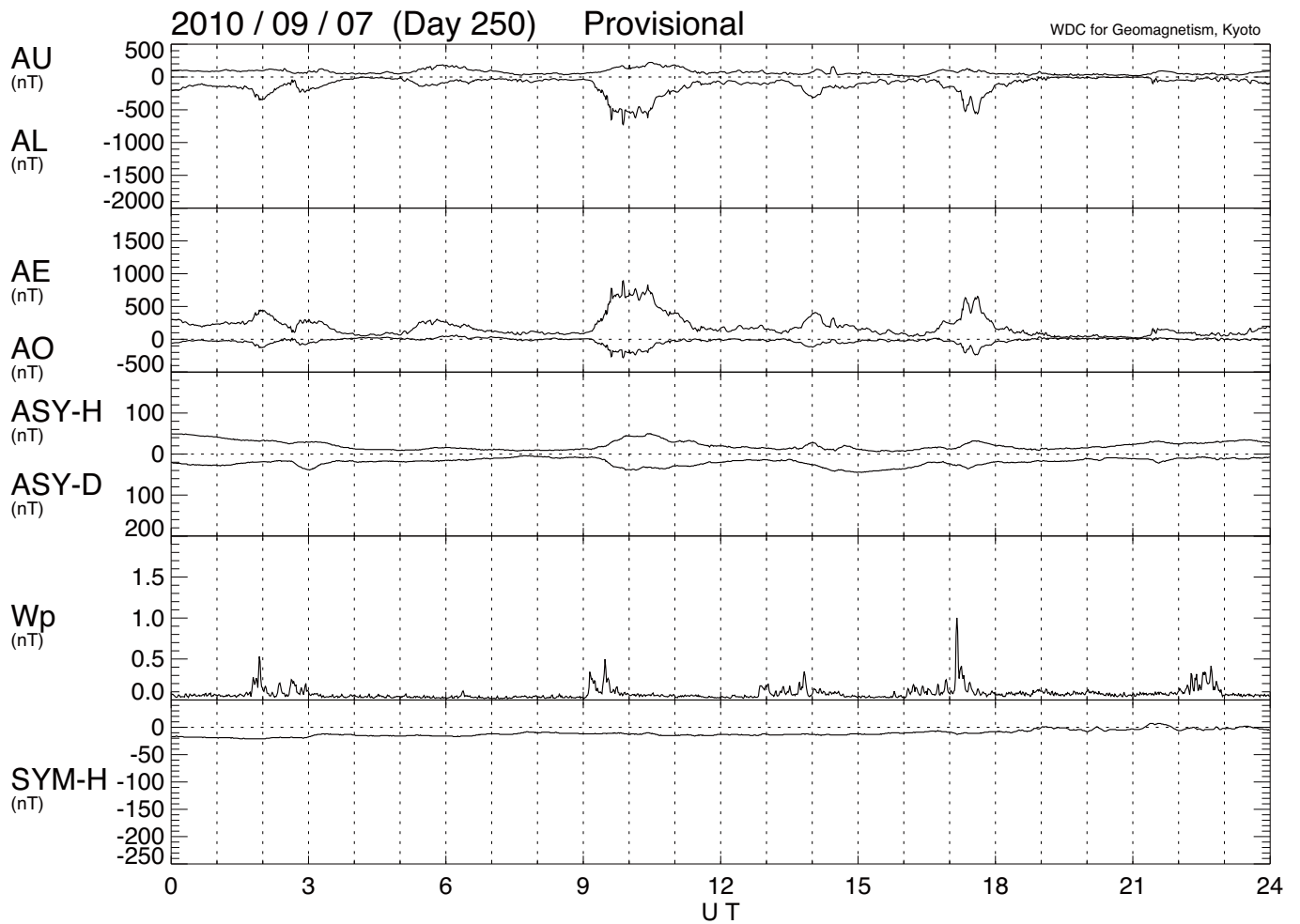


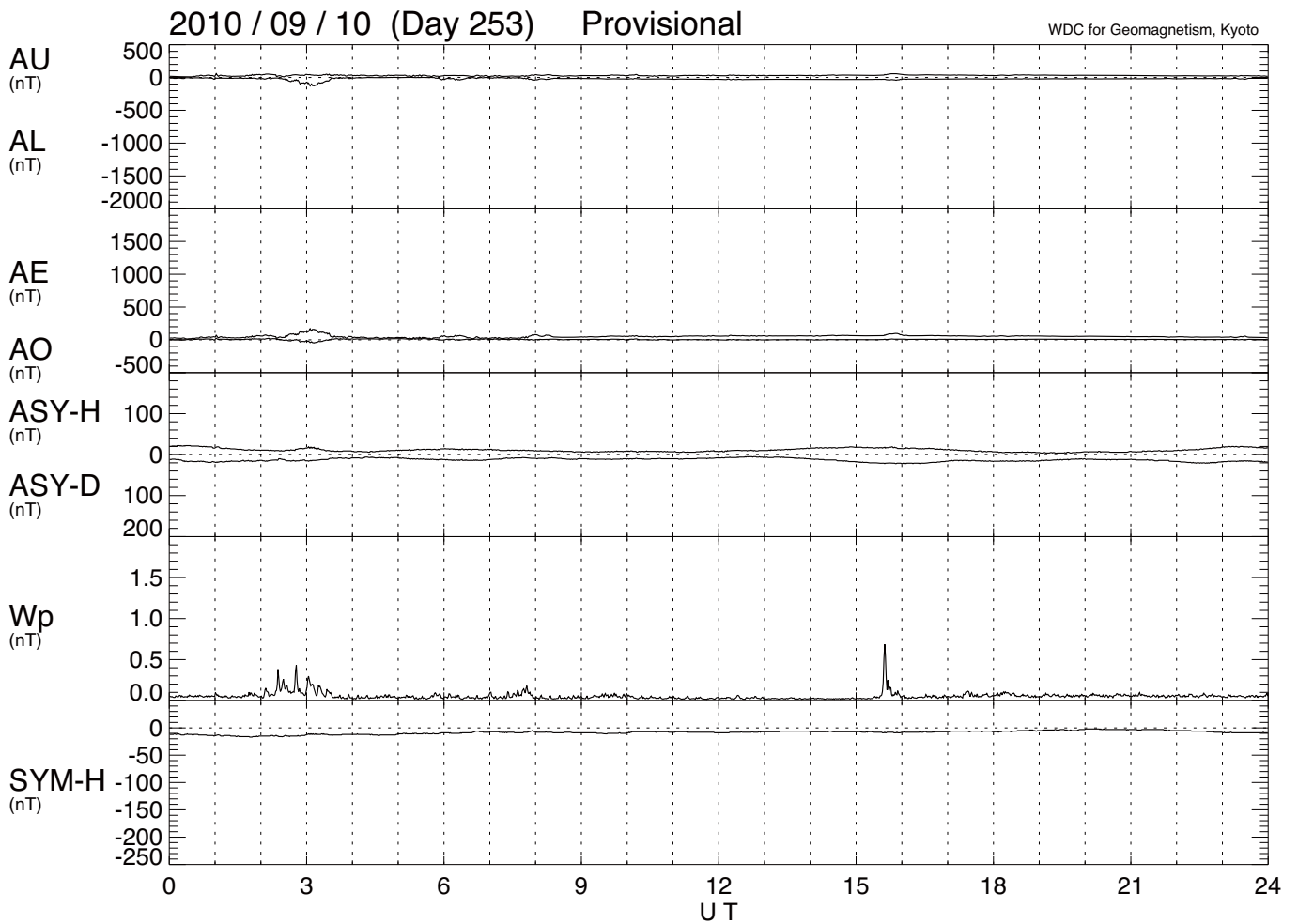
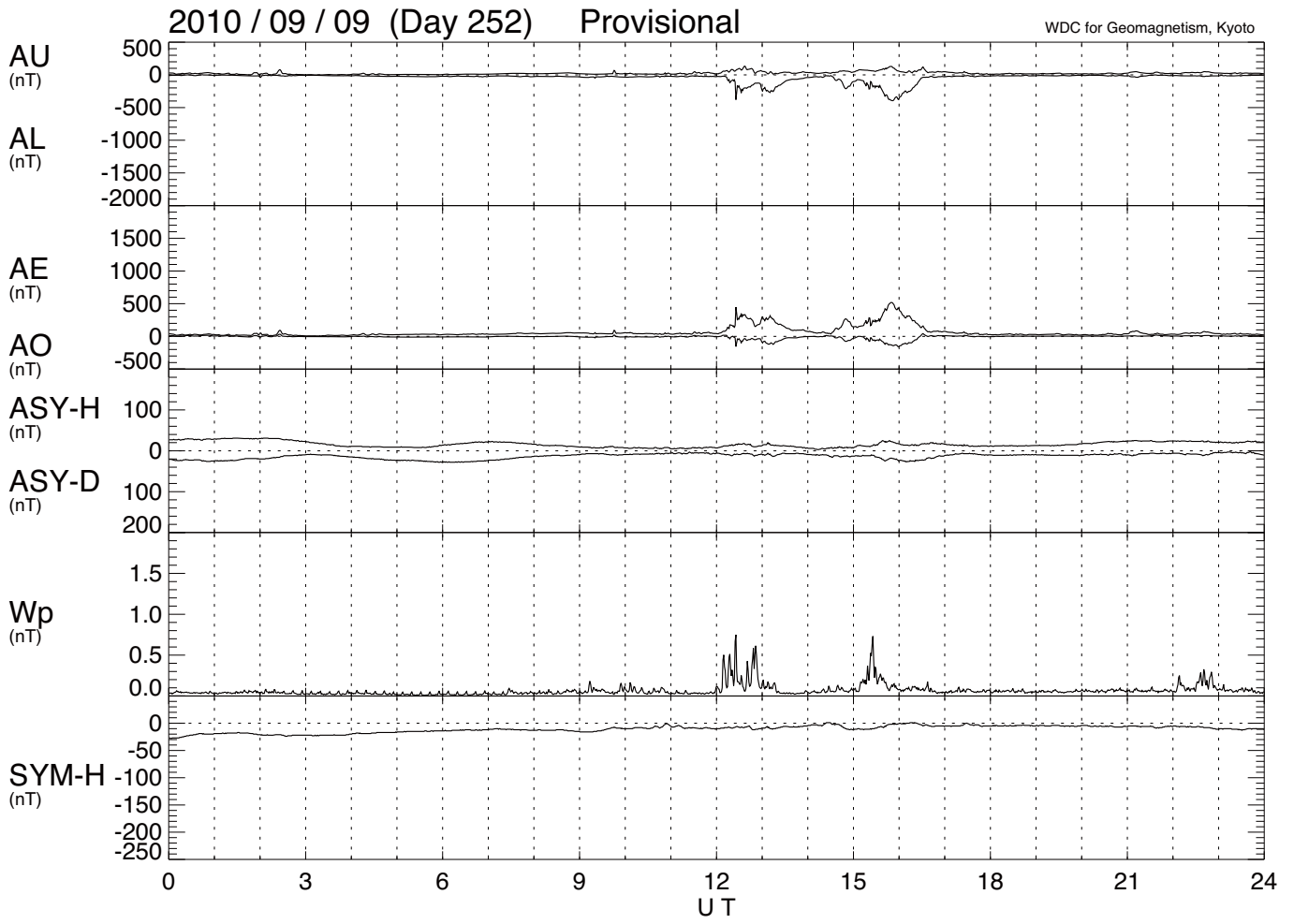


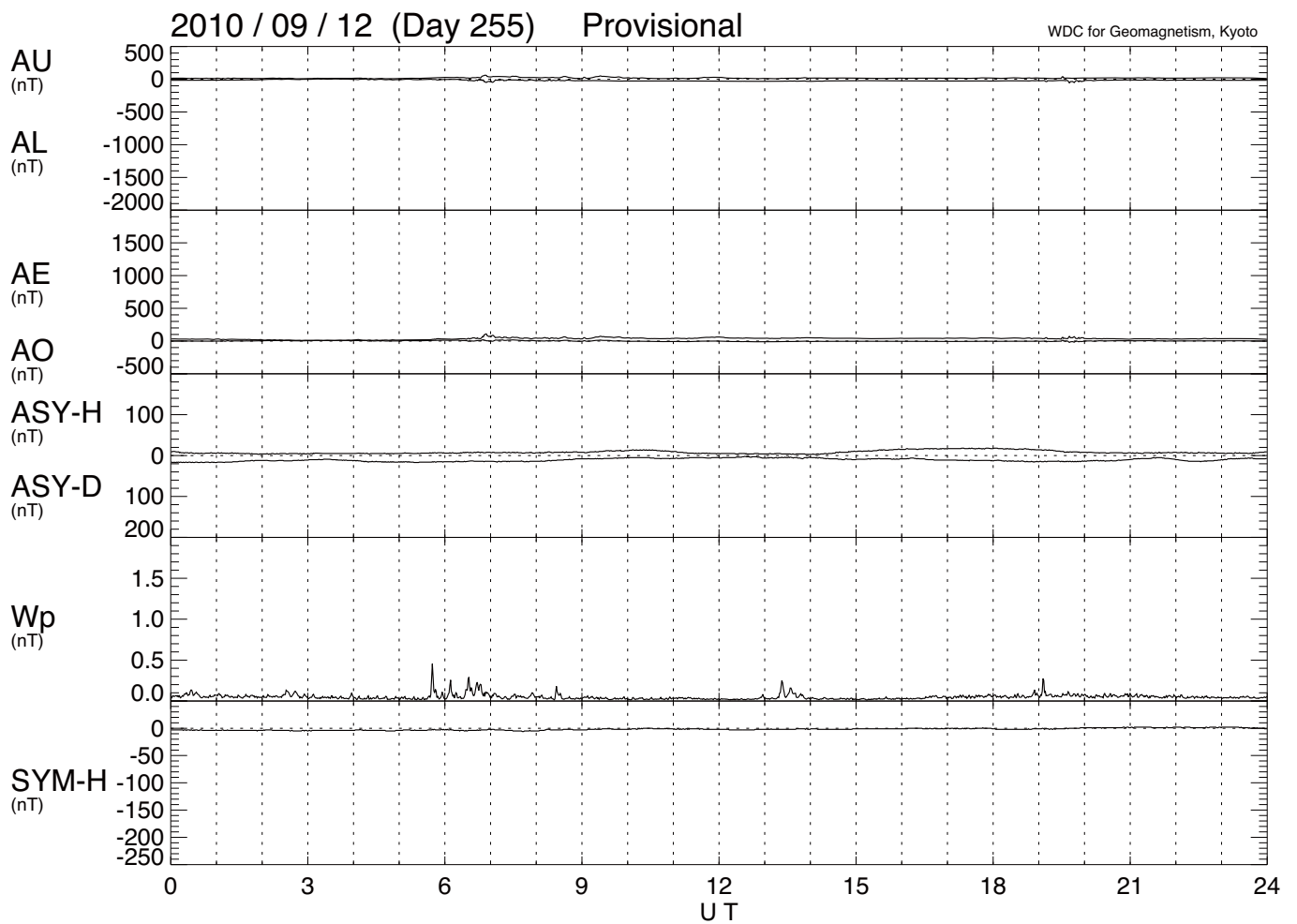
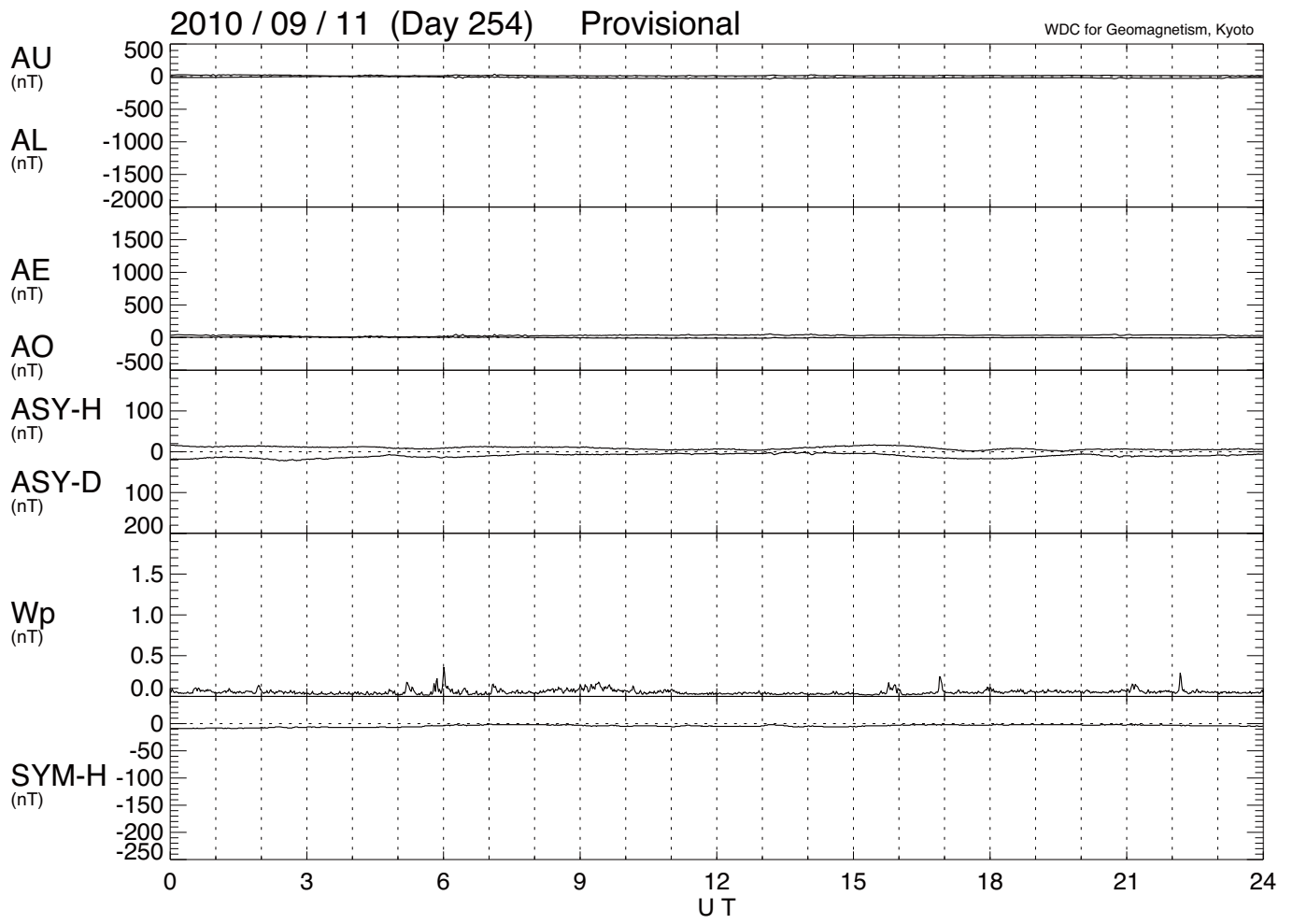


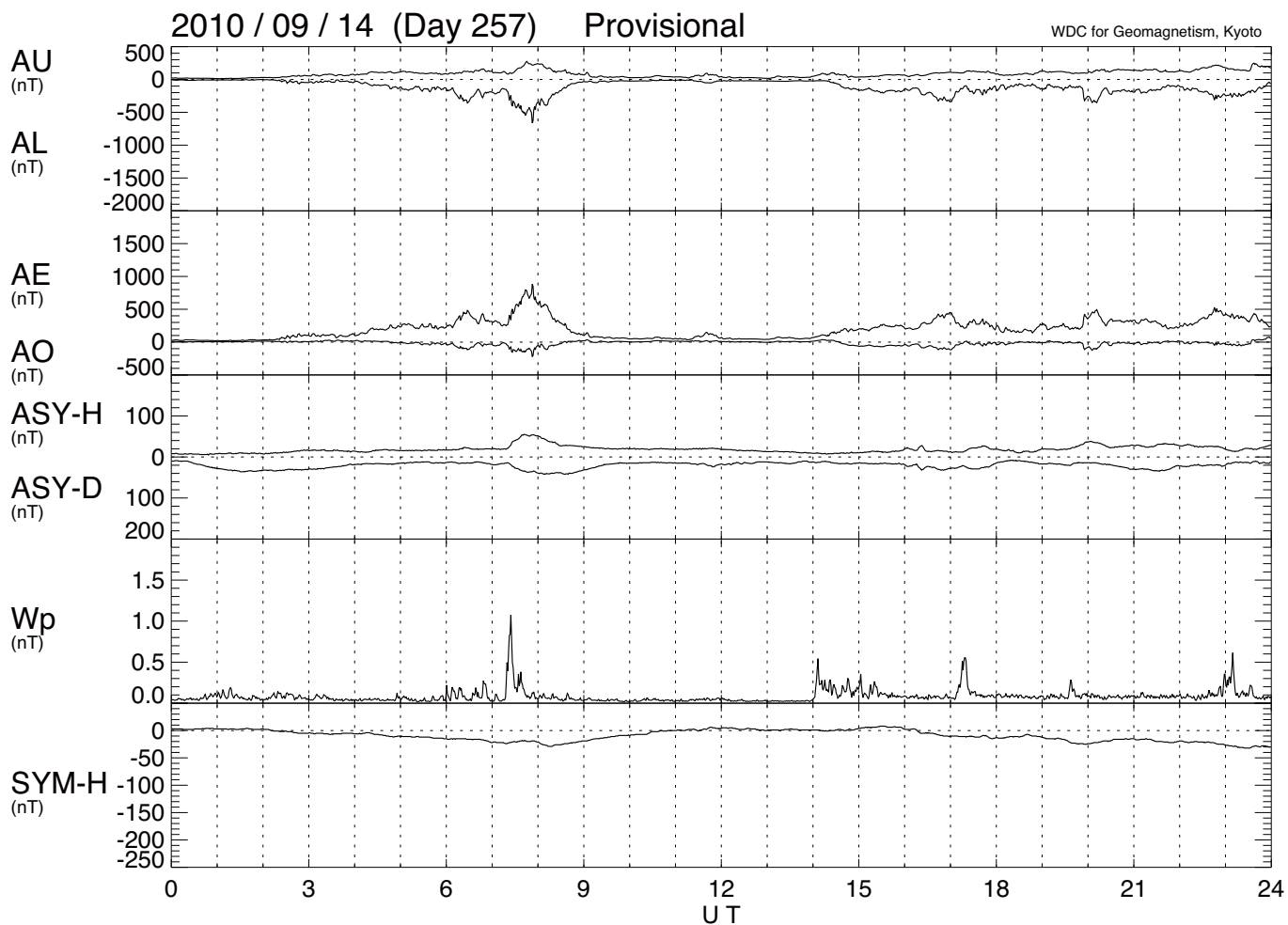
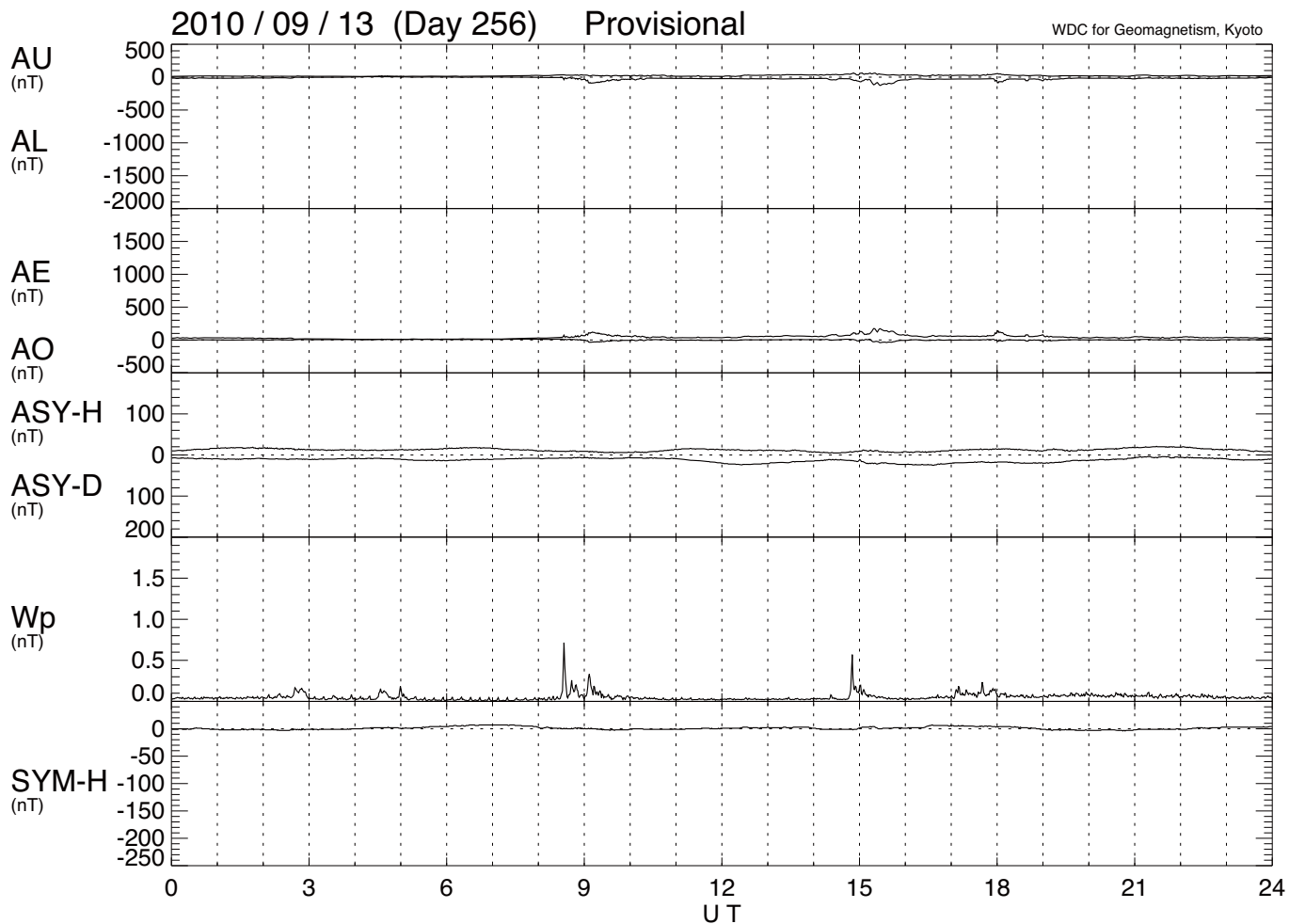


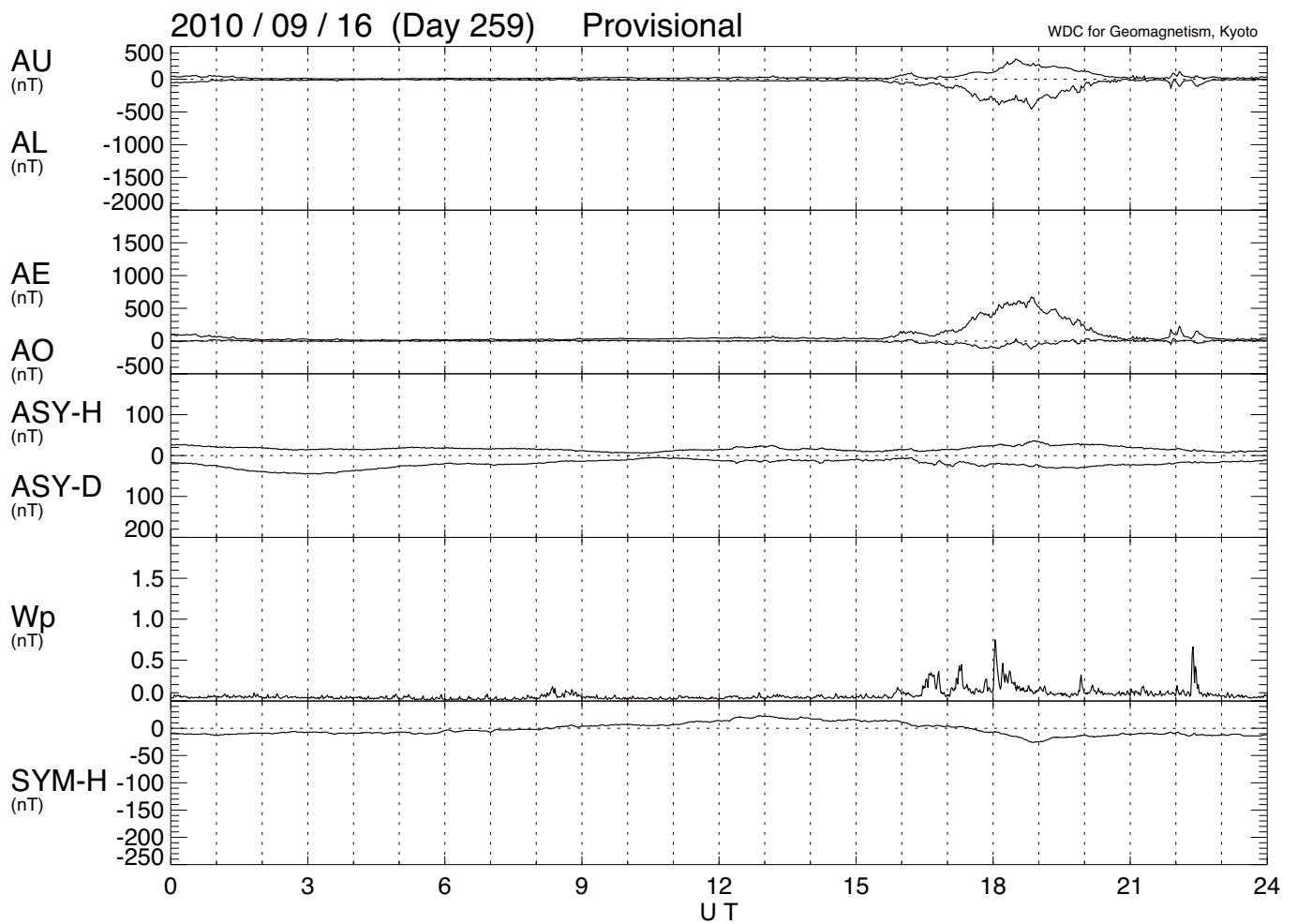
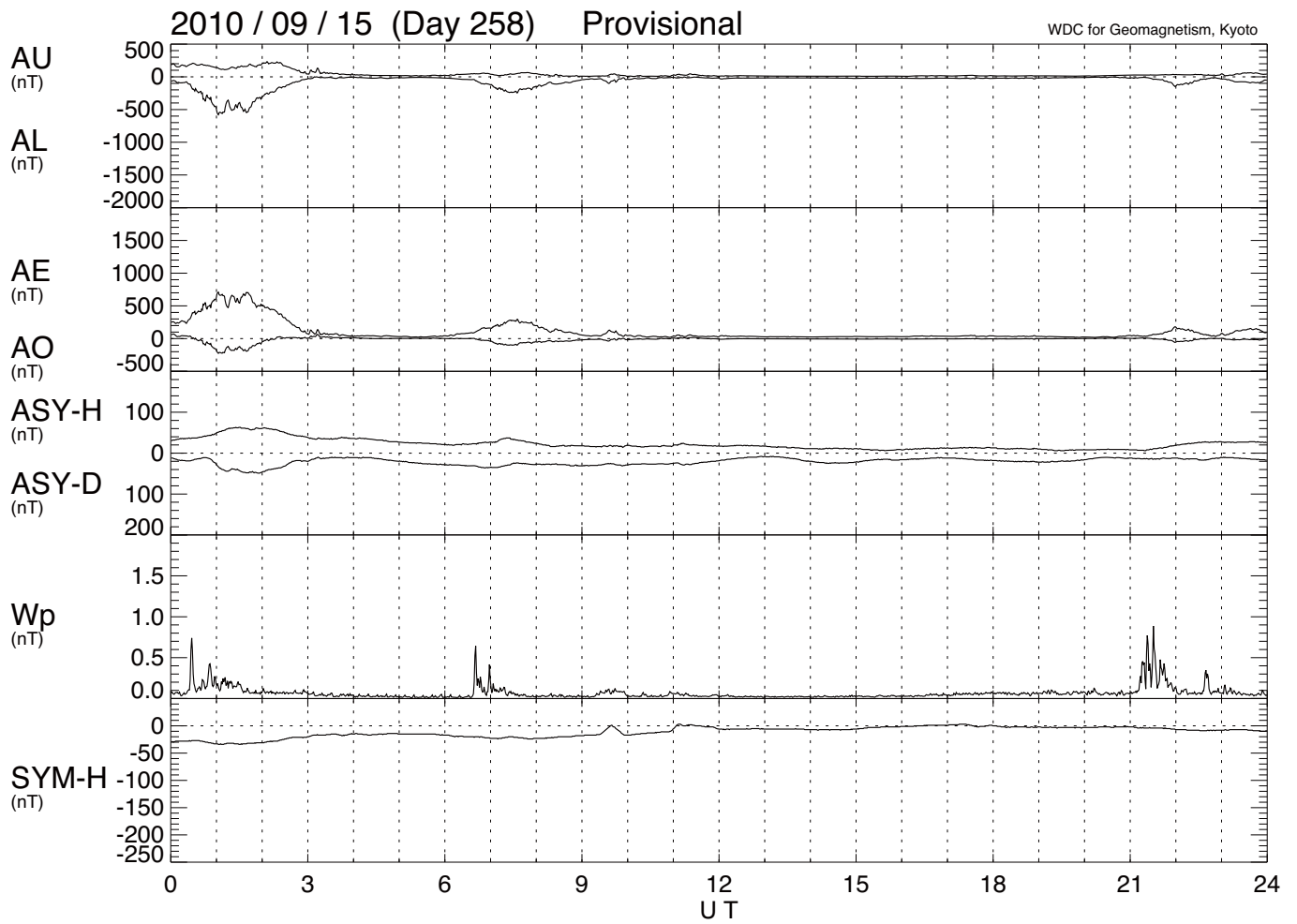


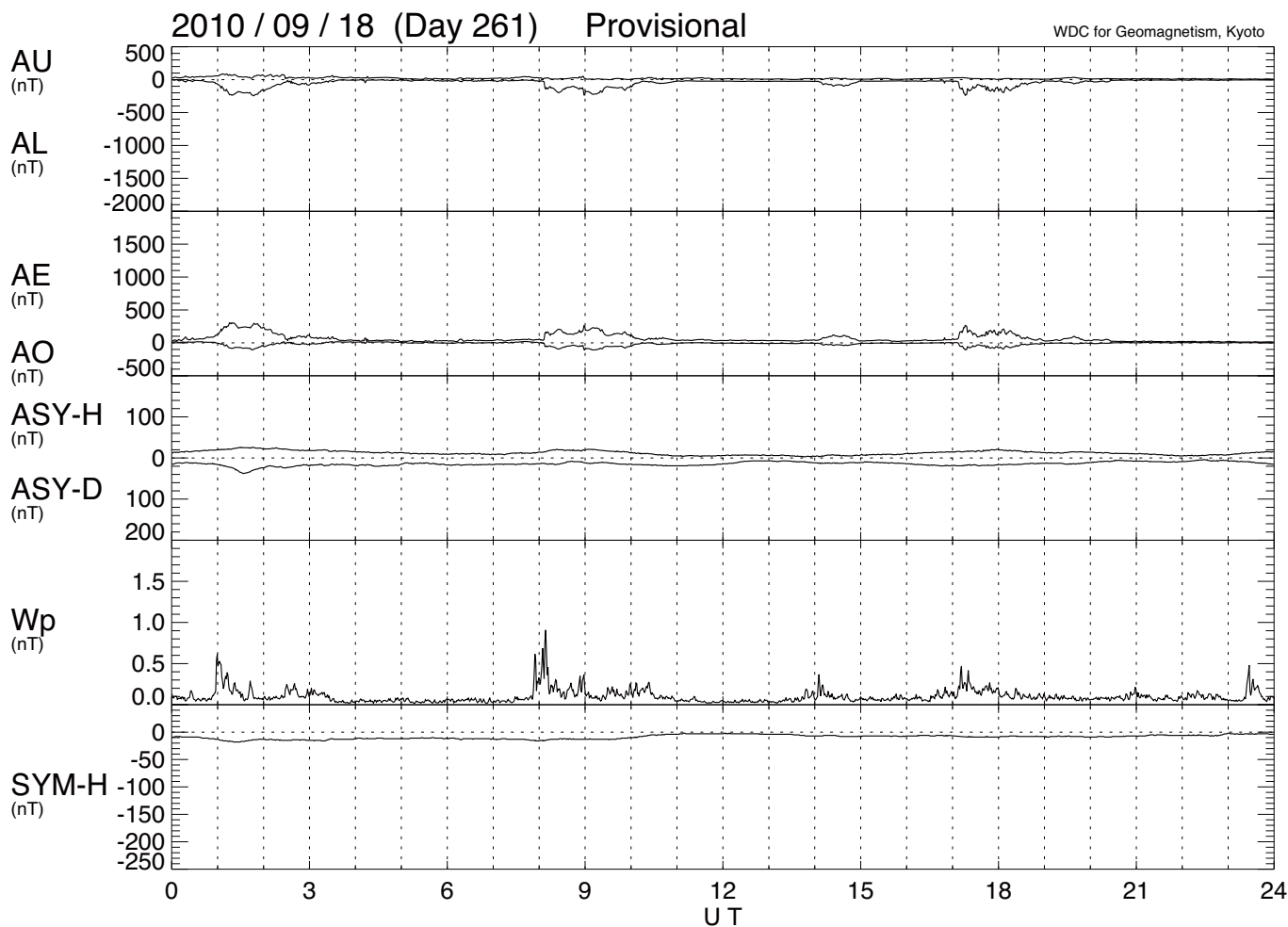
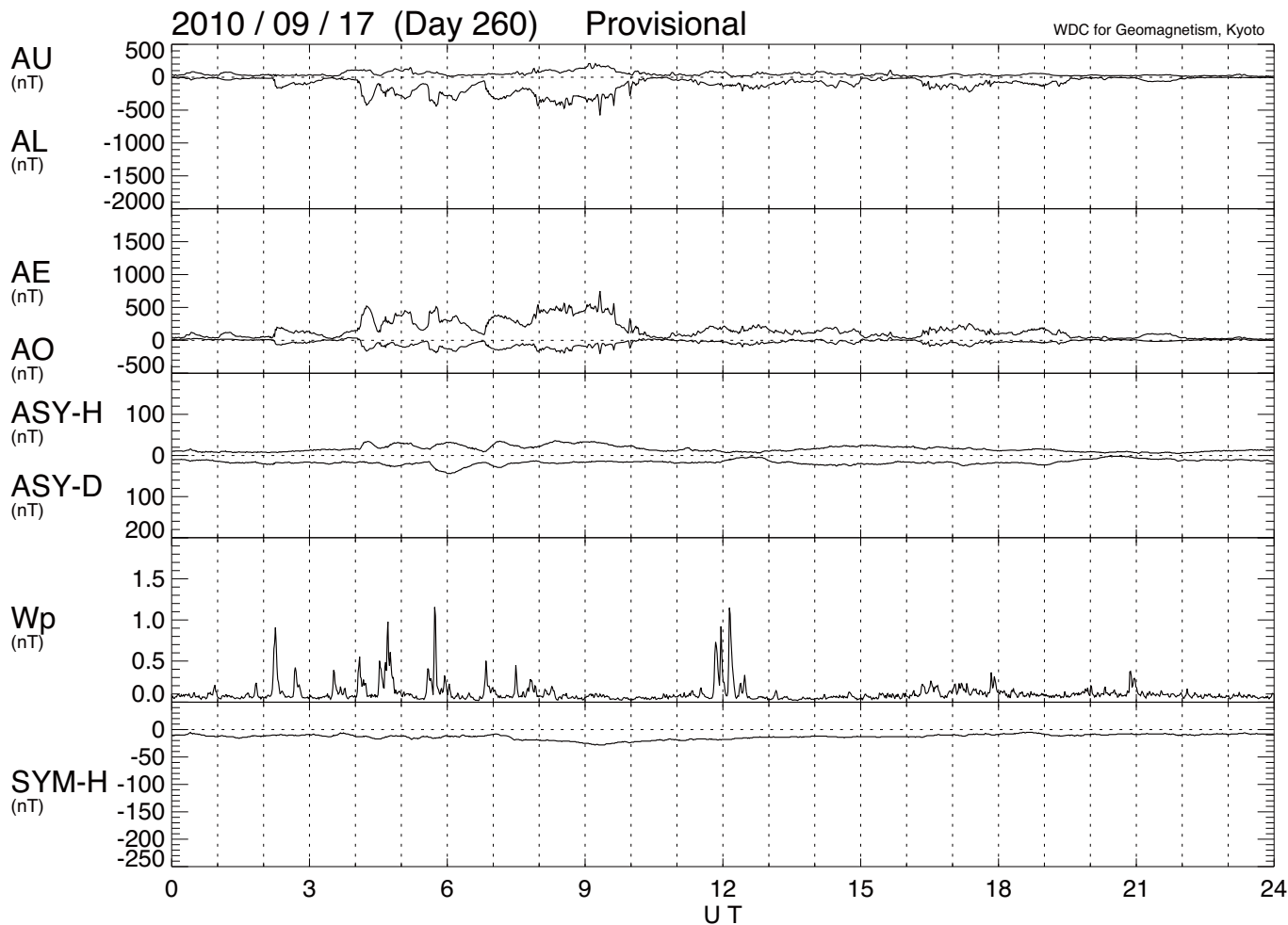


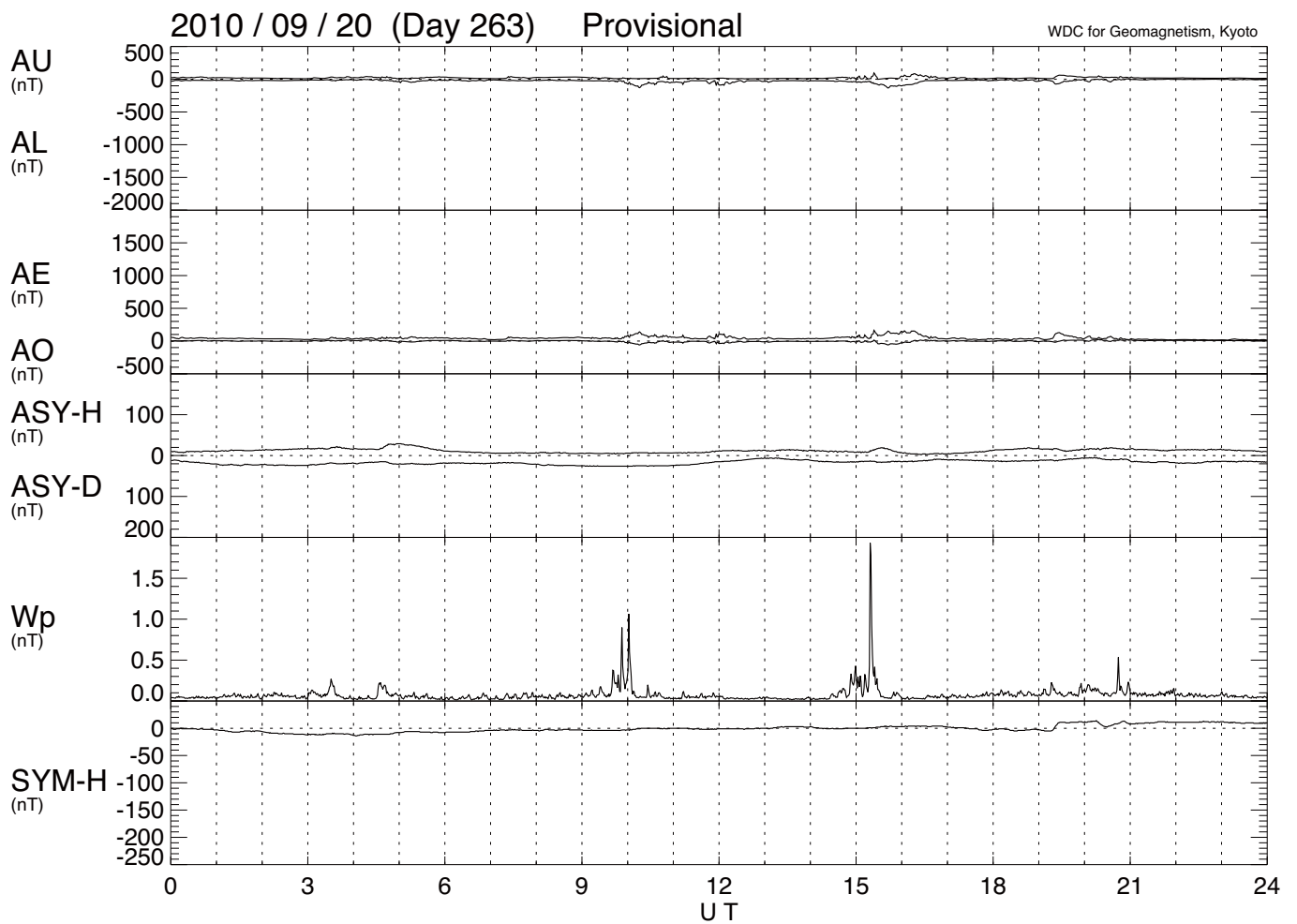
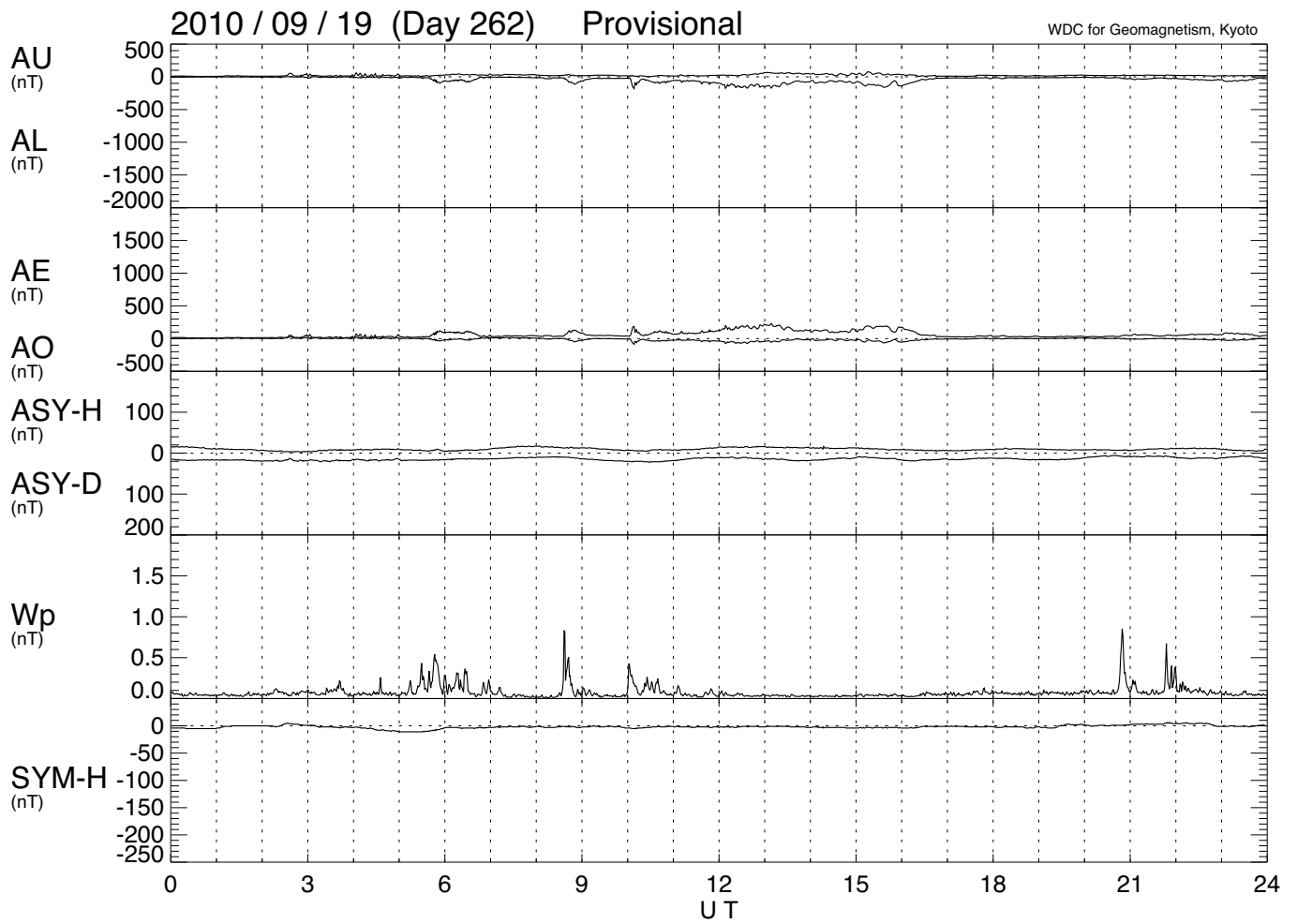


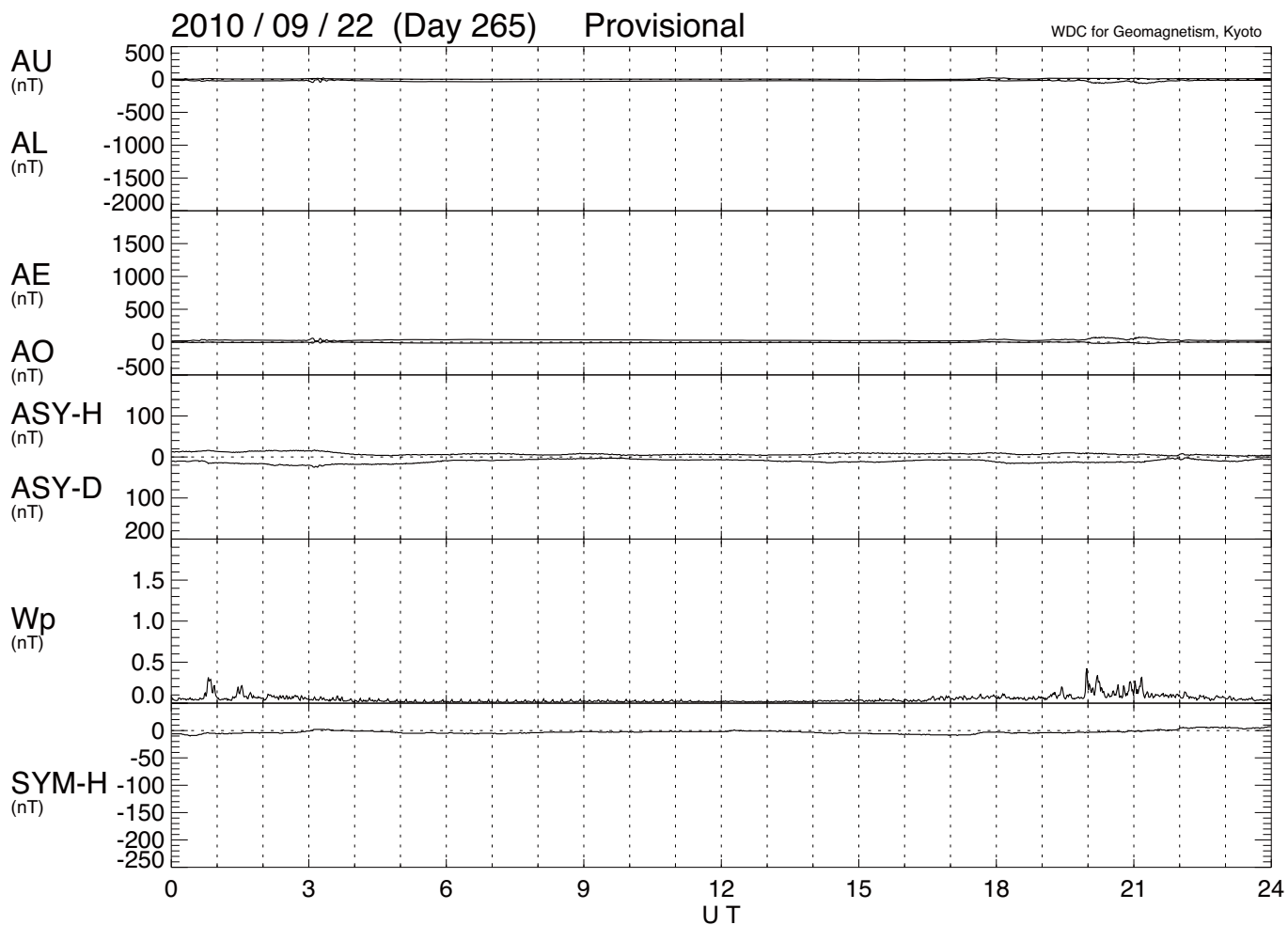
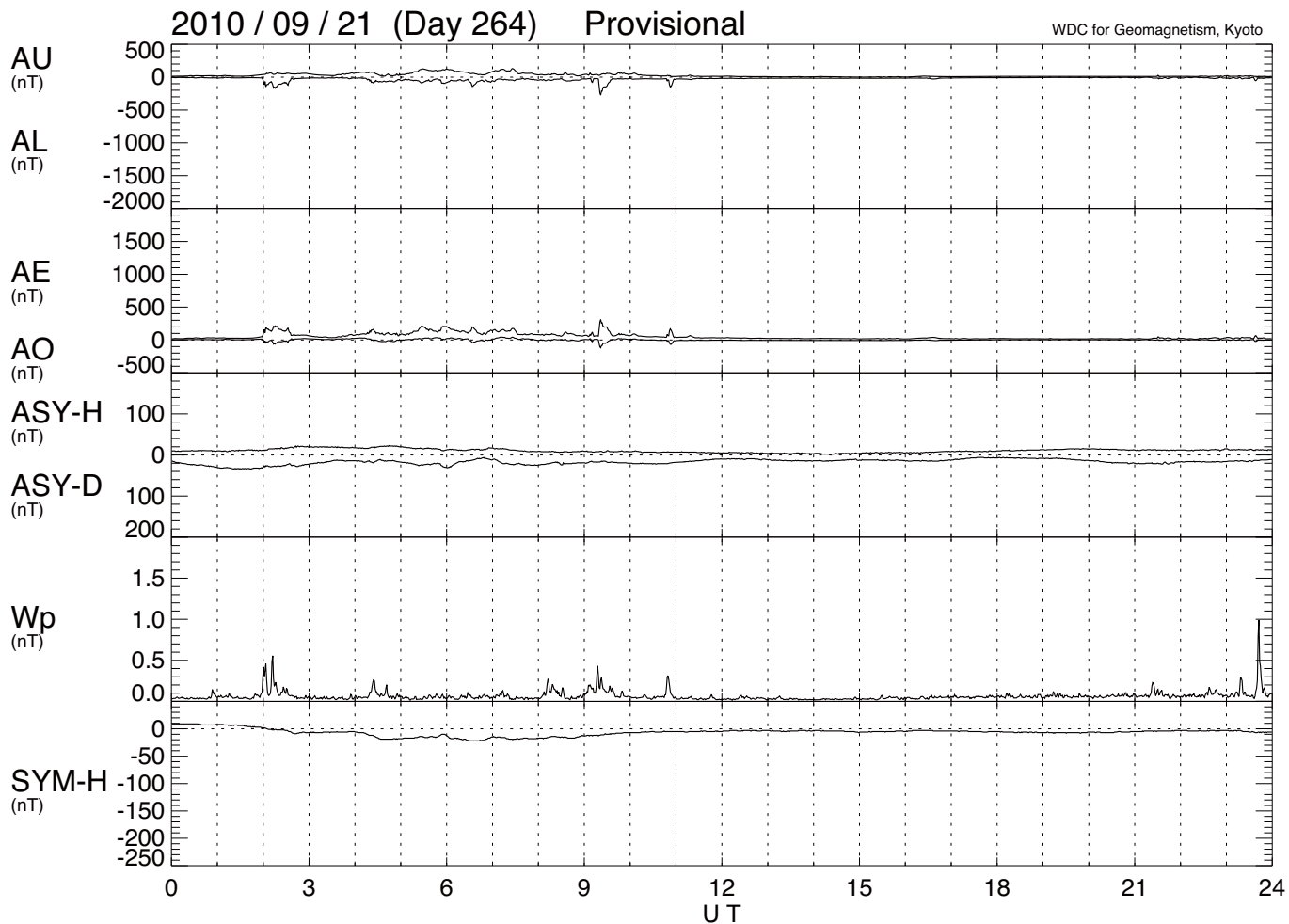


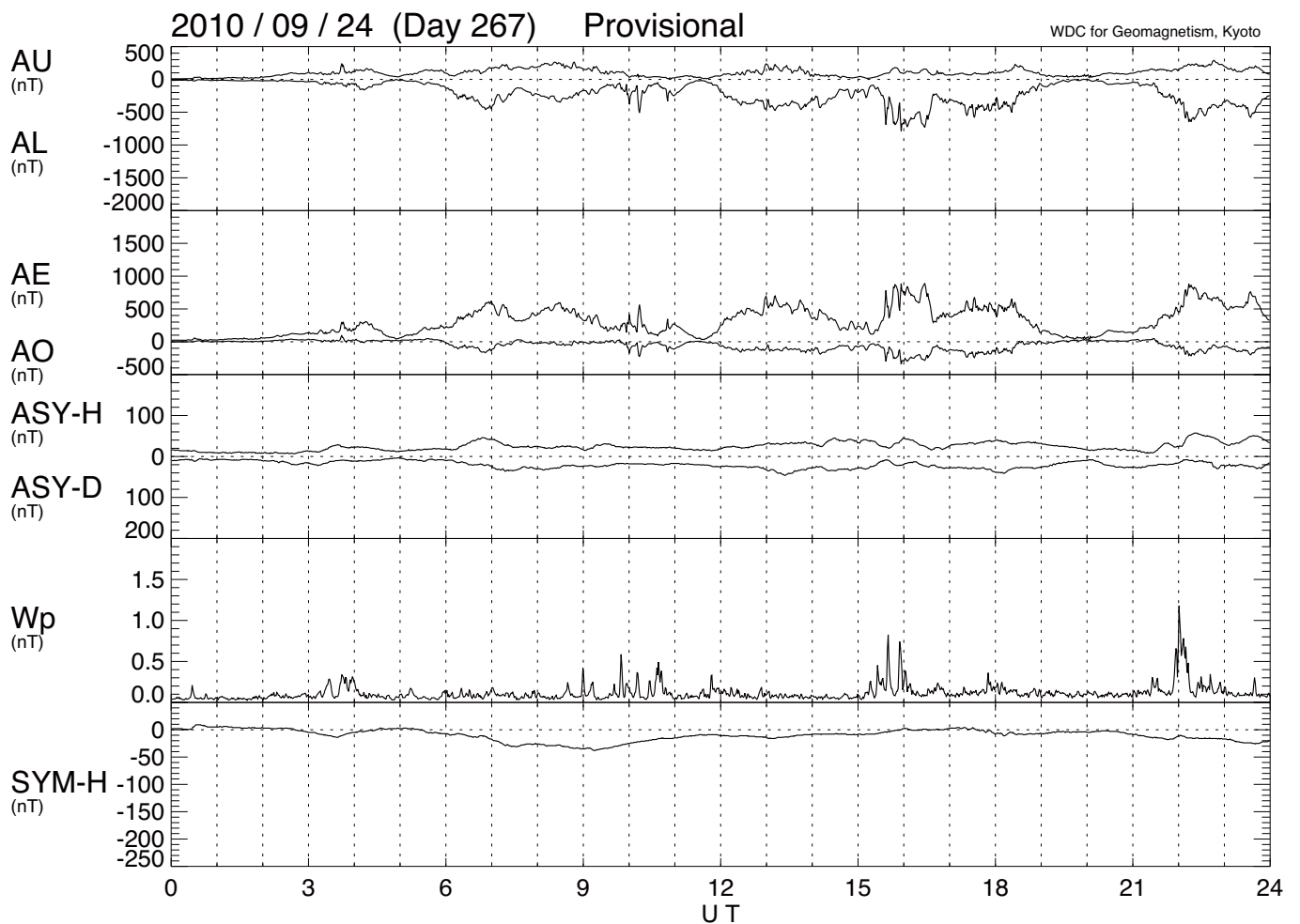
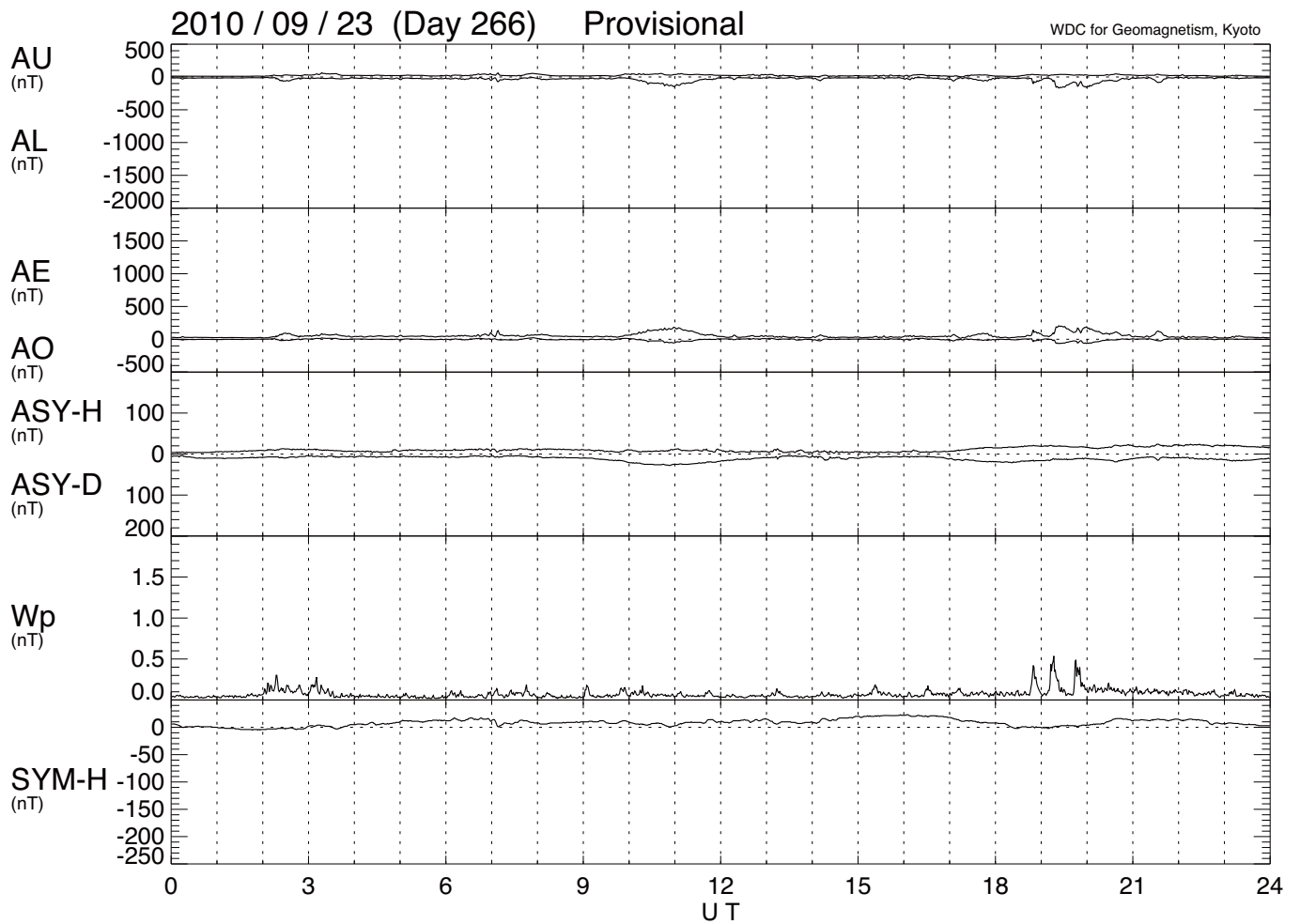


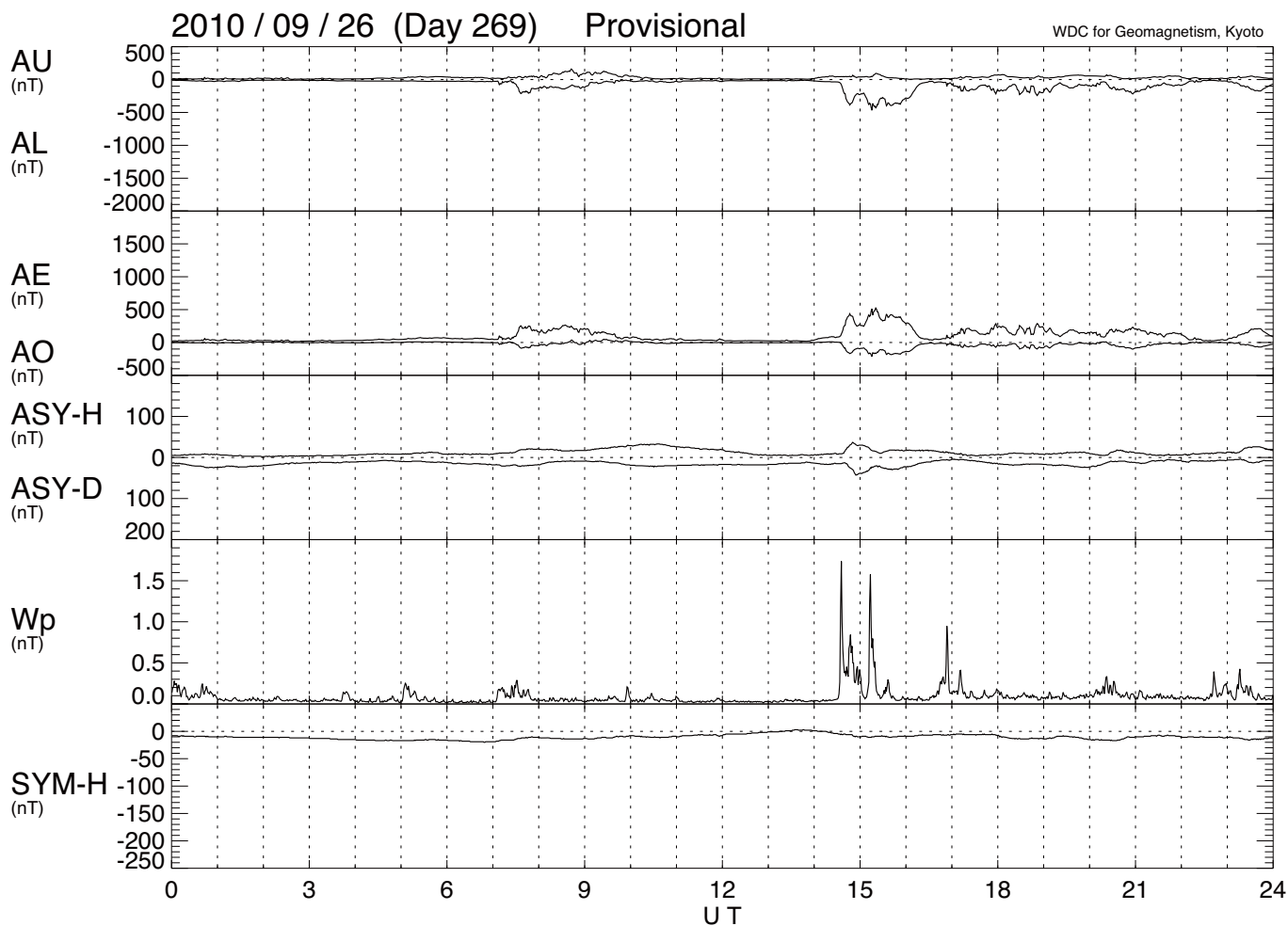
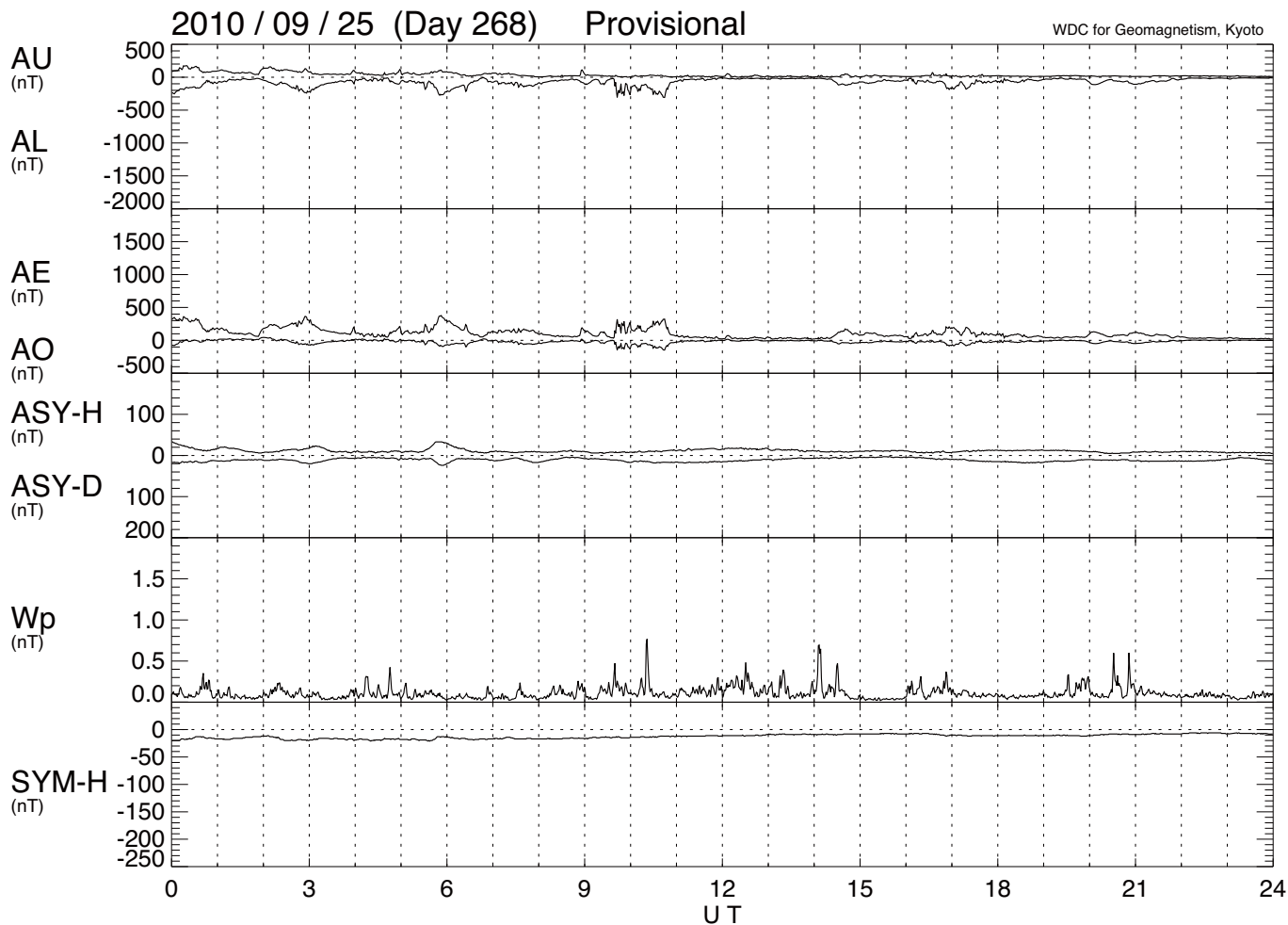


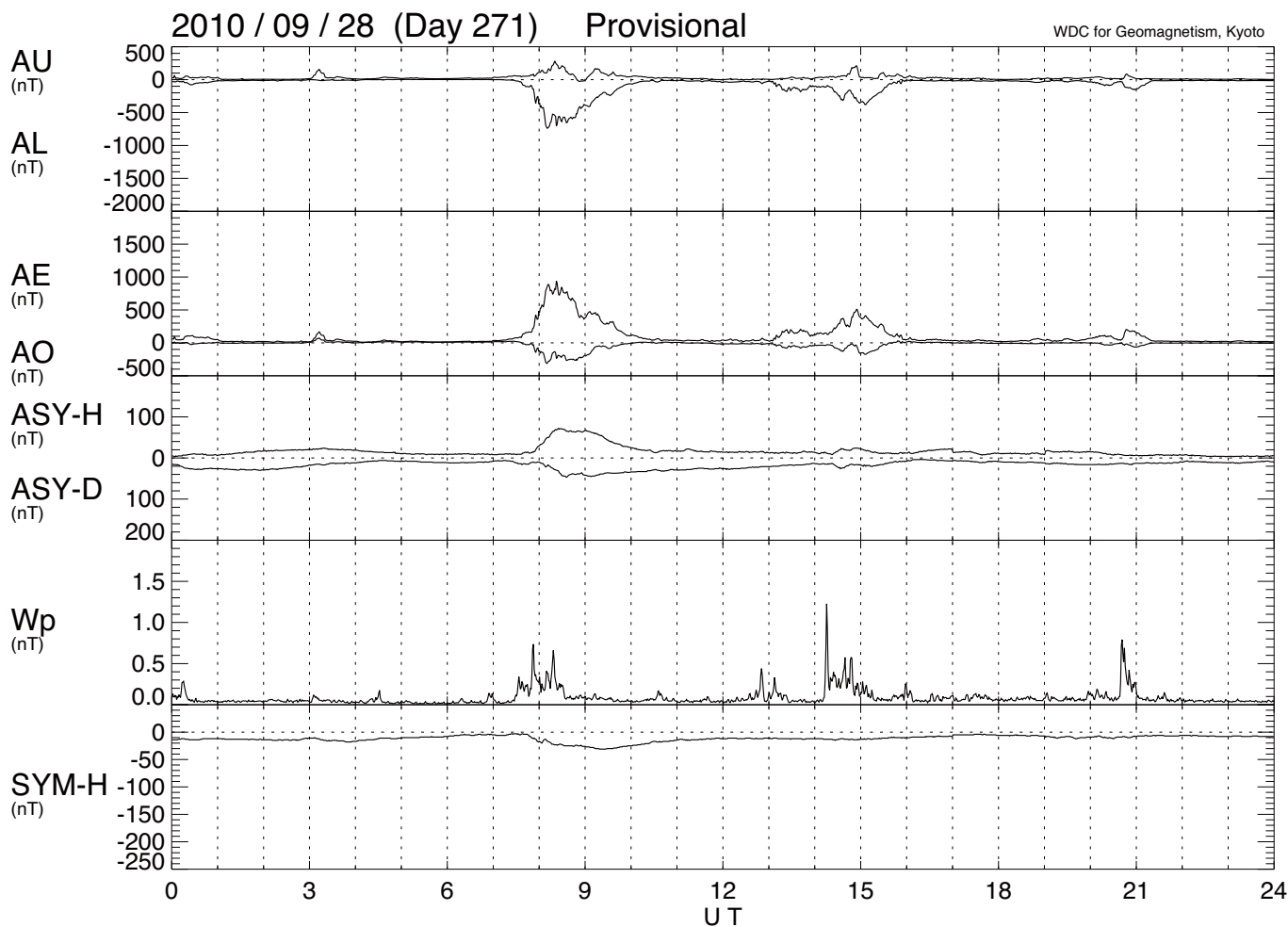
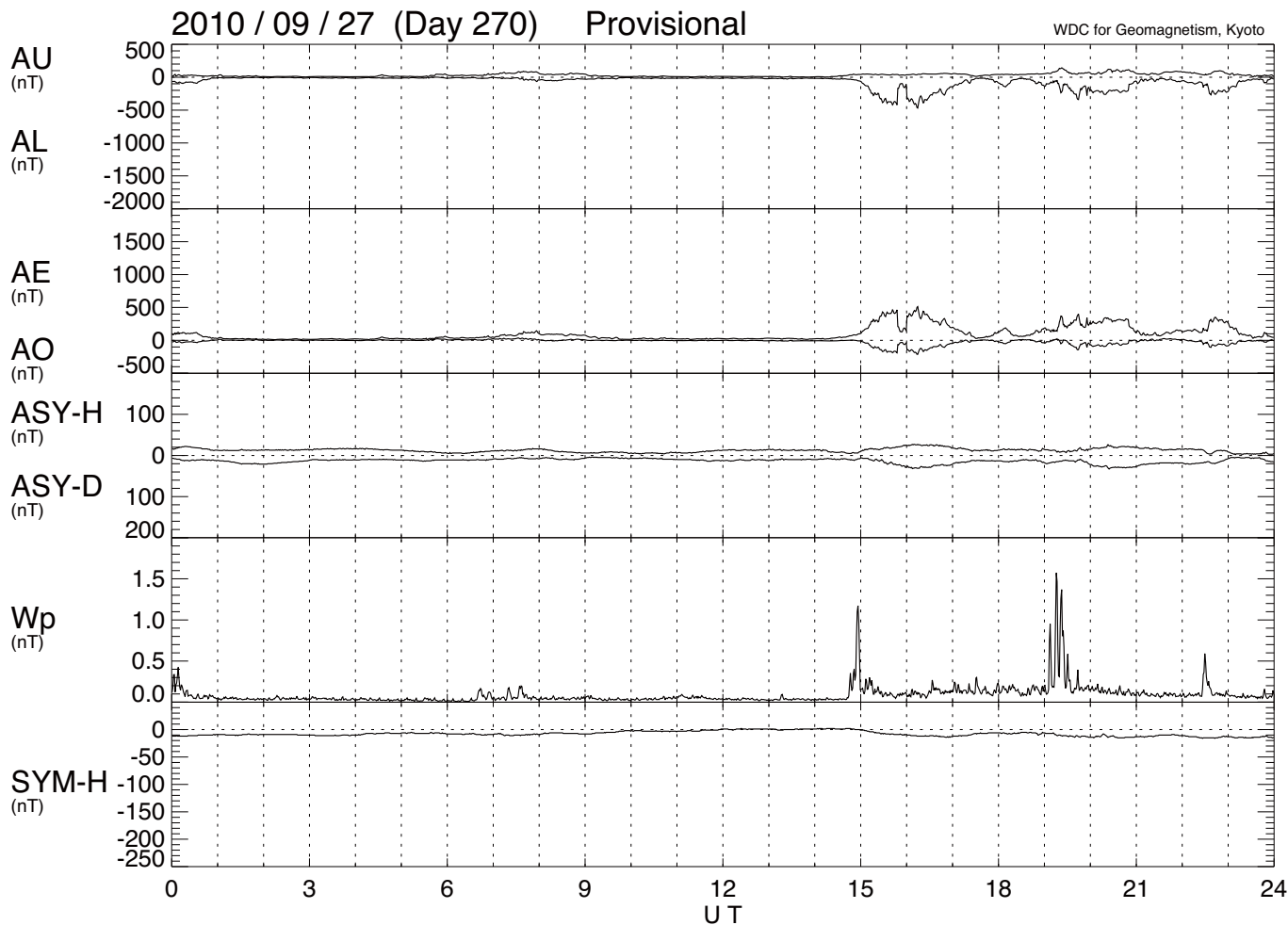


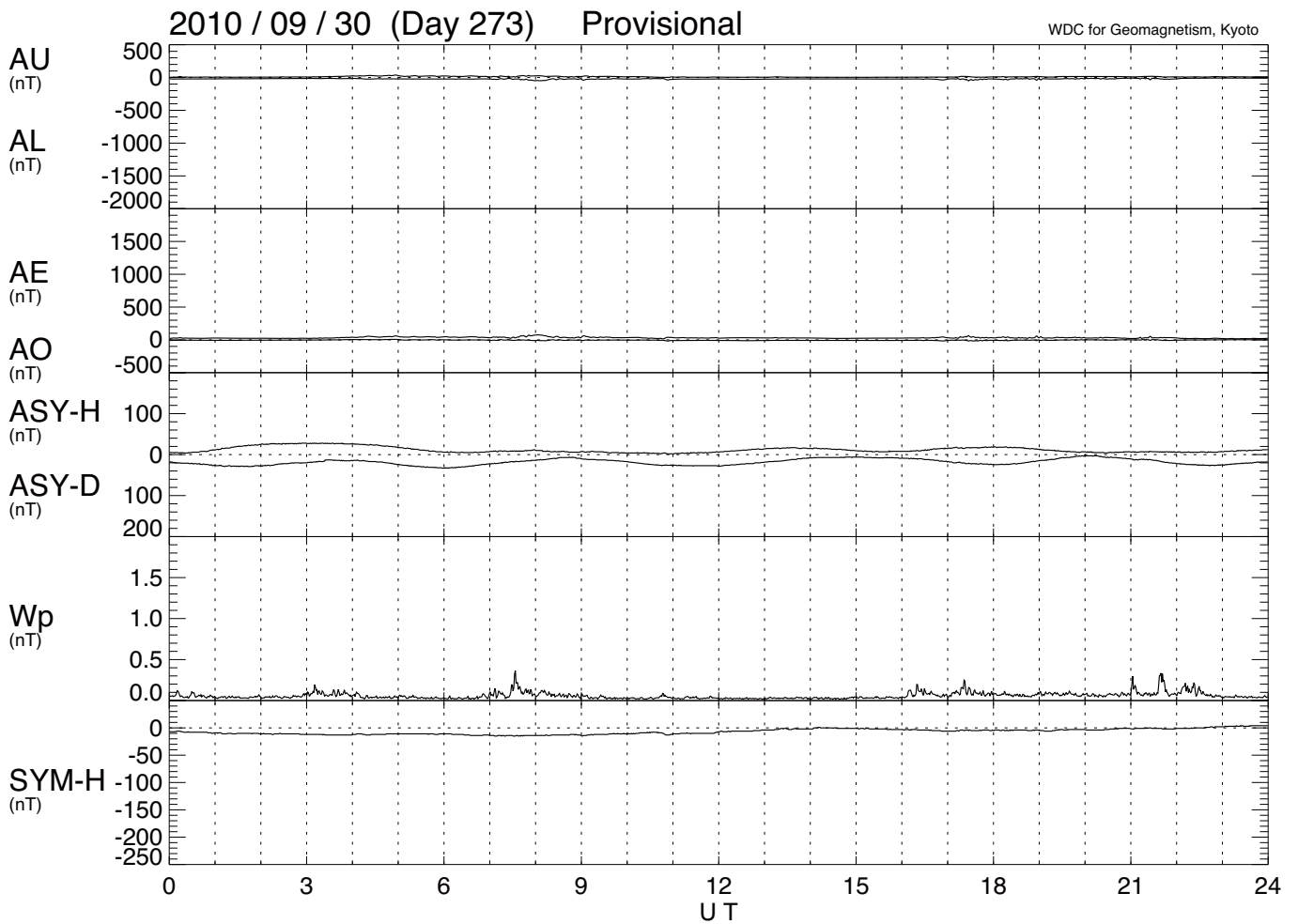
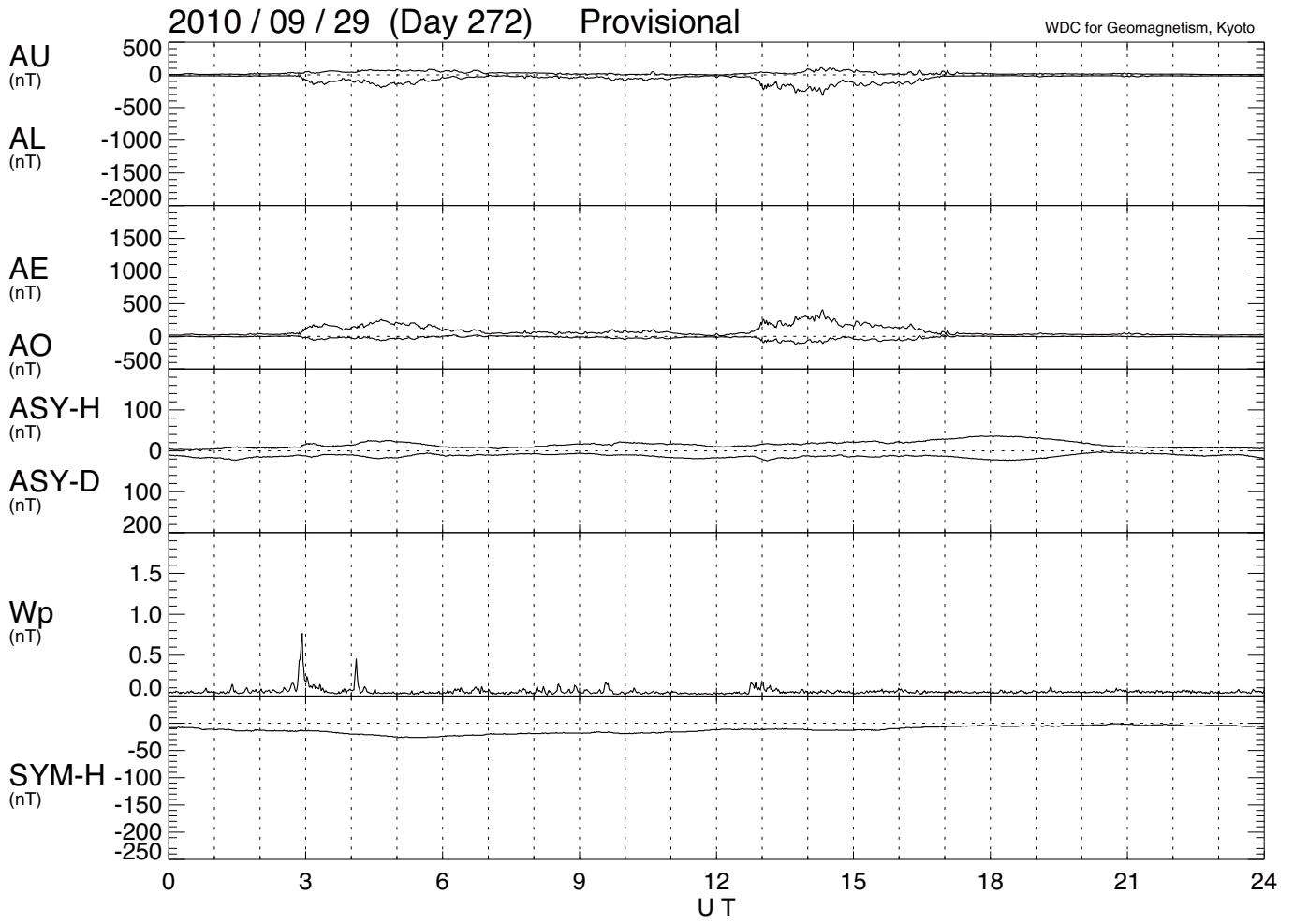


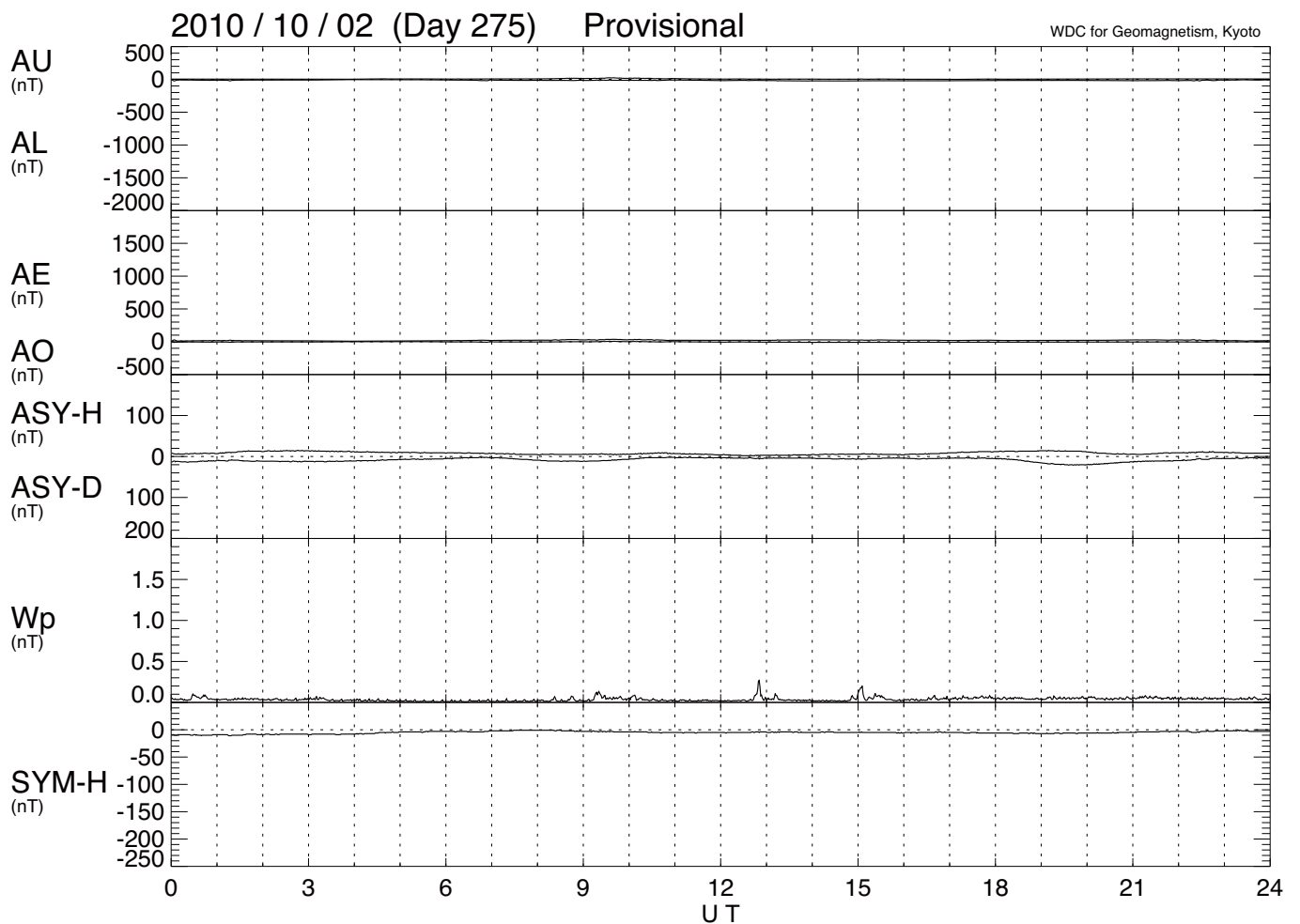
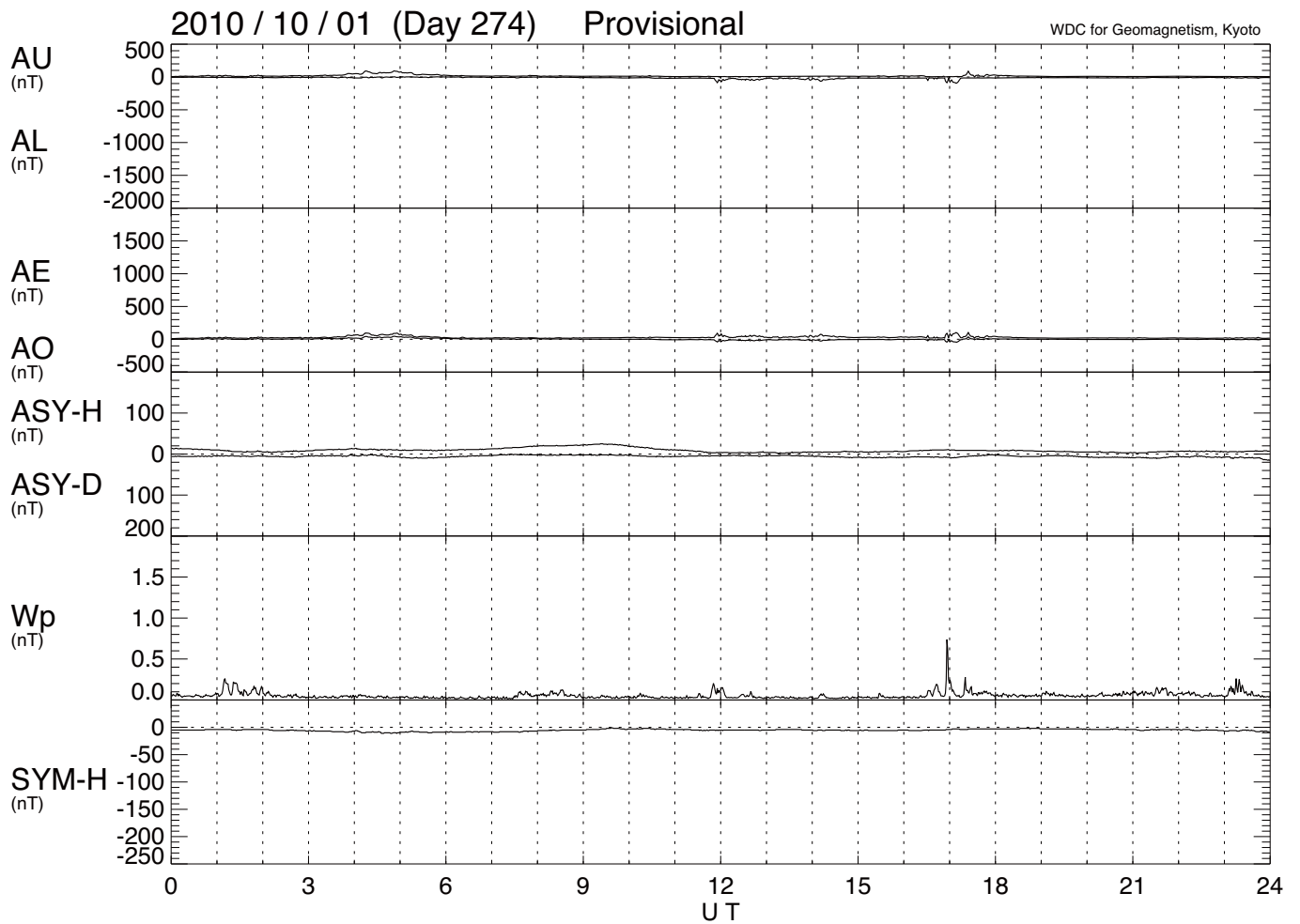


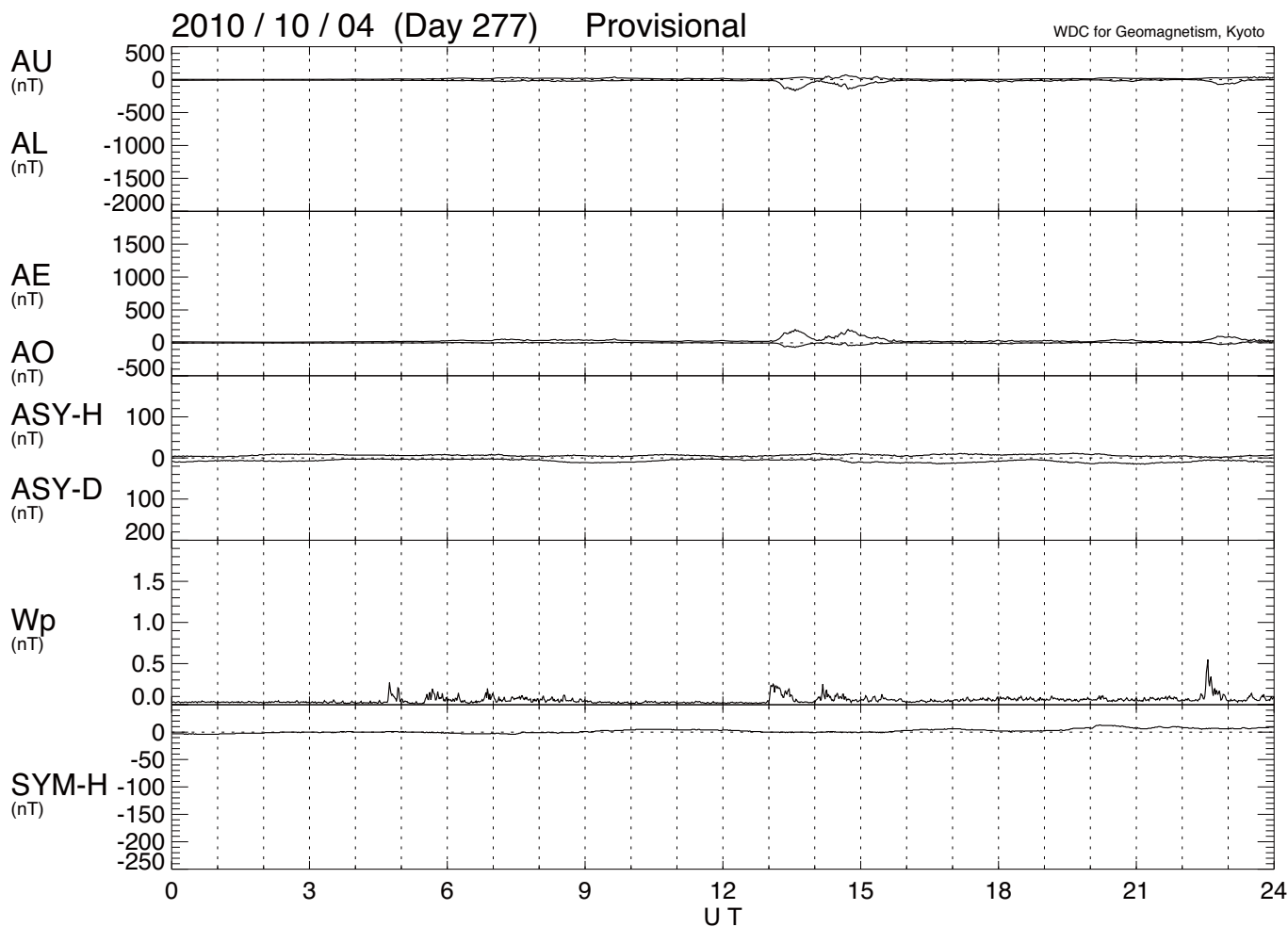
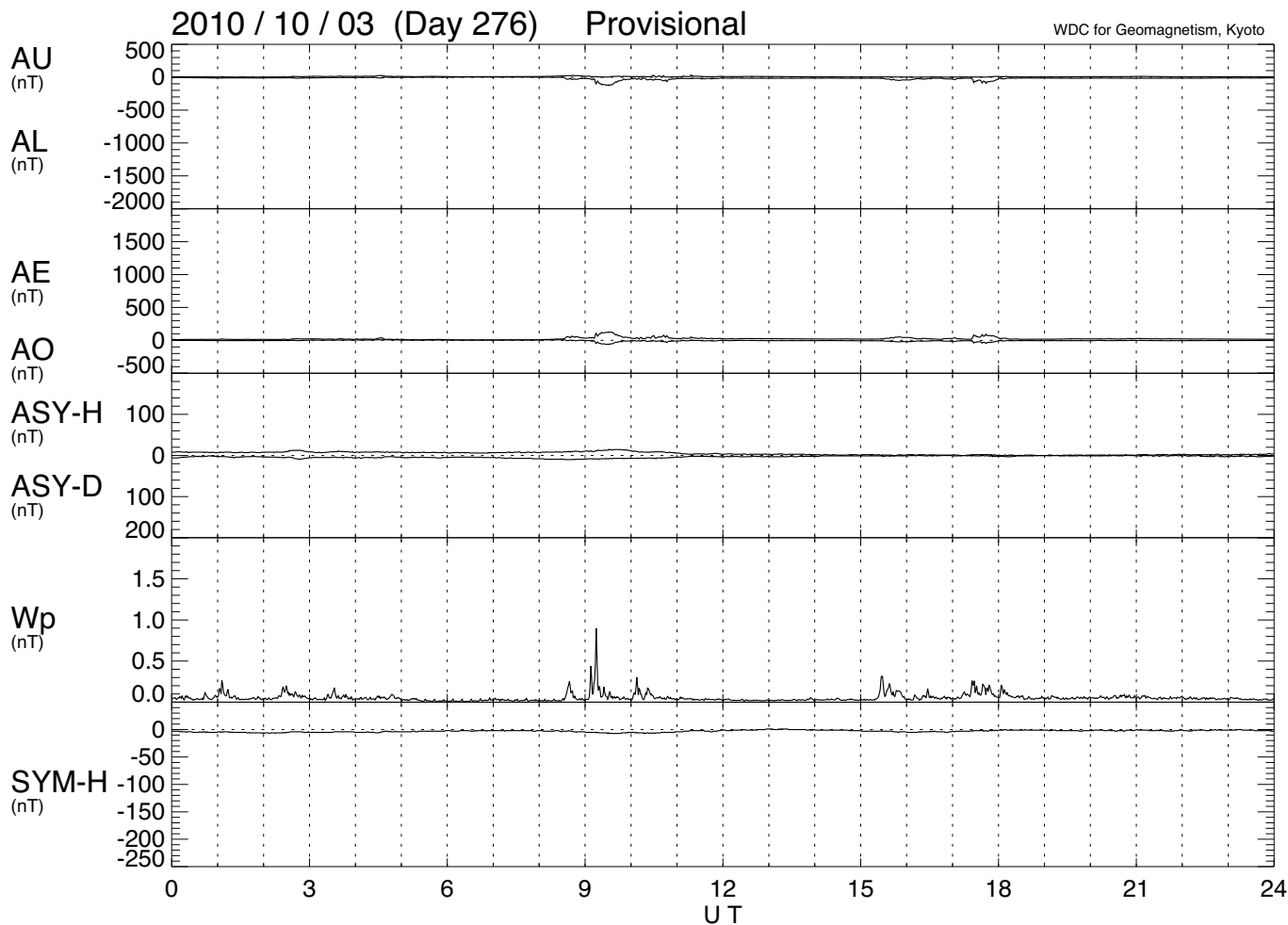


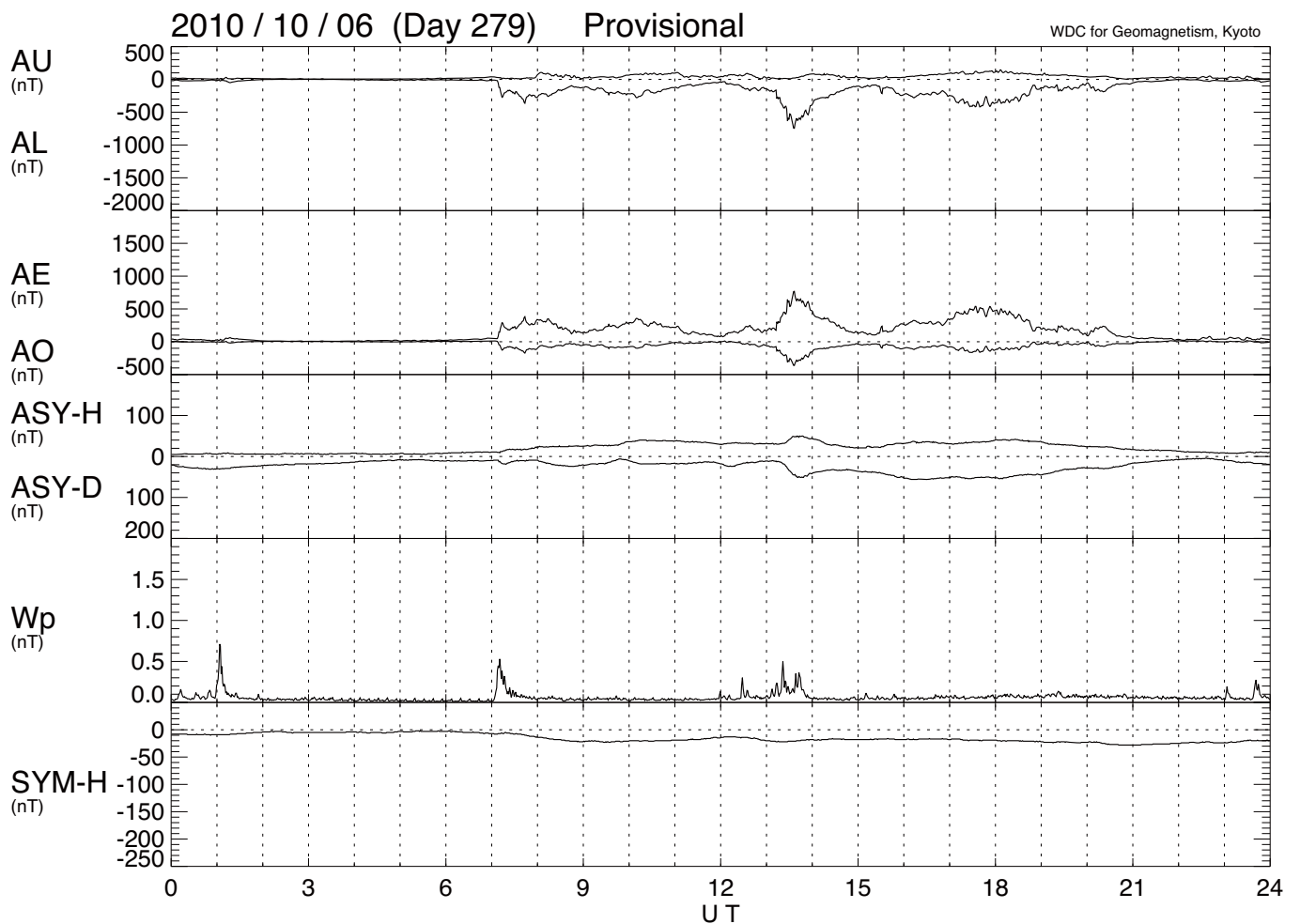
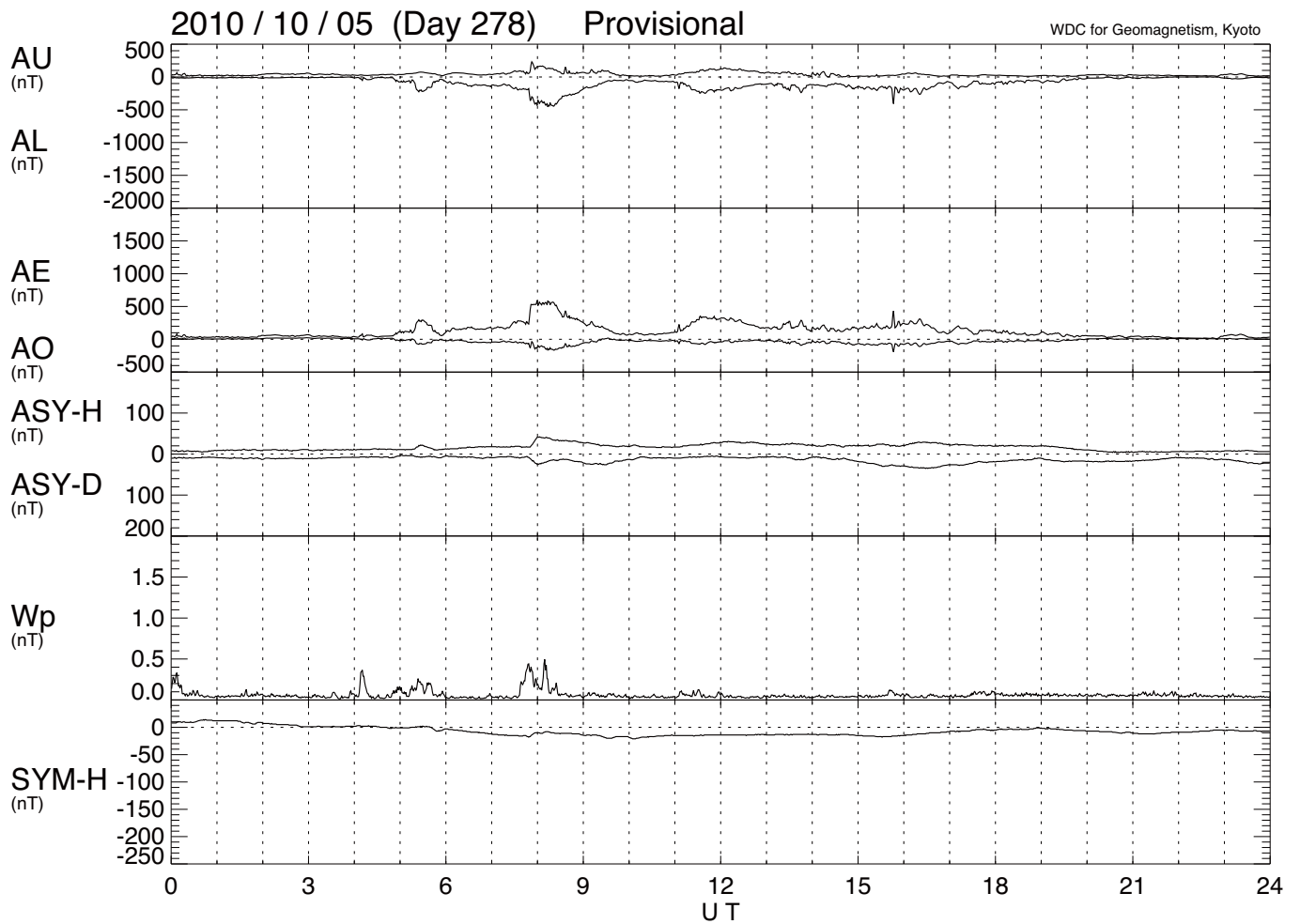


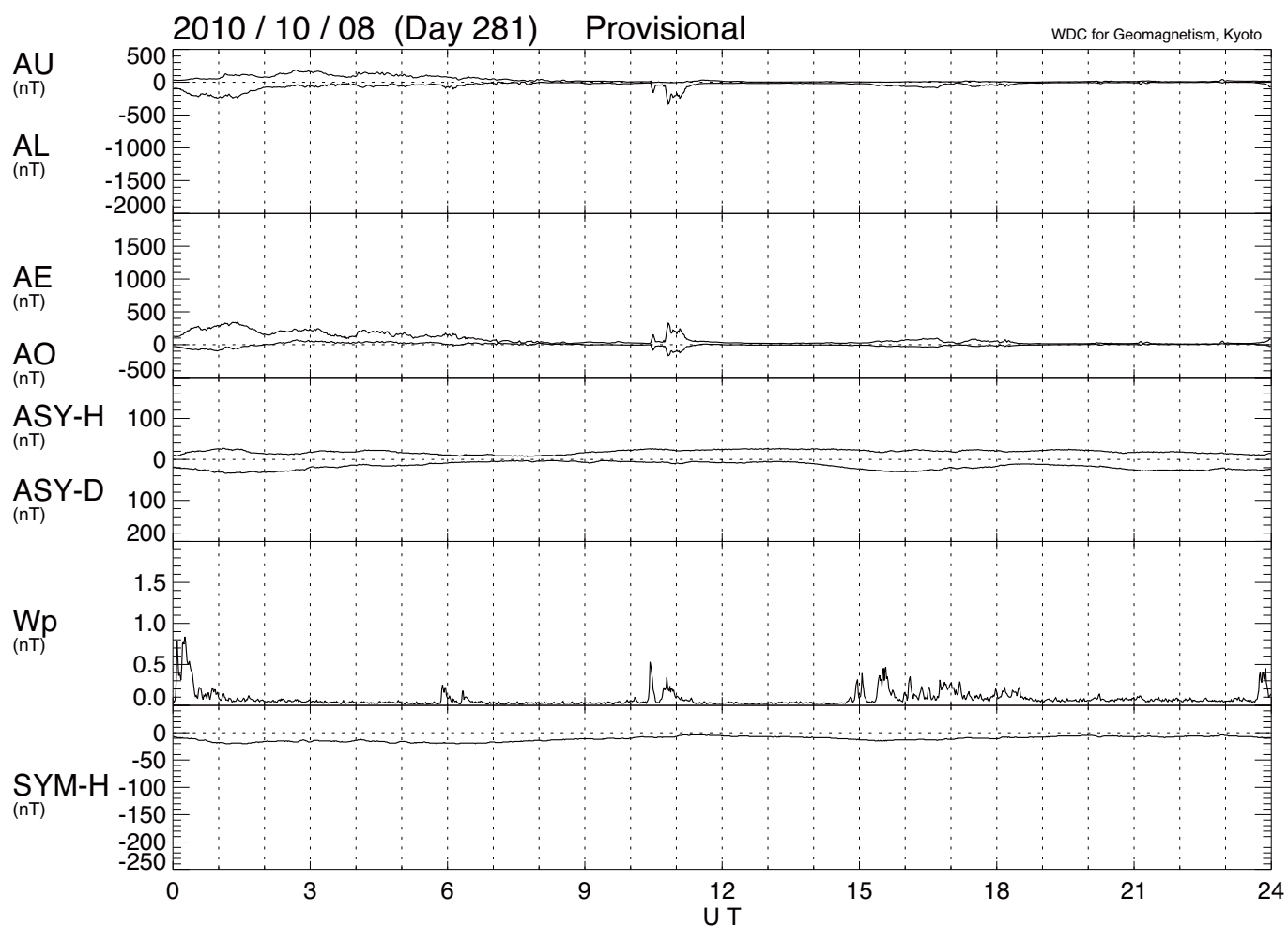
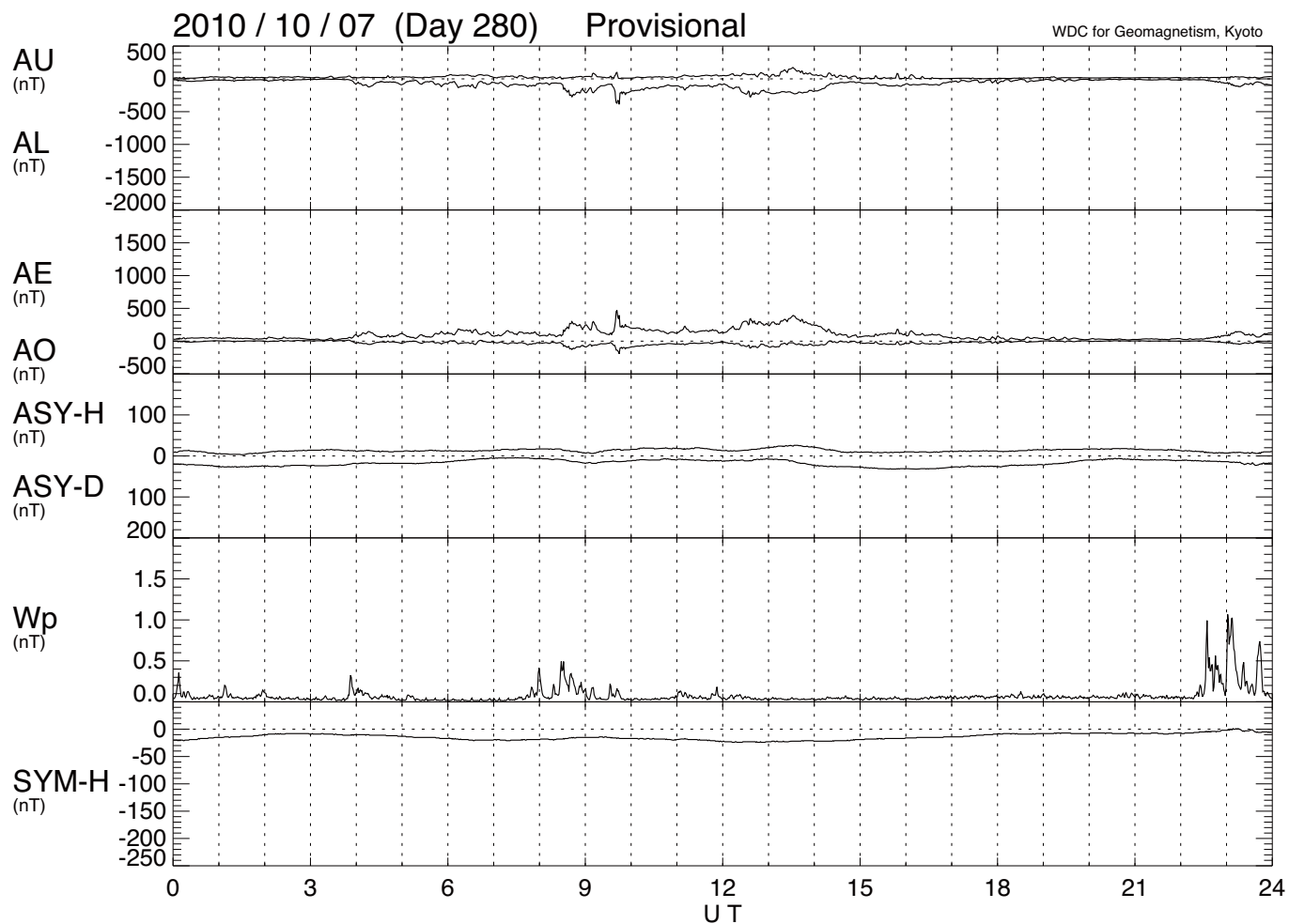


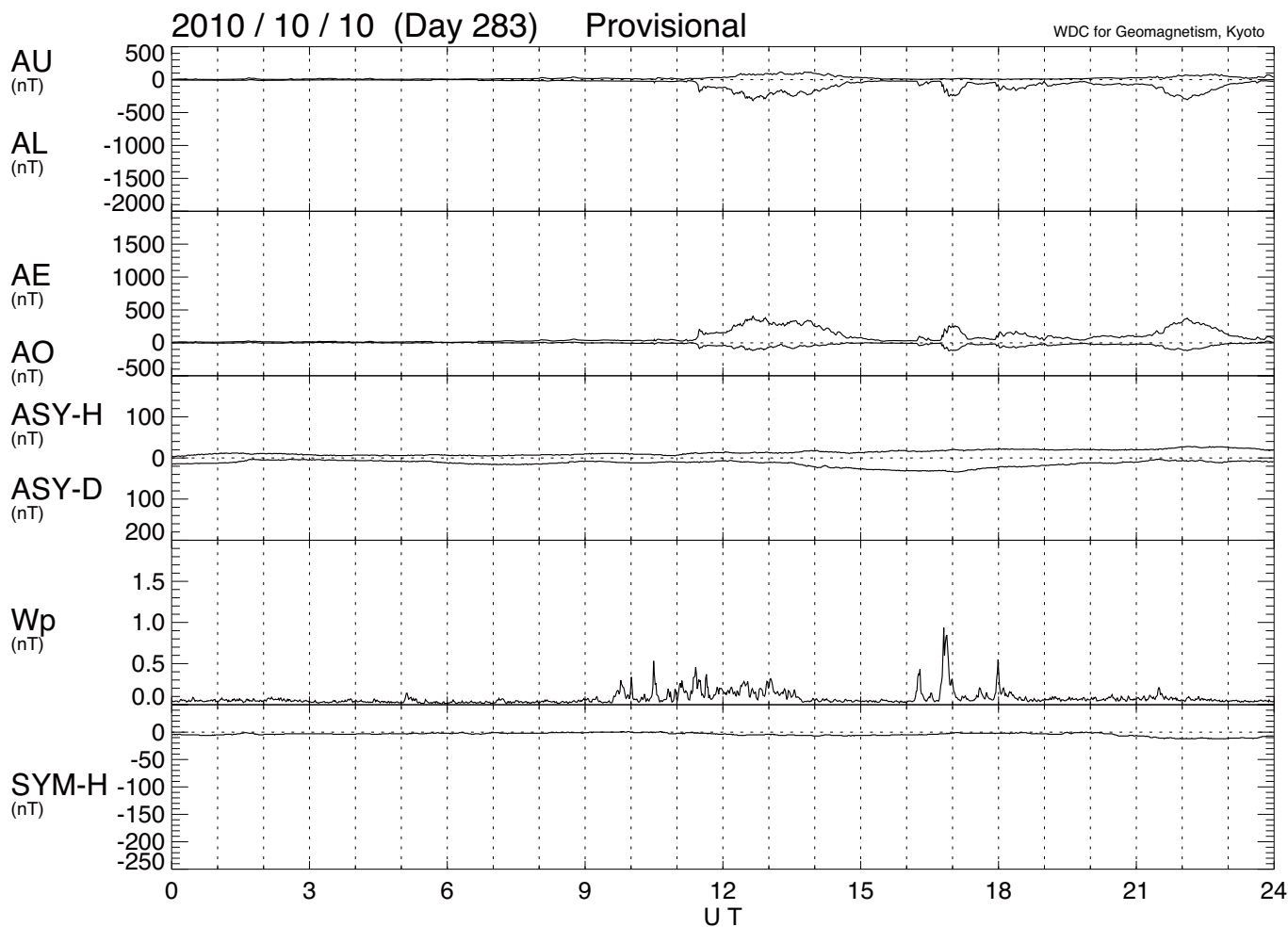
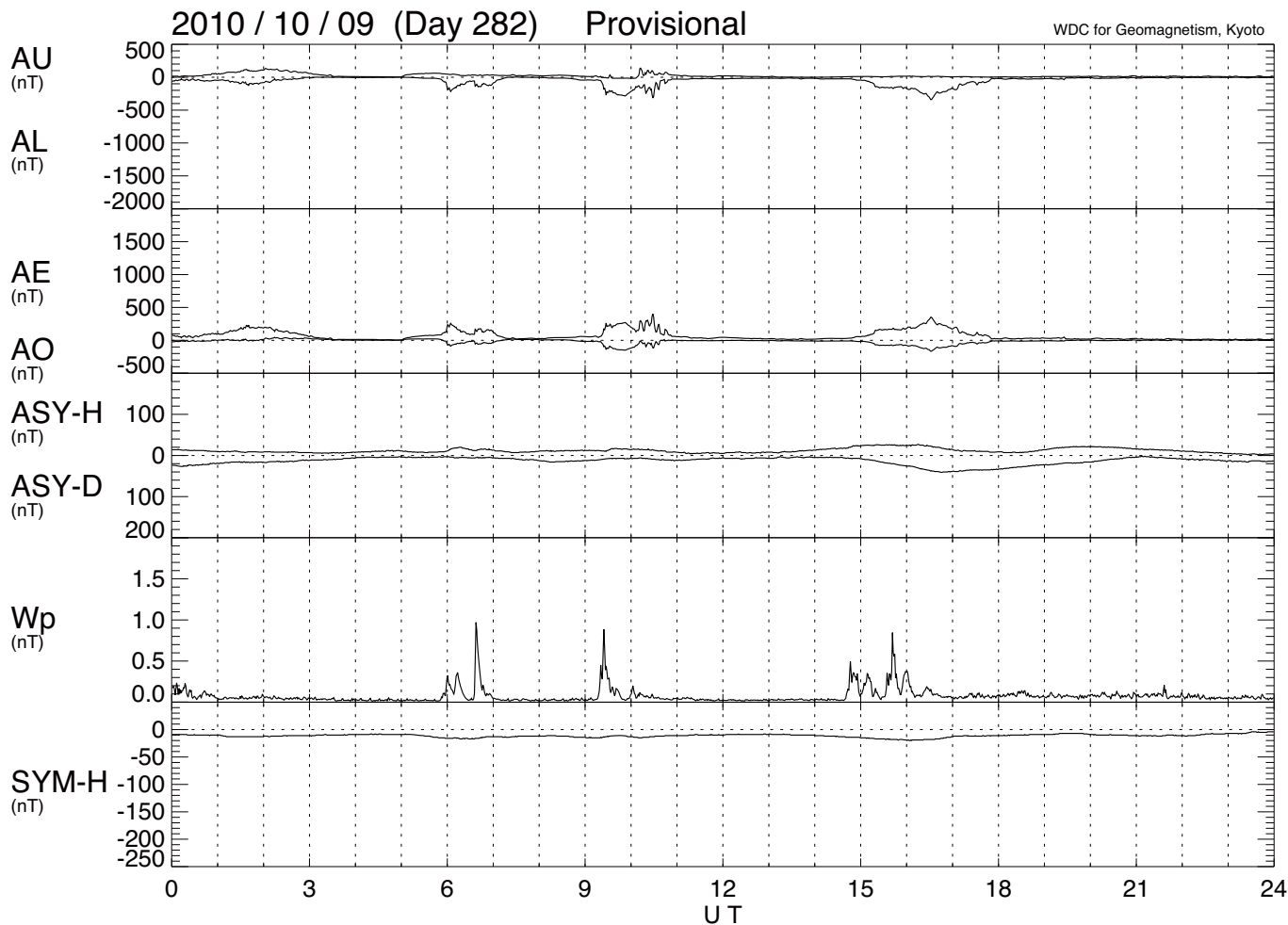


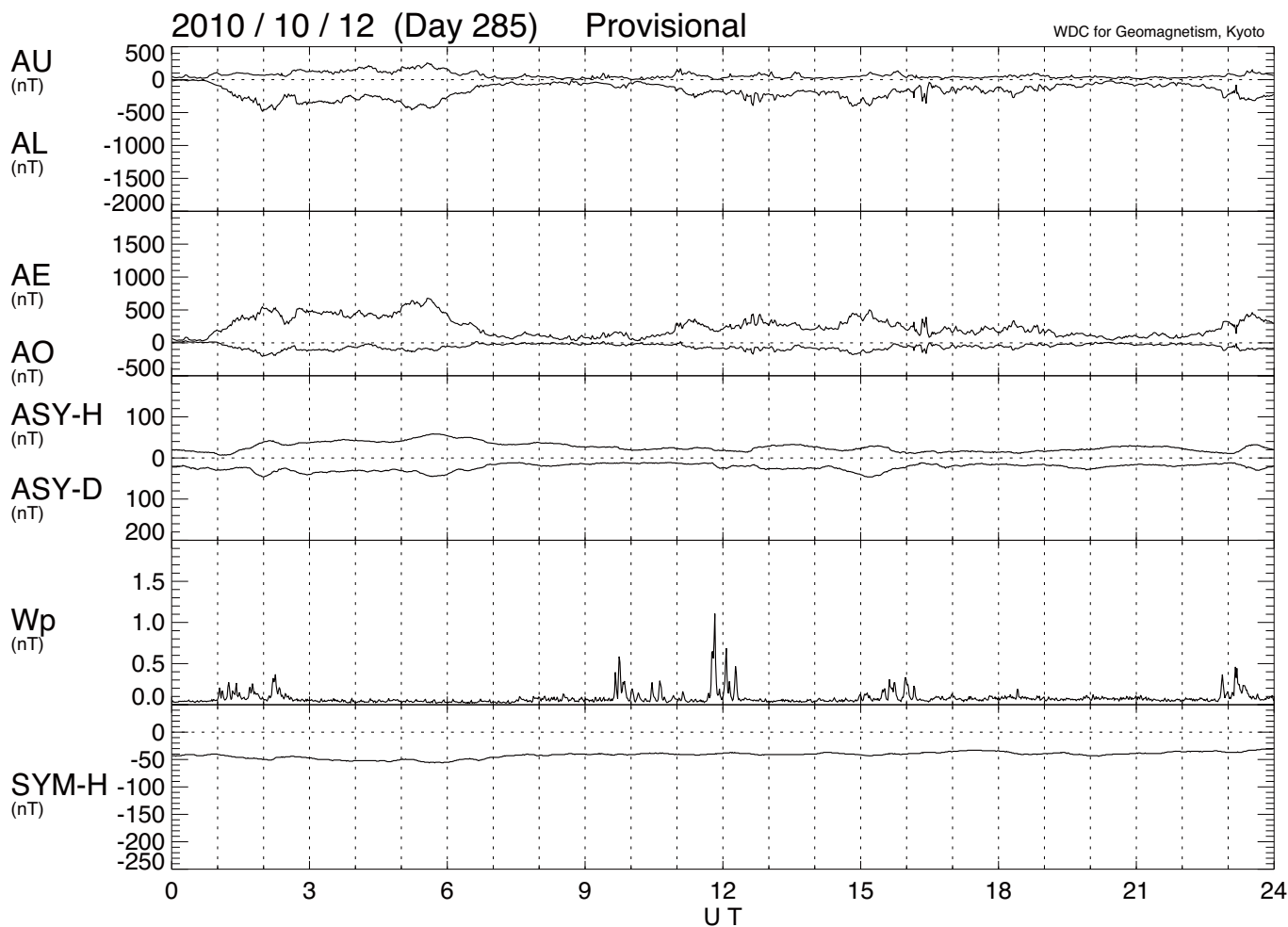
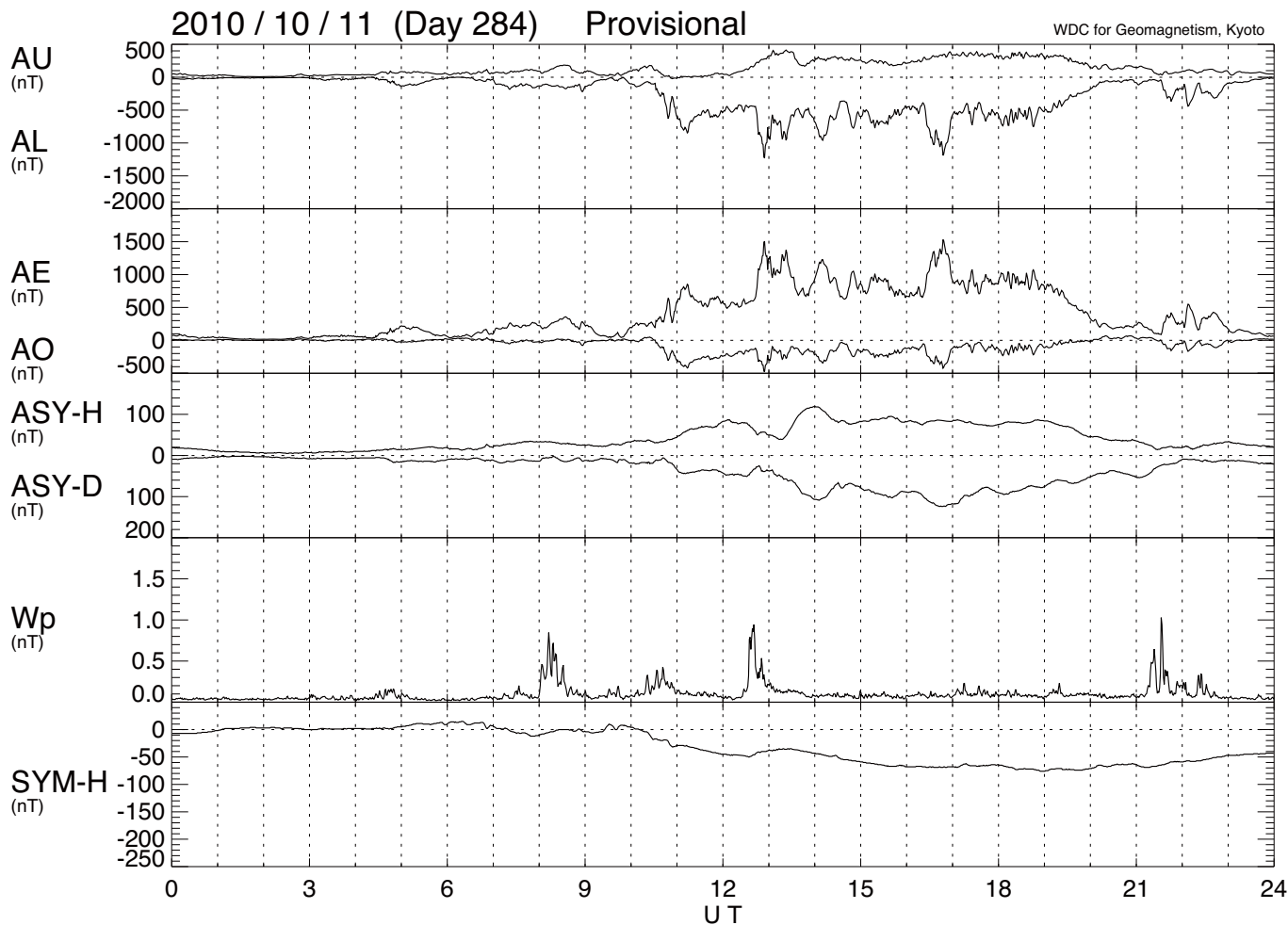


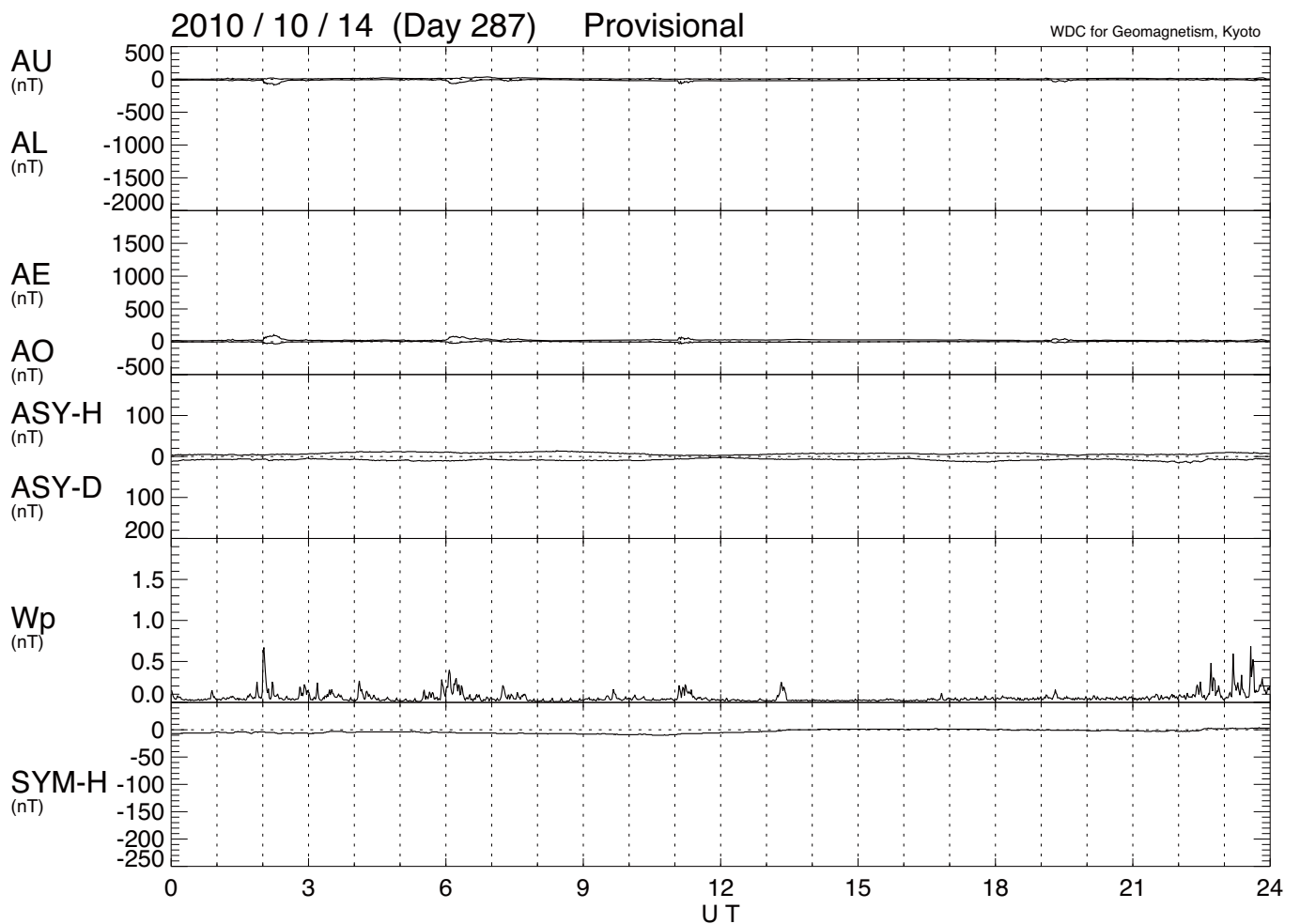
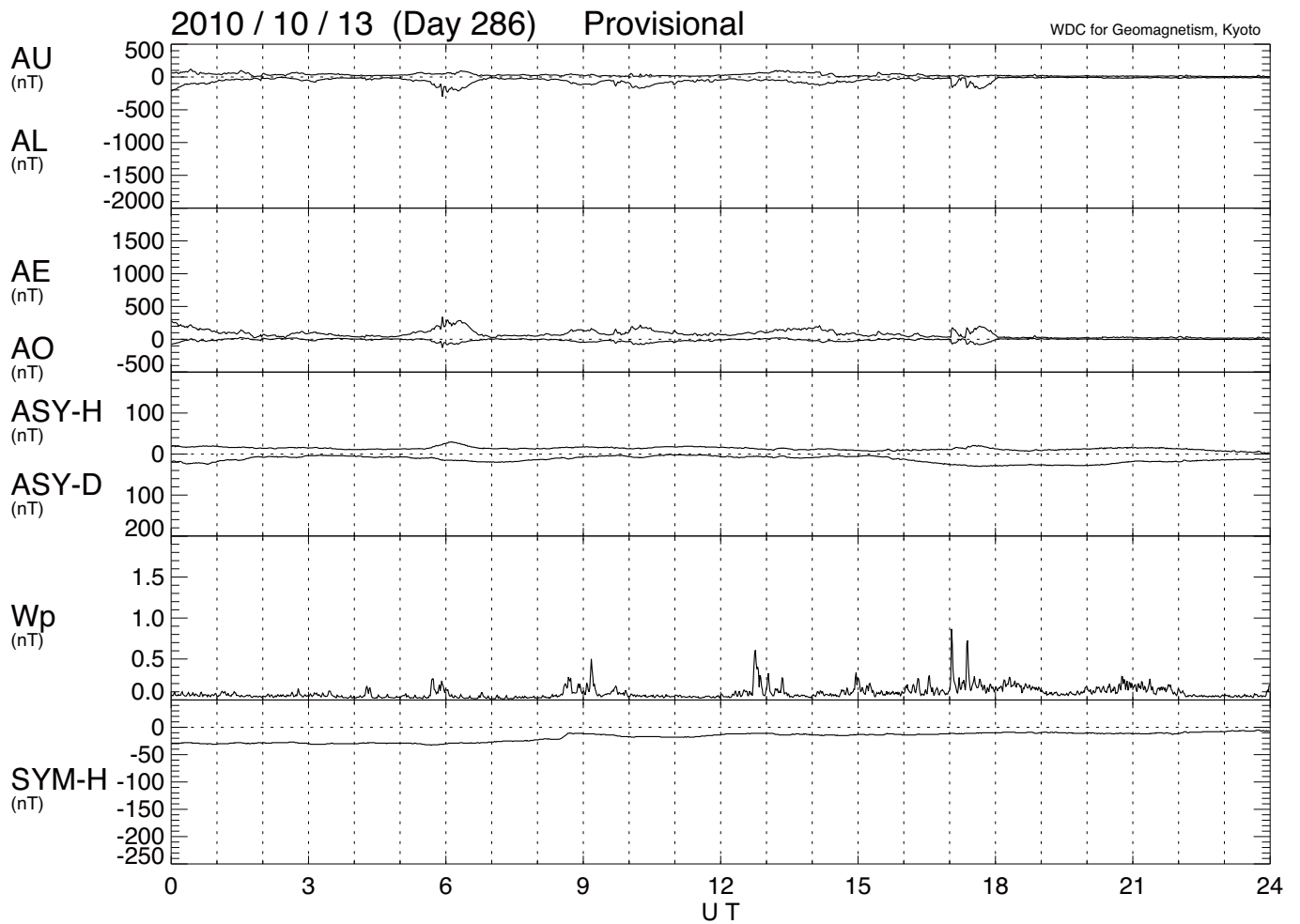


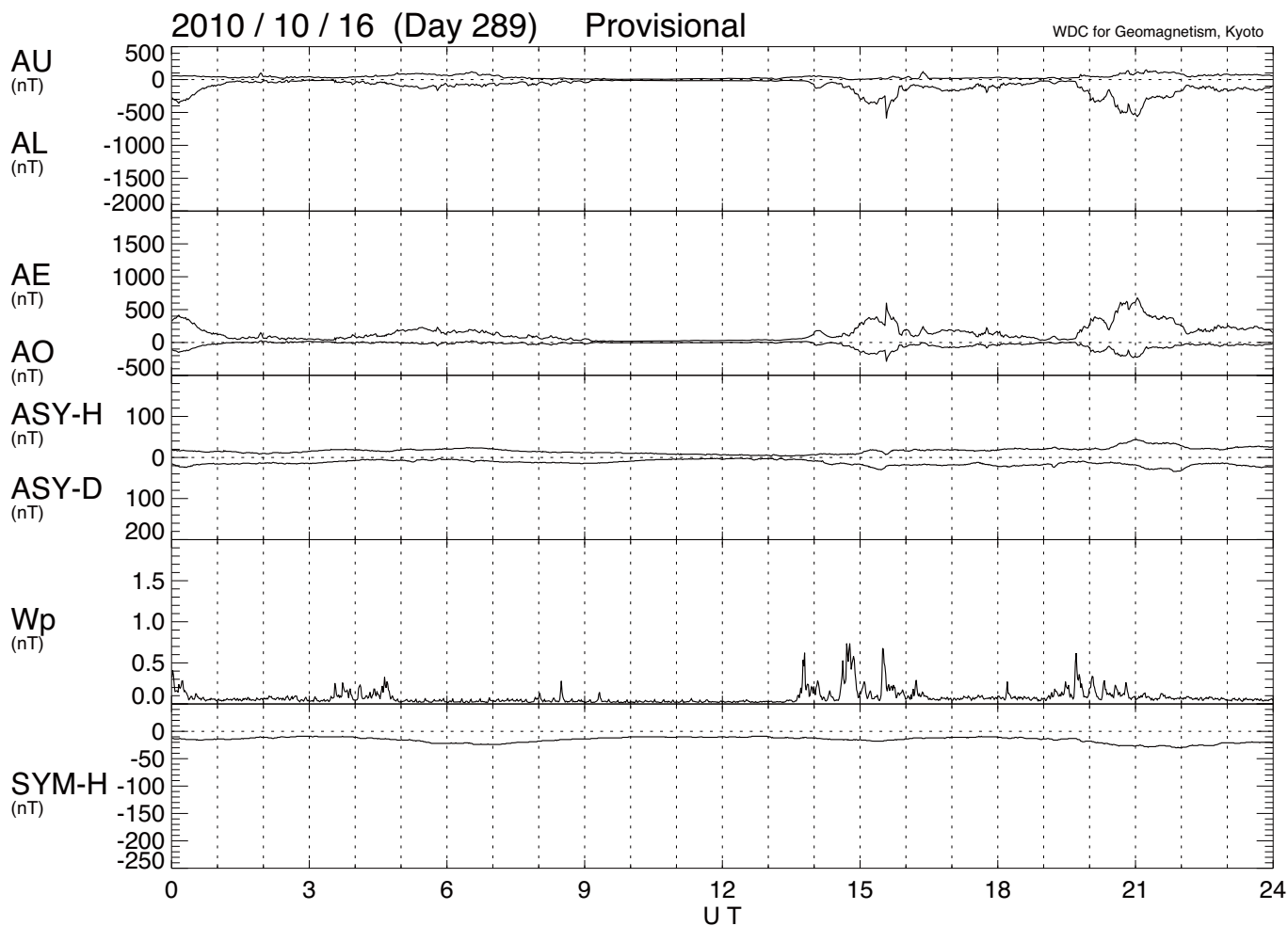
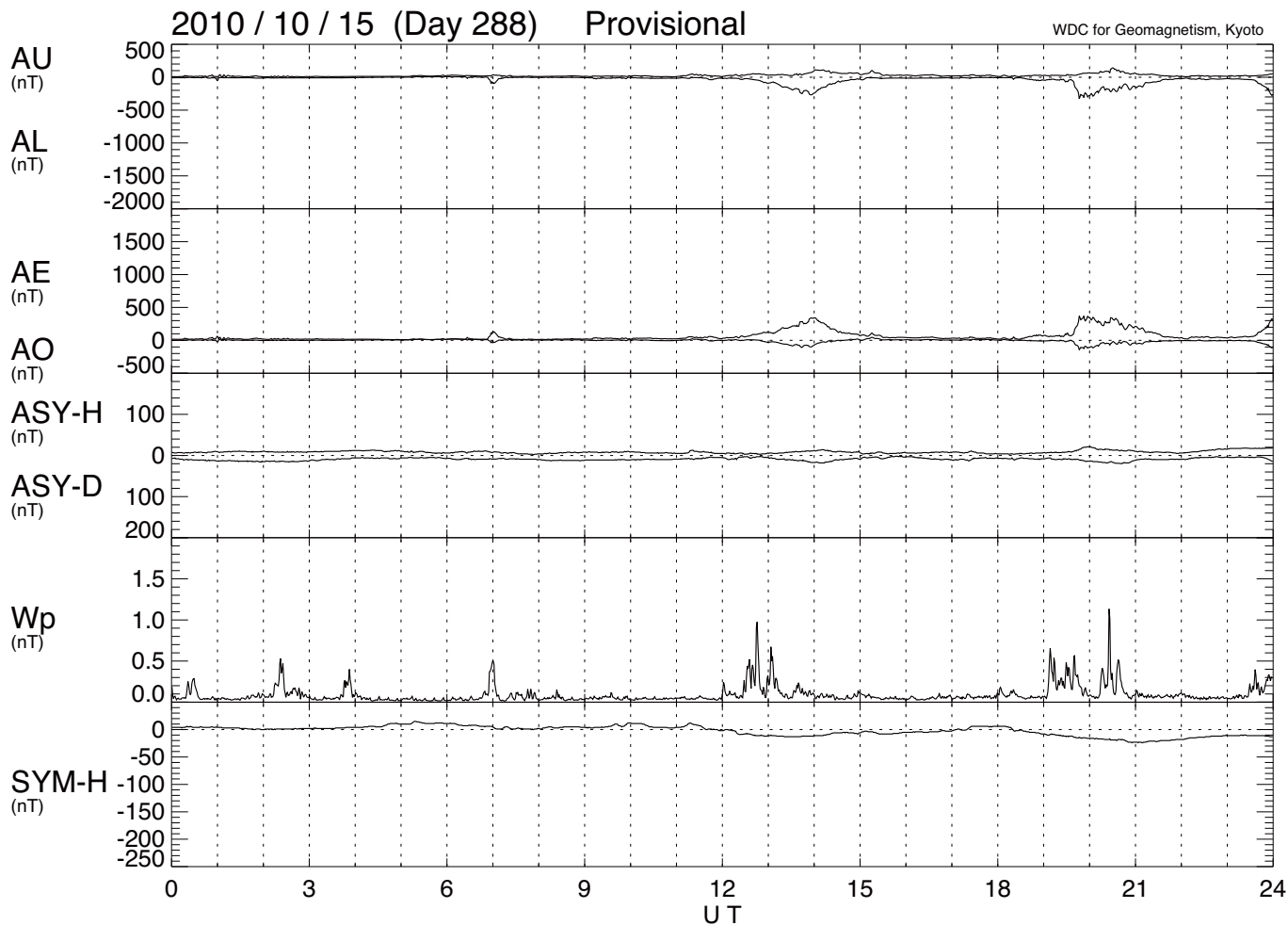


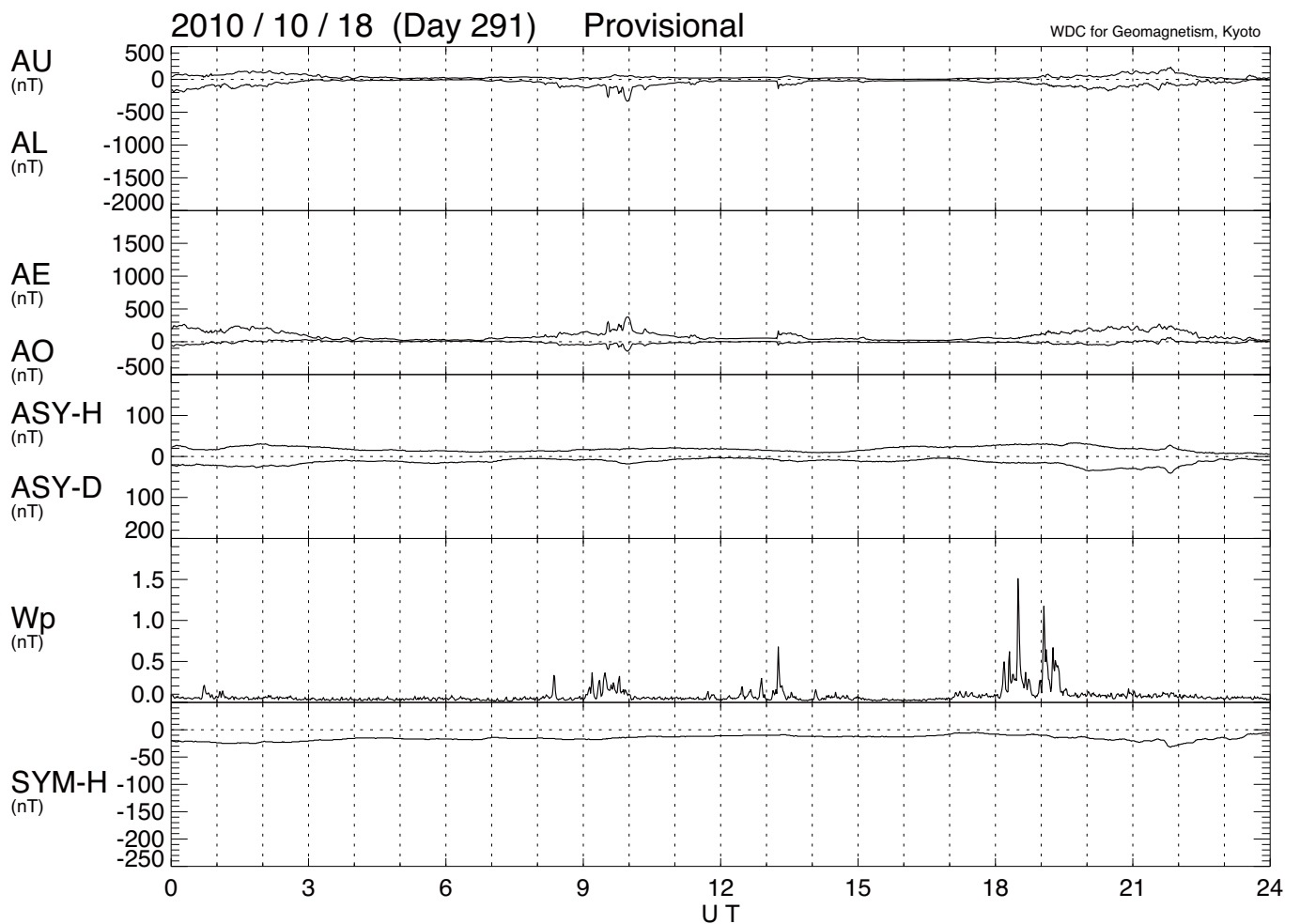
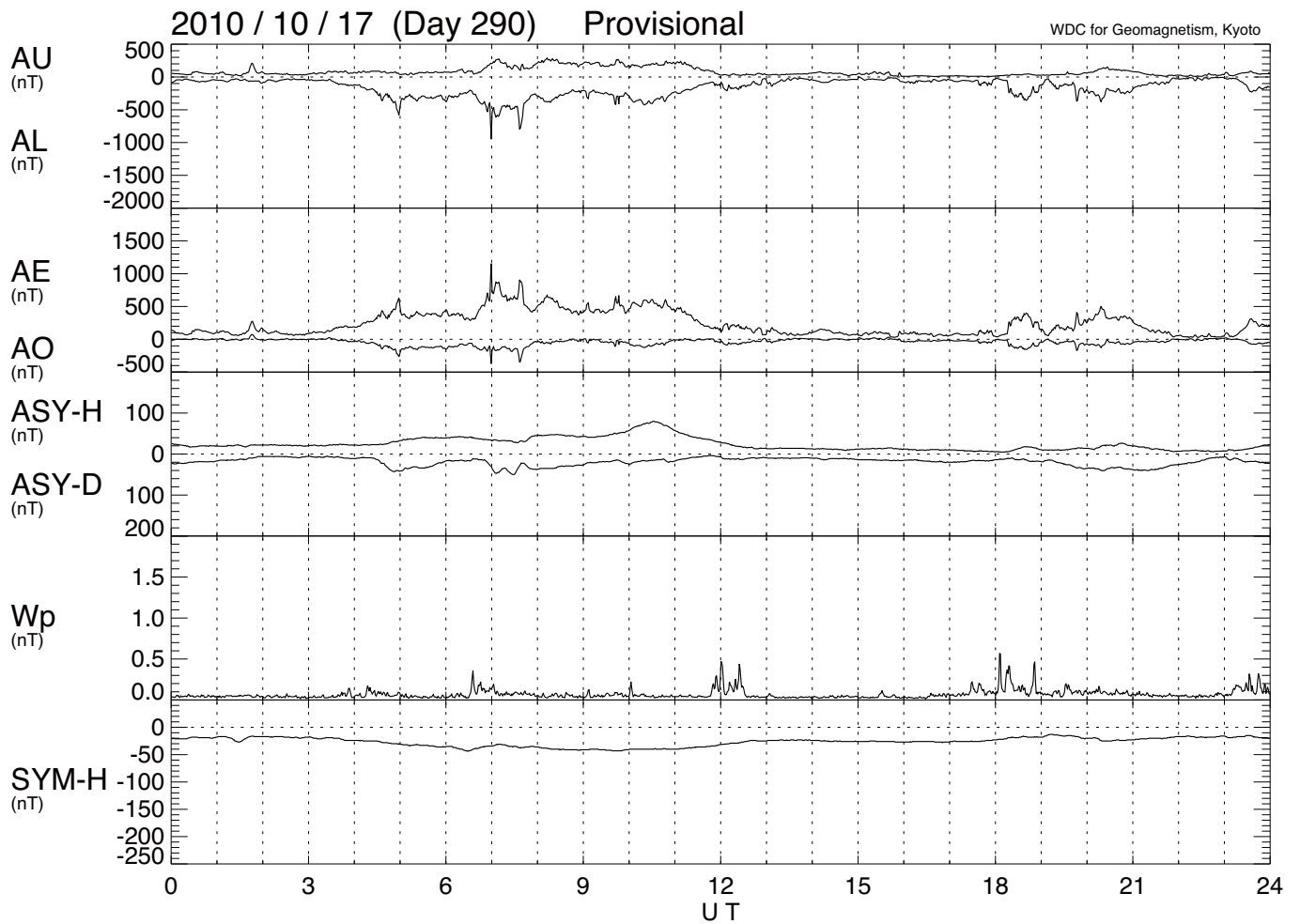


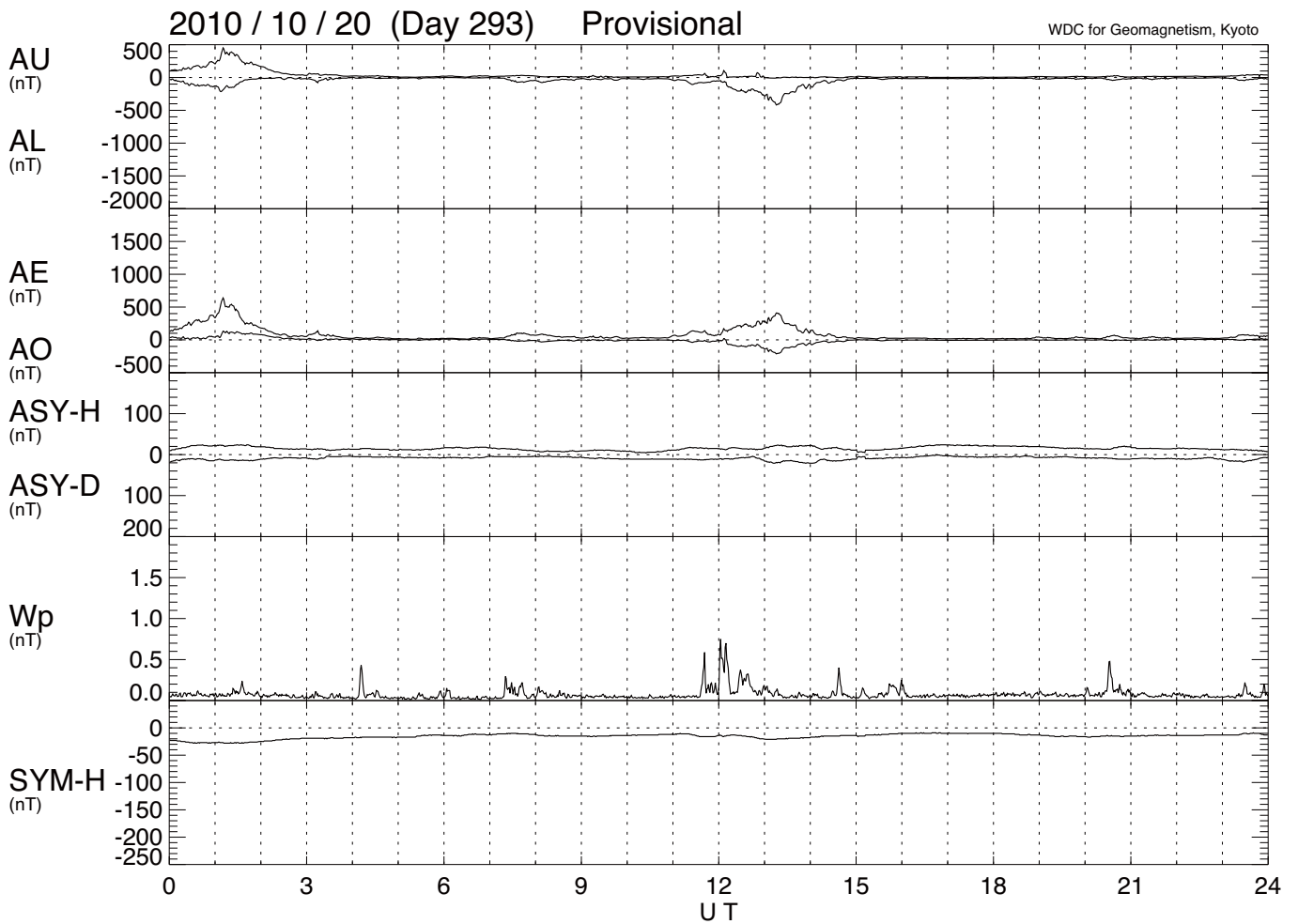
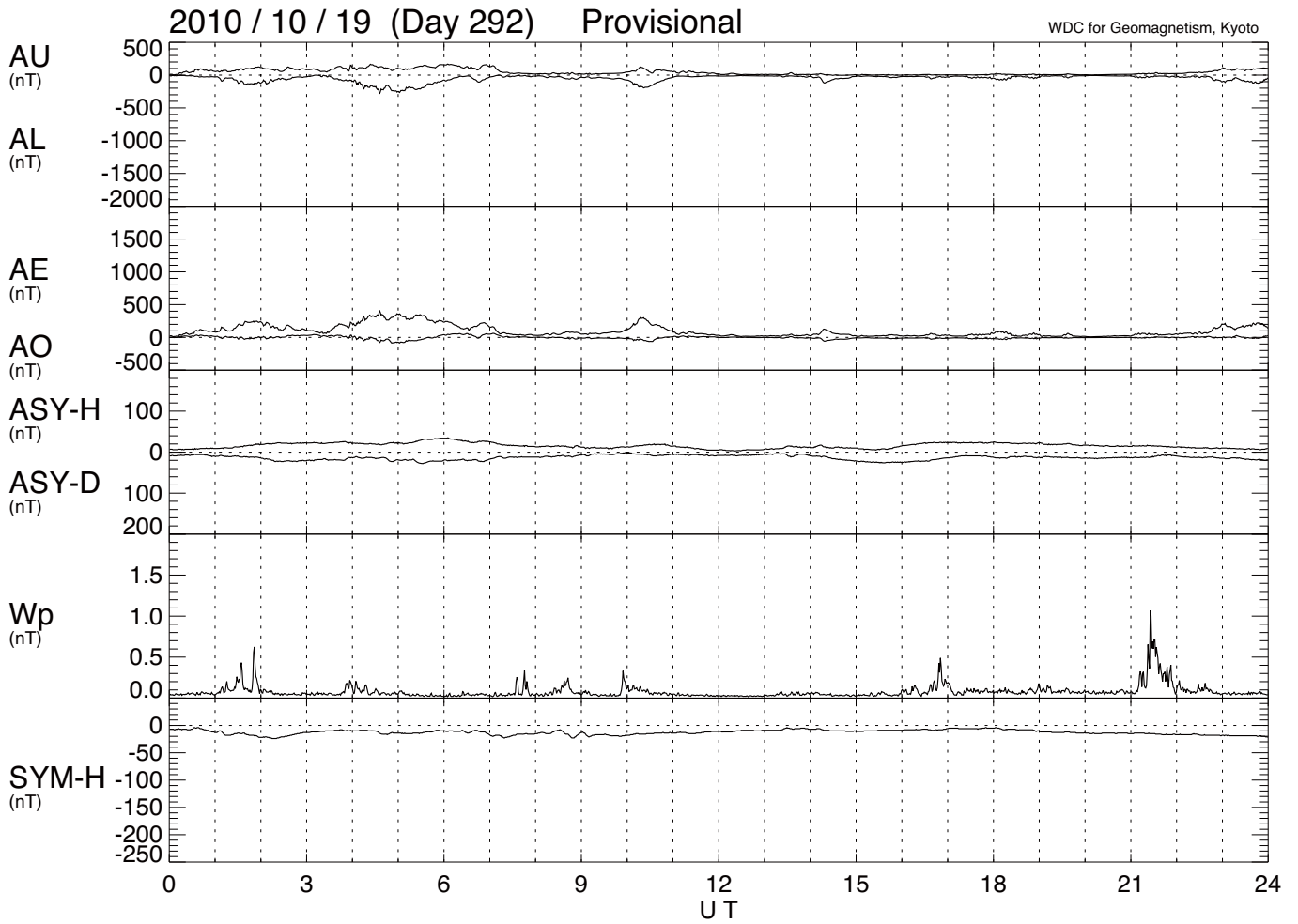


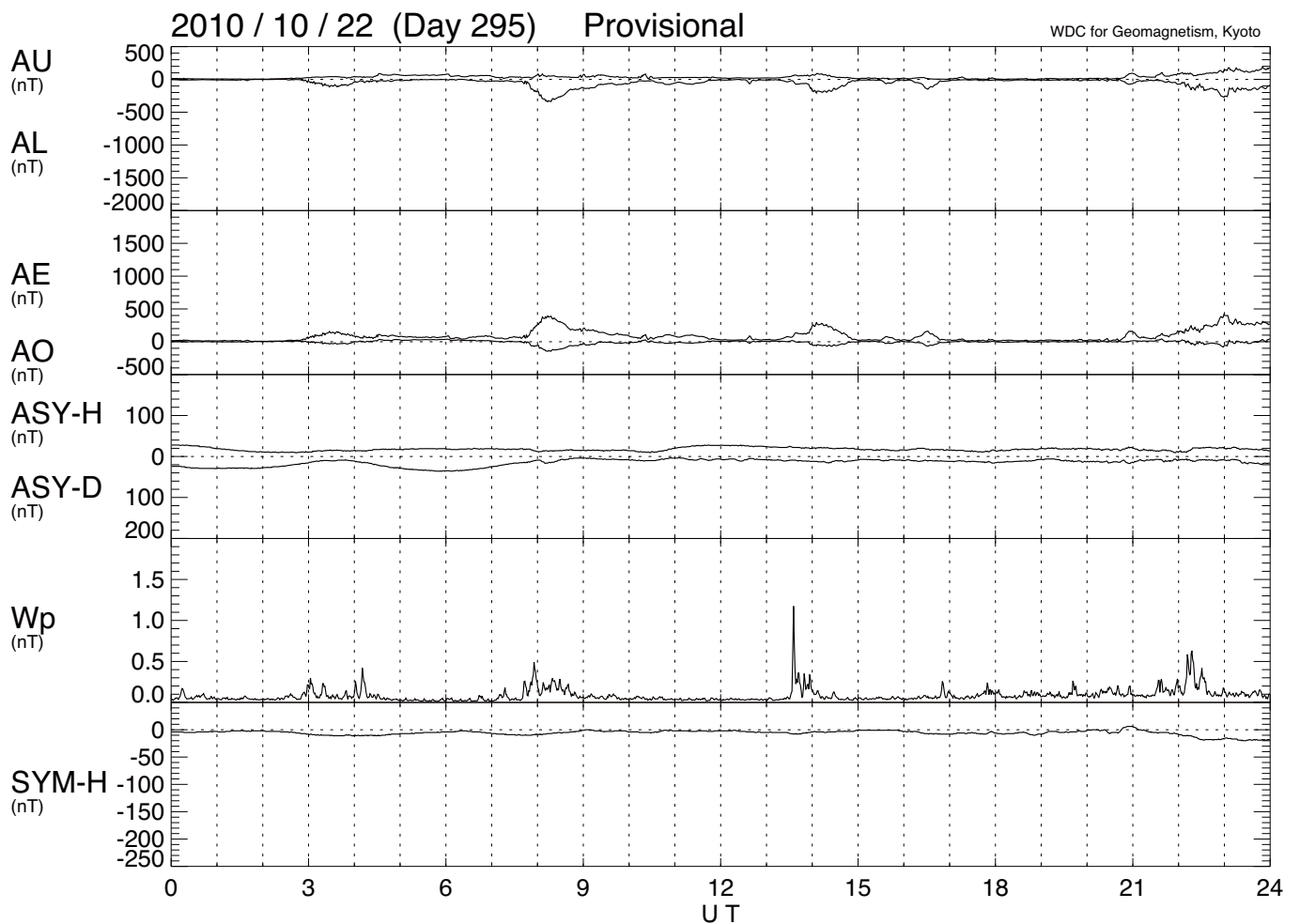
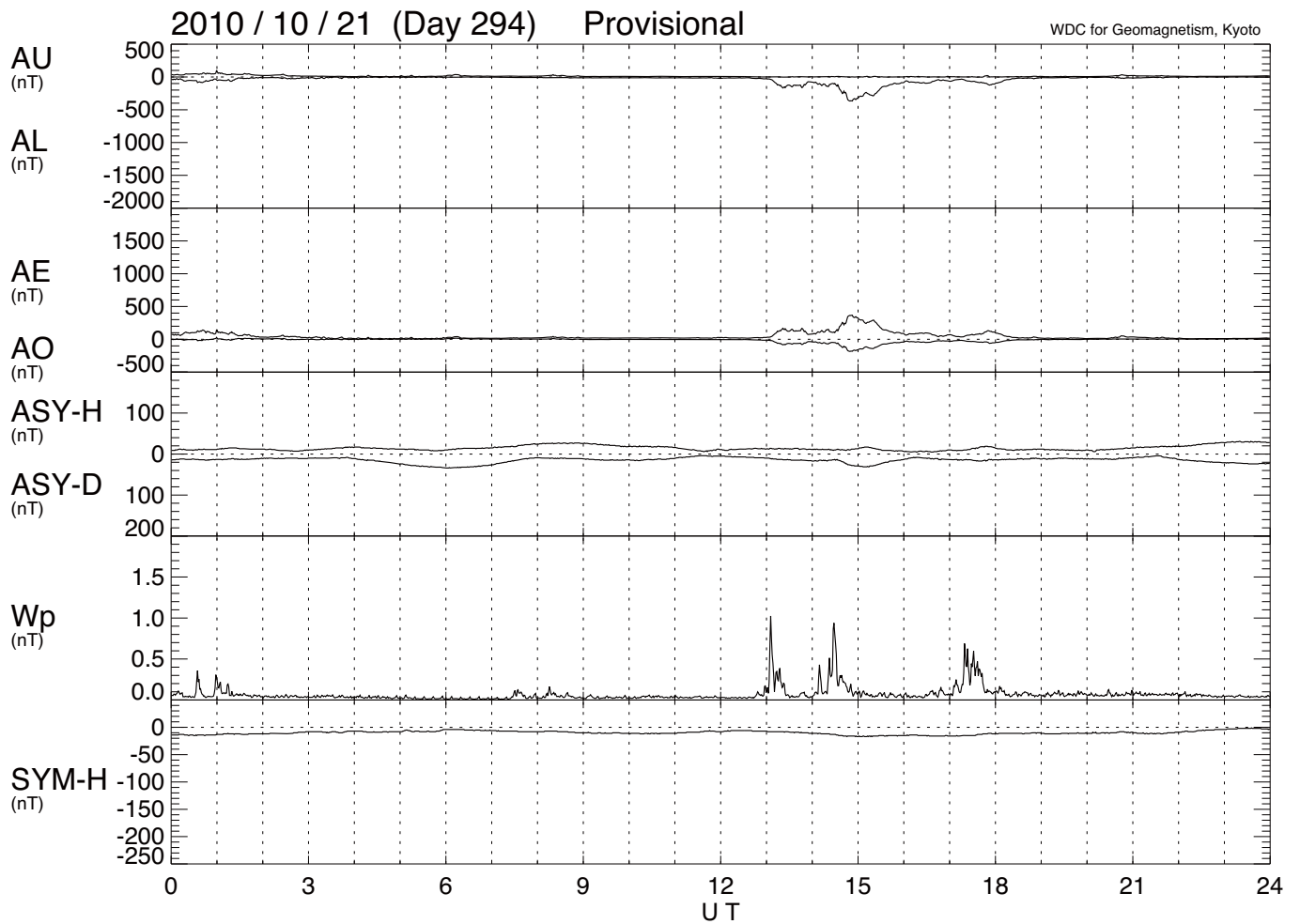


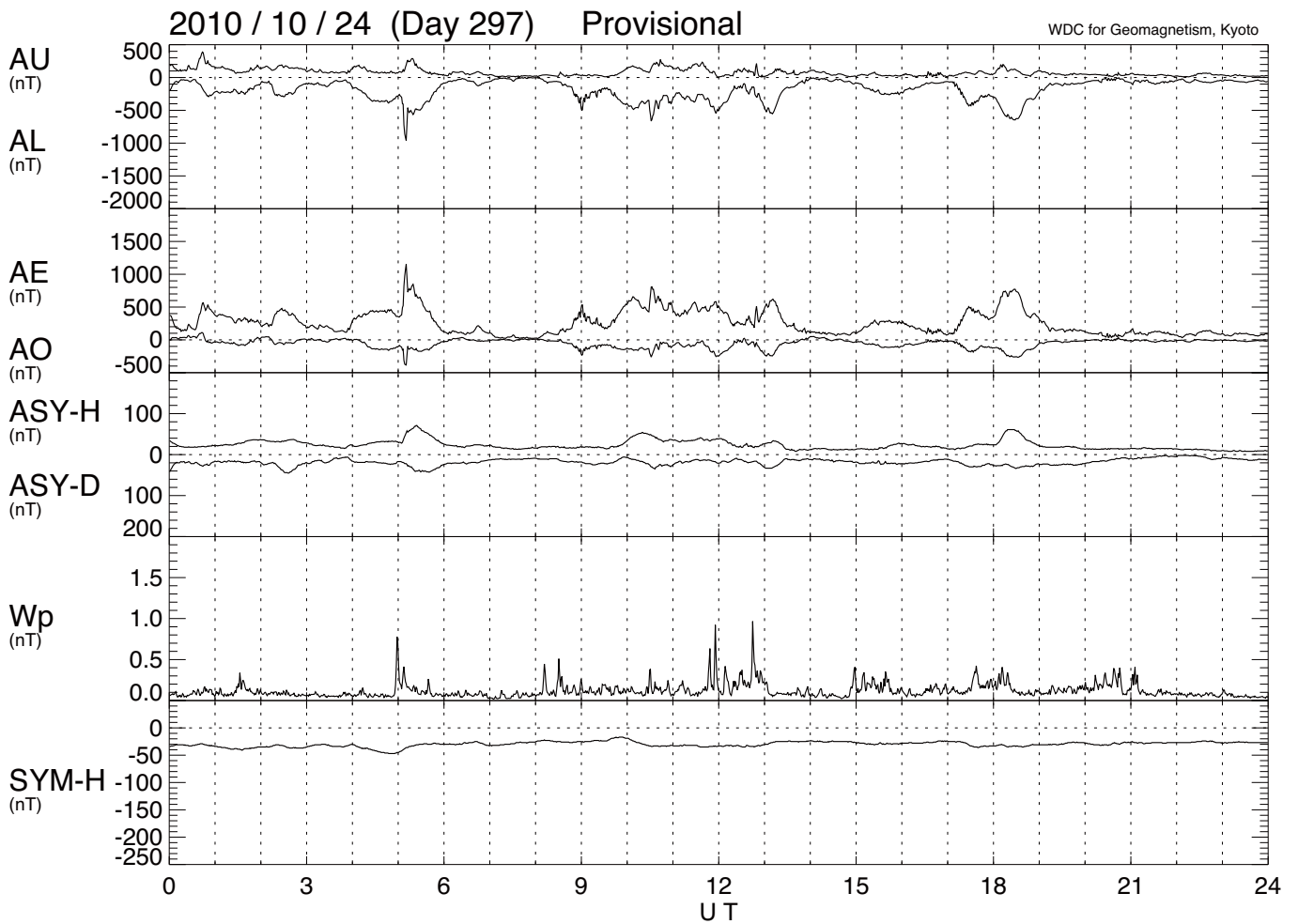
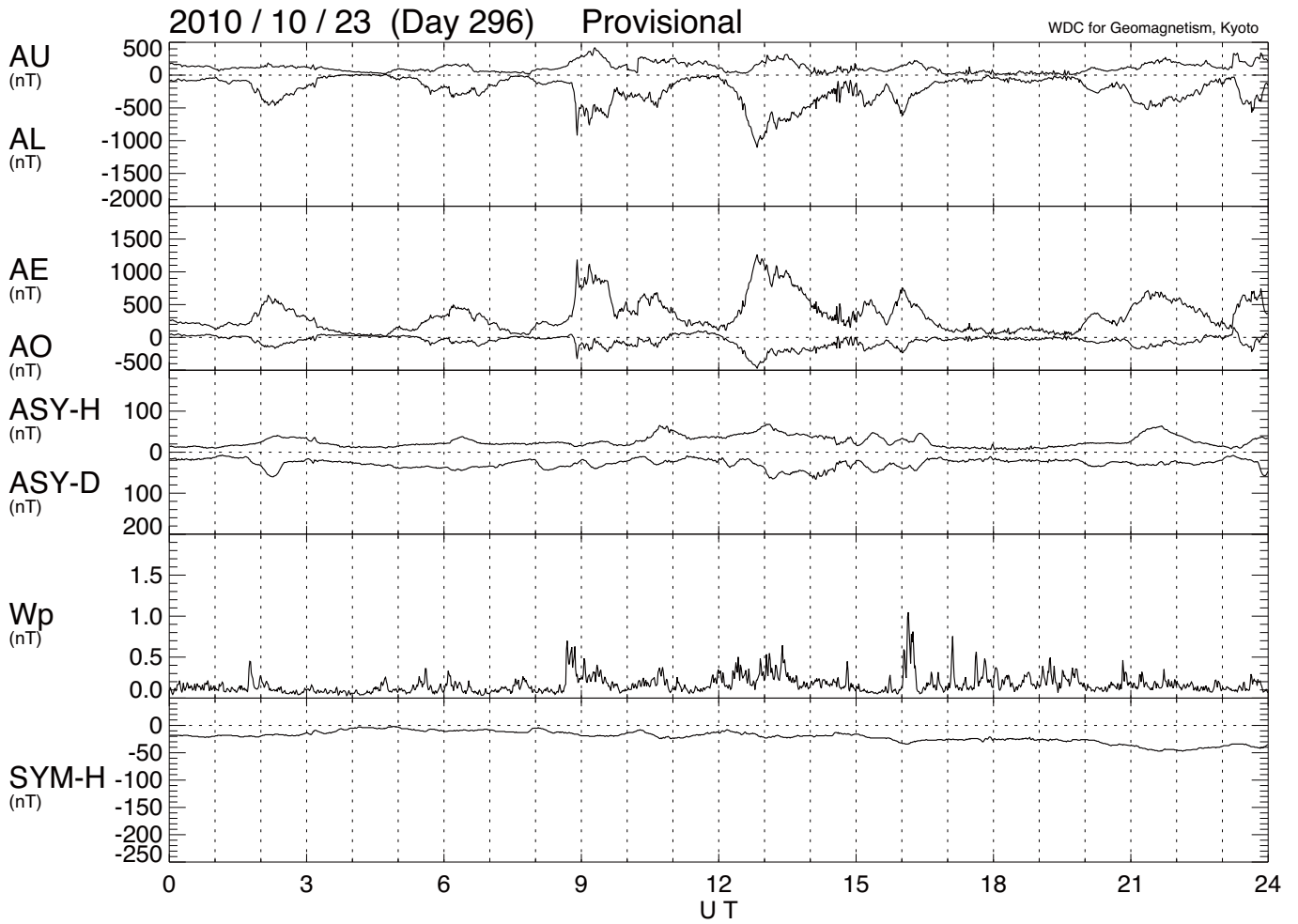


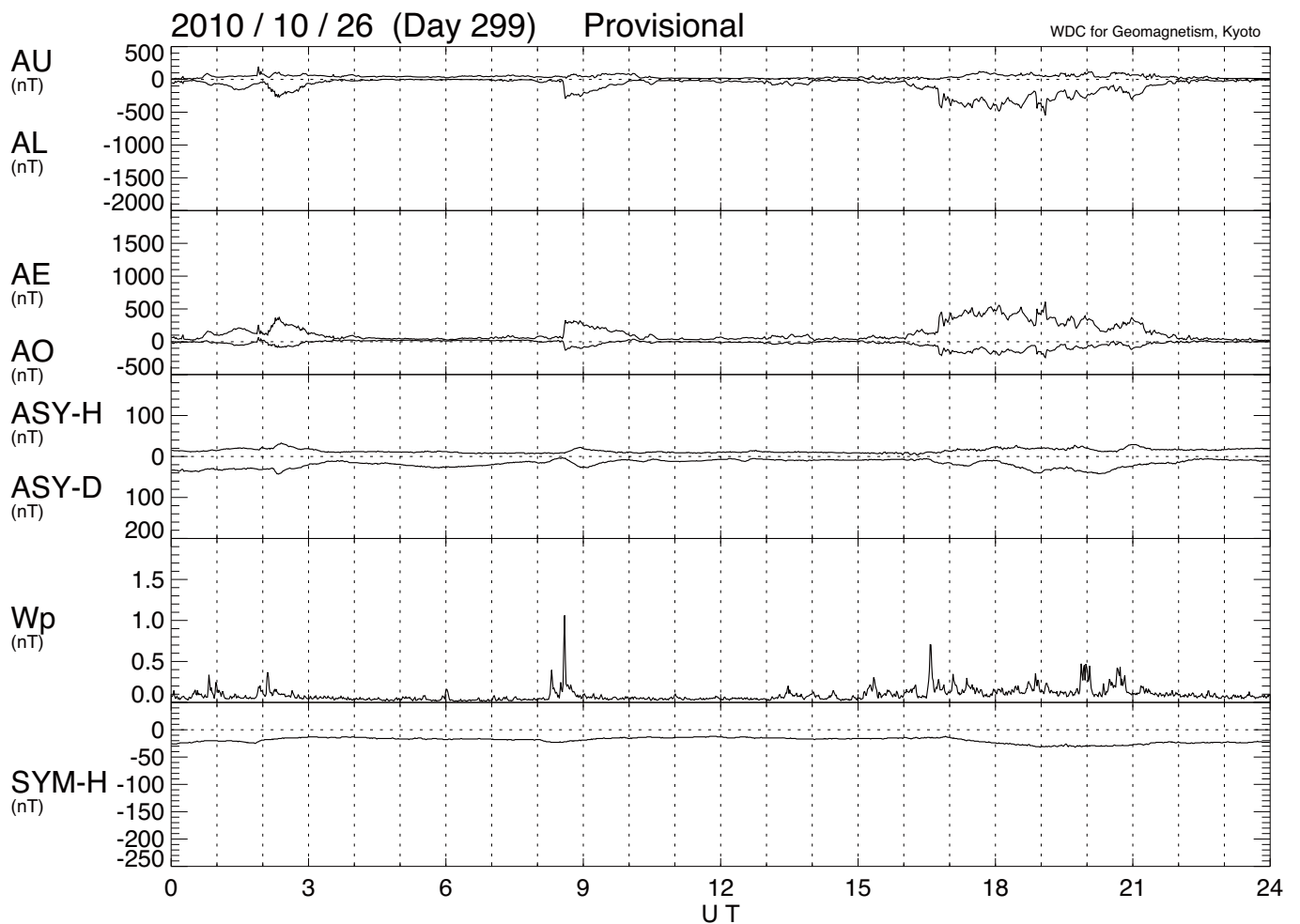
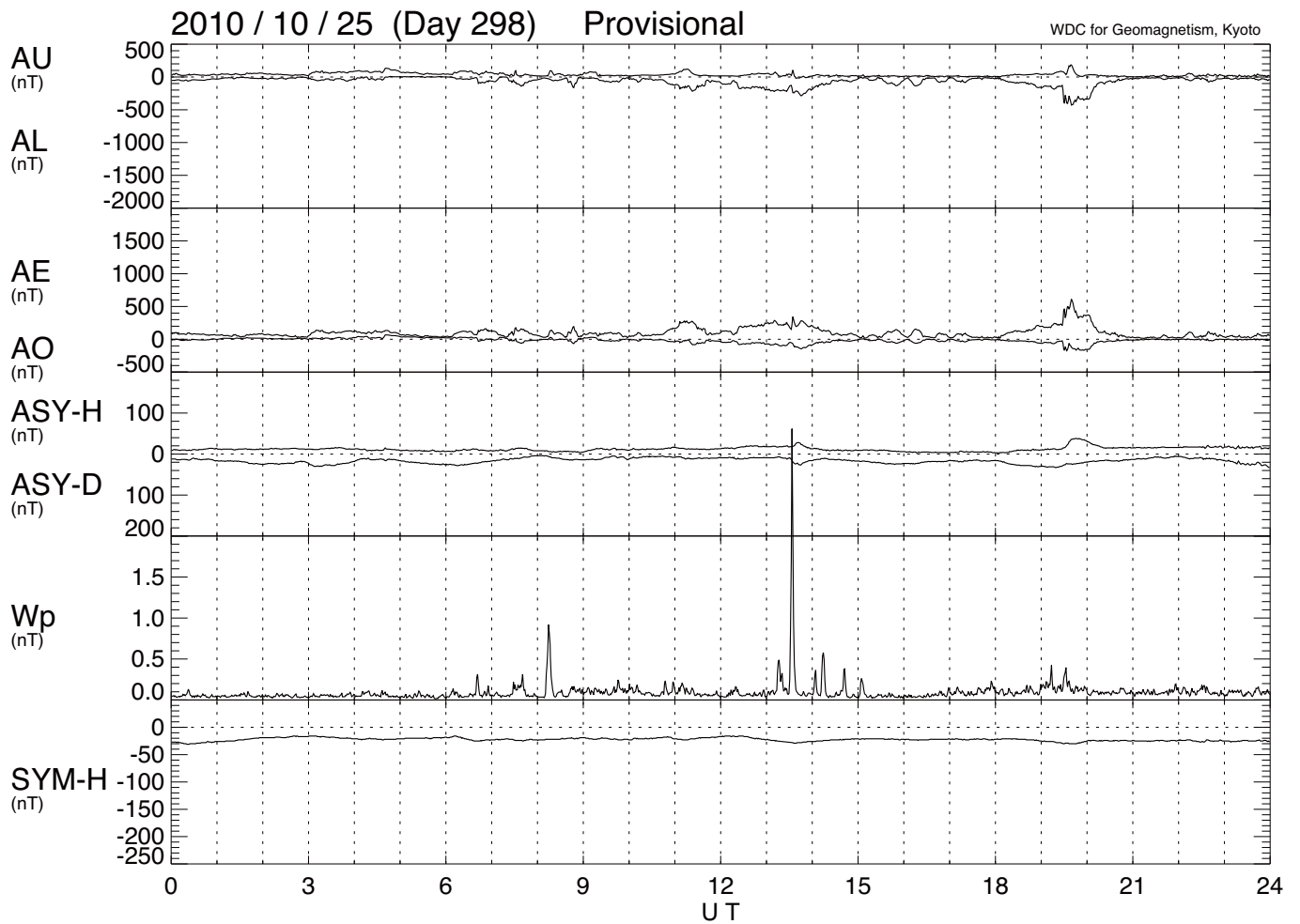


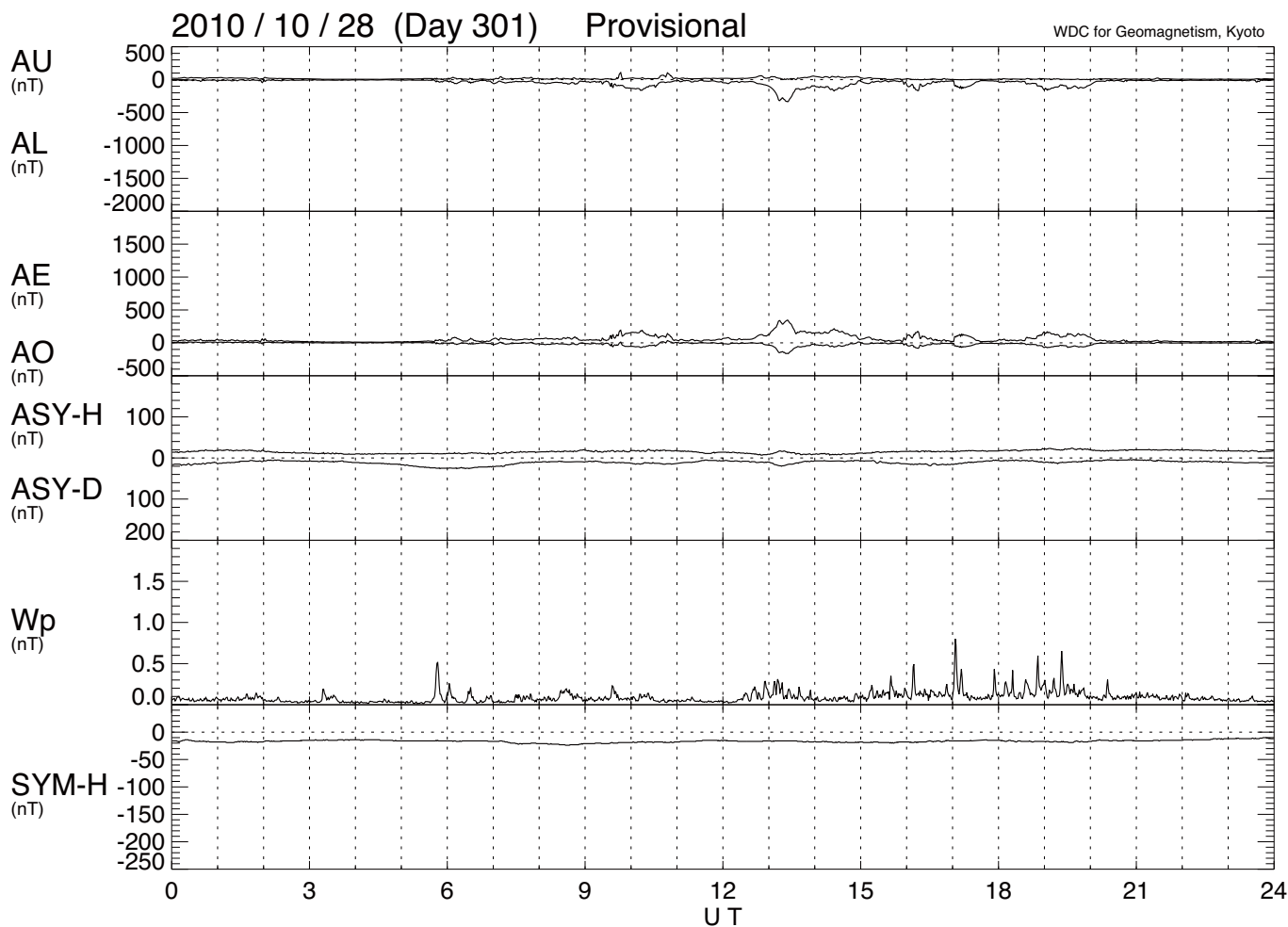
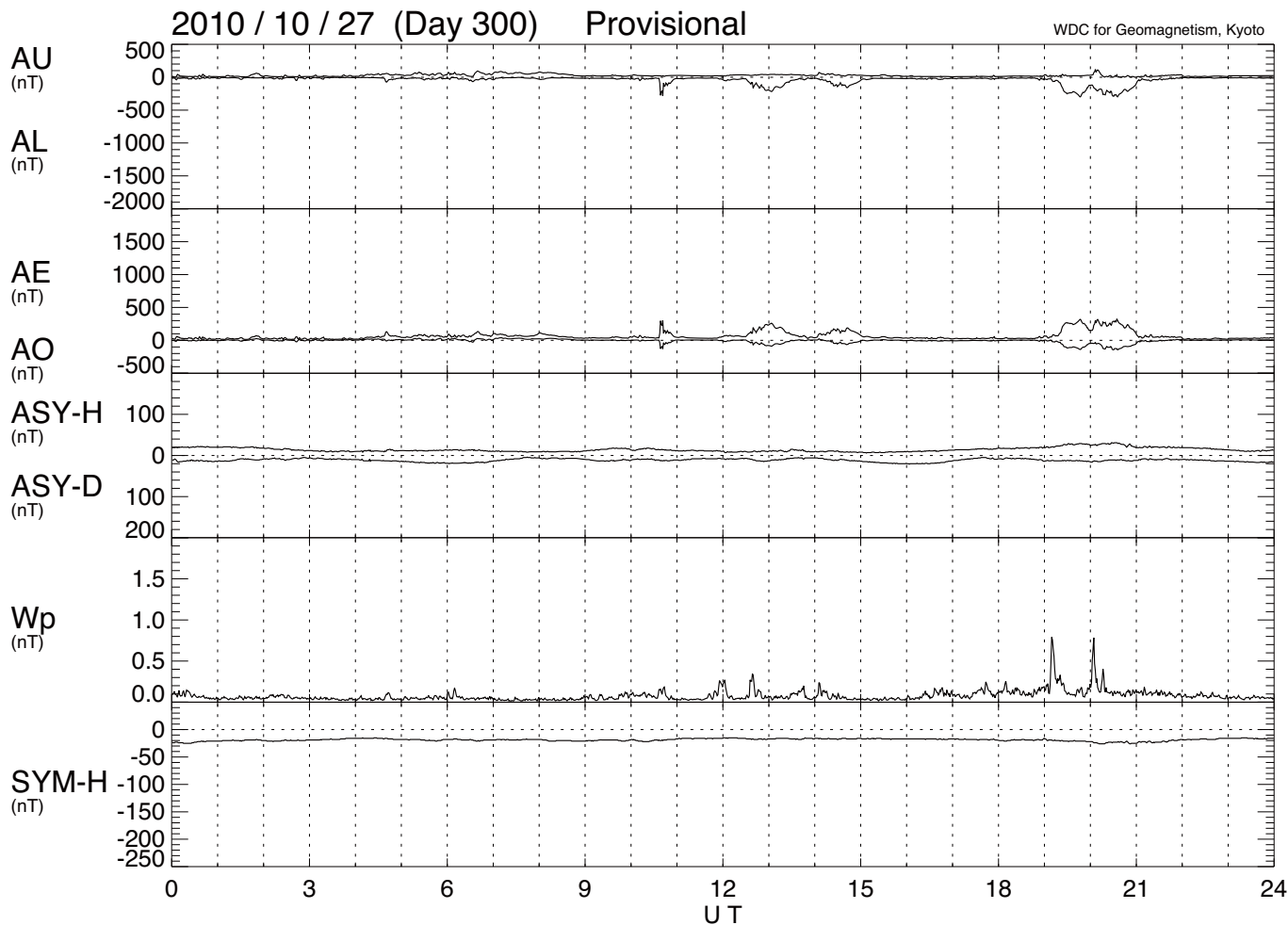


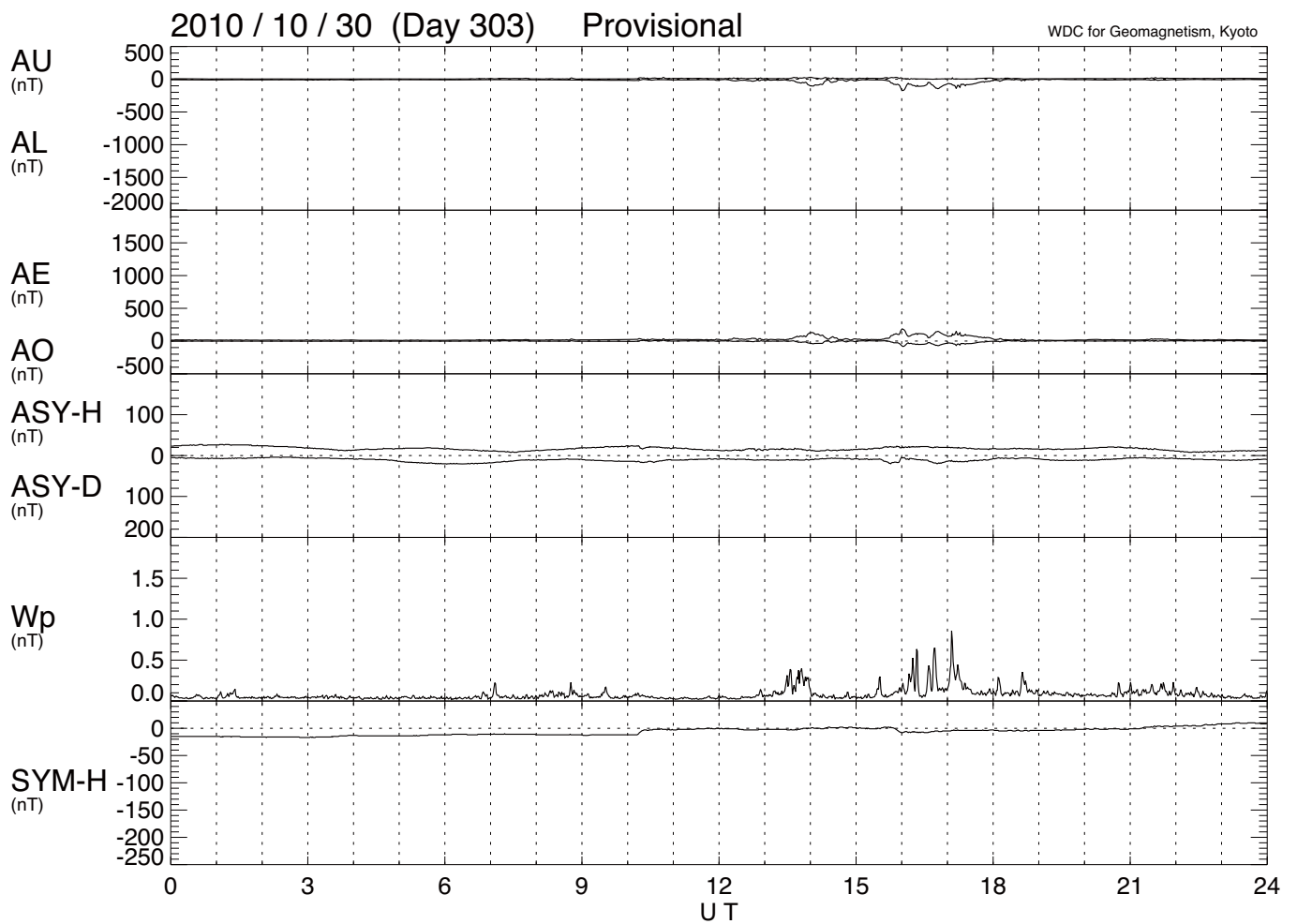
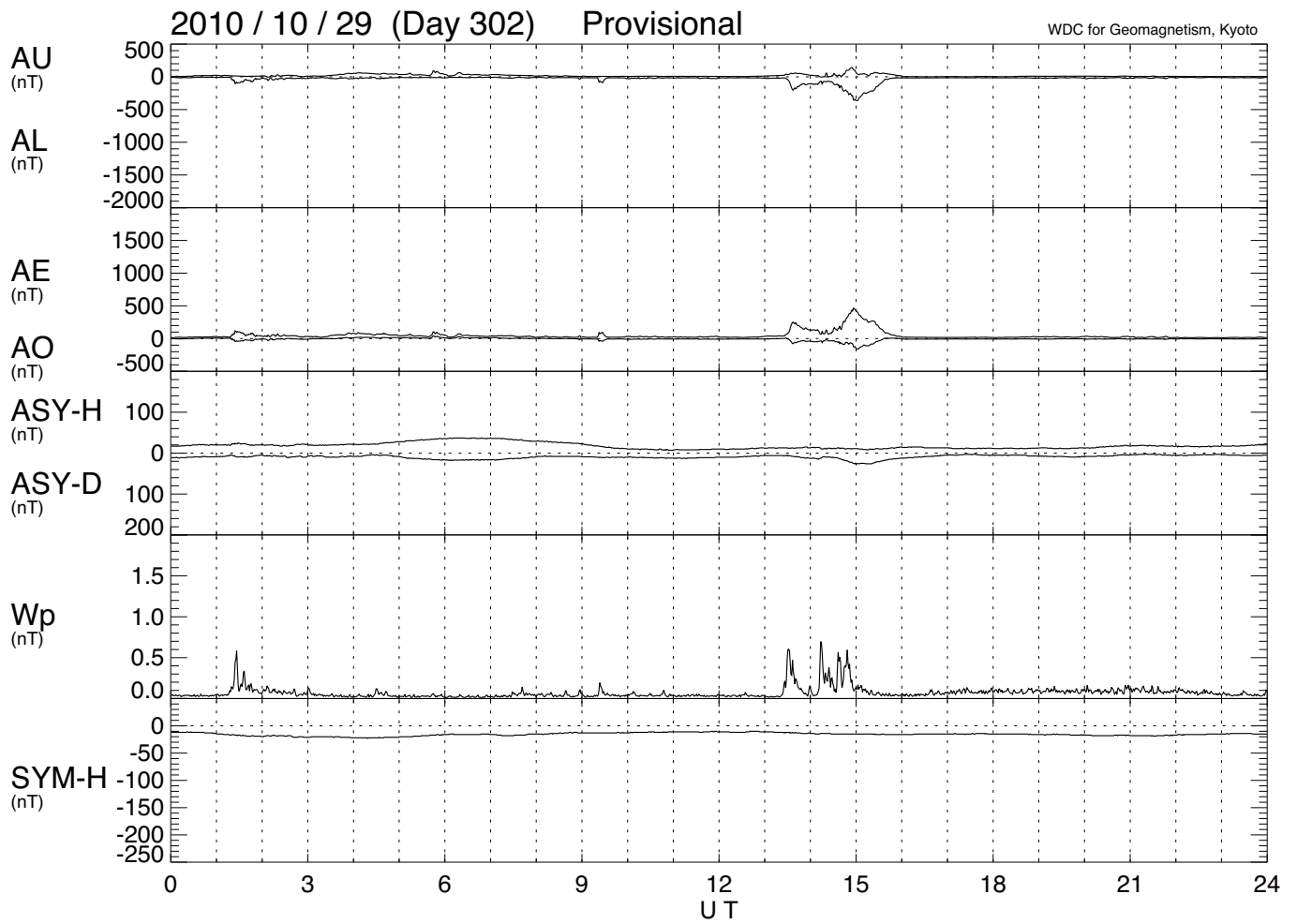












2010 / 10 / 31 (Day 304) Provisional

WDC for Geomagnetism, Kyoto

